

Functional textiles for improved performance, protection and health

The Textile Institute and Woodhead Publishing

The Textile Institute is a unique organisation in textiles, clothing and footwear. Incorporated in England by a Royal Charter granted in 1925, the Institute has individual and corporate members in over 90 countries. The aim of the Institute is to facilitate learning, recognise achievement, reward excellence and disseminate information within the global textiles, clothing and footwear industries.

Historically, The Textile Institute has published books of interest to its members and the textile industry. To maintain this policy, the Institute has entered into partnership with Woodhead Publishing Limited to ensure that Institute members and the textile industry continue to have access to high calibre titles on textile science and technology.

Most Woodhead titles on textiles are now published in collaboration with The Textile Institute. Through this arrangement, the Institute provides an Editorial Board which advises Woodhead on appropriate titles for future publication and suggests possible editors and authors for these books. Each book published under this arrangement carries the Institute's logo.

Woodhead books published in collaboration with The Textile Institute are offered to Textile Institute members at a substantial discount. These books, together with those published by The Textile Institute that are still in print, are offered on the Woodhead web site at: www.woodheadpublishing.com. Textile Institute books still in print are also available directly from the Institute's website at: www.textileinstitutebooks.com.

A list of Woodhead books on textile science and technology, most of which have been published in collaboration with The Textile Institute, can be found towards the end of the contents pages.

Woodhead Publishing Series in Textiles: Number 120

Functional textiles for improved performance, protection and health

Edited by
N. Pan and G. Sun



The Textile Institute

WP

WOODHEAD
PUBLISHING



Oxford

Cambridge

Philadelphia

New Delhi

Published by Woodhead Publishing Limited in association with The Textile Institute,
Woodhead Publishing Limited,
80 High Street, Sawston, Cambridge CB22 3HJ, UK
www.woodheadpublishing.com

Woodhead Publishing, 1518 Walnut Street, Suite 1100, Philadelphia,
PA 19102-3406, USA

Woodhead Publishing India Private Limited, G-2, Vardaan House, 7/28 Ansari Road,
Daryaganj, New Delhi – 110002, India
www.woodheadpublishingindia.com

First published 2011, Woodhead Publishing Limited

© Woodhead Publishing Limited, 2011

The authors have asserted their moral rights.

This book contains information obtained from authentic and highly regarded sources. Reprinted material is quoted with permission, and sources are indicated. Reasonable efforts have been made to publish reliable data and information, but the authors and the publisher cannot assume responsibility for the validity of all materials. Neither the authors nor the publisher, nor anyone else associated with this publication, shall be liable for any loss, damage or liability directly or indirectly caused or alleged to be caused by this book.

Neither this book nor any part may be reproduced or transmitted in any form or by any means, electronic or mechanical, including photocopying, microfilming and recording, or by any information storage or retrieval system, without permission in writing from Woodhead Publishing Limited.

The consent of Woodhead Publishing Limited does not extend to copying for general distribution, for promotion, for creating new works, or for resale. Specific permission must be obtained in writing from Woodhead Publishing Limited for such copying.

Trademark notice: Product or corporate names may be trademarks or registered trademarks, and are used only for identification and explanation, without intent to infringe.

British Library Cataloguing in Publication Data

A catalogue record for this book is available from the British Library.

Library of Congress Control Number: 2011929806

ISBN 978-1-84569-723-5 (print)

ISBN 978-0-85709-287-8 (online)

ISSN 2042-0803 Woodhead Publishing Series in Textiles (print)

ISSN 2042-0811 Woodhead Publishing Series in Textiles (online)

The publisher's policy is to use permanent paper from mills that operate a sustainable forestry policy, and which has been manufactured from pulp which is processed using acid-free and elemental chlorine-free practices. Furthermore, the publisher ensures that the text paper and cover board used have met acceptable environmental accreditation standards.

Typeset by Newgen Publishing and Data Services, Chennai, India

Printed by TJI Digital, Padstow, Cornwall, UK

Contents

<i>Contributor contact details</i>	<i>xiii</i>
<i>Woodhead Publishing Series in Textiles</i>	<i>xvii</i>
<i>Preface</i>	<i>xxiii</i>
Part I Functional textiles and clothing for improved performance and protection	1
1 Improved textile functionality through surface modifications	3
R. MORENT and N. DE GEYTER, Ghent University, Belgium	
1.1 Introduction	3
1.2 Types of surface modification	4
1.3 Physical and chemical characterization of surface modifications	8
1.4 Applications for functional textiles	19
1.5 Future trends	23
1.6 References	24
2 Antistatic and conductive textiles	27
X. ZHANG, North Carolina State University, USA	
2.1 Introduction	27
2.2 Principles of antistatic and conductive textiles	28
2.3 The role of antistatic and conductive textiles	33
2.4 Types of antistatic and conductive textiles	33
2.5 Evaluation of antistatic and conductive textiles	39
2.6 Future trends	41
2.7 Sources of further information and advice	42
2.8 References	43

3	Ultraviolet protection of clothing	45
	T. GAMBICHLER, Ruhr University Bochum, Germany	
3.1	Introduction	45
3.2	<i>In vitro</i> and <i>in vivo</i> testing of the UV protection factor	48
3.3	Standards for sun-protective clothing	50
3.4	Type and construction of fabric	51
3.5	Fabric color, dyes and UV absorbers	53
3.6	Effects of environment and fabric use on UV protection factor	55
3.7	Conclusions and outlook	56
3.8	References	58
4	3D body imaging and fit for functional textiles	64
	B. XU, University of Texas at Austin, USA	
4.1	Introduction	64
4.2	3D body imaging – stereovision	66
4.3	Surface modeling	72
4.4	Virtual dressing	80
4.5	Sewability and fit assessment	91
4.6	Future trends	93
4.7	Acknowledgement	94
4.8	References	94
5	Flame retardant functional textiles	98
	S. GAAN, V. SALIMOVA, P. RUPPER, A. RITTER and H. SCHMID, Swiss Federal Laboratories for Materials Testing and Research (EMPA), Switzerland	
5.1	Introduction	98
5.2	Factors affecting flammability and thermal behavior of textile fibers and fabrics	99
5.3	Types, chemistry and mode of action of flame retardant additives	103
5.4	Flame retardation of textile materials	105
5.5	Environmental issues related to flame retardants	121
5.6	Test standards for flame retardant textiles	122
5.7	References	123

6	Functional shape memory textiles	131
	J. HU and Q. MENG, Hong Kong Polytechnic University, Hong Kong	
6.1	Introduction	131
6.2	Shape memory mechanisms of SMAs	132
6.3	Applications of SMAs in textiles	133
6.4	Shape memory mechanisms of SMPs	138
6.5	Applications of SMPs in textiles	140
6.6	Future trends	155
6.7	Sources of further information and advice	157
6.8	References	157
7	Thermo-regulating textiles with phase-change materials	163
	S. MONDAL, The University of Queensland, Australia	
7.1	Introduction	163
7.2	Concept of thermal comfort and clothing for cold environments	164
7.3	How PCMs work	166
7.4	Thermo-physiological comfort for PCM incorporated textiles	168
7.5	Different types of PCMs	168
7.6	Incorporation of PCM in textile structure	172
7.7	Applications of PCM incorporated textiles	175
7.8	Challenges of PCM in textiles	177
7.9	Acknowledgement	178
7.10	References	178
8	Infrared functional textiles	184
	J. DYER, AgResearch Ltd, New Zealand	
8.1	Introduction and overview	184
8.2	Principles of IR	185
8.3	FIR therapy	186
8.4	The role of FIR in relation to functional textiles	190
8.5	Applications	192
8.6	Benefits and limitations	193
8.7	Conclusions and future trends	194
8.8	Sources of further information	194
8.9	Acknowledgements	195
8.10	References	195

viii	Contents	
9	Functional smart textiles using stimuli-sensitive polymers	198
	A. K. AGRAWAL and M. JASSAL, Indian Institute of Technology, India	
9.1	Introduction	198
9.2	Stimuli-sensitive polymers	198
9.3	Drawbacks and limitations of current SSP/hydrogels	204
9.4	Smart functional textiles	205
9.5	Conclusions	221
9.6	References	221
10	Development and design of performance swimwear	226
	J. WU, Georgia State University, USA	
10.1	Introduction	226
10.2	Development of performance swimwear	227
10.3	Biomechanics of swimming	231
10.4	Effect of innovative swimwear on swimming performance	236
10.5	Future trends in innovative performance swimwear	245
10.6	Sources of further information and advice	246
10.7	Acknowledgements	246
10.8	References	247
11	Key elements of protection for military textiles	249
	J. R. OWENS, Air Force Research Laboratory, USA	
11.1	Introduction	249
11.2	Camouflage	250
11.3	Ballistics	253
11.4	Toxic chemicals	255
11.5	Conclusions	266
11.6	References	267
12	Developments in clothing protection technology	269
	W. ZHONG, University of Manitoba, Canada and N. PAN, University of California, Davis, USA	
12.1	Introduction	269
12.2	Key issues of protective clothing	270
12.3	Developments in clothing protection	274

12.4	Future trends	284
12.5	References	285
Part II	Functional textiles for improved medical and health purposes	291
13	New developments in functional medical textiles and their mechanism of action J. V. EDWARDS, ARS-USDA, USA and S. C. GOHEEN, Pacific Northwest National Laboratory, USA	293
13.1	Introduction	293
13.2	Extracorporeals and implantables	294
13.3	Structure and composition: role of functionality in implantables	297
13.4	The role of biomolecules in conferring bioactive function	301
13.5	Non-implantables: wound dressings, pressure ulcers, hemorrhage control	303
13.6	References	314
14	Improving superhydrophobic coatings for textiles through chemical modifications C. H. XUE, University of California, Davis, USA	320
14.1	Introduction	320
14.2	Key principles of superhydrophobic textiles	321
14.3	Chemical modifications for fabricating rough surfaces on textiles	323
14.4	Hydrophobization for lowering the surface energy of roughened textiles	327
14.5	Nanoscaled coating of materials with low surface energy	329
14.6	Applications	331
14.7	Future trends	334
14.8	References	335
15	Improving superhydrophobic textile materials H. J. LEE, North Carolina State University, USA	339
15.1	Introduction	339
15.2	Physical modification for superhydrophobic textiles	340
15.3	Applications	353

x	Contents	
15.4	Future trends	356
15.5	References	357
16	Antibacterial textile materials for medical applications	360
	G. SUN, University of California, Davis, USA	
16.1	Introduction	360
16.2	Principles of antimicrobial textiles	361
16.3	The development of antibacterial textiles	363
16.4	Performance of antibacterial textiles	368
16.5	New antimicrobial technologies	369
16.6	Applications of antimicrobial textiles	371
16.7	Future trends	371
16.8	Acknowledgments	372
16.9	References	372
17	Antibacterial colorants for textiles	376
	F. ALIHOSSEINI and G. SUN, University of California, Davis, USA	
17.1	Introduction	376
17.2	Synthetic antibacterial colorants	378
17.3	Natural antimicrobial colorants	381
17.4	Antimicrobial colorants from micro-organisms	393
17.5	Photo-activated antimicrobial colorants	395
17.6	References	396
18	Pyrethroid-laden textiles for protection from biting insects	404
	D. G. HAYES, University of Tennessee, USA	
18.1	Introduction	404
18.2	Key issues of insecticide-laden textiles	414
18.3	Factory-produced LLINs and textiles for protection from biting insects	414
18.4	<i>In situ</i> treatment of bednets and other textiles to enable protection from biting insects	424
18.5	Future trends	425
18.6	Sources of further information and advice	426
18.7	References	426

19	Improving the functionality of clothing through novel pesticide protection	434
	S. K. OBENDORF, Cornell University, USA	
19.1	Introduction to human exposure	434
19.2	Mechanisms for chemical protection	436
19.3	Development of novel pesticide-protective clothing	445
19.4	References	456
20	Biomechanics in skin/clothing interactions	462
	M. XING and W. ZHONG, University of Manitoba, Canada and N. PAN, University of California, Davis, USA	
20.1	Introduction	462
20.2	An explicit finite element model of skin/sleeve interactions during arm rotation	465
20.3	Skin friction blistering: computer model	477
20.4	References	486
21	Transdermal permeation of textile dyes and chemicals	489
	W. ZHONG and M. XING, University of Manitoba, Canada and N. PAN, University of California, Davis, USA	
21.1	Introduction	489
21.2	Key issues of textile dyes/chemicals and skin irritations	490
21.3	An <i>in vitro</i> study of transdermal drug permeation	491
21.4	Stochastic modeling for transdermal drug delivery	496
21.5	Conclusion	502
21.6	References	504
	<i>Index</i>	<i>507</i>

Contributor contact details

(* = main contact)

Editors

N. Pan and G. Sun*
Division of Textiles and
Clothing
University of California,
Davis
CA 95616
USA

E-mail: ningpan.pan@gmail.com;
gysun@ucdavis.edu

Chapter 1

R. Morent* and N. De Geyter
Research Unit Plasma Technology
(RUPT)
Department of Applied
Physics
Faculty of Engineering and
Architecture
Ghent University
Jozef Plateaustraat 22
9000 Ghent
Belgium

E-mail: Rino.Morent@UGent.be

Chapter 2

X. Zhang
Department of Textile Engineering,
Chemistry and Science
College of Textiles
North Carolina State University
Campus Box 8301
2401 Research Drive
Raleigh
NC 27695-8301
USA

E-mail: xiangwu_zhang@ncsu.edu

Chapter 3

T. Gambichler
Department of Dermatology
Ruhr University Bochum
Gudrunstrasse 56
44791 Bochum
Germany
E-mail: t.gambichler@
klinikum-bochum.de

Chapter 4

B. Xu
School of Human Ecology
University of Texas at Austin
Gearing Hall 225
Austin
TX 78712
USA
E-mail: bxu@mail.utexas.edu

Chapter 5

S. Gaan*, V. Salimova, P. Rupper,
A. Ritter and H. Schmid
Laboratory for Advanced Fibers
Empa
Swiss Federal Laboratories for
Materials Testing and Research
(EMPA)
Lerchenfeldstrasse 5
CH-9014 St. Gallen
Switzerland
E-mail: sabyasachi.gaan@empa.ch

Chapter 6

J. Hu* and Q. Meng
Institute of Textiles and Clothing
Hong Kong Polytechnic
University
Kowloon
Hong Kong
E-mail: tchujl@inet.polyu.edu.hk

Chapter 7

S. Mondal
Australian Institute for
Bioengineering and
Nanotechnology
The University of Queensland
St Lucia
Queensland 4072
Australia
E-mail: subratamondal@yahoo.com

Chapter 8

J. Dyer
Protein Quality and Function
Lincoln Research Centre,
AgResearch Ltd
Cnr Springs Road and Gerald
Street
Private Bag 4749
Christchurch 8140
New Zealand
E-mail: Jolon.Dyer@agresearch.
co.nz

Chapter 9

A. K. Agrawal* and M. Jassal
Research Group on Smart and
Innovative Textile Materials
Department of Textile
Technology
Indian Institute of Technology
Hauz Khas
New Delhi 110 016
India
E-mail: ashwini@smita-iitd.com;
manjeetjassal@gmail.com

Chapter 10

J. Wu
Department of Kinesiology and
Health
Georgia State University
PO Box 3975
Atlanta
GA 30302-3975
USA
E-mail: jwu11@gsu.edu

Chapter 11

J. R. Owens
Air Force Research Laboratory
Tyndall AFB
FL 32404
USA

E-mail: Jeffery.owens@
tyndall.af.mil

Chapter 12

W. Zhong*
Department of Textile Sciences
University of Manitoba
Winnipeg
Manitoba R3T 2N2
Canada

E-mail: zhong@cc.umanitoba.ca

N. Pan
Division of Textiles and Clothing
University of California, Davis
CA 95616
USA

E-mail: ningpan.pan@gmail.com

Chapter 13

J. V. Edwards*
Agricultural Research Service
US Department of Agriculture
Southern Regional Research Center
New Orleans
LA 70179
USA
Vince.Edwards@ARS.USDA.GOV

S. C. Goheen
Chemical and Physical Sciences
Division
National Security Directorate
Pacific Northwest National
Laboratory
Richland
WA 99352
USA
steve.goheen@pnl.gov

Chapter 14

C. H. Xue
Division of Textiles and Clothing
University of California, Davis
CA 95616
USA

E-mail: chxue@ucdavis.edu

Chapter 15

H. J. Lee
College of Textiles
North Carolina State University
Raleigh
NC 27695-8301
USA

E-mail: hoonjoo_lee@ncsu.edu

Chapter 16

G. Sun
Division of Textiles and Clothing
University of California, Davis
CA 95616
USA

E-mail: gysun@ucdavis.edu

Chapter 17

F. Alihosseini* and G. Sun
Division of Textiles and Clothing
University of California, Davis
CA 95616
USA

E-mail: fhosseini@ucdavis.edu;
gysun@ucdavis.edu

Chapter 18

D. G. Hayes
Department of Biosystems
Engineering and Soil Science
University of Tennessee
2506 E. J. Chapman Drive
Knoxville
TN 37996-4531
USA

E-mail: dhayes1@utk.edu

Chapter 19

S. K. Obendorf
Fiber Science
Martha Van Rensselaer Hall
Cornell University
Ithaca
NY 14853
USA

E-mail: sko3@cornell.edu

Chapter 20

M. Xing* and W. Zhong
Department of Textile Sciences
University of Manitoba
Winnipeg
Manitoba R3T 2N2
Canada

E-mail: xing@cc.umanitoba.ca;
zhong@cc.umanitoba.ca

N. Pan
Division of Textiles and Clothing
University of California, Davis
CA 95616
USA

E-mail: ningpan.pan@gmail.com

Chapter 21

W. Zhong* and M. Xing
Department of Textile Sciences
University of Manitoba
Winnipeg
Manitoba R3T 2N2
Canada

E-mail: zhong@cc.umanitoba.ca;
xing@cc.umanitoba.ca

N. Pan
Division of Textiles and Clothing
University of California, Davis
CA 95616
USA

E-mail: ningpan.pan@gmail.com

Woodhead Publishing Series in Textiles

- 1 **Watson's textile design and colour** Seventh edition
Edited by Z. Grosicki
- 2 **Watson's advanced textile design**
Edited by Z. Grosicki
- 3 **Weaving** Second edition
P. R. Lord and M. H. Mohamed
- 4 **Handbook of textile fibres Vol 1: Natural fibres**
J. Gordon Cook
- 5 **Handbook of textile fibres Vol 2: Man-made fibres**
J. Gordon Cook
- 6 **Recycling textile and plastic waste**
Edited by A. R. Horrocks
- 7 **New fibers** Second edition
T. Hongu and G. O. Phillips
- 8 **Atlas of fibre fracture and damage to textiles** Second edition
J. W. S. Hearle, B. Lomas and W. D. Cooke
- 9 **Ecotextile '98**
Edited by A. R. Horrocks
- 10 **Physical testing of textiles**
B. P. Saville
- 11 **Geometric symmetry in patterns and tilings**
C. E. Horne
- 12 **Handbook of technical textiles**
Edited by A. R. Horrocks and S. C. Anand
- 13 **Textiles in automotive engineering**
W. Fung and J. M. Hardcastle
- 14 **Handbook of textile design**
J. Wilson
- 15 **High-performance fibres**
Edited by J. W. S. Hearle
- 16 **Knitting technology** Third edition
D. J. Spencer
- 17 **Medical textiles**
Edited by S. C. Anand

- 18 **Regenerated cellulose fibres**
Edited by C. Woodings
- 19 **Silk, mohair, cashmere and other luxury fibres**
Edited by R. R. Franck
- 20 **Smart fibres, fabrics and clothing**
Edited by X. M. Tao
- 21 **Yarn texturing technology**
J. W. S. Hearle, L. Hollick and D. K. Wilson
- 22 **Encyclopedia of textile finishing**
H-K. Rouette
- 23 **Coated and laminated textiles**
W. Fung
- 24 **Fancy yarns**
R. H. Gong and R. M. Wright
- 25 **Wool: Science and technology**
Edited by W. S. Simpson and G. Crawshaw
- 26 **Dictionary of textile finishing**
H-K. Rouette
- 27 **Environmental impact of textiles**
K. Slater
- 28 **Handbook of yarn production**
P. R. Lord
- 29 **Textile processing with enzymes**
Edited by A. Cavaco-Paulo and G. Gübitz
- 30 **The China and Hong Kong denim industry**
Y. Li, L. Yao and K. W. Yeung
- 31 **The World Trade Organization and international denim trading**
Y. Li, Y. Shen, L. Yao and E. Newton
- 32 **Chemical finishing of textiles**
W. D. Schindler and P. J. Hauser
- 33 **Clothing appearance and fit**
J. Fan, W. Yu and L. Hunter
- 34 **Handbook of fibre rope technology**
H. A. McKenna, J. W. S. Hearle and N. O'Hear
- 35 **Structure and mechanics of woven fabrics**
J. Hu
- 36 **Synthetic fibres: nylon, polyester, acrylic, polyolefin**
Edited by J. E. McIntyre
- 37 **Woollen and worsted woven fabric design**
E. G. Gilligan
- 38 **Analytical electrochemistry in textiles**
P. Westbroek, G. Priniotakis and P. Kiekens
- 39 **Bast and other plant fibres**
R. R. Franck

- 40 **Chemical testing of textiles**
Edited by Q. Fan
- 41 **Design and manufacture of textile composites**
Edited by A. C. Long
- 42 **Effect of mechanical and physical properties on fabric hand**
Edited by Hassan M. Behery
- 43 **New millennium fibers**
T. Hongu, M. Takigami and G. O. Phillips
- 44 **Textiles for protection**
Edited by R. A. Scott
- 45 **Textiles in sport**
Edited by R. Shishoo
- 46 **Wearable electronics and photonics**
Edited by X. M. Tao
- 47 **Biodegradable and sustainable fibres**
Edited by R. S. Blackburn
- 48 **Medical textiles and biomaterials for healthcare**
Edited by S. C. Anand, M. MirafTAB, S. Rajendran and J. F. Kennedy
- 49 **Total colour management in textiles**
Edited by J. Xin
- 50 **Recycling in textiles**
Edited by Y. Wang
- 51 **Clothing biosensory engineering**
Y. Li and A. S. W. Wong
- 52 **Biomechanical engineering of textiles and clothing**
Edited by Y. Li and D. X-Q. Dai
- 53 **Digital printing of textiles**
Edited by H. Ujiie
- 54 **Intelligent textiles and clothing**
Edited by H. R. Mattila
- 55 **Innovation and technology of women's intimate apparel**
W. Yu, J. Fan, S. C. Harlock and S. P. Ng
- 56 **Thermal and moisture transport in fibrous materials**
Edited by N. Pan and P. Gibson
- 57 **Geosynthetics in civil engineering**
Edited by R. W. Sarsby
- 58 **Handbook of nonwovens**
Edited by S. Russell
- 59 **Cotton: Science and technology**
Edited by S. Gordon and Y-L. Hsieh
- 60 **Ecotextiles**
Edited by M. MirafTAB and A. R. Horrocks
- 61 **Composite forming technologies**
Edited by A. C. Long

- 62 **Plasma technology for textiles**
Edited by R. Shishoo
- 63 **Smart textiles for medicine and healthcare**
Edited by L. Van Langenhove
- 64 **Sizing in clothing**
Edited by S. Ashdown
- 65 **Shape memory polymers and textiles**
J. Hu
- 66 **Environmental aspects of textile dyeing**
Edited by R. Christie
- 67 **Nanofibers and nanotechnology in textiles**
Edited by P. Brown and K. Stevens
- 68 **Physical properties of textile fibres Fourth edition**
W. E. Morton and J. W. S. Hearle
- 69 **Advances in apparel production**
Edited by C. Fairhurst
- 70 **Advances in fire retardant materials**
Edited by A. R. Horrocks and D. Price
- 71 **Polyesters and polyamides**
Edited by B. L. Deopura, R. Alagirusamy, M. Joshi and B. S. Gupta
- 72 **Advances in wool technology**
Edited by N. A. G. Johnson and I. Russell
- 73 **Military textiles**
Edited by E. Wilusz
- 74 **3D fibrous assemblies: Properties, applications and modelling of three-dimensional textile structures**
J. Hu
- 75 **Medical and healthcare textiles**
Edited by S. C. Anand, J. F. Kennedy, M. Miraftab and S. Rajendran
- 76 **Fabric testing**
Edited by J. Hu
- 77 **Biologically inspired textiles**
Edited by A. Abbott and M. Ellison
- 78 **Friction in textile materials**
Edited by B. S. Gupta
- 79 **Textile advances in the automotive industry**
Edited by R. Shishoo
- 80 **Structure and mechanics of textile fibre assemblies**
Edited by P. Schwartz
- 81 **Engineering textiles: Integrating the design and manufacture of textile products**
Edited by Y. E. El-Mogahzy
- 82 **Polyolefin fibres: Industrial and medical applications**
Edited by S. C. O. Ugbohue

- 83 **Smart clothes and wearable technology**
Edited by J. McCann and D. Bryson
- 84 **Identification of textile fibres**
Edited by M. Houck
- 85 **Advanced textiles for wound care**
Edited by S. Rajendran
- 86 **Fatigue failure of textile fibres**
Edited by M. MirafTAB
- 87 **Advances in carpet technology**
Edited by K. Goswami
- 88 **Handbook of textile fibre structure Volume 1 and Volume 2**
Edited by S. J. Eichhorn, J. W. S. Hearle, M. Jaffe and T. Kikutani
- 89 **Advances in knitting technology**
Edited by K-F. Au
- 90 **Smart textile coatings and laminates**
Edited by W. C. Smith
- 91 **Handbook of tensile properties of textile and technical fibres**
Edited by A. R. Bunsell
- 92 **Interior textiles: Design and developments**
Edited by T. Rowe
- 93 **Textiles for cold weather apparel**
Edited by J. T. Williams
- 94 **Modelling and predicting textile behaviour**
Edited by X. Chen
- 95 **Textiles, polymers and composites for buildings**
Edited by G. Pohl
- 96 **Engineering apparel fabrics and garments**
J. Fan and L. Hunter
- 97 **Surface modification of textiles**
Edited by Q. Wei
- 98 **Sustainable textiles**
Edited by R. S. Blackburn
- 99 **Advances in yarn spinning technology**
Edited by C. A. Lawrence
- 100 **Handbook of medical textiles**
Edited by V. T. Bartels
- 101 **Technical textile yarns**
Edited by R. Alagirusamy and A. Das
- 102 **Applications of nonwovens in technical textiles**
Edited by R. A. Chapman
- 103 **Colour measurement: Principles, advances and industrial applications**
Edited by M. L. Gulrajani
- 104 **Fibrous and composite materials for civil engineering applications**
Edited by R. Figueiro

- 105 **New product development in textiles**
Edited by B. Mills
- 106 **Improving comfort in clothing**
Edited by G. Song
- 107 **Advances in textile biotechnology**
Edited by V. A. Nierstrasz and A. Cavaco-Paulo
- 108 **Textiles for hygiene and infection control**
Edited by B. McCarthy
- 109 **Nanofunctional textiles**
Edited by Y. Li
- 110 **Joining textiles: principles and applications**
Edited by I. Jones and G. Stylios
- 111 **Soft computing in textile engineering**
Edited by A. Majumdar
- 112 **Textile design**
Edited by A. Briggs-Goode and K. Townsend
- 113 **Biotextiles as medical implants**
Edited by M. King and B. Gupta
- 114 **Textile thermal bioengineering**
Edited by Y. Li
- 115 **Woven textile structure**
B. K. Behera and P. K. Hari
- 116 **Handbook of textile and industrial dyeing. Volume 1: Principles processes and types of dyes**
Edited by M. Clark
- 117 **Handbook of textile and industrial dyeing. Volume 2: Applications of dyes**
Edited by M. Clark
- 118 **Handbook of natural fibres. Volume 1: Types, properties and factors affecting breeding and cultivation**
Edited by R. Kozlowski
- 119 **Handbook of natural fibres. Volume 2: Processing and applications**
Edited by R. Kozlowski
- 120 **Functional textiles for improved performance, protection and health**
Edited by N. Pan and G. Sun
- 121 **Computer technology for textiles and apparel**
Edited by Jinlian Hu
- 122 **Advances in military textiles and personal equipment**
Edited by E. Sparks
- 123 **Specialist yarn, woven and fabric structure: Developments and applications**
Edited by R. H. Gong
- 124 **Handbook of sustainable textile production**
Edited by M. Tobler-Rohr

Clothing materials have at least two major functions: protection and decoration. Which of these is the primary, most important function is a matter of some debate. This book, through all its chapters, focuses solely on the functional performance of clothing materials related to protection of the human body. There is a long tradition of scientific research on this extremely important topic, but the related knowledge and information has been more or less scattered. This book therefore represents an attempt to collect all the relevant and up-to-date information in this field and to introduce the cutting edge scientific research to the potential audience.

Not many people would associate clothing design and manufacture with high tech or great scientific rigor. The wide range of coverage in this book, along with the theoretical depth of the problems and challenges involved, may consequently come as something of a surprise to them. We hope, therefore, that this book may also serve to attract the attention and interest of scientists from other non-textile fields, with a view to finding topics appropriate for interdisciplinary collaboration and future research.

The book itself can be divided into two parts – one focused on the topics more associated with chemical structures and modifications, and the other on properties related to physics – broadly aligned to the backgrounds of the two editors. Of the topics covered in this book, those with a longer history of research include antistatic and conductive textiles, anti-ultraviolet protection of clothing, flame retardant functional textiles, and infrared textiles. Other topics are relatively new, such as surface modifications for super-hydrophobic textiles, antimicrobial textile materials for medical applications, and to a lesser degree, insect (mosquito) repellent textiles, and pesticide protective clothing. Still others focus on specific types of textiles in sportswear and swimwear, military protective clothing systems, and medical textiles. Advances in material development have led to significant progress in new types of textiles which are also discussed here, including textiles with phase-change materials, functional shape memory textiles, and smart textiles, or wearable electronics, as they are often called. In addition, the book addresses some general scientific issues in textiles such as 3D body scanning

and fit for functional textiles, biomechanics in skin/clothing interactions, and transdermal permeation of textile dyes/chemicals.

We are very grateful to all the contributors of this book for their time and effort in putting together the most up-to-date information in each subject area. We also hope that we have put together a book that serves not only the scientific research community but also the industries on functional textile investigation and development.

Needless to say this book would not have been possible without tremendous help from other people, especially from our Publications Coordinator Mr Adam Hooper, the Commissioning Editor Mrs Kathryn Picking, the Project Editor Miss Vicki Hart, and of course the institution behind them, Woodhead Publishing Limited.

Gang Sun and Ning Pan

Improved textile functionality through surface modifications

R. MORENT and N. DE GEYTER,
Ghent University, Belgium

Abstract: This chapter discusses some important surface modification techniques employed for improved functional behavior of textiles. Through technological innovations, the textile industry has experienced rapid development with miscellaneous new applications. Some of these techniques are briefly introduced. The behavior of these functional textiles is strongly governed by the chemical and physical characteristics of their surface. Progress in understanding this functional behavior is only possible when these characteristics are known and therefore surface analysis is a crucial and necessary step. As a result, advanced surface characterization techniques are used and developed. The most important techniques are described in this chapter. To conclude this chapter, some applications including biomedical applications, antistatic behavior, and water and oil repellency are discussed.

Key words: surface modification, PVD, CVD, plasma, electroless deposition, grafting, sol-gel, XPS, FT-IR, contact angle, SEM, AFM.

1.1 Introduction

This chapter will provide an introductory review of improved functionality of textiles through surface modifications. The focus will be on the surface modification techniques and the appropriate surface characterization techniques.

Section 1.2 will give a brief overview of the most commonly used surface modification techniques for functionalization of textiles. Taking into account the scope of this chapter, this overview is restricted to the techniques most commonly described in the literature, and moreover it is not our goal to discuss these techniques in great detail. A more detailed overview of surface modification techniques in relation to textiles can be found in Wei (2009). Section 1.3 presents the most widely used characterization techniques. Section 1.4 gives different examples of functionalized textiles achieved with the described surface modification techniques.

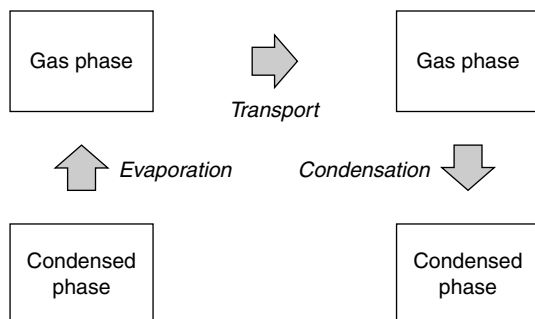
1.2 Types of surface modification

1.2.1 Vapor deposition

Physical vapor deposition

Physical vapor deposition (PVD) is a coating process and is an umbrella term used to describe a variety of methods to deposit thin films by the condensation of a vaporized form of a solid material onto various substrates (Mattox, 2010). A typical PVD process is carried out in vacuum. The most important steps involved in a PVD process are presented in Fig. 1.1.

- **Evaporation:** a target, typically a metal, consisting of the material to be deposited is bombarded by a high-energy source (beam of electrons or ions). Atoms are dislodged from the target surface, so they are vaporized.
- **Transport:** the vaporized atoms travel from the target to the substrate to be coated. In some applications, coatings will consist of, for example, metal oxides, nitrides or carbides. In such cases, the metal atoms evaporated from the target will then react with the appropriate gas during the transport stage. For the above examples, the reactive gases may be oxygen, nitrogen and methane. However, when the coating only consists of the target material, these reaction processes during transport will not occur.
- **Condensation:** the coating builds up at the surface of the substrate. This is the deposition of the coating. Depending on the actual process, some reactions between the target material and the reactive gases may also take place at the substrate surface simultaneously with the deposition process.



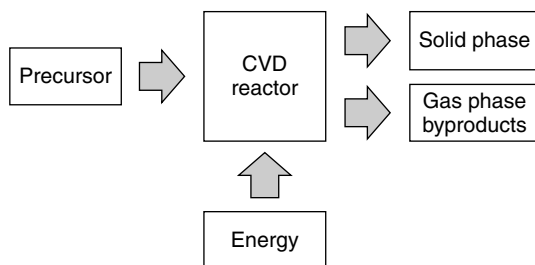
1.1 Schematic representation of a PVD process.

Chemical vapor deposition

Chemical vapor deposition (CVD) is a generic name for a group of processes that involve reactions which transform gaseous molecules, called precursors, into a solid material in the form of a thin film or powder on the surface of a substrate. It is similar in some respects to PVD. The main difference with CVD is that the precursors are solid in PVD, with the material to be deposited being vaporized from a solid target and deposited onto the substrate. Figure 1.2 gives a schematic representation of the CVD process. In a typical CVD process, the substrate is exposed to one or more volatile precursors, which react and/or decompose on the substrate surface to produce the desired deposit. Different types of CVD reactors have already been developed and are in wide use (Hitchman and Jensen, 1993). One important difference between them is the way in which energy is delivered to the reactor: thermal energy, photo energy, and so on. Frequently, volatile by-products are also produced, which are removed by gas flow through the reaction chamber. In most CVD techniques, the temperature of the substrate is a critical issue. Precursor gases (often diluted in carrier gases) are delivered into the reaction chamber at approximately ambient temperatures. As they pass over or come into contact with a heated substrate, they react or decompose forming a solid phase which is deposited onto the substrate. Therefore, the substrate temperature is critical and can influence what reactions will take place.

The process steps involved in CVD can be summarized as follows:

- Transport of precursor molecules into the reactor.
- Diffusion of precursor molecules to the surface.
- Adsorption of precursor molecules to the surface.
- Reactions at the surface: decomposition of precursor molecules on the surface and incorporation into a solid coating.
- Recombination of molecular by-products and desorption into the gas phase.



1.2 Schematic representation of the CVD process.

1.2.2 Wet surface modification techniques

Many surface modification techniques are applied in a wet environment. Despite the possible ecological drawbacks (e.g. water contamination), these wet-chemical techniques are still frequently used in industry for surface modification of textiles. Moreover, the majority of textile surface modifications are achieved using aqueous solutions. There are two types of wet surface modifications:

- Physical interaction with the fibers: typically fiber impurities are removed that resulted from the production process of the fiber or fabric. Desizing of cotton is a common example of such a physical interaction (Cai *et al.*, 2003). Such processes will not be discussed in this chapter.
- Chemical interaction with the fibers: new functional groups will be introduced on the surface of the fibers to change the properties of the fiber or fabric.

Although some authors (Wang and Liu, 2009) also consider the deposition of a material as a physical interaction, in most cases the deposited layer will chemically interact with the substrate. If not, the deposited layer will not adhere well to the substrate.

In the following paragraphs, some of the most common wet-chemical surface modification techniques are discussed.

Grafting

There are two possible methods for the creation of grafted surfaces (Uyama *et al.*, 1998):

- Direct coupling reaction of polymer molecules to the surface: this is only possible if the polymer surface to be modified possesses reactive groups capable of bonding with other components.
- Graft polymerization of monomers to the surface: an effective grafting of molecules onto the surface of textiles needs the creation of free radical sites within the macromolecules of the substrate. These free radical sites are used as initiators for copolymerization reactions with monomers from a grafting solution. Possible techniques to introduce free radicals are chemical graft polymerization, oxidizing agents, high-energy radiation or plasma-induced grafting (Abidi, 2009).

Electroless deposition

Textiles are usually non-conductive and therefore cannot be immersed in a plating solution to be coated in the way that metallic materials can. Electroless deposition or electroless plating of copper and nickel (Mallory

and Hajdu, 1990) is a chemical reduction process which depends upon the catalytic reduction process of metal ions in an aqueous solution and the subsequent deposition of metal without the use of electrical energy. The aqueous solution contains a chemical reducing agent that is the driving force for the reduction of metal ions and their deposition. This driving potential is essentially constant at all points of the surface of the component. Therefore, electroless deposited coatings are very uniform in thickness and are interesting when used for objects with irregular shapes.

Sol-gel

A sol is a colloidal suspension of solid particles in a liquid medium. This liquid is typically an alcohol. Typical precursors are metal alkoxides and metal chlorides, which undergo hydrolysis and polycondensation reactions to form a colloidal suspension. In the sol-gel process, the sol gradually evolves towards the formation of a wet gel-like network containing both a liquid phase and a solid phase. Curing or drying of the gel leads to a so-called xerogel after the solvent is completely removed (Brinker and Sherer, 1990).

1.2.3 Plasma technology: a versatile technique

The pre-treatment and finishing of textiles by non-thermal plasma technologies has become more and more popular as a surface modification technique (Morent *et al.*, 2008; Shishoo, 2007). It offers numerous advantages over conventional processes. Plasma surface modification does not require the use of water, resulting in a more economical and ecologically friendly process. The enormous advantage of plasma processes is the drastic reduction in pollutants and a corresponding cost reduction for effluent treatment. Therefore, it can be considered as an environmentally benign technology. A non-thermal (or cold or low temperature) plasma is a partially ionized gas with electron temperatures much higher than ion temperatures. The high-energy electrons and low-energy molecular species can initiate reactions in the plasma volume without excessive heat causing substrate degradation. Non-thermal plasmas are particularly suited to apply to textile processing because most textile materials are heat sensitive polymers. In addition, it is a versatile technique, where a large variety of chemically active functional groups can be incorporated into the textile surface. Moreover, the versatility of plasma technology is shown by the fact that it is used in combination with or as part of other techniques such as magnetron sputtering PVD, plasma enhanced CVD and plasma-induced grafting.

1.3 Physical and chemical characterization of surface modifications

1.3.1 Microscopic techniques

Resolution

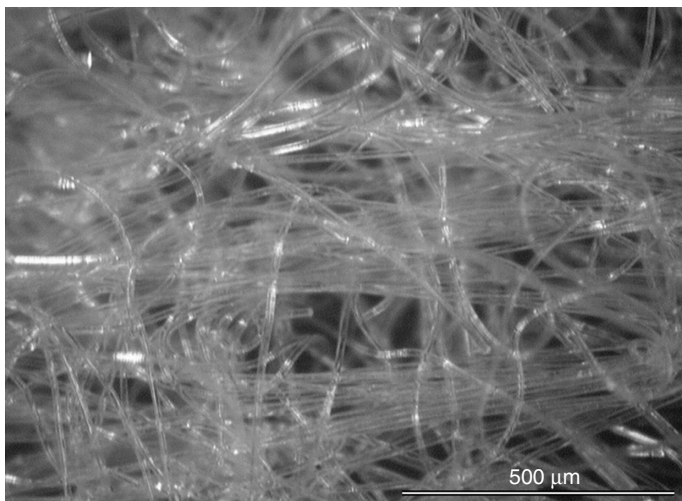
The resolving power or resolution of a microscope is determined by the smallest distance between two points on a surface that can be detected separately. At the lower limit of resolution, images formed by electromagnetic radiation or electrons are limited by diffraction. The resolution of two points is rigorously determined by the Rayleigh criterion and the resolution distance l (m) is given by Roth (2001) as:

$$l = \frac{1.22\lambda}{2n\sin(\varphi/2)} \quad [1.1]$$

where λ is the wavelength of the probing radiation, n is the refractive index of the medium in which the lens operates and φ is the angle subtended at the surface under observation by the edges of the last lens. The quantity $n\sin(\varphi/2)$ is the numerical aperture and may be as much as 1.60 for optical oil-immersion microscopes. In material science, measurements are mostly performed in air and, in that case $n \approx 1.00 \Rightarrow n\sin(\varphi/2) < 1$, the resolution distance l (m) is never less than:

$$l \approx 0.61\lambda \quad [1.2]$$

An image of a non-woven PET obtained with an optical microscope can be seen in Fig. 1.3.



1.3 Microscopic image of a polyester non-woven.

Scanning electron microscopy

Scanning electron microscopy (SEM) was developed in the 1930s (Knoll, 1935) and brought a different way of imaging solids. As stated in the previous section, a modern optical microscope has a magnification of about 1000× and enables the eye to resolve objects separated by 0.275 μm. In the continuous struggle for better resolution, it was found that the resolution of the optical microscope was not only limited by the number and the quality of the lenses, but also by the wavelength of the light used for illumination. In the 1920s, it was discovered that accelerated electrons in vacuum behave like light. Furthermore, it was found that electric and magnetic fields have the same effect on electrons as glass lenses and mirrors have on visible light. These characteristics resulted in the first electron microscope, which images the sample surface by scanning it with a high-energy beam of electrons. When electrons strike the specimen, several phenomena occur:

- emission of secondary electrons by inelastic scattering
- reflection of high-energy electrons by elastic scattering (backscattered electrons)
- absorption of electrons by the sample
- emission of X-rays by the sample
- emission of photons by the sample

All these phenomena are interrelated and all of them depend to some extent on the topography, the atomic number and the chemical state of the specimen. The number of backscattered electrons, secondary electrons and absorbed electrons at each point of the specimen depends on the specimen's topography to a much greater extent than the other phenomena mentioned. Therefore, in SEM, the backscattered, secondary and absorbed electrons will be detected to produce the image.

Many specimens can be examined using SEM without preparation of any kind. Non-conducting specimens (such as polymers) will charge up under electron bombardment and need to be coated with a conducting layer. Because a heavy element like gold also gives a good yield of secondary electrons and thereby a good quality image, this is the favorite element for coating. In addition, it gives a fine grain coating and is easily applied in a sputter coater. The layer required to ensure a conducting layer is quite thin (about 10 nm).

The resolution of SEM can be calculated as follows: the electrons behave as a wave phenomenon with the corresponding energy-dependent de Broglie wavelength λ_{dB} (m) given by:

$$\lambda_{dB} = \frac{h}{p} \quad [1.3]$$

with h (J.s) the Plank constant and p the linear momentum of the electron (kg.m.s^{-1}). If E' is the kinetic electron energy determined by the acceleration voltage of the SEM, then equation [1.3] becomes

$$\lambda_{\text{dB}} = \frac{h}{\sqrt{2m_e E'}} \quad [1.4]$$

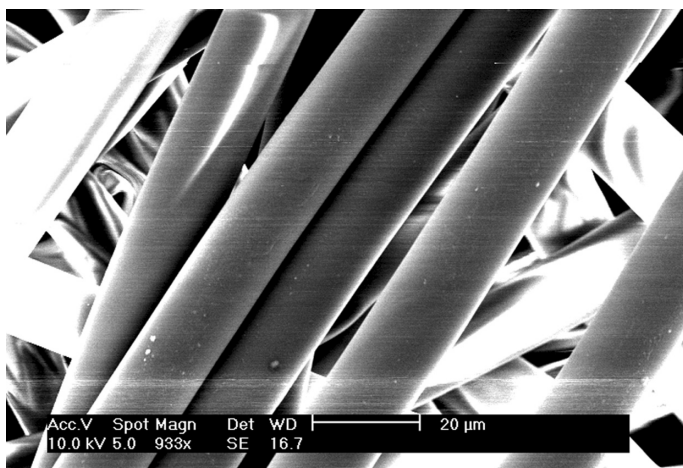
with m_e (kg) the electron mass. Substituting equation [1.4] into equation [1.1] yields the resolution distance l (m):

$$l = \frac{0.61\lambda_{\text{dB}}}{n\sin(\varphi/2)} = \frac{0.61h}{\sqrt{2m_e E'} n\sin(\varphi/2)} = \frac{2.995 \times 10^{-19}}{\sqrt{E'} n\sin(\varphi/2)} \quad [1.5]$$

Assuming a SEM typical electron energy E' of 200 keV ($1 \text{ eV} = 1.602 \times 10^{-19} \text{ J}$) and if the numerical aperture $n\sin(\varphi/2) \approx 1$, then equation [1.5] suggests that $l \approx 1.67 \text{ pm} = 0.00167 \text{ nm}$. This is one hundred times smaller than atomic dimensions. In practice, it will not be possible to form and focus electron beams to such small dimensions, since in real experiments the numerical aperture is smaller than 1. Depending on the instrument, the resolution can fall somewhere between less than 1 and 20 nm. Figure 1.4 shows a typical SEM picture of a polypropylene (PP) non-woven.

Atomic force microscopy

The previously discussed microscopes create a magnified image of an object by focusing electromagnetic radiation, such as photons or electrons, on its surface. Optical and electron microscopes can easily generate



1.4 SEM image of a PP non-woven.

two-dimensional magnified images of an object's surface, with a magnification as great as $1000\times$ for an optical microscope, and as large as $100000\times$ for an electron microscope. Although these microscopes are powerful tools, the obtained images are typically in the plane horizontal to the surface of the object. Such microscopes do not readily supply the vertical dimensions of an object's surface, the height and depth of the surface features.

Unlike traditional microscopes, atomic force microscopy (AFM) does not rely on electromagnetic radiation such as photon or electron beams to create an image. An atomic force microscope is a mechanical imaging instrument that measures the three-dimensional topography as well as physical properties of a surface with a sharpened probe. This probe is typically less than 50 nm in diameter and is placed at the end of a microscale cantilever, typically made out of Si_3N_4 . The probe is positioned close enough to the surface such that it can interact with the force fields associated with the surface. Then the probe is scanned across the surface such that the forces between the probe remain constant. An image of the surface is then reconstructed by monitoring the precise motion of the probe as it is scanned over the surface. Typically the probe is scanned in a raster-like pattern.

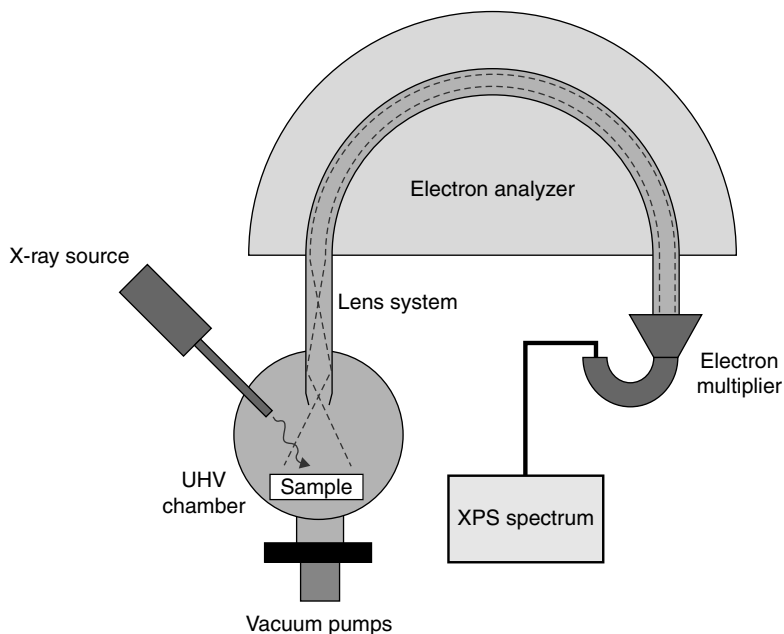
AFM has several advantages compared to SEM: unlike the scanning electron microscope, which provides a two-dimensional image of a sample, AFM provides a three-dimensional surface profile. Moreover, an electron microscope requires a vacuum environment for proper operation, while an atomic force microscope can work perfectly in ambient air. In addition, AFM can provide a higher resolution compared to SEM, since typical AFM resolutions are much lower than 1 nm. Imaging of individual atoms has been possible, although in most applications this level of resolution is not required.

The development of the scanning tunneling microscope in 1981 earned Binnig and Rohrer (1986) the Nobel prize for physics in 1986.

1.3.2 Spectroscopic techniques

X-ray photoelectron spectroscopy

X-ray photoelectron spectroscopy (XPS) is a very powerful surface analysis technique in which chemical states can be determined in near surface regions (Flewitt and Wild, 1994). It is also known as electron spectroscopy for chemical analysis (ESCA). This technique provides a quantitative analysis of the atomic surface composition and can detect different types of chemical bonds at the surface. Photons are used to ionize surface atoms and the energy of the ejected photoelectrons is detected and measured. Figure 1.5 shows the experimental set-up for the XPS measurements. XPS requires an ultra-high vacuum ($<10^{-6}$ Pa) to prevent contamination of the surface of the specimen and to avoid as much as possible collisions of the emitted electrons with the

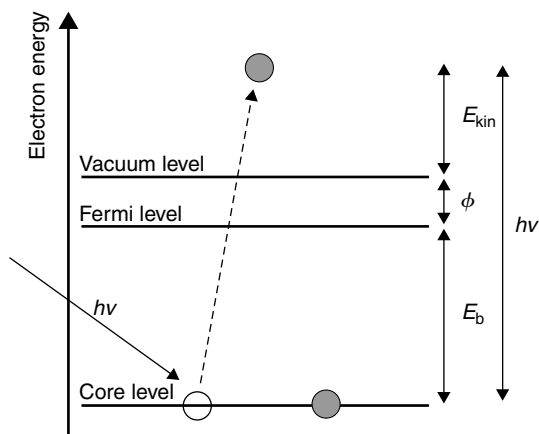


1.5 Schematic set-up for XPS measurements (UHV = ultra high vacuum).

background gas. Therefore the instrument normally consists of a preparation chamber to carry out initial manipulations and an analytical chamber at ultra-high vacuum with a photon source, an electron analyzer and a detector. When placed in the analytical chamber, a monochromatic source of radiation is focused on the specimen. The most commonly employed X-ray sources are $\text{MgK}\alpha$ and $\text{AlK}\alpha$ radiation with corresponding energies of 1253.6 and 1486.6 eV respectively. An X-ray photon with fixed energy ($h\nu$) is absorbed by an atom at the surface of the sample and an electron is ejected from either a valence electron shell or an inner core electron shell (see Fig. 1.6). The ejected photoelectrons are focused onto the entrance slit of an electrostatic analyzer by an electromagnetic lens system. The electrons then pass through the hemispherical electron energy analyzer which can disperse the emitted electrons according to their kinetic energy, and thereby measure the flux of emitted electrons of a particular energy. These electrons are detected using an electron multiplier, which is essentially a tube with the internal surface coated with a material which produces a large number of electrons when an electron is incident upon it.

The kinetic energy E_{kin} of the emitted electron is given by the following relation:

$$E_{\text{kin}} = h\nu - E_{\text{b}} - \phi \quad [1.6]$$



1.6 General energy diagram of the photoionization process.

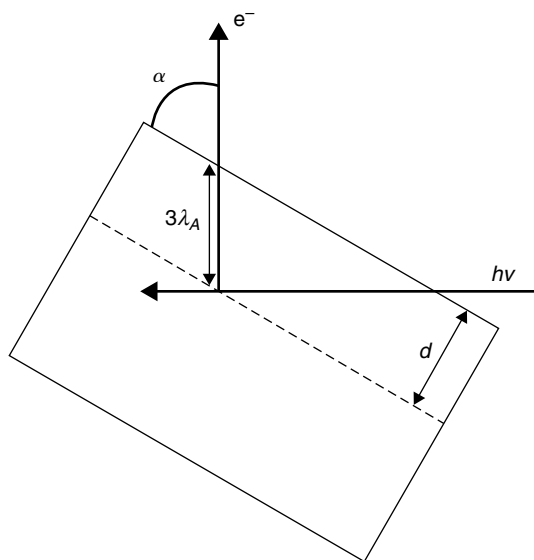
where ν is the frequency of the incident monochromatic X-ray photons, E_b the binding energy of the electron to the atom and ϕ the work function of the specimen. The work function is the minimum energy that must be given to an electron to liberate it from the surface of a particular material. In the photoelectric effect if a photon with an energy greater than the work function is incident on a metal photoelectric emission occurs. Any excess energy is given to the electron as kinetic energy (see also Fig. 1.6). By measuring the energy of the ejected electron and knowing the energy of the incident photons, the electron binding energy can be determined. It is this binding energy that permits the atom to be identified and that provides information concerning its chemical state.

For each atomic element, there will be a characteristic binding energy associated with each core atomic orbital, i.e. each element will give rise to a characteristic set of peaks in the photoelectron spectrum at kinetic energies determined by the photon energy and the respective binding energies. The presence of peaks at particular energies therefore indicates the presence of a specific element in the sample under study. The exact binding energy of an electron depends not only on the electron shell from which photoemission occurs, but also on the local chemical and physical environment. A major strength of XPS is the ability to identify chemical state changes that occur at a surface when two or more atoms combine. When two atoms combine to form a compound, electron transfer occurs between the atoms, one becoming more positive, the other more negative. This results in a shift of the electron binding energies of the electrons by a small amount, usually between a fraction of an eV and a few eV. These small shifts in the peak position are responsible for peak broadening.

In this way, XPS can also provide information on the type of bonds formed at the surface.

The intensity of the peaks is expressed by the peak area and is proportional to the relative abundance of the element within the analyzed region of the sample surface. A quantitative analysis of the atomic surface composition can be determined through a so-called survey scan, i.e. an XPS spectrum with a wide energy frame and a relatively low resolution. When doing XPS experiments this is the first spectrum recorded. For an accurate determination of the binding energy of a specific electron level, a narrow energy frame is placed around a specific XPS peak, where the spectrum is recorded with a high resolution and a small energy step. In this high-resolution spectrum, deconvolution of overlapping peaks is performed to resolve the different types of chemical bonds.

The intensity of the XPS peak is only determined by the photoelectrons that reach the detector without energy loss. The photoelectrons that lose energy through elastic or inelastic collisions within the sample surface contribute to the background or deviate from the detection line. Consequently, an XPS spectrum only provides information on the top atomic layers (up to 5–10 nm, or roughly 20–40 atomic layers). The spectra can be strongly influenced by the relative orientation of the source, sample and detector. The reason for this effect is simply demonstrated by referring to Fig. 1.7. If λ_A is the attenuation length of the emerging electron, then 95% of the



1.7 The effective depth d is determined by the attenuation length λ_A and the take-off angle α between the sample and the detection line.

signal intensity is derived from a distance $3\lambda_A$ within the solid (Briggs, 1990). However, the vertical depth is clearly given by

$$d = 3\lambda_A \sin \alpha \quad [1.7]$$

with α the take-off angle between the photoelectron emission direction and the plane of the sample. This depth is maximum when $\alpha = 90^\circ$ according to equation [1.7]. The attenuation length depends on the kinetic energy of the photoelectron.

Fourier-transform infrared spectroscopy

In Fourier-transform infrared spectroscopy (FT-IR), IR radiation is passed through a sample. Part of the infrared radiation is absorbed by the sample and part of it passes through (is transmitted through) the sample. The resulting spectrum represents the molecular absorption and transmission and creates a molecular fingerprint of the sample. Like a fingerprint, no two unique molecular structures produce the same infrared spectrum. Therefore, the presence or absence of a large number of functional groups can be identified at the sample surface with FT-IR and makes this technique a useful tool to be used in combination with XPS. The sampling depth of FT-IR is typically around 1 μm .

In conjunction with FT-IR, attenuated total reflectance (ATR) is often used as a sampling technique. This technique enables samples to be examined directly in the solid, liquid or gas state without special preparation. The sample is brought into contact with a crystal with high refractive index. ATR is based on the principle of total internal reflection. An infrared light beam passes through the ATR crystal in such a way that it reflects at least once off the internal surface in contact with the sample. This reflection forms the evanescent wave which extends into the sample. The penetration depth into the sample is determined by the wavelength of the infrared beam, the angle of incidence and the refraction index of the ATR crystal together with the characteristics of the sample to be measured. This penetration depth typically ranges between 500 nm and 2 mm. The number of reflections may be controlled by varying the angle of incidence. As the beam exits the crystal, it is then collected by a detector. To achieve this evanescent effect, the crystal is made of an optical material with a higher refractive index than the sample being studied. Otherwise light is lost to the sample. Typical materials for ATR crystals include diamond, germanium and zinc selenide. Diamond is often used due to its excellent mechanical properties and its chemical inertness.

1.3.3 Determining the wetting and wicking of modified textiles

The transport of perspiration is an important contributor to the thermal comfort of fabrics worn next to the skin (Harnett and Mehta, 1984; Korner,

1979; Leach, 1957; Piller, 1979). The wearer perspires due to bodily activity and material worn next to the skin will get wet. Body heat is reduced by these moistened fabrics. Hence, material worn next to the skin should be capable of quick moisture release to the atmosphere. Fabric should therefore be able to:

- evaporate the perspiration from the skin surface
- transfer the moisture to the atmosphere (wicking) (Ramachandran and Kesavaraja, 2004)

Therefore, the measurement of wetting and wicking in fabrics is of topical interest.

A clear distinction between wetting and wicking was made by Kissa (1996). Fiber wettability (Wong *et al.*, 2001) is a prerequisite for wicking, since a liquid that does not wet fibers cannot wick into a fabric. Wicking can only occur when fibers with capillary spaces in between them are wetted by a liquid. The resultant capillary forces drive the liquid into the capillary spaces. The surface properties of the fibers and the wetting liquid completely determine wetting, whereas wicking is also affected by the way the fibers or yarns are arranged into fabrics (Van der Meeren *et al.*, 2002).

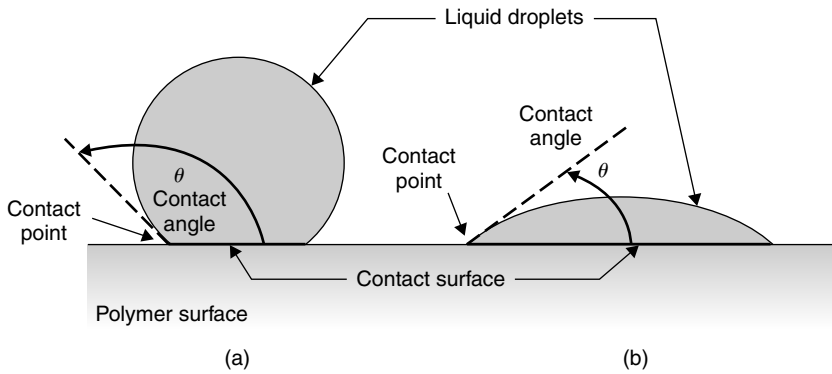
A lot of test methods, like contact angle measurements (Le *et al.*, 1996) or the use of the Wilhelmy technique (Hsieh and Yu, 1992) on individual fibers only provide information on the wetting behavior and do not allow evaluations of fabric wicking characteristics.

Below, the most common techniques to measure wetting or wicking behavior of textiles will be discussed briefly.

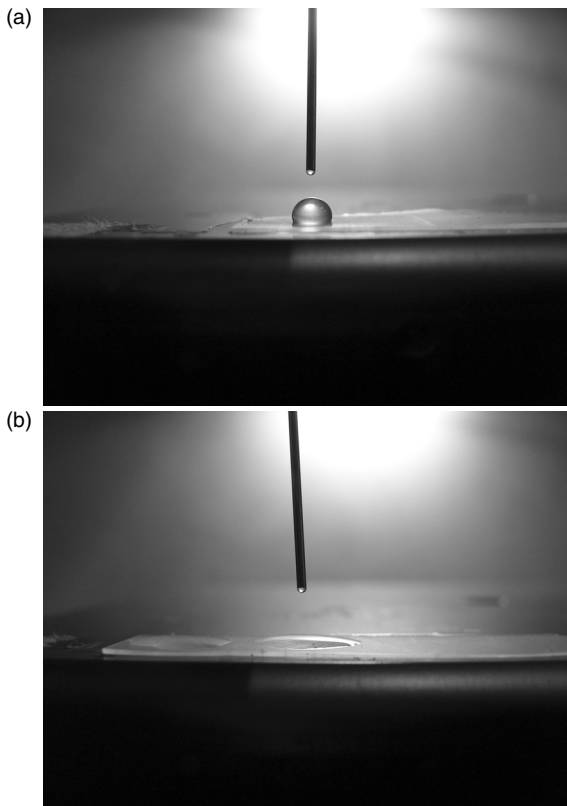
Contact angle measurement

For surfaces with a closed structure (e.g. polymer foils), the surface energy can be derived from the measurement of the static contact angle of small droplets of distilled water or other liquids on the polymer surface. For surfaces with a more open structure, such as woven and non-woven fabrics, the changes in wettability are measured by means of liquid absorptive capacity (see Section 1.4).

A simple and widely used test to evaluate the wettability of polymer films is the measurement of the static contact angle of small droplets of distilled water or other liquids on the polymer surface. Figure 1.8 shows how the contact angle is determined: the contact angle θ is geometrically defined as the angle on the liquid side of the tangential line drawn through the three-phase boundary, where a liquid, gas and solid intersect. Figure 1.8 (a) and (b) show the contact angle for an unwettable and wettable liquid-surface combination respectively. As an example, Fig. 1.9 shows contact angle images of an untreated ($\theta = 108^\circ$) and a plasma-treated ($\theta = 17^\circ$) silicone surface. The



1.8 Principle of contact angle measurement: (a) hydrophobic surface and (b) hydrophilic surface.



1.9 Water droplet on (a) an untreated and (b) a plasma-treated silicone surface.

contact angle is a measure of the relative amounts of adhesive (liquid-to-solid) and cohesive (liquid-to-liquid) forces acting on a liquid and varies over the range $0^\circ \leq \theta \leq 180^\circ$.

Wettability and repellency of polymers against water are basic properties of the polymers. A surface can be hydrophilic or hydrophobic. Hydrophilic and hydrophobic surfaces are results of interactions at an interface between the polymer and water layers and are closely related to the surface energy of polymers. On a hydrophilic surface, polar groups exist and strong interactions between water and these polar groups occur. As a result, the water contact angle of the polymer is small. If the surface energy of the polymer is more than the surface tension of water (72.8 mN/m), the surface of the polymer will completely contact with water, and the contact angle will be zero (Inagaki, 1996). A value of the polymer surface energy lower than the surface tension of water gives rise to a non-zero contact angle. A hydrophobic surface means weak interactions with water at the polymer surface, since the surface mainly consists of non-polar groups. The contact angle of the polymer against water is as large as 90° , in some cases more than 100° .

Liquid absorptive capacity

As the contact angle can only be measured on smooth surfaces, the induced changes in wettability of fabrics are quantified by measuring the liquid absorptive capacity W_A (Zamfir *et al.*, 2002), according to DIN 53 923 (EDANA 10.1–72). W_A is defined as the amount of water that a fabric has absorbed after one minute of immersion in water, relative to its own weight.

First, a dry sample is weighed (M_k). This sample is then immersed in distilled water of a constant temperature for 60 s, 20 mm below the liquid surface. After the wet sample is suspended to vertically drain for 120 s, it is weighed again (M_n). The liquid absorptive capacity W_A is given by:

$$W_A = 100 \frac{M_n - M_k}{M_k} \quad [1.8]$$

In the determination of W_A the temperature of the distilled water strongly influences the value of the measured liquid absorptive capacity (Temmerman *et al.*, 2005). Therefore, the water temperature needs to be kept constant.

This technique is rather time-consuming and depends on a highly accurate weight balance. A droplet that remains on the surface can significantly alter the sample weight, making this procedure very sensitive to misinterpretations.

Capillary rise method

The measurement of wicking in fabrics is mostly done using the capillary rise method (Ferrero, 2003). In this technique, a fabric strip is kept vertically with the lower end of the strip immersed in a water-dye liquor. A spontaneous wicking occurs due to capillary forces (Rice, 1989). The absorption height is recorded as a function of time and the absorption rate is calculated (Ferrero, 2003; Minor *et al.*, 1960). However, during vertical upward wicking, the gravity influences the flow of liquid (Wong *et al.*, 2001). Moreover, wicking goes on in a single dimension, causing differences in wicking behavior in warp and weft direction. To avoid these drawbacks, a horizontal wicking technique was developed by Morent *et al.* (2006). By continuous registration of the wicking area, the technique is able to quantify the wicking rate and it measures wicking in all dimensions. Moreover, this method is a horizontal wicking experiment and, therefore, the influence of gravity can be neglected. The developed image processing algorithms succeed in calculating the wicking area semi-automatically.

1.4 Applications for functional textiles

1.4.1 Biomedical applications

The most imaginative applications of functional textiles are those in the field of biomedical engineering. A typical application is the enhancing of the antibacterial activity of textiles. In most cases, fibers are coated with a metal containing layer. The antibacterial mechanism of the metal is a result of the effect of metallic particles on the external membrane of the bacteria; i.e. the metallic particles block their respiratory capacities, thereby preventing them from breeding (Jiang and Guo, 2009). Wang *et al.* (2008) deposited nanostructured silver films at room temperature on polypropylene (PP) non-wovens by a PVD process to obtain a fabric with antibacterial properties. They investigated the relationship between sputter parameters and antibacterial properties. The effects of a silver film deposition on surface morphology were characterized using SEM and AFM. The test bacteria were *Staphylococcus aureus* and *Escherichia coli*. All silver coated PP non-wovens were very effective against both test bacteria. The results also revealed that the silver coated samples were significantly more effective against *Staphylococcus aureus* than against *Escherichia coli*. Increased film thickness significantly improved the antibacterial performance. It is believed that increasing the coating thickness leads to the release of a larger amount of silver ions, which contributes to the antibacterial performance. However, because silver is quite expensive and because when the silver coating thickness exceeds 28 nm, it may be toxic to certain human

cells (Yuranova *et al.*, 2003), Wang *et al.* (2008) proposed an optimal coating thickness of approximately 3 nm to achieve excellent antibacterial properties and to reduce the cost. Similar results were obtained by Ford (1998) for electroless copper- and nickel-plated polyester fabrics. For *Staphylococcus aureus*, the bacteria reduction for copper- and nickel-plated polyester fabrics reached 99.6% and over 99.9% respectively; for *Escherichia coli*, the bacteria reduction was 99.9% and 94.4%, respectively. So, the copper-plated polyester fabric had a high antibacterial effect for both types of bacteria, whereas the nickel-plated polyester fabric showed a better antibacterial activity against *Staphylococcus aureus* than against *Escherichia coli*. Another research group (Scholz *et al.*, 2005) investigated the PVD deposition of different metals (silver, copper, gold, platinum and platinum/rhodium) on SiO₂ fibers for their performance against bacteria and fungi. It was found that copper was most effective against bacteria and fungi. Silver was also effective against bacteria, but against fungi its effectiveness proved to be limited. The other tested metals did not achieve this effectiveness. The bonding strength between the coatings and the substrates was enhanced by an air plasma treatment before the metal deposition.

1.4.2 Increasing the hydrophilic character

The application of surface modification techniques for improved wettability has been done on all possible fiber types, with varying success. The treatment aims at the introduction of water compatible functional groups such as -COOH, -OH and -NH₂. As mentioned in Section 1.3, when evaluating the wettability of a treated fiber surface, it is in most cases not possible to determine the surface energy directly from contact angle measurements. The irregular surface of a textile reduces the accuracy of (large) contact angle values, while for lower contact angles their porous structure immediately absorbs the liquid drop. That is why wettability of textile (fiber) surfaces is usually monitored by indirect methods such as absorption time and wicking.

De Geyter *et al.* (2006; Morent *et al.*, 2007) modified polyethylene terephthalate (PET) and PP non-wovens by a 10 kHz dielectric barrier discharge (DBD) in air, helium and argon at medium pressure (5.0 kPa). The helium and argon discharges contained a fraction of air smaller than 0.1%. Surface analysis and characterization were performed using XPS, liquid absorptive capacity measurements and SEM. The non-woven, modified in air, helium and argon, showed a significant increase in liquid absorptive capacity due to the incorporation of oxygen-containing groups, such as C-O, O-C=O and C=O. It was shown that an air plasma was more efficient in incorporating oxygen functionalities than an argon plasma, which was more efficient than a helium plasma. An air plasma treatment was

the most efficient in incorporating oxygen on the surface due to the fast reaction between the radicals on the textile surface and the oxygen species present in the discharge. In an argon and helium plasma containing oxygen traces, plasma treatment led to an oxidized cross-linked structure on the textile surfaces. Since the cross-linking reaction inhibits the incorporation of oxygen and since only traces of oxygen were present, a helium and argon plasma were less efficient in oxidation of the textile surfaces. The used argon plasma contained more ions than the helium plasma resulting in a higher degree of cross-linking and a faster incorporation of oxygen-containing groups. SEM pictures of the plasma-treated non-wovens showed that the hydrophilicity of the non-wovens could be increased to a saturation value without causing physical degradation of the surface. The ageing behavior of the plasma-treated textiles after storage in air was also studied in detail. The ageing effect was the smallest for the argon plasma-treated fabrics, followed by the helium plasma-treated fabrics, while the air plasma-treated fabrics showed the largest ageing effect. During the ageing process, the induced oxygen-containing groups reorientated from the surface into the bulk of the material. A restriction of the polar group motion and therefore of the ageing process can be obtained by cross-linking of the polymer chains during plasma treatment. An air-plasma-treated non-woven was not cross-linked and therefore showed a large ageing effect. A helium plasma treatment of the non-wovens led to cross-linked textile surfaces resulting in a less pronounced ageing effect. Argon plasma-treated non-wovens had a higher degree of cross-linking resulting in an even smaller ageing effect. Borcia *et al.* (2003, 2006) studied a 80 kHz DBD in air for the treatment of PET and nylon fabrics and recently, a DBD in air, nitrogen and argon for the treatment of natural, synthetic and mixed fabrics. The wettability and wickability appeared to be strongly increased within the first 0.1–0.2 s of treatment. Any subsequent surface modification following longer treatment (>1.0 s) was less important. The increased wettability could be attributed to the increased level of oxidation where supplementary polar functionalities are created on the fabric fiber surface, as observed by XPS.

1.4.3 Water and oil repellency

Next to enhancing the hydrophilic character of textiles, the opposite goal to increase water repellency also has important applications. Water repellency is important, for example, in outdoor applications of textiles: clothing, car tops, umbrellas, and so forth. Moreover, imparting water, oil and stain repellency to a textile is already a well-established application for napkins, curtains, and so forth. Because the water or oil does not diffuse into the fabric, the cost of washing these textiles is reduced. Such a treatment

introduces certain functional groups via a coating or a graft co-polymer, removes hydrophilic functional groups or changes hydrophilic groups into non-hydrophilic ones. The most commonly used hydrophobic groups contain fluorine. Huang *et al.* (2007) reported on the functionalization of woven silk fabrics in a PVD process with a polytetrafluorethylene (PTFE) coating to improve the hydrophobic property of the silk fabric. The wettability of the fabric was characterized through measuring the surface contact angle and the contact angle of the PTFE coated fabric showed a significant increase from 68° to about 138° . In order to impart water and oil repellency, Louatie *et al.* (1999) chemically grafted polyester fibers with perfluorooctyl-2 ethanol acrylic monomer.

Superhydrophobicity is an effect induced on a surface so that the water contact angle becomes greater than 150° . It depends on reducing the surface energy, as for regular hydrophobic surfaces, but with the addition of rough texture on a nanoscale to trap air and prevent wetting. Superhydrophobic surfaces that are self-cleaning were achieved by a CVD process by Li *et al.* (2007). A nanoscale silicone layer was deposited on cotton fabric resulting in contact angles of 157° .

1.4.4 Conductivity and antistatic properties

Preventing the build-up of static charge on a fabric requires increased conductivity or decreased resistivity. Oh *et al.* (2001) reported on the effect of plasma treatment gas on the electrical conductivity of polyaniline-nylon-6 fabrics. Plasma surface modifications with oxygen, ammonia and argon were performed at low pressure on the nylon-6 fabrics to improve the adhesion and the rate of polymerization. Afterwards the plasma-treated fabrics were immersed in an aqueous hydrochloride solution of aniline. Successive polymerization was initiated with a mixture of an oxidant/dopant solution containing ammonium peroxydisulfate and HCl. The fabrics treated with an oxygen plasma showed the highest conductivity. The conductivity of the oxygen plasma-treated polyaniline-nylon-6 fabric was more stable with repeated washing and abrasion cycles than polyaniline-nylon-6 fabric without plasma pre-treatment.

Hautojärvi and Laaksonen (2000) studied on-line corona treatment of PP fibers during melt-spinning. Corona treatment resulted in a substantial decrease in contact angles. Treated fibers had considerably better antistatic properties than untreated fibers. Treated fibers had an electrical resistance an order of magnitude lower and about 50% less static charge built up during carding than untreated fibers.

Recently, Liu *et al.* (2006) modified the morphology and composition of acrylic fibers with a low-pressure nitrogen glow plasma. The overall surface

roughness increased with increasing treatment time. XPS analysis showed that hydrophilic groups were inserted at the surface. Next to an increase in hydrophilicity, a drastic increase in antistatic ability was reported due to changes in surface morphology and due to the introduction of polar groups at the surface.

1.4.5 UV protection

Prolonged and repeated exposure to UV radiation from sunlight has been identified as the cause of an increase in the incidence of skin cancer in humans. Limiting the skin's exposure to sunlight is not possible for everyone, especially for people working outdoors. Therefore, textiles blocking UV-light are the most suitable alternative. Deng *et al.* (2007) prepared PET non-woven in a PVD process with a ZnO coating. This coating was able to significantly reduce the transmittance in the UV-region, while the transmittance in the visible light range was only slightly reduced.

1.4.6 Photocatalytic coatings

TiO₂ thin films have been deposited on textiles and offer great potential for applications involving the decomposition of various environmental pollutants in both gaseous and liquid phases. Daoud and Xin (2004) reported on the creation of titania coatings via a sol-gel process on cotton fabrics. These fabrics could be used as a self-cleaning antibacterial photocatalyst for the decomposition of organic dirt, environmental pollutants and harmful microorganisms. Degradation of red wine and coffee stains by titania coated fabrics was reported by Bozzi *et al.* (2005a, 2005b) and by Qi *et al.* (2006).

1.5 Future trends

There is a great deal of research to improve the functional properties of textiles, and new technologies have been adopted for the modification of textiles in order to achieve new properties. The newly developed functional textiles find application in fields such as environmental protection and biomedicine. The ideal surface modification techniques introduce a thin uniform layer of a desired functional group without damaging the fiber surface. Moreover, these techniques should also be environmentally friendly. Therefore, some older established surface modification techniques that are not environmentally benign will need to be replaced by sustainable techniques with good results and environmental benefits. For example, the consumption of water and energy of conventional wet treatments of textiles should be drastically

reduced. In addition, progress in surface analysis is essential to develop new functionalities for textiles. This progress will lead to a better understanding of the behavior of textiles, necessary for further improvement.

1.6 References

- ABIDI, N. (2009) Surface grafting of textiles. In: WEI, Q. (ed.) *Surface Modifications of Textiles*. Texas Tech University, USA: Woodhead Publishing Limited.
- BINNIG, G. and ROHRER, H. (1986) Scanning tunneling microscopy – from birth to adolescence. *Nobel Lecture*.
- BORCIA, G., ANDERSON, C. A. and BROWN, N. M. D. (2003) Dielectric barrier discharge for surface treatment: application to selected polymers in film and fibre form. *Plasma Sources Science and Technology*, 12: 335–344.
- BORCIA, G., ANDERSON, C. A. and BROWN, N. M. D. (2006) Surface treatment of natural and synthetic textiles using a dielectric barrier discharge. *Surface & Coatings Technology*, 201: 3074–3081.
- BOZZI, A., YURANOVA, T., GUASQUILLO, I., LAUB, D. and KIWI, J. (2005a) Self-cleaning of modified cotton textiles by TiO₂ at low temperatures under daylight irradiation. *Journal of Photochemistry and Photobiology A-Chemistry*, 174: 156–164.
- BOZZI, A., YURANOVA, T. and KIWI, J. (2005b) Self-cleaning of wool-polyamide and polyester textiles by TiO₂-rutile modification under daylight irradiation at ambient temperature. *Journal of Photochemistry and Photobiology A-Chemistry*, 172: 27–34.
- BRIGGS, D. (1990) Applications of XPS in polymer technology. In: BRIGGS, D. and SEAH, M. P. (eds.) *Practical Surface Analysis – Volume 1 – Auger and X-ray Photoelectron Spectroscopy*. West Sussex, England: John Wiley & Sons Ltd.
- BRINKER, C. J. and SHERER, G. (1990) *Sol-Gel Science: The Physics and Chemistry of Sol-Gel Processing*. Boston: Academic Press.
- CAL, Z. S., QIU, Y. P., ZHANG, C. Y., HWANG, Y. J. and MCCORD, M. (2003) Effect of atmospheric plasma treatment on desizing of PVA on cotton. *Textile Research Journal*, 73: 670–674.
- DAOUD, W. A. and XIN, J. H. (2004) Nucleation and growth of anatase crystallites on cotton fabrics at low temperatures. *Journal of the American Ceramic Society*, 87: 953–955.
- DEGEYTER, N., MORENT, R. and LEYS, C. (2006) Surface modification of a polyester non-woven with a dielectric barrier discharge in air at medium pressure. *Surface and Coatings Technology*, 201: 2460–2466.
- DENG, B. Y., YAN, X., WEI, Q. F. and GAO, W. D. (2007) AFM characterization of nonwoven material functionalized by ZnO sputter coating. *Materials Characterization*, 58: 854–858.
- FERRERO, F. (2003) Wettability measurements on plasma treated synthetic fabrics by capillary rise method. *Polymer Testing*, 22: 571–578.
- FLEWITT, P. E. and WILD, R. K. (1994) *Physical Methods for Materials Characterisation*. Bristol and Philadelphia: Institute of Physics Publishing (IOP).
- FORD, J. E. (1998) Metallized textiles. *Textiles*, 17: 58–62.
- HARNETT, P. R. and MEHTA, P. N. (1984) A survey and comparison of laboratory test methods for measuring wicking. *Textile Research Journal*, 54: 471–478.

- HAUTOJÄRVI, J. and LAAKSONEN, S. (2000) On-line surface modification of polypropylene fibers by corona treatment during melt-spinning. *Textile Research Journal*, 70: 391–396.
- HITCHMAN, M. L. and JENSEN, K. F. (eds.) (1993) *Chemical Vapor Deposition: Principles and Applications*. San Diego, CA: Academic Press.
- HSIEH, Y. L. and YU, B. L. (1992) Liquid wetting, transport, and retention properties of fibrous assemblies. 1. Water wetting properties of woven fabrics and their constituent single fibers. *Textile Research Journal*, 62: 677–685.
- HUANG, H. C., YE, D. Q. and HUANG, B. C. (2007) Nitrogen plasma modification of viscose-based activated carbon. *Surface and Coatings Technology*, 201: 9533–9540.
- INAGAKI, N. (1996) *Plasma Surface Modification and Plasma Polymerization*, Lancaster, PA: Technomic Publishing Company Inc.
- JIANG, S. Q. and GUO, R. H. (2009) Modification of textile surfaces using electroless deposition. In: WEI, Q. (ed.) *Surface Modification of Textiles*. Manchester, England: Woodhead Publishing Limited.
- KISSA, E. (1996) Wetting and wicking. *Textile Research Journal*, 66: 660–668.
- KNOLL, M. (1935) Aufladepotential und Sekundäremission elektronenbestrahler Körper. *Zeitschrift für technische Physik*, 16: 467–475.
- KORNER, W. (1979) Dunova – an absorbent synthetic fiber for high wear comfort. *Chemiefasern/Textilindustrie*, 29: 452–462.
- LE, C. V., LY, N. G. and STEVENS, M. G. (1996) Measuring the contact angles of liquid droplets on wool fibers and determining surface energy components. *Textile Research Journal*, 66: 389–397.
- LEACH, L. L. (1957) Fibres, fabrics and body comfort. *Canadian Textile Journal*, 74: 59–65.
- LI, S. H., XIE, H. B., ZHANG, S. B. and WANG, X. H. (2007) Facile transformation of hydrophilic cellulose into superhydrophobic cellulose. *Chemical Communications*, 46: 4857–4859.
- LIU, Y. C., XIONG, Y. and LU, D. N. (2006) Surface characteristics and antistatic mechanism of plasma-treated acrylic fibers. *Applied Surface Science*, 252: 2960–2966.
- LOUATI, M., ELACHARI, A., GHENAIM, A. and CAZE, C. (1999) Graft copolymerization of polyester fibers with a fluorine-containing monomer. *Textile Research Journal*, 69: 381–387.
- MALLORY, G. O. and HAJDU, J. B. (eds.) (1990) *Electroless Plating: Fundamentals and Applications*. New York: Noyes Publications/William Andrew Publishing, LLC.
- MATTOX, D. M. (2010) *Handbook of Physical Vapor Deposition (PVD) Processing*, 2nd edition. Norwich, NY: William Andrew.
- MINOR, F. W., SCHWARTZ, A. M., BUCKLES, L. C. and WULKOW, E. A. (1960) Pathways of capillary migration of liquids in textile assemblies. *American Dyestuff Reporter*, 49: 37–42.
- MORENT, R., DEGEYTER, N., LEYS, C., GENGEMBRE, L. and PAYEN, E. (2007) Surface modification of non-woven textiles using a dielectric barrier discharge operating in air, helium and argon at medium pressure. *Textile Research Journal*, 77: 471–488.
- MORENT, R., DEGEYTER, N., LEYS, C., VANSTEENKISTE, E., DE BOCK, J. and PHILIPS, W. (2006) Measuring the wicking behavior of textiles by the combination of a horizontal wicking experiment and image processing. *Review of Scientific Instruments*, 77(9): 093502.

- MORENT, R., DEGEYTER, N., VERSCHUREN, J., DECLERCK, K., KIEKENS, P. and LEYS, C. (2008) Non-thermal plasma treatment of textiles. *Surface and Coatings Technology*, 202: 3427–3449.
- OH, K. W., KIM, S. H. and KIM, E. A. (2001) Improved surface characteristics and the conductivity of polyaniline-nylon 6 fabrics by plasma treatment. *Journal of Applied Polymer Science*, 81: 684–694.
- PILLER, I. B. (1979) Applying textured yarns to new knitting applications. *Knitting Times*, 48: 16–20.
- QI, K. H., DAOUD, W. A., XIN, J. H., MAK, C. L., TANG, W. Z. and CHEUNG, W. P. (2006) Self-cleaning cotton. *Journal of Materials Chemistry*, 16: 4567–4574.
- RAMACHANDRAN, T. and KESAVARAJA, N. (2004) A study of influencing factors for wetting and wicking behaviour. *IE (I) Journal-TX*, 84: 37–41.
- RICE, J. E. (1989) Fluid transport characteristics of absorbent structures. In: TURBAK, A. F. and VIGO, T. L. (eds.) *Nonwovens: An Advanced Tutorial*. Atlanta, GA, USA: Tappi Press.
- ROTH, J. R. (2001) *Industrial Plasma Engineering – Volume 2: Applications to Nonthermal Plasma Processing*. Bristol and Philadelphia: Institute of Physics Publishing.
- SCHOLZ, J., NOCKE, G., HOLLSTEIN, F. and WEISSBACH, A. (2005) Investigations on fabrics coated with precious metals using the magnetron sputter technique with regard to their anti-microbial properties. *Surface and Coatings Technology*, 192: 252–256.
- SHISHOO, R. (2007) *Plasma Technologies for Textiles*. Cambridge: Woodhead Publishing Limited in association with The Textile Institute.
- TEMMERMAN, E., AKISHEV, Y., TRUSHKIN, N., LEYS, C. and VERSCHUREN, J. (2005) Surface modification with a remote atmospheric pressure plasma: dc glow discharge and surface streamer regime. *Journal of Physics D-Applied Physics*, 38: 505–509.
- UYAMA, Y., KATO, K. and IKADA, Y. (1998) Surface modification of polymers by grafting. *Grafting/Characterization Techniques/Kinetic Modeling*. Berlin 33: Springer-Verlag Berlin.
- VAN DER MEEREN, P., COCQUYT, J., FLORES, S., DEMEYERE, H. and DECLERCK, M. (2002) Quantifying wetting and wicking phenomena in cotton terry as affected by fabric conditioner treatment. *Textile Research Journal*, 72: 423–428.
- WANG, H. B., WEI, Q. F., WANG, J. Y., HONG, J. H. and ZHAO, X. Y. (2008) Sputter deposition of nanostructured antibacterial silver on polypropylene non-wovens. *Surface Engineering*, 24: 70–74.
- WANG, J. and LIU, J. (2009) Surface modifications of textiles by aqueous solutions. In: WEI, Q. (ed.) *Surface Modification of Textiles*. Manchester, England: Woodhead Publishing Limited.
- WEI, Q. (ed.) (2009) *Surface Modification in Textiles*. Manchester, England: Woodhead Publishing Limited.
- WONG, K. K., TAO, X. M., YUEN, C. W. M. and YEUNG, K. W. (2001) Wicking properties of linen treated with low temperature plasma. *Textile Research Journal*, 71: 49–56.
- YURANOVA, T., RINCON, A. G., BOZZI, A., PARRA, S., PULGARIN, C., ALBERS, P. and KIWI, J. (2003) Antibacterial textiles prepared by RF-plasma and vacuum-UV mediated deposition of silver. *Journal of Photochemistry and Photobiology A-Chemistry*, 161: 27–34.
- ZAMFIR, M., VERSCHUREN, J. and KIEKENS, P. (2002) Medical sponge-bonded and hydroentanglement nonwovens modified by plasma treatment. In: *Proceedings of Joint INDA-TAPPI International Nonwovens Technical Conference*, Atlanta, Georgia.

X. ZHANG,
North Carolina State University, USA

Abstract: The generation of static charges on the surface of textiles can lead to serious consequences, such as handling problems during textile processing, breaking down of sensitive electronic devices, ignition of flammable vapors and dusts in certain environments, clinging tendency and annoying electrical shocks during consumer use. This chapter introduces the fundamentals of static charge generation on textile materials and the key principles of antistatic and conductive textiles. The roles, types, evaluation methods and future trends of antistatic and conductive textiles are discussed.

Key words: static charge, antistatic textile, conductive textile.

2.1 Introduction

All materials in essence are composed of atoms containing positive charges in the nucleus and an equal amount of negative charges orbiting the nucleus in the form of electrons. The contact of two different materials allows the transfer of electrons across the interface. Such redistribution of electrons causes the formation of charges on both materials after they are separated. One material has negative charge (i.e. excess electrons) and the other material has positive charge (i.e. insufficient electrons). If the materials are conductive, the charges can equalize themselves by the backflow of electrons immediately after the separation of two surfaces. However, for most textile materials, electrons are not free to flow because they are bound to the nucleus or shared in the covalent bonds. As a result, charges can survive on textile materials for a measurable length of time and they are hence named static charges. The generation of static charges on the surface of textiles can lead to serious consequences. For example, charged fiber and yarns may repel each other, which makes further processing difficult or even impossible. Charges generated on fibers and fabrics may interfere with the operation of sensitive electronic devices, and sometimes overload and break down these devices. Discharges of sufficient magnitude may cause fires or explosion in an operating room since the spark generated during discharging can ignite flammable vapors and dusts. Therefore, it is important to

develop antistatic and conductive textiles to either avoid the formation of static charges or dissipate them quickly during the processing and use of textile products.

This chapter introduces the fundamental of the static charge generation on textile materials and the key principles of antistatic and conductive textiles. Antistatic and conductive textiles play significant roles during manufacturing and consumer use. Three different types of antistatic and conductive textiles are discussed here based on their intended use. This chapter also describes three categories of evaluation methods for antistatic and conductive textiles. In addition, future trends and additional sources of information are provided.

2.2 Principles of antistatic and conductive textiles

2.2.1 Mechanisms of static charge generation

The effects of static charges are familiar to most people because we can feel, hear and even see the sparks as excess charges are neutralized when brought close to a grounded conductor, or a region with excess charges of the opposite polarity. The familiar phenomenon of a static ‘shock’ is caused by the neutralization of charges. Before addressing the key principles of antistatic textiles, the mechanisms of static charge formation must be understood. In the introductory section, the generation of static charges has been briefly discussed. However, in the real world, there are actually many mechanisms that can lead to the formation of static charges, and the following are some common ones. Any one of these mechanisms can lead to static charging on textile materials, but in many cases, more than one mechanism may work together to generate static charges.

The most important mechanism is contact-induced charge separation (i.e. triboelectric effect). As discussed in the introduction, electrons can be exchanged between textile materials on contact. Materials with sparsely filled outer orbital shells tend to gain excess electrons, while materials with weakly bound electrons tend to lose them. This causes one material being negatively charged and the other positively charged. In addition to electrons, other charged species can also be exchanged between materials. For example, in textiles made of acidic or basic polymers, or polymers with space charge layers, ions can be exchanged at the interface of two contacted textile materials. In this case, charges redistribute according to Boltzmann statistics, i.e. charges move between the two contact materials in numbers (n) that depend on the activation energy ΔG :

$$n = n_0 \exp(-\Delta G / kT) \quad [2.1]$$

where n_0 is the pre-exponential constant, k the Boltzmann's constant and T the absolute temperature.

In the contact-induced charge separation mechanism, the polarity of static charges generated on the materials depends on their relative positions in the triboelectric series. The triboelectric series is an empirically compiled list where materials are arranged from top to bottom depending on their relative ability to lose or gain electrons, beginning with the most positively charged material and ending with the material carrying the most negative charge. Table 2.1 shows several triboelectric series that are often used in the textile field (Adams, 1987; Ballou, 1954; Henniker, 1962; Henry, 1953; Hersh and Montgomery, 1955; Lehmicke, 1949). Although these series do not agree with each other completely, there are some similarities. For example, wool and nylon fibers typically appear at the positive end of the series, cellulose in the middle, and the synthetic fibers other than nylon at the negative end.

According to the triboelectric series shown in Table 2.1, the polarity of static charge generated on a material can be determined. For example, when wool fibers contact cotton fibers, wool acquires positive charge and cotton acquires negative charge because cotton has a better ability to gain electrons than wool. In contrast, the same cotton fibers acquire positive charge when contacting polyethylene fibers because cotton has a greater tendency to lose electrons as compared to polyethylene.

The contact-induced charge separation does not necessarily involve relative motion of the two contact materials. However, motion can certainly enhance the formation of static charges. In many cases, rubbing two textile materials produces temperature gradients, and charges can move from hot spot to cold surrounding area due to the thermoelectric effect.

The contact-induced charge separation is the main cause of static charges as observed during the processing and consumer use of textiles; however, other static charge generation mechanisms, such as pressure-induced charge separation (i.e. piezoelectric effect), also play important roles. Pressure-induced charge separation is determined by the ability of textile materials to generate static charges in response to applied mechanical stress or strain.

The nature of the pressure-induced charge separation is closely related to the formation of electric dipole moments in materials. The electric dipole moments can either be induced in crystal lattice sites with asymmetric charge surroundings or can be carried directly by molecular groups. The dipole density or polarization can be calculated for crystals by summing up the dipole moments per unit cell volume. The change of polarization under a mechanical stress or strain can either be caused by the reconfiguration of the dipole-inducing surrounding or by the reorientation of molecular dipole moments under the influence of the external stress or strain. As a result,

Table 2.1 Triboelectric series

Lehmicke (1949)	Henry (1953)	Ballou (1954)	Hersh and Montgomery (1955)	Henniker (1962)	Adams (1987)
More positive (+)					
Glass	Platinum	Wool	Wool	Nylon 11	Nylon
Human hair	Formvar	Nylon	Nylon	Nylon 6.6	Wool
Nylon yarn	Filter paper	Silk	Viscose	Wool, knitted	Silk
Nylon polymer	Cellulose acetate	Viscose	Cotton	Silk, woven	Paper
Wool	Cellulose triacetate	Cordura®	Silk	Polyethylene glycol	Cotton
Silk	Polyethylene	Human skin	Acetate	Cellulose acetate	Wood
Viscose	Aluminum	Fiber glass	Lucite®	Cotton, woven	Hard rubber
Cotton	Polystyrene	Cotton	Polyvinyl alcohol	Polystyrene	Acetate, rayon
Paper	Copper	Glass	Dacron®	Polyisobutylene	Polyester
Ramie	Nature rubber	Ramie	Dynel®	Polyvinyl butyral	Styroform®
Steel		Dacron®	Velon®	Natural rubber	Orlon®
Hard rubber		Chromium	Polyethylene	Polyacrilonitrile	Saran®
Acetate		Orlon®	Telfon®	Polyethylene	Polyethylene
Synthetic rubber		Polyethylene		Polyvinyl chloride	Polypropylene
Orlon®					Polyvinyl chloride
Polyethylene					Telfon®
More negative (-)					

pressure-induced charge separation can occur when there is variation in the polarization strength, polarization direction or both, depending on: (i) the orientation of polarization within the crystal, (ii) crystal symmetry and (iii) the applied mechanical stress. It must be noted that, although the change in polarization appears as a variation of surface charge density upon the crystal faces, pressure-induced charge separation is not caused by the change in charge density on the surface, but by the change of dipole density in the bulk.

The pressure-induced charge separation is often observed in natural fibers, such as wool and silk. In synthetic fibers, polyvinylidene fluoride (PVDF) exhibits piezoelectricity several times greater than other textile materials.

Like stress or strain, heating can also generate a separation of charge in the atoms or molecules of certain materials. This is so-called heat-induced charge separation (i.e. pyroelectric effect). The atomic or molecular properties of heat and pressure response are closely related. Therefore, heat-induced charge separation is also a mechanism that is related to the change of dipole density or polarization in textile materials. All pyroelectric materials are also piezoelectric (Warner, 1995).

Charge-induced charge separation (i.e. electrostatic induction) is another mechanism for the static charge generation. In non-conductive textile materials, although the electrons are bound to atoms and are not free to flow between atoms, they can move within the atoms. For example, if a positively charged object is brought near a textile material, the electrons in each atom are attracted towards it, and move to the side of the atom facing the charge, while the positive nucleus is repelled and moves slightly to the opposite side of the atom. Since the negative charges are now closer to the external object than the positive charges, their attraction is greater than the repulsion of the positive charges, resulting in a small net attraction towards the inducing charge. This effect is microscopic, but since there are so many atoms, it could add up to significant static charges.

2.2.2 Key principles of antistatic and conductive textiles

Most textile materials are non-conductive, and hence the most important principle for antistatic textiles is to increase either the ionic or electronic conductivity of the materials. The conductivities of both hydrophobic and hydrophilic textile materials are significantly lower than those of pure water and water containing impurities capable of transporting charges such as ions. The relatively high conductivity of water explains why the introduction of even small amounts of water can increase significantly the conductivities of textile materials, especially those of hydrophilic nature. The presence of

water molecules provides transport carriers for electrical charges by facilitating the migration of ions on moisture-absorbed textile surfaces. Therefore, humidity control is a common practice in many textile processing facilities. However, even for hydrophilic natural fibers such as cotton, wool and silk that are capable of high degrees of hydrogen bonding with water molecules, they may not have sufficient conductivity on some occasions. In addition, when the relative humidity reduces, these hydrophilic textiles become insulators and static charges can build up easily. Therefore, it is important to introduce antistatic functionality to both hydrophobic and hydrophilic textiles, depending on the intended use.

The application of antistatic agents is the most common approach to obtain antistatic textiles. Most of the known antistatic agents are hydroscopic compounds that improve the ionic conductivity of textiles by ensuring the presence of water molecules and dissolved ions. Antistatic agents can be ionic or non-ionic; however, ionic agents are generally more effective. Non-ionic agents serve mainly as vehicles for carrying ions of other sources, such as impurities. Ionic agents are typically ionic group-containing molecules that can establish their functionality without relying on other ion sources. Both ionic and non-ionic agents are typically hydroscopic, and they thus need water to realize their antistatic functionality. The main roles of water molecules are to: (i) lower the activation energy for the ionization of ionic groups, (ii) increase the number of the resultant ions and (iii) facilitate the transportation of ions. Many researchers believe that, for maximum efficiency, the water must be present as a continuous phase, preferably on the surface, rather than in the bulk (Sello and Stevens, 1984). Therefore, most antistatic agents are applied on the surface of textile materials to increase the surface conductivity rather than the volume conductivity. However, in some stages of processing, antistatic agents can be absorbed into the textile material and they are no longer just on the surface (Slade, 1998). In addition, internal antistatic agents that are added to the bulk of the material are also used in some applications (Pionteck and Wypych, 2007).

In addition to ionic conductivity, antistatic textiles can also be prepared by enhancing the electronic conductivity. Electronically conductive textiles can be obtained by: (i) dispersing conductive carbon or metal particles into synthetic polymers before or during fiber spinning, (ii) coating the textile surface with a thin layer of electronically conducting materials such as silver, copper, aluminum or gold, (iii) using conductive fibers made of metals such as stainless steel, aluminum, copper and carbon and (iv) blending non-conductive textile fibers with conductive fibers. The advantages of these approaches are that the resultant antistatic properties are durable and do not rely on the presence of water molecules. However, the conductive component added is typically either black or colored, and may affect the appearance of the final textile product.

2.3 The role of antistatic and conductive textiles

Antistatic and conductive textiles play significant roles during manufacturing and consumer use. The following are some examples.

- The introduction of antistatic agents makes high-speed fiber processing possible. For example, during the extrusion of synthetic fibers, a finish is typically used shortly after the extrusion of fibers from the spinnerets. This finish contains lubricating agents and other components, including antistatic agents. The high-speed spinning of synthetic fibers will be difficult or even impossible without this finish.
- Antistatic agents are also used to solve static charge problems during yarn making, knitting, weaving and non-woven manufacturing. The use of antistatic agents can help in positioning textile fibers and yarns and keeping fabrics lint- and dust-free during processing.
- During consumer use, antistatic and conductive textiles can avoid some annoying problems, such as dust and lint pick-up, the clinging of garments to each other and to the human body, and the generation of electric shocks when walking on carpets that are not antistatic.
- The use of antistatic and conductive textiles can also avoid interference with the operation of computers and other sensitive electronic instruments in or around which such textiles are used.
- The use of antistatic and conductive textiles can improve the safety of working environments where flammable gases, liquids and powder solids are present.
- In hospital operating rooms, the use of antistatic and conductive textiles can reduce the risk of injuries due to electric discharge to a conductor leading into the heart or major blood vessels of a patient and injuries due to involuntary movement of surgical personnel receiving a static shock during a critical moment of surgery.

2.4 Types of antistatic and conductive textiles

Antistatic textiles can be classified according to the antistatic agents used during the fabrication of textile products. Depending on how the antistatic agents are applied, they include internal and external finishes. Internal antistatic agents are the ones that are added to the bulk of the material, from where they need to migrate to the material surface (Pionteck and Wypych, 2007).

External antistatic agents are more commonly used and they are applied externally from solutions to the textile surface through a variety of methods including padding, spraying, vapor deposition and plasma grafting. Many external antistatic agents have hydrophobic and hydrophilic parts in their

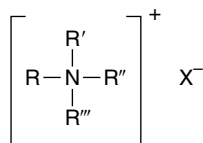
molecular structure. The hydrophilic part orients itself towards the air and promotes the absorption of moisture, thereby leading to increased ion mobility and dissipation. Conventional antistatic agents are typically classified to non-durable and durable finishes according to their ease of removal. The following sections discuss non-durable finishes and durable finishes, respectively. Conductivity textiles, which are obtained by introducing an electronically conducting component, instead of antistatic agents, are also discussed.

2.4.1 Non-durable antistatic textiles

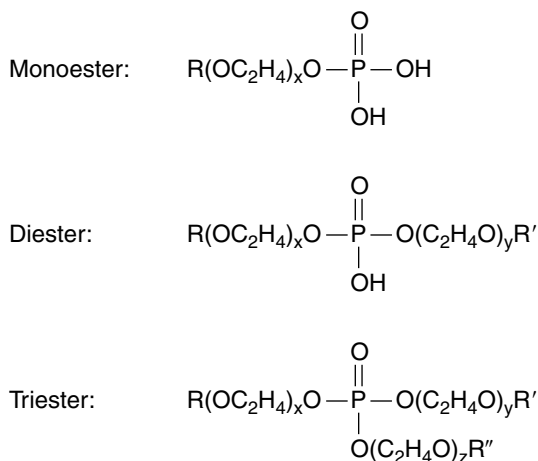
Non-durable antistatic agents are used to treat textiles that only require temporary antistatic ability. They are preferred for fiber and yarn processing since ease of removal is important. They are also used in textile products that do not undergo repeated or any laundering in their lifetime: for example, conveyor belts, driving cords and transport bands (Schindler and Hauser, 2004).

One important type of non-durable antistatic agent for textile materials is quaternary ammonium compounds (Fig. 2.1), which have a good combination of high antistatic efficiency and softening effect on textiles (Sello and Stevens, 1984). Many quaternary ammonium compounds can improve pigment dispersibility and have fast and efficient migration properties. They generally exhibit good thermal stability. Many quaternary ammonium compounds impart softness to the fabric, which makes them extremely capable of value addition in the consumer sector. For example, ditallowdimethylammonium chloride and dehydrogenated tallowdimethylammonium chloride are common ingredients in laundry and dryer softener-antistatic products.

Esters of phosphoric acid (Fig. 2.2) are also widely used as non-durable antistatic agents. Most phosphoric acid esters are produced by reacting the base alcohol with either polyphosphoric acid or phosphorus oxychloride (Burnett, 1966). The reactions typically result in a mixture of mono-, di- and smaller amount of triesters. When polyphosphoric acid is used as the phosphorylating agent, the yield of monoester is at a relatively high ratio. When phosphorous oxychloride is used, a higher yield of trimester can be obtained. The potassium salt versions of phosphoric acid esters are also



2.1 Quaternary ammoniums.



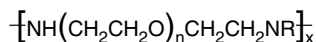
2.2 Phosphoric acid esters.

effective as fiber and fabric antistatic agents (Slade, 1998). Unlike regular phosphoric acid esters, these salts have the advantage of not requiring neutralization.

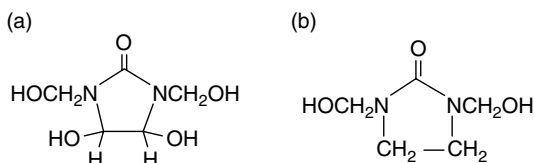
Both quaternary ammoniums and phosphoric acid esters are ionic compounds. Many non-ionic compounds, such as polyethylene glycols, ethoxylated fatty alcohols and sorbitan fatty acid esters, etc., can also be used as antistatic agents. These non-ionic agents are also hygroscopic and can attract water molecules to improve the conductivity of textile materials. Non-ionic compounds are often mixed with ionic agents to obtain superior properties that either cannot achieve alone. In this case, the non-ionic compounds enhance the absorption of water molecules and the ionic compounds provide the ionic species for improving the ionic conductivity of textile materials.

2.4.2 Durable antistatic textiles

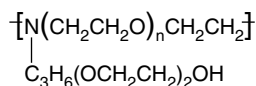
Obtaining antistatic textiles that are durable to repeated launderings and prolonged use from a single treatment is not easy to achieve (Schindler and Hauser, 2004). However, they can be obtained by: (i) forming a cross-linked polymer network containing hydrophilic groups around the textile fibers, (ii) grafting hydrophilic polymer chains through covalent bonds onto the textile surface and (iii) combining both approaches. The antistatic properties of the treated textiles are related to the amount of moisture that the hydrophilic groups can attract. Typically, the larger the hydrophilic portion, the more moisture is absorbed and the greater the antistatic effect obtained.



2.3 Polyamines containing polyoxyethylene groups.



2.4 Dimethyloldihydroxyethyleneurea (a) and dimethylolethyleneurea (b).



2.5 Polyhydroxypolyamines.

However, at high levels of absorbed moisture, the polymer surface film swells and can be more easily removed by abrasion during laundering or other processes. Therefore, the major challenge in developing durable antistatic finishing is to achieve an acceptable balance between the antistatic properties and finishing durability.

Many durable antistatic finishes are based on polyamines containing polyoxyethylene segments (Valko and Tesoro, 1959), which are still widely used in today's durable antistatic finishing. Figure 2.3 shows a typical chemical structure of durable polyamine antistatic finishes. Polyamines achieve antistatic properties by forming cross-linked networks around the textile fibers, which can be realized by many approaches. For example, polyepoxides can be used to obtain cross-linked polyamine-based antistatic surfaces (Schindler and Hauser, 2004). Other multifunctional cross-linking agents, such as dimethyloldihydroxyethyleneurea and dimethylolethyleneurea (Fig. 2.4), can also be used (Latta *et al.*, 1978). The resultant cross-linking structure can be manipulated by selectively adjusting ratios of different chemicals and other treatment conditions. In addition to the simple structure shown in Fig. 2.3, more complicated polyamines can also be used. For example, polyhydroxypolyamines (PHPA, Fig. 2.5) contain both hydrophilic oxyethylene and amino groups, and they can be prepared by reacting polyethyleneglycol dihalide and polyglycolamine. Compared with regular polyamines, PHPA has more hydrophilic oxyethylene groups, which can also serve as additional cross-linkable hydroxyl sites. Therefore, PHPA can

- (a) $\text{CH}_2=\text{CHCONH}_2$
- (b) $\text{CH}_2=\text{C}(\text{CH}_3)\text{COO}(\text{CH}_2\text{CH}_2\text{O})_n\text{OCH}_3$
- (c) $\text{CH}_2=\text{C}(\text{CH}_3)\text{COO}(\text{CH}_2)_2\text{N}(\text{CH}_3)_2$
- (d) $\text{CH}_2=\text{CHCONHC}(\text{CH}_3)_2\text{CH}_2\text{SO}_3\text{H}$
- (e) $\text{CH}_2=\text{C}(\text{CH}_3)\text{COOCH}_2\text{CH}(\text{OH})\text{CH}_2\text{N}(\text{CH}_3)_3\text{Cl}$

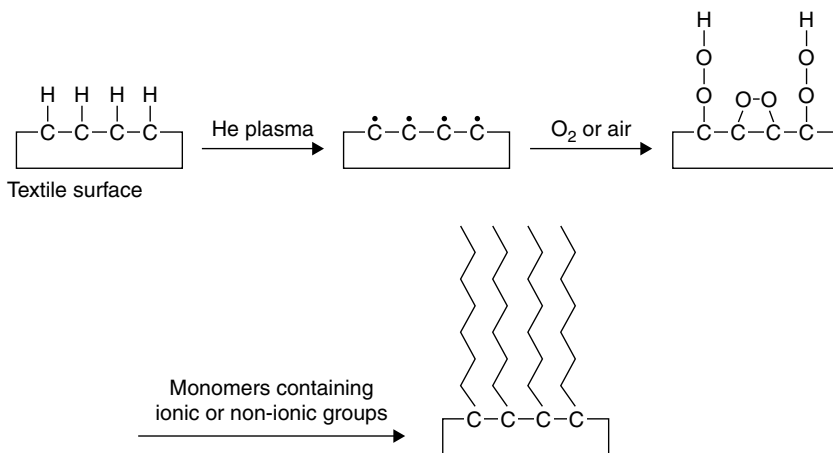
2.6 Monomers containing non-ionic or ionic groups. (a) Acrylamide, (b) polyethyleneglycol methacrylate, (c) dimethylaminoethyl methacrylate, (d) 2-acrylamide-2-methyl propane sulfonic acid, and (e) 2-hydroxy-3-methacryloyloxy propyl trimethyl ammonium chloride.

provide a good balance between hydrophilicity and durability for some applications.

Hydrophilic monomers with ionic or non-ionic groups can also be used to achieve durable antistatic properties. Figure 2.6 gives examples of such monomers. The simplest way to use these monomers is to polymerize them to form an antistatic coating on the surface of textile materials using free-radical initiators such as potassium persulfate. Due to the lack of cross-linking, such antistatic properties are not durable. Copolymerizing them with other multifunctional monomers can form highly cross-linked networks around textile fibers. However, early work shows that although the cross-linked coatings are durable during laundering, the resultant antistatic performance is relatively poor possibly because of the lack of ion mobility at high cross-linking densities (Sello and Stevens, 1984).

Grafting hydrophilic monomers with ionic or non-ionic groups onto textile surfaces can achieve durable antistatic properties. For example, both ionic and non-ionic monomers have been used to produce antistatic polyester fabrics through UV-induced graft polymerization, and the antistatic properties of these fabrics can be maintained without significant loss after washing and storage (Uchida *et al.*, 1991). In addition, these grafted antistatic polyester fabrics have similar softness to the untreated ones.

Among various grafting technologies, plasma treatment is gaining attention because plasma processes are relatively environmentally friendly and can reduce wet chemical and energy consumption (Hwang *et al.*, 2005). Plasma is often characterized by its dissociative interactions, in which molecules first dissociate, and then become ionized (positive or negative) (Eliasson and Kogelschatz, 1991). Plasma can create a highly unusual and reactive chemical environment, which can be used to modify substrates of various geometries. Recent work shows that the treatment of polyester fabric with plasma alone can generate antistatic properties by changing the physical structure and chemical composition on the textile surface (Kan, 2007). Durable antistatic textiles can be produced by using plasma treatment



2.7 Schematic of graft polymerization of hydrophilic monomers containing ionic or non-ionic groups using plasma treatment.

to graft hydrophilic monomers with ionic or non-ionic groups onto the surface of textile materials. A schematic presentation of the plasma grafting process is shown in Fig. 2.7.

2.4.3 Conductive textiles

Conductive textiles are typically prepared by incorporating conductive materials, such as carbons, metals and metal oxides, into traditional textiles. Carbon and metal materials have high conductivities, and they are often corrosion and chemical resistant. Hence, they are the most used conductive materials in the production of conductive textiles. The conductivities of metal oxides, such as SnO_2 , ZnO and Sb_2O_3 , are not as high as those of carbon and metal materials, but they are still useful in making conductive or semi-conductive textiles for some specific applications. The advantage of using carbons, metals and metal oxides is that their conductivities are independent of humidity. However, the introduction of these conductive materials has significant impact on the appearance of textile products since they can often be seen in most textiles. For example, the use of a small amount of carbon can turn the entire textile product black. Therefore, conductive textiles are typically produced mainly for specialty applications such as sensors, antennas, flexible heaters, EMI shielding and specialized apparel.

The introduction of carbons, metals and metal oxides can be realized by: (i) dispersing their particulates into synthetic fibers before or during the fiber extrusion, (ii) using them to coat the textile surface or (iii) blending conventional synthetic fibers with conductive fibers of carbons, metals or metal oxides during knitting, weaving or other textile assembling processes.

The challenge of extruding conductive particulate-added synthetic fibers is the difficulty in achieving homogeneous dispersion of particulates; however, this could be solved by selectively controlling the extrusion condition and/or appropriately modifying the particulate surface. The coating of textile surfaces with conductive materials may involve hazardous chemicals depending on the coating method used, and this problem is being addressed by new research and development. Conductive fibers made of carbons, metals and metal oxides are different in nature from synthetic fibers, which leads to difficulties during blending and usage. In addition, the manufacturing of conductive fibers with small diameters is still costly.

2.5 Evaluation of antistatic and conductive textiles

Many methods have been designed and developed to evaluate the electrostatic properties of textiles so as to establish a pattern for their antistatic behavior. Four major organizations that publish electrostatic test standards are the American Society of Testing and Materials (ASTM), the Electrostatic Discharge (ESD) Association, the American Association of Textile Chemists and Colorists (AATCC) and the International Standards Organization (ISO). These organizations have developed test methods to assess resistivity, and static charge generation, accumulation and decay. There are three accepted categories of test methods that can be used to evaluate the antistatic properties of textile materials: (i) the direct method, (ii) the indirect method and (iii) the simulation method (Holme *et al.*, 1998). Since the antistatic properties of textile materials are sensitive to humidity, all these methods require the test samples to be appropriately conditioned, and the measurements should be carried out in a temperature- and humidity-controlled chamber or room.

2.5.1 Direct methods

The direct method category typically consists of measuring electrical properties such as electrical field, potential, charge amount, or the rate of ESD after developing charges on the material by certain treatments. One example of commercial devices that can be used to evaluate the antistatic properties of yarns and fabrics of almost any denier and construction is the static Honestometer (Slade, 1973). Using this device, charge developed on the textile sample is detected by a receiver connected to the input of an oscilloscope. The charge accumulation and decay on the textile material are shown as sine wave pulses on the oscilloscope. The data from the static Honestometer are typically analyzed using several different methods, such as (i) the oscilloscope face figures, (ii) the initial peak-to-peak charge,

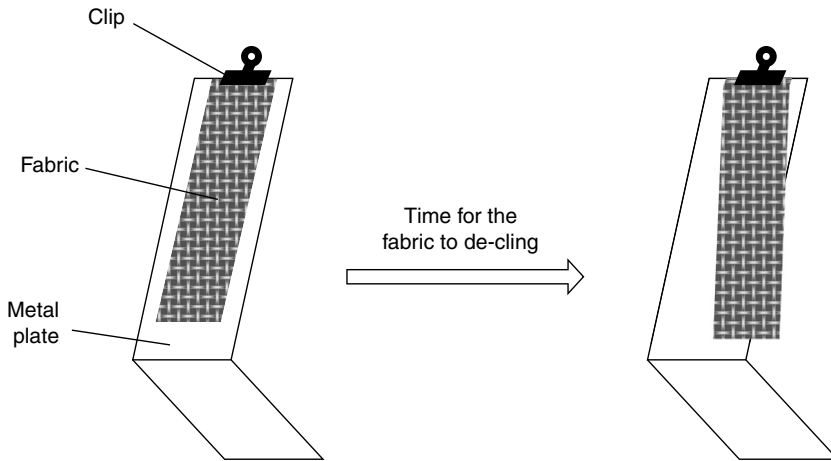
(iii) the half-life for the initial charge to decay and (iv) the percentage of the initial charge retained after a certain time.

2.5.2 Indirect methods

The indirect method generally involves the use of other indicators such as electrical resistivity or conductivity of the textile materials. Resistivity is the inability of a material to conduct electric current. Conductivity is the opposite of resistivity, and it refers to the ability of the material to allow current to flow when a potential difference is applied. Since the static charges are generated on the surface of textile materials, most work focuses on the measurement of the surface resistivity and conductivity. Surface resistivity or conductivity can be measured by using either concentric ring electrodes or parallel plate electrodes. However, the use of a parallel plate electrode requires two sets of tests, in both length and width directions. For a concentric ring electrode, one set is enough because properties of both length and width directions have been taken into consideration during the measurement.

2.5.3 Simulation methods

The third category, simulation, consists of methods that study the behavior of textile materials in a situation simulating the end-use for which they are intended, instead of actual electrostatic properties. For example, in the fabric cling test, the fabric sample is charged by rubbing with another fabric of nylon or polyester, and then allowed to cling to a grounded, inclined metal plate, which is used to simulate the problems of clinging observed between charged garments and the human body (AATCC Test Method 115–2005). The time required for the fabric sample to de-cling from the metal plate indicates that the charge on the fabric surface has decayed to a level where the electrical attractive force between the fabric sample and the metal plate is overbalanced by the gravitational force of the sample (Fig. 2.8). To simulate the static charge formation on a person walking across a carpet, a person wearing sandals manufactured with Neolite soles walks on a carpet sample carrying a probe connected to an electrometer (AATCC Test Method 134–2006). The maximum body voltage generated in one minute is measured. The ash test is another method that can give a rough estimate of antistatic properties by rubbing the fabric sample against another surface to generate static charge and then holding the fabric over a container filled with ash (Slade, 1998). The amount of static charge generated can be estimated by the amount of ash attracted to the charged fabric surface.



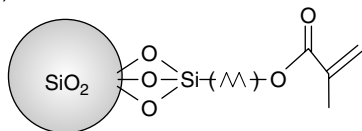
2.8 Schematic of fabric cling test.

2.6 Future trends

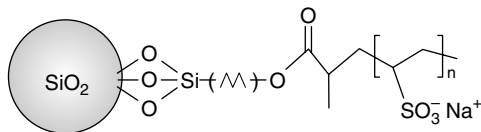
Global competition is requiring antistatic and conductive textiles that can be produced at lower cost and with ‘greener’ processes. It is also attractive to have textiles that are not only antistatic, but also have other functionalities, such as soil and stain resistibility, flame retardancy, water and/or oil repellency and antimicrobial ability.

The use of new technologies in different fields is also encouraging a trend for producing antistatic and conductive textiles with low cost and high performance. One such example is using ceramic nanoparticles to obtain novel durable antistatic textiles. Ceramic nanoparticles have large surface areas and abundant active surface groups. For example, Degussa® R711 silica nanoparticles have a surface area of $150 \text{ m}^2/\text{g}$ and ~ 570 methacrylate group per particulate (Technical Bulletin Pigments #11). They can be covalently linked to the fiber surface and can significantly improve the antistatic properties by grafting a large amount of ionic chains. Figure 2.9 shows the surface chemistry of untreated R711 nanoparticles and those grafted with poly(sodium vinylsulfonate) and poly(sodium 2-acrylamido-2-methyl-1-propanesulfonate), respectively. In addition, these inexpensive silica nanoparticles can serve as cross-link centers and increase the fabric surface roughness, and hence they can improve the durability of the fiber finishing during washing and abrasion. As a result, the use of R711 nanoparticles leads to durable antistatic coatings (Fig. 2.10) that can increase the conductivity of textile fabrics by several orders of magnitude. The methacrylate groups on these silica particulates also allow the easy introduction of other functionalities. Therefore, ceramic nanoparticles

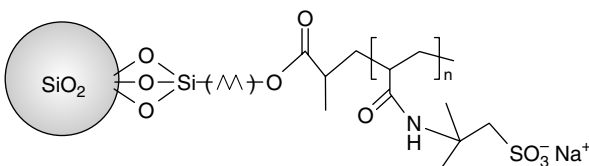
(a) R711



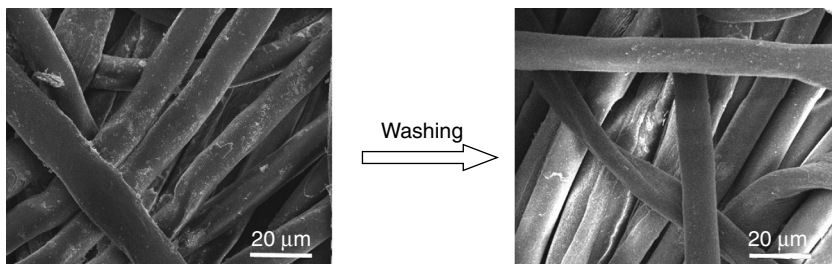
(b) R711-poly(lithium vinylsulfonate)



(c) R711-poly(lithium 2-acrylamido-2-methyl-1-propanesulfonate)



2.9 Surface chemistry of R711 nanoparticulates: (a) untreated, (b) grafted with poly(sodium vinylsulfonate), and (c) grafted with poly(sodium 2-acrylamido-2-methyl-1-propanesulfonate).



2.10 Effect of washing on the surface antistatic coating of cotton/polyester fabric grafted with R711 silica nanoparticulates and poly(sodium vinylsulfonate). The morphology of surface coating does not change significantly after washing.

present an opportunity to develop high-performance durable antistatic textiles.

2.7 Sources of further information and advice

This chapter is a brief introduction to the key principles, roles, types and evaluation methods of antistatic and conductive textiles. More in-depth

understanding on the fundamental of static charges can be obtained from: N. Jonassen, *Electrostatics*, 2nd edition (Norwell, MA: Kluwer Academic Publishers, 2002).

Although the approaches for achieving antistatic properties on different textiles are similar, the technical details can vary depending on the nature and use of the materials. The following two review books provide detailed information on the use of different antistatic compositions based on the types of textile materials: K. Johnson, *Antistatic Agents Technology and Applications* (Park Ridge, NJ: Noyes Data Corporation, 1972) and K. Johnson, *Antistatic Compositions for Textiles and Plastics* (Park Ridge, NJ: Noyes Data Corporation, 1976). More recent advances and future trends in antistatic textiles can be found in: W. D. Schindler and P. J. Hauser, *Chemical Finishing of Textiles* (Cambridge: Woodhead Publishing Ltd, 2004). Another recent book, J. Pionteck and G. Wypych, *Handbook of Antistatics* (Toronto, Ontario: ChemTec Publishing, 2007), gives a detailed discussion on all aspects of antistatic materials, including textiles.

2.8 References

- AATCC Test Method 115–2005, Electrostatic Clinging of Fabrics: Fabric-to-Metal Test.
- AATCC Test Method 134–2006, Electrostatic Propensity of Carpets.
- ADAMS, C. K. (1987) *Nature's Electricity*. Blue Ridge Summit, PA: TAB Books.
- BALLOU, T. W. (1954) Static electricity in textiles. *Textile Research Journal*, 24(2): 146–155.
- BURNETT, L. W. (1966) Nonionics as ionic surfactant intermediates. In: Schick, M. J. (ed.) *Non-Ionic Surfactants*. New York: Marcel Dekker Inc.
- ELIASSON, B. and KOGELSCHATZ, U. (1991) Nonequilibrium volume plasma chemical processing. *Plasma Science, IEEE Transactions*, 19(6): 1063–1077.
- HENNIKER, J. (1962) Triboelectricity in polymers. *Nature*, 196: 474.
- HENRY, P. S. H. (1953) Survey of generation and dissipation of static electricity. *British Journal of Applied Physics*, 4 Suppl.2: S6–S11.
- HERSH, S. P. and MONTGOMERY, D. J. (1955) Static electrification of filaments: experimental techniques and results. *Textile Research Journal*, 25(4): 279–295.
- HOLME, I., MCINTYRE, J. E. and SHEN, Z. J. (1998) Electrostatic charging of textiles. *Textile Progress*, 28: 1–85.
- HWANG, Y. J., AN, J. S., MCCORD, M. G., *et al.* (2005) The effects of helium atmospheric pressure plasma treatment on low-stress mechanical properties of polypropylene nonwoven fabrics. *Textile Research Journal*, 75: 771–778.
- KAN, C. W. (2007) Evaluating antistatic performance of plasma-treated polyester. *Fibers and Polymers*, 8: 629–634.
- LATTA, B. M., STEVENS, C. V. and DENNIS, B. E. (1978) Antistatic finish for textiles material, US Patent 4,104,443.
- LEHMICKE, D. J. (1949) Static in textile processing. *American Dyestuff Reporter*, 38: 853.
- PIONTECK, J. and WYPYCH, G. (2007) *Handbook of Antistatics*. Toronto, Ontario: Chemtec Publishing.

- SCHINDLER, W. D. and HAUSER, P. J. (2004) *Chemical Finishing of Textiles*. Cambridge: Woodhead Publishing Ltd.
- SELLO, S. B. and STEVENS, C. V. (1984) Antistatic treatments. In: LEWIN, M. and SELLO, S. B. (eds.) *Handbook of Fiber Science and Technology: Volume II. Chemical Processing of Fibers and Fabrics. Functional Finishes Part B*. New York: Marcel Dekker Inc.
- SLADE, P. E. (1973) The static Honestometer: a new approach to static measurements. *Modern Textiles*, 54: 68.
- SLADE, P. E. (1998) *Handbook of Fiber Finish Technology*. New York: Marcel Dekker Inc.
- TECHNICAL BULLETIN PIGMENTS #11. (1967) *Basic Characteristics of AEROSIL Fumed Silica*. Degussa.
- UCHIDA, E., UTAMA, Y. and IKADA, Y. (1991) Antistatic properties of surface-modified polyester fabrics. *Textile Research Journal*, 61: 483–488.
- VALKO, E. I., and TESORO, G. C. (1959) Polyamine resins for finishing of hydrophobic fibers. *Textile Research Journal*, 29: 21–31.
- WARNER, S. B. (1995) *Fiber Science*. London: Prentice Hall.

T. GAMBICHLER,
Ruhr University Bochum, Germany

Abstract: This chapter discusses the main aspects playing a role in the prevention of ultraviolet (UV)-induced skin cancer and photodermatoses by means of clothing. The chapter first reviews the *in vitro* and *in vivo* test methods and standards on sun-protective clothing. It then describes various fabric parameters (e.g. composition, construction, dye) and other factors that can have an influence on the UV-blocking properties of clothing. The chapter concludes with a brief outlook on the future of sun-protective garments.

Key words: ultraviolet radiation, skin cancer, photodermatoses, textiles, clothing.

3.1 Introduction

Skin cancer is the most common type of cancer in the United States. In 2006, more than one million people were diagnosed as having basal cell carcinoma (BCC) or squamous cell carcinoma (SCC), resulting in approximately 2200 deaths from both cancers combined. Malignant melanoma (MM), the third and most often fatal type of skin cancer, was diagnosed in approximately 59 940 people and accounted for about 8110 deaths in 2007. Between 1975 and 2004, the annual age-adjusted incidence rate for MM (new cases diagnosed per 100 000 people) nearly tripled, from 6.8 to 18.5 cases per 100 000. The rate of deaths attributed to MM also increased by about 60%, from 1.6 to 2.6 per 100 000 people (Cho and Chiang, 2010; Greenlee *et al.*, 2000; Gruber and Armstrong, 2006; Lucas *et al.*, 2008; Tucker, 2009).

Solar ultraviolet (UV) radiation is ubiquitous during daylight hours. Ambient ground-level UV comprises mainly UVA (400–315 nm) plus a small proportion (<10%, variable by time of day, season and location) of UVB (315–280 nm). Within-person and between-person UV doses vary greatly, depending on location, time of day and season, clothing habits and behavior and skin pigmentation (Holick and Jung, 1999). Exposure to UV radiation on the skin results in clearly demonstrable mutagenic effects. The p53 suppressor gene, which is frequently mutated in skin cancers, is

believed to be an early target of the UV-radiation-induced neoplasms (Soehnge *et al.*, 1997). Although there is no direct way that the active wavelengths for the development of skin cancer in human beings can be determined, there is indirect evidence demonstrating probable ranges. In terms of SCC in albino hairless mice, the action spectrum has been determined to have a strong peak at 293 nm with secondary peaks at 354 and 380 nm. The primary wavelength influencing melanoma risk appears to be in the UVB range. However, studies in fish and opossums have also shown a small effect on MM development as a result of exposure to UVA wavelengths (De Gruijl *et al.*, 1993; Ouhtit *et al.*, 1998; Soehnge *et al.*, 1997; Trappey *et al.*, 2010). Fair-skinned individuals who are more sensitive to the effects of exposure at these wavelengths are at higher risk for the development of skin cancer. In addition, skin cancer rates are also increased in persons with increased artificial UV exposure through tanning salons. The amount of average annual UV radiation correlates with the incidence of skin cancer. There is a direct relationship between the incidence of non-melanoma skin cancer and latitude. The closer an individual is to the equator, the greater the UV energy to which they are exposed (Boniol *et al.*, 2005; Setlow *et al.*, 1993). It has been demonstrated that there is a direct correlation between BCC and SCC incidence and latitude. In terms of melanoma, the relationship is not as clear-cut. MM mortality in the United States and Canada has also been shown to directly correlate with ambient UV exposure. The correlation of MM incidence to UV-radiation exposure is greater when ambient UVA radiation is also included. High-altitude regions tend to have a higher melanoma rate that may be related to the higher UV fluences noted at these sites. MM risk has also been noted to be directly related to annual UV exposure (Boniol *et al.*, 2005; Moan *et al.*, 1999; Rigel *et al.*, 1999; Setlow *et al.*, 1993).

Apart from avoidance of the sun – particularly in peak hours – the most frequently used form of UV protection is the application of sunscreens. The use of textiles as a means of sun protection has been underrated in previous education campaigns, even though suitable clothing potentially offers usually simple and effective broadband protection against the sun (Altmeyer *et al.*, 1997; Gies, 2007; Glanz *et al.*, 2008; Hatch and Osterwalder, 2006; Hoffmann *et al.*, 2001a). However, following comments over years by patients, usually from fair-skinned men, that they sunburnt or developed photosensitive disorders through their clothing, it was decided first of all in Australia, to undertake systematic investigations to study UV-protective properties of clothing. In Australia cancer council education campaigns have long urged the use of clothing in conjunction with hats, sunglasses and sunscreens as UV protection (Dobbinson *et al.*, 2008). However, a number of studies have recently shown that, contrary to popular opinion, some textiles provide insufficient UV protection. These studies showed that more

than one third of commercial summer clothing gives a UV protection factor (UPF) of less than 15 (Dummer and Osterwalder, 2000; Gambichler *et al.*, 2001b; Gies *et al.*, 1999). Analogous to the sun protection factor (SPF) of sunscreens, the UPF is a multiplying factor which permits calculation of one's extended time in the sun, when protected by clothes.

Not only skin cancer formation but also photoaging and photosensitive disorders (e.g. polymorphous light eruption, lupus erythematosus, porphyrias, solar urticaria and phototoxic/photoallergic reactions) may be prevented by UV-protective clothing. Consequently, the use of suitable textiles, which block UVB as well as UVA radiation, has been recommended for photosensitive patients (Gambichler *et al.*, 2002b, 2009a; O'Quinn and Wagner, 1998; Roelandts, 2000). Most of the photosensitive diseases are predominantly provoked by wavelengths in the UVA range (Gambichler *et al.*, 2009a) and in some of these disorders (e.g. solar urticaria, chronic actinic dermatitis) even extremely small UV doses can lead to exacerbation. The latter conditions can also be triggered by visible light. Interestingly, the use of optical whiteners in clothing potentially transforms UVA radiation into visible light, so that in particular cases solar urticaria may be even enhanced through clothing (Gardeazabal *et al.*, 1998). Van den Keybus *et al.* (2006) attempted to determine whether or not the UPF of a particular textile is a good parameter for gauging its protection in the visible light range and concluded that a protection factor of textile materials against visible light needs to be developed. The authors concluded that this development should go beyond the protection factor definition used in this chapter, which has some limitations, and should take into account the exact action spectrum for which the protection is needed.

In addition to the human suffering caused by skin cancer and photosensitive diseases, there is also a significant economic burden due to the costs of preventive efforts, diagnosis, treatment and care of terminally ill patients. Although people are aware of the hazards of sunlight, under-protection because of inadequate application of sunscreen (e.g. amount < 2 mg/cm²; no reapply; skipping ears, neck, etc.) and insufficient textile photoprotection, coupled with overexposure to the sun (prolonging duration of sun exposure by using inadequate UV-protective tools) may partially explain why skin cancer incidences still increase. The data of several studies indicate that some aspects of sun protection are being practiced consistently, while others, such as the use of UV-protective clothing, are not (Barankin *et al.*, 2001; Robinson *et al.*, 2000). As recommended by the American Academy of Dermatology and other organizations, for example, avoiding deliberate tanning with indoor and outdoor light, seeking shade and limiting exposure during peak hours need to be included to sun-protective strategies (Goldsmith *et al.*, 1996; Hall *et al.*, 1997; Holman *et al.*, 1983; Miles *et al.*, 2005).

3.2 *In vitro* and *in vivo* testing of the UV protection factor

Direct and diffuse UV transmittance through a fabric is the crucial factor determining the UV protection of textiles. Simple radiometric broadband UV dosimetry is only suitable for measurements where the relative variation in the UPF is required. By contrast, spectroradiometers and spectrophotometers are suitable for the assessment of the spectral irradiance. These devices collect both transmitted and scattered radiation with the aid of an integrating sphere positioned behind the textile sample. Although spectrophotometers fitted with a double monochromator have a large dynamic range and high accuracy, regular scans of the UV source, e.g. deuterium or xenon arc lamps, are required to provide reference data (Capjack *et al.*, 1994; Gies *et al.*, 1994, 1997). As suggested by Australian, American and European standard documents the spectrophotometer should be fitted with a fluorescence filter, e.g. UG-11 (Schott, Mainz, Germany) to minimize errors caused by fluorescence from whitening agents (AATCC, 183–1998, 2000; AS/NZS 4399, 1996; EN 13758–1, 2002).

The spectrophotometric measurements are usually performed in the wavelength range of 290–400 nm in 5 nm steps or less (Laperre and Gambichler, 2003). Spectrophotometric measurements of textiles are generally made under ‘worst-case’ conditions, with collimated radiation beams at right angles to the fabric. For UPF determination, at least four textile samples must be taken from a garment – two in the machine direction and two in the cross-machine direction. To determine the *in vitro* UPF the spectral irradiance (both source* and transmitted† spectrum) is weighted against the erythral action spectrum (Diffey, 1998)‡, and the UPF is calculated as follows:

$$\text{UPF} = \int E_{\lambda} S_{\lambda} d\lambda / \int E_{\lambda} S_{\lambda} T_{\lambda} d\lambda$$

where E_{λ} = relative erythral spectral effectiveness‡; S_{λ} = solar spectral irradiance in W/m² (Albuquerque, New Mexico, 37.8° S, 17 January 1990)*; T_{λ} = spectral transmission of the sample‡; $d\lambda$ = bandwidth in nm; λ = wavelength in nm; the integrals (\int) are calculated over the wavelength range of 290–400 nm.

As mentioned before, the UPF is defined as the ratio of the average effective UV-radiation irradiance calculated for unprotected skin to the average effective UV-radiation irradiance calculated for skin protected by the test fabric (AS/NZS 4399, 1996). Intra- and interlaboratory comparative trials indicate that spectrophotometry is a precise test method for the determination of the UPF, in particular for samples with UPFs below 50 (Gies *et al.*, 1994; Hoffmann *et al.*, 2001b; Laperre *et al.*, 2001). UPFs greater than 50 are only of theoretical interest as even in Australia the maximum daily UV exposure is less than 40 minimal erythema doses (MEDs). Moreover, Gies

et al. (2003) recently presented results from an intercomparison involving ten independent testing laboratories and 11 different UVR transmission measurement instruments. In addition to comparing the measured UPF, this intercomparison also incorporates detailed scan results from all ten laboratories and highlights differences in performance of the various instruments in different wavelength regions. Careful examination of these differences can indicate where changes to the systems could be made to allow improvements both in equipment performance and in agreement of the final results. The variability in the measurements of UPF in the study of Gies *et al.* (2003) suggests that the protection categories in standards may need to be broadened.

Analogous to SPF testing of sunscreens *in vivo* measurements in human volunteers with the sun as UV source are extremely impracticable for the determination of the UPF. In general, xenon arc solar simulators with collimated radiation beams are used with filters to absorb wavelength below 290 nm and to reduce visible and infrared radiation. Stanford *et al.* (1997) and Gies *et al.* (2000) reported *in vivo* test protocols which are not based on previous *in vitro* testing. In most studies, however, the *in vivo* method has been conducted by *in vivo* checking of the UPF values measured *in vitro* (Gambichler *et al.*, 2001a, 2002a, 2002b; Gies *et al.*, 2000; Greenoak and Pailthorpe, 1996; Hoffmann *et al.*, 2000; Lowe *et al.*, 1995; Menzies *et al.*, 1991). Based on the skin phototype the MED is determined with incremental UVB doses on the upper back of a subject and is read after 24 h. To measure the MED of the protected skin the textile is placed on the skin of the other side of the back (Gambichler *et al.*, 2001a). The incremental UVB doses for determination of the MED of unprotected skin are multiplied with UPF determined *in vitro* resulting in incremental UVB doses for the MED testing of the protected skin. If the *in vitro* method is in agreement with the *in vivo* method, the ratio of the MED of protected skin to the MED of unprotected skin results in the original *in vitro* UPF. Several studies (Gambichler *et al.*, 2001a; Greenoak and Pailthorpe, 1996; Hoffmann *et al.*, 2000; Menzies *et al.*, 1991), however, have shown that the UPFs determined with the *in vivo* method are significantly lower than the UPF values obtained *in vitro* when the fabric samples were tested 'on skin'. By contrast, Césarini *et al.* (2001) and Gies *et al.* (2000) observed no difference between UPF values obtained by *in vitro* and *in vivo* testing. In two studies, *in vivo* testing was also performed in the 'off skin' modus which corresponds rather to a real wearing condition. It was shown that UPF values obtained by the *in vivo* 'off skin' testing differed insignificantly from UPF values obtained by the *in vitro* method (Gambichler *et al.*, 2001a; Menzies *et al.*, 1991). The data inconsistency of these studies is certainly due to different methodology (e.g. different test protocols, UV sources and textile materials).

UV dosimetry has been used to measure erythral UV exposures beneath and above textile materials. Similarly, polysulphone films have been employed in *in vivo* simulated studies as small portable badges monitoring UV doses on manikins and mobile subjects (Holman *et al.*, 1983; Moehrle and Garbe, 2000; Parisi *et al.*, 2000; Ravishankar and Diffey, 1997). Ravishankar and Diffey (1997) concluded that the protection provided by textiles worn in sunlight is, on average, 50% higher than obtained by conventional *in vitro* testing using collimated radiation beams. Thin film polymer such as polysulphone degrades after exposure to UV radiation, especially in the UVB range. The optical absorbance increases in a dose-dependent manner. The polysulphone and CR-39 films show high sensitivities compared to the MED curve between 312 and 330 nm. However, sensitivity is low at wavelength below 305 nm and above 335 nm. In contrast, the sensitivity curve of biological UV dosimeters such as DLR biofilm (*B. subtilis*) provides good similarity to the action spectrum for UV-induced erythema in human skin. The DRL biofilm is a wavelength and time integrating biological UV dosimeter which weights the UV radiation according to its DNA-damaging potential (Quintern *et al.*, 1997). Prior to measurement, the UV dosimeters have to be calibrated to the UV source (e.g. sun, solar simulator). The effective UV doses are calculated using the calibration curve. The UPF is then calculated by dividing the UV dose recorded on the textile-unprotected site by the dose received through the textile at the adjacent skin site. It was shown that cycling jerseys have comparable UPF values when tested spectrophotometrically according to the Australian standard or under stationary sun exposure with DRL biofilms (AS/NZS 4399, 1996; Moehrle and Garbe, 2000). In accordance with results reported by Ravishankar and Diffey (1997), however, the jerseys revealed a much higher UPF when tested under 'real' conditions during cycling. We also conducted a field-based study with biofilms and found that the UPF of a garment worn during outdoor activities is significantly higher than the UPF measured in the laboratory (Gambichler *et al.*, 2002c). Furthermore, we observed in the laboratory-based study that biological dosimetry performed with solar-simulated radiation revealed significantly lower UPFs than spectrophotometric measurements (Gambichler *et al.*, 2002c).

3.3 Standards for sun-protective clothing

The first standard for sun-protective clothing was published jointly by Standards Australia and Standards New Zealand in 1996. This standard, referred to as AS/NZS 4399 has set requirements for determining and labeling the UPF of sun-protective fabrics and other items that are worn in close proximity to the skin (AS/NZS 4399, 1996). Based on the standard, spectrophotometrically assessed UPF is for a fabric material and does not

address the degree of protection that is afforded by the design of a garment. The effects of stretch, wetness, wear and use are not included in the AS/NZS 4399. According to the Australian standard, UPFs are classified in three categories: UPFs of 15–24 (ratings 15 and 20) offer good protection; UPFs of 25–39 (ratings 25, 30 and 35), very good protection; and UPFs of 40 and higher (ratings 40, 45, 50 and 50+), excellent protection. Fabrics with a UPF of less than 15 are not labeled. About ten years ago, three standard documents that pertain to the testing and labeling of UV-protective textile products were published by the American Society for Testing and Materials (ASTM) and the American Association of Textile Chemists and Colorists (AATCC). The titles of these documents, which are available for purchase at www.astm.org and www.aatcc.org are: ASTM D 6544 ‘Standard Practice for the Preparation of Textiles Prior to UV Transmission Testing’, AATCC 183 ‘Test Method for Transmittance or Blocking of Erythemally Weighted Ultraviolet Radiation Through Fabrics’, and ASTM 6603 ‘Standard Guide to Labeling of UV-protective Textiles’ (AATCC 183–1998, 2000; ASTM D 6544, 2000; ASTM 6603, 2003). More recently, the European Committee for Standardization (CEN) has developed a standard on requirements for test methods and labeling of sun-protective garments. The first part of the standard (EN 13758–1) deals with all details of test methods (e.g. spectrophotometric measurements) for textile materials and part 2 (EN 13758–2) covers the classification and marking of apparel textiles. UV-protective clothing for which compliance with the European standard is claimed must fulfill all stringent instructions of testing, classification and marking including a UPF larger than 40 (UPF 40+), average UVA transmission lower than 5%, and design requirements as specified in part 2 of the standard. A pictogram, which is marked with the number of the standard EN 13758–2 and the UPF of 40+, shall be attached to the garment if it is in compliance with the standard (Gambichler *et al.*, 2006). Moreover, British, Canadian, South African and multinational groups, including the Commission on Illumination (CIE) and also the International Organization for Standardization (ISO) have been engaged in writing UV-protective fabric standard documents.

3.4 Type and construction of fabric

For un-dyed fabrics there are differences in the UV absorbing properties of the fiber. Summer clothing is usually made of cotton, viscose, rayon, linen and polyester or combinations thereof. Other types of materials such as nylon or elastane are also found in steps applications such as bathing suits and nylon stockings. In general, consumers consider lightweight non-synthetic fabrics, e.g. cotton, viscose and linen, the most comfortable for summer textiles (Gambichler *et al.*, 2009b). Comparison of the different types of material in relation to the UPF is difficult and only possible

in a limited number of cases. In the case of synthetic fibers (e.g. polyester, polyamide) the analysis is even more difficult because the UV protection of these materials will depend on the type and amount of additives, such as antioxidants or UV stabilizers, to the fiber. In particular, polyester has usually good UV-blocking properties, since this fabric provides relative low UVB transmission probably due to a large conjugated system in the polymer chains (Crews *et al.*, 1999; Davis *et al.*, 1997). Polyester or polyester blends may be the most suitable fabric type for UV-protective garments. However, its permeability for wavelength in the UVA range is frequently higher in comparison to other fiber types (Gambichler *et al.*, 2002b); this could be of significance for many wearers suffering from photosensitive disorders. Bleached cotton and viscose rayon provide relatively low UV protection and are thus transparent to UV radiation. This was recently confirmed by a study of Crews *et al.* (1999) who reported that bleached cotton print cloth had a UV transmission of 23.7%, whereas unbleached cotton print cloth had a UV transmission of only 14.4%. The influence of bleaching was also evident among the silk fabrics in their study. In comparison to bleached textiles unbleached fabrics such as cotton and silk have better UV-protective properties due to UV absorbing natural pigments and other impurities. Very few studies have taken the 'fiber-fabric construction-processing' history of fabrics into consideration to fully elucidate the UV protection abilities of fabrics. Sarkar (2007) recently reported the effect of fabric processing treatments, both chemical and biochemical, on the transmission of UV radiation through selected white and un-dyed fabrics. Sarkar (2007) observed that physical characteristics of fabrics such as thickness, weight and cloth cover were shown to be only partly useful in explaining the UV-protective abilities of fabrics in that the data show anomalies when only physical features of fabrics are considered without considering processing history. However, by taking into account the processing history of fabrics, the UPF values obtained can be fully explained. Sarkar (2007) concluded that chemical processing methods such as desizing and bleaching have a deleterious effect on UV transmission through fabrics. Biochemical processing such as the use of enzymes is comparatively benign and does not adversely impact the UV-protective ability of cotton fabric. Grifoni *et al.* (2009) recently studied the UV protection properties of two fabrics made of natural fibers (flax and hemp) dyed with some of the most common natural dyes. UV transmittance of fabrics was measured by two methods: one based on the utilization of a spectrophotometer equipped with an integrating sphere (*in vitro* test), and the other based on outdoor measurements taken by a spectroradiometer. Transmittance measurements were used to calculate the UPF. Experimental results revealed that natural dyes could confer good UV protection, depending mainly on their different UV absorbing properties, provided that the fabric construction already guaranteed good

cover. An increase in cover factor caused by the dyeing process was also detected. Weld-dyed fabrics gave the highest protection level. The authors also confirmed that comparison the UPFs calculated by *in vitro* measurements were generally lower than those based on outdoor data, indicating an underestimation of the actual protection level of tested fabrics assessed by the *in vitro* test (Grifoni *et al.*, 2009). Sarkar (2004) investigated the UV protection properties of natural fabrics dyed with natural colorants. Three cotton fabrics were dyed with three natural colorants. Fabrics were characterized with respect to fabric construction, weight, thickness and thread count. Sarkar (2004) observed a positive correlation between the weight of the fabric and their UPF values. Similarly, thicker fabrics offered more protection from UV rays. Thread count appears to negatively correlate with UPF. Dyeing with natural colorants dramatically increased the protective abilities of all three fabric constructions. Additionally, within the same fabric type UPF values increased with higher depths of shade. Sarkar (2004) concluded that dyeing cotton fabrics with natural colorants increases the UV-protective abilities of the fabrics and can be considered as an effective protection against UV rays. The UPF of natural fabrics is further enhanced with colorant of dark hues and with high concentration of the colorant in the fabric (Sarkar, 2004).

The fabric construction is a primary determinant of fabric porosity followed by fabric weight and thickness of the textile (Crews *et al.*, 1999). The denser the weave or knitting (smaller yarn-to-yarn spaces), the less the fabric's porosity – consequently, less UV radiation is transmitted. Spaces between the yarns are frequently larger in a knit than in a woven textile. Further, plain woven textiles have a lower porosity than textiles woven using other weaves (Capjack *et al.*, 1994). For an 'ideal' fabric (fibers opaque to UV light) of a particular fiber content and fabric construction, an increase in weight per unit area decreases the fabric porosity – the spaces between the yarns will be smaller in a heavier textile; therefore, less UV radiation is transmitted. However, yarns are usually not opaque to UV radiation and the UPFs of 'real' fabrics are therefore lower than the ideal fabric. In most of the studies thickness measurements for the fabrics were not undertaken or reported. However, thickness is a useful parameter for understanding differences in UV protection between fabrics. Crews *et al.* (1999) reported that thicker, denser fabrics transmit less UV radiation and they concluded that thickness is most useful in explaining differences in UV transmission when differences in percentage cover are also accounted for (Pailthorpe, 1994).

3.5 Fabric color, dyes and UV absorbers

The fabric color may influence the UPF since some dyes have an absorption spectrum extending into the UV spectrum. Enhanced UV protection of

dyed textiles depends on the position and intensity of the absorption bands of the dyes in the UV wavelength and the concentration of the dye in the textile. The absorbance of UV radiation can influence many substrate attributes, e.g. fluorescence, photodegradation and UV protection. Generally, dark colors provide better UV protection due to increased UV absorption. This only holds true for the same UV absorbent dye and provided that other characteristics of the textile, e.g. fabric type and construction, are the same. However, dyes within particular hue types can vary considerably in the degree of UV protectiveness due to their individual transmission/absorption characteristics (Srinivasan and Gatewood, 2000). In order to improve UV protection, UV absorbers have recently been added with different techniques. UV absorbers are colorless compounds that absorb in the wavelength range from 280 to 400 nm. Hilfiker *et al.* (1996) found the cover factor to be useful in predicting the maximum UPF that could be achieved by treating the yarns with UV absorbers. Thus, fabrics could be made opaque to UV radiation with a sufficient level of UV absorber impregnation, and the corresponding UPFs approached the theoretically predicted levels based on the cover factor. Osterwalder and Rohwer (2002) demonstrated that a UV absorber can be brought into contact with a fabric during the wash or rinse cycle of a laundry operation. The high UV transmittance of 30% of a thin, bleached cotton swatch in the dry state (UPF 3) can be reduced tenfold to about 3% (UPF >30) in ten washes cycles. This is more than the effect achieved by dyestuffs. The authors suggested that the detergent should contain about 0.1–0.3% of the special UV absorber (Osterwalder and Rohwer, 2002; Osterwalder *et al.*, 2000). The same effect can be achieved as early as after one wash cycle with a higher concentration provided by a special laundry additive. Yet another form of application is via rinse cycle fabric conditioner.

Titan dioxide is frequently used as a UV-blocking substance in fabrics. However, the absorptive and scattering properties of titan dioxide particles in the UVA wavelength range are different and depend mainly on the particle size and geometry. Other manufactured UV absorbers also provide less protection from UVA radiation, which should be considered when counseling patients with photosensitive disorders. Nevertheless, UV absorbers are suitable for significantly increasing UPF, especially that of non-dyed lightweight summer fabrics, such as cotton and viscose fabrics (Eckhardt and Rohwer, 2000; Hilfiker *et al.*, 1996; Hoffmann 1998; Hoffmann *et al.*, 1998). Recently, Wang *et al.* (2005) presented a facile process to prepare uniform dumbbell-shaped ZnO crystallites. They discovered a unique morphological effect on the UV-blocking property. The as-prepared ZnO crystallites were characterized by different criteria including UV-blocking and Raman scattering spectra. The as-prepared structural material demonstrated a significant advance in protective functional treatment and provided a potential

commercialization. Furthermore, Behler *et al.* (2009) showed that the use of electrospun nanofibers with a high load of nanodiamond can provide UV protection and scratch resistance to a variety of surfaces, especially in applications where a combination of mechanical, thermal and dielectric properties is required.

3.6 Effects of environment and fabric use on UV protection factor

Woven textiles do not stretch significantly; however, knitted textiles are prone to stretch causing an increase of fabric porosity with a consequent decrease in UPF. Moon and Pailthorpe (1995) showed that stretching elastane-based garments about 10%, in both the machine and the cross-machine directions, causes a dramatic decrease in the measured UPF of a textile. Their consumer survey also showed that, on average, about 15% stretch is achieved when these textiles are worn. However, the 15% is for power-stretch, which is only a small segment of the clothing market, and elastane-based textiles for ‘tight-fitting’ should not be considered as defined UV-protective clothing. Kimlin *et al.* (1999) reported that the UPF of 50 denier stockings decreased 868% when stretched 30% from their original size. Notably, the most popular type of stockings (15 denier) provides a UPF less than 2 (Sinclair and Diffey, 1997). The maximum stretch point on the body for tight-fitting garments is the upper back, where textiles can be stretched up to 15%. However, realistically, the effect of stretch on the UPF of a textile may be of significance only for garments with a non-stretched UPF of less than 30, particularly leggings, women’s stockings and swimsuits.

When textiles become wet, by air hydration, perspiration or water, UV transmission through the fabric can significantly change (Khazova *et al.*, 2007). A marked reduction of the UPF was observed for textiles made from cotton and cotton blends. In a field-based study it was recently shown that significant UV exposures may occur beneath the garments, particularly for white cotton fabrics in the wet state. Similar results were also observed in *in vivo* measurements of cotton and polyester blends (Gambichler *et al.*, 2002a; Jevtic, 1990; Moon and Pailthorpe, 1995). One explanation for this is that the presence of water in the interstices of a fabric reduces optical scattering effects and, hence, increases the UV transmission of the textile. The analogy in the visible spectral range is that T-shirts become see-through when wet. In case of fabrics made of viscose or silk, or in fabrics that have been treated with broadband UV absorbers, the UPF frequently increases when the textile becomes wet. This was also observed in a recent study of modal fabrics treated with titan dioxide (Gambichler *et al.*, 2002a; Hoffmann *et al.*, 1998). Thus, UV protection of wet garments is not necessarily poor.

Most of the fabrics will undergo a combination of relaxation shrinkage and consolidation shrinkage when washed (Kaskel *et al.*, 2001). Thus the spaces between the yarns will decrease and UV protection increases. The effect of laundering on the UPF puts into perspective other fabric parameters and factors which decrease the UPF. Stanford *et al.* (1995a) conducted laundering trials using cotton T-shirts. They showed that UPFs increased after the first washing and did not change significantly with subsequent washing. For example, the original UPF rating of a new cotton T-shirt was 15, increasing to UPF 35 after the first laundering. These UPFs were also obtained when participants were instructed to wear their T-shirt for 4–8 h per week and to wash their T-shirt once per week for ten wash-and-wear cycles (Stanford *et al.* 1995b). Wang *et al.* (2001) observed only a moderate increase of the UPF of cotton fabrics after laundering. They found that adding UV absorbing agents during laundering substantially enhances UPF (Osterwalder *et al.*, 2000; Wang *et al.*, 2001). Recently, Zhou and Crews (1998) reported that UPF of cotton cotton/polyester blend fabrics can be significantly enhanced by repeated laundering of the garment in a detergent containing optical brightening agent. This was not true for fabrics comprised entirely of polyester or nylon. Prolonged wear and tear beyond the 'standard' lifetime of a garment may eventually cause thinning of the individual fibers and so alter the UPF. Photostability of a textile and its UV protectiveness is an important requirement for sun-protective clothing (Khazova *et al.*, 2007). Unfortunately, there are only limited data on the stability of the UV protectiveness of a textile against UV radiation or infrared. Below particular wavelengths, photolytic processes of fibers have been observed in various fabrics (linen < 360 nm; cotton < 350 nm; viscose < 340 nm; silk and polyester < 310 nm), independent of other factors, such as temperature, oxygen and hydration. Photo oxidation of fibers can occur above these wavelengths in association with oxidative and hydrolytic processes. For most of the fabrics, durability against thermic effects decreases above 80°C (Bobeth, 1993).

3.7 Conclusions and outlook

Defined UV-blocking fabrics are not only an important element in the campaign against skin cancer, but also in prevention of photosensitive disorders and photoaging. A lot of work has been done around the world on the test methods of the UPF and factors that affect the UV protection provided by clothing. Because parameters are rarely independent, systematic research to quantify the effect of various manufacturing methods is difficult. The UPF of a garment depends on a number of parameters, including fabric construction, type, color, weight, thickness, finishing processes and presence of additives such as UV absorbing substances (e.g. titan dioxide, brightening

agents). Moreover, UV protection of a garment during use depends on wash and wear, including stretch and hydration. Hence, the UPF of a textile is influenced by fabric properties and so complex is the interactive influence of these properties that it is neither possible to predict the UPF or to make generalizations concerning, for example, cotton *vs.* polyester, nor is it sufficient to hold a fabric to the light and assess the amount of light seen through the spaces. Apparel textiles assigned for UV-protective clothing will therefore be measured and labeled in accordance with a standard document (AATCC 183–1998, 2000; AS/NZS 4399, 1996; EN 13758–1, 2002). Principally, sun-protective clothing needs to be designed with special types of complex weaves allowing the passage of air to promote wearer comfort but to block the passage of sunlight through the textile. Fabrics may include UV absorbers of various types to increase UV protection. It will of course be essential to select substances that have a low potential for irritation and sensitization. Moreover, stringent requirements for the design should be complied with in garments assigned for sun-protective clothing (EN 13758–2, 2003).

A recent German study indicate that more counseling on UV-protective clothing is needed for young, male and lower educated individuals (Eichhorn *et al.*, 2008; Gambichler *et al.*, 2009b). The textile industry should be aware of the increasing demand for labeled sun-protective clothing in particular clothing segments such as baby wear, children wear and leisure wear. Lightweight, breathable, natural fabrics made of cotton and linen are the most frequently preferred textiles. The textile industry may consider these fabrics for the production of labeled sun-protective clothing. However, the UV-blocking capacities of cotton and linen have significantly to be improved (e.g. addition of UV absorbers) before these fabrics can be used for proper sun protection. For all sun-aware consumers, who request definitive UV-protective summer clothing that provides sufficient sun protection both under extreme wearing conditions and in all geographical areas, labeling of a garment in compliance with a standardized test and labeling method is a simple aid in selecting the ‘right’ garment. Indeed, clothing does not suffer from the uncertainties of sunscreen application, including thickness and frequency of application and potential skin sensitization and irritation. Nevertheless, people’s compliance in buying and wearing sun-protective clothing may be impaired by several factors such as price, lack of knowledge and desire to tan.

In conclusion, garments assigned for UV-protective clothing play a significant role in the prevention of skin cancer, photodermatoses and premature skin aging. Further education efforts are necessary to change people’s sun behavior and raise awareness for the use of adequate sun-protective clothing. Clearly, whether there will be a market for labeled UV-protective clothing strongly depends on acceptance and demand from the consumer.

3.8 References

- ALTMAYER P., HOFFMANN K. and STÜCKER, M. (1997) *Skin Cancer and UV Radiation*. Berlin and New York: Springer.
- AMERICAN ASSOCIATION OF TEXTILE CHEMISTS AND COLORISTS (AATCC) (2000) AATCC TM 183–1998. Transmittance or blocking of erythemally weighted ultraviolet radiation through fabrics. AATC Tech Manual. Research Park, NC: AATCC.
- AMERICAN SOCIETY FOR TESTING AND MATERIALS (ASTM) (2000) ASTM D 6544: Standard Practice for the Preparation of Textile Prior to UV Transmittance Testing. Conshohocken, PA: ASTM.
- AMERICAN SOCIETY FOR TESTING AND MATERIALS (ASTM) (2003) ASTM D 6603: Standard Guide for Labeling of UV-protective Textiles. Conshohocken, PA: ASTM.
- AUSTRALIAN/NEW ZEALAND STANDARDS AS/NZS (1996) AS/NZS 4399: Sun protective clothing – evaluation and classification. Homebush, NSW, Australia and Wellington, New Zealand.
- BARANKIN, B., LIU, K., HOWARD, J. and GUENTHER, L. (2001) Effect of a sun protection program targeting elementary school children and their parents. *Journal of Cutaneous Medicine and Surgery*, 5: 2–7.
- BEHLER, K. D., STRAVATO, A., MOCHALIN, V., KORNEVA, G., YUSHIN, G. and GOGOTSI, Y. (2009) Nanodiamond-polymer composite fibers and coatings. *ACS Nano*, 3: 363–369.
- BOBETH, W. (1993) *Textile Faserstoffe: Beschaffenheit und Eigenschaften*. Berlin: Springer.
- BONIOL, M., DE VRIES, E., COEBERGH, J. W. and DORE, J. F. (2005) Seasonal variation in the occurrence of cutaneous melanoma in Europe: influence of latitude. An analysis using the EURO CARE group of registries. *European Journal of Cancer*, 41: 126–132.
- CAPJACK, L., KERR, N., FEDOSEJEVS, R., HATCH, K. L. and MARKEE, N. L. (1994) Protection of humans from ultraviolet radiation through the use of textiles: a review. *Family & Consumer Sciences Research Journal*, 23: 198–218.
- CÉSARINI, J. P., OSTERWALDER, U., SCHLENKER, W., ROHWER, H. and BASCHONG, W. (2001) In vivo/in vitro comparison of ultraviolet radiation protection of fabrics. The 8th World Congress on Cancers of the Skin, Zurich, 18–21 July, poster no. 31.
- CHO, Y. R. and CHIANG, M. P. (2010) Epidemiology, staging (new system), and prognosis of cutaneous melanoma. *Clinics in Plastic Surgery*, 37: 47–53.
- CREWS, P. C., KACHMANN, S. and BEYER, A. G. (1999) Influences on UVR transmission of undyed woven fabrics. *Textile Chemist and Colorist*, 31: 17–26.
- DAVIS, S., CAPJACK, L., KERR, N. and FEDOSEJEVS, R. (1997) Clothing as protection from ultraviolet radiation: which fabric is most effective? *International Journal of Dermatology*, 36: 374–379.
- DE GRUIJL, F. R., STERENBORG, H. J. C. M., FORBES, P. D., DAVIES, R. E., COLE, C. and KELFKENS, G. (1993) Wavelength dependence of skin cancer induction by ultraviolet irradiation of albino hairless mice. *Cancer Research*, 52: 1–8.
- DIFFEY, B. L. (1998) The CIE ultraviolet action spectrum for erythema. In: MATHES, R. and SLINEX, D. (eds.) *Measurements of Optical Radiation Hazards*. München: Märkl-Druck, pp. 63–67.
- DOBBINSON, S., WAKEFIELD, M., HILL, D., GIRGIS, A., AITKEN, J. F., BECKMANN, K., REEDER, A. I., HERD, N., FAIRTHORNE, A. and BOWLES, K. A. (2008) Prevalence and determinants of Australian adolescents' and adults' weekend sun protection and sunburn, summer 2003–2004. *Journal of the American Academy of Dermatology*, 59: 602–614.

- DUMMER, R. and OSTERWALDER, U. (2000) UV transmission of summer clothing in Switzerland and Germany. *Dermatology*, 200: 81–82.
- ECKHARDT, C. and ROHWER, H. (2000) UV protector for cotton fabrics. *Textile Chemist and Colorist*, 32: 21–23.
- EICHHORN, C., SEIBOLD, C., LOSS, J., STEINMANN, A. and NAGEL, E. (2008) Knowledge about UV-radiation and sun protection: survey of adolescents and young adults in Bavaria. *Hautarzt*, 59: 821–827.
- EN 13758–1: Fabrics – solar UV protective properties – Method of test for apparel fabrics. Brussels, European Standard, CEN, 2002.
- EN 13758–2: Fabrics – solar UV protective properties – classification and marking of apparel, Brussels, European Standard, CEN, 2003.
- GAMBICHLER, T., AVERMAETE, A., BADER, A., ALTMAYER, P. and HOFFMANN, K. (2001a) Ultraviolet protection by summer textiles. Ultraviolet transmission measurements verified by determination of the minimal erythema dose with solar-simulated radiation. *British Journal of Dermatology*, 144: 484–489.
- GAMBICHLER, T., ROTTERDAM, S., ALTMAYER, P. and HOFFMANN, K. (2001b) Protection against ultraviolet radiation by commercial summer clothing: need for standardised testing and labelling. *BMC Dermatology*, 1: 6.
- GAMBICHLER, T., HATCH, K. L., AVERMAETE, A., ALTMAYER, P. and HOFFMANN, K. (2002a) Influence of wetness on the ultraviolet protection factor (UPF) of textiles: in vitro and in vivo measurements. *Photodermatology, Photoimmunology & Photomedicine*, 18: 29–35.
- GAMBICHLER, T., LAPERRÉ, J., ALTMAYER, P. and HOFFMANN, K. (2002b) UVA and UVB transmission of fabrics: critical wavelength based on absorbance and effective dose. *Exogenous Dermatology*, 1: 290–295.
- GAMBICHLER, T., HATCH, K. L., AVERMAETE, A., BADER, A., HERDE, M., ALTMAYER, P. and HOFFMANN, K. (2002c) Ultraviolet protection factor of fabrics: comparison of laboratory and field-based measurements. *Photodermatology, Photoimmunology & Photomedicine*, 18: 135–140.
- GAMBICHLER, T., LAPERRÉ, J. and HOFFMANN, K. (2006) The European standard for sun-protective clothing: EN 13758. *Journal of the European Academy of Dermatology and Venereology*, 20: 125–130.
- GAMBICHLER, T., AL-MUHAMMADI, R. and BOMS, S. (2009) Immunologically mediated photodermatoses: diagnosis and treatment. *American Journal of Clinical Dermatology*, 10: 169–180.
- GAMBICHLER, T., DISSEL, M., ALTMAYER, P. and ROTTERDAM, S. (2010) Evaluation of sun awareness with an emphasis on ultraviolet protection by clothing: a survey of adults in Western Germany. *Journal of the European Academy of Dermatology and Venereology*, 24(2):155–162.
- GARDEAZABAL, J., GONZALEZ-PEREZ, R., BILBAO, I., ALVAREZ-HERNANDEZ, M. I., AGUIRRE, A. and DIAZ-PEREZ, J. L. (1998) Solar urticaria enhanced through clothing. *Photodermatology, Photoimmunology & Photomedicine*, 14: 164–166.
- GIES, P. (2007) Photoprotection by clothing. *Photodermatology, Photoimmunology & Photomedicine*, 23: 264–274.
- GIES, H. P., ROY, C. R., ELLIOTT, G. and ZONGLI, W. (1994) Ultraviolet radiation protection factors for clothing. *Health Physics*, 67: 131–139.
- GIES, H. P., ROY, C. R., MCLENNAN, A., DIFFEY, B. L., PAILTHORPE, M., DRISCOLL, C., *et al.* (1997) UV protection by clothing: an intercomparison of measurements and methods. *Health Physics*, 73: 456–464.

- GIES, P., ROY, C., TOOMEY, S. and TOMLINSON, D. (1999) Ambient solar UVR, personal exposure and protection. *Journal of Epidermiology*, 9: 115–122.
- GIES, H. P., ROY, C. R. and HOLMES, G. (2000) Ultraviolet radiation protection by clothing: comparison of in vivo and in vitro measurements. *Radiation Protection Dosimetry*, 91: 247–250.
- GIES, P., ROY, C., MCLENNAN, A., PAILTHORPE, M., HILFIKER, R., OSTERWALDER, U., MONARD, B., MOSELEY, H., SLINEY, D., WENGRAITIS, S., WONG, J., HUMAN, S., BILIMIS, Z. and HOLMES, G. (2003) Ultraviolet protection factors for clothing: an intercomparison of measurement systems. *Photochemistry and Photobiology*, 77: 58–67.
- GLANZ, K., YAROCH, A. L., DANCEL, M., SARAIYA, M., CRANE, L. A., BULLER, D. B., MANNE, S., O'RIORDAN, D. L., HECKMAN, C. J., HAY, J. and ROBINSON, J. K. (2008) Measures of sun exposure and sun protection practices for behavioral and epidemiologic research. *Archives of Dermatology*, 144: 217–222.
- GOLDSMITH, L. A., KOH, H. K., BEWERSE, B. A., REILLEY, B., WYATT, S. W., BERGFELD, W. F., *et al.* (1996) Full proceedings from the national conference to develop a national skin cancer agenda. *Journal of the American Academy of Dermatology*, 35: 748–756.
- GREENLEE, R. T., MURRAY, T., BOLDEN, S. and WINGO, P. A. (2000) Cancer statistics, 2000. *CA Cancer Journal for Clinicians*, 50: 7–33.
- GREENOAK, G. E. and PAILTHORPE, M. (1996) Skin protection by clothing from the damaging effects of sunlight. *Australasian Textiles*, 16: 61.
- GRIFONI, D., BACCI, L., ZIPOLI, G., CARRERAS, G., BARONTI, S. and SABATINI, F. (2009) Laboratory and outdoor assessment of UV protection offered by flax and hemp fabrics dyed with natural dyes. *Photochemistry and Photobiology*, 85: 313–320.
- GRUBER, S. and ARMSTRONG, B. K. (2006) Cutaneous malignant melanoma. In: Schottenfeld, D. and Fraumeni, J. F. (eds) *Cancer Epidemiology and Prevention*, 3. New York: Oxford University Press, pp. 1230–1250.
- HALL, H. I., MAY, D. S., LEW, R. A., KOH, H. K. and NADEL, M. (1997) Sun protection behaviors of the U.S. white population. *Preventive Medicine*, 26: 401–407.
- HATCH, K. L. and OSTERWALDER, U. (2006) Garments as solar ultraviolet radiation screening materials. *Dermatologic Clinics*, 24: 85–100.
- HILFIKER, R., KAUFMANN, W., REINERT, G. and SCHMIDT, E. (1996) Improving sun protection factors of fabrics by applying UV-absorbers. *Textile Research Journal*, 66: 61–70.
- HOFFMANN, K. (1998) UV protective clothing in Europe: recommendation of European working party. *Journal of the European Academy of Dermatology and Venereology*, 11: 198–199.
- HOFFMANN, K., HOFFMANN, A., HANKE, D., BÖHRINGER, B., SCHINDLING, G. and SCHÖN, U. (1998) Sun protected from optimally designed fabrics. *Hautarzt*, 49: 10–16.
- HOFFMANN, K., KASPAR, K., GAMBICHLER, T. and ALTMAYER, P. (2000). In vitro and in vivo determination of the UV protection factor for lightweight cotton and viscose summer fabrics: a preliminary study. *Journal of the American Academy of Dermatology*, 43: 1009–1016.
- HOFFMANN, K., LAPPERE, J., AVERMAETE, A., ALTMAYER, P. and GAMBICHLER, T. (2001a) Defined UV protection by apparel textiles. *Archives of Dermatology*, 137: 1089–1094.
- HOFFMANN, K., KESNERS, P., BADER, A., AVERMAETE, A., ALTMAYER, P. and GAMBICHLER, T. (2001b) Repeatability of in vitro measurements of the ultraviolet protection factor (UPF) by spectrophotometry with automatic sampling. *Skin Research and Technology*, 7: 223–226.

- HOLICK, M. F. and JUNG, E. G. (1999) Biologic effects of light 1998. Proceedings of a symposium, Basel, Switzerland, 1–3 November 1998. Norwell: Kluwer Academic Publishers.
- HOLMAN, C. D. J., GIBSON, I. M., STEPHENSON, M. and ARMSTRONG, B. K. (1983) Ultraviolet irradiation of human body sites in relation to occupation and outdoor activity: field studies using personal UVR dosimeters. *Clinical and Experimental Dermatology*, 8: 269–277.
- JEVITIC, A. P. (1990) The sun protective effect of clothing, including beachwear. *Australasian Journal of Dermatology*, 31: 5–7.
- KASKEL, P., ROHWER, H., OSTERWALDER, U. and PETER, R. U. (2001) Improving textile sun protection by regular washing of clothing. *Fortschritte der Medizin Originalien* 119 (Suppl. 2): 91–94 [in German].
- KHAZOVA, M., O'HAGAN, J. B. and GRAINGER, K. J. (2007) Radiation and chemical degradation of UVR protection characteristics of fabrics. *Radiation Protection Dosimetry*, 123: 369–377.
- KIMLIN, M. G., PARISI, A. V. and MELDRUM, L. R. (1999) Effect of stretch on the ultraviolet spectral transmission of one type of commonly used clothing. *Photodermatology, Photoimmunology & Photomedicine*, 15: 171–174.
- LAPERRE, J. and GAMBICHLER, T. (2003) Sun protection offered by fabrics: on the relation between effective doses based on different action spectra. *Photodermatology, Photoimmunology & Photomedicine*, 19: 11–16.
- LAPERRE, J., GAMBICHLER, T., BÖHRINGER, B., DRISCOLL, C., VARIERAS, S. and GASSAN, U. (2001) Determination of the ultraviolet protection factor of textile materials: measurement reliability. *Photodermatology, Photoimmunology & Photomedicine*, 17: 223–229.
- LOWE, N. J., BOURGET, T. D., HUGHES, S. N. and SAYRE, R. M. (1995) UV protection offered by clothing: an in vitro and in vivo assessment of clothing fabrics. *Skin Cancer*, 10: 89–96.
- LUCAS, R. M., MCMICHAEL, A. J., ARMSTRONG, B. K. and SMITH, W. T. (2008) Estimating the global disease burden due to ultraviolet radiation exposure. *International Journal of Epidemiology*, 37: 654–667.
- MENZIES, S. W., LUKINS, P. B., GREENOAK, G. E., WALKER, P. J., PAILTHORPE, M. and MARTIN, J. M. (1991) A comparative study of fabric protection against ultraviolet-induced erythema determined by spectrophotometric and human skin measurements. *Photodermatology, Photoimmunology & Photomedicine*, 8: 157–163.
- MILES, A., WALLER, J., HIOM, S. and SWANSTON, D. (2005) SunSmart? Skin cancer knowledge and preventive behaviour in a British population representative sample. *Health Education Research*, 20: 579–585.
- MOAN, J., DAHLBACK, A. and SETLOW, A. B. (1999) Epidemiological support for a hypothesis for melanoma induction indicating a role for UVA radiation. *Photochemistry and Photobiology*, 70: 243–247.
- MOEHRLE, M. and GARBE, C. (2000) Solar UV-protective properties of textiles. *Dermatology*, 201: 82.
- MOON, R. and PAILTHORPE, M. (1995) Effect of stretch and wetting on the UPF of elastane fabrics. *Australasian Textiles*, 15: 39–42.
- O'QUINN, R. P. and WAGNER, R. F. JR. (1998) Unusual patterns of chronic photodamage through clothing. *Cutis*, 61: 269–271.
- OSTERWALDER, U. and ROHWER, H. (2002) Improving UV protection by clothing – recent developments. *Recent Results in Cancer Research*, 160: 62–69.

- OSTERWALDER, U., SCHLENKER, W., ROHWER, H., MARTIN, E. and SCHUH, S. (2000) Facts and fiction on UV protection by clothing. *Radiation Protection Dosimetry*, 91: 255–260.
- OUHTIT, A., NAKAZAWA, H., ARMSTRONG, B. K., KRICKER, A., TAN, E. and YAMASAKI, H. (1998) UV radiation specific p53 mutation frequency in normal skin as a predictor of risk of basal cell carcinoma. *JNCI: Journal of the National Cancer Institute*, 90: 523–531.
- PAILTHORPE, M. (1994) Textile and sun protection: the current situation. *Australasian Textiles*, 14: 54–66.
- PARISI, A. V., KIMLIN, M. G., MULHERAN, L., MELDRUM, L. R. and RANDALL, C. (2000) Field-based measurements of personal erythema ultraviolet exposure through a common summer garment. *Photodermatology, Photoimmunology & Photomedicine*, 16: 134–138.
- QUINTERN, L. E., FURUSAWA, Y., FUKUTSU, K. and HOLTSCHMIDT, H. (1997) Characterization and application of UV detector spore films: the sensitivity curve of a new detector system provides good similarity to the action spectrum for UV-induced erythema in human skin. *Journal of Photochemistry and Photobiology B, Biology*, 37: 158–166.
- RAVISHANKAR, J. and DIFFEY, B. L. (1997) Laboratory testing of UV transmission through fabrics may underestimate protection. *Photodermatology, Photoimmunology & Photomedicine*, 13: 202–203.
- RIGEL, D. S., RIGEL, E. G. and RIGEL, A. C. (1999) Effects of altitude and latitude on ambient UVB radiation. *Journal of the American Academy of Dermatology*, 40: 11411–11416.
- ROBINSON, J. K., RIGEL, D. S. and AMONETTE, R. A. (2000) Summertime sun protection used by adults for their children. *Journal of the American Academy of Dermatology*, 42: 746–753.
- ROELANDTS, R. (2000) The diagnosis of photosensitivity. *Archives of Dermatology*, 136: 1152–1157.
- SARKAR, A. K. (2004) An evaluation of UV protection imparted by cotton fabrics dyed with natural colorants. *BMC Dermatology*, 4: 15.
- SARKAR, A. K. (2007) On the relationship between fabric processing and ultraviolet radiation transmission. *Photodermatology, Photoimmunology & Photomedicine*, 23: 191–196.
- SETLOW, R. B., GRIST, E., THOMPSON, K. and WOODHEAD, A. D. (1993) Wavelengths effective in induction of malignant melanoma. *Proceedings of the National Academy of Sciences USA*, 90: 6666–6670.
- SINCLAIR, S. A. and DIFFEY, B. L. (1997) Sun protection provided by ladies stockings. *British Journal of Dermatology*, 136: 239–241.
- SOEHNGE, H., OUHTIT, A. and ANANTHASWAMY, O. N. (1997) Mechanisms of induction of skin cancer by UV radiation. *Frontiers in Bioscience*, 2: D538–D551.
- SRINIVASAN, M. and GATEWOOD, B. M. (2000) Relationship of dye characteristics to UV protection provided by cotton fabric. *Textile Chemist and Colorist*, 32: 36–43.
- STANFORD, D. G., GEORGOURAS, K. E. and PAILTHORPE, M. T. (1995a) The effect of laundering on the sun protection afforded by a summerweight garment. *Journal of the European Academy of Dermatology and Venereology*, 5: 28–39.
- STANFORD, D. G., GEORGOURAS, K. E. and PAILTHORPE, M. T. (1995b) Sun protection afforded by a summer weight garment: effect of wash and wear. *Medical Journal of Australia*, 162: 422–425.

- STANFORD, D. G., GEORGOURAS, K. E. and PAILTHORPE, M. T. (1997) Rating clothing for sun protection: current status in Australia. *Journal of the European Academy of Dermatology and Venereology*, 8: 12–17.
- TRAPPEY, A., FERNANDO, A., GAUR, R., RAJ, M. and OUHTIT, A. (2010) The shady side of sunlight: current understanding of the mechanisms underlying UV-induction of skin cancers. *Frontiers in Bioscience (Schol Ed.)*, 2: 11–17.
- TUCKER, M. A. (2009) Melanoma epidemiology. *Hematology/Oncology Clinics of North America*, 23: 383–95.
- VAN DEN KEYBUS, C., LAPERRÉ, J. and ROELANDTS, R. (2006) Protection from visible light by commonly used textiles is not predicted by ultraviolet protection. *Journal of the American Academy of Dermatology*, 54: 86–93.
- WANG, R. H., XIN, J. H. and TAO, X. M. (2005) UV-blocking property of dumbbell-shaped ZnO crystallites on cotton fabrics. *Inorganic Chemistry*, 44: 3926–3930.
- WANG, S. Q., KOPE, A. W., MARX, J., BOGDAN, A., POLSKY, D. and BART, R. S. (2001) Reduction of ultraviolet transmission through cotton T-shirt fabrics with low ultraviolet protection by various laundering methods and dyeing: clinical implications. *Journal of the American Academy of Dermatology*, 44: 767–74.
- ZHOU, Y. and CREWS, P. C. (1998) Effect of OBAs and repeated launderings on UVR transmission through fabrics. *Textile Chemist and Colorist*, 30: 19–24.

3D body imaging and fit for functional textiles

B. XU,
University of Texas at Austin, USA

Abstract: This chapter is focused on how to apply 3D body scanning technology to improve the comfort of functional clothing, which often looks bulky, is ill-fitting and in a one-size-fits-all design. 3D body imaging technology offers solutions to many of the fitting problems for protective clothing. Stereovision techniques were used to construct a low-cost body imaging system, a mesh subdivision algorithm was adapted for generating smooth body surface based on scanned data clouds, and simulation techniques were implemented for creating realistic virtual clothing on a reconstructed model. The portability and high speed of the scanner allow large-scale body surveys. The sewability and fit of designed pattern pieces can be assessed and adjusted prior to production.

Key words: body imaging, stereovision, surface modeling, virtual dressing, fit assessment.

4.1 Introduction

Functional clothing provides protection from hazardous or unhealthy environment risks (extreme climates, fire, bacteria, toxic gases, etc.) to the wearer, but often results in heat stress, work inefficiency and limited range of motion in the case of bulky, ill-fitting and often one-size-fits-all garments [1]. Design based on a more realistic sizing system or personalized-fitting information is the key to improve the wear comfort in mass-produced garments. 3D body imaging technology offers solutions to many of the fitting problems for protective clothing.

Efforts have been made worldwide to develop 3D body scanning systems and their applications in digital body modeling, fit assessment, size survey and virtual clothing [2–10]. Various body scanning systems have taken advantage of different depth-sensing techniques, including structure light triangulation [11–15], phase measurement profilometry [16], moiré fringes [17], infrared position-sensitive detectors [18] and stereovision [19, 20]. Because they differ in resolution, speed, size, price and output, these scanners have found different levels of acceptance from the industry. Overall, the use of body scanning

technology to solve the apparel sizing and fit problem lags behind the expectation of apparel designers, producers and consumers, although the concepts associated with the technology are sound and convincing. The primary reason for this lag is that body scanning systems have not been effectively integrated with apparel CAD, virtual design and modeling systems to create compelling applications, such as size-matching, size-prediction and fit-checking.

A body scanning system usually outputs a set of scattering range data (data clouds) of the scanned body surface. The data clouds often have varying sampling densities over the body and need a substantial storage space. The mathematical modeling of a body surface can eliminate gaps or discrepancies that may exist in the scan data, and can create organized structures that facilitate the further process. For unorganized range data of an arbitrary topology, several modeling algorithms have been attempted. Amenta *et al.* [21] presented an algorithm based on 3D Voronoi diagrams, capable of reconstructing piecewise-linear models from unorganized 3D points. Krishnamurthy and Levoy [22] devised a method to fit tensor product B-spline patches to dense polygon meshes so as to describe the fine surface detail by a displacement map. Hoppe *et al.* [23] explored using sign distance functions to automatically determine the topological type of the surface. Li and Jones [24] made use of a B-spline skinning scheme to construct the human torso from 32 cross-sectional slices with 32 points on each slice. The skinning calculation can be further reduced from 32 slices to eight slices which are located at key geometric positions of the torso. Dekker *et al.* [25] used B-spline curves to approximate all body cross-sections, and demonstrated that 25 control points could provide sufficient accuracy for each cross-section. Douros *et al.* [26] presented an algorithm that constructs a body model with several smooth B-spline surfaces using global interpolation. The body scan data were segmented into several body parts (torso, arms, etc.), and each part was sampled at a regular grid to form a control net for the B-spline interpolation. Xu *et al.* [27] presented another B-spline algorithm to model a human body from unorganized range data. The B-spline-based modeling algorithms usually need a large number of control points to generate surfaces/patches that can retain enough details of the data. Recently, piecewise subdivision surfaces were used to allow more flexible representation [28]. Based on mesh subdivision and optimization, Yu and Xu [29] developed an effective body modeling algorithm specifically for a two-view body scanner.

From a reconstructed body model, 3D dressing can be simulated to create a virtual garment to verify the style and fit of a designed pattern before the garment is actually made. A robust simulation system often includes the key functions that perform fabric modeling, sewing scheme, accurate and fast collision detection/response and size stability maintenance [30].

Of the various methods of fabric modeling [31–40], the mass-spring model has gained wide acceptance for its simplicity and efficiency [38]. In such

a system, a sheet of fabric is discretized into mass particles networked by springs, and the deformation of the fabric is visualized through the movement of each particle that is governed by various external and internal forces. If the mass of the particle and the stiffness and viscosity of the spring are selected properly, this model can demonstrate cloth-like deformations for different types of fabrics with specific fiber contents and structures.

However, a mass-spring system is likely to produce the ‘super-elastic’ effect [38]. Since the fit assessment of a virtual garment on a particular model is one of the important applications of virtual dressing, the strain (elongation/compression rate) of the meshes should not exceed a given tolerance. Caramana *et al.* [41] specified that any edge of a triangular mesh should not change by more than 10% in a single time step of the integration. To rectify the super-elastic behavior, two algorithms were developed based on the position adjustment [38] or velocity adjustment of the end points of the spring that suffers the over-elongation/compression [42]. Though the position adjustment algorithm can effectively restrain the strain within the limit, its possibility to introduce extra intersections between cloth mesh and subject surface and self-intersection among cloth meshes makes it unsuitable for strain control in the virtual dressing procedure, where unpredicted penetration may introduce unacceptable visual effects. Since the velocity adjustment scheme can be integrated into the framework of collision processing routine, it is more reliable in maintaining real-time size stability.

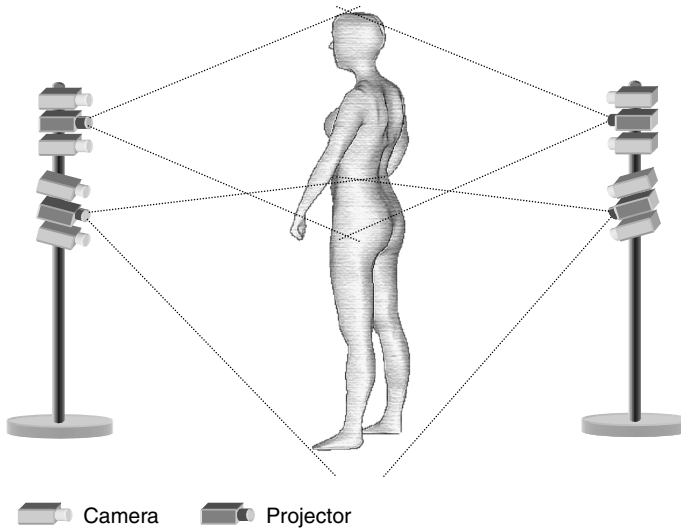
In this chapter, we focus on reporting a stereovision system for 3D body imaging, a mesh subdivision algorithm for body modeling and 3D simulation techniques for virtual dressing.

4.2 3D body imaging – stereovision

A stereovision system employs off-the-shelf cameras to capture body images from different perspectives, and has potential for better portability, affordability and data-acquisition time of scanning [19, 20].

4.2.1 System setup

In a basic stereovision system, two slightly separated cameras reconstruct the visible surface of an object. Since the two cameras observe the object from slightly different viewpoints, the captured left and right images are not identical. The relative displacement of the object in the two images is called the disparity, which is used to calculate the depth. The basic components of a stereo head consist of a pair of cameras and a projector. The projector is used to shed artificial texture onto the body that can enhance matching accuracy. Four stereo heads mounted on two steady stands are needed to a space of $2 \times 1.2 \times 0.8$ m for whole body imaging (Fig. 4.1). Compared to some existing

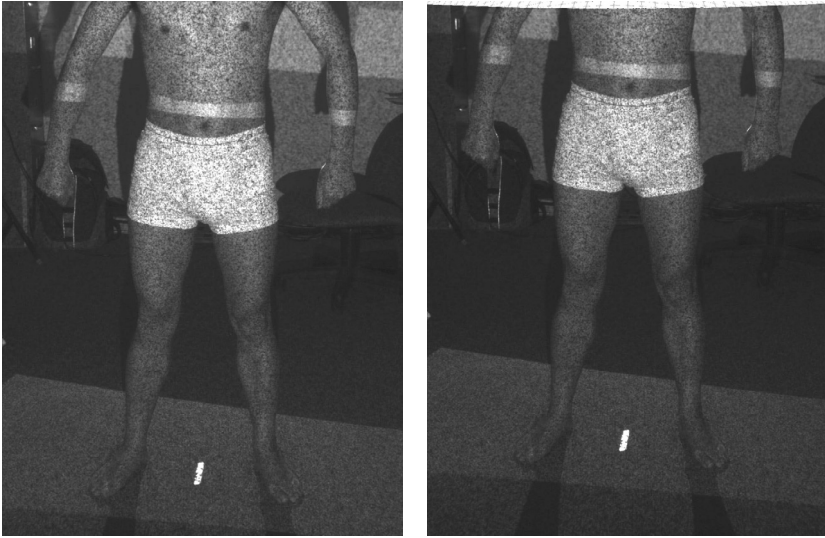


4.1 Schematic of the stereo imaging system setup.

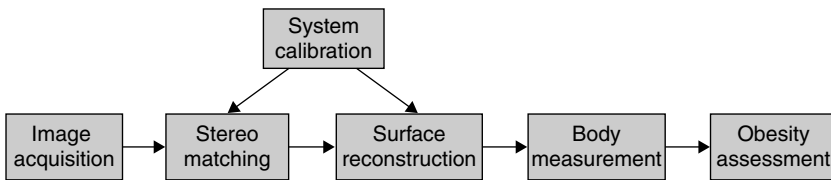
whole body scanners, the unique setup of the system has greatly improved its affordability and portability. The four pairs of images were captured simultaneously when the body was illuminated by the projectors. The entire image acquisition procedure was completed in 200 ms, and thus, the artifacts caused by involuntary body movements were drastically reduced. As an example, a stereo image pair captured by one of the stereo heads is shown in Fig. 4.2. The procedures of data processing in the system are illustrated in Fig. 4.3.

4.2.2 System calibration

The system was calibrated in two separate stages: camera calibration and 3D registration. Camera calibration is a procedure for determining the intrinsic and extrinsic camera parameters. The intrinsic parameters correct the distortion induced in each individual camera by imperfect lens and lens displacement, and more specifically, include the effective horizontal and vertical focal lengths, the principal point describing the center offset of the lens, and the radial and tangential lens distortion coefficients. The extrinsic parameters describe the position and orientation of the each individual camera in a reference coordinate system, and can be represented by a rotation matrix and a translation vector. Based on the extrinsic parameters of the two cameras of a stereo head, their relative position and orientation was determined. The Small Vision System shipped with the cameras provided a toolbox of plane-based calibration routines, using the algorithm originally proposed by Zhang [43].



4.2 Example of a pair of stereo images.



4.3 Data flow diagram of the system.

The above camera calibration procedure was performed separately on each individual stereo head, and each stereo head had its own camera coordinate system. The goal of 3D registration is to transform each camera coordinate system into a common world coordinate system so that 3D data from each view can be merged to complete surface reconstruction. This transformation followed the rigid body model since it does not change the Euclidean distance between any points. To determine a rigid body transformation, three non-collinear points are sufficient. For this purpose, we designed a planar board target. There are six dots on each side of the board, and each stereo head needs only three of them. The world coordinates of the centers of the dots were measured manually. The images of the target were first rectified, and then the dots were identified and sorted. Next, the centers of the dots were estimated and the camera coordinates of each point could be calculated from its disparity.

Within the two stages, camera calibration is relatively complicated, but there is no need to repeat the process frequently since the relative position

of two cameras in a stereo head can be readily fixed and intrinsic camera parameters can be stabilized using locking lenses. Therefore, only 3D registration is required when the system is transported. This property contributes to the portability and also reduces cost of maintenance.

4.2.3 Stereo matching

Stereo matching [44, 45] solves the correspondence problem in stereovision. For the stereovision system developed in this study, a matching algorithm with sub-pixel accuracy was needed to reach the quality of 3D data demanded by body measurements, and to locate the boundaries of foreground objects accurately.

The stereo matching algorithm involves two major phases. In the first phase, foreground objects are accurately segmented from the background of the scene, and meanwhile, a disparity map with integer-pixel accuracy is computed. In the second phase, the disparity map is iteratively refined to reach sub-pixel accuracy. The flowchart of the algorithm is shown in Fig. 4.4, and is explained as follows.

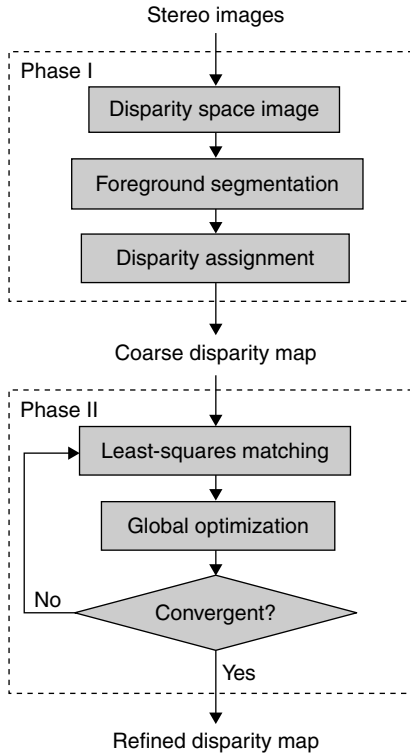
The first step is to compute a disparity space image (DSI) which is a matching cost function defined in the reference image and at each possible disparity [44]. Let $I_l(x, y)$ and $I_r(x, y)$ be the left and right intensity images, respectively. Taking the left image as the reference, a match is denoted as $(x, y)_l \leftrightarrow (x + d(x, y), y)_r$, where $d(x, y)$ is the disparity map to be solved. Suppose the images have been rectified so that the disparity exists only in the horizontal scanline. In this work, a match is measured by normalized cross-correlation (NCC), since NCC is less sensitive to photometric distortions by the normalization in the local mean and standard deviation [46]. Accordingly, the matching cost can be defined by

$$C(x, y, d) = 1 - \rho(x, y, d), \quad [4.1]$$

where $\rho(x, y, d)$ is the NCC coefficient. Since $-1 \leq \rho(x, y, d) \leq 1$, we have $0 \leq C(x, y, d) \leq 2$. Here the trivariate function $C(x, y, d)$ is called the DSI. For the sake of conciseness, we will also denote the DSI as $C_p(d)$ with the subscript p being a pixel.

Then foreground segmentation is performed in the DSI. Let P denote the pixel set of the reference image. We define $L = \{F, B\}$ as a label set with F and B representing the foreground and background, respectively. Then the goal is to find a segmentation (or labeling) $f(P) \mapsto L$ that minimizes an energy function $E(f)$ which usually consists of two terms [47],

$$E(f) = \sum_{i \in P} D_p(f_p) + \sum_{(p,q) \in N} V_{p,q}(f_p, f_q), \quad [4.2]$$



4.4 Flowchart of the stereo matching algorithm.

where $N \subset P \times P$ is the set of all neighboring pixel pairs; $D_p(f_p)$ is derived from the input images that measures the cost of assigning the f_p to the pixel p ; and $V_{p,q}(f_p, f_q)$ imposes the spatial coherence of the labeling between the neighboring pixels p and q .

To derive $D_p(f_p)$, we assume the disparity space can be divided into two subspaces: the foreground space and the background space that contain the object and the background, respectively. The interface between the two subspaces can be readily determined from the known geometrical configuration of the system, as described in [19, 20]. Denote the interface as $d^*(P)$. Now we define $C_p^F = \min_{d_{\min} \leq d \leq d_p^*} C_p(d)$, $C_p^B = \min_{d_p^* < d \leq d_{\max}} C_p(d)$, and thus $C^F(P)$ and $C^B(P)$ represent the minimum surfaces in the foreground and background subspaces, respectively. If $C_p^F < C_p^B$, then we can expect that there is a good chance that the pixel p belongs to the foreground. The same applies to $C_p^B < C_p^F$ and the background. Therefore, we can define $D_p(f_p)$ by

$$D_p(f_p) = \begin{cases} C_p^F, & f_p = F \\ C_p^B, & f_p = B \end{cases} \quad [4.3]$$

Since there are only two states in the label space L , the Potts model [19, 20] can be used to define the spatial coherence term in Equation [4.2], i.e.

$$V_{p,q}(f_p, f_q) = \begin{cases} \beta_{p,q}, & f_p \neq f_q \\ 0, & f_p = f_q \end{cases} \quad [4.4]$$

In the 8-neighborhood system, we set $\beta_{p,q} = \beta_0$ if p and q are horizontal or vertical neighbors, and $\beta_{p,q} = \beta_0/\sqrt{2}$ if they are diagonal neighbors.

As a binary segmentation problem, the global minimum of the energy function $E(f)$ can be searched by using the graph-cuts method [48]. Once the pixels are labeled, each pixel in the foreground is assigned a disparity to minimize the cost function, i.e.

$$d(x, y) = \arg \min_d C(x, y, d) = \arg \max_d \rho(x, y, d). \quad [4.5]$$

In practice, the obtained disparity map can be noisy, so median filtering is used to quench the impulse noise. Furthermore, morphological closed and open operators are used to smooth the contour.

The disparity map from the first phase only takes discrete values, and it should be refined to achieve sub-pixel precision. The refinement process is iterative and involves two steps: local least-squares matching and global optimization. For the first step, the amount of update is estimated locally for each pixel. The estimation can be made by minimizing the matching cost function defined in Equation [4.1]. However, the process is difficult since the NCC function ρ is highly non-linear. So instead, the sum of squared differences (SSD) is applied to define the matching cost as in the least-squares matching algorithm [49]. If the SSD takes into account the gain and bias factors between cameras, it is essentially equivalent to NCC. Now the matching cost is defined as

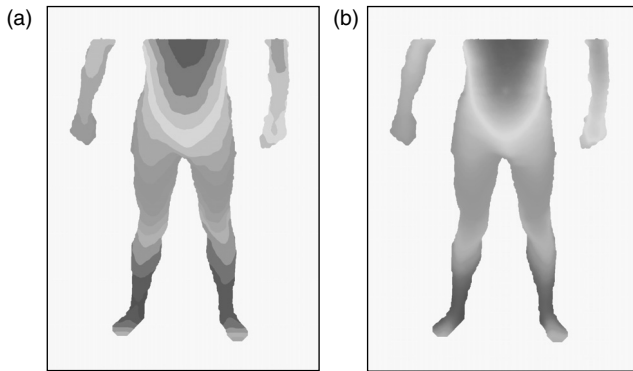
$$C_{\text{SSD}}(x, y, d) = \sum_{(u,v) \in W(x,y)} \left(I_r(u+d, v) - (aI_l(u, v) + b) \right)^2, \quad [4.6]$$

where $W(x, y)$ is a matching window around (x, y) , and a and b are the gain and bias factors, respectively. Then the local estimate of the disparity \tilde{d} is obtained by minimizing the above equation.

In the second step, the following energy function based on the disparity map is minimized,

$$E(d) = \iint \left(d(x, y) - \tilde{d}(x, y) \right)^2 dx dy + \lambda \iint \left(d_x^2 + d_y^2 \right) dx dy, \quad [4.7]$$

where d_x, d_y are the disparity gradients. The first term of the function measures the consistency with the local estimation, and the second term imposes



4.5 Example of stereo matching. (a) Foreground segmentation and coarse disparity map; (b) refined disparity map.

smoothness constraints on the solution. λ is called the regularization parameter that weighs the smoothness term. This process follows the principles of regularization theory [50].

The above two steps are repeated until a convergence is reached. The advantage of this method is that high accuracy can be reached by the least-squares matching. Meanwhile, stability is maintained and potential errors are corrected by the global optimization.

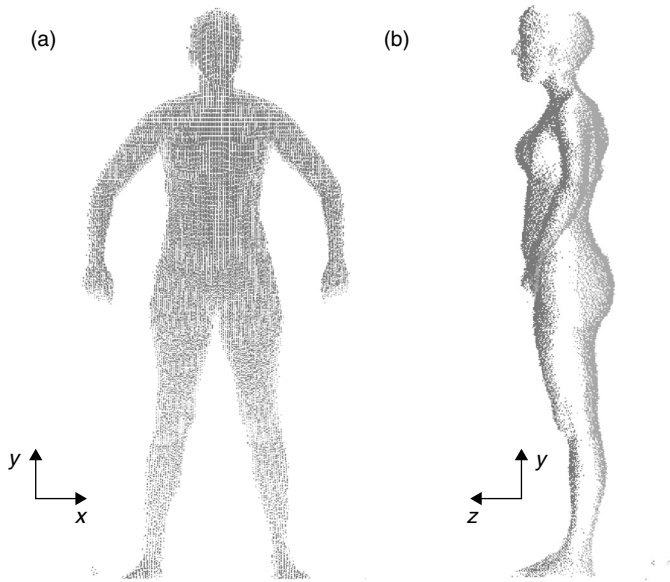
The results of stereo matching on the images of Fig. 4.3 are shown in Fig. 4.5. The disparities are coded with the standard cold-to-hot color mapping that corresponds to 'far-to-close' to the cameras. In this figure, the coarse and refined disparity maps are shown in (a) and (b), respectively. The results show that the algorithm is effective in both foreground segmentation and sub-pixel matching, and is promising for our application. Figure 4.6 presents a typical output of the scanner, which comprises of around 36 000 scattered 3D points. The data are not ready for body measurements because they are incomplete, non-uniformly distributed, and have a big gap between the front and rear views due to occlusions.

4.3 Surface modeling

Surface modeling is a step to produce a complete surface which is a good approximation to the original data with holes/gaps being filled and outliers being filtered.

4.3.1 Data resampling

To facilitate the generation of an initial mesh, the data are resampled on a regular grid and thus explicit neighborhood information can be extracted. The data set of both the front and back views can be regarded as samples on



4.6 Original scan data of a subject in the anterior (a) and lateral (b) views. In (b), data points from the front (back) are shown in black (light grey).

a bivariate surface defined in the frontal projection plane, i.e. the x - y plane in the (x, y, z) Cartesian coordinates as shown in Fig. 4.6. The projections of the data in the x - y plane have irregular distributions because of the varying scanning resolution across the body. The grid density, i.e. the sampling intervals in the x and y directions, is selected. The sampling intervals can be determined as $\Delta y = (y_{\max} - y_{\min}) / (1.2 \times N)$, and $\Delta x = \Delta y / 1.5$, where y_{\min} and y_{\max} are the minimum and maximum y values, and N is the average of the numbers of scanlines in the front and back views. A smaller Δx is selected considering the original data are much denser in the x direction.

At each grid point, the z value is estimated by linear interpolation among neighboring original data points. The neighborhood information can be obtained by triangulation on each data set. Due to the defects of the original data and the irregular contour of a human body, it is difficult to use the Delaunay triangulation algorithm [51] to create a mesh. Fortunately, we can use the partially organized characteristic of the scanlines to perform triangulation between each pair of neighboring scanlines. Since a scanline may come from different parts of the body, e.g. the arms and the torso, a threshold is needed to determine whether two adjacent points in a scanline should be connected. Here the threshold is set to be three times the mean horizontal distance between adjacent points. The local criterion for creating a triangle is the minimum edge length. Once the triangulation is completed,

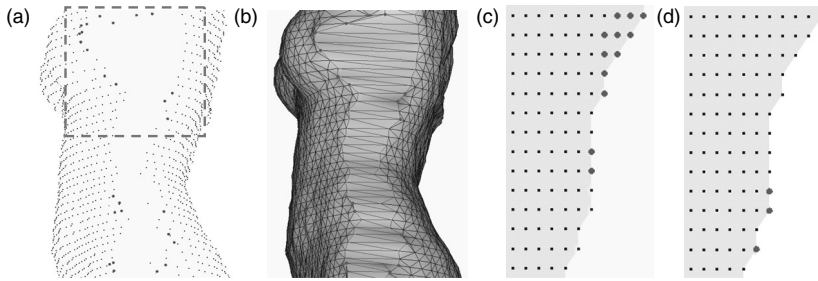
a fast algorithm is used to perform linear interpolation. All triangles are traversed to check whether they hit a grid point or not. It should be pointed out that a triangle might hit more than one grid point. If a grid point is hit by a triangle, then its z value is estimated by a linear combination of the three vertices of the triangle. If a grid point is not hit by any triangle, then it is marked as an empty point. It can be seen that the output of resampling is actually a range image for each data set.

4.3.2 Initial mesh generation

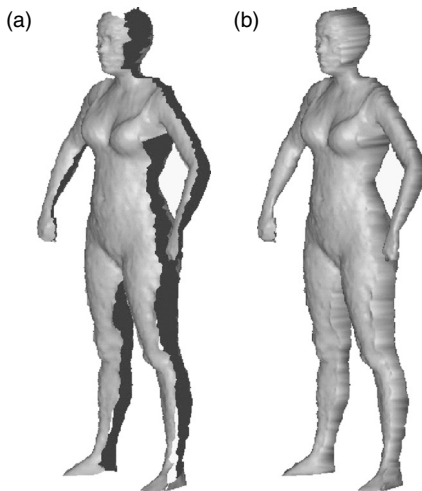
Prior to mesh generation, we need to process the resampled data to fill holes and remove outliers. We define a mask for each view. The mask is actually a binary version of the range image; 1s are assigned to the occupied grid points, and 0s to the empty points. Then, the front and back masks are combined by a logical OR operation. Small blobs in the combined mask are removed as outliers, and only the largest connected region is kept as the body. If there are holes in the remaining region, they are filled by flooding. The combined mask will serve as a reference in the following triangulation process.

The neighborhood information is explicit in a range image, and a triangle mesh can be produced by triangulation between adjacent rows of data, which is similar to the triangulation procedure used in the last step. But a problem arises when we try to merge the front and back meshes to form a complete one, because the mesh contours are so irregular that some conventional tiling algorithms (e.g. reference 52) would fail. To tackle this problem, a technique called Add-Delete is developed in this study. First, some points are padded to both range images according to the combined mask so that their contours have the same projection in the x - y plane. The z values of the added points are set by interpolating their nearest neighbors. With this procedure, holes are also filled. Then triangulation is performed separately on both modified range images. To merge the two triangle meshes, the modified contours are tiled by simply connecting corresponding points. When the meshes are merged, a vertex collapse algorithm can be used to delete these added points. In vertex collapse, a vertex is removed, and its adjacent vertices are re-triangulated to form a new mesh. However, a smarter method is used in this work. We assign a small weight to the added points, and consequently, these points will tend to be deleted first in the following mesh simplification phase. Experiments have shown that the 'soft deletion' strategy gives a more natural appearance of the reconstructed surface.

An example of mesh triangulation is shown in Fig. 4.7. We can see the frontal projections of the front and back meshes completely overlap after padding some points. The generated initial mesh of the whole body is shown in Fig. 4.8. Gaps are closed after merging the contours.



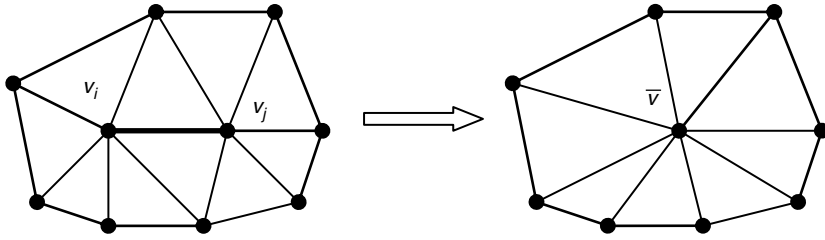
4.7 Triangulation of the torso. (a) Resampled and padded (larger dots) data points. (b) The front and back meshes are merged by tiling the modified contours. Frontal projections of the modified front and back contours, corresponding to the region marked with a dashed box in (a), are shown in (c) and (d), respectively.



4.8 Generation of the initial mesh. Shaded models of the mesh before (a) and after (b) closing the gaps.

4.3.3 Mesh simplification

The purpose of mesh simplification is to reduce the number of triangles and create a control mesh for the model. The simplification algorithm devised by Garland [53] is employed in this work. This algorithm can produce high-quality approximations by using quadric error metrics. It is realized by edge collapse as shown in Fig. 4.9, where the new vertex \bar{v} is evaluated by minimizing the weighted sum of its squared distances (the cost of contraction) to all triangles around vertices v_i and v_j . An edge with the smallest cost of contraction will be collapsed first.



4.9 Edge collapse. A new vertex is created by collapsing the edge.

The quadric measure of the distance of a point v to a plane determined by a point p and a unit normal n is given by

$$D^2(v) = \left((v-p)^T n \right)^2 = v^T n n^T v - 2(n n^T p)^T v + p^T n n^T p.$$

If we define $A = n n^T$, $b = n n^T p$, and $c = p^T n n^T p$, then the quadric error metric can be expressed in this form

$$Q(v) = v^T A v - 2b^T v + c,$$

where the quadric Q is defined as a triple

$$Q = (A, b, c).$$

The quadric for a given vertex v in the original mesh can be expressed as a weighted sum of the fundamental quadrics of its adjacent faces,

$$Q = \sum_k w_k Q_k,$$

where Q_k is the quadric of the k th adjacent face, and the associated weight w_k is set as the face area.

For an edge to be collapsed, such as the edge (v_i, v_j) in Fig. 4.9, the quadric is $Q = Q_i + Q_j$, and the cost of contraction is $Q(\bar{v}) = Q_i(\bar{v}) + Q_j(\bar{v})$, where \bar{v} is the new vertex after collapse. By minimizing the function, we can get the optimal position of \bar{v} ,

$$\bar{v} = A^{-1}b,$$

and the cost

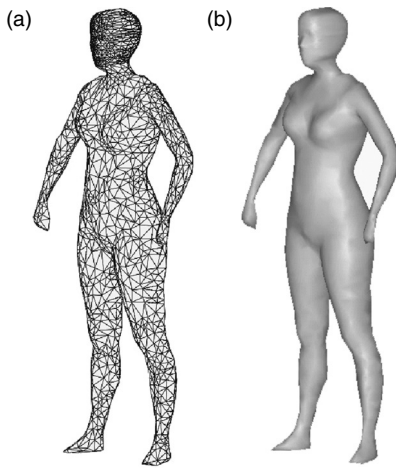
$$Q(\bar{v}) = -b^T A^{-1}b + c.$$

In implementation, all candidate edges are sorted in a heap based on costs. At each step, the edge with minimum cost is removed from the heap and collapsed, and then the heap is updated. This procedure is iteratively repeated until enough simplification is achieved. It is worth noting that, to realize the

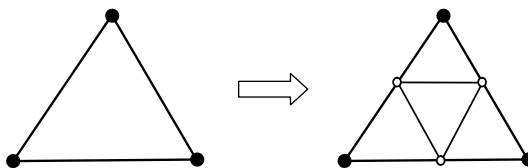
aforementioned ‘soft deletion’ strategy, the cost for an artificially added vertex should be scaled down, so that its associated edges will move upwards in the heap and gain a higher priority for collapse. An example for mesh simplification is shown in Fig. 4.10, where the mesh was obtained by collapsing 80% edges of the model in Fig. 4(b).

4.3.4 Mesh subdivision and optimization

Loop’s subdivision algorithm [54] is used to produce a piecewise smooth mesh. This algorithm is based on edge split, as shown in Fig. 4.11. At each level of subdivision, each edge is split into two, and thus each face is split into four. The surface obtained by an infinite refinement process is called the limit surface of the control mesh. For our applications, a single level of subdivision is enough to obtain a sufficiently dense mesh, which includes two types of points. The first type is called vertex points which are the displacements of the control vertices. The other type is called edge points which are the inserted points on edges.



4.10 A simplified mesh (a) and its shaded model (b).



4.11 Mesh subdivision by edge split.

The evaluation rule for a vertex point p with a valence of n as shown in Fig. 4.12 is given by

$$p = \frac{c_0 v_0 + c_1 v_1 + \cdots + c_n v_n}{c_0 + c_1 + \cdots + c_n},$$

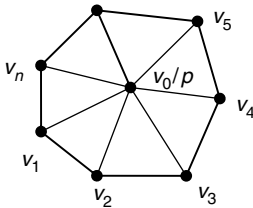
where v_0, \dots, v_n are control vertices, $c_0 = (3/8)n/a(n)$ with $a(n) = (5/8) - (3 + 2\cos(2\pi/n))^2/(64)$, and $c_1 = \cdots = c_n = 1$.

According to the Loop's subdivision rules, the evaluation of an edge point will involve all 2-neighborhood vertices. For an edge point in an ordinary mesh with a valence of six for each vertex, the number of 2-neighborhood vertices is 14, as shown in Fig. 4.13. In our work, to simplify computation, especially in mesh traversal, we only consider 1-neighborhood vertices, which are highlighted in red in Fig. 4.13. Our results show that this simplification still provides a good approximation. The approximate evaluation rule for an edge point p is given by

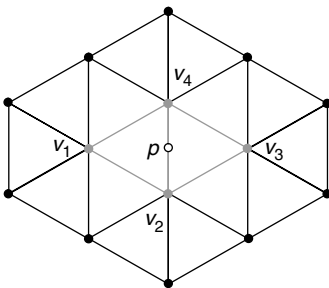
$$p = \frac{c_1 v_1 + c_2 v_2 + c_3 v_3 + c_4 v_4}{c_1 + c_2 + c_3 + c_4},$$

where $c_1 = c_3 = 15$, and $c_2 = c_4 = 32$.

Loop's subdivision algorithm is an approximating scheme, which indicates the limit surface does not pass through the control vertices. In our



4.12 Loop's evaluation rule for a vertex point.



4.13 Modified Loop's evaluation rule for an edge point.

case, it means the resulting model will pull away from the original scanner data. Therefore, the control vertices should be optimized so that the final model can more accurately approximate the original data. This optimization process can be realized by minimizing the distance between the limit surface and the original data. The idea is similar to that in Hoppe *et al.*'s work [55].

The distance can be represented by an energy function as defined by

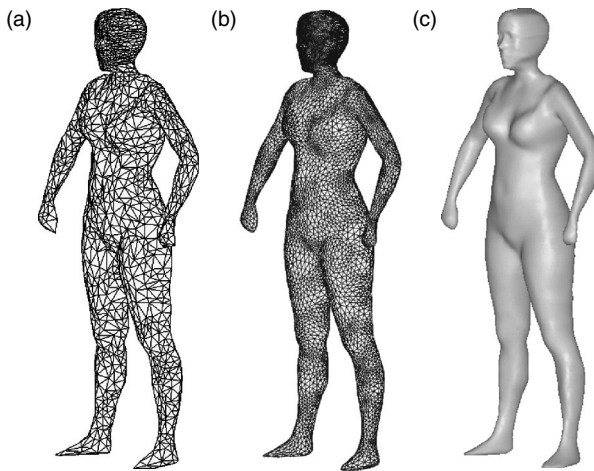
$$E = \sum_i \|q_i - p_i\|^2,$$

where q_i is an original data point, and p_i is its closest point on the limit surface. Since p_i is a weighted combination of the control vertices, the energy function can be rewritten as

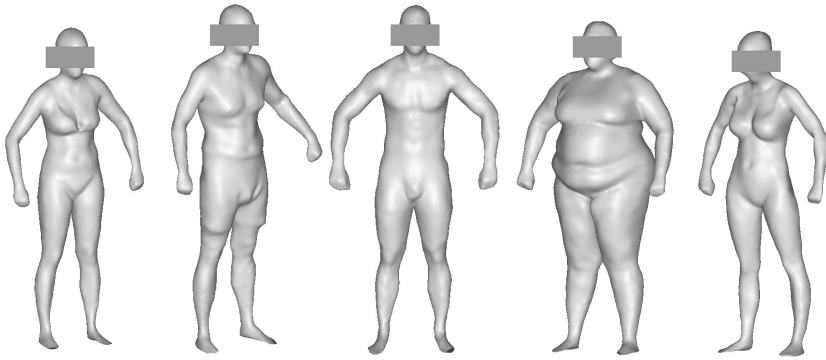
$$E = \sum_i \|q_i - f_i(V)\|^2,$$

where V represents the control mesh, and f_i is a weighting function for p_i . Then, the optimization of V can be achieved by iteratively minimizing E . During each iteration, the V is updated by the conjugate gradient method [56], and the f_i should also be updated to reflect the displacement of the control mesh for the next iteration.

The optimized subdivision mesh for the control mesh in Fig. 4.10 is shown in Fig. 4.14. Some examples of reconstructed 3D surface models of human subjects with various sizes and shapes are shown in Fig. 4.15.



4.14 An optimized control mesh (a), and its subdivision mesh (b) and the shaded model (c).



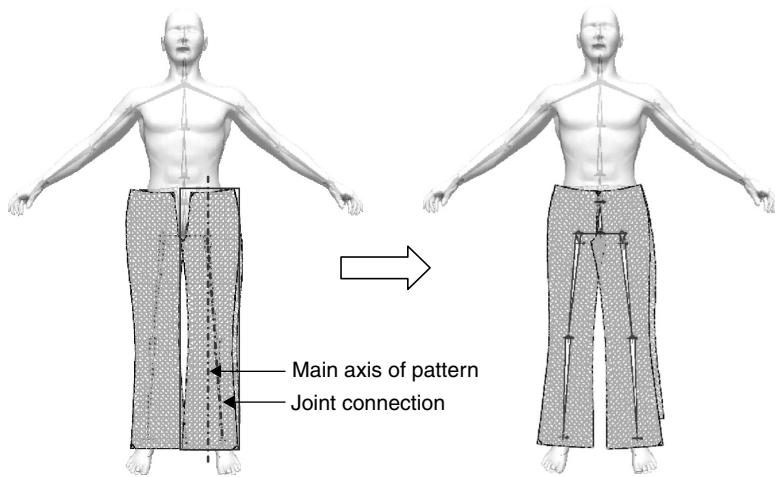
4.15 Examples of 3D surface models of human subjects.

4.4 Virtual dressing

Dressing simulation can be divided into three stages: initial positioning, wrapping and draping. In the first stage, an optimal initial position for each ‘to be sewn’ panel is determined based on the body shape and posture. The appropriate settings of the panels around the body can greatly reduce the computing time in the following stage. In the wrapping stage, the gravity force on the particles of the panel mesh is temporarily removed, and only the attractive force on each particle is imposed to wrap the panels towards the body surface. The force is adaptive to the distance between the particle and the body at each time step of the integration. The particles on the seam-lines of two matching panels (front and back) are pulled together to form a 3D garment. In the last stage, the gravity and surface frictions are added so that the draping effect of a virtual garment can be generated. Since the dressing simulation is an intricate process, this discussion focuses on only a few important issues, such as initial position, adaptive sewing force, collision detection and response and strain control.

4.4.1 Initial positioning and rolling of panels

To wrap pattern panels onto a digital human model, the panel should be positioned in accordance with the pose of the model, which can be defined by the skeleton structure of the human model. The skeleton structure is constructed through the connections of several joints that follow the principle of anatomical landmarking, as shown in Fig. 4.16. The detailed information for acquiring a skeleton from a human model was reported in a previous paper [27].



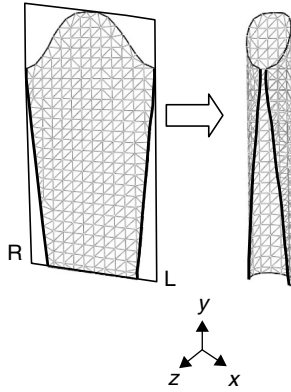
4.16 Body skeleton and initial positioning of panels.

Once a panel is placed in the front of the relevant body part, a bounding box is formed and the axis of the bounding box is regarded as the axis of the panel. To position the panel around a body part of the model, an affine transformation matrix is computed to transform the main axis (either in the transversal direction or in the longitudinal direction) of the bounding box into the orientation of the two joint connection that the panel is laid along. Suppose that the position vector of a mass particle before the transformation is \mathbf{P}_0 , and the affine transformation matrix of the main axis is \mathbf{M} . Hence, the corresponding position \mathbf{P} of the particle on the transformed panel will be:

$$\mathbf{P} = \mathbf{M} \cdot \mathbf{P}_0.$$

Sometimes, a panel faces several skeleton joints, and the joint connections may not be a straight line. In this case, the main axis of the bound box will target the average orientation of the multiple joint connections when computing the affine transformation matrix.

The initial configuration of a panel in the 3D space is a flat panel. Before the wrapping, some pattern can be tube-shaped by a self-rolling process, which can greatly shorten the time of wrapping these pieces. The self-rolling pieces normally have two seamlines that need to be sewn together. Figure 4.17 displays an example of a self-rolled sleeve piece. The key requirement of the self-rolling process is to keep the dimensions of the panel unchanged. This can be fulfilled through a cylindrical mapping method. Let x_{\min} and x_{\max} be the minimum and maximum x coordinates, and



4.17 Self-rolling through cylindrical mapping.

z_{\min} be the minimum z coordinate of the panel, respectively. The radius of the cylinder is

$$r = \frac{x_{\max} - x_{\min}}{2\pi} + \zeta,$$

where ζ is the gap between the left side (L) and the right side (R) on the cylindrical surface (Fig. 4.17). The x and z coordinates of the cylinder axis are given by

$$O_x = \frac{x_{\max} + x_{\min}}{2}, \text{ and } O_y = z_{\min} - r.$$

If the rolling of the flat panel occurs in the $+z$ direction, the new coordinates of particle P_0 can be calculated by

$$\begin{aligned} P_x &= \alpha \cdot r \cdot \sin \theta + O_x \\ P_z &= r \cdot \cos \theta + O_z, \\ P_y &= P_{0y} \end{aligned}$$

where $\theta = (\sqrt{(P_{0x} - O_x)^2 + (P_{0z} - z_{\min})^2}) / (r)$, and $\alpha = \begin{cases} 1 & P_{0x} > O_x \\ -1 & P_{0x} \leq O_x \end{cases}$.

The self-rolling moves the seamlines of the two panels close to each other, and therefore reduces the sewing time in the wrapping stage. Figure 4.18 gives one example for initial positioning of panels around a digital model before the wrapping.

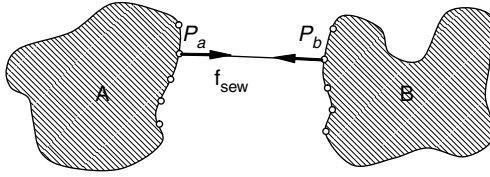


4.18 Initial positioning of multi-panels.

4.4.2 Adaptive sewing force

A robust sewing procedure often requires three basic tasks: (1) associating the corresponding seamlines of panels that need to be sewn together, (2) preventing oscillations of the particles on the seamlines when they approach each other, and (3) keeping the sewn panels untorn (surface penetration) during the entire simulation. These tasks can be achieved by using an adaptive sewing force with acceleration corrections [57] and a particle-merging scheme to secure the seamline when being pulled into a distance tolerance.

As shown in Fig. 4.19, the sewing forces \mathbf{f}_{sew} are imposed on the particles on the seamlines of two panels, and their directions are determined by the directional vectors between two corresponding nodes, P_a and P_b . The sewing force applied on P_a is in the direction of vector $\mathbf{x}_{ab} = \mathbf{x}_b - \mathbf{x}_a$, where \mathbf{x}_a and \mathbf{x}_b



4.19 Illustration of sewing force.

are the position vectors of P_a and P_b , respectively. Similarly, the sewing force on P_b is in the direction of \mathbf{x}_{ba} . To bring P_a and P_b together smoothly, \mathbf{f}_{sew} on P_a is constructed as a function of the distance ($\varepsilon \mathbf{x}_{ab}$), air resistance ($-\tau \mathbf{v}_a$) and an oscillation stabilizer ($\Delta \mathbf{A}_a$).

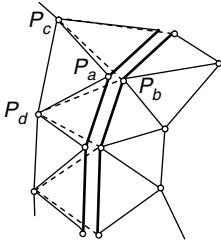
$$\mathbf{f}_{\text{sew}} = \begin{cases} \varepsilon \mathbf{x}_{ab} - \tau \mathbf{v}_a + \Delta \mathbf{A}_a & |\mathbf{x}_{ab}| > \delta \\ c \frac{\mathbf{x}_{ab}}{|\mathbf{x}_{ab}|} & |\mathbf{x}_{ab}| \leq \delta \end{cases}$$

where ε , τ and c are the coefficients, and δ is the distance tolerance, and $\Delta \mathbf{A}_a$ is the acceleration correction at P_a , which can be derived from the total acceleration correction $\Delta \mathbf{A}_{ab}$ [57]. $\Delta \mathbf{A}_{ab}$ is defined as follows,

$$\begin{aligned} \Delta \mathbf{A}_{ab} &= (\lambda_f + \lambda_{\text{damp}_n}) \mathbf{x}_{ab} + (\lambda_f + \lambda_{\text{damp}_n}) \mathbf{v}_{ab}^N + \lambda_{\text{damp}_t} \mathbf{v}_{ab}^T \\ &\quad + \lambda_{\text{atten}_n} \mathbf{a}_{ab}^N + \lambda_{\text{atten}_t} \mathbf{a}_{ab}^T; \\ \Delta \mathbf{A}_a &= \frac{m_a^{-1}}{m_a^{-1} + m_b^{-1}} \Delta \mathbf{A}_{ab}, \text{ and } \Delta \mathbf{A}_b = -\frac{m_b^{-1}}{m_a^{-1} + m_b^{-1}} \Delta \mathbf{A}_{ab}. \end{aligned}$$

where \mathbf{v}_{ab}^N , \mathbf{v}_{ab}^T , \mathbf{a}_{ab}^N and \mathbf{a}_{ab}^T are the relative velocities and relative accelerations of P_a to P_b in \mathbf{x}_{ab} and its transversal direction, respectively. The coefficients, λ_{damp_n} , λ_{damp_t} , λ_{atten_n} and λ_{atten_t} , represent the damping effects on the sewing force, the relative velocity and acceleration. m_a and m_b are the masses of P_a and P_b . Different combinations of the coefficients in computing \mathbf{f}_{sew} can provide different sewing results, and it needs trial tests to determine an optimal combination. When $|\mathbf{x}_{ab}|$ is greater than δ , the magnitude of the sewing force \mathbf{f}_{sew} changes with $|\mathbf{x}_{ab}|$. When $|\mathbf{x}_{ab}|$ is smaller than δ , the two nodes are about to be sewn together, and the magnitude of \mathbf{f}_{sew} should be kept at a lower level ($c < 1$), facilitating the final sewing procedure. We choose $c = 0.8$ after several tests.

To ensure the sewn panels stay together, the next action is to merge P_a and P_b geometrically and change the spring connections accordingly, as shown in Fig. 4.20. When P_a and P_b get close enough ($< 10^{-5} \text{ m}$), it is believed that these two nodes have been sewn together, the sewing force is removed, and the spring connections to node P_a are replaced by the new



4.20 Merging the nodes/particles on the seamlines.

spring connections to node P_b , that is, springs P_cP_a and P_dP_a are replaced by springs P_cP_b and P_dP_b . This change causes two nodes (P_a and P_b) to be glued together all the time, so that the merged panels can be treated as one panel in the subsequent procedures. The masses of the merged particles are combined, and the mass matrix of the mass-spring system needs to be changed accordingly.

4.4.3 Collision detection and response

The virtual dressing may involve wrapping multi-layer panels, which is conducted layer-by-layer. The surface of a human model is always regarded as the first layer, and the garment layers are regarded as the second, the third layer, etc. The geometrical surface of a previous layer is called a subject surface, which is deemed to be motionless. The final 3D configuration of a virtual garment is dictated by the interactions of the particles of the garment pattern with those of the subject surface (cloth/object collisions) and among themselves (self-collisions). These two basic collisions can be further divided into point-triangle collisions and edge-edge collisions. The point-triangle collision occurs when a panel node collides with a triangle facet on the subject surface or a subject surface vertex collides with a panel triangle. Both need the same ray/triangle collision detection procedure, but different collision response mechanisms. In edge-edge collision detections, one edge of a panel triangle collides with an edge of a subject surface triangle.

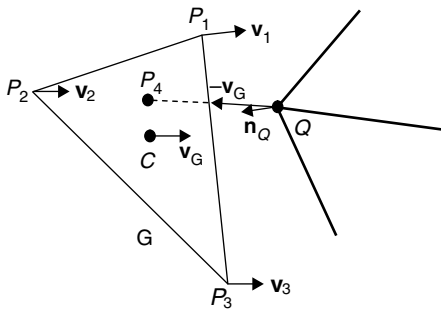
To accelerate the collision detection between a garment surface and a subject surface, an AABB (axis-aligned bounding box) hierarchy tree is pre-calculated by recursive subdivisions of the subject surface [36, 58, 59]. At each time step, the proximity status between the garment surface and the AABB tree is checked. The checking starts with the root node of the AABB tree. If a collision occurs (i.e. the proximity condition is met), the collisions with its subsequent nodes. The checking is performed recursively until all the branching nodes of the AABB tree are checked. The found branching nodes lead to the actual triangles of the subject surface where further collision detections need to be performed.

Point-triangle collision detection and response

The first type of point-triangle collision is the collision between a panel particle and a triangle facet of the subject surface. At one instant of time, if the position of a panel particle P is \mathbf{x} and the instant velocity vector is \mathbf{v} , an incident ray (\mathbf{x}, \mathbf{v}) can be constructed to test whether particle P has a tendency to intersect a triangle facet on the subject surface. A collision is announced when the distance between P and the intersection point is within a given tolerance ξ . Physically, particle P cannot pass through the subject surface. P needs to be bounced back when the collision is detected. This is the so-called collision response. Let v_{rel}^{n-} and v_{rel}^{n+} be the magnitude of the relative velocities in the normal direction of the triangle before and after the colliding, respectively. A coefficient of restitution λ ($0 \leq \lambda \leq 1$) is employed to denote the energy loss for the frictionless collision model, i.e. $v_{\text{rel}}^{n+} = -\lambda v_{\text{rel}}^{n-}$. Since the subject surface is motionless, the new relative velocity of P equals its absolute velocity in the 3D space.

The second type of point-triangle collision is the collision between a panel triangle and a vertex of the subject surface, which is depicted in Fig. 4.21. To detect whether a panel triangle $P_1P_2P_3$, will collide with a vertex Q on the subject surface, the velocity \mathbf{v}_G of the triangle centroid C_G is calculated, and then an incident ray $(Q, -\mathbf{v}_G)$ is drawn at Q . This is based on the assumption that at one instant of time, the moving direction of triangle $P_1P_2P_3$ can be represented by the moving direction of its centroid C_G . If $(Q, -\mathbf{v}_G)$ intersects with triangle $P_1P_2P_3$ at an interior point P_4 , and the distance between P_4 and Q is smaller than ξ , a collision is announced.

After calculating the barycentric coordinates of P_4 in triangle $P_1P_2P_3$ as w_1, w_2 , and w_3 , the velocity of P_4 relative to Q before the collision can be computed as $\mathbf{v}_{4_rel}^- = w_1 \mathbf{v}_1^- + w_2 \mathbf{v}_2^- + w_3 \mathbf{v}_3^-$, and its magnitude in the collision normal direction \mathbf{n}_Q is $v_{4_rel}^{n-} = \mathbf{v}_{4_rel}^- \cdot \mathbf{n}_Q$. Here, the collision normal \mathbf{n}_Q equals to the normal of the vertex Q in the subject surface, and is set to be the



4.21 Collision between a subject surface vertex and a panel triangle (point-triangle).

average normal of all the facets that shared vertex Q . According to the frictionless collision model, the magnitude of the relative velocity of P_4 in the collision normal direction after the collision is $v_{4\text{rel}}^{n+} = -\lambda v_{4\text{rel}}^{n-}$. Therefore, the velocity of P_4 after collision can be synthesized in terms of the collision normal \mathbf{n}_Q . Since Q is motionless, the relative velocity difference of P_4 equals its absolute velocity difference.

Governed by the momentum conservation law, the impulse \mathbf{I} in direction \mathbf{n}_Q equals the momentum change during the collision:

$$\mathbf{I} = m_4 \mathbf{v}_4^+ - m_4 \mathbf{v}_4^- = (w_1 m_1 + w_2 m_2 + w_3 m_3)(\mathbf{v}_4^+ - \mathbf{v}_4^-).$$

Assume that all the particles have the same mass m , and $w_1 + w_2 + w_3 = 1$. We have

$$\mathbf{I} = m(\mathbf{v}_4^+ - \mathbf{v}_4^-) = m\Delta\mathbf{v}_4.$$

Due to the nature of the mass-spring system, the velocity is specified only for the triangle vertices. If one point inside the triangle or on the edge collides with other objects, the collision impulse can be distributed to the triangle vertices in terms of the affine deformation rule. According to Bridson *et al.* [60], the adjusted impulse $\tilde{\mathbf{I}}$ applied on the triangle vertices P_1, P_2 , and P_3 is given by

$$\tilde{\mathbf{I}} = \frac{2\mathbf{I}}{1 + w_1^2 + w_2^2 + w_3^2} = \frac{2m\Delta\mathbf{v}_4}{1 + w_1^2 + w_2^2 + w_3^2}$$

and the new velocity of each vertex is

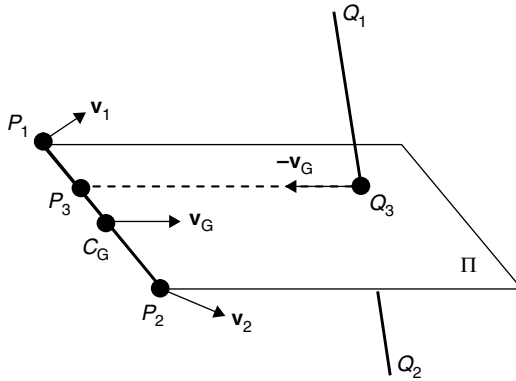
$$\mathbf{v}_i^+ = \mathbf{v}_i^- + w_i \left(\frac{\tilde{\mathbf{I}}}{m} \right) = \mathbf{v}_i^- + \frac{2w_i}{1 + w_1^2 + w_2^2 + w_3^2} (\Delta\mathbf{v}_4); \quad i = 1, 2, \text{ and } 3.$$

Edge–edge collision detection and response

In the edge–edge collision (see Fig. 4.22), the instant velocity of centroid C_G of edge P_1P_2 of a panel triangle is employed as the moving direction towards the triangle edge Q_1Q_2 in the subject surface. The possible colliding point between P_1P_2 and Q_1Q_2 can be found on a plane Π that is formed by using P_1P_2 and \mathbf{v}_G . \mathbf{v}_G stands for the velocity vector of C_G that can be determined by the masses and velocities of P_1 and P_2 as follows,

$$\mathbf{v}_G = (m_1 \mathbf{v}_1 + m_2 \mathbf{v}_2) / (m_1 + m_2),$$

when $m_1 = m_2$, $\mathbf{v}_G = (\mathbf{v}_1 + \mathbf{v}_2)/2$. Assume that Q_1Q_2 intersects with the moving plane Π at point Q_3 . The incident ray $(Q_3, -\mathbf{v}_G)$ will intersect with P_1P_2 at P_3 , which is the potential collision point on edge P_1P_2 . If the distance



4.22 Edge-edge collision.

between Q_3 and P_3 is smaller than the tolerant distance ξ , a collision is announced.

To evaluate the new velocities of P_1 and P_2 after the collision, the velocity change at P_3 needs to be calculated. Before the collision, the velocity at P_3 is calculated as

$$\mathbf{v}_3 = (1-w_1)\mathbf{v}_1 + w_1\mathbf{v}_2,$$

where $w_1 = |\mathbf{x}_1 - \mathbf{x}_3| / |\mathbf{x}_1 - \mathbf{x}_2|$, and $\mathbf{x}_1, \mathbf{x}_2, \mathbf{x}_3$ stand for the position vectors of P_1, P_2 and P_3 , respectively. Here the collision normal at P_3 is defined by the cross product of the two colliding edges. Because the edge orientations of P_1P_2 and Q_1Q_2 are not pre-defined, it is necessary to test the dot product of the normal and the moving direction \mathbf{v}_G . If it is positive, it then needs to invert the normal before making a correct collision response. If the collision normal is \mathbf{n} , the magnitude of P_3 's relative velocity in the collision normal direction before the collision is $v_{3_rel}^{n-} = \mathbf{v}_{3_rel}^- \cdot \mathbf{n}$. The magnitude of P_3 's relative velocity in the collision normal direction after the collision is $v_{3_rel}^{n+} = -\lambda v_{3_rel}^{n-}$, from which the velocity difference of P_3 caused by the collision can be obtained.

When distributing the impulse onto P_1 and P_2 , we have

$$\tilde{\mathbf{I}} = \frac{2\mathbf{I}}{w_1^2 + (1-w_1^2) + w_2^2 + (1-w_2^2)} = \frac{2m\Delta\mathbf{v}_3}{w_1^2 + (1-w_1^2) + w_2^2 + (1-w_2^2)},$$

where $w_2 = |\mathbf{y}_1 - \mathbf{y}_3| / |\mathbf{y}_1 - \mathbf{y}_2|$, and $\mathbf{y}_1, \mathbf{y}_2, \mathbf{y}_3$ stand for the position vectors of Q_1, Q_2 and Q_3 , respectively. Therefore, the new velocities of P_1 and P_2 are calculated as

$$\mathbf{v}_1^+ = \mathbf{v}_1^- + (1-w_1) \left(\frac{\tilde{\mathbf{I}}}{m} \right) = \mathbf{v}_1^- + \frac{(1-w_1)}{w_1^2 + (1-w_1^2) + w_2^2 + (1-w_2^2)} (\Delta\mathbf{v}_3), \text{ and}$$

$$\mathbf{v}_2^+ = \mathbf{v}_2^- + w_1 \left(\frac{\tilde{\mathbf{f}}}{m} \right) = \mathbf{v}_2^- + \frac{w_1}{w_1^2 + (1 - w_1^2) + w_2^2 + (1 - w_2^2)} (\Delta \mathbf{v}_3).$$

4.4.4 Strain control and size stability

The size stability of a pattern means the changes in its perimeter and area remain in the given limits in the entire transformation. The size stability is essential for assessment of a virtual garment fit. To ensure the size stability of the pattern, the strains of all the connecting springs have to be controlled under a tolerance. Although some other researchers had chosen 10% as a strain limit for a mass-spring system [38, 60], we found that only when the strain limit is set as low as 1% can the stability of a pattern be effectively maintained. A spring may incur an ‘over-elongation’ or ‘over-compression’ problem due to a loose strain limit [38].

Figure 4.23(a) shows the positions (\mathbf{x}_0 and \mathbf{x}_1) and velocities (\mathbf{v}_0 and \mathbf{v}_1) of the two end points of a spring at time t . Their next positions at $t + \Delta t$ can be estimated using the Euler integration, i.e.

$$\mathbf{x}_0(t + \Delta t) = \mathbf{x}_0(t) + \mathbf{v}_0(t) \cdot \Delta t, \text{ and}$$

$$\mathbf{x}_1(t + \Delta t) = \mathbf{x}_1(t) + \mathbf{v}_1(t) \cdot \Delta t.$$

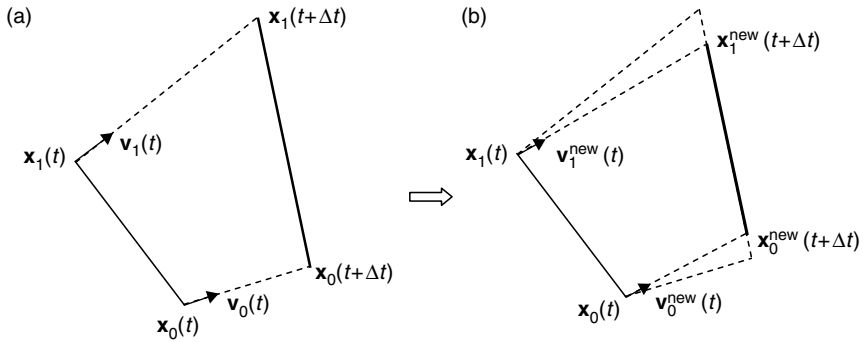
The spring strain at the new position will be $|\mathbf{x}_0(t + \Delta t) - \mathbf{x}_1(t + \Delta t)|/l$ (l is the natural length of the spring). If the strain at $t + \Delta t$ exceeds the strain limit (1%), $\mathbf{x}_0(t + \Delta t)$ and $\mathbf{x}_1(t + \Delta t)$ can be moved along the same direction until the strain falls into the limit (see Fig. 4.23(b)). To ensure the two endpoints to reach their required new positions $\mathbf{x}_0^{\text{new}}(t + \Delta t)$ and $\mathbf{x}_1^{\text{new}}(t + \Delta t)$ at $t + \Delta t$, the velocities of the two endpoints at t need to be adjusted as follows,

$$\mathbf{v}_0^{\text{new}}(t) = [\mathbf{x}_0^{\text{new}}(t + \Delta t) - \mathbf{x}_0(t)] / \Delta t, \text{ and}$$

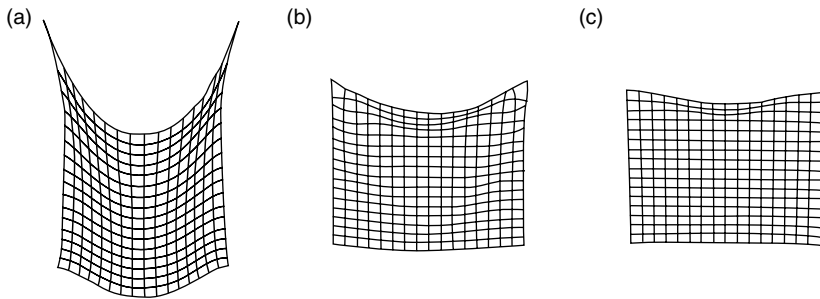
$$\mathbf{v}_1^{\text{new}}(t) = [\mathbf{x}_1^{\text{new}}(t + \Delta t) - \mathbf{x}_1(t)] / \Delta t.$$

To prevent a potential penetration, the routine of the collision detection and response needs to be invoked when the new positions $\mathbf{x}_0^{\text{new}}(t + \Delta t)$ and $\mathbf{x}_1^{\text{new}}(t + \Delta t)$ are calculated.

According to the momentum conservation law, the changes of the velocities induce impulses on the two endpoints of the spring. Theoretically, these impulses will have impacts on other nodes of the mass-spring network, and therefore should be spread throughout the whole system with an iteration method, such as the well-known Jacobi iteration or Gauss–Seidel iteration, to reach an ideal situation such that changing the strain on one spring does



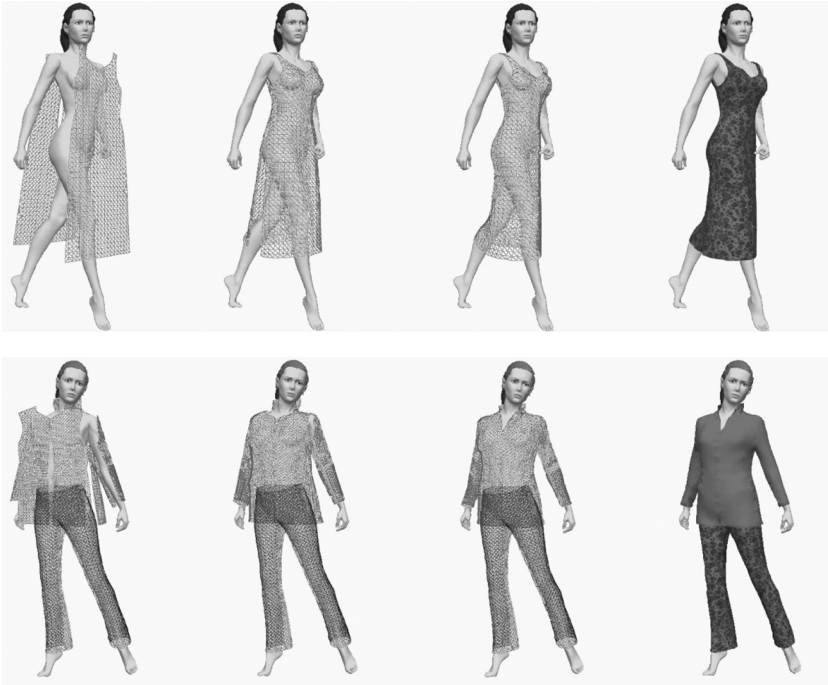
4.23 Strain control through velocity adjustment: (a) particle positions before the adjustment; (b) particle positions after the adjustment.



4.24 A hanging cloth with different strain control methods: (a) no strain control; (b) strain control with the position adjustment; (c) strain control with the velocity adjustment.

not change the strains on others. In practice, since the strain control is executed at every step, the velocity changes at one particular step do not have to be significant. Therefore, the average of the three iterations of velocity adjustments at one time step can be used as the final adjusted velocity for the sake of simplicity. The actual experimental results confirm that this simplification neither causes any instability nor compromises the effectiveness of the strain control scheme.

To verify the strain control performance of the velocity adjustment, we tested it with a 17×17 mesh model of a hanging cloth, which was also done by Provot with the position adjustment scheme [38]. Because of the stress concentration at the hanging corners, the springs connected to the corners are over-elongated when no strain control scheme is implemented, as shown in Fig. 4.24(a). Figure 4.24(b) displays the hanging effect reproduced using the position correction scheme in which the strain limit was set at 10%, and Fig. 4.24(c) is the strain control result of using the velocity adjustment scheme. Both methods demonstrate that the over-elongations



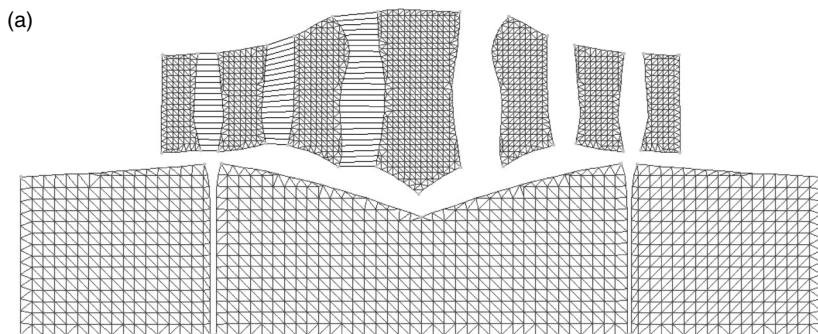
4.25 Image series of virtual dressing.

are curtailed effectively at the hanging corners, while the visual effect of the velocity adjustment seems to be ‘stiffer’ than that of the position adjustment. This is because the velocity adjustment allows a more strict strain control (1%).

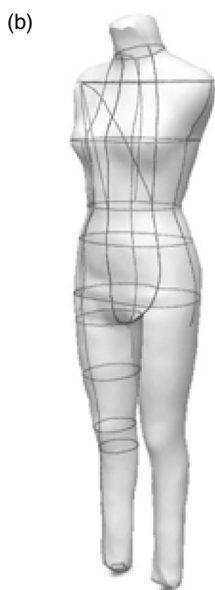
To check the visual effects of the 3D garment dressing, we performed the dressing of different styles of garments onto different poses of a digital human model. As shown in Fig. 4.25, the first series of images demonstrate a single layer dressing of a dress on a walking pose, while the second series of images present a multi-layer dressing of a pant and a jacket on a standing pose. The pant is dressed prior to the jacket. Both image series prove that the virtual dressing methods discussed in this chapter can provide vivid, realistic dressing effects.

4.5 Sewability and fit assessment

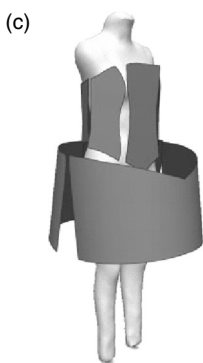
Figure 4.26 presents images from an integrated 3D scanning and dressing system developed at the University of Texas at Austin. The system can automatically generate the mass-spring meshes for the pattern of a garment [61] (Fig. 4.26(a)), scan and reconstruct a subject surface [14, 27] (Fig. 4.26(b)), perform the virtual dressing of the pattern on the scanned



Meshing the input patterns



Body scanning
and modeling



Initial positioning



Wrapping



Draping

Virtual dressing



Photo



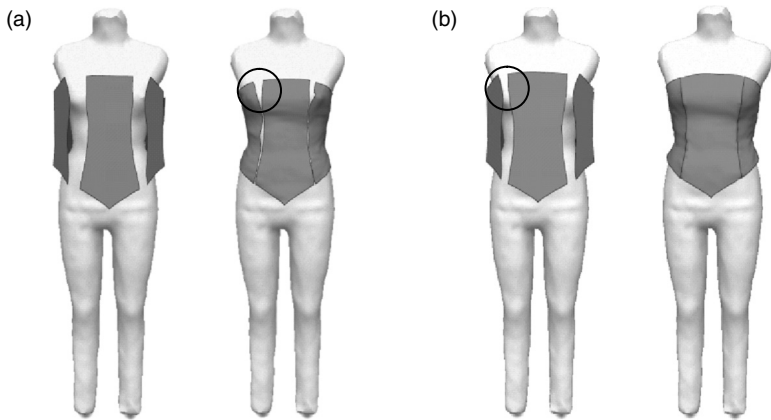
Simulation



Ease map

Fit analysis with the ease map

4.26 An integrated system for virtual dressing.



4.27 Sewability of the pattern: (a) unsewable; (b) sewable.

subject (Fig. 4.26(c)), and analyze the fit using an ease map that illustrates the localized gaps between the garment surface and the subject surface (Fig. 4.26(d)). The garment example included in the pictures is a woman's dress that has ten separate panels. After the mesh generation [61], the system also provides an interactive interface for the user to specify the sewing relationships among the seamlines. The number of the nodes (mass particles) on a pair of associated seamlines must be identical. The body dimension data can be extracted at the defined landmarks [62], which are needed for the fit analysis. Figure 4.26(c) exhibits the three phases of the virtual dressing – initial positioning of the panels, wrapping and draping. Figure 4.26(d) includes a real photo of the mannequin and the dress made with the same pattern, and a simulated picture of the bodice panels of the dress; both appear to have a good match. The ease map gives the quantitative data for the fit analysis.

Since the strain control can facilitate maintaining the designed dimensions of the pattern, the virtual garment can be used to assess the sewability of the pattern before the garment is physically produced. If two associated seamlines cannot be sewn together around a targeted body, the panels are considered unsewable (Fig. 4.27(a)), and their dimensions must be increased based on the corresponding body dimensions. Unsewable panels can be revealed visually and modified immediately until they are sewable and a desired fit is realized (Fig. 4.27(b)).

4.6 Future trends

Currently, 3D body scanning systems have not been seamlessly integrated with apparel CAD, virtual design and modeling systems to create more convenient and effective applications for various users. Most scanning systems

are still considered price-prohibitive for widespread use. They are currently affordable only for trial projects or centralized operations. In addition, they have not fully met the operational requirements concerning their portability, calibration, speed and repeatability. Portability is important for the sizing survey because a system needs to be transported frequently to locations where the targeted consumers are available. An easy calibration procedure permits the quick reinstallation and the desired precision of the system. A high scanning speed helps reduce errors arising from involuntary body movements and throughput time. Further research in 3D body scanning should be directed towards solving these practical problems.

4.7 Acknowledgement

The author expresses his appreciation to the people who worked on the project, especially to Drs Wurong Yu and Yueqi Zhong for their contributions to the research reported in this chapter.

4.8 References

1. LERCH, T., MACGRILLIVRAY, M. and DOMINA, T., 3D laser scanning: a model of multidisciplinary research. *Journal of Textile and Apparel, Technology and Management*, 5(4) (2007): 1–22.
2. ASHDOWN, S. P. (ed.), *Sizing in Clothing: Developing Effective Sizing Systems for Ready-to-Wear Clothing*. Cambridge: Woodhead Publishing Limited, 2007.
3. DEKKER, L., 3D human body modeling from range data. Doctoral thesis, University College London, 2000.
4. ISTOOK, C., Enabling mass customization: computer-driven alteration methods for customized garments. Private communication, 2002.
5. GU, J., CHANG, T., MAK, I., GOPALSAMY, S., SHEN, H. C. and YUEN, M. M. F., A 3D reconstruction system for human body modeling. In: *CAPTECH'98*, Springer-Verlag, Berlin, Heidelberg, 1998, pp. 229–241.
6. KANG, T. J. and KIM, S. M., Development of three-dimensional apparel CAD system part II: prediction of garment drape shape. *International Journal of Clothing Science and Technology*, 12(1) (2000): 39–49.
7. PAQUETTE, S., 3D scanning in apparel design and human engineering. *IEEE Computer Graphics and Applications*, 16(5) (September 1996): 11–15.
8. PARGAS, R., STAPLES, N. and DAVIS, J., Automatic measurement extraction for apparel from a three-dimensional body scan. *Optics and Lasers in Engineering*, 28 (1997): 157–172.
9. PETROV, M., TALAPOV, A., ROBERTSON, T., LEBEDEV, A., ZHILYAEV, A. and POLONSKIY, L., Optical 3D digitizers: bringing life to the virtual world. *IEEE Computer Graphics and Applications*, 18(3) (May/June, 1998): 28–37.
10. PECHOUX, B. L. and GHOSH, T. K., *Apparel Sizing and Fit*. Textile Progress Series, 32(1). Cambridge: Woodhead Publishing, 2002.
11. Cyberware, Whole Body Color 3D Scanner, <http://www.cyberware.com>.

12. Human Solutions, VITUS – 3D Body Scanner, http://www.human-solutions.com/apparel/technology_scanning_en.php.
13. XU, B., HUANG, Y. and YU, W., A 3D body scanning system for apparel mass customization. *Optic Engineering*, 41(7) (2002): 1475–1479.
14. XU, B. and HUANG, Y., 3D technology for apparel mass customization, part I: rotary body scanning. *Journal of Textile Institute*, 94(1) (2003): 72–80.
15. Telmat, SymCAD, www.telmat-net.fr.
16. Textile/Clothing Technology Corporation, [TC]²'s Body Scanner, http://www.tc2.com/index_3dbodyscan.html.
17. Wicks and Wilson Limited, TriForm™ BodyScanner, www.wwl.co.uk/tfmbody-scanner.htm.
18. Hamamatsu Corporation, Body Line Scanner, <http://usa.hamamatsu.com/sys-industrial/blscanner/default.htm>.
19. XU, B., YU, W., YAO, M., PEPPER, R. and FREELAND-GRAVES, J., 3-D surface imaging system for assessing human obesity. *Optical Engineering*, 48(10) (2009): 107204–1–107204–11.
20. YU, W. and XU, B., A portable stereo vision system for whole body surface imaging. *Image and Vision Computing*, 28(3) (2010): 605–613.
21. AMENTA, N., BERN, M. and KAMVYSELIS, M., A new Voronoi-based surface reconstruction algorithm. In: *Proceedings of ACM SIGGRAPH'98*, 1998, pp. 415–421.
22. KRISHNAMURTHY, V. and LEVOY, M., Fitting smooth surfaces to dense polygon meshes. In: *Proceedings of ACM SIGGRAPH'96*, August 1996, pp. 313–324.
23. HOPPE, H., DEROSE, T., DUCHAMP, T., MCDONALD, J. and STUETZLE, W., Surface reconstruction from unorganized points. In: *Proceedings of ACM SIGGRAPH'92*, July 1992, pp. 71–78.
24. LI, P. and JONES, P. R. M., Anthropometry-based surface modeling of the human torso. In: *Computers in Engineering 1994: Proceedings of the 1994 ASME International Computer in Engineering Conference*, The American Society of Mechanical Engineers, Minneapolis, USA, pp. 469–474.
25. DEKKER, L., KHAN, S., WEST, E. and BUXTON, B., Models for understanding the 3D human body form. In: *Proceedings of the IEEE International Workshop on Model-Based 3D Image Analysis*, January 1998, pp. 65–74.
26. DOUROS, I., DEKKER, L. and BUXTON, B., Reconstruction of the surface of the human body from 3D scanner data using B-splines. *SPIE Proceedings*, Vol. 3640, San Jose, California, January 1999.
27. XU, B., YU, W. and CHEN, T., 3D technology for apparel mass customization, part II: human body modeling from unorganized range data. *Journal of Textile Institute*, 94(1) (2003): 81–911.
28. WARREN, J. and WEIMER, H., *Subdivision Methods for Geometric Design: A Constructive Approach*. San Francisco, CA: Morgan Kaufmann Publishers, 2002.
29. YU, W. and XU, B., Surface reconstruction from two-view body scanner data. *Textile Research Journal*, 78(5) (2008): 457–466.
30. ZHONG, Y. and XU, B., 3-D garment dressing simulation. *Textile Research Journal*, 79(9) (2009): 792–803.
31. BARAFF, D. and WITKIN, A., Large steps in cloth simulation. *ACM Transactions on Graphic, SIGGRAPH 1998, Computer Graphics Proceeding*, 1998: 43–54.

32. BREEN, D., HOUSE, D. and WOZNY, M., PREDICTING THE DRAPE OF WOVEN CLOTH USING INTERACTING PARTICLES. *ACM Transactions on Graphic, SIGGRAPH 1994, Computer Graphics Proceeding*, 1994: 365–372.
33. CARIGNAN, M., YANG, Y., Magenat-THALMANN, N. and THALMANN, D., Dressing animated synthetic actors with complex deformable clothes. *ACM Transactions on Graphic, SIGGRAPH 1992, Computer Graphics Proceeding*, 1992: 99–104.
34. CHOI, K. and KO, H., Stable but responsive cloth. *ACM Transactions on Graphic, SIGGRAPH 2002, Computer Graphics Proceeding*, 2002: 604–611.
35. EBERHARDT, B., WEBER, A. and STRASSER, W., A fast, flexible, particle-system model for cloth draping. *IEEE Computer Graphics and Applications*, 16(3) (1996): 52–59.
36. GOTTSCHALK, S., LIN, M. and MANOCHA, D., OBB-tree: a hierarchical structure for rapid interference detection. *ACM Transactions on Graphic, SIGGRAPH 1996, Computer Graphics Proceeding*, 1996: 171–179.
37. MEYER, M., DEBUNNE, G., DESBRUN, M. and BARR, A., Interactive animation of cloth-like objects in virtual reality. *Journal of Visualization and Computer Animation*, 12(1) (2001): 1–12.
38. PROVOT, X., Deformation constraints in a mass-spring model to describe rigid cloth behavior. *Graphics Interface* (1995): 147–154.
39. TERZOPOULOS, D. and FLEISCHER, K., Deformable models. *Visual Computer*, 4(6) (1988): 306–331.
40. TERZOPOULOS, D., PLATT, J., BARR, A. and FLEISCHER, K., Elastically deformable models. *ACM Transactions on Graphic, SIGGRAPH 1987, Computer Graphics Proceeding*, 1987: 205–214.
41. CARAMANA, E., BURTON, D. SHASHKOV, M. and WHALEN, P., The construction of compatible hydrodynamics algorithms utilizing conservation of total energy. *Journal of Computational Physics*, 146 (1998): 227–262.
42. BRIDSON, R., FEDKIW, R. and ANDERSON, J., Robust treatment of collisions, contact and friction for cloth animation. *ACM Transactions on Graphic, SIGGRAPH 2002, Computer Graphics Proceeding*, 21(3) (2002): 594–603.
43. ZHANG, Z., A flexible new technique for camera calibration. *IEEE Transactions on Pattern Analysis and Machine Intelligence*, 22(11) (2000): 1330–1334.
44. SCHARSTEIN, D. and SZELISKI, R., A taxonomy and evaluation of dense two-frame stereo correspondence algorithms. *International Journal of Computer Vision*, 47(1) (2002): 7–42.
45. BROWN, M. Z., BURSCHKA, D. and HAGER, G. D., Advances in computational stereo. *IEEE Transactions on Pattern Analysis and Machine Intelligence*, 25(8) (2003): 993–1008.
46. SUN, C., Fast stereo matching using rectangular subregioning and 3D maximum-surface techniques. *International Journal of Computer Vision*, 47(1) (2002): 99–117.
47. BOYKOV, Y., VEKSLER, O. and ZABIH, R., Fast approximate energy minimization via graph cuts. *IEEE Transactions on Pattern Analysis and Machine Intelligence*, 23(11) (2001): 1222–1239.
48. KOLMOGOROV, V. and ZABIH, R., Computing visual correspondence with occlusions using graph cuts. *Proceedings of the IEEE International Conference on Computer Vision*, 2001: 508–515.

49. LUCAS, B. D. and KANADE, T. An iterative image registration technique with an application to stereo vision. *Proceedings of Imaging Understanding Workshop*, 2001: 121–130.
50. POGGIO, T., TORRE, V. and KOCH, C. Computational vision and regularization theory. *Nature*, 317(6035) (1985): 314–319.
51. WATSON, D. F., Computing N-dimensional Delaunay tessellation with application to Voronoi polytopes. *Computer Journal*, 24(2) (1981): 167–172.
52. FUCHS, H., KEDEM, Z. M. and USELTON, S. P., Optimal surface reconstruction from planar contours. *Communications of the ACM*, 20(10) (1977): 693–702.
53. GARLAND, M., Quadric-based polygonal surface simplification. Ph.D. thesis, Carnegie Mellon University, School of Computer Science, 1999.
54. LOOP, C., Smooth subdivision surfaces based on triangles. Master's thesis, University of Utah, Department of Mathematics, 1987.
55. HOPPE, H., *et al.*, Piecewise smooth surface reconstruction. *Computer Graphics Proceedings, Annual Conference Series*, 1994: 295–302.
56. SHEWCHUK, J. R., *An Introduction to the Conjugate Gradient Method Without the Agonizing Pain*. Pittsburgh, PA: Carnegie Mellon University, 1994.
57. VOLINO, P. and MAGNENAT-THALMANN, N., *Virtual Clothing: Theory and Practice*. Berlin, Heidelberg: Springer-Verlag, 2000.
58. BAREQUET, G., CHAZELLE, B., GUIBAS, L., MITCHELL, J. and TAL, A., Boxtree: a hierarchical representation for surfaces in 3D. *Computer Graphics Forum*, 15(3) (1996): 387–396.
59. BERGEN, G., Efficient collision detection of complex deformable models using AABB trees. *Journal of Graphics Tools*, 2(4) (1997): 1–14.
60. BRIDSON, R., FEDKIW, R. and ANDERSON, J., Robust treatment of collisions, contact and friction for cloth animation. *ACM Transactions on Graphic, SIGGRAPH 2002, Computer Graphics Proceeding*, 21(3) (2002): 594–603.
61. XU, B. and ZHONG, Y., 3D technology for apparel mass customization, part III: visualization of 3D garments. *Journal of Textile Institute*, 94(1) (2003): 92–102.
62. ZHONG, Y. and XU, B., Automatic segmenting and measurement on scanned human body. *International Journal of Clothing Science and Technology*, 18(1) (2006): 19–30.

Flame retardant functional textiles

S. GAAN, V. SALIMOVA, P. RUPPER,
A. RITTER and H. SCHMID,
Swiss Federal Laboratories for Materials
Testing and Research (EMPA), Switzerland

Abstract: This chapter is a brief review of research and developments in the field of flame retardant textiles. The review focuses mainly on the currently available flame retardant solutions for different kinds of textiles. It gives insights into the general mode of action of flame retardants, types of flame retardant fibers, flame retardant additives for fibers and surface treatments and standard test methods for flame retardant textiles. The existing commercial flame retardant treatments for textiles are over 50 years old and some of them have created environmental concerns. Over the past few decades there have been considerable developments in inherently flame retardant synthetic fibers but effective and environmentally friendly flame retardant coatings or finishing solutions for textiles still elude us.

Key words: flame retardant, inherently flame retardant fiber, textile, phosphorus, polymer.

5.1 Introduction

Textiles are manufactured from fiber forming natural polymers such as cellulose and protein and a wide variety of synthetic polymers such as polyesters, polyolefin, polylactide, polyamides, polyaramids, polyetherketones, polyacrylonitrile and cellulose acetate. All of these polymers are suitable for use in textiles because of excellent fiber-forming properties, but they share a common problem, namely that most of them are combustible under normal environmental conditions and pose serious fire hazards in case of fire accidents. These organic polymers are a rich source of hydrocarbons and thus they are an excellent source of fuel during the burning process. The term ‘flame retardant textiles’ usually refers to textiles or textile-based materials that inhibit or resist the spread of fire. The hazards and risks associated with textiles are well documented elsewhere (Horrocks, 2001) and will not be discussed in this review. Flame retardant textiles find use in various areas such as (a) manufacturing of uniforms for fire fighters (Prezant *et al.*, 1999), military/police personnel (Adanur and Tewari, 1997; Duran

et al., 2007; Rodie, 2008) and industrial workers; (b) high-performance sports applications (Stegmaier *et al.*, 2005); (c) upholstery for home furnishing (Kamath *et al.*, 2009), office/commercial infrastructure and transportation (Flambard *et al.*, 2005); and (d) sleepwear for children and elderly people (Horridge and Timmons, 1979; Horrocks *et al.*, 2004). Flame retardant (FR) textile materials help save lives, prevent injuries and property losses and protect the environment by helping to prevent fires from starting and limiting fire damage. Flame retardant textiles can be constructed from inherently flame retardant fibers such as Nomex, Kevlar, wool, Trevira CS, modacrylics, melamine fibers and polyvinyl chloride (Marsden, 1991; Weil and Levchik, 2008). Alternatively, flame retardant textiles can also be manufactured either by surface treatments with flame retardant compounds with various chemistries or by incorporating fire retardant additives in polymer bulk before fiber spinning.

5.2 Factors affecting flammability and thermal behavior of textile fibers and fabrics

The flammability of a textile material is a very complex phenomenon and depends on many factors such as the polymer itself, construction of the textile (i.e. weave/knit of fabric, yarn construction), weight/unit volume, additives in the fiber, the type of chemical treatments and the test conditions (Nair, 2000; Ozcan *et al.*, 2003). All textiles can burn provided they are exposed to the right conditions of flame, heat, oxygen concentration and time of exposure to flame.

5.2.1 Fabric construction

In flammability tests, the inherent resistance of polymers to burning was the major factor affecting fabric performance with weight, weave and thickness being secondary. Fabric structure, weight and thickness were more important when measuring thermal protective capability. A combination of fiber non-flammability and optimum fabric structure should be used to achieve maximum non-flammability with the lightest weight for the specific fabric application (Barker and Brewster, 1982; Ross and Stanton, 1973).

Availability of oxygen is a critical factor in determining the flammability of a fabric. The construction of a fabric can play an important role as it determines the amount of air present, the active surface area and the flow of air through the fabric (Hendrix *et al.*, 1972). Fabrics with open constructions may be more combustible and the flame propagation will also be faster. A fabric with raised surface (e.g. fleece-style fabrics, flannelettes and terry toweling) and containing fiber protruding out to the surface needs special care during processing and use. The flammability hazard with raised fiber

surface fabrics involves the phenomenon called ‘surface flash’ whereby a flame can travel rapidly over the fabric surface, singeing the fiber ends. This flash, in itself, may not be dangerous unless the intensity of the flame is sufficient to ignite the base fabric. In testing, this is known as timed surface flash with base burn. The twist of a yarn may also affect the porosity of the fabric. A tightly woven fabric with higher density, constructed from yarns with high twist will provide better flame protection. Fabric blends can also play a crucial role in defining the flammability of fabrics. Blends of fabric made from two different fibrous polymers may show flammability characteristics quite different from what is exhibited by each component of blend independently. For example, fabrics made from polyester are less flammable than cotton fabrics, but polyester/cotton blended fabrics burn more rapidly. This is because of the ‘scaffolding’ effect, where the charred cotton in the blend acts as a support for the polyester fibers. The melting polyester in the blend does not drip away as it may do in 100% polyester fabrics, and continues to burn (wicking effect). The flammability and thermal shrinkage are relatively independent of the fabric weight and weave design and primarily dependent on the thermal stability of component fibers (Minister of Health, 2009; Stepniczka and Dipietro, 1971).

5.2.2 Type of textile fiber

The fibers used in textiles may be broadly classified based on natural polymers or synthetic polymers. Cotton, wool, silk and flax are some of the major natural textile fibers while viscose, TencelTM and cellulose acetate are derived from natural polymers. The synthetic textile fibers owe their origin to several polymer classes such as polyester, polyamide, polyacrylonitrile, polyolefins, polylactide, polyaramid, melamine based, polyurethane, etc.

The flammability properties of the textile fibers differ and can be grouped based on their burning characteristics into the following (Minister of Health, 2009):

- Readily flammable: these fibers ignite readily and burn rapidly, leaving a light ash residue (e.g. cotton acetate, triacetate, rayon and ramie).
- Moderately flammable: these fibers are more difficult to ignite. The synthetics tend to melt and drip, sometimes self-extinguishing upon removal of the ignition source (e.g. acrylic, nylon, polyester, olefin and silk).
- Relatively non-flammable: in general, these fibers will not support combustion after removal of the ignition source (e.g. wool, modacrylic, vinyon and aramids).

Burning behavior of fibers is related to the thermal transition temperatures and thermodynamic parameters such as glass transition temperature (T_g)

and melting point (T_m). Chemically related transitions such as temperature for onset of pyrolysis (T_p) and combustion (T_c) are also very important. The lower the T_c values and the higher the flame temperature, the higher is the flammability of a fiber. The limiting oxygen index (LOI) of fibers is also an important property which determines the flammability of the fibers. Fibers with LOI values greater than 21% burn slowly and LOI values of 26–28% are sufficient to pass small burning tests. The thermal and flammability properties of fibers are discussed in detail elsewhere (Horrocks, 2001; Stegmaier *et al.*, 2005). All cellulose-based fibers have very low LOI values (<19%) and are thus easy to burn. Among the natural fibers wool has relatively high LOI value (approx. 25%) and is a common component in manufacturing flame retardant clothing for firefighters in some countries such as Australia. Another criterion which determines the flammability of fibers is the heat release rates of fibers (i.e. the speed at which the heat is released during thermal decomposition) (Horrocks, 2001; Yang *et al.*, 2009). Peak heat release rates of some common fibers like cotton, rayon, cellulose acetate, silk, nylon, polyester, polypropylene, acrylic fibers, Nomex and Kevlar have been recently measured using micro-scale combustion calorimetry. Cellulose-based fibers, polypropylene, nylon and polyester have relatively high peak heat release rates (>200 W/g) whereas m-aramid (Nomex), a commonly used fiber in manufacturing flame retardant fabrics, has very low values (~80 W/g) (Yang *et al.*, 2009).

5.2.3 Thermal behavior of polymers

The polymer composition of the textile materials is the most important factor determining their flammability. Understanding the thermal behavior of polymers alone and in the presence of additives is useful in designing an effective flame retardant system. Subjecting polymers to elevated temperatures may lead to several physical and chemical changes which are related to the physical and chemical structure of the polymer. Physical changes like T_g and T_m are quite important in case of thermoplastics and may also influence the flammability of the polymers. Details of physical changes for polymers commonly used in textiles are discussed elsewhere (Hischler, 2000; Horrocks, 2001). Thermoplastic polymers like polyesters have T_m values much lower than the decomposition temperature (T_d) values, and thus tend to become fluids before they start to decompose. This physical property of the polymer greatly influences its fire performance. Under certain fire tests where the flame source is static, such as LOI and vertical flammability tests, once the polymer is subjected to flame the polymer melts away from the flame and stops burning. Thus one has to be careful in determining the real fire performance of polyester-based textiles.

Thermal decomposition of polymers leads to extensive changes in the chemical structure of the polymer, whereas the thermal degradation of a polymer may lead to the loss of physical, electrical or mechanical properties of the polymer. When a polymer is subjected to a temperature greater or equal to T_p or T_c , the polymer chains start to break up into smaller fragments, some of which could be volatile flammable products. These flammable products break down further to finally release hydroxyl (OH^\cdot) and hydrogen (H^\cdot) radicals, which will combine with oxygen to release heat and light. The resultant heat could be released to the environment or could feed back into the burning cycle to cause further decomposition of the polymer. The burning process is a feedback process and will continue until the whole polymer has been consumed. The presence of flame retardant additives or absence of oxygen could interrupt this feedback process. The thermal decomposition of polymer is a very complex phenomenon and could lead to formation of several products such as flammable volatiles, non-flammable volatiles and solid residues. The flammable volatiles could be low molecular weight alkanes, alkenes, alkynes, aldehydes, ketones, ethers, etc. Water vapor and carbon dioxide are commonly formed non-combustible gases. The solid residue could be carbonaceous or inorganic in nature or even a combination of both (Horrocks, 2001). Some polymers like cellulose (wood), protein (wool) or aramids (Kevlar) tend to form carbonaceous chars upon heating. Some, like olefins, polyester and polyamides, do not leave any residues. Presence of additives may influence the amount of residue formed during the thermal decomposition process. Some phosphorus-based compounds would react with the substrate to accelerate formation of char. Presence of inorganic additives like silica derivatives can form protective glassy layers which could insulate the inner layers from further decomposition.

Thermal decomposition of polymers can happen via one or more of the following routes (Hischler, 2000):

- (a) random-chain scission where chain breakage happens along the chain length at random places;
- (b) end-scission: the scission of polymer happens at the chain end mainly in the form of monomers;
- (c) chain stripping: the main polymer chain remains more or less intact with removal of atoms or groups linked to the backbone;
- (d) cross-linking: new bonds are formed between functional groups of adjacent chains.

Most of the vinyl polymers break down via routes (a) and (b) whereas route (c) is more common for halogenated olefins and acrylonitriles.

5.3 Types, chemistry and mode of action of flame retardant additives

Flame retardant additives used in textiles can be classified according to their elemental composition or their mode of action. Flame retardant additives are typically made up from compounds containing elements such as (i) phosphorus (in various organic and inorganic forms); (ii) halogens (brominated, chlorinated organics, fluorides of zirconium); (iii) silicon (organic or inorganic forms); (iv) boron; (v) metals (hydroxides of Al, Mg, Ca, phosphinates of Al, Zn and Ca and Zinc borates, fluorides of zirconium); (vi) nitrogen (either alone or together with phosphorus, inorganic or organic); (vii) antimony (oxides together with halogens).

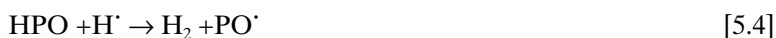
Flame retardants can also be grouped by their mode of action, i.e. gas-phase action and condensed phase action.

(a) Gas-phase action is characterized by evolution of reactive species during the burning process. This action is mostly exhibited by halogen (Georlette *et al.*, 2000) and phosphorus-based flame retardants (Brauman, 1977; Huang *et al.*, 2008). The reactive species could be radicals of halogen (X^\cdot) or phosphorus derivatives which act as free radical scavengers in the vapor phase. Halogen-based flame retardants may release halogen radical which may form hydrogen halide (HX) by abstracting hydrogen from the flame retardant (RX) or the polymer (PH). The hydrogen halide may react further with the hydrogen and hydroxyl radicals (reactions 5.1 and 5.2, respectively) formed from decomposition of polymers and thus interfere with the burning cycle.



Flame retardant activity of halogen compounds can be further enhanced (synergistic interaction) by addition of antimony compounds (Sb_2O_3). This may be because of the formation of volatile antimony halogen compounds such as SbX_3 , which act as an efficient inhibitor of the gas-phase oxidation in the flame (Camino *et al.*, 1991).

Certain phosphorus species have also been found to have gas-phase action. Using direct mass spectrometric investigations of flames, researchers have identified phosphorus species like PO, HPO_2 , PO_2 and P_2 with PO being the major constituent. On the molecular basis, the phosphorus species act by third-body mechanism, catalyzing the recombination of hydrogen atoms according to equations [5.3] and [5.4] (Granzow, 1978).



More recently the gas-phase mechanisms of trimethyl phosphate and triphenyl phosphate derivatives have been studied using Fourier-transform infrared spectroscopy (FTIR). Acidic intermediates (phosphoric acid and its derivatives) formed during the thermal decomposition could also have gas-phase action (Clive and Ed, 2000).

(b) Condensed phase action is characterized by the formation of a protective barrier between the pyrolyzing polymer and the heat source. This protective barrier/char is mostly formed by reaction of the flame retardant additive with the polymer during the thermal decomposition of the polymer. The reaction of flame retardant additive with the polymer is catalytic in nature and causes the decomposition of the polymer at lower temperatures. The action of flame retardant is such that it either changes the pyrolytic pathways of thermal decomposition or it could change the rate of formation of combustible materials. In case of hydroxyl-containing polymers such as cellulose, a large amount of water molecules are released by reaction of phosphorus acidic species with the cellulose. In some instances the phosphorus compounds decompose to form a polyphosphoric acid which forms a thermal insulation barrier on the surface of decomposing polymers (Granzow, 1978; Horrocks, 1983, 2006). The condensed phase action of phosphorus flame retardants could be further enhanced (P-N Synergism) in presence of external nitrogen additives such as urea, guanidine and melamine. The enhanced action of phosphorus flame retardant was attributed to possible chemical reactions between decomposed products of nitrogen additive and phosphorus compound to form a protective coating on the surface of char (Gaan *et al.*, 2008).

(c) Other actions like intumescent and heat sink effects are also mechanisms by which some flameretardant systems work. Intumescent systems are characterized by formation of a foam-like thermal insulation barrier when exposed to flame. A typical phosphorus–nitrogen-based intumescent system consists of a blowing agent (nitrogen-containing compounds like urea, guanidine and melamine), acid source (phosphorus-based flame retardants capable of forming phosphoric acid during thermal decomposition) and char former (generally polyhydroxyl compounds such as pentaerythritol are used). The intumescent effect is due to the combined effect of charring (reaction of phosphorus flame retardants with polyhydroxy compounds), and foaming (evolution of gases like ammonia from nitrogen source) (Camino and Lomakin, 2006). During the burning process the gases evolving from the thermal decomposition of blowing agent get trapped in the char, which is being formed simultaneously, thus forming foam of char on the surface of the material. A heat sink effect is commonly exhibited by additives such as metal hydroxides (aluminum hydroxide) which decompose to release water at elevated temperatures. The heat sink effect could be due to several factors such as endothermic decomposition, heat absorption by

water formed and dilution of gases formed due to pyrolysis of polymers (Weil and Levchik, 2009).

5.4 Flame retardation of textile materials

Flame retardant textiles can be manufactured via the following routes:

(a) *Using inherently flame retardant fibers*

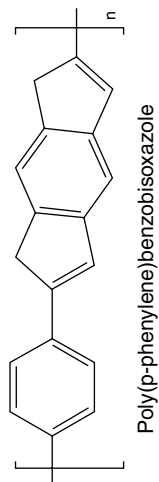
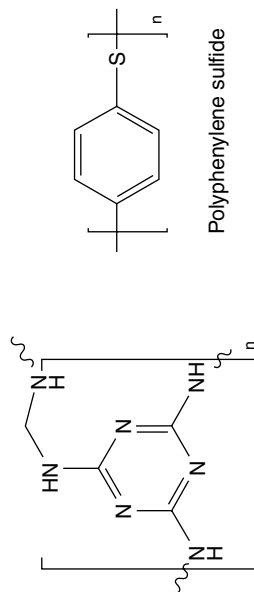
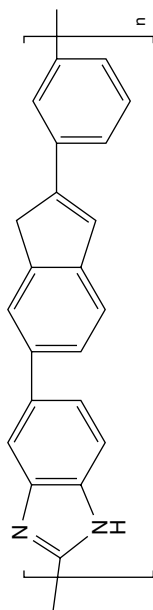
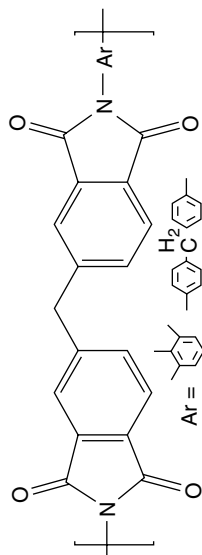
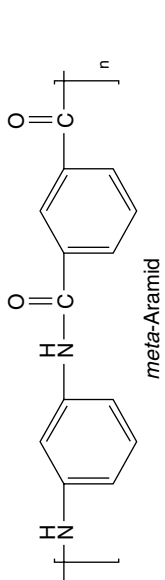
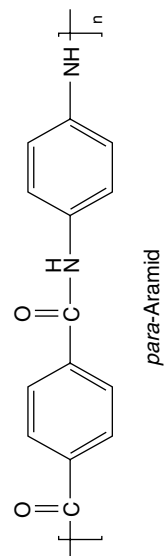
- (i) Fibers from inherently flame retardant polymer. These kinds of flame retardant fibers owe their flame retardant property to the polymer. Aramids, polyimide, melamine, glass, basalt, halogen-containing olefins, oxidized polyacrylonitrile and polyphenylene sulfide-based fibers are some examples of inherently flame retardant polymers. Figure 5.1 shows chemical structures of inherently flame retardant polymers.
- (ii) Fibers from polymers containing special flame retardant comonomers. Modified polyester such as Trevira CS and modacrylics are common examples of fibers containing special monomers with flame retardant characteristics.
- (iii) Fibers containing special non-reactive flame retardant additives. Viscose fibers such as Viscose FR[®] and Visil[®] are flame retardant cellulosic fibers containing very high concentration of flame retardant additives (~30%).

(b) *Finishing or coating*

Application of flame retardants at fabric stage by a finishing process and subsequent fixation by various techniques such as thermal and ammonia curing, UV and plasma polymerization, etc.

5.4.1 Fibers from inherently flame retardant polymers

Aromatic polyamides or *aramids*, which were first developed in 1960s, are one of the most commonly used polymers for developing flame retardant textiles now. These fibers find usage in manufacturing firefighters' uniforms, uniforms for industrial workers, military clothing and accessories. Dupont, USA (Nomex[®] and Kevlar[®]), Teijin, Japan (Twaron[®], Technora[®], Teijinconex[®]) and SRO Group, China (X-Fiber[®]), Yantai Spandex Co. Ltd, China (Newstar[®]), Kermel, France (Kermel[®]) are some major manufacturers of different kinds of aramid fibers. Para-aramid fibers have high tenacity and tensile modulus, heat resistance and dimensional stability and find applications mostly in automotive brake pads and other friction materials, tire cords and protective clothing and are also used as alternatives to asbestos. Meta-aramid fibers are characterized by their long-term heat and flame resistance, and are favored for such applications as heat-resistant filters and



Melamine based polymer

5.1 Inherently flame retardant polymers.

other industrial materials and fireproof clothing for firefighters. Details of aramid fiber production, application and properties can be found elsewhere (Rebouillat, 2001; Yang, 1993).

Melamine fibers are produced by Basofil Fibers LLC, Enka, NC and marketed under the trade name Basofil® Fiber (TNC Global Inc, 2010). Melamine fibers are manufactured from fiber-forming synthetic polymer composed of at least 50% by weight of a cross-linked melamine polymer. The cost of melamine fiber is comparatively low for similar properties. These fibers can operate at high temperatures; they have high LOI values and typically target hot gas filtration and safety and protective apparel markets. Melamine fibers are weak and generally need blending with stronger fibers such as aramids to improve their processing. The major application of melamine fibers is in areas of the bedding industry, upholstery manufacturing of seats for automobiles and aircrafts, protective clothing for firefighters and industrial workers and in the filtration industry involving high temperature applications.

While there are different kinds of commercial polyimide polymers, only some are used in manufacturing textile fibers. P84 is a *polyimide fiber* manufactured by Evonik fibers GmbH, Austria (Weinrotter, 1988). The polymer structure of this fiber is shown in Fig. 5.1. P84 polyimide fiber is derived from aromatic dianhydrides and aromatic diisocyanates and exhibits outstanding thermal stability. The polymer is non-melting and has a glass transition temperature of 315°C. This fiber finds application in different areas such as high temperature filtration, protective clothing, braided packing and insulating material (Evonik Industries, 2010). Fibers based on *polyetherimide* resin (Ultem®) have been recently developed by General Electric (Dris *et al.*, 2008). GE's Ultem® resin is an amorphous, high-performance polymer that exhibits outstanding high heat resistance, strength, modulus and broad chemical resistance. This fiber has a high glass transition temperature of 217°C, a relative thermal index (RTI) of 170°C, is inherently flame resistant and has a very low smoke evolution.

Polybenzimidazole (PBI) is an organic fiber with excellent thermal resistant properties and a good hand. The Federal Trade Commission definition for PBI fiber is 'A manufactured fiber in which the fiber-forming substance is a long chain aromatic polymer having recurring imidazole groups as an integral part of the polymer chain'. PBI does not burn in air and does not melt or drip. PBI Performance Products Inc. is the world's only producer of high-performance PBI fiber (Performance Products Inc, 2010). The high LOI coupled with its good chemical resistance and good moisture regain makes PBI an excellent fiber for fire blocking end uses such as safety and protective clothing and flame retardant fabrics. Its physical properties are relatively inferior, but PBI can be processed on most types of textile equipment. It blends well with other materials such as carbon and aramid fibers and is most often done for performance reasons as well as cost. PBI has

had significant success in the firefighters's apparel market, where, blended in a 60/40 para-aramid/PBI mixture, it has become the standard 'premium' material. PBI's characteristic gold color blends well with other materials for a pleasing appearance.

Glass fibers are made up on a basis of inorganic amorphous polymer and were commercialized in the late 1930s. They find application in insulation (glass batts in home insulation and industrial insulation in mats and fabric form) and are widely used in reinforcing thermoplastic composites in products from circuit boards to boat hulls. They are also used in the manufacturing of barrier fabrics for furniture and military applications and high temperature filtration applications.

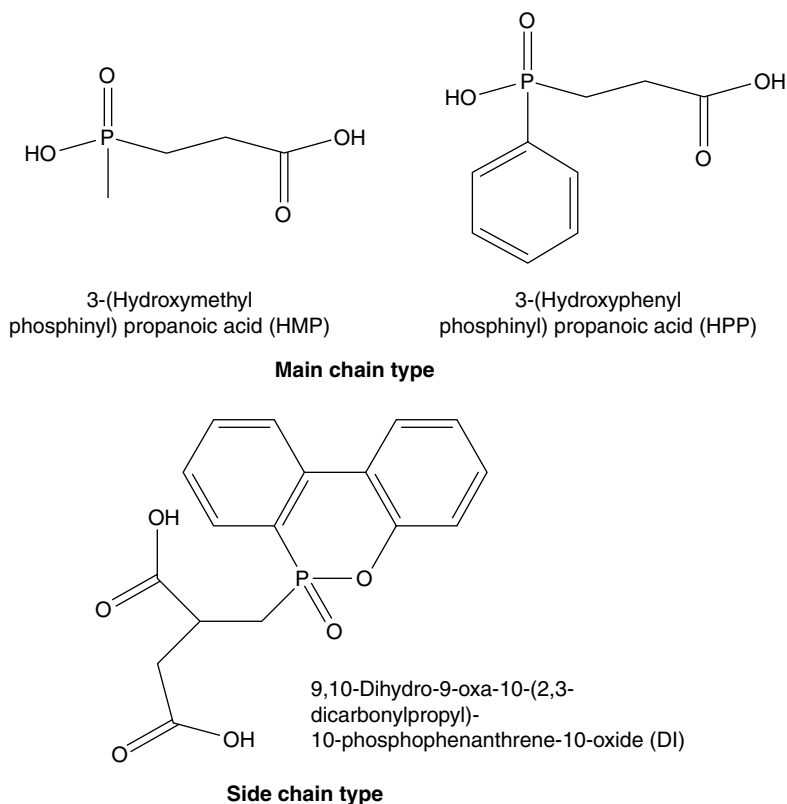
Halogenated fibers based on *modacrylics* and *polyvinyl chlorides* find specialized uses in the development of home furnishings and industrial applications which need fire protection and excellent chemical resistance. These fibers owe their flame retardancy to the presence of chlorine and may liberate large amount of toxic gases during the burning process. Shrinkage problems in the presence of heat, corrosive monomers and environmental regulations make them less attractive nowadays.

Polyphenylene sulfide fibers are known for their moderate temperature resistance and excellent chemical resistance. The polymer is produced by several manufacturers such as Chevron Phillips Chemical Company LP (Ryton®) (Chevron Phillips Chemical Company LLC, 2008), Toboyo (Procon®), Toray (Toray PPS®) (Toray Industries, 2006) and Celanese (Fortron®). The low moisture regain of PPS often prevents its use in protective apparel; the fiber has an uncomfortable hand, but the good chemical resistance makes it very attractive for industrial applications, especially for filtration.

Poly-phenylene benzobisoxazole is a new high-performance organic fiber first introduced by Toyobo in 1999 as Zylon® (Zylon-Department, 2010). It possesses outstanding thermal properties and has almost twice the tensile strength of conventional para-aramid fibers. Its high modulus makes it an excellent candidate for composites reinforcement. PBO has a very high LOI value, more than twice the LOI of meta-aramid fibers.

Oxidized polyacrylonitrile fibers are partially carbonized fibers which can be further converted into carbon or graphite fiber when subjected to further carbonization in an inert atmosphere at high temperature (Rahaman *et al.*, 2007). These fibers do not burn, melt or drip; instead, they char and self-extinguish. Oxidized polyacrylonitrile fiber is relatively weak and has limited abrasion resistance and is thus often blended with other high-performance fibers such as aramid, polyvinyl halide, PBI, flame retardant rayon and polyester fibers creating a strong durable product with excellent flame resistance (Smith, 2007). Zoltek corporation (PYRON®) manufactures oxidized polyacrylonitrile in different forms such as fibers, fabrics and felts (Zoltek Corporation, 2010).

Inherently *flame retardant polyesters* are commercially available from various manufacturers such as Trevira GmbH (Trevira CS[®]), Invista (Avara[®]) and Toyobo (Heim[®]). These kinds of fibers contain reactive organophosphorus additives based on phosphonic acid derivatives. Structures of various reactive co-monomers used in manufacturing commercial flame retardants are shown in Fig. 5.2. A phosphorus content of 0.7–1% is sufficient to achieve satisfactory levels of flame retardancy. The mechanism of flame retardant action of these phosphorus compounds may be due to reduction in melt viscosity caused by acid hydrolysis. The phosphorus atom in these polyesters could be an integral part of the main backbone or it could be present as a pendant group to the main chain. The positioning of phosphorus atom in the polyester does not have any effect on the flammability of the fiber, but it does affect the hydrolysis stability of the polymer. Studies have shown that the main-chain-type hydrolyzes about two times faster than the side-chain type (Maki *et al.*, 2000). Further studies on reaction kinetics have shown that main-chain-type phosphorus-containing monomer like 3-(hydroxymethyl



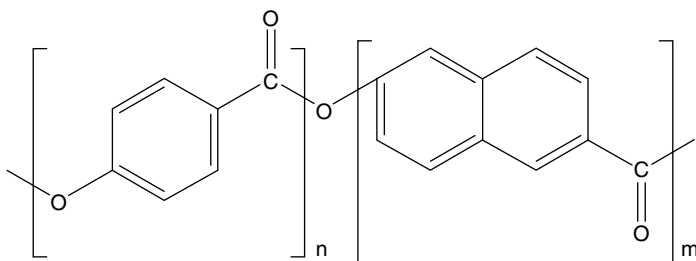
5.2 Phosphorus-containing monomers for polyester.

phosphinyl) propanoic acid (HMP) showed higher chemical reactivity in esterification reactions than the side-chain-type monomer, 9,10-dihydro-9-oxa-10-2,3-dicarbonylpropyl)-10-phosphophenanthrene-10-oxide (DI).

In addition, for production of polyester having the same phosphorous content in commercial scale, it is more beneficial to apply HPP than DI, because of low input of FR due to low molecular weight (Seung-Cheol and Jae Pil, 2007). Polyesters with HPP in the backbone had a higher amount of ethylene glycol in the main chain, thus resulting in lower thermal stabilities. Highly sterically hindered DI was more stable against thermal degradation and alkaline attack, and the DI polyester showed similar stability to that of the normal polyester. For higher phosphorous content polymer production, it is profitable to adopt main-chain-type phosphorous FRs rather than pendant types, because of their lower molecular weight and higher reactivity (Yang and Kim, 2007). The polymer chain of main-chain-type polyester fiber is more flexible than that of pendant type; it adsorbs the dyestuff at lower temperatures and reaches exhaustion more quickly (Seung-Cheol and Jae Pil, 2008). More recently Neopentyl glycol and 3-(hydroxyphenylphosphinyl) propionic acid have been used as the third and fourth co-monomers to synthesize phosphorus-containing poly[(ethylene terephthalate)-*co*-(neopentyl terephthalate)] (PENT) with both flame retardancy (LOI, 25–34%) and low melting temperature (170°C) properties (Xin-Ke *et al.*, 2009).

Fully *aromatic polyester fiber* (Fig. 5.3) developed by Celanese Acetate LLC and now manufactured by Kuraray Co., Ltd (Vectran®) (Kuraray America Inc, 2010) is one of the newest high-performance polymers used for manufacturing textile materials where high thermal and flame protection is important. Vectran HT® and Vectran UM® fibers exhibit high LOI values of 28% and 30%, respectively. These fibers are characterized by low smoke generation and don't drip in vertical flammability tests (Beers and Ramirez, 1990).

Important physical and flame retardant properties of the above-mentioned high-performance synthetic fibers are given in Table 5.1. A detailed review of these properties can be found elsewhere (Greer, 2000–2002).



Structure of Vectran fiber

5.3 Aromatic polyester.

Table 5.1 Properties of fibers made from inherently flame retardant polymers

Fiber	Tenacity (g/den)	Elongation (%)	Limiting oxygen index (LOI)	Chemical resistance	Operating temperature (°C)
Meta-aramid	3.8–7.2	25.0–40.0	30	Mild–good	200
Para-aramid	22.0–26.0	2.4–4.4	25–28	Mild–good	280
Polyphenylene sulfide	3.5–4.5	32.0–49.0	34	Very good	500
Melamine	2.0	18.0	32	Mild–good	400
Polyphenylene benzobis- oxazole	42.0	3.5	68	Mild–good	550–600
PBI	2.7	29.0	41	Good– excellent	250
Polyphenylene sulfide	3.5–7.0	35.0	34	Excellent	190
Polyimide	4.2	30.0	38	Good	500
Oxidized PAN fibers	2.1	25.0	40–52	Good– excellent	570–1000

PAN, polyacrylonitrile.

5.4.2 Flame retardant fibers made from addition of non-reactive additive to polymer

Melt additives

Adding flame retardants during polymer processing is the most widespread and efficient method of FR protection of polymeric materials, since this method does not require new equipment and is economically efficient. However, application of this method is limited by the requirements for an additive: it should be thermally stable up to 300°C under mechanical force for considerable time, should dispense easily and have a suitable melting point and a high degree of dispersion, without degrading or reacting detrimentally with the polymer (Lawton and Setzer, 1975). Halogen-containing organic compounds and organophosphorous compounds are the most commonly used flame retardant additives for poly(ethylene terephthalate) (PET) fibers. Halogen compounds are inert to polyesters under thermal conditions. All phosphorous organic compounds can produce phosphorous-containing acids like H_3PO_4 , H_3PO_3 , H_3PO_2 , which can cause degradation of the polyester by hydrolysis, leading to reduction of mechanical stability. If phosphinates or other P-compounds are used alone or in combination with other flame retardants in polyesters, there is generally some degree of polymer degradation, and this has an adverse effect on the mechanical properties of the polymer system. The melt viscosity of PET is lowered by addition of these compounds. Halogen compounds, typically

hexabromocyclododecane (HBCD), were mainly used as a flame retardant for polyester fibers. However, the use of these compounds is being regulated, because they are persistent and bio-accumulative in nature. Use of many types of halogenated flame retardants, especially brominated compounds (2,2',4,4',5,5'-hexabromobiphenyl), are banned due to toxicity and environmental issues. Some cyclophosphazene derivatives have been developed in the past as melt additives for polyester fibers. Cyclophosphazene phenyl and phenoxy derivatives were incorporated (5–10%) into polyester fibers before spinning to impart flame retardancy without harming their dyeing properties. PET chips were melted at 280°C, combined with 60% hexaphenylcyclotriphosphazene and spun into yarn which was self-extinguishing in nature (Clutter, 1975). Salts of phosphinic acid have been developed as an additive for thermoplastic polyester (Schlosser *et al.*, 2008; Yao *et al.*, 2006). The FR polyester fibers have been produced by the incorporation of FRs using blending or copolymerization (Levchik and Weil, 2004, 2005). A dialkylphosphinate salt has been recently introduced as a melt spinning additive in polyester (Weil and Levchik, 2008). The availability and commercial success of most of these phosphorus-based non-reactive melt additives are not known yet. Flame retardant polyester fibers are manufactured mostly from reactive additives or monomers containing a phosphorus component.

Unlike polyester fibers there are no inherently flame retardant fibers from *polyamides* that are commercially available. There are different kinds of polyamide in commercial use. They vary in their melting points: PA6 (220°C), PA6.6 (260°C), PA6.10 (240°C), PA6.12 (218°C), PA11 (198°C) and PA12 (178°C). There is a temperature range of about 60°C between the melting points which gives the possibility to use different thermo-stable flame retardant additive systems for melt-spun fibers. Other polyamides like thermoplastic fibers, even when flame retarded using either co-monomeric, modifications or additives introduced during polymerization and/or fiber extrusion stages, melt drip and/or form holes when exposed to flame. They cannot, therefore, be used in applications such as protective clothing and barrier textiles, where sustained thermal protection via char formation is an essential requirement (Horrocks, 1996). Some additives like low molecular weight phosphorous compounds, chlorinated polyethylene, brominated pentaerythritol, boric acid and antimony oxide have been used in the spinning dope of polyamides. Calcium zinc molybdate (KemGard 425, Sherwin-Williams Company) and a mixture of brominated pentaerythritol, antimony oxide and boric acid were introduced to nylon 6 melt without change of physical mechanical properties. Melt extrusion of nylon 6 at 230°C with red phosphorous has been reviewed elsewhere (Subbulakshmi *et al.*, 2000). Compounds such as phosphorylated pentaerythritol, lead methylphosphonate and a complex compound of an alkylphosphonic acid and antimony have been investigated as thermally stable flame retardant additives for

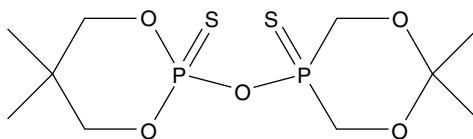
fiber spinning (Butylkina *et al.*, 1989). Ammonium polyphosphate (APP) has been applied on different kinds of nylons and thermal decomposition and flame retardant behavior have been studied in detail. During the burning process APP acts as an intumescent agent and also forms a thermally stable polyphosphoric acid layer on the surface of decomposing polymer (Levchik *et al.*, 1994, 1995). Resorcinol bis(diphenyl phosphate) and bisphenol A bis(diphenyl phosphate) have been used as fire-retardant additives on nylon 6 and nylon 6,6. It was shown that aromatic phosphates promoted charring of the nylons, but the char yield was insufficient to rapidly extinguish the flame (Levchik *et al.*, 2001).

Recently phosphinic acid derivative additives have been developed as melt additive for application on nylon fibers (Yao *et al.*, 2006). In spite of much research and development in flame retardant melt additives, there exist no successful commercial flame retardant additives for nylon melt spinning.

Polyolefin fibers are traditionally made flame retardant by adding brominated additives containing antimony or phosphorus (Zhang and Horrocks, 2003). These brominated flame retardants may adversely affect the light stability of olefins and also have shown to have adverse environmental effects. Tris (tribromoneopentyl) phosphate is a thermally stable, effective flame retardant additive for polypropylene fibers. More recently halogen- and phosphorus-free flame retardant has been introduced by Ciba (Flamestab® NOR™ 116). It requires an addition of 1–1.5% to achieve some degree of flame retardancy (Weil and Levchik, 2009).

Additives for wet spun fibers

Flame retardant *viscose fibers* such as manufactured by Lenzing, Austria (Viscose FR®) and Sateri International Group (Visil®) are the only inherently flame retardant fibers developed from cellulose. Both these fibers use different technology to achieve flame retardant property. Viscose FR® is made by incorporating ~30% organophosphorus-based pigment additive whereas Visil® fiber contains up to 35% SiO₂ as a flame retardant additive. The development of flame retardants for viscose is very challenging as the flame retardant has to withstand severe alkaline and acidic conditions during the fiber manufacturing process. Studies on several kinds of phosphorus-based flame retardants have shown that 1,3,2-dioxaphosphorinane, 2,2'-oxybis 5,5-dimethyl-, 2,2'-disulfide (Fig. 5.4) is the most suitable flame retardant additive for viscose fiber (Wolf, 1981). This compound is a white pigment, practically insoluble in water and very stable to acid and alkaline hydrolysis. It is currently manufactured by Clariant and sold under the trade name Exolit 5060. Visil fibers are manufactured by adding sodium silicate in the alkaline spinning solution and regenerating it as polysilicic acid in the coagulating bath.



1,3,2-Dioxaphosphorinane, 2,2'-oxybis 5,5-dimethyl-, 2,2'-disulfide

5.4 Phosphorous-containing flame-retardant additive for viscose manufacturing.

5.4.3 Application of flame retardants on fabrics by finishing treatments

Application on synthetic fiber fabrics

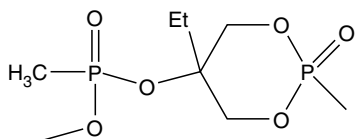
Synthetic fabrics made from nylon, polyester and acrylic fibers are difficult to ignite but once ignited they exhibit severe melting and dripping.

Nylon fabrics are commonly used in manufacturing of fabrics for military applications, upholsteries and carpet, because of their excellent mechanical property. Several flame retardant treatments based on brominated compounds, thiourea formaldehyde resins (Horrocks, 2003) and cyclic phosphonate esters have been discussed in the literature (Weil and Levchik, 2004). Back coating formulations containing polyvinyl chloride, chloroparaffin wax emulsions, brominated flame retardants and antimony oxides with polymeric binders were also suggested in the literature (Weil and Levchik, 2004). Treatments of nylon–cotton blended fabrics with hydroxyfunctional oligomers have also been reported. Durability of the treatments (up to ten laundry cycles) was ensured by the use of melamine- and urea-based cross-linkers. The treatments improved the char formation and reduced the decomposition temperature and heat release rates of the fabrics (Yang *et al.*, 2009). Treatments with urea formaldehyde resin and brominated compounds lead to very high LOI values, but the treated fabrics could not pass vertical flame tests due to enhanced dripping effect. Non-durable anti-dripping flame retardant treatments of nylon 6,6 fabrics have been obtained by the use of intumescent formulations containing pentaerythritol and melamine (Li *et al.*, 2009). Hydroxymethylation of nylon 6 fabrics with formaldehyde and subsequent treatments with N-methylol-3-(dimethoxy)phosphonopropionamide resulted in increased LOI values (Kang De *et al.*, 1992).

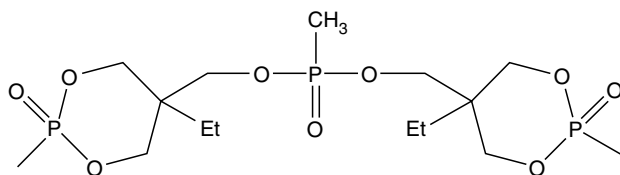
Polyester fabrics owing to unavailability of reactive functional groups are difficult to make flame retardant by conventional finishing treatments. The most common method for making flame retardant polyester is by applying either phosphorus or halogen-based flame retardants by the thermosol method (Weil and Levchik, 2008). The fabrics are generally treated with aqueous solutions of flame retardants (2–15%), dried at around 100°C and cured at 185–195°C (knitted fabrics) or 190–205°C (woven fabrics)

for 120–160 s. Durable flame retardant treatments can be obtained by this method. The flame retardants are believed to diffuse into the soft polymer during the curing operation. Once the fabrics are cooled, the flame retardant gets trapped and excess flame retardant on the surface is washed off. A common phosphorus flame retardant composition for polyester fabric is a mixture of cyclic phosphonate compounds (Fig. 5.5) and is sold as Kappaflam P 31 by Kapp-Chemie GmbH, Germany. Diphosphonate products are also available from Thor (Afflamit) or Zschimmer & Schwarz (Flammex). They are slightly acidic in nature, therefore an application solution needs buffering of the pH to 6.5. Usually a final fixation of 1.5% of the compound is quite sufficient to achieve satisfactory flame retardancy. Halogen-containing novel organophosphorus compound such as dichlorotribromophenyl phosphate (DCTBPP) has been synthesized and applied to polyester fabrics by thermosol method to obtain self-extinguishing fabrics with durability up to 50 laundry cycles (Yoo-Hun *et al.*, 2001). A novel anti-dripping flame retardant, poly(2-hydroxypropylene spirocyclic pentaerythritol bisphosphonate) (PPPBP) was synthesized and applied by the thermosol method to impart flame retardancy and dripping resistance to PET fabrics (Chen *et al.*, 2005). Polyester fabric has also been treated with inorganic salts like sodium polymetaphosphate (Mostashari, 2007) and ammonium chloride to achieve non-durable treatments which could pass vertical flammability tests (Mostashari and Mostashari, 2008).

Polyacrylonitrile fabrics unlike modacrylics are rarely used for manufacturing fabrics which might be of use in areas that require flame protection. Nevertheless, one can find several research articles related to flame proofing



Phosphonic acid, P-methyl-, (5-ethyl-2-methyl-2-oxido-1,3,2-dioxaphosphorinan-5-yl) methyl ester



Phosphonic acid, P-methyl-, bis[(5-ethyl-2-methyl-2-oxido-1,3,2-dioxaphosphorinan-5-yl)] methyl ester

5.5 Cyclic phosphonate compounds for thermosol application.

of polyacrylonitrile fabrics with various phosphorus- and halogen-containing compounds. Several compounds such as decabromodiphenyl oxide and ammonium bromide, urea and phytic acid, hydrazine hydrate, hydroxylamine sulfate, and metal salts have been used as flame retardants (Bajaj *et al.*, 2000). More recent investigations have shown that polyacrylonitrile fabrics can be made flame retardant by grafting of acrylic-based organophosphorus compounds using environmentally friendly plasma technologies. In this research argon plasma-induced graft polymerization of four acrylate monomers containing phosphorus, diethyl(acryloyloxyethyl)phosphate (DEAEP), diethyl-2-(methacryloyloxyethyl)phosphate (DEMEP), diethyl(acryloyloxymethyl)phosphonate (DEAMP) and dimethyl(acryloyloxymethyl)phosphonate (DMAMP) was performed. The treatments resulted in moderate flame retardant properties for the fabrics with limited durability to several laundry cycles (Tsafack and Levalois-Grützmacher, 2006).

Application on natural fiber fabrics

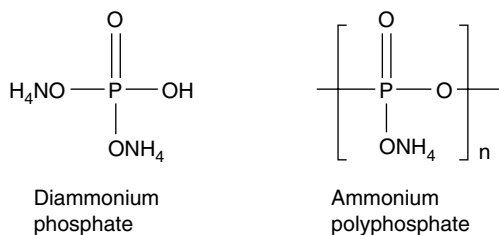
Attempts to impart flame retardant properties to cellulose- and protein-based natural fibers have been made since the early nineteenth century. Since then considerable efforts have been made to develop newer flame retardant solutions for these natural fibers. Production of flame retardant cellulose-based textiles has been the most challenging task. Cellulose is a natural polymer and exists in different fibrous forms such as cotton, jute and linen. The only way to produce fire-resistant cellulosic textiles from these fibers is via a chemical finishing treatment. The intrinsic properties of textiles like the tensile strength, tactile properties, air permeability and dyeability should not be affected by the treatment. Moreover, the flame retardant should meet health requirements and not produce toxic gases when burned. It is also important that the flame retardant treatment should last at least 50 industrial washing cycles. These requirements make the development of flame retardants for cellulosic fibers very challenging. Textiles made from natural fibers like cotton and silk are highly flammable whereas wool-based textiles are self-extinguishing in nature. The LOI values of untreated cotton, silk and wool are 18.4, 22.8 and 25, respectively (Horrocks, 2001).

Finishing treatments for *cellulose-based textiles* can be grouped into the following:

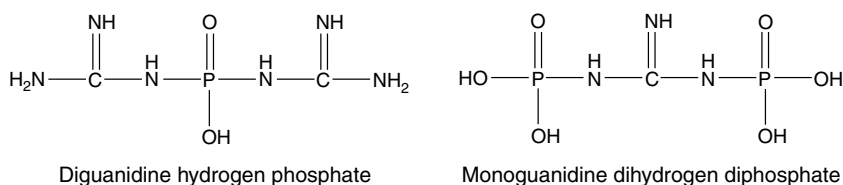
(a) Finishes with inorganic phosphates

Examples of inorganic salts that are used as flame retardants for cellulose are ammonium phosphates, polyphosphates (Fig. 5.6), bromides and borate-boric acid mixtures.

Typically, 1–2% of the phosphorus content relative to the weight of the fabric is enough to obtain flame retardant cotton. Ammonium bromide can also be used in combination with ammonium phosphates to provide



5.6 Ammonium salts of phosphoric and polyphosphoric acid.

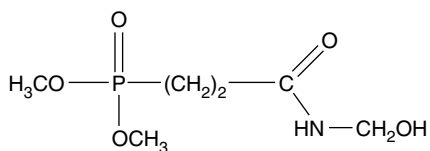


5.7 Guanidine phosphate salts.

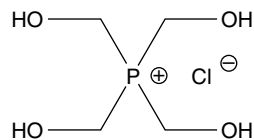
some vapor-phase flame retardant action, particularly helpful for blends (Chellapa and Shah, 1989; Davies *et al.*, 2002). Ammonium sulfamate or sulfate is also included in some ammonium phosphate formulations (Weil and Levchik, 2009). The use of APP is reviewed in the literature (Davies *et al.*, 2005; Horrocks, 2003). Attempts have also been made to achieve durable coatings on cellulose by using these organic salts (Hawkes *et al.*, 2009; Webb *et al.*, 2007). Monoguanidine dihydrogen phosphates (Fig. 5.7) and diguanidine hydrogen phosphate are further examples of phosphates used for non-durable cotton treatment (Vroman *et al.*, 2004). Some flame retardants like Flovan[®] CGN (Ciba), Flammentin[®] FMB (Thor Specialities) and Pyrovatim[®] PBS (Weil and Levchik, 2009) have been used to produce semi-durable coatings. Treatments with these flame retardant agents will survive water soaking or leaching to various degrees, but have poor stability to laundering. Semi-durable finishes with these inorganic phosphates are not durable to alkaline laundering conditions. When phosphoric acid groups are chemically attached and neutralized by ammonium cations, the finish can become fairly durable to water washing.

(b) *Finishes with organophosphorus compounds*

The two most successful products with more than 60 years' history for flame retardation of cellulose are Pyrovatex[®] CP (Ciba) and Proban[®] CC (Rhodia). The basic molecule in Pyrovatex formulation is 3-(dimethylphosphono)-N-methylolpropionamide (DMPMP) (Fig. 5.8), and in Proban – tetraakis (hydroxymethyl) phosphonium chloride (THPC) (Fig. 5.8). Durable



3-(Dimethylphosphono)-N-methylolpropionamide



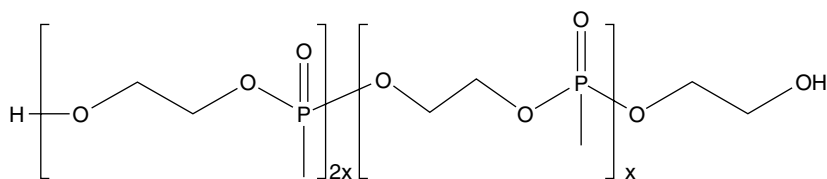
Tetrakis (hydroxymethyl) phosphonium chloride

5.8 Organophosphorus flame retardants for durable treatment on cellulose.

treatments of DMPMP on cellulose-based fabrics are generally obtained by the use of a formaldehyde-based cross-linker such as melamine formaldehyde. Presence of formaldehyde in DMPMP and the cross-linker creates environmental problems during the application process due to the release of formaldehyde fumes. Formaldehyde may also be released during the subsequent use of the treated fabric. Fixation of THPC on cellulosic textiles requires the use of patented ammonia curing process which limits its widespread usage. These compounds are presently the best solutions for flame retardant finishing of cellulose-based textiles.

Recent studies on the flame retardant action of DMPMP have shown that it has superior action to some phosphates and phosphoramidate compounds. The superior action of DMPMP has been attributed to the formation of acidic intermediates during the thermal decomposition process, which could further catalyze the char formation of cellulose (Gaan and Sun, 2007a). DMPMP treated cotton has higher activation energy of decomposition, higher char content, lower heat of combustion and forms a protective coating on the char surface (Gaan and Sun, 2007b). Application of THPC as a flame retardant on cellulose-based textiles has been extensively investigated by many researchers. THPC was applied together with urea and melamine on cotton, cotton–polyester blends and viscose to obtain finishes which could withstand 20 laundering cycles (Donaldson *et al.*, 1973, 1975; Guthrie *et al.*, 1955; Hamalainen *et al.*, 1956; Reeves and Guthrie, 1953, 1954; Reeves *et al.*, 1957).

Recently the use of oligomeric hydroxyl functional organophosphorus compound has been investigated in durable flame retardant finishing of cellulose (Fig. 5.9). HFPO has been used to make flame retardant cotton and cotton/nylon blends (Yang and Wu, 2006). In this study HFPO was shown to significantly lower the thermal decomposition temperature of cotton and increases the amount of char formed during the burning process. HFPO was used in combination with various cross-linkers such as trimethylolmelamine and dimethyloldihydroxyethyleneurea. The cotton fabric treated with this system maintained satisfactory flame retarding performance (LOI more than 29%) after 40 home laundering cycles (Stowell and Yang, 2003; Yang



Hydroxy functional organophosphorus oligomer (HFPO)

5.9 Hydroxy functional oligomeric organophosphorus compound.

and Wu, 2004). Numerous studies have been performed in order to improve the durability of the chemical finishing to washing. Eco-friendly cross-linkers such as multifunctional carboxylic acids (phosphorus-containing maleic acid, polycarboxylic acids) have also been used as finishing agents for cotton since the late 1980s (Blanchard and Graves, 2002, 2005; Welch, 2001; Wu and Yang, 2008).

Developments in organophosphorus flame retardants for cellulose have focused on novel phosphoramidate compounds (Gaan *et al.*, 2009b). Phosphoramidates have been shown to have superior flame retardant action to the analogous phosphates (Gaan *et al.*, 2009a). Phosphoramidates with hydroxyl terminating alkyl groups (Gaan *et al.*, 2009a; Rupper *et al.*, 2010) and methyl ester phosphoramidates have been shown to have superior flame retardant action (Gaan, 2008).

(c) Flame retardancy with sulfur derivatives

The sulfur derivatives are used mainly for treating cellulose with ammonium, aluminium or other metallic sulfates and produce limited non-durable flame retardant coatings. Sulfation treatments with urea sulfamates yielded fabrics that withstood 50 hard and soft water launderings. However, the treatments suffered from drawbacks like reduced tensile strengths and after-glow effect (Lewin, 2005).

(d) Grafting flame retardant monomers to cellulose

Some attempts have been made to develop flame retardant cellulose by chemical graft polymerization techniques. Methacryloyloxyethyl orthophosphorotetra ethyl diamidate was used as flame retardant for graft polymerization on cellulose. Durability to about 50 washing cycles has been achieved by varying the parameters of graft polymerization (Abdel-Mohdy, 2003). Other researchers have used radiation graft polymerization technique to flame retard cotton fabrics. Orthophosphoric acid was used as a flame retardant, where the treatments had limited durability (Reddy *et al.*, 2005). 4-Vinyl pyridine has been used as flame retardant with benzophenone as photoinitiator for grafting onto cellulose fabrics using UV radiation

technique. The thermogravimetric analysis (TGA) of the grafted fabrics showed lower decomposition temperatures with slight increase in char yield (Kaur *et al.*, 2007a). Methacrylamide has also been grafted onto cotton with the use of low energy UV irradiation technique to introduce functionalities that can react with phosphorus-containing compounds to impart flame retardancy. Subsequent phosphorylation of grafted fabric showed improved flame retardant behavior in comparison to grafted fabric (Kaur *et al.*, 2007b). More recently plasma technology has been used as an environmentally benign technique to produce flame-resistant textiles. Grafting and polymerization of fire-retardant monomers on the cotton fabrics have been carried out using microwave argon plasma to produce durable flame retardant coatings (Tsafack and Levalois-Grützmacher, 2006, 2007). It is postulated that the flame retardant properties of treated cotton depend primarily on the structure of the FR monomer and not on the phosphorus content of the fabrics. The durability of the coatings obtained has been attributed to the covalent bond formed between flame retardant molecule and cellulose during plasma-induced polymerization. Sodium silicate has been applied onto cellulose textiles using radio frequency low pressure non-equilibrium oxygen plasma to produce phosphorus-free fire-resistant fabrics. It was observed that samples treated in plasma withstood 50 laundering cycles due to the cross-linked structure of the coatings (Totolin *et al.*, 2009).

Wool textiles have the highest inherent non-flammability and pass the required flame-retardancy tests untreated, because of its highly cross-linked chemical structure, high amino- and amido-nitrogen content (16%) and moisture content (10–14%). Hexafluorozirconate (Zirpro® treatment) has been the basis for the widely used and commercial flame retardant system for wool textiles, which was developed by Benisek in the early 1970s. The Zirpro® treatments act in the solid phase by producing char around the fibers. A detailed review of flame retardant treatments for wool is discussed elsewhere (Horrocks, 1986). In 2005 a new flame retardant for wool was introduced (Noflan®). It is based on amidoalkylphosphonic acid and contains about 14% phosphorus. It is claimed, that Noflan® enhances char formation in the solid phase, thus minimizing smoke and toxic gas emissions (Benisek and Andrews, 2004, 2005). In addition, Noflan® is an environmentally benign flame retardant, and can be applied by continuous pad-dry technique.

Silk is widely used in apparel and home furnishing for its luxurious appearance, soft handle, high wearing comfort and other desirable aesthetic appearances (Currie, 2001; Robson, 1998). Treatment of silk with a mixture of phosphoric acid resulted in high level flame retardancy (LOI more than 28%) with limited wash durability (Achwal *et al.*, 1987). Pyrovatex CP has also been used to render silk flame retardant. Treated silk is claimed to have LOI values greater than 30%. The flame retardant properties were retained

to some extent even after 50 washing cycles (Guan and Chen, 2006). Graft copolymerization of a vinyl phosphorus-based monomer such as DEMEP has also been carried out on silk fabrics. Treated silk fabrics were found to be stable to 30 hand washing cycles (Guan and Chen, 2008). Hydroxyfunctional organophosphorus polymer in combination with 1,2,3,4-butanetetracarboxylic acid has been used as a formaldehyde-free flame retardant finishing system for silk. Treated fabrics were claimed to be stable to 15 washing cycles (Guan *et al.*, 2009). Metal oxides and salts such as antimony oxide, lead monoxide, manganese dioxide and ammonium chloride have also been used in flame retardant treatments on silk fabrics. Antimony oxide has been shown to have better flame retardant effect than lead monoxide (Tarafer and Singh, 2007).

5.5 Environmental issues related to flame retardants

During the last few decades the knowledge about toxicity and environmental impact of chemicals has rapidly grown and people have become more aware of potential dangers associated with them. A large number of flame retardant compounds are on special lists of national or international environmental committees because of their harmful properties. Many of these substances are either banned or their use has been restricted. Currently tetrabromobisphenol A (TBBPA), decabromodiphenyl ether (DecaBDE) and HBCD are the most widely used brominated flame retardants worldwide. DecaBDE is mainly used as flame retardant for plastic casing of electrical and electronic equipments, for furniture and textiles. TBBPA is mainly used in manufacturing circuit boards and plastics. HBCD is mainly used in expanded and extruded polystyrene insulations, textiles and to a lesser extent for plastic casings of electrical and electronic equipments (Ittershagen, 2008).

Scientific and political discussions have focused on these products because of their growing worldwide presence in sediments, dust in buildings, micro-organisms, fish and animals such as polar bears, seals, raptors and their eggs and even in human blood, tissues and breast milk (D'Silva *et al.*, 2004; Hardy *et al.*, 2009; Kang *et al.*, 2009; La Guardia *et al.*, 2007; Lilienthal *et al.*, 2009; Schecter *et al.*, 2009; Smolarz and Berger, 2009; Stapleton *et al.*, 2009; Uddin, 2003).

Environmental risks associated with pentabromodiphenyl ether (PentaBDE), octabromodiphenyl ether (OctaBDE) and DecaBDE, have been assessed in the recent past and resulted in an EU Directive (Official Journal of the European Union, 2003). This Directive prohibits the application and use of PentaBDE and OctaBDE. More recently (2008) the use of DecaBDE in electrical and electronic devices has been banned in Europe. In Norway and Sweden there are national prohibitions for the use of DecaBDE. The US EPA has recently (2009) reached an agreement

with three manufacturers of DecaBDE to voluntarily phase out its production and use in all consumer products by the end of 2013. Studies have shown that DecaBDE persists in the environment, potentially causes cancer and may impact brain functions. DecaBDE can also degrade to form more toxic by-products which are frequently found in the environment (Environmental Protection Agency, 2009). According to the new European REACH-Regulation, all persistent, bio-accumulating and toxic compounds will be assessed and their substitution by less hazardous chemicals encouraged. The basic goal of REACH (Registration, Evaluation, Authorization and Restriction of Chemicals) is the protection of human health and the environment from the risks posed by chemicals (Kemmlein *et al.*, 2009). The following halogenated flame retardants for fireproofing garments are restricted (European Commission, 2008):

- tris(2,3-dibromo-1-propyl)-phosphate
- tris-(aziridiny)-phosphin oxide
- polybrominated biphenyls.

The use of antimony trioxide as synergist together with halogenated-based flame retardants (e.g. in textile back coatings, flame retarded paints, rubber, textiles) is also under review within the European Union Commission. The International Antimony Association opposes the ban of antimony oxides under the European Union's Restriction of Hazardous Substances (RoHS) regulation as there is no conclusive evidence regarding the toxicity or environmental impact of antimony oxides (International Antimony Association, 2009).

Local legislations in some countries may not be able to induce a broad sustainable protection of mankind and the environment as many chemicals remain unchanged in nature for a long period of time and may also spread over large regions of the planet. The Stockholm Convention with more than 160 member states will decide on the possible ban of POPs (persistent organic pollutants) which have shown toxicity and environmental risks (Secretariat of the Stockholm Convention, 2009). Thus stronger cooperation between countries and international organizations is required to tackle the problems associated with the use of harmful chemicals.

5.6 Test standards for flame retardant textiles

There are several kinds of standard test methods to determine the fire risks of textile materials. The use of any particular standard test method is based on the end use of the textile material and the country where the material is to be used. The test method generally outlines various specifications such as the type and size of a sample, source of the flame/heat, and duration of the application of the flame/heat to the substrate. Table 5.2 outlines several important test methods for various kinds of textiles.

Table 5.2 List of standard test methods for flame retardant textiles

Textile type	Standard test methods	Comments
Furnishing fabrics	BS 5852: Pts 1 and 2: 2006	Cigarette and simulated match flame (20 s ignition)
	BS 5852: 1990(1998)	Small flames and wooden cribs applied to small and full scale tests
	ISO 8191: Pts 1 and 2 (same as BS 5852: 1990)	
	BS EN 1021-1: 2006	Cigarette
	BS EN 1021-2: 2006	Simulated match flame (15 s ignition)
	BS 6807: 2006	Ignitability of mattresses or divans
Nightwear	BS 5867: Part 2: 1980 (1990)	Small flame test for curtains and drapes
	BS 5722: 1991 AS1249	Small flame Australian Standard for children's nightwear
Bedding	BS 7175: 1989 (1994)	Ignitability of bed covers and pillows
	BS ISO 12952-1/4: 1999 BS ISO 12952-2/3: 2001	Ignitability of bedding items by cigarette and small flame sources
	France Decree 2000-164	French Standard for bedding (cigarette resistance)
Protective clothing	EN 533, NF P92 503 (M1), BS 7175 Crib 5	
Carpet	DIN 4102(B1), FAR25-853	
Non-woven	NF P92 503	
Textiles in aircrafts	ASTM E 906 1983, uses Ohio State University heat release calorimeter	Irradiate under 35 kW/m ² with small flame igniter
	NF P 92501: 1995 French 'M test'	Irradiate with small burner

5.7 References

- ABDEL-MOHDY, F. A. (2003) Graft copolymerization of nitrogen- and phosphorus-containing monomers onto cellulose for flame- retardant finishing of cotton textiles. *Journal of Applied Polymer Science*, 89: 2573-2578.
- ACHWAL, W. B., MAHAPATRAO C. R., *et al.* (1987) Flame retardant finishing of cotton and silk fabric. *Colourage*, 6: 16-30.

- ADANUR, S. and TEWARI, A. (1997) An overview of military textiles. *Indian Journal of Fibre & Textile Research*, 22: 348–352.
- BAJAJ, P., AGRAWAL, A. K., *et al.* (2000) Flame retardation of acrylic fibers: an overview. *Polymer Reviews*, 40: 309–337.
- BARKER, R. L. and BREWSTER, E. P. (1982) Evaluating the flammability and thermal shrinkage of some protective fabrics. *Journal of Industrial Fabrics*, 1: 7–17.
- BEERS, D. E. and RAMIREZ, J. E. (1990) Vectran high-performance fiber. *Journal of the Textile Institute*, 81: 561–574.
- BENISEK, L. and ANDREWS, J. (2004) Noflan – a new flame retardant for wool. *DWI Reports*, 128: 1–5.
- BENISEK, L. and ANDREWS, J. (2005) New flame retardant for wool. *Melliand International*, 11: 337–339.
- BLANCHARD, E. J. and GRAVES, E. E. (2002) Polycarboxylic acids for flame resistant cotton/polyester carpeting. *Textile Research Journal*, 71: 39–43.
- BLANCHARD, E. J. and GRAVES, E. E. (2005) Improving flame resistance of cotton/polyester fleece with phosphorous based polycarboxylic acids. *AATCC Review*, 5: 26–30.
- BRAUMAN, S. K. (1977) Phosphorus fire retardance in polymers: 1. General mode of action. *Journal of Fire Retardant Chemistry*, 4: 18–37.
- BUTYLKINA, N. G., IVANOVA, A. A., *et al.* (1989) Polycaproamide fibres with reduced combustibility. *Fiber Chemistry*, 20: 14–15.
- CAMINO, G., COSTA, L., *et al.* (1991) Overview of fire retardant mechanisms. *Polymer Degradation and Stability*, 33: 131–154.
- CAMINO, G. and LOMAKIN, S. (2006) Intumescent materials. In: Horrocks, A. and Price, D. (eds.) *Fire Retardant Materials*. Cambridge: Woodhead Publishing, pp. 128–130.
- CHELLAPA, K. L. and SHAH, M. C. (1989) Ammonium bromide as a fireproofing agent for cellulosic materials, US 4888136.
- CHEN, D.-Q., WANG, Y.-Z., *et al.* (2005) Flame-retardant and anti-dripping effects of a novel char-forming flame retardant for the treatment of poly(ethylene terephthalate) fabrics. *Polymer Degradation and Stability*, 88: 349–356.
- CHEVRON PHILLIPS CHEMICAL COMPANY LLC (2008) Rayton PPS Fiber, Woodlands, TX. Available at: http://www.cpchem.com/enu/ryton_pps_p_what_is_pps.asp [accessed 29 January 2010].
- CLIVE, S. S. and ED, M. (2000) A study of fire-retardant mechanisms in the gas phase by FTIR spectroscopy. *Polymer International*, 49: 1169–1176.
- CLUTTER, R. J. (1975) Flame-retardant polyester, US3865783.
- CURRIE, R. (2001) *Silk, Mohair, Cashmere and Other Luxury Fibres*, ed. Franck, R. R. Cambridge: Woodhead Publishing.
- D'SILVA, K., FERNANDES, A., *et al.* (2004) Brominated organic micropollutants – igniting the flame retardant issue. *Critical Reviews in Environmental Science and Technology*, 34: 141–207.
- DAVIES, P. J., HORROCKS, A. R., *et al.* (2002) Possible phosphorus/halogen synergism in flame retardant textile backcoatings. *Fire and Materials*, 26: 235–242.
- DAVIES, P. J., HORROCKS, A. R., *et al.* (2005) The sensitisation of thermal decomposition of ammonium polyphosphate by selected metal ions and their potential for improved cotton fabric flame retardancy. *Polymer Degradation and Stability*, 88: 114–122.

- DONALDSON, D. J., NORMAND, F. L., *et al.* (1973) Flame-retardant organic fibrous materials, US 365896.
- DONALDSON, D. J., NORMAND, F. L., *et al.* (1975) Flame-retardant blend materials, US 618188.
- DRIS, I., LAK, A. M., *et al.* (2008) Filtered polyetherimide polymer for use as a high heat fiber material and fiber manufacture, US2008006970.
- DURAN, K., BAHTIYARI, I., *et al.* (2007) Protective nonwoven technical textiles. *Tekstil Ve Konfeksiyon*, 17: 174–177.
- ENVIRONMENTAL PROTECTION AGENCY (2009) DecaBDE Phase-Out Initiative, Washington DC, United States Environmental Protection Agency. Available at: <http://www.epa.gov/oppt/existingchemicals/pubs/actionplans/deca-dbe.html> [accessed 8 February 2010].
- EUROPEAN COMMISSION (2008) Textiles Background Product Report, Brussels, European Commission, DG Environment-G2, B-1049. Available at: http://ec.europa.eu/environment/gpp/pdf/toolkit/textiles_GPP_background_report.pdf [accessed 8 February 2010].
- EVONIK INDUSTRIES (2010) P84 Polyetherimide Fibers, Austria. Available at: <http://www.p84.com/products/p84/> [accessed 5 February 2010].
- FLAMBARD, X., BOURBIGOT, S., *et al.* (2005) Progress in safety, flame retardant textiles and flexible fire barriers for seats in transportation. *Polymer Degradation and Stability*, 88: 98–105.
- GAAN, S. (2008) *Novel Phosphoramidate Flame Retardants*. European Coatings Conference, Fire Retardant Coatings III, 18–19 September, Vincentz Network GmbH, Berlin, Germany, pp. 135–146.
- GAAN, S., RUPPER, P., *et al.* (2009a) Thermal decomposition and burning behavior of cellulose treated with ethyl ester phosphoramidates: effect of alkyl substituent on nitrogen atom. *Polymer Degradation and Stability*, 94: 1125–1134.
- GAAN, S., SALIMOVA, S., *et al.* (2009b) Phosphoramidate flame retardants, WO2009153034.
- GAAN, S. and SUN, G. (2007a) Effect of phosphorus and nitrogen on flame retardant cellulose: a study of phosphorus compounds. *Journal of Analytical and Applied Pyrolysis*, 78: 371–377.
- GAAN, S. and SUN, G. (2007b) Effect of phosphorus flame retardants on thermo-oxidative decomposition of cotton. *Polymer Degradation and Stability*, 92: 968–974.
- GAAN, S., SUN, G., *et al.* (2008) Effect of nitrogen additives on flame retardant action of tributyl phosphate: phosphorus-nitrogen synergism. *Polymer Degradation and Stability*, 93: 99–108.
- GEORLETTE, P., SIMONS, J., *et al.* (2000) Halogen-containing fire-retardant compounds. In: Grand, A. F. and Wilkie, C. A. (eds.) *Fire Retardancy of Polymeric Materials*. New York: Marcel Dekker Inc, pp. 245–284.
- GRANZOW, A. (1978) Flame retardation by phosphorus compounds. *Accounts of Chemical Research*, 11: 177–183.
- GREER, S. C. (2000–2002) The ITA-High Performance Fiber Chart. Available at: <http://www.intexa.com/hitemp.htm> [accessed 19 January 2011].
- GUAN, J. P. and CHEN, G. Q. (2006) Flame retardancy finish with an organophosphorus retardant on silk fabric. *Fire and Materials*, 30: 415–424.
- GUAN, J. P. and CHEN, G. Q. (2008) Flame resistant modification of silk fabric with vinyl phosphate. *Fibers and Polymers*, 9: 438–443.

- GUAN, J. P., YANG, C. Q., *et al.* (2009) Formaldehyde-free flame retardant finishing of silk using a hydroxyl-functional organophosphorus oligomer. *Polymer Degradation and Stability*, 94: 450–455.
- GUTHRIE, J. D., DRAKE, G. L. Jr., *et al.* (1955) Application of the tetrakis(hydroxymethyl) phosphonium chloride flame-retardant process to cotton fabrics. *American Dye-stuff Reporter*, 44: 328–332.
- HAMALAINEN, C., REEVES, W. A., *et al.* (1956) Cotton made flame-resistant with bromine-containing phosphonitrilates in combination with THPC resins. *Textile Research Journal*, 26: 145–149.
- HARDY, M. L., BANASIK, M., *et al.* (2009) Toxicology and human health assessment of decabromodiphenyl ether. *Critical Reviews in Toxicology*, 39: 1–44.
- HAWKES, J. A., WEBB, P., *et al.* (2009) Method of treating materials, especially cotton and wool textiles to improve flame retardancy, WO 2009030947 A1.
- HENDRIX, J. E., DRAKE, G. L., Jr., *et al.* (1972) Effects of fabric weight and construction on oxygen index (OI) values for cotton cellulose. *Journal of Fire & Flammability*, 3: 38–45.
- HISCHLER, M. M. (ed.) (2000) *Chemical Aspects of Thermal Decomposition of Polymeric Materials*. Fire Retardancy of Polymeric Materials, Marcel Dekker Inc.
- HORRIDGE, P. and TIMMONS, M. B. (1979) Blend for children's sleepwear incorporating inherently flame-retardant fiber. *Journal of Consumer Product Flammability*, 6: 218–227.
- HORROCKS, A. R. (1983) An introduction to the burning behavior of cellulosic fibers. *Journal of the Society of Dyers and Colourists*, 99: 191–197.
- HORROCKS, A. R. (1986) Flame retardant finishing of textiles. *Review in Progress Coloration*, 16: 62–101.
- HORROCKS, A. R. (1996) Developments in flame retardants for heat and fire resistant textiles – the role of char formation and intumescence. *Polymer Degradation and Stability*, 54: 143–154.
- HORROCKS, A. R. (2001) Textiles. In: Horrocks, A. R. and Price, D. (eds.) *Fire Retardant Materials*. Cambridge: Woodhead Publishing, pp. 128–81.
- HORROCKS, A. R. (2003) Flame-retardant finishes and finishing. In: Heywood, D. (ed.), *Textile Finishing*. Bradford, UK: Society of Dyers and Colorists, pp. 214–250.
- HORROCKS, A. R., NAZARE, S., *et al.* (2004) The particular flammability hazards of night-wear. *Fire Safety Journal*, 39: 259–276.
- HUANG, N. H., ZHANG, Q., *et al.* (2008) A mechanistic study of flame retardance of novel copolyester phosphorus containing linked pendant groups by TG/XPS/direct Py-MS. *Chinese Chemical Letters*, 19: 350–354.
- INTERNATIONAL ANTIMONY ASSOCIATION (2009) Downstream user exposure scenarios being prepared for REACH, Brussels, International Antimony Association VZW. Available at: <http://www.antimony.be/newsletter/docs/i2a/i2a-newsletter-december-2009.pdf> [accessed 8 February 2010].
- ITTERSHAGEN, M. (2008) Brominated flame retardants: guardian angels with a bad streak? Dessau-Rosslau, Germany, Umweltbundesamt. Available at: <http://umweltbundesamt.de/uba-info-presse-e/hintergrund/flammschutzmittel.pdf> [accessed 10 February 2010].
- KAMATH, M. G., BHAT, G. S., *et al.* (2009) Processing and characterization of flame retardant cotton blend nonwovens for soft furnishings to meet federal flammability standards. *Journal of Industrial Textiles*, 38: 251–262.

- KANG DE, Y., WEIPING, H., *et al.* (1992) Flame-retarding modification of nylon 6 textile. *Journal of Applied Polymer Science*, 46: 467–470.
- KANG, M. J., KIM, J. H., *et al.* (2009) Nephrotoxic potential and toxicokinetics of tetrabromobisphenol A in rat for risk assessment. *Journal of Toxicology and Environmental Health Part A-Current Issues*, 72: 1439–1445.
- KAUR, I., RAJNEESH, S., *et al.* (2007a) Flame-retardant cotton fabric through graft copolymerization. *Defence Science Journal*, 57: 249–258.
- KAUR, I., SHARMA, V., *et al.* (2007b) Development of flame retardant cotton fabrics through grafting and post-grafting reactions. *Indian Journal of Fibre and Textile Research*, 32: 312–318.
- KEMMLEIN, S., HERZKE, D., *et al.* (2009) Brominated flame retardants in the European chemicals policy of REACH – regulation and determination in materials. *Journal of Chromatography A*, 1216: 320–333.
- KURARAY AMERICA INC (2010) Vectran Fiber, USA Vectran Division. Available at: http://www.vectranfiber.com/pdf/9Pages%20from%20Vectran_broc_final61206.pdf [accessed 8 February 2010].
- LA GUARDIA, M. J., HALE, R. C., *et al.* (2007) Evidence of debromination of decabromodiphenyl ether (BDE-209) in biota from a wastewater receiving stream. *Environmental Science & Technology*, 41: 6663–6670.
- LAWTON, E. L. and SETZER, C. J. (1975) Flame-retardant polyethylene terephthalate fibers. In: Pearce, E. (ed.) *Flame-Retardant Polymeric Materials*. New York: Springer, pp. 193–221.
- LEVCHIK, S. V., COSTA, L., *et al.* (1994) Effect of the fire-retardant ammonium polyphosphate on the thermal decomposition of aliphatic polyamides. Part III – polyamides 6.6 and 6.10. *Polymer Degradation and Stability*, 43: 43–54.
- LEVCHIK, S. V., LEVCHIK, G. F., *et al.* (1995) Mechanism of action of phosphorus-based flame retardants in nylon 6. II. Ammonium polyphosphate/talc. *Journal of Fire Sciences*, 13: 43–58.
- LEVCHIK, S. V., LEVCHIK, G. F., *et al.* (2001) Phosphorus-containing fire retardants in aliphatic nylons. In: Nelson, G. L. and Wilkie, C. A. (eds.) *Fire and Polymers: Materials and Solutions for Hazard Prevention*. Washington, DC: American Chemical Society, pp. 214–227.
- LEVCHIK, S. V. and WEIL, E. D. (2004) A review on thermal decomposition and combustion of thermoplastic polyesters. *Polymers for Advanced Technologies*, 15: 691–700.
- LEVCHIK, S. V. and WEIL, E. D. (2005) Flame retardancy of thermoplastic polyesters – a review of the recent literature. *Polymer International*, 54: 11–35.
- LEWIN, M. (2005) Unsolved problems and unanswered questions in flame retardancy of polymers. *Polymer Degradation and Stability*, 88: 13–19.
- LI, L., CHEN, G., *et al.* (2009) The anti-dripping intumescent flame retardant finishing for nylon-6,6 fabric. *Polymer Degradation and Stability*, 94: 996–1000.
- LILIENTHAL H., VAN DER VEN, L. T. M., *et al.* (2009) Effects of the brominated flame retardant hexabromocyclododecane (HBCD) on dopamine-dependent behavior and brainstem auditory evoked potentials in a one-generation reproduction study in Wistar rats. *Toxicology Letters*, 185: 63–72.
- MAKI, S., SEIJI, E., *et al.* (2000) The flame-retardant polyester fiber: improvement of hydrolysis resistance. *Journal of Applied Polymer Science*, 78: 1134–1138.
- MARSDEN, W. H. (1991) Thermal performance of wool and inherently flame-retardant fiber-blend fabrics. *High-Tech Fibrous Materials*, 457: 260–269.

- MINISTRY OF HEALTH (2009) Flammability of textile products in Canada, Ontario, Ministry of Health. Available at: <http://www.hc-sc.gc.ca/cps-spc/pubs/indust/flammability-inflammabilite/index-eng.php> [accessed 29 January 2010].
- MOSTASHARI, S. M. (2007) Synergistic effect of sodium polymetaphosphate-urea on the flame-retardancy imparted to a polyester fabric. *International Journal of Polymeric Materials*, 56: 759–767.
- MOSTASHARI, S. M. and MOSTASHARI, S. Z. (2008) Ammonium chloride as a flame retardant in a polyester fabric and its detection. *International Journal of Polymeric Materials*, 57: 355–361.
- NAIR, G. P. (2000) Flammability in textiles and routes to flame retardant textiles – II. Important factors in fabric flammability studies – decomposition and burning of textile fibers; complex nature of fabric flammability; variety and multiplicity of flammability and burning testing methods and their significance. *Colourage*, 47: 39–40, 42–44.
- OFFICIAL JOURNAL OF THE EUROPEAN UNION (2003) Directive 2003/11/EC of the European Parliament and of the Council, Brussels. Available at: http://eur-lex.europa.eu/LexUriServ/site/en/oj/2003/l_042/l_04220030215en00450046.pdf [accessed 10 February 2010].
- OZCAN, G., DAYIOGLU, H., *et al.* (2003) Effect of gray fabric properties on flame resistance of knitted fabric. *Textile Research Journal*, 73: 883–891.
- PERFORMANCE PRODUCTS INC (2010) PBI Fibers, North Carolina. Available at: <http://www.pbigold.com/en/> [accessed 8 February 2010].
- PREZANT, D. J., KELLY, K. J., *et al.* (1999) Impact of a modern firefighting protective uniform on the incidence and severity of burn injuries in New York City firefighters. *Journal of Occupational and Environmental Medicine*, 41: 469–479.
- RAHAMAN, M. S. A., ISMAIL, A. F., *et al.* (2007) A review of heat treatment on polyacrylonitrile fiber. *Polymer Degradation and Stability*, 92: 1421–1432.
- REBOUILLAT, S. (2001) Aramids. In: Hearle, J. W. S. (ed.) *High Performance Fibers*. Woodhead Textiles Series. Cambridge: Woodhead Publishing, pp. 23–61.
- REDDY, P. R. S., AGATHIAN, G., *et al.* (2005) Ionizing radiation graft polymerized and modified flame retardant cotton fabric. *Radiation Physics and Chemistry*, 72: 511–516.
- REEVES, W. A., DRAKE, G. L. J., *et al.* (1957) Flame retardants for cotton using APO- and APS-THPC resins. *Textile Research Journal*, 27: 260–266.
- REEVES, W. A. and GUTHRIE, J. D. (1953) Flameproofing of cotton with THPC resins. *United States, Records of the Bureau of Agricultural and Industrial Chemistry, Mimeographed Circular*. Ser. AIC-364: 11.
- REEVES, W. A. and GUTHRIE, J. D. (1954) Flameproofing with tetrakis(hydroxymethyl) phosphonium chloride. *Dyer*, 111: 567.
- ROBSON, R. M. (1998) Silk: composition, structure, and properties. In: Lewin, M. and Pearce, E. M. (eds.) *Handbook of Fiber Chemistry*, 2nd edn. New York: Marcel Dekker, pp. 415–464.
- RODIE, J. B. (2008) Armored up with textiles. *Textile World*, March/April, 35.
- ROSS, J. H. and STANTON, R. M. (1973) Relation of fabric flammability to fabric structure. *Applied Polymer Symposia*, 21: 109–119.
- RUPPER, P., GAAN, S., *et al.* (2010) Characterization of chars obtained from cellulose treated with phosphoramidate flame retardants. *Journal of Analytical and Applied Pyrolysis*, 87: 93–98.
- SCHECTER, A., SHAH, N., *et al.* (2009) PBDEs in US and German clothes dryer lint: a potential source of indoor contamination and exposure. *Chemosphere*, 75: 623–628.

- SCHLOSSER, E., HOEROLD, S., *et al.* (2008) Flame-retardant compounded polyester materials, US2009088512.
- SECRETARIAT OF THE STOCKHOLM CONVENTION (2009) Information Request for Chemicals under Review by the POPs Review Committee, Geneva, The Persistent Organic Pollutants Review Committee. Available at: <http://chm.pops.int/Home/tabid/36/mctl/ViewDetails/EventModID/1007/EventID/73/xmid/1855/mret/t/language/en-US/Default.aspx> [accessed 7 February 2010].
- SEUNG-CHEOL, Y. and Jae PIL, K. (2007) Flame retardant polyesters. I. Phosphorous flame retardants. *Journal of Applied Polymer Science*, 106: 2870–2874.
- SEUNG-CHEOL, Y. and Jae PIL, K. (2008) Flame retardant polyesters. III. Fibers. *Journal of Applied Polymer Science*, 108: 2297–2300.
- SMITH, N. W. J. (2007) Flame retardant yard blend, US4865906.
- SMOLARZ, K. and BERGER, A. (2009) Long-term toxicity of hexabromocyclododecane (HBCDD) to the benthic clam *Macoma balthica* (L.) from the Baltic Sea. *Aquatic Toxicology*, 95: 239–247.
- STAPLETON, H. M., KELLY, S. M., *et al.* (2009) Metabolism of polybrominated diphenyl ethers (PBDEs) by human hepatocytes in vitro. *Environmental Health Perspectives*, 117: 197–202.
- STEGMAIER, T., MAVELY, J., *et al.* (2005) High performance and high functional fibres and textiles. In: Shishoo, R. (ed.) *Textiles in Sport*. Cambridge: Woodhead Publishing, pp. 89–119.
- STEPNICZKA, H. and DIPIETRO, J. (1971) Flammability characteristics of cotton and polyester fibers. *Journal of Applied Polymer Science*, 15: 2149–2172.
- STOWELL, J. K. and YANG, C. (2003) A durable low-formaldehyde flame retardant finish for cotton fabrics. *AATCC Review*, 3: 17–20.
- SUBBULAKSHMI, M. S., KASTURIYA, N., *et al.* (2000) Production of flame-retardant nylon 6 and 6.6. *Journal of Macromolecular Science – Reviews in Macromolecular Chemistry and Physics*, 40: 85–104.
- TARAFDER, N. and SINGH, S. S. (2007) Effect of flame retardant finishes on silk and polyester fabrics. *Man-Made Textiles in India*, 50: 69–75.
- TNC GLOBAL INC (2010) Basofil Fibers, TNC Global, Inc., North Carolina. Available at: <http://www.basofil.com/index.html> [accessed 8 February 2010].
- TORAY INDUSTRIES (2006) PPS Fiber, Japan. Available at: <http://www.toray.co.jp/english/plastics/products/pps/index.html> [accessed 12 January 2010].
- TOTOLIN, V., SARMADI, M., *et al.* (2009) Low pressure, nonequilibrium-plasma-assisted generation of flame retardant cotton. *AATCC Review*, 9: 32–37.
- TSAFACK, M. J. and LEVALOIS-GRÜTZMACHER, J. (2006) Plasma-induced graft-polymerization of flame retardant monomers onto PAN fabrics. *Surface and Coatings Technology*, 200: 3503–3510.
- TSAFACK, M. J. and LEVALOIS-GRÜTZMACHER, J. (2007) Towards multifunctional surfaces using the plasma-induced graft-polymerization (PIGP) process: flame and waterproof cotton textiles. *Surface and Coatings Technology*, 201: 5789–5795.
- UDDIN, F. (2003) Bedenken bei bromhaltigen Flammhemmern. Concerns of brominated flame retardant. *Industrial Fabrics Bulletin*, Band 13: 55–56.
- VROMAN, I., LECOUEUR, E., *et al.* (2004) Guanidine hydrogen phosphate-based flame-retardant formulations for cotton. *Journal of Industrial Textiles*, 34: 27–38.
- WEBB, P., LEWIS, D. M., *et al.* (2007) A wash durable flame-retardant composition and method, WO 2007099343 A1.

- WEIL, E. D. and LEVCHIK, S. (2004) Current practice and recent commercial developments in flame retardancy of polyamides. *Journal of Fire Sciences*, 22: 251–264.
- WEIL, E. D. and LEVCHIK, S. V. (2008) Flame retardants in commercial use or development for textiles. *Journal of Fire Sciences*, 26: 243–281.
- WEIL, E. D. and LEVCHIK, S. V. (2009) *Flame Retardants for Plastics and Textiles: Practical Applications*. Cincinnati: Hanser Publications, pp. 241–250.
- WEINROTTER, K. (1988) *The New Polyimide Fiber P84/Properties and Applications*. TAPPI Nonwovens Conference, St Petersburg, FL.
- WELCH, C. M. (2001) Formaldehyde-free durable press finishing. In: Pastore, C. M. and Kiekens, P. (eds.) *Surface Characteristics of Fibers and Textiles*. New York: Marcel Dekker, pp. 1–32.
- WOLF, R. (1981) Flame retardant viscose rayon containing a pyrophosphate. *Industrial & Engineering Chemistry Product Research and Development*, 20: 413–420.
- WU, X. and YANG, C. (2008) Flame retardant finishing of cotton fleece fabric. Part III. The combination of maleic acid and sodium hypophosphite. *Journal of Fire Sciences*, 26: 351–368.
- XIN-KE, J., XIN-GUO, G., *et al.* (2009) A novel phosphorus-containing copolyester with low melting temperature and high flame retardancy. *Polymer International*, 58: 1202–1208.
- YANG, C. and WU, W. (2004). Applications of a hydroxyl-functional organophosphorus oligomer as a durable flame retarding finishing agent for cotton and cotton/polyamide blends. Recent Advances in Flame Retardancy of Polymeric Materials Conference, Business Communications Co.
- YANG, C. and WU, W. (2006) Comparative of reactive organophosphorus flame retardant finishes for cotton. Annual Conference and Exhibition of AATCC, Atlanta, GA.
- YANG, C. Q., HE, Q., *et al.* (2009) Investigation of the flammability of different textile fabrics using micro-scale combustion calorimetry. *Polymer Degradation and Stability*, 95: 108–115.
- YANG, H., YANG, C. Q., *et al.* (2009) The bonding of a hydroxy-functional organophosphorus oligomer to nylon fabric using the formaldehyde derivatives of urea and melamine as the bonding agents. *Polymer Degradation and Stability*, 94: 1023–1031.
- YANG, H. H. (1993) *Kevlar Aramid Fiber*. Chichester: John Wiley.
- YANG, S. C. and KIM, J. P. (2007) Flame-retardant polyesters. II. Polyester polymers. *Journal of Applied Polymer Science*, 106: 1274–1280.
- YAO, Q., LEVCHIK, S. V., *et al.* (2006) Phosphorus-containing flame retardant for thermoplastic polymers, WO2006009983.
- YOO-HUN, K., JINHO, J., *et al.* (2001) Durable flame-retardant treatment of polyethylene terephthalate (PET) and PET/cotton blend using dichlorotribromophenyl phosphate as new flame retardant for polyester. *Journal of Applied Polymer Science*, 81: 793–799.
- ZHANG, S. and HORROCKS, A. R. (2003) A review of flame retardant polypropylene fibres. *Progress in Polymer Science*, 28: 1517–1538.
- ZOLTEK CORPORATION (2010) PYRON, USA. Available at: <http://www.zoltek.com/products/pyron.php> [accessed 8 February 2010].
- ZYLON-DEPARTMENT (2010) PBO Fiber Zylon, Toyobo Company Ltd, Osaka. Available at: http://www.toyobo.co.jp/e/seihin/kc/pbo/menu/fra_menu_en.htm [accessed 8 February 2010]. Available at: <http://www.toyobo.co.jp/e/seihin/kc/pbo/technical.pdf>.

J. HU and Q. MENG,
Hong Kong Polytechnic University, Hong Kong

Abstract: This chapter introduces different mechanisms of shape memory materials (SMMs), strategies for applying SMMs to textiles and the applications of the resultant shape memory textiles. New functions of textiles created by integrating them with SMMs are also presented. The chapter mainly focuses on shape memory alloys (SMAs) and shape memory polymers (SMPs), which have been widely used in textiles. In addition to the present achievements of the SMM application research, the future of SMMs in textile applications is also discussed.

Key words: shape memory polymer, shape memory alloy, smart textiles.

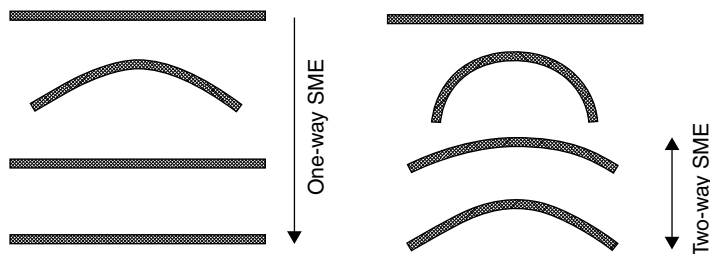
6.1 Introduction

Shape memory materials (SMMs) can rapidly change their shapes (configuration or dimensions) under appropriate stimuli such as heat (Hu, 2007b), moisture/water (Yang *et al.*, 2006), pH value (Feil *et al.*, 1992), electricity (Asaka and Oguro, 2000), light (Jiang *et al.*, 2006), magnetic field (Makhosaxana *et al.*, 2000) and solvent (Siegal and Firestone, 1988). Smart and functional textiles have developed very quickly in recent decades. Textiles with new functions such as luminescent textiles (Kongolo, 2008), electronic display (Lee and Starner, 2008), heat sensing textiles (Zhu *et al.*, 2009), self-cleaning textiles (Qi *et al.*, 2007) and shape recovery textiles (Hu *et al.*, 2007b) have been invented in the past decade. The ability of SMMs to sense and respond to environmental signals such as temperature, humidity and pH value inspires people to create smart textiles with self-regulating structures and performance.

SMMs include shape memory alloys (SMAs), shape memory polymers (SMPs) and shape memory ceramics. Shape memory ceramics have not been used in textiles because they are very brittle and difficult to process. This chapter will introduce the mechanisms of the shape memory effect (SME) of versatile SMAs and SMPs, the strategies for applying them to textiles, and the functions of SMMs in textiles. Existing problems with the application of SMMs to textiles are discussed and future applications of SMMs in textiles are presented.

6.2 Shape memory mechanisms of SMAs

The shape recovery of SMAs arises from the crystal lattice change of a specific martensite variant to its parent single crystal phase. Nickel-titanium (NiTi), copper-aluminum-nickel alloys and copper-zinc-aluminum-nickel are the three main types of SMAs. During the shape deformation and recovery cycles, SMAs show two phases; the austenite phase (A) with a body centered cubic structure at high temperature, and the martensite phase (M) with a tetragonal, orthorhombic or monoclinic crystal lattice structure at low temperature. NiTi alloys change from austenite to martensite upon cooling and change from martensite to austenite upon heating. The phase transformation from austenite to martensite upon cooling is not caused by the diffusion of atoms, but by shear lattice distortion. Upon cooling, the austenite transforms to martensite, resulting in the formation of several martensitic variants, up to 24 for NiTi. This arrangement of martensite variants does not show any macroscopic shape change to the materials. At a temperature below the martensite transformation finish temperature, however, deformation stress can cause the transformation of other variants of the martensite phase into a specific variant accompanied by macroscopic shape changes. The deformation strain is usually below 10% – any higher and it will cause a slippage of the lattice, which is unrecoverable. If the alloy is increased to a temperature above the starting temperature of the austenite phase, the specific martensite variant transforms into the lattice of the original austenite phase, which leads to the one-way shape recovery of the SMA. Figure 6.1(a) shows the shape deformation and recovery process of a one-way SME. In order to obtain a temporary shape in the one-way SME an external force has to be employed. Figure 6.1(b) shows the two-way SME of SMAs. The two-way SME can be imparted to SMAs by training so that SMAs can remember two different shapes at a low temperature and at a high temperature respectively. The two-way SME is caused by the residual stress in the SMAs after specific training processes using specific heat treatment, and



6.1 (a) One-way SME; (b) two-way SME.

complicated thermomechanical cycles. Two-way SMAs have a much lower recoverable strain and the recovery stress is very low in comparison with that of one-way SME.

Another important property of SMAs, which has been widely applied, is pseudoelasticity. The pseudoelasticity mechanism of SMAs works as follows: At a temperature slightly above the martensite transformation starting temperature, outer mechanical stress can cause the phase transformation of SMAs from the austenite to the martensite phase. The martensite variant (stress induced martensite) grows in the direction most favorable for the applied stress, which causes the shape deformation of the SMA. At a temperature above the austenite phase, if the external stress is released, the material recovers its original shape because of the transformation of SMAs from the specific martensite phase to the austenite phase.

6.3 Applications of SMAs in textiles

SMAs have been used in a number of applications from industrial applications such as aircraft, piping and robotics, to medical applications such as optometry, orthopedic surgery and dentistry and from everyday items such as glasses frames and coffee-pot thermostats to high-performance devices such as satellite antennas and vascular stents.

6.3.1 Applications of SMA pseudoelasticity in textiles

SMAs, after an apparent plastic deformation, can return to their original shape, which is ascribed to the pseudoelasticity of SMAs. The recoverable strain in a certain temperature range can be up to 10%. Composite materials reinforced with SMA fibers having superior ductility and energy absorption capacity, also known as damping properties, due to the pseudoelasticity of SMAs (Soroushian, 1997) SMA reinforced fabrics with a good damping effect (energy absorption) can be used in armor textiles (Boussu and Petitniot, 2002). By incorporating SMAs into polyparaphenylene terephthalamide and high tenacity polyethylene fabrics, the high-velocity impact resistance was substantially improved.

The pseudoelasticity of SMAs can also be used for the underwire of brassieres to improve comfort (Wu and Schetky, 2000). Shape memory underwire is more comfortable because of the lower elastic modulus of SMAs compared to those made of other steel wires. Furthermore, it is reported that the SMA underwire is resistant to permanent deformation because washing and drying the brassieres can trigger the shape recovery of deformed underwire.

6.3.2 Effect of SMAs on textiles

Shape memory yarn

SMAs, after suitable training, can attain a two-way SME, meaning that the shape change of textile products with two-way SMAs can be reversible and repeatable. Stylios *et al.* (2005) (Stylios and Wan, 2007) used NiTi wires after a solution treatment at 650°C for 60 min and an ageing treatment at 480°C for 1 h and 40 min followed by air-cooling to fabricate shape memory yarn. The two-way shape memory training process is as follows:

- (1) The TiNi wires were wound on a cylindrical jig, and then annealed at 500°C for 30 min followed by air-cooling.
- (2) The springs were annealed at 350–450°C for 1 h during which time the springs were constrained by a frame.
- (3) The constrained springs were thermomechanically trained for several cycles, at a temperature of 5°C (in a martensitic state) before relaxing the force and again heating up to 100–300°C, a temperature slightly higher than the austenite state finished temperature.

Yarns with trained NiTi SMA wires as their core component were developed. The SMA yarns were wrapped with polyester, viscose or polyamide. Stylios' research group designed many yarns with different twist levels and structures (Stylios, 2006).

Shape memory fabrics

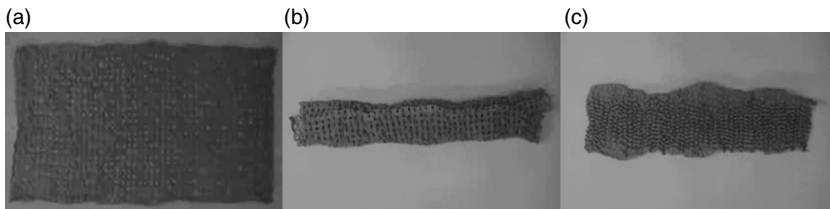
Many woven and knitted fabrics were prepared by using the yarns with SMA wires. Three aims can be achieved by using SMA wires (Chan and Stylios, 2003)

- Movement of fabrics, for the purposes of visual wave effects and other textural changes on the surface of fabrics.
- F020 opening and closing of apertures in fabric structures to alter properties for the purposes of opacity, insulation, diffusion of light and air flow.
- F020 opening and closing of fabric structures to create smart structures that can open and close such as for smart interior screens or curtains.

Various designs and structures can be used to incorporate SMA wires with textiles to prepare shape memory fabrics. Figure 6.2 shows the shape recovery of a shape memory fabric embedded with SMA wires (Oclaciro, 2010). The fabric is first compressed into a small size. Then with increasing temperature, the fabric became fluffy and unfolds.



6.2 The shape recovery of a fabric with nitinol SMA wires.



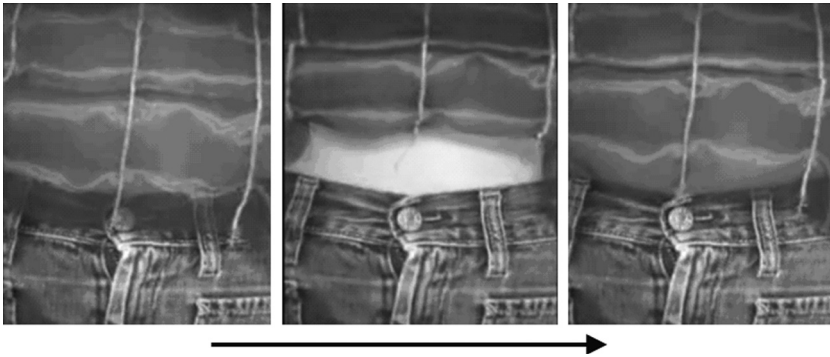
6.3 Shape memory of a fabric with SMA wires. For explanation see text.

Stylios and Wan (2007) demonstrated the shape recovery of a fabric with trained SMA wires which had a two-way SME. The trained SMA wires were blended with two kinds of polymer yarn. The fabric changed from a flat to a curled shape in 50 s when it was heated to a temperature of 50°C which was slightly above the austenite transformation starting temperature. By cooling the fabric from above 50°C to room temperature, the fabric recovered from the curled state to its original flat state. Figure 6.3 presents another shape memory fabric with two-way SMA wires (Leenders, 2010). The fabric was originally flat as shown in Fig. 6.3(a). When heated, the fabric rolled up as shown in Fig. 6.3(b). Finally, the fabric was cooled to room temperature which caused it to recover its original flat shape as shown in Fig. 6.3(c).

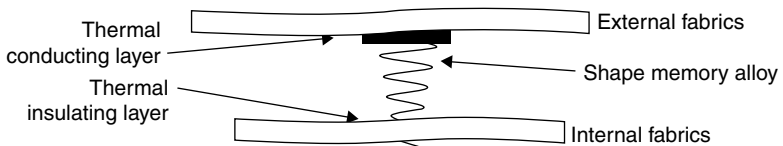
Shape memory clothing

Various shape memory clothing items and accessories have been designed for their aesthetic interactive and functional effects on textiles. An Italian design house based in Florence, Corpo Nove, designed 'lazy shirt' fabric which was joined with SMA wires and nylon fiber. When outside temperatures are high, the shirtsleeves can quickly wind up from wrist to elbow. When the temperature drops the sleeves automatically return to their original shape (Marks, 2001).

Figure 6.4 shows another interesting design of shape memory dress (Leenders, 2010). The under layer of the dress is made of fabric embedded with SMA wires. As shown in Fig. 6.4, the under layer of the dress shrinks



6.4 A shape memory dress with SMA wires.



6.5 Schematic showing the functionality of the insulating property (reprinted with permission from: J. Hu, *Shape Memory Polymers and Textiles*, 2007, Woodhead Publishing Limited, UK).

when the dress is heated using a hair dryer. The dress recovers its original length when the dryer is removed.

Figure 6.5 illustrates the external and internal layers of a fabric incorporated with springs made of two-way SMAs (Hu, 2007b). The two-way shape memory spring with a switching temperature of $\sim 50^{\circ}\text{C}$ extends when subjected to a temperature above 50°C . At a high temperature, above the switching temperature, the two layers separate from one another as the length of the shape memory spring increases. This increases the air gap between the two layers which acts as a barrier against flames and intense heat. At low or normal temperatures, the two layers approach each other because the length of the spring decreases at a temperature below its switching temperature.

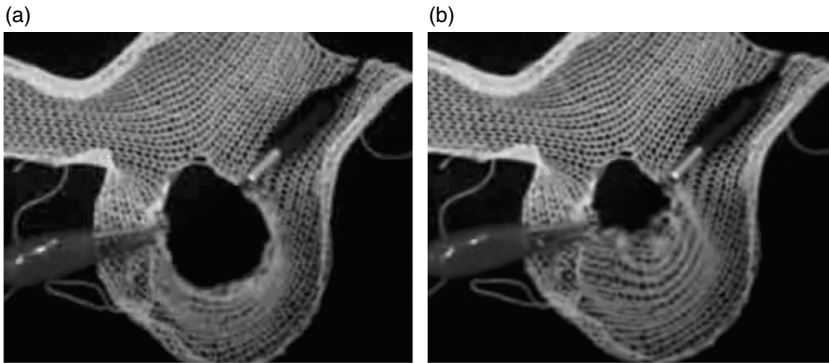
Other shape memory textile products

Fabric with two-way SMA wires is not only useful in clothing for aesthetic and novel functions; it can also be used for practical purposes in many other textile products. Shape memory fabrics were used in the intelligent window curtain applications proposed by Stylios and Wan (2007; Stylios *et al.*, 2005). The two-way shape memory curtains can self-regulate their structures and performances in response to the room temperature.

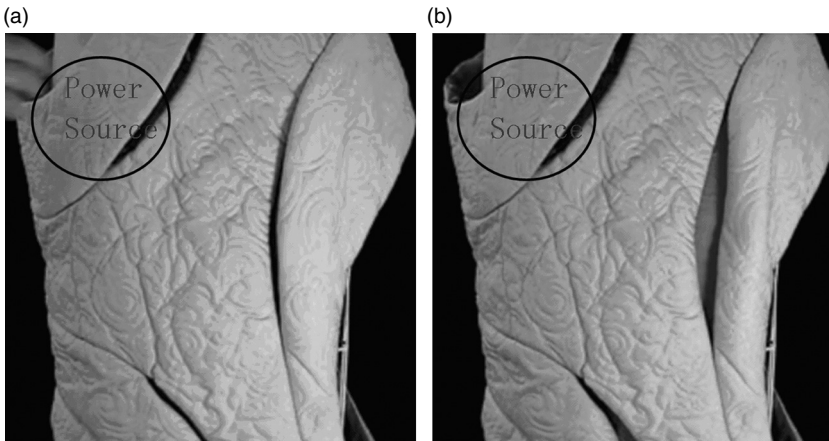
Electro-active shape memory textile products

SMA is an electro-conductive intermetallic alloy. They can be heated using an electrical current via Joule heating. Shape change driven by an electrical current is easier and more efficient than that caused by direct heating. Figure 6.6 shows the shape recovery of a knitted fabric with SMA wires (Labs, 2010). The pre-designed hole, which is much larger at the beginning (see Fig. 6.6(a)), shrinks to a smaller size (see Fig. 6.6(b)) when the fabric is charged with an electrical current.

Figure 6.7 shows a garment incorporated with SMA wires and a power source (Xslabs, 2010). The designed gaps on the garment can open and close as a result of the increasing and decreasing temperature of the SMA wires by Joule heating. The power is supplied by the power source embedded within the garment.



6.6 Electrical-active shape memory fabric. The hole size changes between (a) and (b) reversibly when electrical stimulation is applied alternately.



6.7 Smart garment with SMA wires. Upon electrical stimulation, the small gaps (a) on the garment open into big gaps (b); the gaps recover once the electrical stimulation is removed.

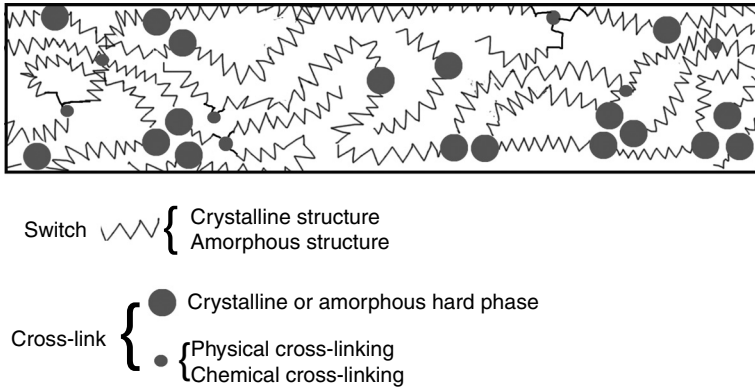
Problems of textile products with SMAs

Although many shape memory textiles with different structures and functions have been designed and developed by incorporating SMAs, there are still some minor problems. First, because of the significant mechanical difference of SMA wires and traditional textile fibers, SMA wires have a tendency to protrude from the garment. Complicated textile structures are therefore difficult to accomplish. Second, due to their stiffness and limited extensibility, the knitting of SMA wires is difficult. Finally, if not designed properly, the SMA wires in shape memory fabrics significantly affect the soft hand feel of the garment.

6.4 Shape memory mechanisms of SMPs

In comparison with SMAs, SMPs have the advantages of being lightweight, low cost and easy to process as well as possessing high shape deformability, high shape recoverability and tailorable switching temperatures. The disadvantages of SMPs compared with SMAs, however, are low mechanical and recovery strengths. According to the switch mechanisms of SME, SMPs can be divided into the following categories: (a) those with an SME based on conventional glass or melting transition (Liu *et al.*, 2007a), (b) those with an SME based on anisotropic chain conformation change (Ahir *et al.*, 2006; Qin and Mather, 2009), (c) those with an SME based on thermally reversible Diels-Alder cycloaddition (Ishida and Yoshie, 2008), (d) those with an SME based on carbon nanotube (CNT)/SMP composites (Vaia, 2005) and finally (e) those with an SME based on in-direction heating such as electricity (Koerner *et al.*, 2004), light (Langer and Tirrell, 2004; Small IV *et al.*, 2005) or a magnetic field (Cuevas *et al.*, 2009). SMPs can be used in smart textiles and apparels (Meng *et al.*, 2007a), intelligent medical devices (Nagahama *et al.*, 2009; Wischke *et al.*, 2009), heat shrinkable packages for electronics (Charlesby, 1960), sensor and actuators (Kunzelman *et al.*, 2008; Lan *et al.*, 2008), smart water vapor permeability materials (Mondal *et al.*, 2006), self-deployable structures in spacecraft (Campbell *et al.*, 2006), micro-systems (Eddington and Beebe, 2004), damping materials (Yang *et al.*, 2004), self-peeling reversible adhesives (Xie and Xiao, 2008), vehicle components (Lendlein, 2006), toys (Hayashi *et al.*, 2004), hair treatments (Lendlein and Ridder, 2007) and chemical feeding in chemical reactions (Laroche *et al.*, 2002).

Until now, the SMPs applied in textiles were mostly based on conventional glass or melting transitions. The molecular mechanism of the SME of an SMP, based on glass or melting transition, as a switch, is shown in Fig. 6.8. These SMPs usually have a physical cross-linking structure, crystalline/amorphous hard phase, or chemical cross-linking structure and a low



6.8 The molecular mechanism of thermal active SME.

temperature transition of crystalline, amorphous or liquid crystal phase. They are processed or thermally set to have an 'original' shape. Generally, in the permanent shape, internal stress is zero or very low. If the SMP is subject to deformation, the large internal stress can be stored in the cross-linking structure by cooling the polymer below its switch transition temperature (glass transition or melting temperature). The deformed temporary shape is thus fixed because of the elastic modulus sharp increase once the glass transition or melting temperature is reached. By heating the polymer above the switch transition temperature, the SMP recovers to its permanent shape as a result of releasing internal stress stored in the cross-linking structure. The network to store the internal stress, which is used as a shape recovery driving force, may be a physical cross-linking structure, crystalline/amorphous hard phase or chemical cross-linking structure. The 'molecular switch' to resist the release of internal stress may be a crystallization, glass transition or liquid crystal phase. It is clear then that SME is a result of polymer morphology structures, but not of the properties of specific polymers.

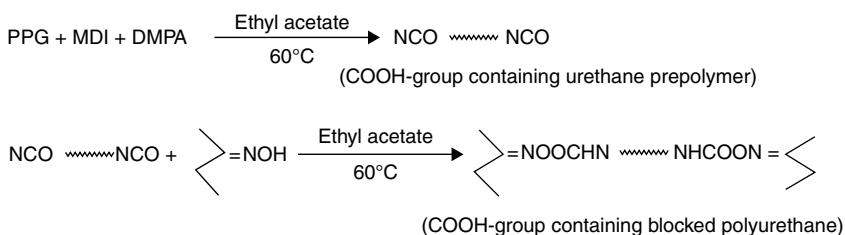
Liu *et al.* (2007a) divided SMP based on glass or melting transition into four categories: class I, covalently cross-linked glassy thermoset networks as SMPs (glass transition as a switch); class II, covalently cross-linked semi-crystalline networks as SMPs (melting transition as a switch); class III, physically cross-linked glassy copolymers as SMPs (glass transition or melting transition as a switch); and class IV, physically cross-linked semi-crystalline block copolymers as SMPs (glass transition or melting transition as a switch). From the view of the application, the prerequisite for thermal sensitive polymers as SMPs is that their switch transitions are above the environment temperature into which they are applied.

6.5 Applications of SMPs in textiles

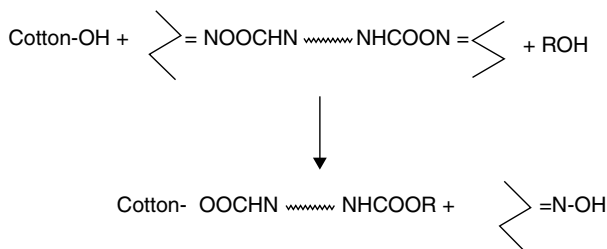
6.5.1 SMP coating

SMPs can be used for garment finishing and fiber spinning using various techniques to impart the SME of SMPs to textiles. Wan and Stylios (2004) finished fabrics with shape memory polyurethane (SMPU). The finishing solution was fabricated by dissolving SMPU chips in dimethylacetamide. The coating was conducted using a traditional finishing method. The SME of the treated fabrics could be trained from being flat at a high temperature to being bent at a low temperature (Stylios and Wan, 2007).

Hu *et al.* (2007a; Liem *et al.*, 2007; Liu *et al.*, 2008) treated cotton and wool fabrics using an SMPU water-borne emulsion. The water-borne emulsion was prepared through solution polymerization following the steps as shown in Fig. 6.9 (Hu, 2007a; Liu *et al.*, 2005). First, SMPU oligomers were prepared with poly (propylene glyols) (PPG), 4, 4,-diphenylmethane diisocyanate (MDI) and dimethylolpropionic acid (DMPA). Then, the –NCO was end-capped with methyl ethyl ketoxime (MEKO). Triethylamine was added to neutralize the free carboxylic groups. The acetone and water mixture was dropped into the reactor to prepare SMPU aqueous emulsions. Finally, the aqueous emulsion was used to finish cotton fabrics by a pad→pre-dry→cure process. During curing at a high temperature, the released isocyanates



6.9 Synthesis of end-capped SMPU oligomers (reprinted with permission from Elsevier Limited).

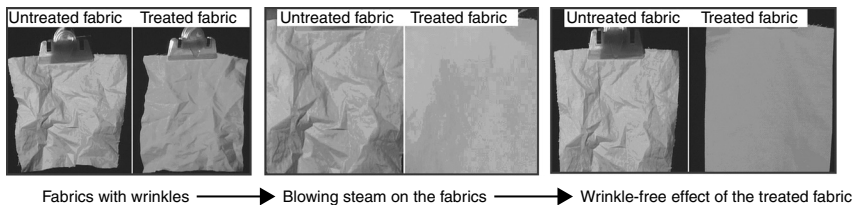


6.10 Reaction of SMPU oligomers with cotton (reprinted with permission from Elsevier Limited).

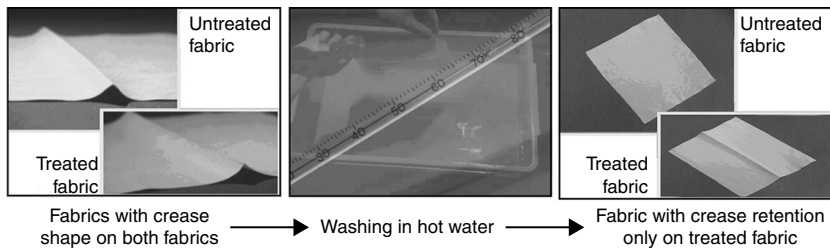
reacted to form cross-linking structures on cotton fabrics following the reaction as shown in Fig. 6.10. To improve the hydrophilicity of the finished textile products, hydrophilic segments such as polyethylene glycol with a molecular weight of 200–600 can be incorporated in SMPUs.

The SMP-treated cotton fabrics showed wrinkle-free properties due to the shape recovery effect of the SMPs (Li *et al.*, 2004). Fabrics, especially cotton fabrics, become very wrinkled during wearing or storing due to the de-bonding and slippage of hydrogen bonding. As shown in Fig. 6.11, the cotton fabric treated with SMP can recover its original flat shape within 1 min simply by steam blowing, while the untreated fabric cannot. Compared with traditional wrinkle-free finishing by formaldehyde agents such as DMDHEU (dimethyloldihydroxyethylene urea), the advantage of SMPU finishing is that it has no harmful formaldehyde. Unlike another kind of wrinkle-free finishing technique which uses polycarboxylic acid finishing agents such as BTCA (1,2,3,4-butane tetra-carboxylic acid), SMPU finishing does not significantly decrease the mechanical strength and whiteness of the fabric. SMPU finishing of cotton increases the mechanical strength of cotton fabrics to some extent. Repeated washing experiments showed that the wrinkle-free effect of SMPU emulsion treated fabric can last for hundreds of laundry cycles.

The ability of SMPs to hold shape well means that cotton fabrics treated with SMPU emulsion have a high crease and pattern retention ability and that aesthetic designs can be easily achieved. Figure 6.12 shows the crease retention effect of a cotton fabric treated with SMPs. In Fig. 6.12, one cotton



6.11 Wrinkle-free effect of fabrics treated with water-borne SMPU.



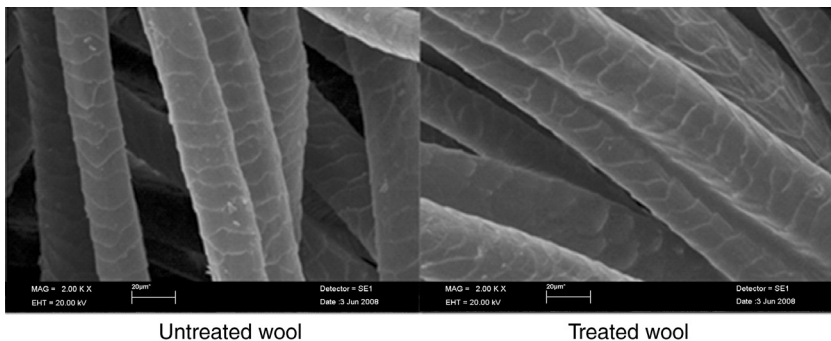
6.12 Crease retention of fabrics treated with SMP (crease shape was produced by ironing).

fabric is treated by SMP; another one is not. Both fabrics have a crease shape in the centre at the beginning by ironing. After washing them in hot water with a temperature around 60°C, the crease shape on the untreated fabric disappears, while the crease shape on the treated fabric remains. Figure 6.13 shows the superior pattern retention of an SMP designed fabric. Even after many laundering cycles the pattern is retained.

We also treated wool fabrics with the SMPU emulsion using a similar reaction mechanism as that used in the shape memory finishing of cotton fabrics. Wool fabrics and sweaters have serious felting and shape shrinkage problems because of the scale friction on wool fiber surfaces. Resin coating, chlorination shrink proofing and oxidation anti-felting can significantly reduce these problems. The SEM images of the SMPU-treated wool fibers are presented in Fig. 6.14. The wool garment treated with SMP emulsion has



6.13 The pattern with good shape retention.



6.14 SEM images of untreated wool and treated wool fabrics.

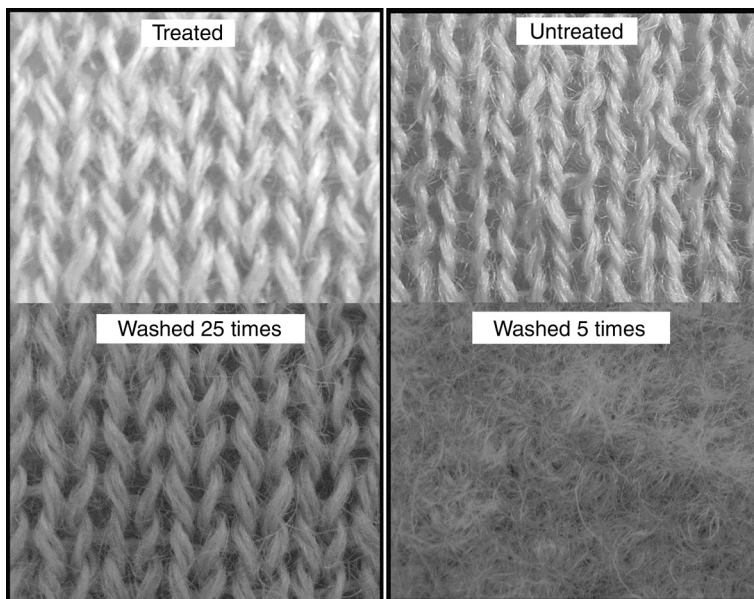
a better dimension stability than that of the untreated garment because the SMPU covers the wool fiber scales and, as a result, reduces the wool's directional frictional effect after the finishing process. As shown in Fig. 6.15, the untreated wool garment shrinks after a certain amount of washing cycles whereas the treated garment maintains its original size.

In addition, the finishing of wool fabrics significantly reduces the felting effect because the coated SMPU resin reduces the friction between wool fibers. The textures of untreated fabric and treated fabric after shape memory finishing are shown in Fig. 6.16. The texture of the treated wool fabric is still clear after 25 washes; in contrast, the texture of the untreated wool fabric shows serious felting after five washes. Both were washed following standard AATCC wool washing procedures.

Though shape memory finishing of fabrics can add new functions to fabrics, there are still some problems which have to be tackled. To obtain good shape memory functions, the coating cannot be too thin. In contrast, SMPU coating which is too thick will significantly decrease the soft hand feel of cotton and wool fabrics. Intrinsically, fabrics of different structures and fabrication specifications have different degrees of elasticity and fixability which affects the shape memory behavior of different SMPU-treated fabrics. For a specific function such as a wrinkle-free effect, high shape recovery ability and high elasticity of the SMPU are required. However, for a shape retention effect, high shape fixability is preferable. There are several areas of the shape memory finishing of fabrics process which would benefit from further study such as the influence of fabric structure on the properties of the SMPU-treated fabrics. The molecular structures of cellulose



6.15 Improved dimensional stability of SMP-treated wool fabrics after washing. The SMP-treated garment maintains its original size (left garment); the untreated garment shrinks significantly after washing (right garment).

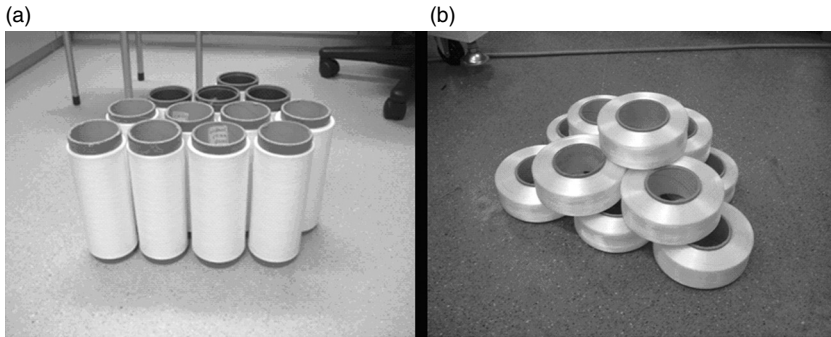


6.16 Texture of untreated and treated wool fabric.

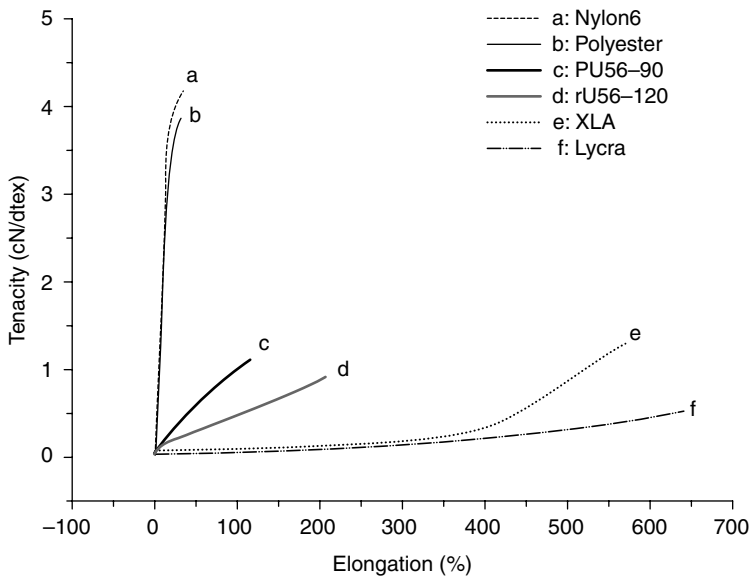
after cross-linking with SMPU need to be investigated. The reaction extent of hydroxyls on cellulose fabrics and the methods used for treating specific fabrics need to be established. The percentage of hydroxyls to be cross-linked by SMPU before the treated fabric obtains optimal SME and hand feel needs to be determined. Finally, the idea that the unsatisfied functions of SMPU-treated fabrics may be partially due to the friction of rigid fibers and fabric structures needs to be examined.

6.5.2 SMP fiber spinning

Hu *et al.* (Hu *et al.*, 2007c, 2008b; Meng and Hu, 2007b; Meng *et al.*, 2007; Zhu *et al.*, 2006) developed different SMPU filaments by using polyol as the soft segment and small size diols and MDI as the hard segment and by using different spinning methods. The switching temperature of the SMP fibers was at around room temperature ($\sim 29\text{--}64^\circ\text{C}$). The polyols used included PBA (poly (buthylene-adipate)) or PEA (poly (ethylene adipate)), PCL (polycaprolactone) and PHA (poly (hexylene adipate)). The polyol species, molecular weight and content significantly affect the spinnability of SMPU. The SMP fibers prepared by wet spinning and melt spinning are shown in Fig. 6.17(a) and (b) respectively. Figure 6.18 (Zhu *et al.*, 2006) shows the stress-strain curves of an SMPU fiber compared with other synthetic fibers. The tenacity of SMPU fibers is in the range of

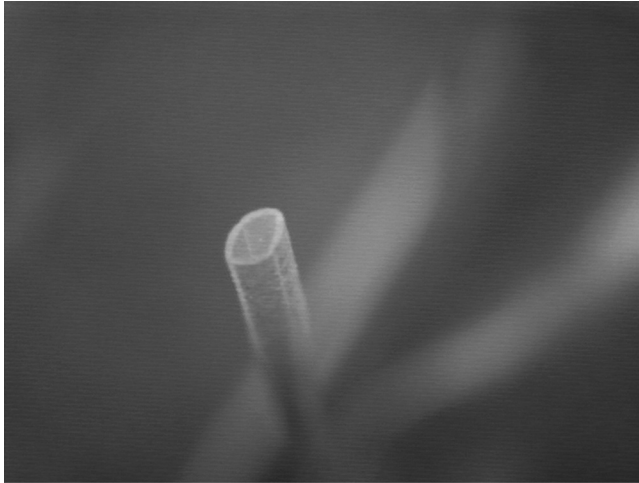


6.17 SMP fibers prepared by wet spinning (a) and melt spinning (b).



6.18 Stress-strain curve of shape memory polyurethane fiber compared with other synthetic fibers.

~6–14cN/tex with maximum strains in the range of ~35–204%. The stress-strain curve of SMPU fibers (PU56–90, PU56–120) is located between the high modulus fiber such as nylon and the high elasticity fiber such as Lycra fiber (Spandex fiber of Du Point). In comparison with SMPU films, SMPU fibers have lower shape fixability, higher shape recovery and higher recovery stress as a result of molecular orientation in SMPU fibers brought about during spinning processes. The recovery ratios of SMPU fibers can be as high as 100% (Zhu *et al.*, 2006). By incorporating CNTs into the SMPU fibers, Hu *et al.* (Meng *et al.*, 2007) developed electro-responsive SMP fibers which could change their shapes under electrical stimulation



6.19 Cross-sectional image of the shape memory hollow fiber.

by Joule heating. At present, the voltage required to produce enough heat to trigger the shape recovery is around 100 volts. For safety reasons, the conductivity of fibers has to be further improved so that a low voltage can trigger shape recovery.

Figure 6.19 shows an SMP hollow fiber prepared by melt spinning by Hu *et al.* (Meng *et al.*, 2009a). The internal diameter of the hollow fiber can noticeably change and recover under thermal stimulation as a result of SME. Because the changes of the internal diameter of hollow fibers affect the physical properties of textile products, smart SMPU hollow fibers can be used for thermal management in garments, or as stuffing for pillows and mattresses, which can adapt to body contours for comfort just like the function of memory foams. Furthermore, this kind of hollow fiber has the potential to be used in smart filtration, controlled drug-release and liquid transportation.

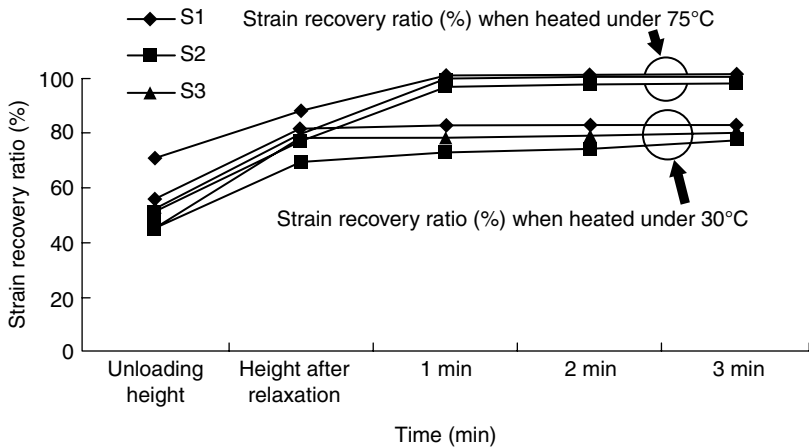
6.5.3 Shape memory functions of SMP fabrics and garments

Shape memory yarns such as blended, warped or core yarns of SMP fibers and natural, regenerated or synthetic fibers have been developed. The shape memory properties of shape memory fabrics were investigated by Hu and her colleagues. Three kinds of knitted fabrics were prepared using (a) 100% shape memory fiber, (b) shape memory core yarns (50% cotton and 50% shape memory fiber) and (c) two-ply yarns (100% cotton). The basic

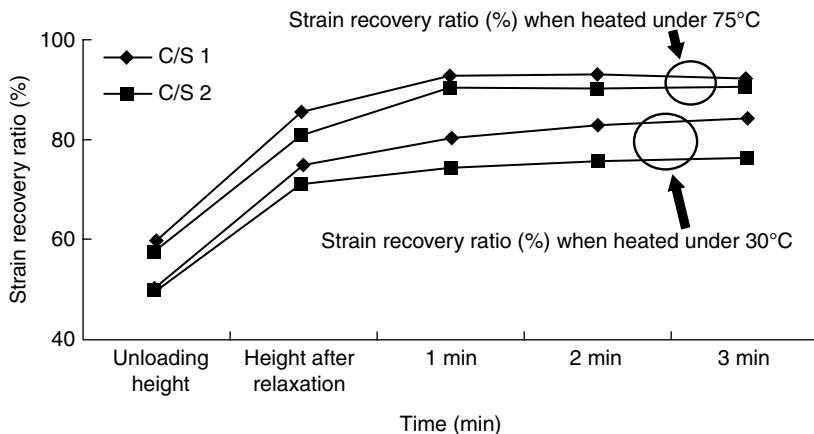
fabricating parameters of the shape memory fabrics are shown in Table 6.1. Shape memory properties were determined using a bagging recovery test (Li, 2007; Liu *et al.*, 2007b). First, a bag shape was produced on every fabric by an Instron machine. Then, the bagged fabric was heated in the oven at a constant temperature of 30°C and 75°C respectively for 3 min. Non-recoverable bagging height was measured every minute after heating. Strain fixity (%) and strain recovery ratio (%) were calculated using the bagging height. The strain recovery curves of shape memory fabrics are shown in Figs 6.20–6.22.

Table 6.1 Basic fabric parameters (plain knit) (90 × 90 mm)

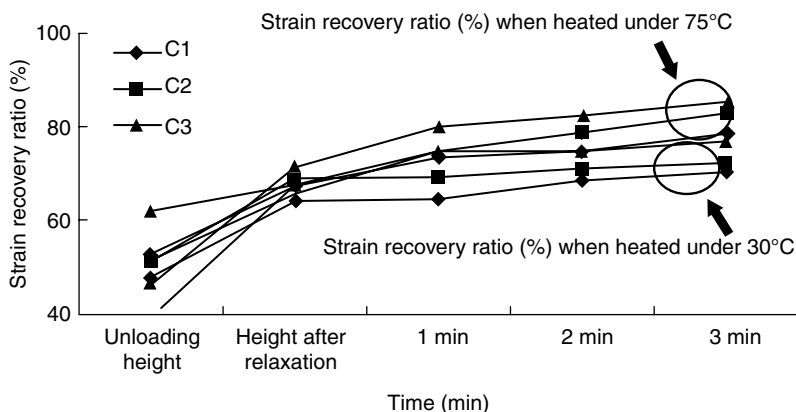
Fabric code	Fiber content	Yarn type	Count (tex)	Tightness factor
S1	100% SM polymer PU56 (Y1)	Shape memory fiber	9	13.72
S2	100% SM polymer PU66 (Y4)	Shape memory fiber	20	12.08
S3	100% SM polymer PU66 (Y4)	Shape memory fiber	20	10.4
C/S 1	50% SM polymer PU66 (Y8) and 50% cotton	Shape memory core yarn	16	13.72
C/S 2	50% SM polymer PU66 (Y8) and 50% cotton	Shape memory core yarn	16	10.4
C1	100% Cotton (Y13)	Two-ply yarn	63	19.25
C2	100% Cotton (Y13)	Two-ply yarn	63	18.04
C3	100% Cotton (Y13)	Two-ply yarn	63	16.75



6.20 Strain recovery ratio (%) of 100% shape memory knitted fabric solely composed of SM fibers (30°C, 75°C).



6.21 Strain recovery ratio (%) of 50% SM fiber and 50% cotton knitted fabric (30°C, 75°C).



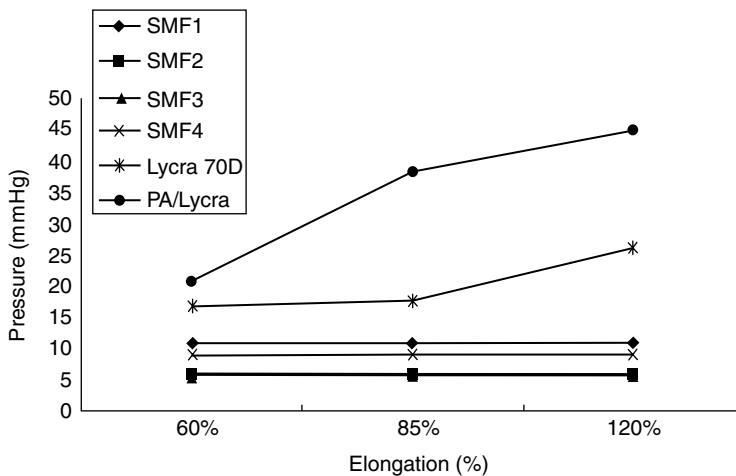
6.22 Strain recovery ratio (%) of 100% cotton knitted fabric (30°C, 75°C).

The knitted fabrics containing 100% shape memory fiber and shape memory core yarn (50% cotton and 50% shape memory fiber) showed a superior thermal sensitive shape memory performance in comparison with the knitted fabric composed only of two-ply yarns (100% cotton). The recovery ratio for knitted fabrics composed of 100% shape memory fibers had a shape recovery ratio of approximately 100% after heating to 75°C which is above the switching temperature of shape memory fibers. The fabrics with 50% shape memory fibers had a recovery ratio above 90% after heating to 75°C.

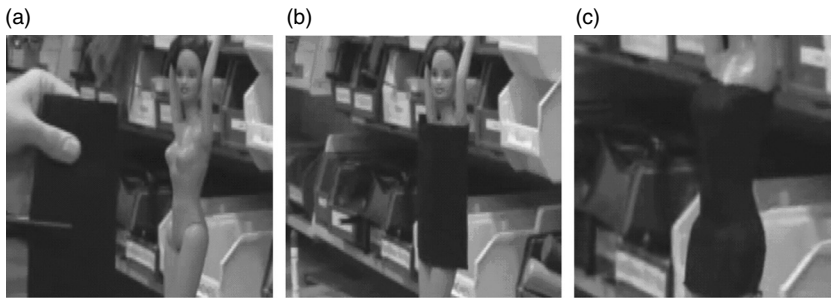
Shape memory fabrics made of SMP fibers can be used in textiles and clothing to create self-adapting textiles with self-regulating structures and performance in response to environmental temperature variation. Apparel

prototypes of shape memory fabrics have been made using knitted and woven SMP fibers (Hu *et al.*, 2009; Liu *et al.*, 2007b). The garments made of SMP fibers can be enlarged to adapt to various wearers' figures (Li, 2007; Liu *et al.*, 2007b). Vertical pressure test results shown in Fig. 6.23 show that, in comparison with fabrics made of Lycra (spandex fibers) or PA/Lycra, the garments made of SMP fibers have a relatively low vertical tension stress. The low tension stress can be ascribed to the shape fixability of SMP fibers to temporary shapes, which diminishes the pressure sensation for wearers. The fabric made with SMP fibers can be used to improve the comfort sensation of textile products such as intimate apparel (Hu *et al.*, 2008b, 2009).

Figure 6.24 (Bonanni, 2010) shows another application of shape memory textiles: they can be made to fit to individual figure size which takes advantage of the SME of shape recovery fibers. Figure 6.24(a) is a columnar shaped memory fabric which can be facially fabricated. First, the diameter of the columnar shaped memory fabric is enlarged to a size larger than the diameter of the model's body so that the columnar fabric can be easily put on the model's body, as shown in Fig. 6.24(b). By using a hair dryer to heat the fabric, the fabric recovers and becomes the same shape as the model's body, as shown in Fig. 6.24(c). Thus a perfect match can be obtained, and different body shapes can be accommodated and shown to their best advantage using shape memory fabrics.



6.23 Pressure (vertical direction to fabric surface) of enlarged fabrics to 'wearer' (testing cylinder) (SMF1, SMF2, SMF3 and SMF4 are fabrics made of shape memory fibers with different composition, Lycra 70D is a fabric made of Lycra fibers of 70 denier, PA/Lycra is a fabric made of polyamide fibers and Lycra fibers).



6.24 Easy wear and perfect match of shape memory garment. The diameter of the columnar shape memory fabric is enlarged to a size larger than the diameter of the model's body (a) so that the columnar fabric can be easily put on the model's body (b); upon heating the columnar fabric recovers, thus a perfect match is obtained (c).

The biological properties of shape memory fabrics with a switching temperature of around body temperature were preliminarily evaluated (Meng *et al.*, 2009b). The results showed that the shape memory fabric was not cytotoxic, hemolytic, insensitive or irritating. With a better compatibility with human bodies than shape memory films or bulks, SMPs in fiber/fabric form may also find applications in biomedical areas such as wound dressing, scaffold materials and orthodontics.

In addition to the self-adaptability of shape fabrics which feel good and are a perfect match for body shape, shape memory fabrics can be used for wrinkle-free effects, and many kinds of artistic designs. Depending on the desired properties, shape memory fabrics can be used on the collars and cuffs of shirts which need a rigid fixed shape, on the elbows and knees of jackets and trousers which need to be hard-wearing, and on denim, velvet and cord which need help holding their shape.

SMP fibers, yarns and fabrics have also been developed by Stylios *et al.* (2005; Vili, 2007). Yarns of different conventional fibers along with SMP fibers were woven sparsely and loosely along the weft to allow room for the SME to take place. Contract (shape recovery) occurs when the environmental temperature is over the glass transition temperature of the SMP. Thus, fabric with SMP yarns can be aesthetically appealing. Shape memory fabrics can also be used for temperature and moisture management of the human body.

It has been found that if the filaments are used solely to make fabrics by knitting or weaving, the fabrics do not have a good hand feel. For this reason SMPU filaments are preferred for use along with other fibers such as cotton. If the filaments are used as core spun yarn, fasciated yarn or wrap yarns with cotton, the SME of the fabrics made of the yarns is not pronounced due to the restriction of the cotton fibers on the movement of the SMP fibers. The elasticity structure of knitting fabrics decreases the shape fixity of the fabrics, while the structure of woven fabrics hinders the shape recovery of

the fabrics. Furthermore, during processing at room temperature, SMPU fibers in fabrics are elongated to some extent due to the low glass transition temperature (slightly above room temperature) of SMPU fibers. This temporary elongation needs to be taken into consideration during the design of shape memory fabrics because it can cause shrinkage.

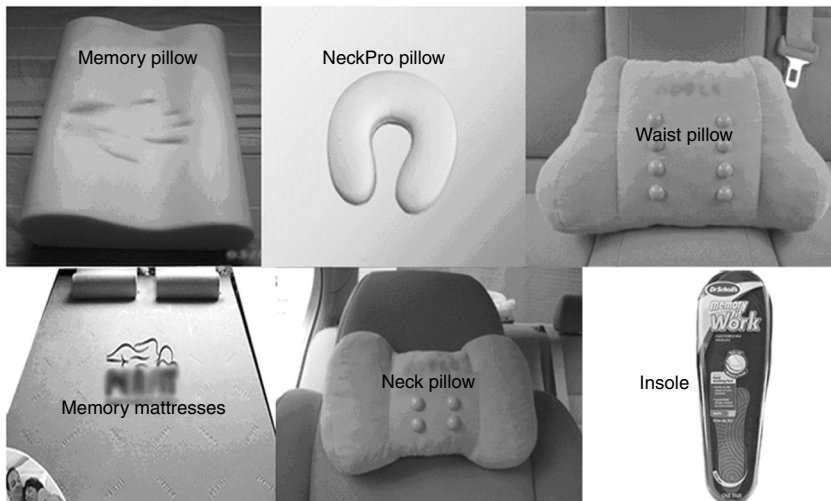
6.5.4 Shape memory nano-fibers

Shape memory nano-fibers have special properties due to their large surface area to volume ratio. Hu *et al.* (Zhuo *et al.*, 2008) coated nano SMPU fiber meshes onto textiles by electrospinning. After the SMPU nano-fibers were coated on fabrics, many unique properties were found on the fabrics due to the surface properties and orientation structure of the nano-fibers, such as good hand feel, good water vapor permeability, waterproofing ability and unusual SME. Krause *et al.* (2007) prepared nano-fibers and thin film of main-chain liquid crystal elastomers, which showed a shape response temperature change. The photo cross-linkable liquid crystal elastomers were cross-linked during the electrospinning process. The prepared nano-fibers had a uniform director alignment along their long axis. SMEs were observed in this kind of material.

Electrospun non-woven meshes have minimal resistance to moisture vapor diffusion and maximal efficiency in trapping aerosol particles in comparison with conventional textiles (Peppas and Kim, 2006). Protective clothing with nano-fiber coating can be fabricated using SMPs. Fabrics coated with nano-fibers from SMPs can neutralize hazard agents without decreasing the air and water vapor permeability of the fabrics. The nano non-woven structure can also provide a strong resistance to the penetration of harmful agents in aerosol forms. SMP nano-fibers can be used not only in textile areas, but also in tissue engineering (Ulijn *et al.*, 2007), scaffolding (Chen and Ma, 2004) and wound dressing (Ignatova *et al.*, 2006).

6.5.5 Shape memory foams

SMP foams have been proposed for use in aerospace applications (Tobushi *et al.*, 2006), weight reducing (Marco and Eckhouse, 2006), drug delivery (Wache *et al.*, 2004) and measuring tools of complex cavities (Huang *et al.*, 2006). Figure 6.25 shows examples of textile products using memory foams. The memory pillow is filled with low resilience polyurethane memory foams developed by Bayer. It can adjust its shape to the contour of the neck and shoulders of the body. SMP foams can also be used as memory mattresses to provide comfort and support for the user's body. SMP foams have also been used to prepare insoles, which can effectively improve shoe fitting. Wearing high-heeled shoes can cause many problems for women, such as calluses, painful bunions and spine deformities (Gefen *et al.*, 2002). Dr Scholl's



6.25 The textile products made of shape memory foams.

Company produces Dr Scholl's® Memory Fit™ (Work) Customizing Insoles (Fig. 6.25) (Scholl, 2010) using memory foams for the balls of the feet or from heel to toe, which can adapt to everybody's unique foot shape with every step and can help tackle the above-mentioned problems effectively.

6.5.6 Shape memory textiles with good damping properties

SMPs can absorb impact energy due to their good damping properties once they reach the glass transition temperature (switching temperature) (Yang *et al.*, 2004). AlliedSignal Inc. (Lim *et al.*, 2002) developed an automotive seatbelt fabric using SMP fibers (Securus fiber) to help increase occupant safety utilizing the damping effect of the SMPs. It is reported that the Securus fiber can absorb energy from the body's forward motion and improves the safety of passengers during a crash. First, the seatbelt holds the passenger securely in place, then elongates slightly and cushions the body as the belt absorbs the energy of the body's forward motion. The Securus fibers are melt spun from shape memory poly (ethylene terephthalate)-poly (caprolactone) block copolymers.

6.5.7 Shape memory textiles with smart breathability

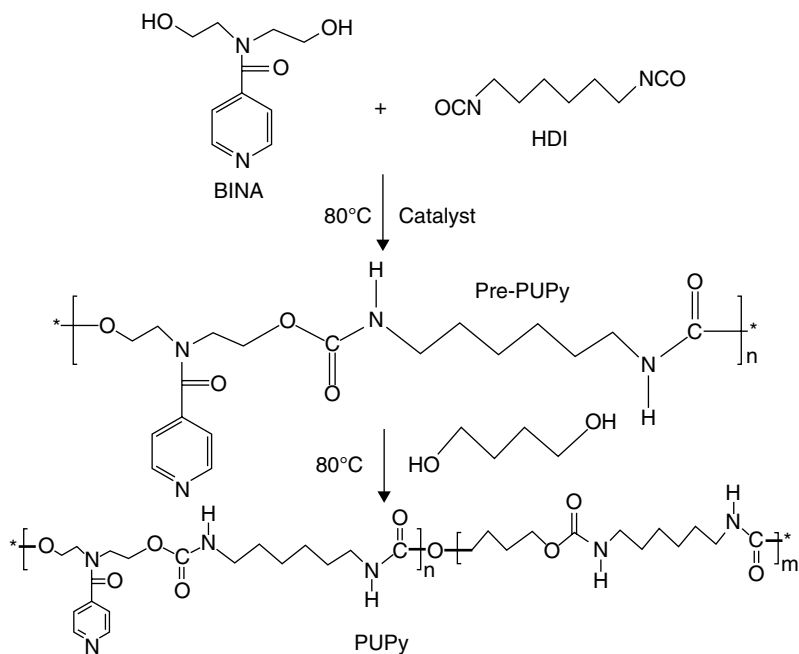
SMPU used as a coating or film in garments can offer temperature-dependent water vapor permeability to improve the comfort of the garment (Hyashi, 1993). SMPUs for breathable fabrics have a glass transition temperature of

about human body temperature. The water vapor permeability of the SMPU dense films changes to correspond with the wearer's temperature variations. When the body temperature is above the glass transition temperature of the polyurethane dense film, the free volume of the film increases significantly which increases the transmission speed of water vapor molecules with an average diameter of 3.5\AA through the SMPU films (Hu *et al.*, 2002). Thus, the heat and vapor from perspiration are transported away from the body into the environment, and comfort can be obtained. When the body temperature is below the glass transition temperature of the SMPU, the free volume decrease, which prevents air and water molecules passing through. Consequently, the film keeps the body warm. By employing hydrophilic segments such as dimethylpropionic acid, diol terminated poly (ethylene oxide) (Jeong *et al.*, 2000; Mondal and Hu, 2006, 2007) in SMPUs, the overall water vapor permeability of dense SMPU films can be improved. The overall water vapor permeability of SMPs can also be significantly increased by forming microfoams in the SMPs. Thermal-responsive SMPU film can be coated, laminated or interlined in traditional fabrics.

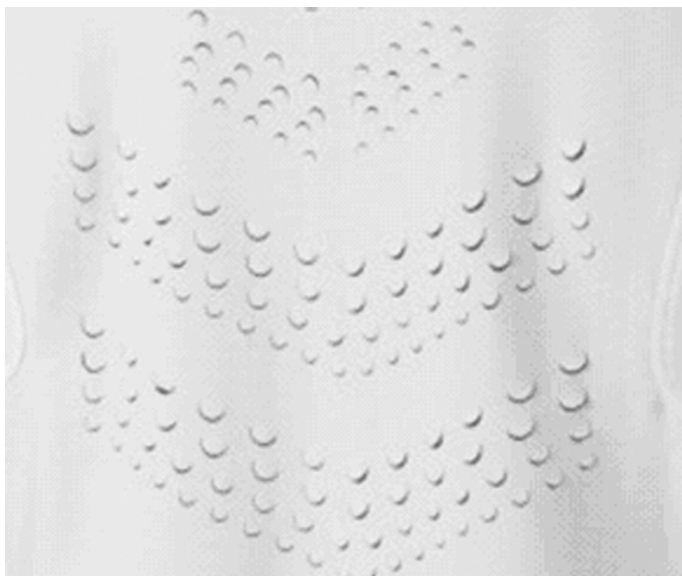
6.5.8 Shape memory textiles with water/moisture-driven SME

The shape recovery of deformed SMPs can be triggered by water or moisture due to the plasticizing effect of water molecules, which increase the flexibility of macromolecule chains (Huang and Yang, 2005; Leng *et al.*, 2008). If an SMP has a hydrophilic or water soluble ingredient, the shape recovery can be accelerated (Chen *et al.*, 2007; Jung *et al.*, 2006). A pyridine unit, which is responsive to moisture, can be used to improve the moisture absorption of polyurethane. Hu *et al.* (Chen *et al.*, 2009) introduced a pyridine unit into SMPU by N-bis(2-hydroxyethyl) isonicotinamine (BINA) and prepared moisture-responsive SMPU. High strain recovery with fast recovery speed was obtained. The synthesis route of SMPU with pyridine unit is presented in Fig. 6.26. First, 1, 6-hexamethylene diisocyanate (HDI) reacts with BINA to form a pre-polymer. Then the pre-polymer is extended with 1, 4-butanediol (BDO). It can be deduced that SMPs sensitive to their suitable solvents can be created just as hydrophilic SMPs can be created to be sensitive to water/moisture. Lv *et al.* (2008) observed the DMF (*N,N'*-dimethylformamide) (a good solvent of SMPU)-responsive SME of SMPUs.

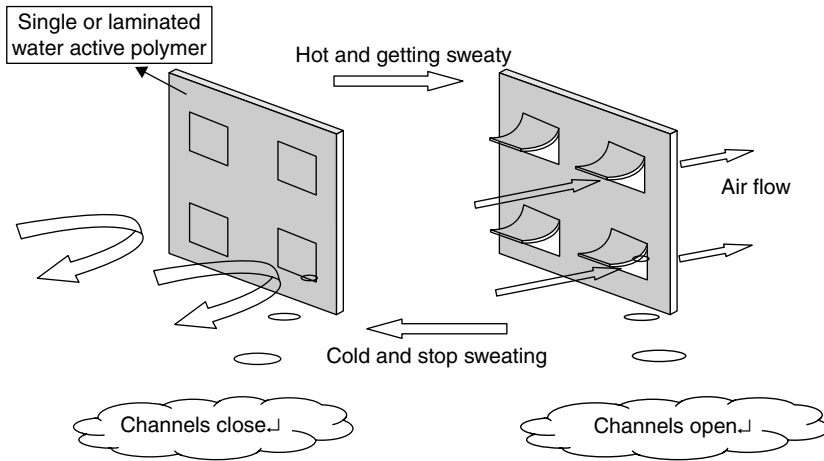
When body temperature is unstable and leads to excess perspiration, wearers will feel uncomfortable. Figure 6.27 shows a smart shirt named 'Sphere React Shirt' with rear vents which can open up to allow perspiration and heat to escape when the wearer sweats. The vents automatically close once the wearer reaches a dry state. It may be very effective to use water/moisture-responsive textiles which can change macro-shape or micro-structures



6.26 Synthesis routine of SMPU with pyridine units (reprinted with permission from Elsevier Limited).



6.27 The back of Nike 'Sphere React' shirt with a smart vent structure.



6.28 The applications of moisture-responsive SMPs for intelligent management of sweat from human bodies.

to achieve such functions for the moisture and heat management of human bodies. Figure 6.28 shows the schematic sketch of a moisture-responsive SMP for the intelligent management of sweat and heat from human bodies. The fabric made of single or laminated moisture-responsive SMPs has many small windows on it. If the wearer becomes hot and gets sweaty after excessive activity, the windows on the fabric open to allow heat and sweat to be released. In a cold situation without sweat, the windows close and keep the wearer warm and comfortable.

The US Patent 6627673 of Kimberly-Clark company (Topolkaraev and Soerens, 2003) disclosed a humidity activated laminate textile for disposable and reusable product applications. The humidity-responsive laminate textile contains an elastomeric polymer and a moisture absorbing polymer. Upon exposure to a high humidity environment, the disposable product transforms to a desired configuration which can guard against leakage. The laminated polymer is deformed at a dry state. In a high moisture situation, the modulus of the material decreases and triggers the shape change of the material because of the moisture absorbed by the moisture absorbing polymer. Thus, this material can change to a desired shape and/or texture during use. The products can therefore be used for disposable and reusable products such as disposable diapers, training pants, incontinence products and feminine care products.

6.6 Future trends

By integrating SMMs into textile structures, we can obtain new functions of textiles for aesthetic design, moisture/temperature management and

protection against extreme climates. Textiles with SMMs can move or change shape to achieve different 3D forms of garments for aesthetic appeal. Curtains with SMMs can open and close automatically to accommodate environmental stimulation. The micro- or macro-structure change of adapting clothing in response to stimuli is a good means for heat and moisture management of human bodies for comfort. The change of fabric structures can also be used for protecting against extreme environments.

At present, most SMMs used in textiles are sensitive only to one specific stimulus signal, namely thermal stimulus with specific stimulus range. In future, SMMs with multiple stimuli-active functions may be achieved by integrating different stimuli-response materials into one material together. Therefore, the SMMs may be able to adapt themselves to different environmental conditions with varying thermal, light, electricity, pH and humidity signals.

In addition to shape change and recovery properties, stimuli-responsive textiles can offer a deformation force which may be used as an aid for physiological performance. Orthopedic suppliers may use such textiles for corrective aids. SMPs with shape change polymers in textiles may also be used for the release of perfume, nutrition and drugs to human skin. These stimuli-responsive textiles will open new opportunities for smart textiles in medicine and medical applications.

The SME of all SMPs which have been used in textiles are one-way. This means that the shape changes of all the shape memory textiles developed are non-reversible and cannot be repeated. Several technologies have been reported to develop SMPs with a two-way SME. Chung *et al.* (2008) reported a two-way SME in cross-linked shape memory poly(cyclooctene). Cooling-induced crystallization under a tensile load results in elongation. Subsequent heating melts the network yields which then contract and recover their shape. However, a tensile load is necessary for the two-way SME and it is difficult to control. Ahir *et al.* (2006) and Qin and Mather (2009) achieved two-way SME through anisotropic chain conformation change of liquid-crystalline polymers. Unfortunately, this process requires a temperature of above 100°C which makes the material unsuitable for clothing applications. Hu *et al.* (Chen *et al.*, 2008) obtained two-way SME by laminating an SMP with an elastic polymer. This laminate material is more suitable for textile applications. The two-way SME was ascribed to the release of an elastic strain of the SMP layer upon heating, and the recovery of the elastic strain induced by the bending force of the elastic polymer layer upon cooling. Hu's research group is also developing bi-component fibers with one component as an SMP and another component as an elastic fiber, and studying the two-way SME of the conjugate fibers.

The study of SMMs for textile applications currently remains largely unexplored. Even though polymer materials can have a good compatibility

with textiles, textile applications pose strict requirements on the original properties of SMMs such as making them safe, lightweight, highly stable, easy to process and with a soft hand feel. Cleaning and washing also need to be taken into consideration for some clothing applications. Extensive and intensive work needs to be conducted to investigate in detail the property parameters of SMMs and to integrate their properties with textile products.

6.7 Sources of further information and advice

Shape memory polymers and textiles, J. Hu (2007), Woodhead Publishing Limited, Cambridge, UK: <http://www.woodheadpublishing.com/en/book.aspx?bookID=917> [accessed 1 January 2010].

Shape Memory Textile Centre: <http://www.shapememory.com> [accessed 1 January 2010].

6.8 References

- AHIR, S. V., TAJBAKSHI, A. R. and TERENTJEV, E. M. (2006) Self-assembled shape-memory fibers of triblock liquid-crystal polymers. *Advanced Functional Materials*, 16: 556–560.
- ASAKA, K. and OGURO, K. (2000) Bending of polyelectrolyte membrane platinum composites by electric stimuli. *Journal of Electro-Analytical Chemistry*, 480: 186–198.
- BONANNI, L. (2010) Fashion on demand or shape memory dress. Available at: <http://www.youtube.com/watch?v=NyF3GcSXTxE> [accessed 15 January 2010].
- BOUSSU, F. and PETITNIOT, J. L. (2002) Development of shape memory alloy fabrics for damping and shape control of composite structures. World Textile Conference, 2nd AUTEX, Conference, Textile Engineering at the Dawn of a New Millennium: An Exciting Challenge, Bruges, Belgium, 3 July.
- CAMPBELL, D., MAJI, A. and ASCE, F. (2006) Failure mechanisms and deployment accuracy of elastic-memory composites. *Journal of Aerospace Engineering*, 19: 184–193.
- CHAN, Y. Y. F. and STYLIOU, G. K. (2003) Engineering the design attributes of woven interior textiles using shape memory polymer. Advanced Flexible Materials and Structures: Engineering with Fibres, The Fibre Society 2003 Spring Symposium. Loughborough.
- CHARLESBY, A. (1960) *Atomic Radiation and Polymers*. New York: Pergamon Press.
- CHEN, M. C., TSAI, H. W., CHANG, Y., LAI, W. Y., MI, F. L., LIU, C. T., WONG, H. S. and SUNG, H. W. (2007) Rapidly self-expandable polymeric stents with a shape-memory property. *Biomacromolecules*, 8: 2774–2780.
- CHEN, S., HU, J., YUEN, C. W. and CHAN, L. (2009) Novel moisture-sensitive shape memory polyurethanes containing pyridine moieties. *Polymer*. DOI: 10.1016/j.polymer.2009.07.031.
- CHEN, S., HU, J., ZHUO, H. and ZHU, Y. (2008) Two-way shape memory effect in polymer laminates. *Materials Letters*, 62: 4088–4090.

- CHEN, V. J. and MA, P. X. (2004) Nano-fibrous poly (L-lactic acid) scaffolds with interconnected spherical macropores. *Biomaterials*, 25: 2065–2073.
- CHUNG, T., ROMO-URIBE, A. and MATHER, P. T. (2008) Two-way reversible shape memory in a semicrystalline network. *Macromolecules*, 41: 184–192.
- CUEVAS, J. M., ALONSO, J., GERMAN, L., ITURRONDORBEITIA, M., LAZA, J. M., VILAS, J. L. and LEON, L. M. (2009) Magneto-active shape memory composites by incorporating ferromagnetic microparticles in a thermo-responsive polyalkenamer. *Smart Materials and Structures*, 18: 075003.
- EDDINGTON, D. T. and BEEBE, D. J. (2004) Flow control with hydrogels. *Advanced Drug Delivery Reviews*, 56: 199–210.
- FEIL, H., BAE, Y. H., FEIJEN, T. and KIM, S. W. (1992) Mutual influence of pH and temperature on the swelling of ionizable and thermosensitive hydrogels. *Macromolecules*, 25: 5228–5230.
- GEFEN, A., MEGIDO-RAVID, M., ITZCHAK, Y. and ARCAN, M. (2002) Analysis of muscular fatigue and foot stability during high-heeled gait. *Gait Posture*, 15: 56–63.
- HAYASHI, S., TASAKA, Y., HAYASHI, N. and AKITA, Y. (2004) Development of smart polymer materials and its various applications. *Mitsubishi Heavy Industries Ltd, Technical Review*, 41: 1–3.
- HU, J. (2007a) Textiles of shape memory polymers, PCT 2007/070172, 25 June.
- HU, J. L. (2007b) *Shape Memory Polymers and Textiles*. Cambridge: Woodhead Publishing.
- HU, J., CHUNG, S. and LI, Y. (2007a) Characterization about the shape memory behaviour of woven fabrics. *Transactions of the Institute of Measurement and Control*, 29: 301–319.
- HU, J. L., DING, X. M. and TAO, X. M. (2002) Shape memory polymers and their applications to smart textile products. *Journal of China Textile University*, 19: 89–93.
- HU, J. L., MENG, Q. H., ZHU, Y., LU, J. and ZHUO, H. T. (2007c) Shape Memory Fibers Prepared by Wet, Reaction, Dry, Melt, and Electro Spinning. *US Patent Office*, Pat. No. 11907012.
- HU, J. L., MENG, Q. H., ZHU, Y., LV, J. and ZHUO, H. T. (2008b) Methods for Preparing Shape Memory Polyurethanes for Textile Products. *US Patent Office*, Pat. No. 61163483.
- HU, J., ZHU, Y., LU, J., YEUNG, L. Y. and YEUNG, K. W. (2007b) Uniqueness of shape memory fibers in comparison with existing man-made fibers. The 9th Asian Textile Conference. Federation of Asian Professional Textile Associations. Taiwan.
- HU, J., ZHU, Y. and LV, J. (2008a) Self Adjustable, Self Repairable Textiles with Shape Memory Fibers. *US Patent Office*, Pat. No. 61/136068.
- HUANG, W. M., LEE, C. W. and TEO, H. P. (2006) Thermomechanical behavior of a polyurethane shape memory polymer foam. *Journal of Intelligent Material Systems and Structures*, 17: 753–760.
- HUANG, W. M. and YANG, B. (2005) Water-driven programmable polyurethane shape memory polymer: demonstration and mechanism. *Applied Physics Letters*, 86: 114105.
- HYASHI, S. (1993) Properties and applications of polyurethane. *International Progress in Urethanes*, 6: 90–115.
- IGNATOVA, M., STARBOVA, K., MARKOVA, N., MANOLOVA, N. and RASHKOV, I. (2006) Electrospun nano-fibre mats with antibacterial properties from quaternised chitosan and poly (vinyl alcohol). *Carbohydrate Research*, 341: 2098–2107.

- ISHIDA, K. and YOSHIE, N. (2008) Two-way conversion between hard and soft properties of semicrystalline crosslinked polymer. *Macromolecules*, 41: 4753–4757.
- JEONG, H. M., AHN, B. K. and KIM, B. K. (2000) Temperature sensitive water vapour permeability and shape memory effect of polyurethane with crystalline reversible phase and hydrophilic segments. *Polymer International*, 49: 1714–1721.
- JIANG, H. Y., KELCH, S. and LENDLEIN, A. (2006) Polymers move in response to light. *Advanced Materials*, 18: 1471–1475.
- JUNG, Y. C., SO, H. H. and CHO, J. W. (2006) Water-responsive shape memory polyurethane block copolymer modified with polyhedral oligomeric silsesquioxane. *Journal of Macromolecular Science, Part B: Physics*, 45: 453–461.
- KOERNER, H., PRICE, G., PEARCE, N. A., ALEXANDER, M. and VAIA, R. A. (2004) Remotely actuated polymer nanocomposites – stress-recovery of carbon-nanotube-filled thermoplastic elastomers. *Natural Material*, 3: 115–120.
- KONGOLO, D. (2008) Luminescent Textiles, WIPO Patent Application WO/2008/148138.
- KRAUSE, S., DERSCH, R., WENDORFF, J. H. and FINKELMANN, H. (2007) Photocrosslinkable liquid crystal main-chain polymers: thin films and electrospinning. *Macromolecular Rapid Communication*, 28: 2062–2068.
- KUNZELMAN, J., CHUNG, T., MATHER, P. and WEDER, C. (2008) Shape memory polymers with built-in threshold temperature sensors. *Journal of Materials Chemistry*, 18: 1082–1086.
- LABS, X. (2010) Nitinol and Felt (test 6): the ‘Anus’ Machine Knit. Available at: <http://www.youtube.com/watch?v=gXu1sT2z5No> [accessed 4 January 2010].
- LAN, X., HUANG, W. M., LIU, N., PHEE, S. Y., LENG, J. S. and DU, S. Y. (2008) Improving the electrical conductivity by forming Ni powder chains in a shape-memory polymer filled with carbon black. *Proceedings of SPIE – The International Society for Optical Engineering*, vol. 6927, San Diego, CA, USA.
- LANGER, R. and TIRRELL, D. A. (2004) Designing materials for biology and medicine. *Nature*, 428: 487–492.
- LAROCHE, F. E. F. G., Fiset, M. and MANTOVANI, D. (2002) Shape memory materials for biomedical applications. *Advanced Engineering Materials*, 4: 91–104.
- LEE, S. and STARNER, T. (2008) Stop burdening your eyes: a wearable electro-tactile display. *Conference Information: 12th IEEE International Symposium on Wearable Computers*, 28 September–1 October, Pittsburgh, PA, pp. 115–116.
- LEENDERS, M. (2010) Shape Memory Textiles. Available at: <http://www.youtube.com/watch?v=HdRRy7hItgI> [accessed 15 February 2010].
- LENDLEIN, A. (2006) Blends of Shape Memory Polymers with Thermoplastic Polymers, PCT, PCT/EP2006/011420.
- LENDLEIN, A. and RIDDER, U. (2007) Method for Hair Treatment with Shape Memory Polymers. *US Patent Office*, Pat No. 2007/0088135 A1.
- LENG, J., LV, H., LIU, Y. and DU, S. (2008) Comment on ‘Water-driven programmable polyurethane shape memory polymer: demonstration and mechanism’ [*Applied Physics Letters* 86: 114105 (2005)]. *Applied Physics Letters*, 92: 206105-1-206105-2.
- LI, Y., K. (2007) *Evaluation of Shape Memory Fabrics*, MPhil thesis, Hong Kong Polytechnic University: Hongkong. p. 219.
- LI, Y., CHUNG, S., CHAN, L. and HU, J. L. (2004) Characterization of shape memory fabrics. *Textile Asia*, 35: 32–37.

- LIEM, H., YEUNG, L. Y. and HU, L. (2007) A prerequisite for the effective transfer of the shape-memory effect to cotton fibers. *Smart Materials and Structures*, 16: 748–753.
- LIM, K. Y., KIM, B. C. and YOON, K. J. (2002) Effect of structural characteristic on physical properties of copolyesters from poly(ethylene terephthalate) oligomer and polycaprolactone. *Journal of Polymer Science: Part B: Polymer Physics*, 40: 2552–2560.
- LIU, C., QIN, H. and MATHER, P. T. (2007a) Review of progress in shape-memory polymers. *Journal of Materials Chemistry*, 17: 1543–1558.
- LIU, X., HU, J., BABU, K. M. and WANG, S. (2008) Elasticity and shape memory effect of shape memory fabrics. *Textile Research Journal*, 78: 1048–1056.
- LIU, Y., CHUNG, A., HU, J. L. and LU, J. (2007b) Shape memory behavior of SMPU knitted fabric. *Journal of Zhejiang University Science A*, 8: 830–834.
- LIU, Y. Q., HU, J. L., ZHU, Y. and YANG, Z. H. (2005) Surface modification of cotton fabric by grafting of polyurethane. *Carbohydrate Polymers*, 62: 276–280.
- LV, H., LENG, J., LIU, Y. and DU, S. (2008) Shape-memory polymer in response to solution. *Advanced Engineering Materials*, 10: 592–595.
- MAKHOSAXANA, X. P., FILIPCEI, G. and ZRINYI, M. (2000) Preparation and responsive properties of magnetically soft poly(n-isopropylacrylamide) gels. *Macromolecules*, 33: 1716–1719.
- MARCO, D. and ECKHOUSE, S. (2006) Biodegradable Self-inflating Intra-gastric Implants for Curbing Appetite. *US Patent Office*, Pat. No. 0156248.
- MARKS, P. (2001) Shirt Rolls up Its Own Sleeves. Available at: <http://www.newscientist.com/article/dn1073-shirt-rolls-up-its-own-sleeves.html> [accessed 3 January 2010].
- MENG, Q. H. and HU, J. L. (2007) Study on poly(ϵ -caprolactone)-based shape memory copolymer fiber prepared by bulk polymerization and melt spinning. *Polymers for Advanced Technologies*. Published online, DOI: 10.1002/pat.985.
- MENG, Q., HU, J. L., SHEN, L., HU, Y. and HAN, J. (2009a) A smart hollow filament with thermal sensitive internal diameter. *Journal of Applied Polymer Science*, 113: 2440–2449.
- MENG, Q. H., HU, J. L. and YEUNG, L. Y. (2007a) An electro-active shape memory fibre by incorporating multi-walled carbon nanotubes. *Smart Materials and Structures*, 16: 830–836.
- MENG, Q. H., HU, J. L., ZHU, Y., LU, J. and LIU, Y. (2007b) Polycaprolactone-based shape memory segmented polyurethane fiber. *Journal of Applied Polymer Science*, 106: 2515–2523.
- MENG, Q., HU, J. L., ZHU, Y., LV, J. and LIU, B. (2009b) Biological evaluations of a smart shape memory fabric. *Textile Research Journal*, 79: 1522–1533.
- MONDAL, S. and HU, J. L. (2006) Structural characterization and mass transfer properties of nonporous-segmented polyurethane membrane: influence of the hydrophilic segment content and soft segment melting temperature. *Journal of Membrane Science*, 276: 16–22.
- MONDAL, S. and HU, J. L. (2007) A novel approach to excellent UV protecting cotton fabric with functionalized MWNT containing water vapor permeable PU coating. *Journal of Applied Polymer Science*, 103: 3370–3376.
- MONDAL, S., HU, J. L. and ZHU, Y. (2006) Free volume and water vapor permeability of dense segmented polyurethane membrane. *Journal of Membrane Science*, 280: 427–432.
- NAGAHAMA, K., UEDA, Y., OUCHI, T. and OHYA, Y. (2009) Biodegradable shape-memory polymers exhibiting sharp thermal transitions and controlled drug release. *Biomacromolecules*, 10: 1789–1794.

- OCLACIRO (2010) Oricalco Fabric – Thermal Shape Memory Textile. Available at: http://www.youtube.com/watch?v=_oGQz-eSIOQ [accessed 12 February 2010].
- PEPPAS, N. A. and KIM, B. (2006) Stimuli-sensitive protein delivery systems. *Journal of Drug Delivery Science and Technology*, 16: 11–18.
- QI, K., CHEN, X. and LIU, Y. (2007) Facile preparation of anatase/SiO₂ spherical nanocomposites and their application in self-cleaning textiles. *Journal of Materials Chemistry*, 17: 3504–3508.
- QIN, H. and MATHER, P. T. (2009) Combined one-way and two-way shape memory in a glass-forming nematic network. *Macromolecules*, 42: 273–280.
- SCHOLL (2010) Dr. Scholl's® Memory Fit® Work Customizing Insoles. Available at: <http://www.drscholls.com/drscholls/productSearch.do?method=doProductDetailsLookup&searchArg=53> [accessed 1 January 2010].
- SIEGAL, R. A. and FIRESTONE, B. A. (1988) PH-dependent equilibrium swelling properties of hydrophobic polyelectrolyte copolymer gels. *Macromolecules*, 21: 3254–3259.
- SMALL IV, W., WILSON, T. S., BENETT, W. J., LOGE, J. M. and MAITLAND, D. J. (2005) Laser-activated shape memory polymer intravascular thrombectomy device. *Optics Express*, 13: 8204–8213.
- SOROUSHIAN, P. (1997) Metal Matrix Materials Reinforced with Shape Memory Fibers for Enhanced Ductility and Energy Absorption Capacity, and Method of Manufacturing Same. *US Patent Office*, Pat. No. 6025080.
- STYLIOU, G. K. (2006) Engineering textile and clothing aesthetics using shape changing materials. In: Mattila, H. and Mattila, H. R. (eds.) *Intelligent Textiles and Clothing*. Cambridge: Woodhead Publishing, pp. 165–190.
- STYLIOU, G. K., CHAN, Y. Y. F., WAN, T., LAM, P. and TANG, S. (2005) Engineering textile aesthetics by shape and colour changing materials. 5th AUTEX World Textile Conference, Portoroz, Slovenia.
- STYLIOU, G. K. and WAN, T. (2007) Shape memory training for smart fabrics. *Transactions of the Institute of Measurement and Control*, 29: 321–336.
- TOBUSHI, H., HAYASHI, S., HOSHIO, K. and MIWA, N. (2006) Influence of strain-holding conditions on shape recovery and secondary-shape forming in polyurethane-shape memory polymer. *Smart Materials and Structures*, 15: 1033–1038.
- TOPOPKARAEV, V. A. and SOERENS, D. A. (2003) Methods of Making Humidity Activated Materials Having Shape-Memory. *US Patent Office*, Pat. No. 6627673.
- ULIJN, R. V., BIBI, N., JAYAWARNA, V., THORNTON, P. D., TODD, S. J., MART, R. J., SMITH, A. M. and GOUGH, J. E. (2007) Bioresponsive hydrogels. *Materials Today*, 10: 40–48.
- VAIA, R. (2005) Nanocomposites: remote-controlled actuators. *Nature Materials*, 4: 429–430.
- VILI, Y. Y. F. C. (2007) Investigating smart textiles based on shape memory materials. *Textile Research Journal*, 77: 290–300.
- WACHE, H. M., TARTAKOWSKA, D. J., HENTRICH, A. and WAGNER, M. H. (2004) Development of a polymer stent with shape memory effect as a drug delivery system. *Journal of Materials Science: Materials in Medicine*, 14: 109–112.
- WAN, T. and STYLIOU, G. K. (2004) Investigating shape memories technologies for SMART fabrics. 2nd International Textile Conference of the North India Section of the Textile Institute, New Delhi, India.
- WISCHKE, C., NEFFE, A. T., STEUER, S. and LENDLEIN, A. (2009) Evaluation of a degradable shape-memory polymer network as matrix for controlled drug release. *Journal of Controlled Release*, 138: 243–250.

- WU, M. H. and SCHETKY, L. M. (2000) Industrial applications for shape memory alloys. *Proceedings of the International Conference on Shape Memory and Superelastic Technologies*, Pacific Grove, California, pp. 171–182.
- XIE, T. and XIAO, X. (2008) Self-peeling reversible dry adhesive system. *Chemistry of Materials*, 20: 2866–2868.
- XSLABS (2010) Luttergill: Kinetic Skorpion Dress. Available at: <http://www.youtube.com/watch?v=uA4L9o2AwVY> [accessed 10 January 2010].
- YANG, B., HUANG, W. M., LI, C. and LI, L. (2006) Effects of moisture on the thermo-mechanical properties of a polyurethane shape memory polymer. *Polymer*, 47: 1348–1356.
- YANG, J. H., CHUN, B. C., CHUNG, Y. C., CHO, J. W. and CHO, B. G. (2004) Vibration control ability of multilayered composite material made of epoxy beam and polyurethane copolymer with shape memory effect. *Journal of Applied Polymer Science*, 94: 302–307.
- ZHU, Y., HU, J. L. and YEUNG, K. (2009) Effect of soft segment crystallization and hard segment physical crosslink on shape memory function in antibacterial segmented polyurethane ionomers. *Acta Biomaterialia*, 5: 3346–3357.
- ZHU, Y., HU, J. L., YEUNG, L. Y., LIU, Y., JI, F. L. and YEUNG, K. W. (2006) Development of shape memory polyurethane fiber with complete shape recoverability. *Smart Materials and Structures*, 15: 1385–1394.
- ZHUO, H., HU, J. L. and CHEN, S. (2008) Electrospun polyurethane nanofibres having shape memory effect. *Materials Letters*, 62: 2074–2076.

Thermo-regulating textiles with phase-change materials

S. MONDAL,

The University of Queensland, Australia

Abstract: Incorporation of phase-change material (PCM) in textiles is an attractive way to make thermo-regulating textiles. This chapter provides a review of PCM for textile applications. The chapter discusses thermal comfort, working principles of PCM, different types of PCMs, incorporation of micro-encapsulated PCMs in textiles and various applications of PCM incorporated textiles. The chapter concludes with a discussion of some of the challenges for PCMs in textile applications.

Key words: thermal comfort, thermal energy storage, phase-change materials, micro-encapsulation, smart textiles.

7.1 Introduction

Smart materials that can respond to external stimuli are now increasingly being applied in the manufacturing of innovative textile products. Garments made from a smart fabric whose functional properties adjust with changes in the external environment can provide superior protection to the wearer in extreme environmental conditions. Phase-change material (PCM) is one such smart material which has the ability to store and release energy in a certain temperature range [1]. Whenever the supply of or demand for energy does not change dependently with time, energy storage is required [2]. The thermal energy storage (TES) system bridges the time gap between energy requirements and energy use [3], and plays an important role in energy management of textile products to enhance thermal comfort [4]. TES by PCM to improve thermal performance of clothing during environmental temperature fluctuation is becoming an attractive option [5]. PCMs absorb energy in the heating cycle as phase change takes place from solid to liquid, and release energy to the environment in the phase-change range from liquid to solid during a reverse cooling process [6]. Incorporation of PCM in textiles to make thermo-regulated smart textiles is of growing interest to researchers. There are many situations where this concept could find applications such as all those professions where a person is affected by extreme changes of external temperature [7].

Wide ranges of PCMs are researched by scientists. However, PCM with a phase-change temperature range of 18–35°C will be most useful for making thermo-regulating textiles [5]. Selection of PCM for the textile substrate depends on the end application of textile materials. For underwear textiles, PCM with a phase-change temperature near skin temperature is appropriate. On the other hand, for lining material of a ski suit, a much lower phase-change temperature of PCM is required [8]. This chapter provides a review of the PCMs for applications in textile fields. Concepts of thermal comfort, clothing for cold environments, PCMs and thermo-physiological comfort are discussed here and different types of PCMs are presented. This is followed by an account of the incorporation of PCM in the textile substrates. Some of the applications of PCM incorporated textiles are introduced. Finally, the chapter concludes with a discussion of some of the challenges for PCMs in textile applications.

7.2 Concept of thermal comfort and clothing for cold environments

Thermal comfort or discomfort is defined as the mental satisfaction or dissatisfaction respectively with the thermal environment. Thermal dissatisfaction may be due to the warm or cool discomfort of the body which is expressed by the predicted mean vote (PMV) and predicted percentage of dissatisfied (PPD) indices. Thermal dissatisfaction may also be caused by local discomfort due to the unwanted cooling or heating of one particular part of the body [9]. Thermal comfort/discomfort engendered by textile materials in direct contact with the skin is a complex phenomenon and depends on the integration of the following groups of sensations: thermal (warm or cold), wetness and tactile (contact). Weather conditions (humidity, temperature, wind, etc.), levels of physical activity, the physical and physiological status of individuals, and the properties of textile materials all influence the level of perceived sensations [10]. The human body attempts to maintain a core body temperature around 37°C. The balance between the heat production by the body and loss of the same is known as the comfort factor. The body will be in a state of comfort when the body temperature is about 37°C and there is no perspiration on the skin surface [11]. For predicting or evaluating the thermal environment, clothing has an important role to play because it determines how much of the heat generated by the human body can be exchanged with the environment [12–13]. There are many studies that have investigated the relationship between clothing properties and thermal environment [14–17]. In a cold environment, thermal insulation is required in order to ensure that the body is sufficiently warm while resting. During extensive physical activity, body temperature increases with enhanced heat

production, and the body will perspire in order to withdraw energy from the body by evaporation of sweat. Overall thermal balance may be attained at numerous combinations of the thermal environmental parameters and clothing properties, even at high atmospheric humidity [18]. The transport of dry heat through textiles is a complex process involving conduction, convection and radiation. The dry heat loss, H_{dry} , from the skin can be calculated from the heat balance equation [19] as follows:

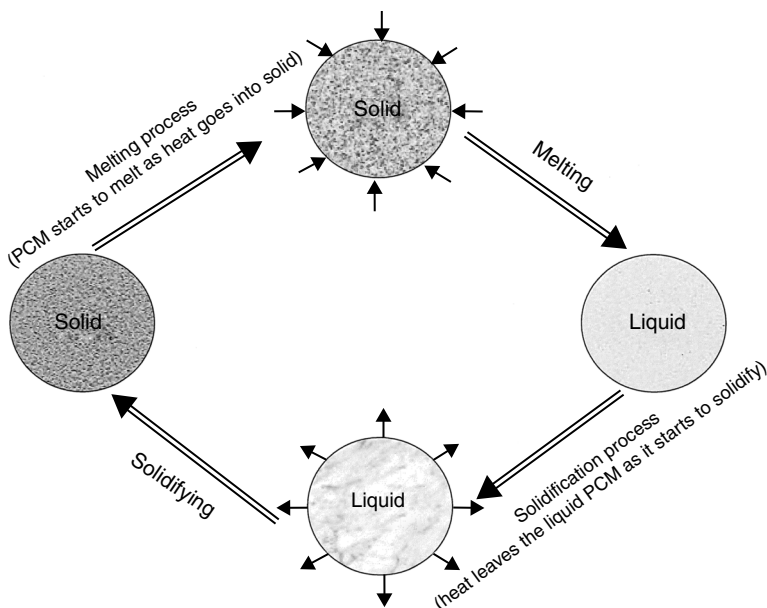
$$H_{\text{dry}} = M - W - C_{\text{res}} - E_{\text{res}} - E - S \quad [7.1]$$

where M is the metabolic rate, W is the external work, C_{res} is the convective respiratory heat loss, E_{res} is the evaporative respiratory heat loss, E is the evaporative heat loss from the skin and S is the change in body heat content. All values in equation [7.1] are expressed in $\text{W}\cdot\text{m}^{-2}$ [19]. A heat balance between the heat produced by human body with heat exchange between the body and the environment maintains the human body temperature [20]. Heat loss through respiration is only around 10% of the total heat loss from the body; therefore clothing plays an important role in the thermal sensations of the human body [21]. In addition to its thermal protection role, clothing also influences the metabolic rate, and therefore plays a prominent role in overall heat balance. Lee and Choi stated that the body's metabolic rate is lower with heavier clothing than with lighter clothing [14].

Heat loss through perspiration evaporation, and heat and water vapor flux through textiles are very important for the comfort of warm weather clothing. Perspiration is transformed into water vapor on the skin surface, and evaporation of moisture from the skin surface through clothing is extremely effective for the removal of body heat when the environmental temperature is greater than skin temperature. On the other hand, thermal insulation is one of the important factors for cold weather clothing. Besides insulation, cold weather clothing should ideally have three main features: it should be perspiration permeable, windproof and waterproof. Two types of fabrics are used in foul weather clothing, namely impermeable fabrics and breathable fabrics. An impermeable fabric is both wind- and waterproof but not perspiration permeable. In contrast, a breathable fabric meets all the features of foul weather clothing and it is perspiration permeable [22]. In cold environments, both general body cooling and local cooling have a negative affect on human work performance due to thermal discomfort and, in more extreme cases, as a result of cold injury. Most probably, the insulation of different body parts is influenced by skin temperatures [16]. Thus, to prevent cooling of the peripheral body parts, clothing insulation is very important for cold weather clothing.

7.3 How PCMs work

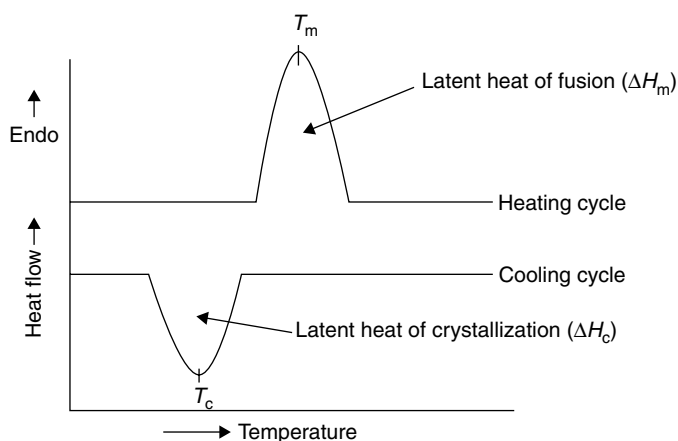
Generally, material may exist in three states: solid, liquid and gas. In the phase-change process, a material converts from one state to another and vice versa. Three kinds of phase change of PCM may occur: (a) solid to liquid, (b) liquid to gas and (c) solid to solid. Relatively few solid–solid PCMs have been identified for the TES system. Due to large volume changes during phase transformation, liquid–gas PCMs are usually not considered for practical applications. Solid–liquid PCMs are useful as TES materials, as they store relatively large quantities of heat over a narrow temperature range, without corresponding significant volume change [23, 24]. The modes of heat transfer are strongly dependent on the phase of the substances involved in the heat transfer processes [25]. For substances that are solid, conduction is the predominant mode of heat transfer. For liquids, convection heat transfer predominates, and for vapors convection and radiation are the primary modes of heat transfer. Heat is absorbed or released during the solid–liquid and vice versa phase-change process of PCMs (Fig. 7.1). This absorbed or released heat content is called latent heat. The latent heat storage PCM can store large amounts of heat with only a small temperature swing as compared to a sensible heat storage system [26]. Small temperature differences between storage and retrieval cycles, small unit sizes and



7.1 Schematic of phase-change cycles of phase-change material.

low weight per unit storage capacity are advantages of PCMs for the TES system [27].

PCMs exist in various forms in nature. The most common example of a PCM is the water which crystallizes as it changes from liquid to solid (ice) at 0°C . A phase change also occurs when water is heated to a temperature of 100°C when it converts to steam [6, 28]. The PCM, which can convert from solid to liquid and vice versa is used as latent heat storage material for the manufacturing of thermo-regulating textiles. Every material absorbs heat during a heating process while its temperature rises constantly. The heat stored in the material is released into the environment through a reverse cooling process. During the complete melting and crystallization process, the temperature of the PCM as well as its surrounding area remains almost constant [6]. During the solid–liquid phase-change process, the PCM absorbs large quantities of latent heat from the surrounding area, and during the reverse phase-change (liquid to solid) process the PCM releases heat to the surrounding area. Therefore, PCMs should be able to repeatedly convert between solid–liquid and vice versa phases to utilize their latent heat of fusion/crystallization to absorb, store and release heat during such phase conversion cycles. The high heat transfer during melting and crystallization processes without significant temperature change makes PCM an interesting candidate for making thermo-regulating textiles. The thermal performance of PCMs can be evaluated by differential scanning calorimetry (DSC) (Fig. 7.2). Simplicity, speed and economy in its sample requirements are the advantages of DSC. The main disadvantage of DSC is that the result obtained is not absolute and it provides relative results [29].



7.2 Schematic of heating and cooling cycles, and their corresponding thermal parameters of PCM in DSC technique.

7.4 Thermo-physiological comfort for PCM incorporated textiles

The thermal comfort provided by clothing primarily depends on the physical activity engaged in, and on the surrounding conditions, such as temperature, relative humidity and wind. The quantity of heat produced by human body depends heavily on the nature of the physical activity involved and can vary from 100 W while resting to over 1000 W during maximum physical activity [22]. The quality of insulation for a garment against cold is largely governed by the thickness and density of its component fabrics. Greater thickness and lower garment density improve insulation due to the air gaps between the garment layers. However, a garment made from a thick fabric will have greater weight, and the freedom of movement of the wearer will be restricted. People wearing heavy clothing in a cold climate need to adjust it frequently to cope with changes in activity and weather, which often causes thermal discomfort [30]. Constant discomfort while wearing such protective garments can lead to reduced work efficiency and the likelihood of accidents. To improve the thermal performance of textiles, clothing with thermo-regulating properties are widely used and based on the application of PCM in textile structure. PCM is a highly effective thermal storage system, which can be used to absorb heat released by the human body under excessive physical activities and stored energy by PCM can be released to keep the body warm when the body/surrounding temperature decreases [31]. The ability of the PCMs to change their physical state (solid to liquid or vice versa) within a certain temperature range makes them ideal for thermo-regulating textile applications. Suitable thermo-regulating properties of textiles depend on the PCM quantity applied to the active-wear garment with the level of physical activity and the duration of the garment use. PCM incorporated textile will be a dynamic and active thermo-responsive substance for some end applications [32].

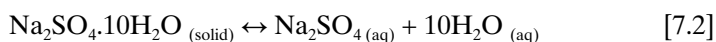
7.5 Different types of PCMs

A classical example of PCM is paraffin wax. Another common PCM is water. Higher hydrocarbons like hexadecane, octadecane, and so forth, have been extensively used as PCMs. Control of the melting point temperature and high latent heat are desirable for a good PCM, and the target temperature will depend on the end application [33]. PCMs can be classified into three major categories: (a) inorganic compounds, (b) organic compounds and (c) eutectic compounds of inorganic–inorganic, organic–organic or inorganic–organic. Salts, salt hydrates, metals and their alloys are some examples of inorganic PCM compounds, whereas paraffin waxes, polyethylene glycols (PEGs) and fatty acids are examples of organic PCMs [23, 34]. In most cases inorganic

PCMs are cheaper than the organic PCMs. However, reliable data and information of life span, stability, toxicity and corrosion of inorganic PCMs are often unavailable [34]. A brief account of the advantages and disadvantages of organic and inorganic PCMs are tabulated in Table 7.1. A wide spectrum of PCMs are available with different heat storage capacity and phase-change temperature as reported in Table 7.2.

7.5.1 Hydrated salts

Hydrated salts are attractive PCMs due to their high volumetric storage density ($\sim 350 \text{ MJ/m}^3$), relatively high thermal conductivity ($\sim 0.5 \text{ W/m} \cdot ^\circ\text{C}$) and relatively low cost as compared to the organic PCMs [35, 43–44]. Hydrated inorganic salts with ‘ n ’ molecules of water usually has a heat-absorbing and heat-releasing temperature interval of about $20\text{--}40^\circ\text{C}$, which can be used for the manufacturing of thermo-regulated textiles. Hydrated sodium sulfate produces or absorbs heat by the following chemical reaction between the decahydrate crystal and the water solution [45]:



Melting and super cooling of most inorganic salt hydrates applied to fabrics withstands several heating/cooling cycles. Salt hydrate PCMs have low material costs, but high packing costs [35].

7.5.2 Long chain hydrocarbons

Hydrophobic linear hydrocarbon is becoming more and more attractive as a PCM (by-product from oil refining). This material has a general

Table 7.1 Advantages and disadvantages of organic and inorganic PCMs [35]

Type of PCMs	Advantages	Disadvantages
Organic	Most organic PCMs are non-corrosive, chemically stable, high latent heat per unit weight, low vapor pressure, exhibit little or no subcooling	Low thermal conductivity, high changes in volume as compared to inorganic PCM on phase-change cycles, flammability
Inorganic	High latent heat per unit volume, high thermal conductivity, non-flammable, low in cost as compared to organic PCMs	Corrosive to most metal, suffer from decomposition and subcooling, higher packing cost

Table 7.2 Latent heat storage materials and their thermal properties

Materials	Melting temperature (°C)	Latent heat (kJ/kg)	References
<i>Inorganic</i>			
Salt hydrates			
Na ₂ SO ₄ ·10H ₂ O	32.4	254	35
Mn(NO ₃) ₂ ·6H ₂ O	26	125.9	36
CaCl ₂ ·6H ₂ O	29	187	37
MgCl ₂ ·6H ₂ O	117.2	168.6	36
AlCl ₃	192	280	23
Si	1415	1654	23
<i>Organic</i>			
Paraffin (C16–C18)	21.2	152	36
PEG (600 g.mol ⁻¹)	21.6/27.7	106.5	32
Stearic acid	54–56	186.5	38
Palmitic acid (97%)	61	203.4	39
Lauric acid	40–43	167–171	40
Butyl stearate	19	200	41
Dimethyl sebacate	21	135	41
<i>Eutectics</i>			
Inorganic–inorganic			
66.6% CaCl ₂ ·6H ₂ O + 33.3% MgCl ₂ ·6H ₂ O	25.2	127	36
58.7% Mg(NO ₃) ₂ ·6H ₂ O + 41.3% MgCl ₂ ·6H ₂ O	59.2	132.2	36
Organic–organic			
Capric–lauric acid	18	140.8	37
Lauric–palmitic acid	32.7	145	42
Lauric–stearic acid	34	150	42
Palmitic–stearic acid	51	160	42
Organic–inorganic			
66.6% Urea + 33.4% NH ₄ Br	76.2	161	36

chemical formula of C_nH_{2n+2}. The melting and crystallization temperature of *n*-alkane depends on the number (odd or even) of carbon atoms in its molecular structure [46–47]. In solid state, pure *n*-alkanes form a single crystal or four crystal system, namely hexagonal (α -phase), rhombic (β -phase), monoclinic (γ -phase) and triclinic (δ -phase), and the system depends on the temperature and the number of carbon atoms in its molecular structure [48]. The melting temperature of hydrocarbon increases with the number of carbon atoms (*n*) in its molecular structure (Table 7.3). A wide range of latent heats, melting points, densities and specific heat of *n*-alkanes offers a good choice for low-temperature TES applications [52].

Table 7.3 Thermal properties of linear hydrocarbons as PCM

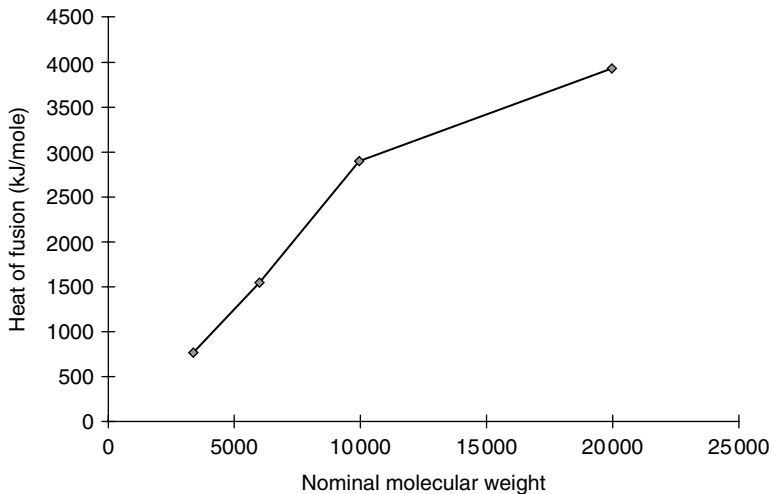
Hydrocarbons	No. of C atoms (<i>n</i>)	Melting temperature (°C)	Latent heat (kJ/kg)	References
n-Tetradecane	14	5.5	215	49
n-Pentadecane	15	9.6	168	50
n-Hexadecane	16	22	185.3	32
n-Heptadecane	17	25	176.4	51
n-Octadecane	18	27.5	241.4	37
n-Nonadecane	19	34.4	177.6	51
n-Eicosane	20	36.4	248	37

7.5.3 Polyethylene glycol

The repeating unit of PEG is oxyethylene ($-\text{OCH}_2\text{CH}_2-$), with either end of the chain containing a hydroxyl group. These water-soluble semi-crystalline polymers are another important candidate of PCMs for making thermo-regulating textiles. The melting temperature of PEG is proportional to the molecular weight, when its molecular weight is lower than 20 000. Its melting point temperature is in the range of 35–63°C when its molecular weight varies from 1000 to 20 000 [7, 53]. The heat of fusion also increases with increasing molecular weight of PEG (Fig. 7.3) [53]. Analysis of the molecular weight of PEG on its melting point and heat of fusion revealed that there is an increased tendency for higher molecular weight PEGs to form in the crystalline phase due to their lower segmental mobility and more convenient geometrical alignment. In the cooling cycle, a higher molecular weight PEG causes an increase in the solidification temperature and heat of crystallization. The advantage of using PEG blends as compared to its pure form is related to the opportunity of changing the phase transition temperature range and heat content associated with melting/crystallization cycles [54].

7.5.4 Others

Melting temperatures of fatty acids (capric, lauric, palmitic and stearic) are in the range of 30–65°C, and their heat of fusion is in the range of approximately 153–182 kJ/kg as reported by Feldman *et al.* [42]. The mixture of 65 mol% capric acid and 35 mol% lauric acid (C–L acid) having a melting temperature of 18°C can be used as potential thermal storage material for textile applications [42]. Polyethylene paraffin compound (PPC) which consists of paraffin as a dispersed PCM and a high density polyethylene



7.3 Influence of molecular weight on heat of fusion of PEG [53].

(HDPE) as a supporting material is reported as a stable PCM. The melting temperatures and latent heat of fusion for composite PCMs are 37.8–55.7°C, and 147.6–162.2 kJ/kg respectively [55]. A new PCM for low-temperature heat storage which consists of a stable mixture of water with water-soluble polymerized and cross-linked monomer such as acrylamide is described by Royon *et al.* [56]. The melting and thawing temperature of this new PCM is 0°C and latent heat is 292 kJ/kg [56].

7.6 Incorporation of PCM in textile structure

One of the major disadvantages of the use of latent heat storage materials is the useful life of a PCM's container system and the number of cycles it can withstand before degradation of its functional properties [35]. Before application of PCM on the textile substrate, PCMs need to be kept in a very small container to protect them while in a liquid state. The microcapsules should be resistant to mechanical action, heat and most types of chemicals. Effective microencapsulation of PCM is defined by particle size, thickness of shell wall, thermal capacity and conductivity, durability, and so forth [32]. It is important to retain as high enthalpy as possible for the microcapsule, whereas the microcapsules should not coalesce during thermal cycles of melting and crystallization [57]. Therefore, a higher core to shell ratio is required to improve the thermo-regulating efficiency of PCM on textiles substrate [58]. In most cases, these microcapsules possess approximate diameters of around 40 µm.

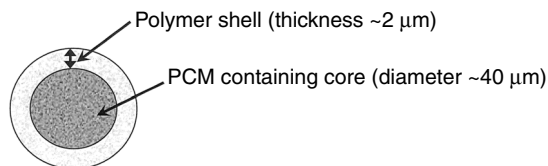
7.6.1 Microencapsulation of PCMs

Microencapsulated PCMs (MicroPCMs) are colloidal particles composed of a protective polymer shell and one or more PCMs in the core [8, 59–61]. Encapsulation is one of the most important parameters for the effective utilization of PCM, and has a significant influence on the formation of capsules and thermo-physics performance [62]. Microencapsulation is opening up new market opportunities for performance textiles. In microencapsulation, tiny particles (small particle with few micrometer) of solids or liquids are surrounded by a coating (Fig. 7.4). The microcapsules are produced by depositing a thin polymer coating on small solid particles or liquid droplets, or on dispersions of solids in liquids [63].

Without encapsulation, the following major problems may be encountered for PCMs in textile application:

- (a) diffusion of low viscous PCM in its liquid state from the surface and subsequent spreading of PCM on the textile substrate;
- (b) changes of PCM properties, for example alteration of the number of hydrates in the salt hydrate PCMs;
- (c) chances of wash out of water-soluble PCM (for example PEG) during washing of PCM treated garments.

With PCM microencapsulation, the ultimate aim is not only to make PCMs easier and safer to handle – but also to reduce reactivity, to improve thermal properties by increasing the heat transfer area and permit the core material to withstand frequent changes in the volume of the storage during the phase-change cycles [35, 64–65]. The solid–liquid and vice versa phase-change temperature and the latent heat associated with phase changes are strongly dependent on the encapsulation ratio, and influence the microcapsules' practical applications [5]. Physical or chemical techniques may be employed to prepare microencapsulation production of PCM. Physical methods include mainly spray drying or centrifugal and fluidized bed processes which are not able to prepare microcapsules smaller than 100 μm [32]. Many chemical methods are developed for microencapsulation of



7.4 Schematic of core-shell microencapsulation of PCM.

PCM, including interfacial polymerization [66], suspension polymerization [67], emulsion method [59], *in situ* polycondensation [66, 68] and complex coacervation [65]. In a recent study, nanoencapsulation of PCMs using ultrasonic technique and mini-emulsion *in situ* polymerization have been reported by Fang *et al.* [62]. The core material is made into droplets and the capsule shell reactive monomers polymerize on the surface of the droplets. When the initially formed oligomers are insoluble at the interface of the droplets, they grow, and a thin monolayer membrane forms around the droplets. The polymerization leads the monolayer membrane to become a microscopic shell around the PCM droplets [59]. Polyurea, polyurethane (PU), polyester, polyamide, polyethylene and amine resin can be used as the shell materials for PCMs.

7.6.2 Incorporation of PCM in textiles

Coating

PCMs can be incorporated into the textile structure by coating application. A typical coating composition includes wetted microspheres containing PCMs dispersed throughout the polymer binder, surfactant, dispersant, anti-foaming agent and thickener. In order to prepare the coating composition, microsphere containing PCMs can be wetted and dispersed in a dispersion of water solution containing surfactant, dispersant, antifoaming agent and polymer binder such as PU or acrylic mixture [69]. The coating paste can then be applied to the textile substrate by a suitable coating method. There are various available coating methods, including knife-over-roll, knife-over-air, pad-dry-cure, gravure, dip coating, transfer coating, and so forth [7].

Lamination

In order to improve the thermo-physiological wear comfort of non-woven protective garments, PCM could be incorporated into the thin polymer film and applied to the inner side of the fabric system by lamination [31]. The quality of lamination primarily depends on the strength of adhesion of films to the textile substrate, which may be lost due to mechanical and/or extreme environmental conditions [70]. PCM laminated textile can be applied in chemical protective suits. Beside chemical protective suits the PCM laminates can also improve the thermo-physiological wearing comfort of other protective garments made of non-wovens such as surgical gowns, uniforms or garments worn in clean rooms [31]. Prior to the lamination, PCM microcapsules can be mixed into a water-blown PU foam mixture. An excellent honeycomb structure is formed during water evaporation. Still air entrapped in the honeycomb structure increases the passive insulation which is an added advantage of the PCM-PU foam laminated system [4].

Fiber technology

MicroPCM can be incorporated into the textile fibers. Micro PCM can be added to the polymer solution before the spinning process starts. The PCM incorporated fibers are able to absorb heat, and store this heat for long periods of time [71]. The composition and properties of sheath/core composite polypropylene fiber non-wovens with different PCM contents in the core have been investigated by Zhang *et al.* The PCM content in the fiber and sheath/core ratio affect the temperature-regulating capability of the fibers [72]. A novel method of sheath–core photo-thermal converted thermo-regulated fibers by using the fiber-forming polymer containing photo-thermal conversion ceramic as sheath and the fiber-forming polymer containing micro PCMs as core is reported by Shi *et al.* Photo-thermal converted and thermo-regulated fibers have better temperature-regulating capabilities when compared with the control one [73].

Others

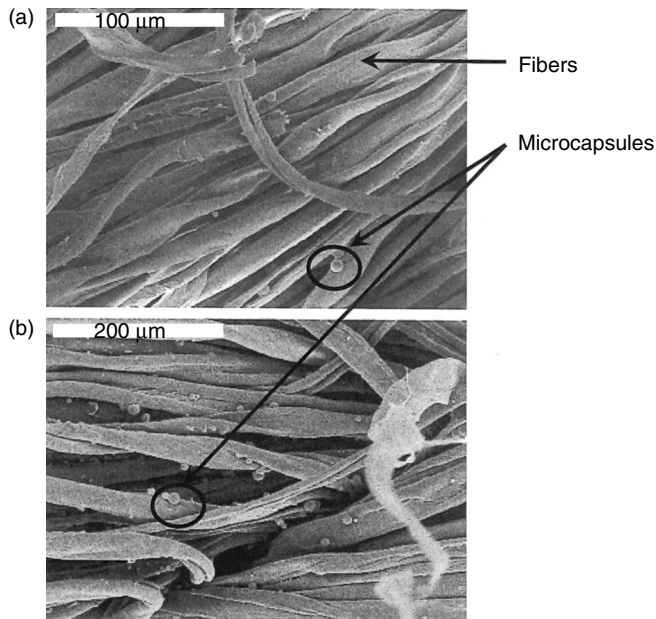
Micro PCMs can be applied on the textile substrate by impregnation or by the exhaustion method with acrylic resin. Treated fabric can then be heat-treated in order to fix the microcapsules on the textile substrate. Significant difference in the number of microcapsules remaining on the fabric was observed by different methods. The number of microcapsules existing on the fabric is higher for the impregnation process than for bath exhaustion (Fig. 7.5) [74]. Onder *et al.* encapsulated PCM by complex coacervation, and 2.5–4.5 times enhancement of energy absorption capacities of the coacervate added fabrics were observed [75].

7.7 Applications of PCM incorporated textiles

PCM incorporated textiles create clothing that keeps the wearer at a comfortable temperature, even in extreme weather conditions, by solid–liquid and vice versa phase-change cycles. PCM incorporated textiles have been used in space, medical, insulation, protective clothing, automotive textile and many more applications [7]. A brief account of the application of PCM incorporated textiles is given in the following paragraphs.

7.7.1 Aerospace textiles

PCMs were first developed in textiles for use in space suits and gloves to protect astronauts from temperature fluctuations while working in space [76]. Phase-change material incorporated textiles keep astronauts comfortable in space due to their thermo-regulating properties [7].



7.5 Scanning electron micrographs of cotton fabrics with microcapsules: (a) applied by bath exhaustion and (b) applied by impregnation method (Reproduced with permission from P. Monllor, M. A. Bonet and F. Cases, Characterization of the behaviour of flavour microcapsules in cotton fabrics. *European Polymer Journal* 43 (2007): 2481–2490 © 2007 Elsevier Ltd [74]).

7.7.2 Active-wear clothing

From the original applications in space, PCMs are now increasingly used in consumer apparel products. The development of PCM technology has made it possible to create fabrics to maintain comfortable temperatures for the wearer without adding significant mass to the bulk of the garment [77]. Active wear needs to provide a thermal balance between the heat generated by the body and the heat released into the environment while engaged in a sports activity to reduce thermal stress. PCM incorporated active wear, lifestyle apparel and outdoor sports apparel can provide an active thermal insulation effect acting in addition to the passive thermal insulation effect of the garment system [78]. Excessive body heat from the wearer can be absorbed by the PCM incorporated apparel during physical activity and released during periods of rest between activities as less heat is generated to keep the human body in a comfortable state. The popularity of cold winter sports such as alpine climbing, ice climbing and recreational skiing has increased the demand for textiles which keep the wearer dry, warm and comfortable [77].

7.7.3 Automotive textiles

Micro PCMs can be applicable in automobile textiles such as seat covers. Paraffin PCM is used in automobile textile applications due to the high capacity of its heat storage capability, low toxicity, lack of hygroscopic properties and low cost, and the target temperature range can be obtained by blending. Application of PCM incorporated textiles in car interiors and seat covers can provide superior thermal control to the passengers [7].

7.7.4 Medical textiles

PCMs interact with the microclimate around the human body, and respond to the fluctuations of temperature which may be caused by changes in physical activity levels and external environment changes [7]. Therefore, the textiles treated with PCM microcapsules have potential applications in surgical apparel, bedding materials, bandages and other medical textiles products to regulate patient temperatures in intensive care units [79].

7.7.5 Other areas in textiles

PCM incorporated fabrics can also be applicable in bedding accessories such as quilts, pillows, bed sheets and mattress covers. PCM incorporated textiles could be used to actively control temperature in bed by absorption of body heat (to cool down) and the release of stored energy (to warm up) when required. The PCMs are also used in footwear, especially in ski boots, mountaineering boots, racing drivers' boots, and so forth [80]. Helmets [81], fishing waders and firefighters' suits are some other examples of potential application of PCMs in the textile field.

7.8 Challenges of PCM in textiles

PCMs found in today's consumer textile products were originally developed to protect astronauts from extreme temperature fluctuations while working in space [7, 76]. There are many challenges facing the use of these smart materials in consumer apparel applications. The use of these interesting materials and their integration into garments requires the development of new types of testing methods and standards. One problem for this kind of smart material is probably its low thermal conductivity [82–86], for example paraffin PCM has thermal conductivity of 0.22 W/m.K as compared to 2–90 W/m.K for graphite powder [85]. Low thermal conductivity decreases the rate of heat storage and release of PCM during the melting and crystallization processes respectively [85]. Hence, thermal conductivity enhancement of core PCM microcapsules and their shell wall may be needed in

order to obtain fast response properties of these smart materials with environmental temperature changes. Furthermore, effective microencapsulation of PCM (such as control of size, stability and shell wall thickness of microcapsules), mechanical properties, durability or functionality of developed PCM incorporated textiles in repeated cycles under various conditions, and flammability of organic PCM should also be evaluated. More research in these areas will offer opportunities for material scientists to make PCM ideal for thermo-regulating textiles.

7.9 Acknowledgement

The author would like to acknowledge Elsevier Ltd for providing the required permission to reproduce Fig. 7.5.

7.10 References

1. LI, W.-D. and DING, E.-Y., Preparation and characterization of cross-linking PEG/MDI/PE copolymer as solid-solid phase change heat storage material. *Solar Energy Materials & Solar Cells*, 91 (2007): 764–768.
2. KÜRKÜ, A., Thermal performance of a tapered store containing tubes of phase change material: cooling cycle. *Energy Conversion and Management*, 38(4) (1997): 333–340.
3. HE, B. and SETTERWALL, F., Technical grade paraffin waxes as phase change materials for cool thermal storage and cool storage systems capital cost estimation. *Energy Conversion and Management*, 43 (2002): 1709–1723.
4. SARIER, N. and ONDER, E., Thermal characteristics of polyurethane foams incorporated with phase change materials. *Thermochimica Acta*, 454 (2007): 90–98.
5. SALAÜN, F., DEVAUX, E., BOURBIGOT, S. and RUMEAU, P., Development of phase change materials in clothing. Part I: Formulation of microencapsulated phase change. *Textile Research Journal*, 80(3) (2010): 195–205.
6. BAJAJ, P., Thermally sensitive materials. In: TAO, X. M. (ed.) *Smart Fibres, Fabrics, and Clothing*. Cambridge: Woodhead Publishing 2001, pp. 58–82.
7. MONDAL, S., Phase change materials for smart textiles – an overview. *Applied Thermal Engineering*, 28 (2008): 1536–1550 (and references therein).
8. SHIN, Y., YOO, D.-H and SON, K., Development of thermoregulating textile materials with microencapsulated phase change materials (PCM). IV. Performance properties and hand of fabrics treated with PCM microcapsules. *Journal of Applied Polymer Science*, 97 (2005): 910–915.
9. FANGER, P. O., Thermal environment – human requirements. *The Environmentalist*, 6(4) (1986): 275–278 (and references therein).
10. CURTEZA, A., FARIMA, D., MACOVEI, L. and FLOREA, A., Method of subjective evaluation of the clothing comfort. *ITC & DC: 4th International Textile Clothing and Design, Conference, Book of Proceedings – Magic World of Textiles* (ISBN: 978-953-7105-26-6). University of Zagreb, Croatia, 2008, pp. 736–741.
11. SEN, A. K., *Coated Textiles: Principle and Applications*, tech. ed. J. Damewood. Lancaster, PA: Technomic Publishing Co., 2001, pp. 133–154.

12. CARLI, M. D., OLESEN, B. W., ZARRELLA, A. and ZECCHIN, R., People's clothing behavior according to external weather and indoor environment. *Building and Environment*, 42 (2007): 3965–3973.
13. SALLOUM, M., GHADDAR, N. and GHALI, K., A new transient bioheat model of the human body and its integration to clothing models. *International Journal of Thermal Sciences*, 46 (2007): 371–384.
14. LEE, J.-Y. and CHOI, J.-W., Influences of clothing types on metabolic, thermal and subjective responses in a cool environment. *Journal of Thermal Biology*, 29 (2004): 221–229.
15. KACZMARCZYK, J., MELIKOV, A. and FANGER, P. O., Human response to personalized ventilation and mixing ventilation. *Indoor Air*, 14 (Suppl 8) (2004): 17–29.
16. GAVHED, D. C. E. and HOLMÉR, I., Thermal responses at three low ambient temperatures: validation of the duration limited exposure index. *International Journal of Industrial Ergonomics*, 21 (1998): 465–474.
17. FAN, J. T. and TSANG, H. W. K., Effect of clothing thermal properties on the thermal comfort sensation during active sports. *Textile Research Journal*, 78(2) (2008): 111–118.
18. TOFTUM, J., JØRGENSEN, A. S. and FANGER, P. O., Upper limits of air humidity for preventing warm respiratory discomfort. *Energy and Buildings*, 28(1) (1998): 15–23.
19. NIELSEN, R., OLESEN, B. W. and FANGER, P. O., Effect of physical-activity and air velocity on the thermal insulation of clothing. *Ergonomics*, 28(12) (1985): 1617–1631.
20. WANG, S. X., LI, Y., HU, J. Y., TOKURA, H. and SONG, Q. W., Effect of phase-change material on energy consumption of intelligent thermal-protective clothing. *Polymer Testing*, 25 (2006): 580–587.
21. FANGER, P. O., Human requirements in future air-conditioned environments. *International Journal of Refrigeration*, 24 (2001): 148–153.
22. HOLMES, D. A., Performance characteristics of waterproof breathable fabrics. *Journal of Industrial Textiles*, 29(4) (2000): 306–316.
23. HASNAIN, S. M., Review on sustainable thermal energy storage technologies, part 1: heat storage materials and techniques. *Energy Conversion and Management*, 39(11) (1998): 1127–1138 (and references therein).
24. HASNAIN, S. M. and ALABBADI, N. M., Need for thermal-storage air-conditioning in Saudi Arabia. *Applied Energy*, 65(1–4) (2000): 153–164.
25. ROLLE, K. C., *Heat and Mass Transfer*. Englewood Cliffs, NJ: Prentice-Hall 2000, pp. 496–547.
26. LAMBERG, P., Approximate analytical model for two-phase solidification problem in a finned phase-change material storage. *Applied Energy*, 77 (2004): 131–152.
27. EL-DESSOUKY, H. and AL-JUWAYHEL, F., Effectiveness of a thermal energy storage system using phase-change materials. *Energy Conversion and Management*, 38(6) (1997): 601–617.
28. PAUSE, B., Textiles with improved thermal capabilities through the application of phase change material (PCM) microcapsules. *Melliand Textilberichte*, 81(9) (2000): E179–E180 and 753–754.
29. HE, B., MARTIN, V. and SETTERWALL, F., Phase transition temperature ranges and storage density of paraffin wax phase change materials. *Energy*, 29 (2004): 1785–1804.

30. BUDD, G. M., Work in cold environments: cold stress and cold adaptation. *Journal of Thermal Biology*, 18(5/6) (1993): 629–631.
31. PAUSE, B., Nonwoven protective garments with thermo-regulating properties. *Asian Textile Journal*, 13(4) (2004): 62–64.
32. SARIER, N. and ONDER, E., The manufacture of microencapsulated phase change materials suitable for the design of thermally enhanced fabrics. *Thermochimica Acta*, 452 (2007): 149–160.
33. SUPPES, G. J., GOFF, M. J. and LOPES, S., Latent heat characteristics of fatty acid derivatives pursuant phase change material applications. *Chemical Engineering Science*, 58 (2003): 1751–1763.
34. NAGANO, K., MOCHIDA, T., TAKEDA, S., DOMAŃSKI, R. and REBOW, M., Thermal characteristics of manganese (II) nitrate hexahydrate as a phase change material for cooling systems. *Applied Thermal Engineering*, 23 (2003): 229–241.
35. FARID, M. M., KHUDHAIR, A. M., RAZACK, S. A. K. and AL-HALLAJ, S., A review on phase change energy storage: materials and applications. *Energy Conversion and Management*, 45 (2004): 1597–1615 (and references therein).
36. DEMIRBAS, M. F., Thermal energy storage and phase change materials: an overview. *Energy Sources, Part B*, 1 (2006): 85–95.
37. VEERAPPAN, M., KALAISELVAM, S., INIYAN, S. and GOIC, R., Phase change characteristic study of spherical PCMs in solar energy storage. *Solar Energy*, 83(8) (2009): 1245–1252.
38. SARI, A. and KAYGUSUZ, K., Thermal energy storage system using stearic acid as a phase change material. *Solar Energy*, 71(6) (2001): 365–376.
39. SARI, A. and KAYGUSUZ, K., Thermal performance of palmitic acid as a phase change energy storage material. *Energy Conversion and Management*, 43(6) (2002): 863–876.
40. ABHAT, A., Low temperature latent heat thermal energy storage: Heat storage materials. *Solar Energy*, 30(4) (1983): 313–332.
41. FELDMAN, D., SHAPIRO, M. M. and BANU, D., Organic phase change materials for thermal energy storage. *Solar Energy Materials*, 13 (1986): 1–10.
42. FELDMAN, D., SHAPIRO, M. M., BANU, D. and FUKS, C. J., Fatty acids and their mixtures as phase-change materials for thermal energy storage. *Solar Energy Materials*, 18 (1989): 201–216.
43. BISWAS, D. R., Thermal-energy storage using sodium sulphate decahydrate and water. *Solar Energy*, 19(1) (1977): 99–100.
44. MARKS, S., An investigation of the thermal energy storage capacity of Glauber salt with respect to thermal cycling. *Solar Energy*, 25(3) (1980): 255–258.
45. SAITO, A., OKAWA, S., SHINTANI, T. and IWAMOTO, R., On the heat removal characteristics and the analytical model of a thermal energy storage capsule using gelled Glauber's salt as the PCM. *International Journal of Heat and Mass Transfer*, 44 (2001): 4693–4701.
46. ZHANG, X.-X., FAN, Y.-F., TAO, X.-M. and YICK, K.-L., Crystallization and prevention of supercooling of microencapsulated n-alkanes. *Journal of Colloid and Interface Science*, 281 (2005): 299–306.
47. MONTENEGRO, R. and LANDFESTER, K., Metastable and stable morphologies during crystallization of alkanes in miniemulsion droplets. *Langmuir*, 19(15) (2003): 5996–6003.
48. HE, B., MARTIN, V. and SETTERWALL, F., Liquid–solid phase equilibrium study of tetradecane and hexadecane binary mixtures as phase change materials

- (PCMs) for comfort cooling storage. *Fluid Phase Equilibria*, 212 (2003): 97–109 (and references therein).
49. ALVARADO, J. L., MARSH, C., SOHN, C., VILCEUS, M., HOCK, V., PHETTEPLACE, G. and NEWELL, T., Characterization of supercooling suppression of microencapsulated phase change material by using DSC. *Journal of Thermal Analysis and Calorimetry*, 86(2) (2006): 505–509.
 50. DIMAANO, M. N. R. and WATANABE, T., The capric-lauric acid and pentadecane combination as phase change material for cooling applications. *Applied Thermal Engineering*, 22(4) (2002): 365–377 (and references therein).
 51. PAUSE, B., Building conditioning technique using phase change materials. US Patent 6230444, 2001.
 52. HIMRAN, S., SUWONO, A. and MANSOORI, G. A., Characterization of alkanes and paraffin waxes for application as phase change energy storage medium. *Energy Sources*, 16(1) (1994): 117–128.
 53. CRAIG, D. Q. M. and NEWTON, J. M., Characterization of polyethylene glycols using differential scanning calorimetry. *International Journal of Pharmaceutics*, 74 (1991): 33–41.
 54. PIELICHOWSKI, K. and FLEJTUCH, K., Differential scanning calorimetry studies on poly(ethylene glycol) with different molecular weights for thermal energy storage materials. *Polymers for Advanced Technologies*, 13(10–12) (2002): 690–696.
 55. SARI, A., Form-stable paraffin/high density polyethylene composites as solid-liquid phase change material for thermal energy storage: preparation and thermal properties. *Energy Conversion and Management*, 45(13–14) (2004): 2033–2042.
 56. ROYON, L., GUIFFANT, G. and FLAUD, P., Investigation of heat transfer in a polymeric phase change material for low level heat storage. *Energy Conversion and Management*, 38(6) (1997): 517–524.
 57. JIN, Z., WANG, Y., LIU, J. and YANG, Z., Synthesis and properties of paraffin capsules as phase change materials. *Polymer*, 49 (2008): 2903–2910.
 58. SHIN, Y., YOO, D.-II. and SON, K., Development of thermoregulating textile materials with microencapsulated phase change materials (PCM). II. Preparation and application of PCM microcapsules. *Journal of Applied Polymer Science*, 96 (2005): 2005–2010.
 59. CHO, J.-S., KWON, A. and CHO, C.-G., Microencapsulation of octadecane as a phase-change material by interfacial polymerization in an emulsion system. *Colloid and Polymer Science*, 280(3) (2002): 260–266.
 60. BOH, B., KNEZ, E. and STARESINIC, M., Microencapsulation of higher hydrocarbon phase change materials by in situ polymerization. *Journal of Microencapsulation*, 22(7) (2005): 715–735.
 61. SANCHEZ-SILVA, L., CARMONA, M., DE LUCAS, A., SANCHEZ, P., RODRIGUEZ, J. F., Scale-up of a suspension-like polymerization process for the microencapsulation of phase change materials. *Journal of Microencapsulation* 27(7)(2010): 583–593.
 62. FANG, Y., KUANG, S., GAO, X. and ZHANG, Z., Preparation of nanoencapsulated phase change material as latent functionally thermal fluid. *Journal of Physics D: Applied Physics*, 42(3) (2009): Article Number: 035407 (8 pp.).
 63. ANONYMOUS, Microencapsulation: for enhanced textile performance, *Performance Apparel Markets*, 12 (2005): 21–39 (abstract through Elsevier Scopus).

64. HAWLADER, M. N. A., UDDIN, M. S. and KHIN, M. M., Microencapsulated PCM thermal-energy storage system. *Applied Energy*, 74(1–2) (2003): 195–202.
65. OZONUR, Y., MAZMAN, M., PAKSOY, H. O. and EVLIYA, H., Microencapsulation of coco fatty acid mixture for thermal energy storage with phase change material. *International Journal of Energy Research*, 30(10) (2006): 741–749.
66. CHEN, L., XU, L. L., SHANG, H. B. and ZHANG, Z. B., Microencapsulation of butyl stearate as a phase change material by interfacial polycondensation in a polyurea system. *Energy Conversion and Management*, 50(3) (2009): 723–729.
67. AI, Y., JIN, Y., SUN, J. and WEI, D. Q., Microencapsulation of n-hexadecane as phase change material by suspension polymerization. *E-Polymers* (2007): Article Number: 098.
68. ZOU, G. L., LAN, X. Z., TAN, Z. C., SUN, L. X. and ZHANG, T., Microencapsulation of n-hexadecane as a phase change material in polyurea. *ACTA Physico-Chimica Sinica*, 20(1) (2004): 90–93.
69. ZUCKERMAN, J. L., PUSHAW, R. J., PERRY, B. T. and WYNER, D. M., Fabric coating containing energy absorbing phase change material and method of manufacturing same (2003), US Patent 6514362.
70. HOLME, I., Innovative coating and lamination. *International Dyer*, 193(2) (2008): 11–12 and 14 (abstract through Elsevier Scopus).
71. NEW FIBERS AS TEMPERATURE-CONTROLLED HEAT-FLOW BARRIER. *Chemiefasern/ Textilindustrie. Technische Textilien/Technical Textiles*, 42–94 (7–8) (1992): T88–T89 and E78 (Abstract through Elsevier Scopus).
72. ZHANG, X. X., WANG, X. C., ZHANG, H., NIU, J. J. and YIN, R. B., Effect of phase change material content on properties of heat-storage and thermo-regulated fibres nonwoven. *Indian Journal of Fibre and Textile Research*, 28(3) (2003): 265–269.
73. SHI, H. F., ZHANG, X. X., WANG, X. C. and NIU, J. J., A new photothermal conversion and thermo-regulated fibres. *Indian Journal of Fibre and Textile Research*, 29(1) (2004): 7–11.
74. MONLLOR, P., BONET, M. A. and CASES, F., Characterization of the behavior of flavour microcapsules in cotton fabrics. *European Polymer Journal*, 43 (2007): 2481–2490.
75. ONDER, E., SARIER, N. and CIMEN, E., Encapsulation of phase change materials by complex coacervation to improve thermal performances of woven fabrics. *Thermochimica Acta*, 467 (2008): 63–72.
76. COOL FABRICS FROM THE WORLD'S FREEZER. *Knitting International*, 111(1321) (2004): 38 (abstract through Elsevier Scopus).
77. TEMPERATURE CONTROL FABRICS. *Performance Apparel Markets*, 4 (2003): 16–42 (abstract through Elsevier Scopus).
78. GEETHAMALINI, R., The role of phase change material in textiles. *Melliand International*, 12(2) (2006): 118–121 (abstract through Elsevier Scopus).
79. PAUSE, B., Phase change materials show potential for medical applications. *Technical Textiles International*, 8(7) (1999): 23–26 (abstract through Elsevier Scopus).
80. PARTHIBAN, M., KUMAR, S. R., KUMAR, K. S. and KUMAR, K. S., PCM – manufacture and applications in the field of textiles. *Asian Textile Journal*, 18(2) (2009): 28–32 (abstract through Elsevier Scopus).
81. TAN, F. L. and FOK, S. C., Cooling of helmet with phase change material. *Applied Thermal Engineering*, 26(17–18) (2006): 2067–2072.

82. LI, J. L., XUE, P., DING, W. Y., HAN, J. M. and SUN, G. L., Micro-encapsulated paraffin/high-density polyethylene/wood flour composite as form-stable phase change material for thermal energy storage. *Solar Energy Materials and Solar Cells*, 93(10) (2009): 1761–1767.
83. FUKAI, J., HAMADA, Y., MOROZUMI, Y. and MIYATAKE, O., Effect of carbon-fiber brushes on conductive heat transfer in phase change materials. *International Journal of Heat and Mass Transfer*, 45 (2002): 4781–4792.
84. ELGAFY, A. and LAFDI, K., Effect of carbon nanofiber additives on thermal behavior of phase change materials. *Carbon*, 43 (2005): 3067–3074.
85. SARI, A. and KARAIPEKLI, A., Thermal conductivity and latent heat thermal energy storage characteristics of paraffin/expanded graphatite composite as phase change material. *Applied Thermal Engineering*, 27 (2007): 1271–1277.
86. NAYAK, K. C., SAHA, S. K., SRINIVASAN, K. and DUTTA, P., A numerical model for heat sinks with phase change materials and thermal conductivity enhancers. *International Journal of Heat and Mass Transfer*, 49 (2006): 1833–1844.

J. DYER,
AgResearch Ltd, New Zealand

Abstract: Far infrared (FIR) textiles are a new category of functional textiles that have putative health and wellbeing functionality. FIR exerts strong rotational and vibrational effects at the molecular level with the potential to be biologically beneficial. The underpinning targeted benefit of FIR textiles is the enhancement of blood circulation. These materials are based on the principle of absorbing energy from sunlight and then radiating this energy back onto the body at specific wavelengths.

This chapter explores the basic principles of electromagnetic radiation as they relate to FIR, examines the putative mechanism and therapeutic effects of FIR therapy, and surveys what objective evidence currently exists of health benefits. The role of FIR fibres and fabrics in functional textiles is also evaluated, together with existing and potential applications of these textile products. A summary of the benefits, limitations and anticipated future trends of current products and technologies is then provided.

Key words: textiles, infrared, circulation, functional textiles, health, bioceramics.

8.1 Introduction and overview

Textiles that offer additional functionality to the user above conventional textiles are increasingly gaining prominence. Far infrared (FIR) textiles are a new category of functional textiles that have putative health and wellbeing functionality. At the molecular level FIR exerts strong rotational and vibrational effects with the potential to be biologically beneficial. The underpinning targeted benefit of FIR textiles is the enhancement of blood circulation. These materials are based on the principle of absorbing energy from sunlight and then radiating this energy back onto the body at specific wavelengths.

This chapter first explores the basic principles of electromagnetic radiation, and in particular infrared (IR) radiation. Then it examines the putative mechanism and therapeutic effects of FIR therapy, and surveys what objective evidence currently exists of health benefits. The role of FIR fibres and fabrics in functional textiles is then explored, focusing on currently commercially available bio-ceramic-based FIR products. Applications of these

textile products are then summarized, along with other, non-FIR, therapy applications of IR properties in textiles. Finally the benefits and limitations of these technologies are highlighted and future trends discussed.

IR textiles represent a growing and exciting area of functional textiles and this area will continue be an interesting one to observe over coming years, as technologies progress.

8.2 Principles of IR

8.2.1 Principles of electromagnetic radiation

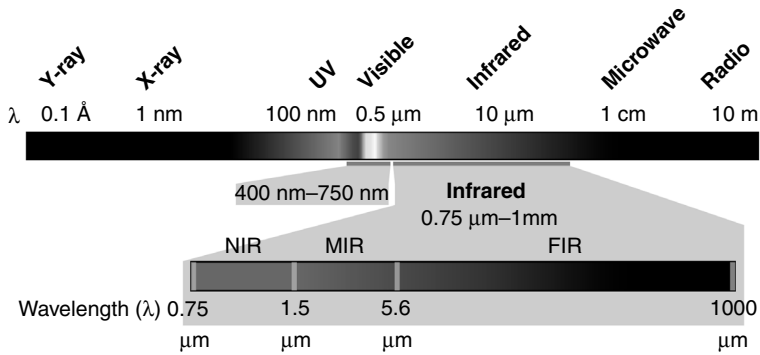
Electromagnetic radiation comprises self-propagating waves, which have electric and magnetic components. The basic unit of electromagnetic radiation is the photon. Electromagnetic waves, or rays, are classified according to their wavelength (Knight, 2004).

Sunlight is made up of both visible and invisible wavelength radiation. The visible range covers red, orange, yellow, green, blue, indigo and violet coloured light. Wavelengths shorter or longer than these colours are invisible to humans and include ultraviolet (UV) light and X-rays at shorter wavelengths, and microwaves and radio waves at longer wavelengths.

Electromagnetic waves between visible light and the microwave region are called IR light. The term infrared literally means below red, because IR has a longer wavelength, and hence lower frequency, than visible red light. The wavelength of IR waves range from 0.75 to 1000 μm . IR is commonly divided into three spectral regions: near (0.75–1.5 μm), mid (1.5–5.6 μm) and FIR (5.6–1000 μm) (Lin *et al.*, 2007). The boundaries between the near, mid and FIR regions are not agreed upon and can vary substantially depending on the context. Figure 8.1 shows the position of IR within the electromagnetic spectrum.

IR radiation is emitted by any object with a temperature above absolute zero. The wavelength at which an object radiates most intensely depends on its temperature. In general, as the temperature of an object cools, it emits farther IR wavelengths.

IR radiation is commonly, but mistakenly, equated to ‘heat’ or ‘thermal radiation’. This misconception is because people often attribute all radiant heating to IR light. In fact, electromagnetic radiation of all frequencies will lead to heating of materials that absorb them. IR radiation from sunlight accounts for half of the heating of the earth, with the other half the consequence of visible light that is absorbed then re-radiated at longer wavelengths (Knight, 2004). Unlike electromagnetic radiation, which can propagate through a vacuum, heat is technically energy that flows due to temperature differences, and is transmitted by thermal conduction or thermal convection.



8.1 The location and breakdown of IR within the electromagnetic spectrum.

8.2.2 Far infrared

The FIR electromagnetic spectrum of wavelengths between 5.6 and 1000 μm is not visible to the human eye. As described earlier, any material above absolute zero emits IR. The FIR region of the spectrum is notable in that materials at room temperature emit radiation that is generally concentrated between 8 and 25 μm (Knight, 2004).

The two key FIR properties of direct relevance to IR textiles are the FIR absorption characteristics of human tissue and the FIR emission properties of the textile.

On absorption, IR energy in general elicits vibrational excitation in molecules through changes in the molecular dipole moment. FIR radiation can penetrate relatively deeply into the human body, reaching as far as 4–7 cm into the tissues, and is readily absorbed by biological materials (Inoue and Kabaya, 1989; Karu, 1998).

With respect to FIR emission, the concept of radiative emission is significant in understanding the relative IR emissions of materials. Emissivity is a material surface property which describes how radiative emissions deviate from that of a theoretical black body. Two objects can be at the same physical temperature, but can have differing emissivities, meaning that they are emitting different electromagnetic radiation profiles (Knight, 2004).

8.3 FIR therapy

8.3.1 Phototherapy

People have long believed that exposure to sunshine can maintain and enhance health and wellbeing. Phototherapy, or light therapy, is a rapidly growing, but often controversial, area of health treatment. In particular,

low-level laser therapy (LLLT), also known as ‘photobiomodulation’, is a relatively new therapeutic option used to relieve pain and inflammation and promote wound healing (Desmet *et al.*, 2006; Karu, 1989). It has been known for many years that low levels of either coherent (waves are in phase with each other, e.g. laser light) or non-coherent (waves are out of phase with each other, e.g. sunlight) radiation in the red or near-IR region can in some situations accelerate some phases of wound healing, reduce pain, inflammation and swelling, and prevent tissue death (Karu, 1998), but the benefits of LLLT in medicine in general are still debated. The Food and Drug Administration (FDA) cleared the first LLLT device for hair growth in January 2007, and light treatment is now being used for a wide range of therapeutic applications (Basford *et al.*, 1998).

The number of clinical studies in the general area of phototherapy is increasing, with mixed results in terms of observed efficacy (Capon and Mordon, 2003; Karu, 2003; Smith, 2005; Yu *et al.*, 2006). Many researchers claim to have achieved positive clinical and pre-clinical results with LLLT, and the evidence for positive therapeutic effects under selected conditions is certainly mounting (Desmet *et al.*, 2006; Zhang *et al.*, 2009b), but others remain sceptical. This scepticism can probably be largely attributed to the introduction into the market of self-treatment light devices with little or no supporting clinical data. However, it seems certain that selected forms of light therapy will continue to grow in popularity and to gain increasing mainstream acceptance and medical usage. It is within this context that FIR therapy must be considered.

8.3.2 FIR health effects

The systemic biological effects of FIR radiation on whole organisms are currently poorly understood. However, the basic principles are established. FIR wavelengths have relatively high penetrability in most biological materials. Absorption by biomolecules, such as proteins and lipids, leads to stimulation of intramolecular bond vibrations and rotations, and this increased molecular kinetic energy leads to an elevation in temperature (Lubart *et al.*, 1992).

The underlying principle of FIR therapeutic approaches is that FIR absorption can be used to elevate local tissue temperature, leading to dilation of blood vessels and therefore enhancing blood microcirculation for targeted regions of the body. Microcirculation refers to the flow of blood through the vascular network lying between the arterioles and venules. The main function of the circulating blood is to transport oxygen and nutrients, and to remove carbon dioxide and other waste materials.

FIR rays in the 4–14 μm range are considered beneficial for cellular growth, and this radiation has been termed by some as the ‘rays of life’

(Voeikov, 2006). FIR can penetrate deeply into tissue and induce a higher skin blood flow. When FIR penetrates through the skin into subcutaneous tissue, it induces the generation of heat energy through resonance effects, essentially stimulating intramolecular micro-vibrations. It can be said that the metabolic rate of an individual is an indicator of health. This resonance process is believed to invigorate cellular activities through expanding capillaries and increasing the circulation of nutrient-rich, oxygenated blood, thereby improving overall metabolism. Other beneficial effects may include assisting the regenerative ability of tissues, activating the immune system and enhancing the removal of cellular waste materials.

On this basis, FIR therapy therefore has a wide range of claimed health and wellbeing benefits. A summary list of the major proposed ways in which FIR therapy can improve human health is presented here (Burton Goldberg, 1993):

- Increasing oxygen in the blood
- Rejuvenating skin and muscle tissue
- Promoting regeneration and rapid healing
- Improving the function of the nervous system
- Reducing lipids in skin tissue
- Enhancing metabolism
- Improving blood circulations
- Enhancing delivery of oxygen and nutrients to soft tissue
- Removing accumulated toxins by improving lymph circulation
- Relaxing muscles.

The question can be asked – What are the advantages of utilising IR over full spectrum sunlight? The potential advantage is that sunlight contains a range of radiation types including UV, visible light and IR. Different wavelengths have different biological effects, with some positive and some negative (Knight, 2004). IR can penetrate tissues (the longer the wavelength, the deeper the penetration) and in principle specifically target selected biomolecules, avoiding damage associated with exposure to other electromagnetic wavelengths (Inoue and Kabaya, 1989; Karu, 1998).

Health conditions that are particularly targeted by FIR therapy, and from which there is significant anecdotal feedback of efficacy, include arthritis, muscle pain and spasm, joint stiffness and Raynaud's syndrome.

The most notable application to date is probably the treatment of arthritis. Arthritis refers to a wide range of different muscle/skeletal conditions, including osteoarthritis, gout, rheumatoid arthritis and fibromyalgia. The symptoms of most forms of arthritis are joint inflammation, pain and stiffness. Arthritis pain and inflammation occurs in nearly everyone as they age, with the majority of people over the age of 50 exhibiting some signs of

arthritis as joints degenerate. FIR therapy is believed to be particularly useful for arthritis because it can be applied directly to the area of pain.

Along with these therapeutic applications, some claim farther-reaching health benefits, including anti-cancer, anti-obesity and anti-pathogen effects. There are even claims that FIR rays can be used not only to inhibit cancer growth, but also to kill existing cancerous cells.

With such a broad range of putative therapeutic effects, the critical question raised is: Is there any clinical proof to back up the claims?

There is an increasing number of supporting studies on the therapeutic effects of FIR therapy, but these are still few in number. For example, one clinical study came to the conclusion that there are significant improvements in subjective measures of pain and discomfort associated with Raynaud's syndrome (Ko and Berbrayer, 2002). Raynaud's syndrome is a disorder that results in discoloration of the fingers and toes. This phenomenon is believed to be the result of decreased blood supply, with emotional stress and cold the classic triggers (Anderson *et al.*, 2007; Hirschl *et al.*, 2006).

Among FIR therapy's putative healing benefits is its ability to relieve inflammation (Lin *et al.*, 2008). Studies have found that FIR therapy can exert a strong anti-inflammatory effect by inducing haem oxygenase-1, an enzyme which catalyses the oxidative degradation of haem. It is noteworthy that induction of haem oxygenase-1 production is also associated with anti-proliferative, antithrombotic and antioxidant effects through generation of carbon monoxide and bilirubin.

Another notable research study investigated whether FIR treatment could improve wound healing in rat models (Toyokawa *et al.*, 2003). This study measured skin wound area, skin blood flow and skin temperature before and during FIR irradiation. Wound healing was observed to be significantly more rapid with than without FIR. Interestingly, skin blood flow and skin temperature were not observed to change significantly. However, histological evaluation revealed greater collagen regeneration and infiltration of fibroblasts that expressed transforming growth factor- β 1 (TGF- β 1) in wounds in the FIR group. Stimulation of the secretion of TGF- β 1 or the activation of fibroblasts can be considered as a possible mechanism for the promotion of wound healing.

Taken as a whole, there is still a relative paucity of objective scientific and clinical data to provide comprehensive support for FIR therapy health benefits in humans, although those studies that have been conducted indicate significant potential. In addition, detailed information on the molecular mechanisms by which FIR exerts beneficial effects is scarce. It is undoubtedly for these reasons that, currently, FIR therapy is generally regarded as an alternative medical approach, and has not yet been fully accepted by mainstream medicine. As further research is conducted and the general field of phototherapy takes on greater acceptance, the indications are that

FIR therapy will continue to grow and become established as a viable therapeutic approach.

With respect to the more extreme claims of therapeutic benefits, such as FIR efficacy in killing cancerous cells and reversing ageing effects, currently there does not appear to be sufficient objective data in support, and these claims must be treated with due caution until further robust clinical trials are undertaken.

8.4 The role of FIR in relation to functional textiles

8.4.1 FIR fibres and fabrics

Textiles represent an excellent means to deliver localized treatment to the human body. FIR fibres are fibres that can transform absorbed energy into the emission of FIR rays. FIR fabrics are generally derived from traditional fibres, but have been functionalized by the incorporation of a material with appropriate electromagnetic absorption and emission properties.

So how can a fibre emit FIR radiation? The human body is continuously emitting thermal energy. The principle behind FIR textiles is that when the fabric is stimulated by this thermal energy, it absorbs the heat and converts it via emission of FIR rays, which are directed back into the human body. So, in theory, FIR textiles are powered by the wearer.

A simplified way in which this putative process can be explained is that the layer of FIR-active material acts as a mirror to the human body, with heat emitted sent back as FIR within a specific range of wavelengths.

FIR functionality can be incorporated into textile products in a variety of ways. The main route for manufacturing an FIR textile is usually to blend the fibre polymer and an FIR ceramic powder together to make the FIR yarn, with the FIR yarn subsequently incorporated into various FIR textile products. The FIR-active materials can be adhered to the textiles or yarn by techniques including impregnating, printing, coating, covering and laminating (Lin *et al.*, 2008). FIR materials can be added during the dyeing or finishing treatment process of an ordinary fabric.

After absorbing either sunlight or heat from the human body, FIR textiles are designed to transform the energy into FIR radiation with a wavelength of 4–14 μm and pass it back to the body. Fabrics with FIR function can effectively achieve thermal retention and are therefore ideal materials for activities that require warmth retention, such as mountaineering and hiking.

It has been reported that skin temperature increases are more rapid for radiant heating than for equivalent conductive or convective heating (Nakajima *et al.*, 2002). This corresponds to increased skin sensitivity and therefore needs to be taken into consideration in the design of textiles with radiant heating functionality.

Of course, the FIR emissivity value of the final product is critical with respect to its function. Studies on the emissivity of various FIR textiles have been performed and have arguably shown that relatively high emissions can be obtained (Zhang, 1994; Zhang *et al.*, 2009a). The critical question with regard to therapeutic applications is – What level of emissivity is required to achieve measurable benefits to the wearer? This is the R&D area where currently there is a paucity of robust supporting data with respect to real-life applications and where the potential to significantly boost the image of FIR textiles exists.

8.4.2 Bio-ceramics

Bio-ceramics is a term applied to ceramics with biological functionality, including those that can emit FIR (Richerson, 1992; Shackleford, 1998). The ceramic is therefore the functional component of the functional textile, and the amount and means by which the bio-ceramic can be incorporated into the fibres determines the overall fabric FIR emissivity (Koo *et al.*, 2007).

FIR textiles are often made through adding nano- or micro-sized ceramic powder to polymers prior to spinning. Bio-ceramic powders that can be incorporated into the structure of textiles to add FIR effects include magnesium oxide, zirconium, iron oxide, silicon carbide and germanium-based compounds (Lee and Lee, 2006; Park *et al.*, 2006). These materials are believed to retain emitted body heat and re-emit as FIR deep into joints and surrounding tissues to increase blood flow.

A common way to manufacture FIR fibres is through blending polypropylene with the active bio-ceramic. The bio-ceramic is ground into micro- or nano-particles and is either inseminated into the polypropylene during the fibre forming process or impregnated through a soaking or coating process. In one example of a coating process, the Fir-Tex line of products are derived from a treated polyamide fabric with a film of composite material based on polyurethane and the chosen bio-ceramic (<http://fir-tex.com/>).

A key challenge in the manufacture of bio-ceramic/polymer-based FIR fibres is to optimize the density of active material within the polymer matrix and thereby maximize the FIR emissivity. As the tensile strength of the fibre polymer tends to decrease with increased ceramic content and because the nozzles often used are abrasively worn down by the ceramic powder, the content of FIR bio-ceramic powder in textiles is limited. In one manufacturing protocol, this potential issue is claimed to be overcome by a sputtering method that forms a transparent and uniform FIR bio-ceramic thin film on the surface of the substrate (Lin *et al.*, 2008).

Another class of FIR fibres are bamboo-carbon modified polyesters (BCMP). Aged bamboo is converted to bamboo-carbon through thermal dissociation processes. The materials thus generated are very dense but

porous, with high surface area. When ground into powders, these can then be incorporated into a polymer matrix, in this case polyester. BCMPs are reported to have good FIR emissivity properties and it is claimed that use of BCMP fabrics can raise body temperature by 4–7°C (Qi *et al.*, 2006).

Bio-ceramic FIR textiles have also been designed by incorporating phase-change material microcapsules (PCMMCs) in combination with silicon carbide to provide additional thermal storage and insulation properties (Koo *et al.*, 2007).

8.5 Applications

As discussed, the key targeted effect of FIR therapy is improved blood microcirculation in order to reduce inflammation and pain in muscles and joints, and to promote regeneration and fast healing. The ideal application for FIR textiles, therefore, has been in a full range of products for localized pain relief and support. This includes therapeutic knee bands, elbow bands, wrist bands, waist bands, gloves, socks, shirts, back-belts and long johns. However, applications for IR textiles are broad. The major categories are summarized below.

8.5.1 Sportswear

FIR medical supports and orthotics worn during exercise are purported to help increase sweating, removal of lactic acid and toxin breakdown. Traditionally, athletes have used supporting textiles made of fibres such as myelin, latex and rubber to achieve some benefit. However, since these fabrics do not breathe well, deleterious effects such as skin irritation and inflammation can result. In contrast, FIR textiles can, in principle, maximize body heat and thereby prevent muscles from feeling over-worked, potentially improve muscle tone and mitigate soreness and muscle spasms while reducing the risk of injury (Babu, 2008). FIR textile products can also assist with the relief of injured or over-worked muscles, tendons and ligaments. Due to their enhanced absorption properties, FIR textiles can also help minimize sun damage during sport and recreation.

8.5.2 Therapeutic

The chief therapeutic function targeted by FIR textile products is promotion of microcirculation. Textiles can be made to adhere closely to body surfaces and are therefore ideal for delivering localized functionality, such as in joint supports. FIR therapeutic products are therefore often designed to relieve arthritis pain, such as rheumatoid arthritis, knee pain, shoulder pain, neck pain, and all kinds of chronic pains.

The range of therapeutic targets for FIR textiles currently on the market is very broad and includes Raynaud's syndrome, sprains, fractures, bunions, gout, athlete's foot, psoriasis, poor circulation, chilblains and RSI (<http://www.farinfraredhealth.com/>). Essentially, FIR textiles are marketed with therapeutic claims to match those of FIR therapy in general.

8.5.3 Warmth

Textiles with strong FIR emission properties make excellent fabrics for warmth retention products. FIR fabrics can keep the body warm in cold environments. For instance, FIR sleeping pads are available offering instant warmth even in cool air temperatures. Similarly, wools and cottons impregnated with ceramic insulating powder are available as socks, gloves, jackets and car seats to promote warmth. For marketing purposes these products are promoted in conjunction with the offer of passive FIR health benefits.

Similar FIR fibres are also used in some advanced heated clothing. For such heated clothing, an additional power source in the form of a battery is used to stimulate the warmth radiating properties of the FIR fibres. This form of clothing is designed to provide a significant heating effect in very cold environments.

8.6 Benefits and limitations

Preliminary evidence is emerging of beneficial health effects from FIR therapy. Particularly for arthritis and pain relief, textiles represent an excellent potential means of delivering localized treatment.

However, FIR textile technology is currently limited by the lack of reputable scientific and clinical trial support for the proposed therapeutic effects of FIR. For this reason, treatment using FIR textiles is still regarded as an alternative therapy, and currently lies outside mainstream health and medical treatments. Further targeted and objective studies are required to provide support for genuine therapeutic claims.

The benefits of IR textiles in non-therapeutic applications are significant and relatively well demonstrated. In particular, utilization in sportswear and warmth clothing offers an excellent route to providing additional functionality over and above conventional fabrics.

A limitation of current FIR textile products and technologies is the amount of FIR-active material that can be incorporated into the fibre, and the level of FIR that can be therefore be directed back to the body. A further limitation are the consumer-care properties. Ceramic pores can be blocked by dirt and sweat, but repeated washing can damage the ceramic layers and limit function. For instance, for the Fir-Tex range of breathable FIR fabrics, the manufacturer recommends that the products

are not washed above 30°C and that fabric softener be avoided (<http://fir-tex.com/>). Development of fibre technologies that are increasingly robust to consumer routine will facilitate enhanced consumer satisfaction with FIR textile products.

8.7 Conclusions and future trends

The general field of phototherapy is well on the path to mainstream acceptance for those applications where efficacy is being robustly demonstrated. It is notable that a recent paper in *Nature* outlined a potential mechanism of actions that could underpin the biological effects of low-level light therapy (Lane, 2006). This study presents evidence that red or near IR light may be able to relieve chronic inflammatory conditions.

Recent studies are also beginning to provide preliminary evidence for potential specific beneficial effects of FIR in particular. Selected forms of FIR therapy are anticipated to gradually take on increasing acceptance in mainstream medicine and science. Lack of full acceptance to date can be attributed to a combination of both general unsubstantiated claims and the fact that many studies have not been conducted with appropriate scientific rigour and methodology (Smith, 2005).

The further development of FIR textiles is likely to parallel that of FIR therapy in general. FIR textile products have an existing consumer base and will continue to occupy a niche in the textile market. To break out of this niche, however, robust data will need to be generated showing therapeutic efficacy. On the other hand, for non-therapeutic applications such as sportswear and warmth retention, FIR textiles have excellent potential for increased utilization and market uptake. This will be supported by continued innovation in FIR-active materials, in particular those technologies allowing increased active density and quantum yield.

As mentioned at the outset of this chapter, IR textiles represent a growing and exciting area of functional textiles. As new technologies and further supporting studies become available, this area will undoubtedly continue to mature and generate ongoing interest.

8.8 Sources of further information

Several avenues are available for further information surrounding IR textiles, with web-based information being the most accessible.

General information on electromagnetic radiation can be found in the 'Electromagnetic Waves' section of the Centre for Remote Imaging, Sensing and Processing website (<http://www.crisp.nus.edu.sg/~research/tutorial/em.htm>) and a historical summary of IR is on the Omega website (<http://www.omega.com/literature/transactions/volume1/historical1.html>). There is also

a simplified explanation of IR on the NASA website for children at <http://science.hq.nasa.gov/kids/imagers/ems/infrared.html>.

The American Society of Photobiology website provides objective background information with respect to the area of phototherapy (http://www.pol-us.net/ASP_Home/index.html), and also provides excellent background information on the nature and effects of electromagnetic radiation in a biological context.

Sources of general information around FIR usage in putative therapeutic applications include the websites <http://www.farinfraredhealth.com/>, <http://www.toolsforwellness.com/far-infrared.html> and www.earthtym.net/ref-far-infrared.htm.

There are still relatively few sources of information specific to FIR textiles. However, the following websites provide a general indication of current FIR textile products available on the market – www.fir-tex.com, www.firheals.com/catalog/infrared_clothing and www.therapygloves.com.

A certification standard for FIR textiles from Taiwan Functional Textiles can be found at tft.ttfapproved.org.tw/e_tft/introduction/fts-fa-010.asp.

8.9 Acknowledgements

I would like to acknowledge and thank Dr Anita Grosvenor for her critical review and editing of this chapter and Dr Duane Harland for preparation of the figure.

8.10 References

- ANDERSON, M. E., MOORE, T. L., LUNT, M. and HERRICK, A. L. (2007) The 'distal-dorsal difference': a thermographic parameter by which to distinguish between primary and secondary Raynaud's phenomenon. *Rheumatology*, 46(3): 533–538.
- BABU, K. M. (2008) Far infrared (FIR) bio-ceramic textiles for health care. *Asian Textile Journal*, April 2008, 37–41.
- BASFORD, J. R., MALANGA, G. A., KRAUSE, D. A. and HARMSSEN, W. S. (1998) A randomized controlled evaluation of low-intensity laser therapy: plantar fasciitis. *Archives of Physical Medicine and Rehabilitation*, 79(3): 249–254, doi: 10.1016/S0003-9993(98)90002-8.
- BURTON GOLDBERG GROUP (1993) *Alternative Medicine – The Definitive Guide*. Future Medicine Pub, Puyallup, WA.
- CAPON, A. and MORDON, S. (2003) Can thermal lasers promote skin wound healing? *American Journal of Clinical Dermatology*, 4(1): 1–12.
- DESMET, K. D., PAZ, D. A., CORRY, J. J., EELLS, J. T., WONG-RILEY, M. T., HENRY, M. M., BUCHMANN, E. V., CONNELLY, M. P., DOVI, J. V., LIANG, H. L., HENSEL, D. S., YEAGER, R. L., MILLSAP, D. S., LIM, J., GOULD, L. J., DAS, R., JETT, M., HODGSON, B. D., MARGOLIS, D. and WHELAN, H. T. (2006) Clinical and experimental applications of NIR-LED photobiomodulation. *Photomedicine and Laser Surgery*, 24(2): 121–128.

- HIRSCHL, M., HIRSCHL, K., LENZ, M., KATENSCHLAGER, R., HUTTER, H. P. and KUNDI, M. (2006) Transition from primary Raynaud's phenomenon to secondary Raunaud's phenomenon identified by diagnosis of an associated disease: results of ten years of prospective surveillance. *Arthritis and Rheumatism*, 54(6): 1974–1981.
- INOUE, S. and KABAYA, M. (1989) Biological activities caused by far-infrared radiation. *International Journal of Biometeorology*, 33: 145–150.
- KARU, T. (1989) Photobiology of low-power laser effects. *Health Physics*, 56: 691–704.
- KARU, T. I. (1998) *The Science of Low Power Laser Therapy*. London: Gordon and Breach Scientific Publications.
- KARU, T. I. (2003) Low power laser therapy. In: Vo-Dinh, T. (ed.) *CRC Biomedical Photonics Handbook*, Vol. 48. Boca Raton, FL: CRC Press, pp. 1–25.
- KNIGHT, R. D. (2004) *Physics for Scientists and Engineers: A Strategic Approach*. San Francisco, CA: Addison-Wesley.
- KO, G. D. and BERBRAYER, D. (2002) Effect of ceramic-impregnated 'thermo-flow' gloves on patients with Raynaud's syndrome: randomized, placebo-controlled study. *Alternative Medicine Review*, 7(4): 327–334.
- KOO, K., CHOE, J. D., CHOI, J. S., KIM, E. A. and PARK, Y. M. (2007) Preparation physical characteristics of high-performance heat storage. Release fabrics with PCMMc: wet coating process. *Journal of the Korean Society of Dyers and Finishers*, 19: 23–30.
- LANE, N. (2006) Cell biology: power games. *Nature*, 443: 901–3, doi: 10.1038/443901a.
- LEE, H.-K. and LEE, K.-M. (2006) Far infrared radiation characteristics of germanium compounds. *Journal of Korean Industrial and Engineering Chemistry*, 17(6): 597–603.
- LIN, C.-C., CHANG, C.-F., LAI, M.-Y., CHEN, T.-W., LEE, P.-C. and YANG, W.-C. (2007) Far-infrared therapy: a novel treatment to improve access blood flow and unassisted patency of arteriovenous fistula in hemodialysis patients. *Journal of the American Society of Nephrology*, 18(3): 985–992, doi: 10.1681/asn.2006050534.
- LIN, C.-C., LIU, X.-M., PEYTON, K., WANG, H., YANG, W.-C., LIN, S.-J. and DURANTE, W. (2008) Far infrared therapy inhibits vascular endothelial inflammation via the induction of heme oxygenase-1. *Arteriosclerosis, Thrombosis, and Vascular Biology*, 28(4): 739–745, doi: 10.1161/atvbaha.107.160085.
- LIN, Y.-S., PAN, H.-C., LEE, C.-T. and LEUNG, T.-K. Manufacturing method for a far-infrared substrate. Available at: <http://www.faqs.org/patents/app/20080217163>. US Patent Appl. 20080217163A1, Sept 11.
- LUBART, R., WOLLMAN, Y., FRIEDMANN, H., ROCHKIND, S. and LAULICHT, I. (1992) Effects of visible and near-infrared lasers on cell cultures. *Journal of Photochemistry and Photobiology B: Biology*, 12(3): 305–310, doi: 10.1016/1011-1344(92)85032-p.
- NAKAJIMA, T., HACHINO, Y. and YAMANO, H. (2002) Effect of thermal radiation from fabrics on human body. *International Journal of Clothing Science and Technology*, 14(3/4): 251–256, doi: 10.1108/09556220210437220.
- PARK, C. H., SHIM, M. H. and SHIM, H. S. (2006) Far IR emission and thermal properties of ceramics coated fabrics by IR thermography. *Journal of Key Engineering Materials, Advanced Non-destructive Evaluation I*: 849–852, doi: 10.4028/www.scientific.net/KEM.321–323.849.
- QI, Q., SHUCAI, H. and LIJUN, M. (2006) Healthy functions of bamboo-carbon modified polyesters. *Meilland Internations: Fibres/Yarns*, 12(3): 177–178.

- RICHERSON, D. W. (1992) *Modern Ceramic Engineering: Properties, Processes, and Use in Design*. New York: Marcel Decker.
- SHACKLEFORD, J. F. (ed.) (1998) *Bioceramics: Applications of Glass and Ceramic Materials in Medicine*. Zurich: Trans-Tech Publications.
- SMITH, K. C. (2005) Laser (and LED) therapy is phototherapy. *Photomedicine and Laser Surgery*, 23(1): 78–80.
- TOYOKAWA, H., MATSUI, Y., UHARA, J., TSUCHIYA, H., TESHIMA, S., NAKANISHI, H., KWON, A.-H., AZUMA, Y., NAGAOKA, T., OGAWA, T. and KAMIYAMA, Y. (2003) Promotive effects of far-infrared ray on full-thickness skin wound healing in rats. *Experimental Biology and Medicine*, 228(6): 724–729.
- VOEIKOV, V. L. (2006) Reactive oxygen species (ROS): pathogens or sources of vital energy? Part 2. Bioenergetic and bioinformational functions of ROS, *Journal of Alternative and Complementary Medicine*, 12(3): 265–270, doi: 10.1089/acm.2006.12.265.
- YU, S.-Y., CHIU, J.-H., YANG, S.-D., HSU, Y.-C., LUI, W.-Y. and WU, C.-W. (2006) Biological effect of far-infrared therapy on increasing skin microcirculation in rats. *Photodermatology, Photoimmunology & Photomedicine*, 22(2): 78–86.
- ZHANG, H., HU, T. L. and ZHANG, J. C. (2009a) Surface emissivity of fabric in the 8–14 μm waveband. *Journal of the Textile Institute*, 100(1): 90–94.
- ZHANG, R., MIO, Y., PRATT, P. F., LOHR, N., WARLTIER, D. C., WHELAN, H. T., ZHU, D., JACOBS, E. R., MEDHORA, M. and BIENENGRAEBER, M. (2009b) Near infrared light protects cardiomyocytes from hypoxia and reoxygenation injury by a nitric oxide dependent mechanism. *Journal of Molecular and Cellular Cardiology*, 46(1): 4–14, doi: 10.1016/j.yjmcc.2008.09.707.
- ZHANG, X. (1994) Study and developments of far-infrared absorbing and emissive fibres and fabrics. *Journal of Textile Research*, 11: Article 12.

Functional smart textiles using stimuli-sensitive polymers

A. K. AGRAWAL and M. JASSAL,
Indian Institute of Technology, India

Abstract: Immense interest has been shown in polymeric systems exhibiting stimuli-sensitive properties due to their wide range of applications. This chapter discusses the general features of stimuli-sensitive polymers. It also introduces the basic chemistry of synthesis of temperature- and pH-responsive polymers. Then, the chapter reviews the different techniques suitable for producing smart textiles using stimuli-responsive polymers. The response of these polymers can be enhanced by integrating to textiles or by conversion to stable, strong thin shapes.

Key words: temperature-responsive textile, transition temperature, poly(*N*-*tert*-butylacrylamide-*ran*-acrylamide), coated yarn, shape changing fibers, pH-responsive fibers, water-vapor transmission rate.

9.1 Introduction

Fibers are flexible, mechanically strong one-dimensional structures and can be converted into a variety of two- and three-dimensional flexible structures such as ligaments (artificial muscles), woven fabrics, non-woven webs and membranes. A smart fiber that changes shape in response to various stimuli from the environment would not only enable development of the above applications in a desirable manner, but also open up a wide window of new applications in areas such as intelligent textiles (both apparel and technical applications), robotics and aerospace. In this chapter, we aim to highlight recent results of stimuli-responsive polymers for converting them to strong responsive structures suitable for making smart textiles.

9.2 Stimuli-sensitive polymers

Stimuli-sensitive polymers (SSP), also known as ‘stimuli-responsive polymers’ or ‘smart-polymers’ or ‘intelligent-polymers’, are a class of polymers that show a reversible transformation from one state to another as a response to various stimuli from the environment. Other than the widely studied temperature stimulus, the other chemical and physical stimuli which

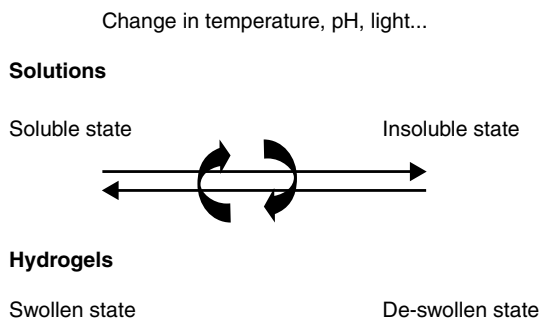
bring about a reversible transition in such polymers include electric field, solvent-composition, light, pressure, sound, stress and magnetic field, and chemical and bio-chemical stimuli (i.e. pH and ions).¹⁻³

Responsive polymers change their individual chain dimensions/size, secondary structure, solubility or the degree of intermolecular association in solution. Generally, the physical or chemical event that causes these responses is limited to formation or destruction of secondary forces (hydrogen bonding, hydrophobic effects, electrostatic interactions, etc.), simple reactions (e.g. acid–base reactions) of moieties pendant to the polymer backbone, and/or osmotic pressure differentials that result from such phenomena (Fig. 9.1). These polymers provide a big opportunity for creating intelligent materials that needs to be exploited.

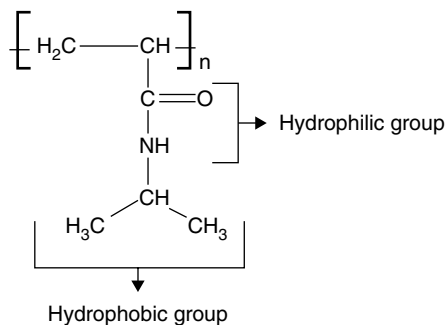
9.2.1 Temperature-responsive polymers

Immense interest has been shown in polymeric systems exhibiting stimuli-sensitive properties, ever since the observation of lower critical solution temperature (LCST) behavior in poly(*N*-isopropylacrylamide) (PNIPAm) solution.^{4,5} The aqueous solutions of the temperature-sensitive polymers change their phase reversibly from a soluble state to an insoluble state across the LCST. A few other polymers for which solution properties similar to PNIPAm have been reported are: poly(*N*, *N*'-dimethylacrylamide), poly(*N*-*n*-butylacrylamide), poly(*N*-acryloylpiperidine), poly(methoxy methyl acrylic acid), poly(propionylethyleneimine), poly(vinyl methyl ether), poly(*N*, *N*'-dimethylaminoethyl methacrylate) (DEAEM).^{1,5,6}

The SSP have both hydrophilic and hydrophobic groups in their structure. For example, PNIPAm has a hydrophobic backbone and a pendant group which has a hydrophilic amide moiety and a hydrophobic isopropyl moiety (Fig. 9.2). Depending upon which among the hydrophilic or hydrophobic interactions dominate, the polymer exists as an extended chain or a collapsed chain. PNIPAm has an LCST in the range of 31–34°C where



9.1 Mechanism of action of SSP.



9.2 Chemical structure of PNIPAm.

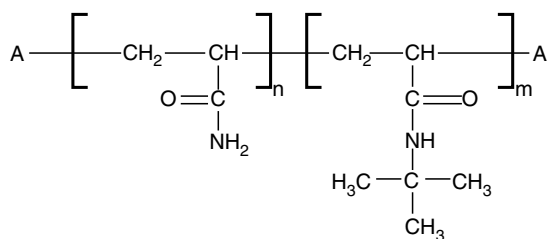
it undergoes transitions in the physical properties, such as mechanical, optical and thermal properties. These changes in temperature-sensitive polymers/gels are used to characterize the transition temperature of polymers/gels by dynamic mechanical measurement, infrared (FTIR), UV-vis-spectrophotometry (UV-vis), differential scanning calorimetry (DSC), nuclear magnetic resonance (NMR), atomic force microscopy (AFM) and X-ray scattering.

These polymers when synthesized in a hydrogel form, exist in a swollen state at temperatures below the transition temperature and in collapsed state at temperatures above the transition. The huge difference in water-holding capacity, which transforms reversibly according to the transition temperatures, has potential to be exploited for different applications. These polymers find various applications¹ in the field of controlled drug-delivery,^{7,8} molecular-separation,⁹ enzyme-activity control,¹⁰ artificial muscles,^{11–13} etc.

Different applications require the transformation to occur at a desired temperature, in order to achieve the switching at that particular temperature. The design of the hydrophilic-hydrophobic balance therefore becomes necessary. The LCST of a polymer can be designed/tuned to a desired value by

- using additives^{14,15}
- designing monomer structure^{16,17}
- copolymerization.^{18–21}

Save *et al.*²² have reported synthesis of series of new temperature-sensitive copolymers based on of *N*-*tert*-butylacrylamide (NTBA) and acrylamide (AM) (Fig. 9.3). Random linear and cross-linked copolymers of NTBA and AM were prepared by solution polymerization method, using regulated dosing of comonomer AM having a higher reactivity ratio ($r_{\text{AM}} = 1.5$) than NTBA ($r_{\text{NTBA}} = 0.5$). Linear copolymers with varying feed ratios of NTBA and AM (80:20 to 20:80 mol%) were synthesized and characterized. For the



9.3 Copolymer structure.

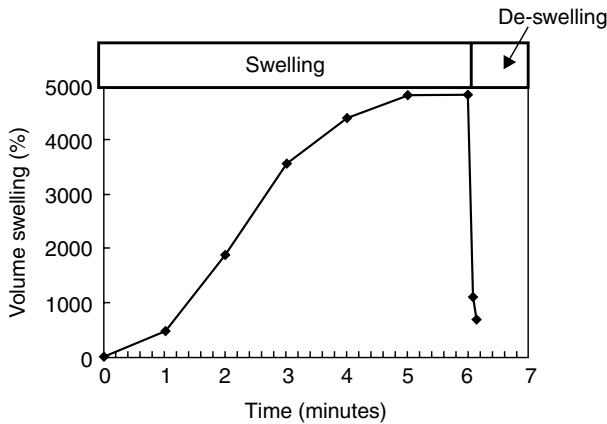
synthesis of copolymer hydrogels, *N*, *N'*-methylenebisacrylamide (MBA) was used along with monomers. The incorporation of a higher percentage of the hydrophilic comonomer AM, in the structure resulted in the shifting of the transition temperature towards a higher value. The transition temperatures of the copolymers synthesized with feed compositions of 80:20, 70:30, 60:40, 50:50, 40:60, 30:70 and 20:80 mol% were found to be 2, 10, 19, 27, 37, 45 and 58°C, respectively. DSC studies confirmed the formation of random copolymers.

Another interesting case of a thermo-responsive polymer is the hyper-branched polyether structure synthesized by Jia *et al.*²³ The reaction proceeded via proton transfer polymerization of a diepoxide and a triol. The LCST could be varied from 19 to 40.3°C depending on the composition of the triol.

9.2.2 pH-responsive polymers

The pH-sensitive polymers²⁴ undergo a change from a hydrophobic state to a hydrophilic state by the change in pH. These polymers consist of ionizable pendant groups (acidic such as carboxylic and sulfonic acids or basic groups like amine) that can accept and donate protons in response to the environmental change in pH. As the environmental pH changes, the degree of ionization in pendant groups undergoes dramatic change at a specific pH called pK_a . This rapid change in the net charge of pendant groups causes an alternation of the hydrodynamic volume of the polymer chains. This results in a transition from collapsed hydrophobic state to soluble hydrophilic state of the polymer.²⁴ The pH-sensitive hydrogels can be weakly acidic (anionic) or weakly basic (cationic) depending on the nature of the ionizable moieties on their polymer backbones. Many systems based on acidic carboxylic acid group comonomers or basic amino group containing comonomers have been reported.^{25–28} The hydrogel swelling and de-swelling properties depend on several factors including their hydrophobic–hydrophilic nature, cross-link density (elasticity), charge density and pK_a .²⁹

In poly(acrylic acid), the carboxyl group gets ionized at alkaline pH and becomes hydrophilic. In this state, the ionized groups mutually repel due to



9.4 Mechanism of action of pH-responsive polymer.

their negative charge and force the polymer chains to unfold and dissolve in the medium. While at a low pH, the carboxylic groups lose their charge and the polymer collapses as it becomes hydrophobic (Fig. 9.4). Since these polymers are in solubilized form when hydrophilic, they are generally produced as a cross-linked structure for many applications. In cross-linked gel form, the polymer network swells when hydrophilic and de-swells when subjected to a pH at which it is hydrophobic. The cationic polymers like *N, N'* diethyl amino ethyl methacrylate exhibit a similar behavior, but collapse at high pH and swell at lower pH. Since the swelling of polyelectrolyte hydrogels is mainly due to the electrostatic repulsion among charges present on the polymer chain, the extent of swelling is influenced by any conditions that reduce electrostatic repulsion such as pH, ionic strength and type of counter ions. The swelling and pH responsiveness of polyelectrolyte hydrogels can be adjusted by using neutral comonomers, such as 2-hydroxyethyl methacrylate, methylmethacrylate and maleic anhydride. Different comonomers provide different hydrophobicity to the polymer chain, leading to different pH-sensitive behavior.

The synthesis of polymeric hydrogels is typically accomplished by one of two well-established schemes:

1. Polymerization of hydrophilic monomers.
2. Modification or functionalization of existing polymers.

Some pH-responsive polymer systems are given in Table 9.1.

9.2.3 Dual-sensitive (temperature and pH sensitive) polymers/hydrogels

These polymers respond to more than one environmental stimulus and are expected to provide more sophisticated responsiveness and greater

Table 9.1 Commonly used polymer systems for pH-sensitive polymers

	Polymer system	Type of response	References
1.	Based on cationic monomers		
A	Based on chitosan		
(i)	Chitosan	pH	30
(ii)	Polyacrylic acid and chitosan	pH and temperature	30,31
(iii)	Grafting of <i>N</i> -isopropylacrylamide (NIPAm) and 2-acrylamido-2-methyl propane sulfonic acid (AMPS) onto chitosan (CS)	pH and temperature	32
(iv)	Hydrolyzed-chitosan-g-PAN	pH	33
(v)	Semi-IPN of chitosan and poly(methacrylic acid)	pH	34
B	Poly(allylaniline)	pH	35
C	Poly(<i>N</i> - <i>N'</i> dimethyl aminoethyl methacrylate) (DEAEM)	pH	
D	Poly(amino benzene sulfonamide)	pH	
E	Poly(2-vinyl pyridine)(PVP)	pH	
F	Poly(ethylpyrrolidine) (PEPyM)	pH and temperature	36
2.	Based on anionic monomers		
A	Acrylic acid (AA) and its derivatives	pH	
(i)	Polymers of: AA, methacrylic acid (MA), propyl acrylic acid (PPA), ethyl acrylic acid (EAA)	pH	37–39
(ii)	Copolymers of AA and acrylonitrile (AN)	pH and temperature	40
(iii)	Copolymers of acrylamide and acrylic acid/sodium acrylate	pH and temperature	
(iv)	PNIPAm-co(methacrylic acid)	pH and temperature	41
(v)	NIPAm and AA	pH and temperature	42
(vi)	Graft copolymers of poly(methacrylic acid) and poly(ethylene glycol)	pH and temperature	28
(vii)	Poly(vinyl alcohol) networks grafted with AA or MA	pH and temperature	
(viii)	Poly(itaconic acid)(IA)	pH	
(ix)	<i>N</i> -vinyl-2-pyrrolidone and IA	pH	43
(x)	Poly(<i>N</i> -isopropylmaleamic acid-co-acrylonitrile) hydrogels	pH and temperature	40
B	Sulfonamide	pH	
C	Barbituric acid	pH	44
D	Cholic acid and derivatives	pH	45

potential for novel applications. Two main approaches have been used to prepare multi stimuli-responsive polymers. One approach involves the copolymerization of different responsive components.⁴⁶ Many studies have been carried out, where the copolymers have been made either for having response to two stimuli, e.g. both temperature and pH, or for adjusting the transition temperature of the resulting copolymer by the design of the

hydrophilic–hydrophobic balance. Though the polymers have response to two different stimuli, e.g. temperature and pH, the presence of the other comonomer also affects the transition value of each stimulus.

In the second approach, the multi-stimuli-sensitive hydrogels are obtained from interpenetrating polymer networks (IPN) of two polymers with independent stimuli responsiveness. This method has been used to make IPNs composed of temperature-responsive poly (*N*-isopropyl acrylamide), or PNIPAAm and a pH-responsive hydrogel composed of either poly (acrylic acid).⁴⁷ By chain interpenetration, one may attain combination of properties from these two polymer networks. Since there is no chemical bonding between the two components networks, each network may retain its own property while the proportion of each network may also lead to much higher mechanical strength with respect to the homopolymer network.

Chitosan-polyacrylic acid IPNs have also been reported⁴⁸ to show response to both alkaline as well as acidic pH. Dual response has also been discovered in acrylonitrile (AN) copolymers with acrylic acid (AA).^{40,49–51}

9.3 Drawbacks and limitations of current SSP/hydrogels

The SSP used in the hydrogel form have poor mechanical properties and hence are used as thick gels when converted to structures. An important factor for application is not only the maximum amount of water absorbed or released but also the rate of swelling and shrinking.

The major drawback of SSP when polymerized in the gel form is their slow response at transition. A disk-shaped gel of PNIPAAm-*co*-poly(ethylene oxide) of 0.7 cm diameter in dry state requires 75 h to attain equilibrium.⁵² In another study, pH and temperature-sensitive hydrogels (thickness 1–1.5 mm) based on *N*-acryloyl-*N'*-methylpiperazine and methyl methacrylate ions have been reported to show a reversible response to pH with a long response time of 150 min.⁵³ The response time which is diffusion controlled is given by:

$$\tau = r^2/D_{\text{coop}}$$

where, τ is the time for diffusion to achieve equilibrium, r represents the smallest gel dimension in the swollen state, and D_{coop} is the cooperative diffusion coefficient of the network in the swelling solvent (D_{coop} for PNIPAAm/water is $3 \times 10^{-7} \text{ cm}^2 \text{ s}^{-1}$).

Due to slow response and poor magnitude of response, the potential applications of these copolymer hydrogel structures have not been fully exploited.

9.3.1 Approaches to improve the response

Several other approaches for making the structure of the polymers which result in a faster response time have been discussed in a review,³ but these studies also report loss in mechanical strength of the hydrogels. Some of the strategies that have been proposed in order to increase the response rate include

- (i) forming a heterogeneous network structure of the hydrogel through a phase separation method
- (ii) graft-copolymerization, where the free ends of the grafts act to accelerate the dehydration rate
- (iii) use of pore-forming agent during the polymerization reaction.

All these modifications lead to improvement in the response time typically ranging by one order of magnitude. Similarly, the swelling ratios of the hydrogels increase from 150% to 3000% based on the thickness and cross-linking density of the hydrogels. However, to date improvements in response time have been limited, because these polymers have not been subjected to processing into mechanically strong thin shapes.

The simplest way to improve the response time is to make hydrogels stronger, thinner and smaller.

SSP are expected to overcome the limitations of slow response, limited transition, weak mechanical properties and find additional numerous novel applications if:

- (a) new series of SSP could be synthesized with a structure that can render them processable,
- (b) these new polymers could be processed into thin-films or fibers with thickness in the range of few microns,
- (c) alternatively, these polymers could be integrated as coatings to non-active substrates such as mechanically strong yarns and fabrics and
- (d) the resultant SSP fiber and SSP-substrate composite could retain the thermo-sensitive property.

9.4 Smart functional textiles

As discussed above, the major drawbacks of the current SSP gel structures are their weak mechanical properties and poor transitional response. Processing of these materials into thin structurally strong shapes or their integration to textile materials (such as mechanically strong yarns and fabrics) is likely to solve the current drawbacks of hydrogels and also develop responsive textile materials for smart textile.

This has been achieved by converting the linear copolymer of poly(*N*-*tert*-butylacrylamide-*ran*-acrylamide) (27:73 mole %) containing polycarboxylic acid cross-linker and catalyst into fibers (30–50 μm), and coatings onto cellulosic yarns and fabrics.^{3,22,54,55} The processed forms were dried and cured at 150–200°C for 5–25 min. The presence of reactive side groups in the monomer has been utilized to introduce cross-links with the help of polyfunctional cross-linkers. This approach of incorporation of responsive polymers in the form of thin film/coating on reactive flexible substrate provides an active polymer layer on top of substrates. Such a structure also results in mechanically strong SSP composites with a large surface area.

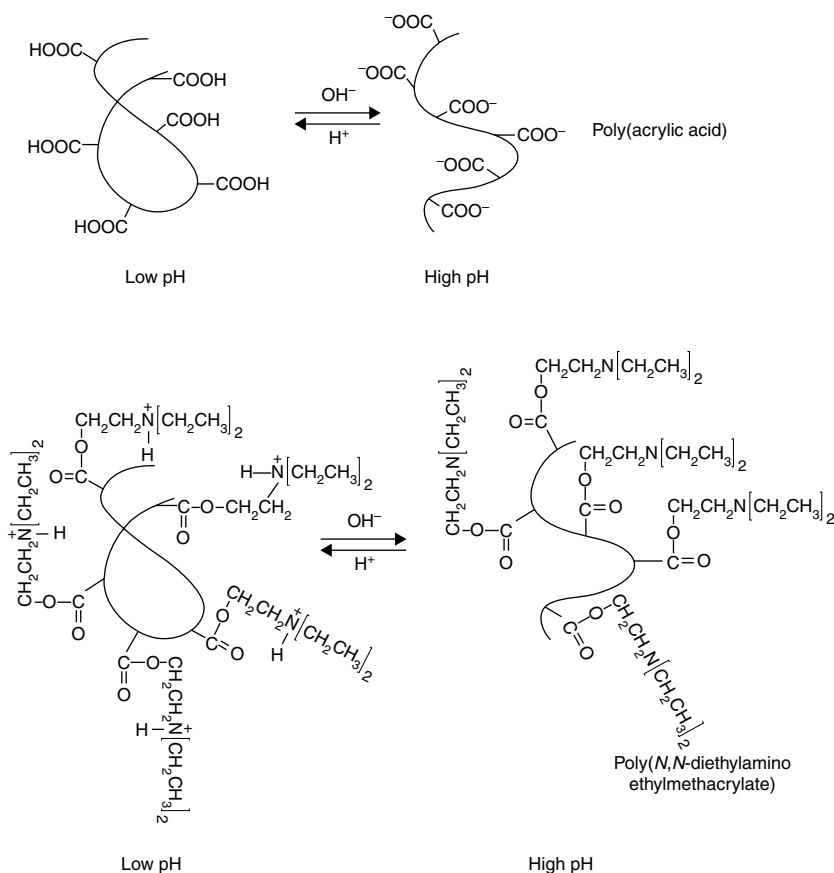
9.4.1 Integration of stimuli-responsive polymers to textiles

The cross-linking appears to result due to condensation between the amide side-groups of the copolymer and carboxylic acid groups of the cross-linker. The carboxylic acid groups of polyfunctional cross-linker also react with hydroxyl groups of the cellulose substrate resulting in chemical bonding of copolymer onto the substrate. This approach of incorporation of responsive polymers in the form of thin film/coating on reactive flexible substrate would provide an active polymer layer on top of substrates. Such a structure would give mechanically strong SSP composites with a large surface area.

Coated yarn structures

The yarn samples were dip-coated with the above coating solution, dried at 120°C for 5 min and cured at 180°C for 6 min. The integrity of the copolymer coating to yarn was found to be excellent.

The transitional behavior of the coated yarn was studied with respect to temperature of the surrounding water bath. The yarn shows volumetric swelling of 4500% at 6°C and collapse to a swelling percentage of 800 at 80°C. A clear transition was observed between a temperature range of 15–35°C with a mean transition temperature of about 25°C. When the coated yarn was subjected to de-swelling, the de-swelling curve with temperature followed the swelling curve with a small hysteresis. The transition was found to be reversible to repeated swelling and de-swelling cycles. During swelling, the equilibrium was achieved within 5 min as shown in Fig. 9.5, while during de-swelling the equilibrium was attained in less than 10 s. The coated yarns showed much faster rates of transition compared to the hydrogels. This may be attributed to the higher surface area to volume ratio of the copolymer–yarn composite. However, the transition observed in coated yarn was broader compared to pure copolymer gel and also shifted to a lower temperature. This broad transition may be a result of localized



9.5 Rate of transition of the coated yarn immersed in a water bath. Swelling rate was studied at 6°C and de-swelling initiated after 6 min of the experiment time by changing the temperature to 80°C.

heterogeneity in the cross-link density of the coated yarn structure. And the shift in transition temperature in coated yarns is due to the decrease in hydrophilicity of the copolymer caused by decrease in the number of amide groups as some of the amide groups are used in the cross-linking reaction.

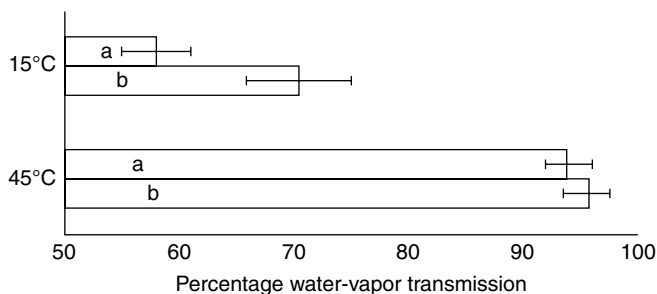
Crespy has described the chemistry of and synthesis of temperature-responsive polymers (TSPs) and their application on textiles.⁵⁶ Alternative methods for integration of SSP to textile substrate by radiation grafting⁵⁷ or photo irradiated grafting (at $\lambda < 300$ nm)⁵⁸ are also reported. In all these cases, the transitions of the integrated PNIPA remain similar to the pure PNIPA; however, it is shown to become significantly broad over a wide temperature range.

Coated fabric: responsive breathable fabric

We thought that it would also be interesting to investigate whether fabrics made from the above coated yarns would show response in air atmosphere as opposed to their tests in water baths, where ample supply of water is available for the transition. A breathable fabric⁵⁵ was prepared by integrating the TSP onto a cotton fabric with 23% add-on. The coating on the fabric showed a swelling ratio of around 800% and a response time of 20 min to equilibrium swelling. The water-vapor transmission rate (WVTR) values of the TSP integrated breathable fabric were measured as a percentage of control uncoated substrate. The transmission percentage at 20% relative humidity for TSP fabrics (Fig. 9.6) were found to change across the transition temperature (15–45°C) from 58% to 94% compared to a comparative non-responsive breathable fabric (made using poly(acrylamide)-coated fabric), which changed only from 70% to 94%. The difference in percentage transmission, due to a change in the environment temperature, shows the responsive (smart) behavior of the TSP fabrics. Similar results were obtained for other relative humidity conditions.

9.4.2 Conversion of SSP to fibers

Stimuli-sensitive fibers are likely to show fast transition and better utilization of functional sites available inside the structure. Stimuli-sensitive fibers would also have an advantage over grafted SSP membranes in that they would not require support of inactive (passive) substrate, and therefore, would be able to show much higher functionality per unit weight of the material used. However, the technology of fiber spinning is complex and



9.6 Water-vapor transmission for coated fabrics shown as a percentage of control (uncoated cotton fabric) at 20% relative humidity. (a) Responsive breathable sample made from TSP-coated cotton fabric and (b) non-responsive breathable sample made from polyacrylamide-coated cotton fabric.

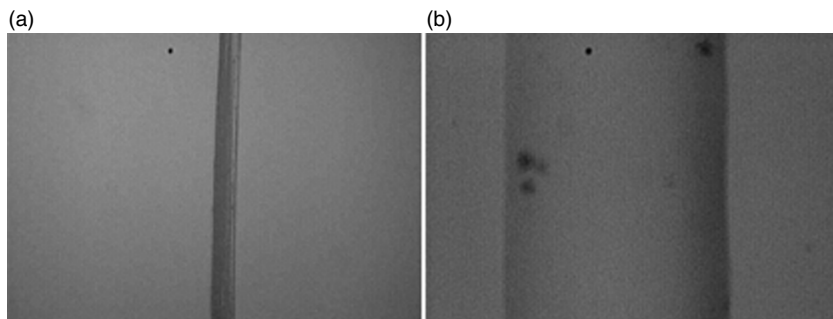
confined to only a few known non-responsive polymers. Therefore, it would be highly desirable to find methods to produce fibers from SSP. Linear SSP can be processed into fibers and then stabilized by cross-linking for producing SSP fibers that are stable during use.

Temperature-responsive fibers

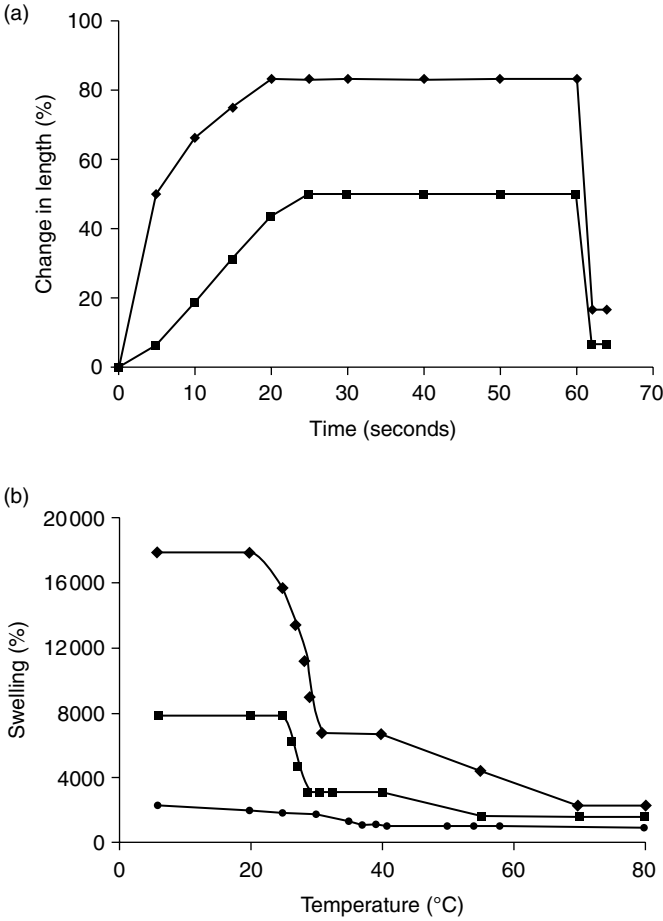
A high molecular weight poly(*N-tert*-butylacrylamide-*ran*-acrylamide::27:73) was converted to insoluble strong fibers with fineness of 30–50 μm by solution spinning, drawing and subsequent cross-linking (using the approach mentioned above for coated yarns and fabric). The mechanism of cross-linking using NMR and FTIR techniques has been separately investigated and published by our group.

The cured fiber was placed at 6°C for 15 min and then transferred to 80°C for 15 min. The SSP fibers were found to change shape (with respect to both diameter and length). Figure 9.7 shows an optical micrograph of the diametric change of the fiber immersed in water. The rate of transition of the fiber is shown in Fig. 9.8(a) and the transition temperature is shown in the Fig. 9.8(b).

The transition was sharp and occurred reversibly in a very narrow range of temperature (3–4 degrees). Also, the transition temperatures of the cross-linked fibers were found to shift towards the lower temperature from 37°C (in linear copolymer) to 22–25°C. As shown in Fig. 9.9, these engineered fibers display sharp temperature sensitivity, extremely high reversible change in dimensions (1000% in diameter and ~70% in length), and extremely fast response time (<20 s for expansion and <2 s for contraction).



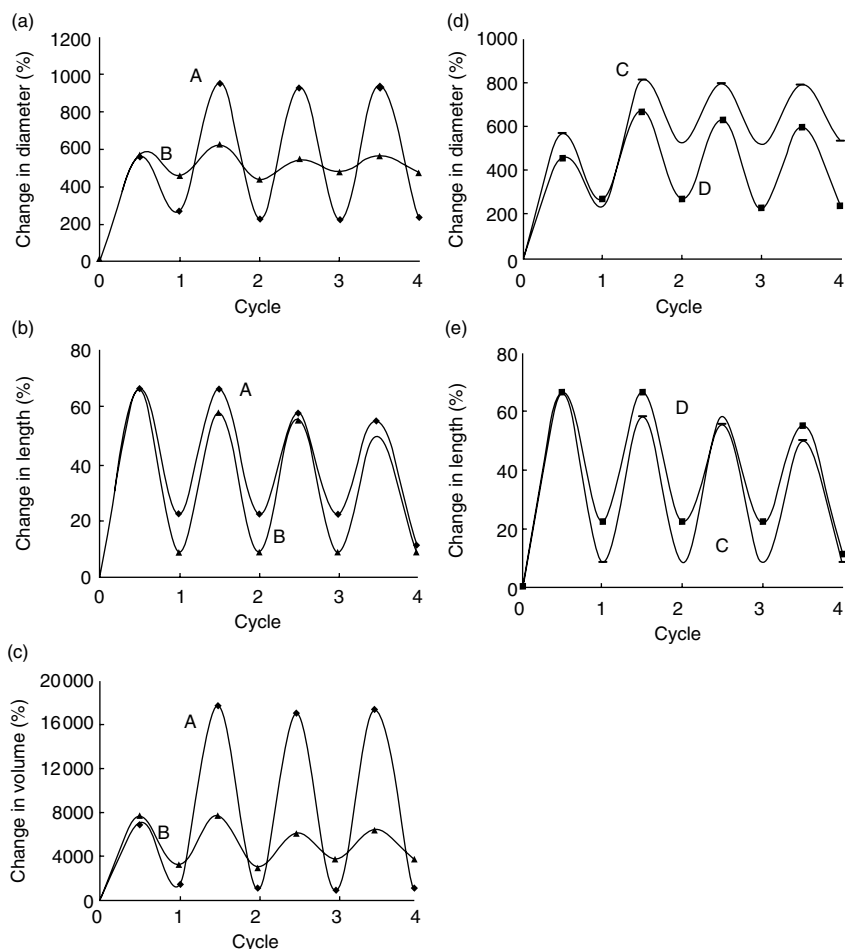
9.7 The optical microscopic view at $\times 100$ of SSP fiber produced from poly(NTBA:Am::27:73) copolymer with 37.9 mol% cross-linker concentration. (a) As-spun and cured fiber and (b) fiber at equilibrium swelling in water at 6°C.



9.8 Rate of transition and transition temperature of SSP fibers. (◆) Fiber with 37.9 mol% cross-linker concentration, (■) fiber with 88.4 mol% cross-linker concentration and (●) copolymer gel of the same composition shown for comparison.

pH-responsive fibers

(a) Hydrogel fibers by chemical cross-linking
PVA/PAA blend fibers have been thermally cross-linked to form hydrogel fibers.^{59,60} The hydrogel fibers exhibit pH-sensitive behavior and show hysteresis loop in the pH range from 2.5 to 12.5. The transition pH value was reported to shift to lower value with increasing content of PAA. The cross-linking of fiber caused a drop in the swelling ratio (i.e. magnitude of response decreased) and a shift in the transition pH to a higher pH value. The oscillatory swelling/contracting behavior of the hydrogel fiber exhibited

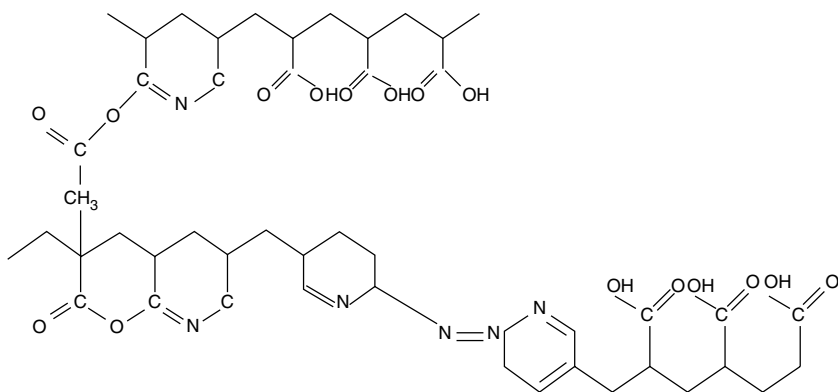


9.9 Change in shape of different SSP fibers when subjected to swelling/de-swelling cycles between 6°C and 80°C, respectively. Trace A, fiber with 37.9 mol% cross-linker concentration; trace B, fiber with 88.4 mol% cross-linker concentration; trace C, fiber with 63.2 mol% cross-linker concentration with draw ratio of 6; and trace D, fiber with 63.2 mol% cross-linker concentration with draw ratio of 3.

a well reversible pH-responsive property. But these fibers have very poor mechanical properties because of the cross-linked structure.

(b) Hydrogel fibers by modification of an existing precursor fiber

It is known that AN and AA copolymers are used as pH-sensitive materials. An interesting approach has been reported to modify the existing poly (acrylonitrile) (PAN) fiber to produce the pH-sensitive fiber.^{23,61} The modification involves two steps:



9.10 Chemical structure of modified PAN fiber.

- (i) Thermal stabilization of fiber at 210°C to impart cross-links that provide the strength and structural integrity.
- (ii) Saponification of nitrile groups to responsive carboxylic acid groups in the stabilized fibers.

Figure 9.10 shows the structure of stabilized and saponified acrylic fiber (pH-responsive fiber).

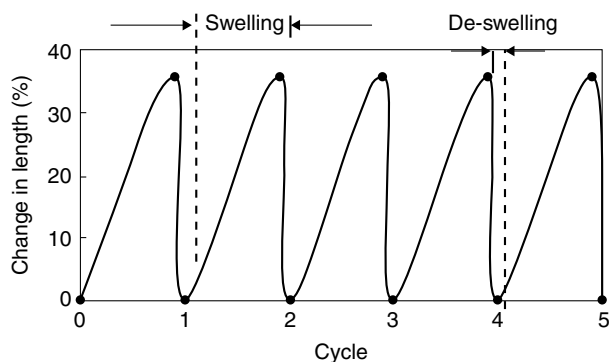
The modified PAN fibers were found to change shape with pH of environmental solution. The structure, properties and response behavior of modified fibers are determined by stabilization and saponification conditions. The modified PAN fiber (stabilized for 5 h and hydrolyzed) exposed to pH 10 attained equilibrium in 180 min with the percentage increase in length of about 55%.

The transition rate for the swelling cycle in 2N NaOH solution was extremely fast and was found to be complete in about 4 s. Compared to swelling, the de-swelling was still faster and the entire change occurred spontaneously (<1 s). The fast transition obtained in the pH-responsive fiber is due to the large surface to volume ratio provided by the fine fiber structure compared to hydrogels.

The fibers could be repeatedly subjected to cycles of elongation and contraction (Fig. 9.11) indicating the stability of structure. And the transition was sharp, stable and occurred reversibly.

This process appears to be simple and involves the modification of an existing precursor fiber but it has some drawbacks:

- (i) pH-sensitive fibers are black in color due to chemical conjugation of nitrile groups to form six membered aromatic rings, which makes them inappropriate for smart textile applications.
- (ii) Production rate of these fibers is considerably slow due to slow oxidation step.



9.11 Cyclability behavior of modified acrylic fiber.

- (iii) The parameters available for controlling the amount of cyclization and cross-linking in the fiber are limited.
- (iv) Production of fibers of varying chemical and physical architecture for tunable response is difficult.

(c) Hydrogel fibers with physical cross-links

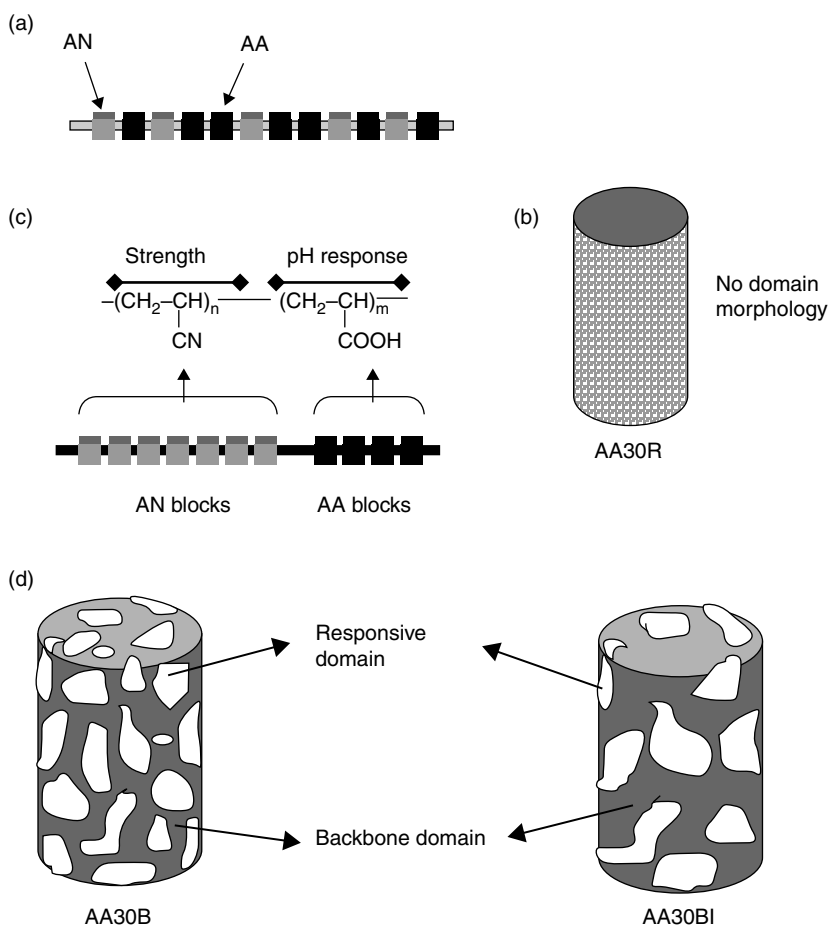
The above limitations of chemically cross-linked responsive fibers can be overcome and these can find additional numerous novel applications if:

- (i) Stimuli-sensitive copolymers could be synthesized with a controlled architecture (enriched segments of strength imparting monomer and enriched segments of responsive monomer).
- (ii) Interestingly, these new polymers could be processed into thin oriented fibers with physical cross-links (instead of chemical cross-links). Rather the physical structure of the fiber has been tuned to give both responsiveness and structural stability.

pH-sensitive copolymers of controlled architecture based on AA and AN have been synthesized by specially designed free radical polymerization. AN was chosen to impart fiber-forming properties to the copolymer while AA was selected to provide pH response. The approach was to control the distribution of both AN and AA (AA) moieties in the polymer chains in such a way that small block segments of each are possible. On wet spinning of the copolymers into fine fibers and their subsequent annealing, it was found that the segments of AN moieties from different chains could come together (phase separate), crystallize and form various tie-points (AN domains) to provide strength to the formed structure, whereas the block segments of AA could form responsive domains which provided pH response through ionization under suitable environment. The mechanical properties as well

as pH response of the fibers could be significantly enhanced by modifying the chemical architecture of the copolymers and the morphology of the resultant fibers, while keeping their physical dimensions fixed. The proposed structure of the copolymers is also shown in Fig. 9.12. Spinning of the copolymers was studied in detail with respect to their (a) thermodynamic behavior during spinning and (b) effect of spinning and post-spinning operations on their pH response and mechanical properties.⁶²

The fibers from block copolymer (AA50B) showed significantly higher strength, extensibility and retractive forces compared to fibers from random type copolymers (AA50R) (Table 9.2). These properties could be further



9.12 Proposed structure of the copolymers and fiber. (a) Chemical structure AA30R, (b) schematic of fibers AA30R, (c) chemical structure of AA30B and (d) schematic of fibers consisting of domain morphology.

Table 9.2 Equilibrium swelling of different pH-responsive fibers without any load and retractive force during de-swelling

Fiber from copolymer	AA or/and MA content in monomer feed (mol%)	% Volumetric swelling at pH 10	Time of swelling at pH 10	Retractive stress during de-swelling (MPa)	Breaking force during swollen condition (MPa)	Breaking force after de-swelling (MPa)
AA50R	50	1723	50	0.058	0.78	13.55
AA50B*	50	3890	45	0.26	3.31	34.29
AA40B	40	3601	45	0.29	8.67	59.38
MA30B	30	5200	30	0.12	3.29	27.40
AA30R	30	775	58	0.13	3.91	22.72
AA30B	30	1508	50	0.36	16.84	72.04
AA30BI	30	6775	20	0.46	20.76	83.32
AA30BII	30	8800	12	0.25	10.47	62.39
AAMA30B	30	3460	20	0.23	11.02	63.51

* AA50B: represents 50 mol% of monomer AA in blocky architecture and R represents random architecture.

improved by increasing the AN content to up to 90 mol% (AA40B–AA10B). Swelling behavior was also superior for fibers from block type copolymers. The extent and rate of swelling was higher while the hysteresis was lower for fibers from block type structures. However, the extent and rate of swelling decreased with increasing AN content. As a result of these changes, the fibers from AA30B (30 mol% AA) were able to show significantly better mechanical properties and retractive forces compared to fibers from AA50R while still maintaining a similar swelling ratio.

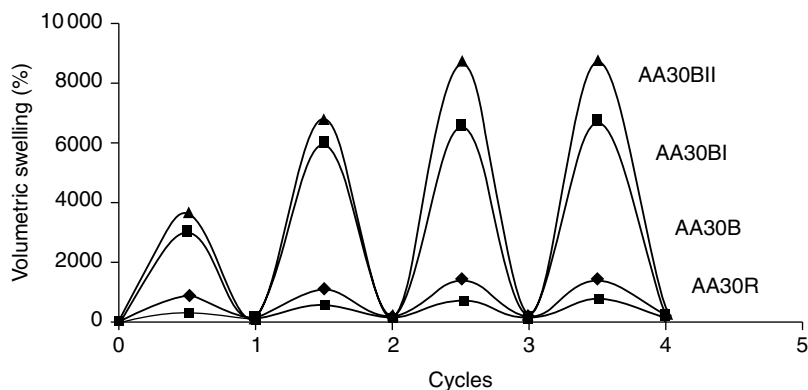
The finer fibers from AA50B (38 μm) showed a stable, reversible transition with significantly higher equilibrium volumetric swelling of 22200% at a pH of 10 compared to their thicker version of 120 μm , which showed volumetric swelling of only 3300–3600%. Also, the finer fibers from AA50B (38 μm) showed significantly higher strength (1.6 times), and higher retractive stress (1.2 times) during the transition compared to the fibers with higher diameter (120 μm). The rate of transition was also found to be higher for the finer fibers and their equilibrium de-swelling time was also significantly lower at 20 s. These changes in properties of the two fibers is attributed to the formation of better domain structure due to higher drawing imparted to the coagulating fiber. The fibers heat-set at 100°C were not able to withstand repeated cycling and were disintegrated in a few cycles, while the fiber heat-set at 150°C could withstand more than 50 cycles without any deterioration in their mechanical properties. However, the increased heat-setting temperature was found to have a negative effect on the equilibrium swelling as well as the response rate. The FTIR spectroscopy of the heat-set samples suggested that though samples had undergone some chemical changes in relation to disappearance of OH groups of COOH, there were no significant indications of formation of cyclized structure at these temperatures.

The effect of block length of individual monomer moieties on response and mechanical properties of the pH-sensitive fibers has also been reported.⁵¹ Copolymers of AN and AA with AA (feed ratio of 30 mol%) but varying average block length of AA were converted to fine fibers by solution spinning in DMF-water system, drawn in coagulation bath, and annealed at 120°C for 2 h to develop domain morphology. The domains formed were of nano dimensions (5–10 nm) possibly because of small segment lengths of AA and AN in the copolymers and were of different sizes as the segment lengths changed from one copolymer to another as evident from changing thermal shrinkage and X-ray diffraction patterns. The fibers with segregated nano-domain morphology (AA30B-AA30BII) were found to have significantly higher swelling percentage, faster response and higher stability to repeated cycling compared to the fiber obtained from random copolymer (AA30R) (Fig. 9.13). Also, the fibers from block copolymers (AA30B-AA30BII) showed better tensile properties during swelling and higher retracting forces during de-swelling.

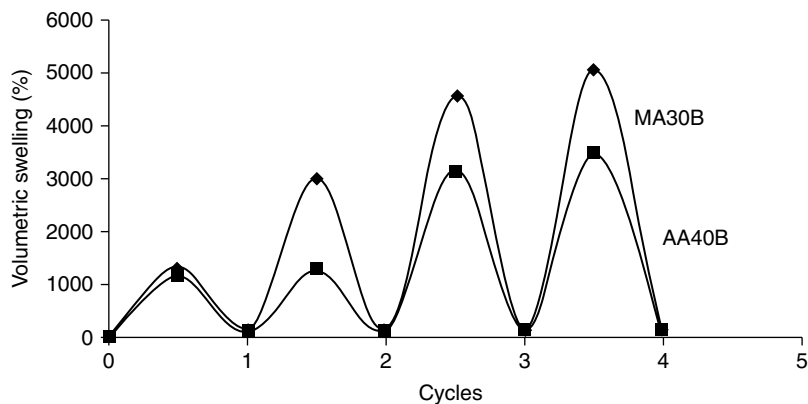
The fibers made from copolymers with higher AA block length showed significantly higher swelling ratio (an increase from 775% in AA30R to 8800% AA30BII) and a much faster response (0.25% per min to 12% per min) having a similar AA content. This was explained based on formation of possibly larger nano domains of AA moieties that allowed better and faster opening of the AA regions during swelling.

To understand the effect of bulky $-\text{CH}_3$ group of methacrylic acid (MA) on the properties of the pH-responsive fibers,⁶³ poly(acrylonitrile-co-methacrylic acid) was synthesized.

The fibers from MA30B showed higher volumetric swelling, faster response and lower mechanical properties compared to AA40B (with ~40mol% AA) possibly because of the bulky $-\text{CH}_3$ group in MA, which opens the responsive domains of the fibers (Fig. 9.14).



9.13 Cycles of swelling and de-swelling of the pH-sensitive fibers (AA30R, AA30B, AA30BI and AA30BII).



9.14 Cycles of swelling and de-swelling of the pH-sensitive fibers (AA40B and MA30B).

Clearly the replacement of AA with MA improved the responsive properties significantly; however, mechanical properties were compromised. Therefore, only a small amount of MA comonomer was incorporated along with AA in the AA30B type block copolymer.

The copolymer of AN and AA containing about 27 mol% AA and about 7 mol% of MA (AAMA30B) was synthesized using the method of regulated dosing. The properties of fibers from AAMA30B were compared with those from polymers having block type architecture with AA (AA30B) and from polymers with random architecture with AA (AA30R), where all copolymers had similar composition of acidic monomer (~30 mol%). The fibers developed from AAMA30B showed swelling values much higher than that of AA30B, which in turn showed higher values than that of AA30R. The fibers from AAMA30B showed swelling of 3103–3305%, which was more than 100% increase over the values of AA30B and gave a response rate of ~12%/min versus ~1.2%/min in AA30B, which was ten times faster. However, the mechanical properties were found to be still a bit lower in AAMA30B compared to AA30B. The retractive stress was 0.23 MPa (a decrease of 50%), tenacity in swollen condition was 11.02 MPa (a decrease of ~45%), and in de-swollen condition was 63.51 MPa (a decrease of ~15%). The reduction in mechanical properties suggested that the introduction of bulky MA moieties in the polymer chains had hampered the formation of proper AN domains, which were responsible for creating the stress bearing backbone of the fiber.

These fibers also exhibited sensitivity to temperature.⁴⁰ When subjected to change in temperature at an alkaline aqueous medium, the fibers showed temperature-dependent swelling behavior. The swelling first increased with increasing temperature and then suddenly decreased to swelling values close to the original state. For example, fibers containing 30 mol% of AA (AA30B) showed a clear and sharp transition temperature between 49°C and 50°C, where the swelling suddenly decreased from 6440% to 4200%. The behavior was reversible and stable to repeated cycling. The transition temperature at pH 10 could be modulated from 40°C to 62°C by varying the composition of the copolymer from 10 mol% AA to 50 mol% AA. While the transition temperature for AA30 B could be changed from 33°C to 61°C as the pH of the medium was increased from 7 to 12. Below pH 7, the thermal transition could not be observed probably due to the poor ionizability of the carboxylic groups.

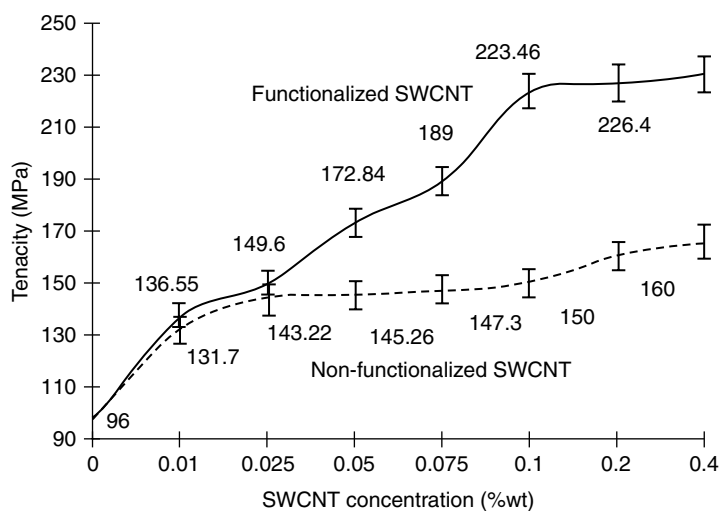
The transition appears to be a result of three simultaneous effects: (a) first increased ionization of carboxylic groups due to increasing pH; (b) increased ionization of carboxylic groups due to increasing temperature, and (c) LCST transition of copolymer while going from lower to higher temperature regime. The dual response to pH and temperature stimulus in acrylic fibers is an important discovery and is expected to support the

development of new application in actuators, smart textiles and related areas.

Electroactuating fibers

Many of the polyelectrolytes/pH-responsive polymers (like Chitosan) have been reported to show actuation to changes in the applied voltage to some extent. The electrical actuation amongst these polyelectrolyte hydrogels is limited due to the insulating nature of the polymeric hydrogels. Attempts, such as blending with a conducting polymer, have been made to improve its sensitivity towards electric voltage,^{64–66} but satisfactory results have not yet been obtained. Another problem that arises is the stability of these materials towards the cyclic changes in the pH. Thus, to improve its stability, blending with some other polymers or copolymerization is carried out which, in turn, adversely affects the response behavior.

When the electric voltage is applied, chitosan fiber is observed to show some response, but the magnitude and the speed of response is less. Therefore to induce the electrical conductivity within the chitosan matrix blending with a conducting filler material has been reported. Suitably functionalized single wall carbon nano-tubes (SWCNT) were dispersed in chitosan and wet spun in an alkaline coagulation system to produce SWCNT/chitosan composite fibers.⁶⁷ The incorporation of SWCNT loading on the mechanical properties of the composite fiber was investigated and the tensile stress–strain curves are shown in Fig. 9.15. The tenacity of neat chitosan fiber was recorded as 96 MPa. The incorporation of functionalized carbon



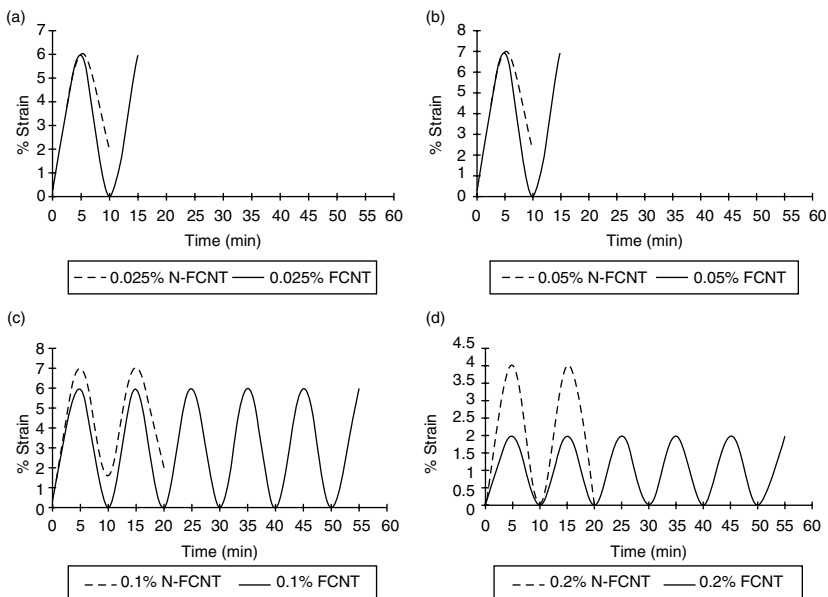
9.15 Effect of SWCNT concentration on the tenacity of SWCNT/chitosan composite fiber.

nano-tubes resulted in continuous and significant improvement in tenacity even at higher SWCNT concentrations.

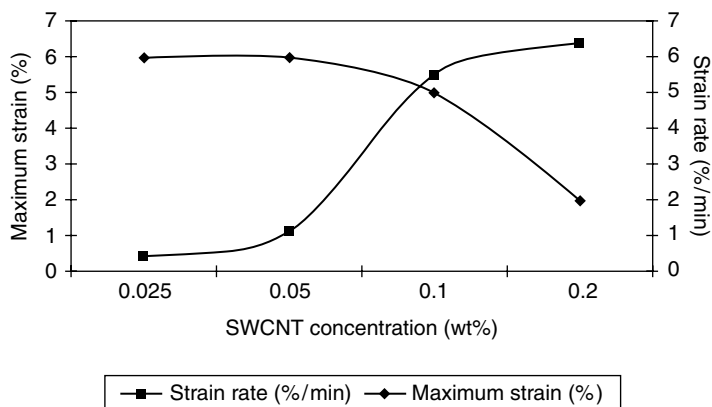
Carbon nano-tube reinforced chitosan fibers were subjected to electric field for a known time interval at constant potential difference of 10 V in a 0.5% NaCl solution. The specimens were connected to cathode and anode alternately after every 5 min.

The pure chitosan fibers remain unaffected even on application of electric voltage or rather it can be assumed to be a too slow response and of very low magnitude. The SWCNT/chitosan composite fibers responded immediately to the change in applied voltage. Figure 9.16 illustrates the behavior of chitosan fibers with the cyclic switching of the potential difference.

Figure 9.17(a) and (b) shows the response behavior towards the applied voltage. With the increase in the carbon nano-tube concentration some strain is observed when the fiber is connected at the cathode, but up to the carbon nano-tube concentration of 0.05% the fiber cannot survive beyond three cycles of switching electric field. As shown in Fig. 9.17(c) and (d), on incorporation of non-functionalized SWCNT, the composite fibers are not able to survive beyond three cycles even at higher concentration of the SWCNT. In case of the functionalized SWCNT, the stability of the fibers can be observed until ten cycles of changing electric field. This can be attributed to the interaction between the amine groups of the chitosan and the



9.16 Response of SWCNT/chitosan composite fibers to the changes in applied voltage (10 V in 0.5% NaCl solution).



9.17 Effect of functionalized SWCNT on the magnitude and strain rate of the composite fibers.

carboxyl groups present on the functionalized carbon nano-tubes. At higher concentration of nano-tubes (0.2% of SWCNT), the strain observed during the changing electric field is lower than that observed for 0.1% concentration. This may be due to the increase in the rigidity of the composite fibers at the higher carbon nano-tube concentration.

It has been observed that the strain rate with respect to the applied voltage and the magnitude of strain are a function of the carbon nano-tube concentration. The presence of carbon nano-tubes introduces a conductive path for free ions in the chitosan hydrogel. Thus with the increase in the SWCNT concentration, the strain rate increases. However, the presence of carbon nano-tubes makes the fiber structure more rigid and therefore the magnitude of strain decreases.

9.5 Conclusions

The study suggested that the control of the chemical architecture and physical morphology of the pH-responsive structure may be the key to producing responsive fibers with both higher mechanical properties and response that are suitable for their applications in artificial muscles, actuators and smart textiles.

9.6 References

1. TAO, X (ed.), *Smart Fibers, Fabrics and Clothing*. Cambridge: Woodhead Publishing.
2. ROY, D., CAMBRE, J. and SUMERLIN, B. S., Future perspectives and recent advances in stimuli-responsive materials. *Progress in Polymer Science*, 35 (2010): 278–301.

3. KUMAR, A., SRIVASTAVA, A., GALAEV, I. Y. and MATTIASSON, B., Smart polymers: physical forms and bioengineering applications. *Progress in Polymer Science* 32(10) (2007): 1205–1237.
4. HESKINS, M. and GUILLET, J. E., Solution properties of poly(*N*-isopropylacrylamide). *Journal of Macromolecular Science Chemistry*, A2(8) (1968): 1441–1455.
5. JASSAL, M., AGRAWAL, A. K. and SAVE, N. S., Thermoresponsive smart textile. *Indian Journal of Fibre and Textile Research*, 31(1) (2006): 52–65.
6. SHIBAYAMA, M., MORIMOTO, M. and NOMURA, S., Phase separation induced mechanical transition of poly(*n*-isopropylacrylamide)/water isochore gels. *Macromolecules*, 27 (1994): 5060–5066.
7. DONG, L. C. and HOFFMAN, A. S., Insulin permeation through thermo-sensitive hydrogels. *Journal of Controlled Release*, 9 (1989): 271–279.
8. KIKUCHI, A. and OKANO, T., Pulsatile drug release control using hydrogels. *Advanced Drug Delivery Review*, 54 (2002): 53–77.
9. FIEL, H., BAE, Y. H., FEIJIN, J. and KIM, S. W., Molecular separation by thermosensitive hydrogel membranes. *Journal of Membrane Science*, 64 (1991): 283–294.
10. LIN, F., TAO, G. L. and ZHU, R. X., Synthesis of thermal phase separating reactive polymers and their applications in immobilized enzymes. *Polymer Journal* 25 (1993): 561–567.
11. KISHI, R., ICHOU, P. and HIROSA, O. J., Thermo-responsive devices using poly(vinyl methyl ether) hydrogels. *Journal of Intelligent Material Systems and Structures* 4 (1993): 533–537.
12. MARRA, S. P., RAMESH, K. T. and DOUGLAS, A. S., Mechanical characterization of active poly(vinyl alcohol)-poly(acrylic acid) gel. *Materials Science and Engineering C*, 14 (2001): 25–34.
13. MARRA, S. P., RAMESH, K. T. and DOUGLAS, A. S., Characterization and modeling of compliant active materials. *Journal of Mechanics and Physics of Solids*, 51 (2003): 1723–1743.
14. LELE, A. K., HIRVE, M. M., BADIGER, M. V. and MASHELKAR, R. A., Predictions of bound water content in poly(*N*-isopropylacrylamide) gel. *Macromolecules* 30 (1997): 157–159.
15. DHARA, D. and CHATTERJEE, P. R., Phase transition in linear and cross-linked poly(*N*-isopropylacrylamide) in water: effects of various types of additives. *Journal of Macromolecular Science – Reviews of Macromolecular Chemistry and Physics*, C40(1) (2000): 51–68.
16. LIU, H. Y. and ZHU, X. X., Lower critical solution temperatures of *N*-substituted acrylamide copolymers in aqueous solutions. *Polymer*, 40 (1999): 6985–6990.
17. MUELLER, K. F., Thermotropic aqueous gels and solutions of *N,N*-dimethylacrylamide-acrylate copolymers. *Polymer*, 33 (1992): 3470–3476.
18. DEBORD, J. D. and LYON, L. A., Synthesis and characterization of pH-responsive copolymer microgels with tunable volume phase transition temperatures. *Langmuir*, 19 (2003): 7662–7664.
19. TAN, Q., ZHAO, X., TANG, X. and ZHANG, Y., Hydrophobic association and temperature and pH sensitivity of hydrophobically modified poly(*N*-isopropylacrylamide/acrylic acid) gels. *Journal of Applied Polymer Science*, 87 (2003): 2406–2413.
20. SHIN, B. C., KIM, S. S., KO, J. K. and KYUNG, J. J., Gradual phase transition of poly(*N*-isopropylacrylamide-co-acrylic acid) gel induced by electric current. *European Polymer Journal*, 39 (2003): 579–584.

21. ZHANG, X. Z., YANG, Y. Y., WANG, F. J. and CHUNG, T. S., Thermosensitive poly(*N*-isopropylacrylamide-co-acrylic acid) hydrogels with expanded network structures and improved oscillating swelling-deswelling properties. *Langmuir*, 18 (2002): 2013–2018.
22. SAVE, N. S., JASSAL, M. and AGRAWAL, A. K., Stimuli sensitive copolymer poly(*N*-tert butylacrylamide-ran-acrylamide): synthesis and characterization. *Journal of Applied Polymer Science*, 95(3) (2005): 672–680.
23. JIA, Z., CHEN, H., ZHU, X. and YAN, D., Backbone-thermoreponsive hyperbranched polyethers. *Journal of American Chemical Society*, 128 (2006): 8144–8145.
24. SCHREYER, H. B., GEBHART, N., KIM, K. J. and SHAHINPOOR, M., Electrical activation of artificial muscles containing polyacrylonitrile gel fibers. *Biomacromolecules*, 1 (2000): 642–647.
25. ZAREIE, H. M., BULMUS, E. V., GUNNING, A. P., HOFFMAN, A. S., PISKIN, E. and MORRIS, V. J., Investigation of a stimuli-responsive copolymer by atomic force microscopy. *Polymer*, 41 (2000): 6723–6727.
26. JIANQI, F. and LIXIA, G., PVA/PAA thermo-crosslinking hydrogel fiber: preparation and pH-sensitive properties in electrolyte solution. *European Polymer Journal*, 38(8) (2002): 1653–1658.
27. JING, J. and MINGZHI, H., Swelling kinetics for gelatin-poly(*N*-isopropylacrylamide) hydrogel. *Gongneng Gaofenzi Xuebao* 15(2) (2002): 177–180.
28. NAKAMURA, K. and PEPPAS, N. A., Uptake and release of budesonide from mucoadhesive, pH sensitive copolymers and their application to nasal delivery. *Journal of Controlled Release*, 61 (1999): 329–335.
29. CHUANMIN, R., KEFENG, Z. and CRAIG, A. G., A mass-sensitive pH sensor based on a stimuli-responsive polymer. *Analytica Chemical Acta*, 497 (2003): 123–131.
30. HU, Y., JIANG, X. and DING, Y., Synthesis and characterization of chitosan-poly(acrylic acid) nanoparticles. *Biomaterials*, 23 (2002): 3193–3201.
31. CHEN, S., LIU, M., JIN, S. and CHEN, Y. J., Synthesis and swelling properties of pH-sensitive hydrogels based on chitosan and poly(methacrylic acid) semi-interpenetrating polymer network, *Applied Polymer Science*, 98 (2005): 1720–1726.
32. GHOLAP, S. G. and BADIGER, M. V., Synthesis and characterization of polyamphoteric hydrogel membrane based on chitosan. *Journal of Applied Polymer Science*, 93(3) (2004): 1454–1461.
33. DEEPAK, A. M. and ASHWANI, K., Solvent and pH resistance of surface crosslinked chitosan/poly(acrylonitrile) composite nanofiltration membranes. *Journal of Applied Polymer Science*, 77 (2000): 1782–1793.
34. POURJAVADI, A., MAHDAVINIA, G. R. and ZOHURIAAN-MEHR, M. J., Modified chitosan. II. H-chitoPAN, a novel pH-responsive superbabsorbent hydrogel. *Journal of Applied Polymer Science*, 90(11) (2003): 3115–3121.
35. KIOUSSIS, D. R., WHEATON, F. W. and KOFINAS, P., Phosphate binding polymeric hydrogels for aquaculture wastewater remediation. *Aquacultural Engineering*, 19 (1999): 163–178.
36. GONZALEZ, N., ELVIRA, C. and ROMAN, J. S., Novel dual-stimuli-responsive polymers derived from ethylpyrrolidine. *Macromolecules*, 38(22) (2005): 9298–9303.
37. THEMIS, R., YRIAKIDES, K., CHEUG, C. Y. and MURTHY, N., pH-sensitive polymers that enhance intracellular drug delivery in vivo. *Journal of Controlled Release*, 78 (2002): 295–303.

38. FANG LIU and MAREK, W., Urban recent advances and challenges in designing stimuli-responsive polymers. *Progress in Polymer Science*, 35(1–2) (2010): 3–23.
39. HOFFMAN, A. S., Conventional and environmentally sensitive hydrogels for medical and industrial uses: a review paper. In: DEROSS, D., KAJIWARA, K., OSADA, Y. and YAMAUCHI, A. (eds.) *Polymer Gels*. New York: Plenum Press, 1991, pp 289–297.
40. SAHOO, A., JASSAL, M. and AGRAWAL, A. K., Discovery of a unique dual response in acrylonitrile copolymers. *Smart Materials and Structures*, 16(5) (2007): 1843–1848.
41. ZHANG, J. and PEPPAS, N. A., Synthesis and characterization of pH- and temperature sensitive poly(methacrylic acid)/poly(*N*-isopropylacrylamide) interpenetrating polymeric networks. *Macromolecules*, 33 (2000): 102–107.
42. WEI, X., SIMON, C., MALCOLM, B. H. and TIMOTHY, G. J., Rapid swelling and deswelling in cryogels of crosslinked poly(*N*-isopropylacrylamide-co-acrylic). *European Polymer Journal*, 40(4) (2004): 703–712.
43. CHEN, K. S., KU, Y. A., LIN, H. R., YAN, T. R., SHEU, D. S., CHEN, T. M. and LIN, F. H., Preparation and characterization of pH-sensitive poly (N-vinyl 2-pyrrolidone/itaconic acid) copolymer hydrogels. *Materials Chemistry and Physics*, 91(2–3) (2005): 484–489.
44. ZHOU, W. J. and KURTH, M. J., Synthesis of a novel pH-responding polymer with pendant barbituric acid moieties. *Polymer*, 42 (2001): 345–349.
45. BENREBOUH, A., AVOCE, D. and ZHU, X. X., Thermo- and pH-sensitive polymers containing cholic acid derivatives. *Polymer*, 42 (2001): 4031–4038.
46. CHEN, G. and HOFFMAN, A. S., Graft copolymers that exhibit temperature-induced phase transitions over a wide range of pH. *Nature*, 373 (1995), 49.
47. SHIN, B. C., JOHN, M. S., LEE, H. B. and YUK, S. H., pH/temperature dependent phase transition of an interpenetrating polymer network: anomalous swelling behavior above lower critical solution temperature. *European Polymer Journal*, 34 (1998): 1675–1681.
48. TALAPATRA, A., SETHI, S., JASSAL, M. and AGRAWAL, A. K., Chitosan polyacrylic acid interpenetrating networks: emerging trends in polymers and textiles. *Proceedings of International Conference*, New Delhi, India, 7–8 January 2005, pp. 201–207.
49. SAHOO, A., RAMASUBRAMANI, K. R. T., JASSAL, M. and AGRAWAL, A. K., Effect of copolymer architecture on the response of pH sensitive fibers based on acrylonitrile and acrylic acid. *European Polymer Journal*, 43(3) (2007): 1065–1076.
50. SAHOO, A., JASSAL, M. and AGRAWAL, A. K., Influence of the copolymer architecture and composition on the response and mechanical properties of pH-sensitive fibers. *Journal of Applied Polymer Science*, 105 (2007): 3171–3182.
51. SAHOO, A., JASSAL, M. and AGRAWAL, A. K., Effect of distribution of monomer moiety on pH response and mechanical properties of poly(acrylonitrile-co-acrylic acid) copolymers. *Smart Materials and Structures*, 19(2) (2010): 025015/1–025015/11.
52. AGRAWAL, A. K., JASSAL, M., VISHNOI, A. and SAVE, N. S., Temperature responsive fibers with anisotropic transitional behavior. *Journal of Applied Polymer Science*, 95 (2005): 681–688.
53. MATSUO, E. S. and TANAKA, T., Kinetics of discontinuous volume-phase transition of gels. *Journal of Chemical Physics*, 89 (1988): 1695–1703.
54. GAN, L. H., ROSHAN, D. G., GAN, Y. Y. and TAM, K. C., Water sorption studies of new pH responsive *N*-acryloyl-*N'*-methyl piperazine and methyl methacrylate gels. *European Polymer Journal*, 37 (2001): 1473–1478.

55. SAVE, N. S., JASSAL, M. and AGRAWAL, A. K., Smart breathable fabric. *Journal of Industrial Textiles*, 34(3) (2005): 39–155.
56. CRESPI, D. and ROSSI, R. M., Temperature-responsive polymers with LCST in the physiological range and their applications in textiles. *Polymer International*, 56 (2007): 1461–1468.
57. JUN, L., JUN, L., MIN, Y. and HONGFEI, H., Solvent effect on grafting polymerization of NIPAAm onto cotton cellulose via γ -preirradiation method. *Radiation Physics and Chemistry*, 60 (2001): 625.
58. XIE, J. and HSIEH, Y., Thermosensitive poly(*N*-isopropylacrylamide) hydrogels bonded on cellulose supports. *Journal of Applied Polymer Science*, 89 (2003): 999.
59. QUI, Y. and PARK, K., Environment-sensitive hydrogels for drug delivery. *Advanced Drug Delivery Review*, 53 (2003): 321–339.
60. XING, J. and HSIEH, Y.-L., pH-responsive swelling behavior of poly(vinyl alcohol)/poly(acrylic acid) bi-component fibrous hydrogel membranes. *Polymer*, 46(14) (2005): 5149–5160.
61. JASSAL, M., AGRAWAL, A. K., GHOSH ARNAB, K., RAMASUBRAMANI, K. R. T. and SAHOO, A., Stimuli sensitive behaviour of modified polyacrylonitrile fibres. *Journal of Textile and Apparel*, 10(2) (2006): 58–68.
62. SAHOO, A., MANJEET, J. and AGRAWAL, A. K., pH-responsive fibers based on acrylonitrile acrylic acid block copolymers: effect of spinning conditions and post-spinning operations on response and mechanical properties. *Journal of Applied Polymer Science*, 109(6) (2008): 3792–3803.
63. SAHOO, A., MANJEET, J. and AGARWAL, A. K., pH responsive fibers based on acrylonitrile copolymers: effect of bulky side group on response and mechanical properties. *Hankook Sumyu Gonghakhoeji*, 44(3) (2007): 149–158.
64. SIDDHANTA, S. K. and GANGOPADHYAY, R., Conducting polymer gel: formation of a novel semi-IPN from polyaniline and crosslinked poly(2-acrylamido-2-methyl propanesulphonic acid). *Polymer*, 46 (2005): 2993–3000.
65. KIM, S. J., SHIN, S. R., LEE, S. M. and KIM, I. Y., Electromechanical properties of hydrogels based on chitosan and poly (hydroxyethyl methacrylate). *Smart Materials and Structures*, 13 (2004): 1036–1039.
66. KAEWPIRON, S. and BOONSANG, S., Electrical response characterisation of poly(ethylene glycol) macromer (PEGM)/chitosan hydrogels in NaCl solution. *European Polymer Journal*, 42 (2006): 1609–1616.
67. SUKRUT, O., JASSAL, M. and AGRAWAL, A. K., pH and electrical actuation of single walled carbon nanotubes/chitosan composite fibers. *Smart Materials and Structures*, 17 (2008), doi: 055016 (8 pp.).

Development and design of performance swimwear

J. WU,
Georgia State University, USA

Abstract: Innovative performance swimwear has been widely used during competitive swimming competitions to reduce drag force and enhance swimmers' performance. This chapter briefly reviews the history of performance swimwear development and focuses on the question of whether performance swimwear can significantly improve swimming performance in collegiate and professional swimmers. Specifically, this chapter provides information on the material and design of performance swimwear, the basic biomechanics of swimming, the measurement of passive and active drag force, and the effect of performance swimwear on drag forces and physiological and biomechanical responses during swimming. A brief discussion deals with the design and impact of performance swimwear in the future.

Key words: performance swimwear, swimming, drag force, biomechanics, physiology.

10.1 Introduction

Swimwear is an article of clothing that is used for swimming and other aquatic activities. Swimwear is usually designed for men, women and children to accommodate their different body configurations. Swimwear design varies drastically in materials, colors, body coverage, level of fit and other factors. Performance swimwear is a type of swimwear that is specially designed to help professional athletes to further improve their swimming performance. Since the Olympic Games in Sydney in 2000, performance swimwear has attracted enormous public attention. Innovative materials and technology have been researched and applied by manufacturers such as Speedo and TYR to revolutionize the design of performance swimwear. The outcome is that a number of new swimming world records have been set over the first decade of the twenty-first century. Although the International Swimming Federation (FINA) banned the usage of full-body performance swimwear starting on 1 January 2010, it is important to review the development of performance swimwear during the last decade and forecast the future direction it might take.

This chapter focuses on the development of performance swimwear and addresses the question of whether performance swimwear can significantly improve swimming performance in collegiate and professional swimmers. Specifically, this chapter provides information on the material and design of performance swimwear, the basic biomechanics of swimming, the measurement of passive and active drag force, and the effect of performance swimwear on drag forces and physiological and biomechanical responses during swimming. Finally, the chapter forecasts the design and impact of performance swimwear in the future.

10.2 Development of performance swimwear

10.2.1 Brief history of the development of swimwear

During the classical period swimming was mainly done in the nude. The earliest swimwear can be traced back to Grecian times and early Pompeii. Wearing a special covering during swimming has occurred for centuries since then. However, no drastic changes in the design of swimwear occurred until the last century or two. The last two decades are the pivotal point in the development of functional and performance swimwear. New materials, designs and technologies have been used collectively to significantly improve the quality of functional and performance swimwear.

When public bathing and swimming became popular in France and England during the eighteenth century, appropriate swimwear was needed to bring men and women together on the beach. However, swimwear at that time was more like bathing gowns rather than functional swimwear. This type of swimwear was far from comfortable due to the materials and designs. To avoid indecent exposure, ladies at that time often sewed additional weights such as lead into the hem of the bathing gown, which in turn reduced the comfort and function of swimwear (Horwood, 2000). With increasing demands for better fit and functional swimwear, the last two centuries have witnessed a revolution in the development of functional and performance swimwear. Specially designed swimwear aimed to protect one's modesty and more importantly to allow one to participate in swimming and water sports freely. Women's typical swimwear at the end of nineteenth century had a two-piece design which included a one-piece blouse and trousers and another piece of skirt extending below the knees to conceal the figure. At the beginning of the twentieth century revolutionary designs of swimwear emerged to make swimwear more transparent and briefer (Davies, 1997). Young women of the 1920s adopted a figure-hugging wool jersey sleeveless tank suit. The next 30 years saw increased popularity for feminine cotton-printed swimwear with small overskirts to hide the thighs (Horwood, 2000). This swimwear design was broadly similar to the swimwear of today. During

the 1950s a bikini or two-piece women's swimsuit became a revolutionary milestone in the development of swimwear. With one piece covering the breasts and the other covering the groin or the entire buttocks region, a bikini exposes the rest of the torso. However, a traditional one-piece (also known as tank suit) swimsuit has been the typical performance (or racing) swimwear for women.

Like the evolutionary process in the development of women's swimwear, men's swimwear also changed over time. Men's swimwear from the beginning showed marked differences to women's swimwear. In contrast to the exaggerated curves used in female swimwear design, boxiness and solidity were the two main characteristics of men's swimwear (Davies, 1997). One controversial issue that was vigorously debated was whether men should be allowed to bare their chests in public swimming and bathing. As a compromise, men's typical swimwear during the 1920s had a skirt or a flannel knee pants which were worn outside of the trunks. By 1933, a convertible-style belted suit emerged which allowed the top to be removed by unzipping the newly invented zipper. However, many arrests were still made for indecent exposure. In the same year the BVD company hired Olympic swimmer Johnny Weismuller to advertise a new swimwear line, the first ever pair of bathing trunks (Cunningham, 2009). It was not until 1937 that men finally had the right to wear only the trunks during swimming. With women's suits becoming more and more daring and flamboyant during the 1950s and beyond, men's swimwear saw an explosion of color patterns and fancy artwork. In contrast to the almost constant transformation of women's swimwear, men's swimwear has been, to a great extent, confined to the basic boxer and brief. This was also the traditional men's performance swimwear used in the second half of the twentieth century.

10.2.2 Materials used in performance swimwear

When swimwear took the form of bathing gown, mainly functioned as covering suit, it was made of natural fibers such as wool. These bathing gowns were extremely heavy in water when fully soaked, making the action of swimming more difficult. For example, the first Jantzen male swimwear weighed about 4 kg (9 lb) when fully soaked and therefore had a tendency to slip down. Although swimwear was often made of wool knit, other materials were also used including silk and cotton. But all of these natural materials still became extremely heavy when fully soaked. Therefore, the revolution in swimwear demanded snug-fitting fabrics that were lightweight, had recoverable elasticity and possessed dye retention and tensile qualities in the most adverse environments. Furthermore, though tight-fitting, the swimwear could not restrict movement during vigorous exercise.

Initially rayon fiber was used, first manufactured in 1889 from an extract of the mulberry leaf and introduced into the United States as artificial silk in 1910. The Jantzen Company produced the first rib knit stitch swimwear in the 1910s, which gave them a technological advantage over their competitors who still used wool jersey and flat stitch (Allender, 1996). During the following decade, American Rubber's Lastex, an extruded rubber surrounded by fiber, became a popular staple, despite its failure to retain color and design when stretched, or retain its flex life when exposed to body oils. For example, in 1930s the Jantzen's Sunsheen fabric was made with Lastex (Allender, 1996), and the BVD's Sea Satin fabric was made of a rayon acetate fabric backed with Lastex for stretch and used a new knitting stitch called the Gulf stream stitch (Cunningham, 2009).

Searching for less expensive manmade fibers during the Great Depression, Wallace Carothers at Du Pont researched a series of polyamides and finally produced nylon 6,6, one of most commonly used polymers. Although nylon hosiery was introduced as early as 1940, it was not until after World War Two that nylon was fully utilized to improve the elasticity of swimwear. Nylon was found to be molded and heat set to a permanent shape and to display differing textures depending on whether it has been woven or knitted. Also, in the 1940s polyester, another commonly used polymer, was invented and used in the manufacture of swimwear. By the end of the 1950s, research scientists had produced a variety of manmade textile filaments such as Du Pont's Dacron, Vyrene, Lycra and Spandex. These new materials, whether used alone or blended with other materials, continued to revolutionize the swimwear industry by improving the comfort, function and fashion of swimwear. The revolution of swimwear manufacture in the first decade of the twenty-first century has seen the inclusion of textured, thin fabric and water-repellent coatings used to reduce the drag force acting on the swimwear.

10.2.3 Design of performance swimwear

In the late nineteenth century swimwear was barely modified summer day-time wear for men and women due to social restrictions. This type of swimwear had the vaguely functional design of sitting on a beach but was not optimal for swimming (Allender, 1996). Johnny Weissmuller, who won five Olympic gold medals in swimming, assisted the BVD Company in developing men's swimwear in the early 1930s. The Weissmuller model that was introduced in 1931 had low cut armholes to free the arms and a high waist for more room from crotch to waist (Cunningham, 2009). This one-piece swimwear was almost identical to the traditional women's performance (or racing) swimwear. Other swimwear from the same company had a two-piece design with shirts and trunks separately made with wool and rayon. The

women's swimwear design was more fashionable with a feature of evening gown backs. Almost all the women's swimwear had the design of a skirted front and back for modesty with minuscule trunks attached underneath (Cunningham, 2009). Performance swimwear, used in general competitive water sports such as swimming, followed the traditional design for the most of the second half of the twentieth century, i.e. boxer trunk or brief for men and one-piece swimwear for women.

The design of traditional men's and women's swimwear changed little until the late 1990s. In 1996, Speedo announced the development of the best and fastest swimwear possible on the basis of their award-winning Aquablade swimwear. A special fabric called Fastskin made of polyester and Lycra was introduced in 2000 and its second version Fastskin FSII made of nylon and Lycra was introduced in 2004. With the goal of reducing the total amount of drag over the surface of the swimwear, Speedo moved away from the traditional manufacture of swimwear and looked to nature to mimic the skin of fast-moving creatures. Sharks, creatures that are fast in water but not naturally hydrodynamic, were chosen as a model for the Fastskin and Fastskin FSII swimwear. Scientific research has indicated that sharks' quickness is to a great extent attributed to the V-shaped ridges on its skin which are called denticles. These denticles decrease surface friction and turbulence on the shark's skin and allow the water to pass the skin more effectively. Similar denticles added to the Fastskin and FSII swimwear parallel to the path of swimming resemble a series of peaks and valleys. When water flows over the body, only the peaks contact with water and therefore reduce the drag force. In contrast to Speedo's denticle design, the TYR Company included ridges or tripwires perpendicular to the path of swimming in their performance swimwear. It was claimed that these additional tripwires would reduce both pressure and wave drag force during competitive swimming.

The design of performance swimwear also broke away from the traditional men's and women's performance (racing) swimwear. Various design models were available on the market which included waist-to-knee, waist-to-ankle, neck-to-knee, neck-to-ankle and full body including arms. Innovative performance swimwear developed during this period also used the super stretch fabric to increase swimwear fit, improve streamlined shape of the body, and enhance muscle efficiency. It was believed that by compressing the skin and muscles, vibrations in the skin and muscles would significantly reduce to increase muscle power. With the revolutionary body scanning technique and 3-D swimwear pattern design, Speedo researchers and engineers were able to make swimwear for individual swimmers while providing them with a full range of motion during swimming. From anatomic and dynamic points of view, Speedo created a swimwear pattern in which seams act like tendons and provide tension in the swimwear while the fabric panels act like muscles and provide power to complete the swimming activity.

To further reduce the drag force of performance swimwear, Speedo manufactured the next generation Fastskin products, LZR racer swimwear in 2008, which became the predominant swimwear in the Beijing Olympic Games that year. A lightweight LZR Pulse fabric, which was exclusive to Speedo, was claimed to provide better water-repellent capability and more skin compression than Fastskin FSII swimwear. This lightweight fabric is woven rather than knitted from chlorine resistant elastane and ultra fine nylon yarns. Water-repellent coating added on the LZR Pulse fabric via a plasma process provided lower water absorption and a fast water drying rate. Polyurethane panels were placed strategically around the parts of the torso, abdomen and lower back that experience high amounts of drag. Ultrasonic welding was also applied to eliminate the traditional seams and smooth the surface of the swimwear. The design of the sleeveless neck-to-ankle pattern became highly popular in the Beijing Olympic Games that year.

10.2.4 Does performance swimwear enhance the performance of swimming?

World records of competitive swimming have been set at an unprecedented rate since the introduction of innovative performance swimwear in 2000. The Aquatic World Championships in Rome, Italy in 2009, observed 28 new world records set by swimmers wearing the bodysuit-type (neck-to-ankle) swimwear. This year was also the last year before the swimming governing body FINA banned the usage of bodysuit-type performance swimwear. The critics have long argued that the new performance swimwear might have benefited some swimmers more than others. Such advantages may be found in the morphology (i.e. more streamlined shape) of the swimmer and a better angle of buoyancy in the water. Although almost all performance swimwear manufacturers claimed that their products significantly reduce the drag force and increase swimming performance, the question that needs to be addressed is whether scientific research findings have supported these claims. This will be the focus of the next few sections in this chapter. The basic biomechanics of swimming will be briefly reviewed in the next section followed by the summary of peer-reviewed scientific papers on the effect of performance swimwear on competitive swimming.

10.3 Biomechanics of swimming

10.3.1 Fluid mechanics: drag force associated with swimming

While traveling through the water a swimmer displaces some water from his or her path. Resistance from the water can usually be defined as either

passive or active drag. Passive drag is the resistance that a swimmer experiences when being towed passively in the water or gliding without other movements underneath the water. In contrast, active drag is the resistance that a swimmer experiences during active swimming. Active drag consists of both passive drag and additional form and wave drags.

When a swimmer displaces water while moving forward, the water reacts to the swimmer by producing three types of resistance: skin friction drag, pressure drag and wave-making drag. This can be written as the formula:

$$F_{\text{total}} = F_{\text{friction}} + F_{\text{pressure}} + F_{\text{wave}} \quad [10.1]$$

Skin friction drag is the frictional force acting between the water and the surface of the body. Its magnitude can be calculated by the formula (Vorontsov and Rumyantsev, 2000):

$$F_{\text{friction}} = \mu \left(\frac{dV}{dZ} \right) S_{\text{friction}} \quad [10.2]$$

where μ is coefficient of viscosity, dV is difference in the velocity of water layers (dV is equivalent to flow velocity V), dZ is difference in the thickness of water layers and S_{friction} is wetted body surface area. This formula shows that skin friction drag is linearly proportional to the velocity. Friction drag is considered a primary part of passive drag and therefore significantly affects the gliding velocity of a swimmer underneath the water.

Pressure drag is also called form drag. It is the resistance generated in the pressure difference between the front and rear portions of the swimmer. When the swimmer swims or is towed at a slow speed, water flows surrounding the swimmer can be viewed as thin laminae or layers of water, which are all parallel to each other and move smoothly without any disturbances. The water layer in contact with the body surface travels with the same speed as the swimmer and the adjoining external layers move at slower speeds due to water viscosity. Because the boundary layers of water move relative to the body and each other, they perform mechanical work and separate from the body surface before they reach the rear portion. When the swimming velocity increases, separating water layers form eddies (i.e. rotating water masses with high velocity and low pressure) behind the rear portion of the swimmer, which is called the wake. Therefore, boundary layers are thinner in the leading portion of the body and thicker towards the trailing portion. This pattern causes general laminar flow in the leading portion of the body and more turbulence in the trailing portion. A swimmer thus experiences high pressure on the front surfaces but low pressure in the wake. This pressure gradient causes pressure (form) drag and can be calculated as (Vorontsov and Rumyantsev, 2000):

$$F_{\text{pressure}} = 0.5C_D \rho A V^2 \quad [10.3]$$

where C_D is coefficient of drag, ρ is density of water, A is the projected frontal area and V is velocity of the swimmer relative to water. It can clearly be seen that pressure drag has a square relationship with the velocity.

Reynolds number (Re) is a criterion used in fluid mechanics to describe whether the flow is laminar or turbulent. It is the ratio of inertial forces to viscous forces. The Reynolds number can be calculated as (Vorontsov and Rumyantsev, 2000):

$$\text{Re} = \frac{\rho VL}{\mu} \quad [10.4]$$

where ρ is density of water, V is flow velocity, L is length of the body and μ is coefficient of dynamic viscosity. A lower Reynolds number denotes a more laminar fluid flow, and a higher Reynolds number denotes a more turbulent fluid flow. The Reynolds number for competitive swimming ranges between 2×10^5 and 2.5×10^6 (Clarys, 1979). Such a higher value of Reynolds number leads the inertial forces to dominate viscous forces. The boundary layer along the swimmer is thus expected to be predominant with turbulent flow.

Wave-making resistance or wave drag is the third type of drag that a swimmer experiences when swimming on the water surface or at a small depth under water. Some water displaced by the swimmer along the body's trajectory moves from a high-pressure zone to a low-pressure zone which still has a pressure level above the undisturbed water. This process forms waves and is accompanied by the swimmer's efforts to work against gravity and lift the water above the surface. Wave formation around a swimmer is clear evidence that certain energy is lost along the swimming path. Wave drag is usually calculated as (Vorontsov and Rumyantsev, 2000):

$$F_{\text{wave}} = \rho \left(\frac{A^3}{\lambda^2} \right) (V \sin \alpha)^3 \cos \alpha \Delta t \quad [10.5]$$

where ρ is density of water, A is amplitude of the wave, λ is length of the wave, V is swimming velocity, α is the angle between the swimming direction and the front of the wave and Δt is time unit. This formula indicates that wave drag has a cube relationship with swimming velocity. Parts of the body such as the head, shoulders, upper trunk and buttocks generate waves during swimming and thus slow down the movement of the body. However, when a swimmer moves at a certain depth such as 0.7 m under water, wave drag is too small to slow down the movement of the body.

Formulas of three types of drag force demonstrate that skin friction drag increases linearly with swimming velocity, while pressure and wave drags have the square and cube relationship, respectively, with swimming velocity. With the increase of swimming velocity, both pressure and wave drags become more dominant contributors to the total hydrodynamic resistance. About 90% of the total hydrodynamic resistance was reported to come

from pressure drag at a flow velocity of 2 m/s (Rumyantsev, 1982). At nearly maximal swimming velocity, wave drag becomes another major component of the total hydrodynamic resistance. In the meantime, as wave drag becomes negligible during a deep glide, it is beneficial to maintain high gliding velocity using a leg kick only under water. Swimming practice has shown that gliding under water is no slower or even faster than swimming on the surface using the full stroke.

10.3.2 Measurement of drag force

Though we can easily define three types of drag force in swimming, it is extremely difficult to accurately measure the friction, pressure and wave drag due to the fact that the propulsion along the water surface can be considered as a collection of numerous traveling pressure points. It is therefore more common to measure the total drag in relation to velocity. The most reliable and practical method is to measure passive drag since passive hydrodynamic drag is fundamental to understanding active drag in the next step. In fact, a swimmer experiences passive drag when being towed on the surface of or under water, or during glide after the start and turns under water, or during transitional postures in breaststroke and butterfly strokes.

In experiment, passive drag can be measured with an electromechanical towing device to tow a swimmer in a water tank or a swimming flume (Vorontsov and Rumyantsev, 2000). The towing device can either be fixed on a stationary platform or attached to a mobile carriage. The towing device provides the towing force parallel to water surface and its electric motor generates varying power to precisely control the towing velocity during towing. A swimmer usually adopts a steady and immobile body posture during the towing experiment. Studies have found that a swimmer's body position and orientation significantly affect the total hydrodynamic resistance during towing. A common posture during towing is a prone, streamlined glide position with both arms extended overhead and feet together. Other postures can significantly increase the total hydrodynamic resistance. For instance, arms placed along the body increases the total hydrodynamic resistance by approximately 30% compared to the streamlined glide position, whereas arms extended forward with hands at shoulder width increases the total hydrodynamic resistance by about 10% (Onoprienko, 1968). It was also found that passive drag is affected, to a great extent, by the maximal frontal area of the swimmer and the circumferences of the head and shoulders (Clarys, 1978). This finding together with equation [10.3] emphasizes the importance of pressure drag in the total hydrodynamic resistance. While examining other anthropometric variables such as proportions of the human body, few correlations were observed between passive drag and anthropometric variables. Part of the explanation is that the human body is not well

streamlined; rather, it has many local pressure points such as the shoulders, knee joints and buttocks.

While passive drag certainly depends upon body shape and orientation in an immobile posture, active drag is associated with swimming techniques and constantly moving body positions. It is thus expected that active drag is much higher than passive drag. Studies with different measuring techniques show that the relationship between active drag and swimming velocity is quadratic (Clarys, 1979; Toussaint *et al.*, 1988). Active drag (F_{DA}) can be established as (Vorontsov and Rumyantsev, 2000):

$$F_{DA} = 0.5C_{DA\rho}AV^2 \quad [10.6]$$

where C_{DA} is the coefficient of active drag, ρ is density of water, A is anthropometric variable and V is swimming velocity. Comparing this equation with equation [10.3], it clearly implies that pressure drag is a major component of the total hydrodynamic resistance in active swimming. Anthropometric characteristics and passive drag contribute predominantly to active resistance at slow swimming velocities, but reduce substantially at high swimming velocities (Toussaint *et al.*, 1988). However, no correlation has been found between the magnitudes of active and passive drag (Clarys, 1978).

Measurement of active drag has been a challenge to biomechanists and sports scientists. Early techniques used the indirect calculation based on oxygen consumption (VO_2) during active swimming (Clarys, 1979; Di Prampero *et al.*, 1974). One of the drawbacks of the indirect method is that it measures aerobic function in swimming and thus is not appropriate for swimming at maximal efforts which include anaerobic function. More recent methods measuring active drag (MAD) include the MAD system (Toussaint *et al.*, 1988) and the velocity perturbation method (Kolmogorov and Duplishcheva, 1992). The MAD method measures the average propulsive force during frontal crawl swimming only. The rationale is that the propulsive force should be equal to active drag acting on the swimmer at constant swimming velocity. The velocity perturbation method, however, can assess active drag in all four swimming strokes. This method manipulates the maximal swimming velocity by using an additional hydrodynamic body with known resistance. The hydrodynamic body is placed behind a swimmer with the distance about four times of the swimmer's body length. The swimmer performs two swims with maximal efforts with and without the hydrodynamic body. Active drag can be estimated with the measured two maximal velocities and the known resistance from the hydrodynamic body. Both methods reached the same conclusion as shown in Clarys's (1979) study such that swimming technique is a more important component in determining active drag compared to body composition.

10.3.3 Swimwear design and drag force

It has long been debated whether skin shaving can reduce drag force in swimming. Swimmers who shaved their skin before a race were reported to consume less energy, produce longer stroke distance and swim faster than those without shaving (Sharp and Costill, 1989). This implies that skin friction drag is influenced markedly by the smoothness of the skin. Another approach to reducing skin friction drag is to develop better designs and fabrics for swimwear. This can be achieved by using a water-repellent and ultra thin elastic fabric to increase body smoothness. Woolen swimwear was found to increase drag force by 3% compared to silk swimwear when a female swimmer was towed at 2 m/s (Onoprienko, 1968).

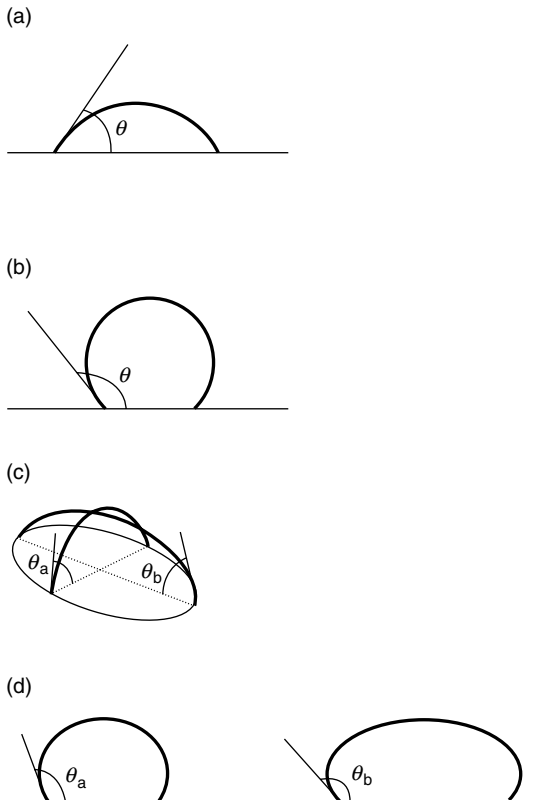
As pressure drag is usually significantly higher than skin friction drag, design of innovative performance swimwear should take pressure drag into consideration. When a well-streamlined swimmer moves at slow velocity, the boundary layers act like smooth laminar flow and little eddy formation occurs behind the body. Skin friction drag is thus the predominant component of the total hydrodynamic resistance. When swimming velocity increases, the boundary layers around the swimmer decrease in thickness and their separation point shifts to the front of the body causing a growing pressure gradient. Many eddies form behind the swimmer and take away kinetic energy from the swimmer. A streamlined swimwear design is therefore warranted to reduce pressure drag during swimming. Compared to fast-swimming fish and sea mammals such as dolphins, the human body with a similar longitudinal contour experiences much greater drag force at the same speed (Vorontsov and Rumyantsev, 2000). This is to a great extent due to many local pressure resistance centers in the human body including the head, shoulders, buttocks, knees and heels. Compression from a tight and fit swimwear is expected to reduce drag force at these local pressure centers and improve the streamline shape of the swimmer. Although swimwear manufacturers have claimed the significant advantages of their innovative performance swimwear, it is still up to carefully designed scientific experiments to verify these claims.

10.4 Effect of innovative swimwear on swimming performance

10.4.1 Water repellency in innovative swimwear

Smoothness and water repellency can significantly affect the physical characteristic of the swimwear fabric surface and therefore reduce drag force. Water repellency is usually measured with contact angle. By definition, contact angle is the angle formed by the water droplet and the fabric surface.

A greater contact angle demonstrates a better water-repellent property of the fabric. Figure 10.1 illustrates contact angles for four different types of fabrics. If a fabric is isotropic (i.e. uniformity in all directions) and hydrophilic (i.e. water loving), the contact angle is usually much less than 90° as depicted in Fig. 10.1(a). For an isotropic and hydrophobic (i.e. water-repelling) fabric, the water droplet maintains to some extent a spherical shape and its contact angle is usually greater than 90° as shown in Fig. 10.1(b). However, often a swimwear fabric is made with different materials such as nylon and Lycra. This fabric may not be considered as isotropic; rather, the fabric shows the anisotropic property (i.e. directionally dependent). Figure 10.1(c) shows the contact angle of an anisotropic and hydrophilic fabric. Since the water droplet does not spread evenly in all directions, an elliptical shape of water



10.1 Illustration of contact angle of water droplets on different fabric surfaces. (a) Isotropic and hydrophilic fabric, (b) isotropic and hydrophobic fabric, (c) anisotropic and hydrophilic fabric and (d) anisotropic and hydrophobic fabric. Note that the fabric of innovative performance swimwear is water repellent and thus more comparable to fabric (d). Contact angle, θ , can be measured along the minor axis, θ_a , or the major axis, θ_b .

spreading can often be observed. Contact angles can be measured along the minor axis (θ_a) and the major axis (θ_b) of this ellipse and both angles are less than 90° . The ratio between these two contact angles is usually calculated to quantify the spreading asymmetry of the fabric. An innovative performance swimwear requires water-repellent and fast drying properties to avoid water accumulation and penetration. Figure 10.1(d) illustrates contact angles of an anisotropic and hydrophobic fabric. Again contact angles θ_a and θ_b can be measured along the minor and major axes, respectively. However, because of the water-repellent property of the fabric, both contact angles should be greater than 90° .

Rogowski *et al.* (2006) investigated the effect of fabric characteristics on the performance of butterfly stroke swimming. Three fabrics were tested including a training fabric made of polyamide, a competition fabric made of polyamide and elastane, and the same competition fabric with additional mechanochemical coating treatment to increase water repellency and anisotropy. The contact angle was measured for each fabric to estimate its water repellency. Results showed that the competition fabrics with and without coating have greater contact angles ($130\text{--}140^\circ$) than the training fabric (about 85°), and the competition fabric with coating had a lower spreading asymmetry than the other two fabrics. In the swimming testing session, nine national French male swimmers performed 50 m butterfly stroke at 85% of effort while wearing a conventional swimwear made of the training fabric and the sleeveless neck-to-ankle long swimwear made with the competition fabrics with and without the coating treatment. It was found that overall hip velocity during the propulsive phase of butterfly stroke swimming was not different among the three swimwear; however, both long swimwear significantly increased hip velocity during the recovery phase (i.e. gliding). Furthermore, the long swimwear made with the competition fabric with the coating treatment provided further improvement. Thus, modification of water repellency (i.e. contact angle) has indirectly shown to significantly reduce drag force during swimming.

10.4.2 Effect of innovative swimwear on drag force and physiological and biomechanical responses

Measurement of passive and active drag forces has been described in the earlier sections. Because the goal of developing innovative swimwear is to enhance a swimmer's performance during competition, it is important to investigate the biomechanical and physiological responses during swimming while wearing innovative swimwear. Physiological responses are usually measured by VO_2 and blood lactate accumulation during or after a swimming event. Biomechanical variables usually include stroke distance, stroke rate and swimming velocity. Stroke distance is the distance that a swimmer

covers per stroke or per complete swimming cycle. Stroke rate is the number of strokes or complete swimming cycles that a swimmer performs per unit time (usually per second). Swimming velocity is equal to the product of stroke rate and stroke distance and can be defined for an entire race or each part of the race such as the start and turns of the race. A particular ratio of stroke rate and stroke distance is required for a swimmer to achieve the maximal velocity. If a stroke rate is too high, it disturbs muscle coordination because the muscles do not have enough time to recover between two bursts and get fatigued rapidly. On the other hand, if a stroke rate is too low, excessive efforts are needed to produce a high stroke distance, which increases anaerobic activity and decreases a swimmer's working capability.

Table 10.1 summarizes the studies on performance swimwear and wetsuits over the past 20 years. Findings on the amount of passive drag during towing and active drag during swimming are not conclusive. Three to ten percent of reduction on drag force has been reported by several studies (Benjanuvattra *et al.*, 2002; Chatard and Wilson, 2008; Mollendorf *et al.*, 2004; Pendergast *et al.*, 2006). A shoulder-to-ankle design was found to further reduce drag force compared to other designs such as shoulder-to-knee, waist-to-ankle and waist-to-knee (Mollendorf *et al.*, 2004). In the meantime, both Speedo Fastskin and TYR swimwear, though with different design philosophies as described in the earlier section, showed evidence of reducing drag force during passive towing (e.g. Mollendorf *et al.*, 2004; Pendergast *et al.*, 2006). However, non-significant difference has also been found between innovative and conventional swimwear (Roberts *et al.*, 2003; Smith *et al.*, 2007; Toussaint *et al.*, 2002). As different methods were used to assess drag force and the experimental setup was not identical across the studies, one should be cautious in evaluating the validity of each study and compare the differences between studies. Nonetheless, none of the studies demonstrates that an innovative performance swimwear would increase passive and active drag force. It may be concluded that an innovative performance swimwear can reduce drag force to some degree which may not be as high as that claimed by some swimwear manufacturers.

Physiological responses to innovative and conventional swimwear have been reported in favor of innovative performance swimwear (see Table 10.1). Most studies (Chatard and Wilson, 2008; Roberts *et al.*, 2003; Starling *et al.*, 1995; Tiozzo *et al.*, 2009) have shown that an innovative performance swimwear can significantly reduce VO_2 by approximately 5% and blood lactate concentration by 10–20%. Three percent of reduction on VO_2 was reported while wearing innovative performance swimwear, even though this reduction was not significant (Smith *et al.*, 2007). Lower VO_2 during swimming indicates that less effort is needed to complete a race, which may suggest that a lower drag force is associated with innovative performance

swimwear. In the meantime, lower blood lactate concentration means that wearing innovative performance swimwear allows muscles to work less hard than when wearing conventional swimwear. In other words, muscles do not get fatigued as rapidly while wearing innovative performance swimwear. In addition, a significant 7% reduction on heart rate was reported after completing a 400 m freestyle swim while wearing innovative performance swimwear (Tiozzo *et al.*, 2009). All of these physiological responses provide positive evidence that innovative performance swimwear can significantly reduce physiological demand and improve swimming performance.

When examining the biomechanical variables, most studies showed significant improvement while wearing innovative performance swimwear (see Table 10.1). While maintaining stroke rate unchanged, stroke distance was found to increase by 2–5% while wearing innovative performance swimwear (Chatard and Wilson, 2008; Roberts *et al.*, 2003; Starling *et al.*, 1995). This finding implies that drag force may be reduced by innovative swimwear so that a swimmer can cover a long distance per stroke at the same stroke rate. It also suggests that stroke distance rather than stroke rate is the variable that a swimmer manipulates first to increase the velocity when less drag force occurs. Swimming velocity was also found to increase markedly while wearing innovative performance swimwear. For example, the velocity of gliding under water significantly increased by 20% due to the contribution from shoulder-to-ankle performance swimwear (Rogowski *et al.*, 2006). This finding is important because innovative swimwear can significantly benefit a swimmer at the start and turns of a race and therefore markedly enhance the swimmer's performance. Also, studies on freestyle swimming at sub-maximal and maximal efforts demonstrate that innovative swimwear can significantly increase swim velocity and decrease swimming time (Chatard and Wilson, 2008; Roberts *et al.*, 2003; Tiozzo *et al.*, 2009). Taken together, research confirms that innovative performance swimwear can significantly improve biomechanical characteristics of swimming.

Performance swimwear reviewed above is usually used during competitions in an indoor swimming pool. With increasing popularity of triathlon around the world, a wetsuit specially designed for this sport has attracted increased attention from athletes, coaches, manufacturers and the general public. A wetsuit is a garment usually made of foamed neoprene and covers the full body including the arms and shoulder-to-ankle. Besides reducing drag force, a wetsuit is designed to provide thermal insulation and increase buoyancy during open water swimming. Table 10.1 also summarizes the studies on the effect of wetsuits on drag force and physiological and biomechanical measures. While wetsuits were reported to reduce drag force by 12–14% (Toussaint *et al.*, 1989), recent studies found non-significant reduction of active drag while wearing a wetsuit (De Lucas *et al.*, 2000; Tomikawa and Nomura, 2009). Similar inconclusive findings were also reported on

Table 10.1 Summary of studies on innovative performance swimwear and wetsuits

Author(s)	Year	Participants	Swimsuit	Swimming activity	Drag force	Physiological responses	Biomechanical measures
Starling <i>et al.</i>	1995	12 American males	Speedo torso swimsuit (80% polyester and 20% polyurethane)	365.8 m front crawl at 90% efforts		VO ₂ reduced by 4.1% and blood lactate reduced by 16.4%	Stroke distance increased by 4.7%
Benjanuvatra <i>et al.</i>	2002	9 Australian males and females	Fastskin shoulder-to-ankle swimsuit	Being towed at 1.6–2.8 m/s while gliding and flutter kick	Reduced drag by 4–10%, and drag increased with speed		
Toussaint <i>et al.</i>	2002	13 Netherlands males and females	Fastskin shoulder-to-ankle swimsuit	Front crawl with arms only at 1–2 m/s	Non-significant 2% reduction of active drag		
Roberts <i>et al.</i>	2003	9 American males	Fastskin shoulder-to-ankle swimsuit	183 m freestyle swimming at different efforts, and being towed at 2–2.5 m/s	Did not decrease passive drag during towing	Increased VO ₂ by 4% and blood lactate by 10% after freestyle swimming	Increased velocity by 2% and stroke distance by 4% and maintained stroke rate in freestyle swimming

Continued

Table 10.1 Continued

Author(s)	Year	Participants	Swimsuit	Swimming activity	Drag force	Physiological responses	Biomechanical measures
Mollendorf <i>et al.</i>	2004	7 American males	Fastskin shoulder-to-ankle, shoulder-to-knee, waist-to-ankle, and waist-to-knee (polyester and Lycra)	Being towed at 0.2–2.2 m/s, and gliding after push-off from the wall	Reduced drag by 3–10% during towing with shoulder-to-knee the best, and decreased coefficient of drag during gliding by 8–15% with shoulder-to-ankle the best		
Rogowski <i>et al.</i>	2006	9 French males and females	Neck-to-ankle swimsuit (polyamide and elasthane)	50 m butterfly at 85% efforts			Hip velocity during gliding increased by 20%
Pendergast <i>et al.</i>	2006	14 American males and females	TYR swimsuit with trip wires (polyester and Lycra)	Being towed at 0.2–2.2 m/s	Additional trip wires reduced drag by 10–15%, primarily from pressure drag reduction		

Smith <i>et al.</i>	2007	8 American males	TYR shoulder-to-ankle swimsuit	Free drop from 1 to 5 m high, being towed at 2 m/s, and 365.8 m freestyle swimming at 90% efforts	Non-significant 2% reduction of passive drag during towing	Non-significant 3% reduction of VO_2	Reduced velocity decay after entering into the water during free drop
Chatard and Wilson	2008	14 New Zealand males and females	Fastskin shoulder-to-ankle and waist-to-ankle swimsuits	Being towed at 1.2–2 m/s, and freestyle swim of 25–800 m at maximal efforts	4.7% reduction with waist-to-ankle swimsuit and 6.2% reduction with shoulder-to-ankle swimsuit in towing	Reduced VO_2 by 5% after swimming	Reduced swimming time by 2–3.5%, increased stroke distance by 2%, and maintained stroke rate
Tiozzo <i>et al.</i>	2009	15 Croatian males	Fastskin shoulder-to-ankle swimsuit	50 m sprint and 400 m swimming		Reduced heart rate by 7% and blood lactate by 21% after 400 m swimming	Reduced race time by 0.4 s in 50 m sprint
Toussaint <i>et al.</i>	1989	12 Netherlands males and females	Triathlon wetsuit	Front crawl at 1.1–1.5 m/s	Reduced active drag by 12–14%		
Cordain and Kopriva	1991	14 American females	Scott Tinley shoulder-to-ankle wetsuit	400 and 1500 m swimming at maximal efforts			Swim time reduced by 5% in 400 m and by 3.2% in 1500 m swim

Continued

Table 10.1 Continued

Author(s)	Year	Participants	Swimsuit	Swimming activity	Drag force	Physiological responses	Biomechanical measures
Trappe <i>et al.</i>	1996	5 American males	Full body, shoulder-to-ankle, and shoulder-to-knee wetsuits	Front crawl at 0.9–1.31 m/s in a swimming flume		Reduced VO_2 by 16–33% with full bodysuit the best	
De Lucas <i>et al.</i>	2000	19 Brazilian males and females	Ironman neoprene shoulder-to-ankle wetsuit	2 x 30 m swim at maximal efforts, 3 x 200 m swim with 85–95% efforts, and 1500 m swim at maximal efforts	Non-significantly reduced active coefficient of drag in 2 x 30 m swim	Increased anaerobic threshold by 5% in 3 x 200 m swim	Increased swimming velocity by 3.4% in 1500 m swim
Tomikawa and Nomura	2009	12 Japanese males and females	Neoprene full-body wetsuit	Continuous swimming to measure VO_2 max, and 2 x 25 m and 400 m maximal swim	Non-significant difference in active drag and coefficient of drag	Non-significant difference in VO_2 max and blood lactate	Increased velocity by 6% at VO_2 max and by 4.3–7% in 25 and 400 m swim

Note that gains in drag force, physiological responses, and biomechanical measures are compared to conventional swimsuit.

physiological responses. Trappe *et al.* (1996) reported that wearing a wetsuit significantly decreased VO_2 by 16–33%, whereas Tomikawa and Nomura (2009) found no reduction on VO_2 and blood lactate while wearing a wetsuit. However, when swimming velocity was examined while wearing a wetsuit, all the studies demonstrated 3–7% increase of velocity in 400 m and 1500 m swimming (Crodain and Kopriva, 1991; De Lucas *et al.*, 2000; Tomikawa and Nomura, 2009). All the evidence indicates that wearing a wetsuit can significantly benefit a triathlon athlete by reducing drag force and VO_2 to some degree and improving swimming velocity.

The evidence from the research studies reviewed above, even though not totally consistent with each other, suggests that innovative performance swimwear developed in the past 20 years can to a great extent reduce drag force and improve the physiological and biomechanical responses during competitive swimming. It is therefore appropriate to continue the development of new innovative performance swimwear to provide further benefits to professional swimmers and possibly collegiate and amateur swimmers.

10.5 Future trends in innovative performance swimwear

Existing research has demonstrated that the full body or sleeveless shoulder-to-ankle swimwear design can significantly reduce drag force compared to both conventional and waist-to-knee swimwear. However, FINA banned the use of full body and sleeveless shoulder-to-ankle design from January 2010. The current performance swimwear allowed by FINA is the waist-to-knee design for men and shoulder-to-knee design for women. Furthermore, FINA required that only textile fabrics made of natural and synthetic yarns can be used for performance swimwear and these fabrics should be manufactured by weaving, knitting or braiding. In addition, FINA produced detailed guidelines for the fabric surface coating and treatment. With these new guidelines for performance swimwear, creative design and technology are needed to bring the development of performance swimwear to the next stage.

Synthetic materials such as nylon, polyester and Lycra have been widely used in manufacturing performance swimwear. This is to a great extent due to their water-repellent capability. Future research will focus on the development of new synthetic materials which should be comparable to or better than the existing synthetic materials. In the meantime, research needs to address how to manufacture thinner synthetic filaments and produce lighter and thinner swimwear fabrics. Obviously, elasticity and compression are the two important characteristics of swimwear fabrics and can significantly affect the streamline shape of a swimmer. As the buttocks are one of the local pressure centers, a better ergonomic swimwear design is warranted to streamline this area. Three-dimensional body scans as used by Speedo will

continue to help individualize the performance swimwear for each swimmer. In addition, theoretical and applied fluid mechanics have been successfully used in developing performance swimwear over the past 20 years. With more advanced computing technology, computational fluid mechanics will be an appropriate tool to help further understand water flow around a swimmer's body and thus accurately estimate passive and active drag force during competition. This knowledge will in turn revolutionize the development of performance swimwear.

10.6 Sources of further information and advice

Readers are recommended to check the website of FINA (www.fina.org) for the guidelines on performance swimwear. The details can be found under bylaws-swimwear in the rules and restrictions of FINA. As guidelines on performance swimwear change from time to time, it is important for researchers and manufacturers to understand these guidelines and incorporate them into the development of next performance swimwear.

To gain more knowledge on the biomechanics of swimming, a helpful book is Vladimir Zatsiorsky (ed.), *Biomechanics in Sport: Performance Enhancement and Injury Prevention* (2000). As manufacturers usually claim remarkable advantages for their new performance swimwear over conventional swimwear, it is important to look at the research studies that employ theoretical modeling and scientific experimental design to study drag force and physiological and biomechanical responses associated with new performance swimwear. The following are some excellent journals (not an exclusive list) for readers who are interested in exploring the effect of performance swimwear on competitive swimming: *Medicine and Science in Sports and Exercise*, *Journal of Biomechanics*, *Journal of Applied Biomechanics* and *Sports Biomechanics*.

In addition, it would be helpful to frequently study the websites and newsletters of the major swimwear manufacturers such as Speedo, TYR and Adidas to follow the new trend of swimwear development. The development of performance swimwear often follows the cycle of the Olympic Games. This means that new performance swimwear is usually released and promoted a year before or in the year of the Olympic Games. As the usage of performance swimwear has expanded from professional swimmers to collegiate and amateur swimmers, the development of new innovative performance swimwear will continue to proceed in the future.

10.7 Acknowledgements

Special thanks are due to Dr Hong Chen and Mr Matthew Bogenberger for their contributions to the literature research and review and for their suggestions and comments on this chapter.

10.8 References

- ALLENDER, M. E. (1996) The Jantzen Company: a classic case of marketing success. *Essays in Economic and Business History*, 14: 219–227.
- BENJANUVATRA, N., DAWSON, G., BLANKSBY, B. A. and ELLIOTT, B. C. (2002) Comparison of buoyancy, passive and net active drag forces between Fastskin™ and standard swimsuits. *Journal of Science and Medicine in Sport*, 5: 115–123.
- CHATARD, J.-C. and WILSON, B. (2008) Effect of Fastskin suits on performance, drag, and energy cost of swimming. *Medicine and Science in Sports and Exercise*, 40: 1149–1154.
- CLARYS, J. P. (1978) Relationship of human body form to passive and active hydrodynamic drag. In: Asmussen, E. and Jorgensen, K. (eds.) *Biomechanics VI-B*. Baltimore: University Park Press, pp. 120–125.
- CLARYS, J. P. (1979) Human morphology and hydrodynamics. In: Terauds, J. and Bedingfield, E. W. (eds.) *Swimming III*. Baltimore: University Park Press, pp. 3–41.
- CRODAIN, L. and KOPRIVA, R. (1991) Wetsuits, body density and swimming performance. *British Journal of Sports Medicine*, 25: 31–33.
- CUNNINGHAM, P. A. (2009) From underwear to swimwear: branding at Atlas and B.V.D. in the 1930s. *Journal of American Culture*, 32: 38–52.
- DAVIES, E. (1997) Engineering swimwear. *Journal of the Textile Institute*, 88: 32–36.
- DE LUCAS, R. D., BALIKIAN, P., NEIVA, C. M., GRECO, C. C. and DENADAI, B. S. (2000) The effects of wet suits on physiological and biomechanical indices during swimming. *Journal of Science and Medicine in Sport*, 3: 1–8.
- DI PRAMPERO, P. E., PENDERGAST, D. R., WILSON, C. W. and RENNY, D. W. (1974) Energetics of swimming in man. *Journal of Applied Physiology*, 37: 1–5.
- HORWOOD, C. (2000) Girls who arouse dangerous passions: women and bathing, 1900–39. *Women's History Review*, 9: 653–673.
- KOLMOGOROV, S. V. and DUPLISHCHEVA, O. A. (1992) Active drag, useful mechanical power output and hydrodynamic force coefficient in different swimming strokes at maximal velocity. *Journal of Biomechanics*, 25: 311–318.
- MOLLENDORF, J. C., II, A. C. T., OPPENHEIM, E. and PENDERGAST, D. R. (2004) Effect of swim suit design on passive drag. *Medicine and Science in Sports and Exercise*, 36: 1029–1035.
- ONOPRIENKO, B. I. (1968) Relationship of hydrodynamic drag and swimmer's body position. *Theory and Practice of Physical Culture*, 9: 12–15.
- PENDERGAST, D., MOLLENDORF, J., CUVIELLO, R. and TERMIN, A. (2006) Application of theoretical principles to swimsuit drag reduction. *Sports Engineering*, 9: 65–76.
- ROBERTS, B. S., KAMEL, K. S., HEDRICK, C. E., MCLEAN, S. P. and SHARP, R. L. (2003) Effect of a FastSkin™ suit on submaximal freestyle swimming. *Medicine and Science in Sports and Exercise*, 35: 519–524.
- ROGOWSKI, I., MONTEIL, K., LEGRENEUR, P. and LANTERI, P. (2006) Influence of swimsuit design and fabric surface properties on the butterfly kinematics. *Journal of Applied Biomechanics*, 22: 61–66.
- RUMYANTSEV, V. A. (1982) *Biomechanics of Sport Swimming*. Moscow: Central State Institute of Physical Culture.
- SHARP, R. L. and COSTILL, D. L. (1989) Influence of body hair removal on physiological responses during breaststroke swimming. *Medicine and Science in Sports and Exercise*, 21: 576–580.

- SMITH, J. W., MOLLOY, J. M. and PASCOE, D. D. (2007) The influence of a compressive laminar flow body suit for use in competitive swimming. *Journal of Swimming Research*, 17: 10–16.
- STARLING, R. D., COSTILL, D. L., TRAPPE, T. A., JOZSI, A. C., TRAPPE, S. W. and GOODPASTER, B. H. (1995) Effect of swimming suit design on the energy demands of swimming. *Medicine and Science in Sports and Exercise*, 27: 1086–1089.
- TIOZZO, E., LEKO, G. and RUZIC, L. (2009) Swimming bodysuit in all-out and constant-pace trials. *Biology of Sport*, 26: 149–156.
- TOMIKAWA, M. and NOMURA, T. (2009) Relationships between swim performance, maximal oxygen uptake and peak power output when wearing a wetsuit. *Journal of Science and Medicine in Sport*, 12, 317–322.
- TOUSSAINT, H. M., BRUININK, L. E. X., COSTER, R., LOOZE, M. D., ROSSEM, B. V., VEENEN, R. v. and GROOT, G. D. (1989) Effect of a triathlon wet suit on drag during swimming. *Medicine and Science in Sports and Exercise*, 21: 325–328.
- TOUSSAINT, H. M., GROOT, G. D., SAVELBERG, H. H. C. M., VERVOORN, K., HOLLANDER, A. P. and SCHENAU, G. J. v. I. (1988) Active drag related to velocity in male and female swimmers. *Journal of Biomechanics*, 21: 435–438.
- TOUSSAINT, H. M., TRUIJENS, M., ELZINGA, M.-J., VEN, A. V. D., BEST, H. D., SNABEL, B. and GROOT, G. D. (2002) Effect of a Fastskin ‘body’ suit on drag during front crawl swimming. *Sports Biomechanics*, 1: 1–10.
- TRAPPE, T. A., PEASE, D. L., TRAPPE, S. W., TROUP, J. P. and BURKE, E. R. (1996) Physiological responses to swimming while wearing a wet suit. *International Journal of Sports Medicine*, 17: 111–114.
- VORONTSOV, A. R. and RUMYANTSEV, V. A. (2000) Resistive forces in swimming. In: Zatsiorsky, V. (ed.) *Biomechanics in Sport: Performance Enhancement and Injury Prevention*. Hoboken, NJ: Wiley-Blackwell, pp. 184–204.
- ZATSIORSKY, V. (ed.) (2000) *Biomechanics in Sport: Performance Enhancement and Injury Prevention*. Hoboken, NJ: Wiley-Blackwell.

Key elements of protection for military textiles

J. R. OWENS,

Air Force Research Laboratory, USA

Abstract: This chapter discusses the currently recognized critical elements of protection for military personnel. A brief discussion of the history, the current state of the art and expectations for the future for each aspect of protection are given. Aspects of protection considered are limited to threats from human adversaries and include camouflage, ballistic protection and protection from toxic vapors, aerosols and liquids.

Key words: protection, chemical warfare agent, ballistic, aerosol, adsorbent, camouflage.

11.1 Introduction

The cornerstone of apparel, aside from imbuing modern societies with a sense of modesty, is protection. This umbrella term includes protection from the elements: sun, rain, snow, heat, cold, and so forth; from nature: insects, abrasion, irritating flora and fauna, and so forth; and – the subject of this chapter – protection from enemies and their wartime technological equipment, such as improvised explosive devices (IED), small fire arms, toxic chemicals, engineered pathogens, and so forth. However, it should be recognized that it is neither economically nor technologically feasible to protect soldiers completely from all threats. Therefore, a level of acceptable risk must be established that is palatable to upper leadership. In the United States the level of risk is indirectly set by public opinion and, in comparison to most other military powers of the world, the level of risk tolerance remains relatively low. Designing a future military protective ensemble is a juggling act to balance cost and performance, while attempting to predict what the future threat profile will entail. Current systems do not adequately protect personnel and assets against threats developed 75 years ago, much less more recently developed threats. Consequently, action is required in the science community to develop technologies that will define the protective systems that can protect against current and future terrorist and other adversarial actions.

This chapter will discuss the currently recognized critical elements of protection for military personnel, beginning with a brief discussion of the

history. The current state of the art and expectations for the future for each aspect of protection will be addressed.

The primary adversarial threats to soldiers include:

- (a) *Detection* – A soldier does not become a target until he/she is detected. Currently the most widely fielded camouflage for US soldiers consists of a digital screen-print pattern that is called *desert marine* (Fig. 11.1(a)).
- (b) *Wounding by small arms or by shrapnel* – The US military currently uses a ballistic vest system consisting of composite, high-strength para-aramid fibers (Kevlar), and boron carbide ceramic plates wrapped in ultra-high-molecular-weight (UHMW) polyolefins (Spectra™/Dyneema™), as depicted in Fig. 11.1(b).
- (c) *Exposure to toxic chemicals or biological agents* – The US currently uses a suit called the Joint-Service Lightweight Integrated Suit Technology (JSLIST). It consists of a 50:50 nylon–cotton shell fabric with a water-repellent treatment, an adsorbent liner of activated carbon beads, and an internal nylon scrim to protect the carbon liner (Fig. 11.1(c)).
- (d) *Being burned by ignited fuels from IED* – Fire-retardant (FR) textiles are used by select military units. Firefighters wear an FR-treated 100% cotton. Other units wear a woven composite consisting of 65% FR rayon, 25% para-aramid and 10% nylon, marketed as Defender-M™. Note that we will not dwell on FR technologies as they are addressed in detail in Chapter 6.

11.2 Camouflage

Prior to the 1800s military uniforms of Western civilizations were designed to protect soldiers from the elements, to intimidate enemies and to easily differentiate between friend and foe. Thus they were typically brightly colored – the iconic British Redcoat uniforms being the classic example (Kannik, 1968). In the late 1800s, after British troops sustained high casualties in several skirmishes due to the high visibility of their uniform and the use of guerrilla tactics by their adversaries, the British and the majority of Western military organizations adopted drabber colors, and the first vestiges of camouflage began to emerge in modern warfare (Kannik, 1968).

Camouflage is a method of avoiding observation that allows an otherwise visible object to remain indiscernible from the surrounding environment through deception. Traditional military camouflage consisted of combining background pattern matching with disruptive coloration in the form of dye patterns on military uniforms in the visible spectrum to allow soldiers to blend into their surroundings (Behrens, 2009). The widespread availability of infrared spectral imaging, night vision technologies, and more recent advances in hyperspectral and multispectral imaging require that the



11.1 (a) USA fielded camouflage; (b) USA fielded ballistic protection; (c) USA fielded chemical and biological warfare (CBW) agent protection.

concept of camouflage be applied across a range of electromagnetic (EM) frequencies. In today's modern warfare camouflage represents a critical component of a military combat uniform and represents a soldier's first line of defense – soldiers are not targets until they are seen/detected.

State-of-the-art camouflage is divided into two categories: passive and active or adaptive camouflage. The differentiating factor between these two technologies is that passive camouflage does not adapt to blend in with its surrounding environment as the surroundings change, whereas active camouflage does. Background pattern matching and disruptive coloration are two examples of traditional passive camouflage that represent the most widely used camouflage for modern warfare for more than a century (Behrens, 2009). More advanced and recent developments in passive camouflage include technologies that mask the human body's natural infrared

signature through a combination of photon absorption and EM scattering (NMAB, 2003). These technologies are commercially available and are already integrated into select military garments.

Although fundamental research on adaptive camouflage dates back almost half a century, applied research in the area required breakthroughs in nearly all the fields of science and engineering. Consequently, up until the mid to early 1990s, applied research into active camouflage was largely relegated to the area of science fiction. Today active camouflage is an important area of research for industry, academia and governments. Currently at least one company is already marketing an active camouflage garment that uses a series of flexible organic light-emitting diodes, in addition to EM scattering and absorption techniques, and claims 'invisibility' to infrared, near infrared, and visible EM frequencies (Crane, 2006).

Unlike humans, for whom the idea of active camouflage is relatively new, nature has been in the game for millions of years, which is why many researchers are turning to bio-mimicry for their inspiration. In nature, no species has mastered the skill of active camouflage better than the cephalopods in their use of dynamic iridescence as active camouflage (Birch, 2010). Iridescence is a reflective optical phenomenon that causes the color of a surface to appear to change depending on the angle of incidence of light onto the iridescent material relative to the observer. Examples include the sheen reflected off an oil slick or soap bubble. Although iridescence is common in natural species – pearls, seashells, wings of butterflies and other insects are examples – these do not exhibit dynamic iridescence because they possess no physiological means to control the reflected colors aside from changing the angle of the iridescent surface. Certain cephalopods, however, effectively employ dynamic iridescence through a complex, continual neurophysiological response, whose cycle begins with a visual stimulus and ends with an environmentally adaptive color change (Chiao *et al.*, 2007). In this manner cephalopods keep their 'cloaking device' perpetually on using this active camouflage strategy. Researchers believe that they can mimic this behavior through a combination of electroactive polymers and nanotechnology (Birch, 2010).

Research in the area of metamaterials, or artificial materials that are designed to interact with and control EM waves, takes the prize for stimulating the imagination and generating the most excitement in the quest to develop active camouflage that requires no power. Researchers have theorized, proven and demonstrated that metamaterials can be designed such that they have a negative refractive index over a specific frequency range (Cho, 2006). This means that light falling within this frequency range will literally bend around the object rendering the object invisible from a specific field of view. In theory the phenomenon can be used to bend any wavelength of light, but in practice, because the negative-refractive-index metamaterials

must possess very ordered structures that correspond in size and frequency to the wavelength of light to be bent, it is currently impractical at visible wavelengths. However, researchers say that because visible light possesses a wavelength range between 390 and 750 nm, one can conceive of fabric coated with negative-refractive-index metamaterials – otherwise known as an invisibility cloak (Cho, 2006).

11.3 Ballistics

Another extremely important component of a protective military duty ensemble is protection from small arms fire and fragmentation from grenades, mines and IED. This type of protection is termed *ballistic and fragmentation protection* and its history is extensive. Materials designed to protect against projectile attacks have co-evolved parallel to the development of ballistic delivery methods. In terms of textiles, ballistic protection can be divided into two broad categories: soft, ‘wearable’ armor, wherein the ballistic protection is provided by the soft, flexible textile, and soft–rigid armor, wherein ballistic protection is provided by a combination of inflexible armor plates that are integrated into a high-modulus textile. In this section we will briefly discuss the ballistic protective elements of soft–rigid composite systems, and then delve into research on fully flexible, soft textile systems.

Various levels of ballistic protection exist, and each level is defined in terms of the velocity and mass of the projectile the ballistic armor will protect against. The most widely used standard for ballistics protection for militaries is the ability to stop a 9.6 g 7.62×51 -mm steel jacketed NATO-standard round (US military designation M80) at a velocity of 847 ± 9.1 m/s, which equates to a kinetic energy of 3444 J (NIJ, 2008). This level of ballistic protection is described as Type III, protection from rifle rounds. At this point in time (2010), there exists no commercially available soft system that can provide Type III ballistic protection. There are, however, multiple soft–rigid composite systems that can.

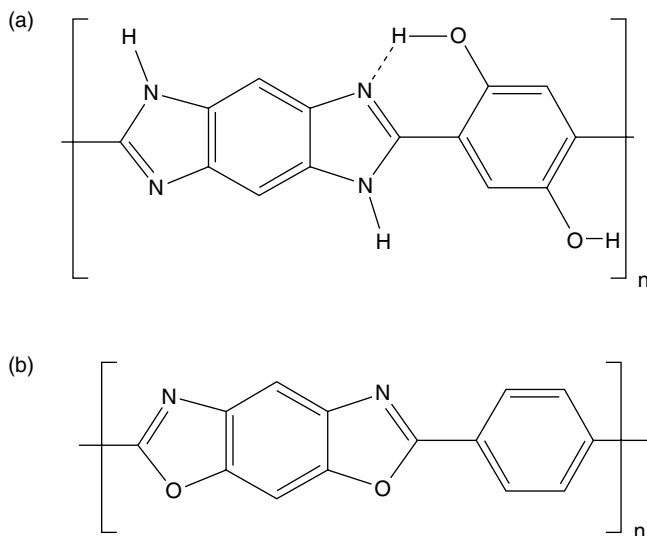
Soft–rigid composite textile systems for ballistics protection typically comprise ceramic armor plates, e.g. boron nitride, tungsten carbide, tungsten disulfide, aluminum nitride, and so forth, coated or contained in high-modulus organic polymers, such as para-aramids e.g. Kevlar™ and Twaron™, or UHMW polyolefins, e.g. Spectra™ and Dyneema™ (NCJRS, 2001). In such systems rigid plates are designed to intercept an incoming projectile and disperse its kinetic energy over a large area, while the soft textile is used to disperse as much kinetic energy as possible and cause deformation of the round prior to it reaching the ceramic plates.

The earliest forms of ballistics protection consisted of multiple layers of metal and hardened, boiled or treated leather components. The commercially

available soft components of anti-ballistics materials of 2010 still consist of layer upon layer of high-strength polymer, and with good reason. These systems rely on their high tensile, specific and shear strength, and elastic moduli to ‘catch’ an incoming projectile and disperse the kinetic energy as heat over a large area via friction as the polymer chains ‘slip’ against one another (Northolt and Baltussen, 2001). In materials such as para-aramids and poly(*p*-phenylene-2,6-benzobisoxazole), or PBO, the high elastic moduli are caused by a combination of intermolecular hydrogen bonding and intermolecular *pi* stacking, while UHMW polyolefins, such as Dyneema™, achieve high moduli through the cumulative Van der Waals interactions resulting from their extremely long polyolefin chains, typically 100 000–250 000 repeating units. UHMW polyolefins are produced by a solvent gel-spinning process (vs. melt-spinning) to produce fibers that are ten times stronger than steel, more durable than polyester, possess a specific strength 40% greater than aramid fibers and are less dense than water (Ward and Ladizesky, 1985). Researchers once hoped that these materials could result in a soft ballistic armor capable of stopping a rifle ballistics round; however, the reliance on the intermolecular kinetic energy dispersion currently prevents this, and thus ceramic plate components are still required to further disperse the kinetic energy over a wider area. While pristine PBO possesses sufficient strength in fiber form to provide Type III ballistic protection in a semi-flexible textile, performance degradation of the polymer via disruption of the intermolecular forces by water, acids and ultraviolet radiation causes unacceptable and unanticipated service life issues (Cunniff and Auerbach, 2003).

Fully flexible soft ballistic protection appears to be on the horizon. Magellan Systems International LLC is working on scaling up production of the high-performance fiber poly{diimidazopyridinylene(dihydroxy)phenylene} or M-5™. Modeling and simulations predict that M-5™ will perform at least equivalent to pristine PBO without the associated degradation issues. More encouraging is that empirical tests indicate that M-5™ fiber will outperform PBO by a considerable margin (Cunniff and Auerbach, 2003). Researchers attribute the unexpected increase in performance compared to computer modeled predictions to M-5’s ability to form hydrogen bonds in the lateral dimension, a trait possessed by no other anti-ballistic fiber. The M-5 fiber’s ability to hydrogen bond becomes apparent upon inspection of the structure compared to the structure of PBO, as seen in Fig. 11.2(a) and (b).

Another technology that has demonstrated the ability to serve in an anti-ballistic capacity is a composite system consisting of a high-performance anti-ballistic fiber combined with a shear-thickening colloidal dispersion. Shear-thickening fluids or STFs are liquids whose viscosity increases as a function of applied stress. A mixture of cornstarch and water is the



11.2 (a) Chemical structure of M-5 fiber; (b) chemical structure of PBO fiber.

classic example of an STF. Researchers at the University of Delaware have produced anti-ballistic yarns possessing STFs intercalated into the fiber (Wagner and Brady, 2009). Ballistic tests of these composite fibers show a 250% increase in stopping power of STF-treated Kevlar fibers compared to Kevlar alone. Production of these STF-enhanced textiles for other applications has already begun by Dow Corning under the name Deflexion™. Now, consider a merger of M-5 fiber with STF technology and it becomes apparent that soft anti-ballistic armor will soon be a reality.

11.4 Toxic chemicals

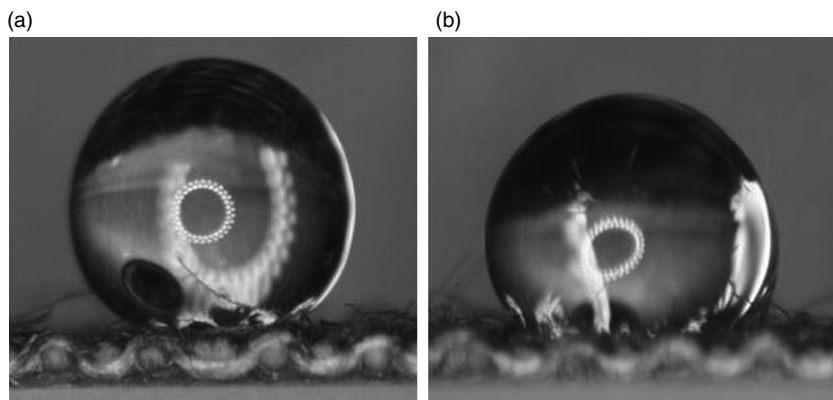
Nobel Laureate Fritz Haber formally introduced the world to chemical warfare at the Battle of Ypres, 22 April 1915 (Cornwell, 2003). The world has not been idle since that time. The dynamic and rapidly evolving science and technology world has driven the threat from newly developed chemical and biological warfare (CBW) agents to new heights (Cordesman, 2001). Moreover, the availability of the Internet and global networking has made it easy and economically feasible for anyone with the inclination and a relatively modest budget to acquire the technology, instrumentation and starting materials to develop both traditional and next-generation threat agents. The challenge lies in developing the capability to deal with the multitude of identified and unidentified threats that will inevitably become available to terrorist organizations and adversaries.

While the enemies' method of choice has traditionally been the use of explosives, events such as the Tokyo subway sarin nerve gas attack, the weaponized anthrax mail attack, and chlorine-laden and fuel-laden IED clearly point to a trend towards CBW (Cordesman, 2001). Unfortunately, while the world of chemistry has advanced exponentially since the 1930s, the systems employed to protect against chemical agents remain essentially the same as they were in the 1930s: passive exclusion barrier materials, such as butyl rubber and poly(vinyl alcohol)s, solid-state adsorbents, such as activated carbon and diatomaceous earth, and hypochlorite solutions for chemical agent decontamination/neutralization (Donahue, 2003). Biological agent protection has come a bit further in the realm of medicine, with the development of new vaccines and antibiotics, but still remains grossly inadequate compared to the wide variety of highly adaptive pathogens available in nature's arsenal, and their availability to practically anyone who has the motivation to use them.

11.4.1 Bulk toxic or burning liquids

Current and past protective ensembles include an outer shell fabric composed of 50:50 nylon-cotton treated with a water-repellent finish. This outer shell fabric represents the first line of defense from incoming threat agents. Unfortunately, in currently fielded systems this shell fabric protects the wearer only from high surface tension liquids such as water. Protection from oils, fuels and other low surface tension liquids – including many chemical threat agents – was and continues (2010) to be provided by the adsorbent activated carbon inner liner. Reliance on the adsorbent liner for protection from bulk liquids is one of the primary reasons why current chemical protective ensembles are heavy, bulky, hot and have a working service life of only 45 days.

By mimicking the surface micro- and nanoscale roughness of the lady's mantle, the lotus leaf and the rose petal, coupled with surface treatments that allow for much lower surface tensions than found in nature, researchers have demonstrated the ability to repel and prevent the absorption of traditional chemical warfare agents, burning fuels and other liquid threat agents into treated textile materials (Lee and Owens, 2010). The high contact angle to water and oil can be clearly seen in Fig. 11.3. Technologies that can deliver this omniphobic quality on an industrial scale will protect the wearer from a wide range of bulk liquid threat agents and, consequently, allow for lightweight chemical protective ensembles that possess a much longer service life – if this property can be sustained over the lifetime of the garment. According to modern theories of how liquids wet surfaces, such feats are not possible on a permanent basis but are said to exist in a meta-stable state (Lee and Owens, 2010). However, this 'transient' state appears sufficiently stable across the majority of militarily relevant threat scenarios.

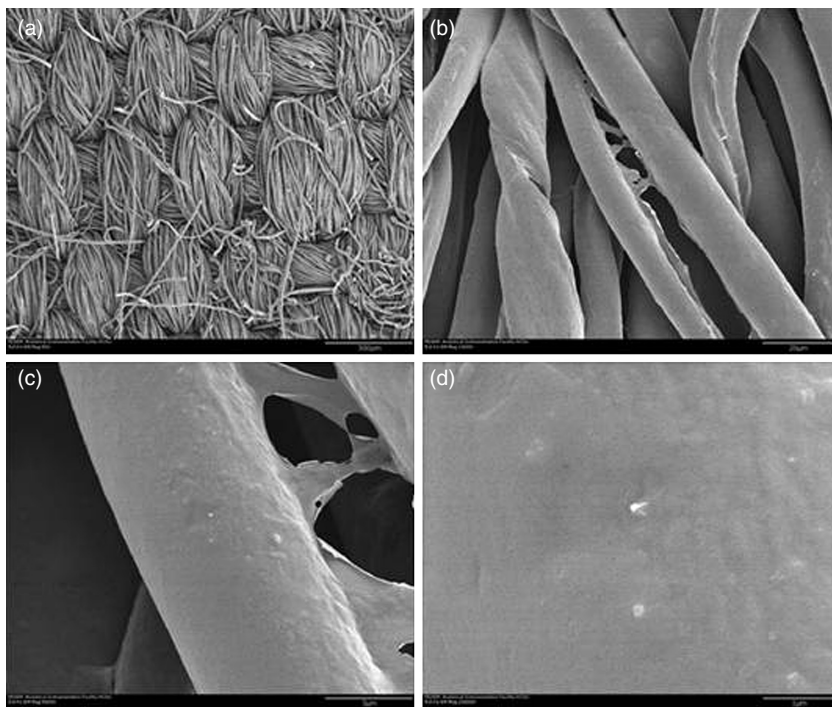


11.3 (a) 5 μL water droplet on treated 50:50 woven nylon–cotton;
(b) 5 μL dodecane droplet on treated 50:50 woven nylon–cotton.

Modification technologies are available to change surface energy, structure, morphology, wettability and other physical properties of treated materials. At least three surface modification techniques have demonstrated the ability to produce omniphobic nylon: plasma deposition of perfluoroacrylates, microwave deposition of perfluorosiloxanes, and pretreatment followed by wet processing of nylon using perfluorosiloxanes (Saraf *et al.*, 2010). Such an engineered coating is illustrated in Fig. 11.4, which shows a coating synthesized using microwave deposition. These durable textile treatments are at the forefront of repellent technologies. Textile treatments and modifications are covered in greater depth in Chapter 2 and wetting behavior in Chapters 15 and 16.

11.4.2 Toxic gases and vapors

Another extremely important aspect of chemical protection is protection from toxic gases and vapors. Unlike aerosols, toxic gases and vapors are too small to trap via mechanical filtration and, unless encapsulation technologies are adopted, require removal by either adsorption, absorption, reaction or a combination of these mechanisms. Adsorption is the most commonly used mechanism and is defined as a process that occurs when a gas or liquid solute accumulates on the surface of a solid or a liquid (adsorbent), forming a molecular or atomic film (the adsorbate) (Rolando and Roque, 2007). It is different from *absorption*, in which process a substance diffuses into a liquid or solid to form a solution. Adsorption is operative in most natural physical, biological and chemical systems, and is widely used in industrial applications. Similar to surface tension, adsorption is a consequence of surface energy. In a bulk material, all the bonding requirements (be they ionic, covalent or metallic) of the constituent atoms of the material are filled.



11.4 Scanning electron micrographs (SEM) of microwave-treated 50:50 nylon-cotton. (a-d), in magnifications of 50, 1000, 5000, and 20,000.

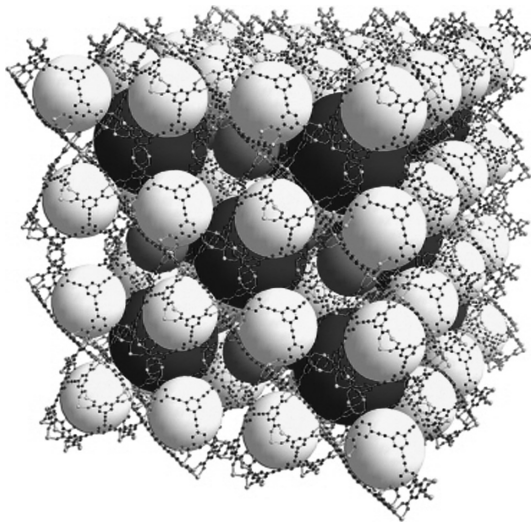
However, atoms on the surface experience a bond deficiency, because they are not wholly surrounded by other atoms. Consequently, it is energetically favorable for these surface features to minimize surface energy by bonding to available compounds. The exact nature of the attachment depends on the details of the species involved, but the adsorbed material is generally classified as exhibiting physisorption or chemisorption. *Physisorption* or physical adsorption is a type of adsorption in which the adsorbate adheres to the surface only through Van der Waals interactions, whereas *chemisorption* is a type of adsorption whereby a molecule adheres to a surface through the formation of a chemical bond, after which a new chemical species is generated (Rolando and Roque, 2007). Unfortunately, physisorption is most common in activated carbon, the most commonly used adsorbent for protection from toxic vapors. Desorption of physisorbed vapors is reversible and is dependent on the mass transfer rate into and out of the adsorbent and on the affinity of the adsorbate for the adsorbent. The mass transfer equilibria of such systems are highly variable depending on the concentration of the target compound in the air vs. concentration of the target compound in the adsorbent, on temperature, and on competitive kinetics of interferents (e.g.

commonly encountered solvents, pesticides, diesel exhaust, fuel vapors, etc.) (Rivin and Kendrick, 1997). Additionally, such systems can reach their saturation point, at which stage they have exhausted their adsorbent capacity for the target compound. The high variability within these materials, coupled with the huge numbers of unknown variables in a practical environment make it extremely difficult to predict the amount of time these systems will function properly before needing to be replaced; consequently, extremely conservative parameters have been established that govern the system's working life based on worst-case environmental conditions.

Because they possess extremely large surface areas per unit weight, activated carbon, silica, alumina and zeolites are the most common commercially available adsorbents. Just one gram of activated carbon has a surface area of 500–1000 m²/g (for comparison, a tennis court is about 260 m²). Activated carbon is produced by pyrolysis and carbonization of organic matter, typically coconut shells or hardwoods. Silica gels are matrices of hydrated silicon dioxide, alumina is mined or precipitated aluminum oxide and hydroxide, and zeolites are highly ordered aluminosilicates that occur naturally and can be synthesized. Activated carbon composite beads are currently used in most chemical warfare agent protective ensembles.

Research in novel adsorbents for protection from toxic vapors has taken two converging directions. One direction involves the development of catalytically reactive adsorbents, wherein the adsorbent decomposes the toxic vapor before it can penetrate the textile. Such an approach has the advantage that the adsorbent no longer needs to prevent breakthrough of the toxic chemical, but only to react with the toxic vapor faster than it can penetrate the adsorbent liner. Literally thousands of reactive adsorbents have been evaluated, but most fall into one of three categories based on mode of decomposition: hydrolysis catalysts, oxidation catalysts and degradative enzymes (Yang *et al.*, 1992). Two major drawbacks of such an approach are that decomposition products are not always non-toxic, and not all toxic vapors undergo the same decomposition pathway or at the same decomposition rate. Thus such systems must be targeted to specific threat agents, typically traditional chemical warfare agents. Unfortunately recent wartime activities suggest that such a narrow approach may be flawed. Consequently, the area of reactive adsorbents is rapidly converging with the development of ultra-high-surface area (UHSA) adsorbents.

Research in UHSA adsorbents is primarily concentrated in the area of highly periodic crystalline structures called metal–organic frameworks or MOFs. An MOF is composed of two major components: a metal ion or cluster of metal ions and an organic linker molecule. An MOF cage filled with adsorbate is shown in Fig. 11.5, clearly depicting the extremely high pore volume and open structure. The organic units are typically multivalent ligands. The choice of metal and linker govern the structure pore geometry,



11.5 Pictorial representation of an MOF filled with adsorbate.

and stability of the MOF (MacGillivray, 2010). This versatility allows for tailored design of MOFs based on desired application. These structures possess theoretical surface areas of $>8000 \text{ m}^2/\text{g}$ – more than five times the surface area of the best activated carbon!

11.4.3 Aerosols

Traditionally military protective textiles do not provide significant percutaneous protection from liquid or solid aerosolized particles. However, with the development of new CBW agents, new dispersion techniques, the use of toxic industrial materials as threat agents, and the threat of bombs laden with radioactive dust, referred to as ‘dirty bombs’, percutaneous protection from aerosols has become a critical aspect of future military protective textiles (Cordesman, 2001). The current goal for aerosol protection is achieving aerosol protection without significantly affecting water vapor transport.

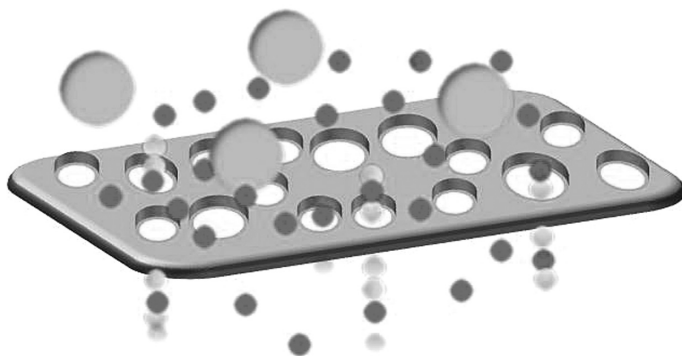
Currently two approaches exist for providing percutaneous aerosol protection: encapsulation and mechanical filtration. Encapsulation, the oldest and crudest form of protection from aerosols and poisonous chemicals, consists of covering the area to be protected with a material that is non-porous, and therefore impermeable to aerosols. While this approach does protect personnel from aerosols and other poisonous threat agents, it also encumbers the wearer with an unacceptable thermal burden that will likely result in more harm than good – note that the majority of both wartime and peacetime casualties in the past 30 years have been heat-stress related. Nonetheless, if the need arose, commercially available encapsulation

technologies are available and include a number of impermeable materials such as butyl rubber and polypropylene suits. As, by definition, encapsulation techniques allow for no improvement in breathability, we will focus primarily on advances in mechanical filtration technologies.

Mechanical filtration, which is defined as the physics of the interactions between fine particles and airstreams with filter fibers, membranes and surfaces, is well understood (Davies, 1973). Particle motion in an air stream depends on the characteristics of the particle and for a typical particle having a density near 1.0 g/cm^3 inertial motion dominates at sizes larger than one micrometer, while diffusional processes dominate at sizes smaller than 100 nm. Aerosols of $<500 \text{ nm}$ typically agglomerate via Brownian coagulation and electrostatic interactions with other aerosols to form particles of $>1 \text{ }\mu\text{m}$. The ability of an aerosol to stay airborne is a function of its mass, inertia, velocity and the velocity and turbulence of the air that the aerosol is suspended in, which can be calculated using the Navier–Stokes equation. In general, aerosols larger than $8 \text{ }\mu\text{m}$ in diameter exhibit rapid gravitational settling in most relevant military scenarios (Hinds, 1999). Therefore, the primary aerosol threat for textiles is in the size range of about 20 nm – $7.0 \text{ }\mu\text{m}$.

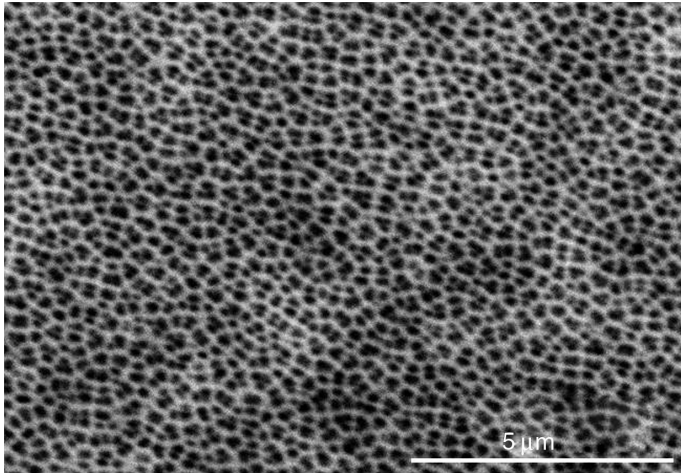
The area of mechanical filtration lends most of its advancements to removal of particles from gases, primarily air, and liquids, primarily water. Mechanical filtration technologies that are adapted for integration into a wearable textile include membrane technologies, fibrous filtration technologies and hybrids that possess aspects of both fibrous and membrane particulate filtration.

A membrane, as defined by the International Union of Pure and Applied Chemistry (IUPAC), is a structure having lateral dimensions that are much greater than its thickness, through which mass transfer may occur under a variety of driving forces – or, from our perspective, a thin sheet of material that is mostly solid, with intermittent holes as in Fig. 11.6 (IUPAC, 1996).

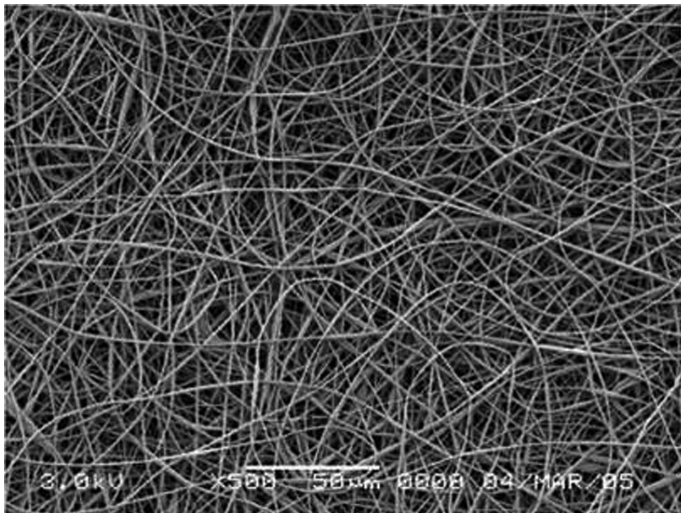


11.6 Pictorial representation of a size exclusion membrane.

Common commercially available, wearable membrane technologies include expanded polytetrafluoroethylene composites, e.g. Gore-tex™, and polyether ether ketone (PEEK) composites. As in the case of encapsulation, the very definition of a membrane – a structure having lateral dimensions much greater than its thickness – significantly limits the rate of mass transport through the membrane. Figure 11.7 shows an actual membrane for comparative purposes with Fig. 11.8. While a membrane serves well from an aerosol protection sense, it makes maintaining adequate water vapor transport difficult.



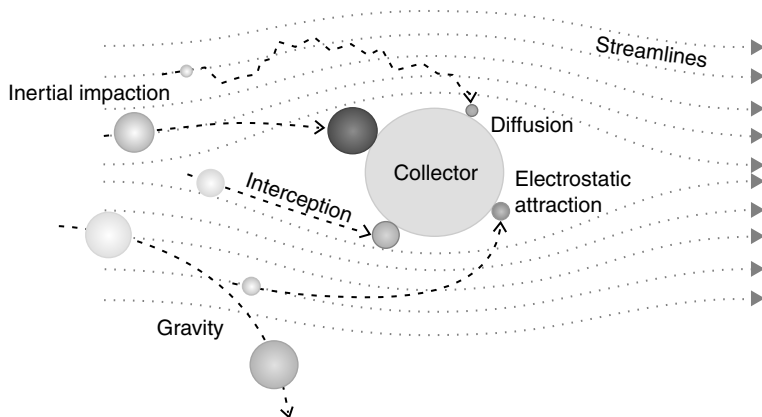
11.7 SEM of an alumina membrane.



11.8 SEM of meltblown glass fiber aerosol filtration media.

Traditional fibrous aerosol filters partially circumvent the water vapor transport difficulty by increasing the air space between individual fibers and relying more heavily on mechanisms other than size exclusion for achieving performance. Fibrous aerosol filters are typically composed of a mat of randomly arranged fibers wherein the air space between individual fibers is typically much greater than $0.3\text{ }\mu\text{m}$. Key factors affecting the function of fibrous filters are fiber diameter, filter thickness, face velocity and electrostatic surface charge. The intuitive assumption that a high-efficiency filter functions based solely on size exclusion, allowing particles smaller than the largest opening to pass through, is incorrect. Unlike membrane filters, in which particles as wide as the largest opening or distance between fibers are prevented from traversing the pore, fibrous high-efficiency filters can capture aerosols that are much smaller than the distance between fibers by relying more on interception, diffusion, and electrostatic attraction than on size exclusion or inertial impaction for capturing submicron aerosols. Consequently, fibrous submicron aerosols. Consequently, fibrous filters are typically much more open than membranes. Figure 11.9 illustrates the combination of mechanisms a fibrous high-efficiency filter employs for capturing aerosols. The four primary mechanisms of aerosol capture are (Hinds, 1999):

1. *Interception* – Particles following a line of flow in the air stream come within one radius of a fiber and adhere to it.
2. *Inertial impaction* – Larger particles are unable to follow the curving contours of the air stream, run into a fiber and stick to it; this mechanism increases in efficiency with diminishing fiber separation and higher air flow velocity.
3. *Diffusion* – The collision with gas molecules by the smallest aerosol particles, especially those below $0.1\text{ }\mu\text{m}$ in diameter, which are thereby



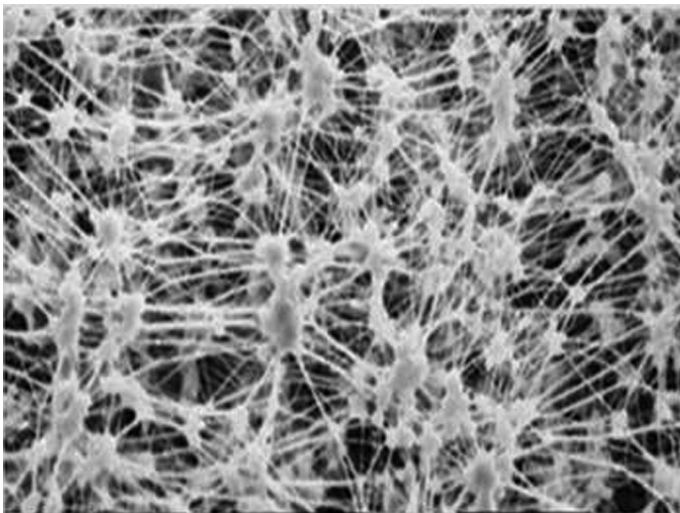
11.9 Pictorial representation of the mechanisms of aerosol capture.

deflected out of the streamline in their path through the filter and onto a fiber. This behavior is similar to Brownian motion and raises the probability that a particle will be stopped by either of the two mechanisms above. Diffusion becomes the dominant capture mechanism at smaller particle sizes, and is more efficient at lower airflow velocities.

4. *Electrostatic attraction* – Particles adhere to a surface due to the build-up of static charge on the *surface* of objects.

Aerosol filtration media created by stretching or expanding membranes so as to dramatically increase the size and volume of their pores are also commercially available. These technologies are essentially fibrous filtration media that are derived from membranes (Fig. 11.10). Commercially available fibrous aerosol filtration methods that can be integrated into a wearable textile are numerous because any technology that can durably deposit a fibrous mat onto a textile represents an improvement to aerosol penetration. Again, as previously stated, the difficulty is providing adequate aerosol protection without significantly reducing the overall breathability of the textile. To accomplish this researchers are turning to nanoscale fibrous materials.

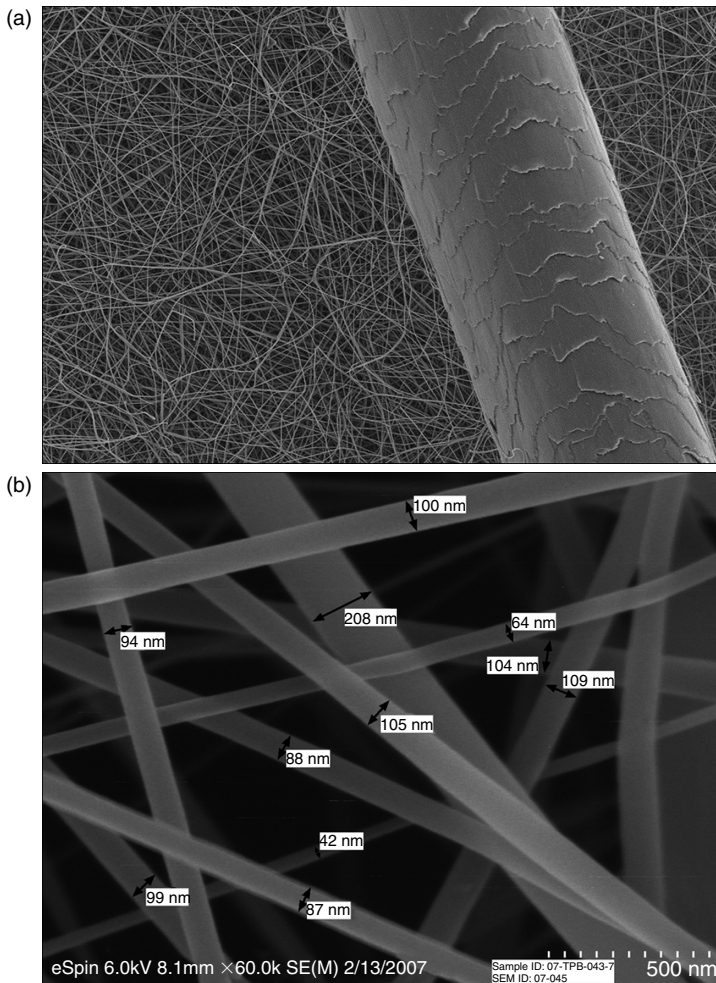
Research in the area of nanotechnology for producing nanoscale aerosol filtration media is currently at the leading edge of research in textile incorporable aerosol filtration. This is because as fiber diameters approach the mean free path of air, 35–65 nm, the mixture of molecules that comprise air enter into the slip-flow regime with respect to passage through the filtration



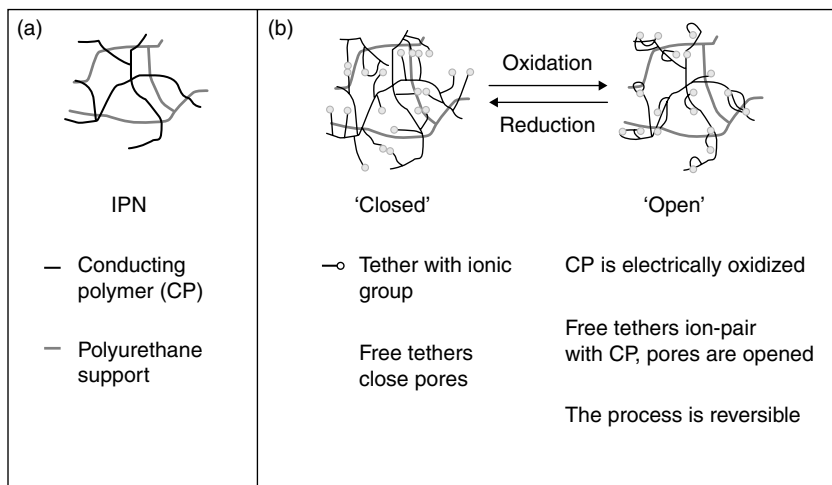
11.10 SEM of expanded polytetrafluoroethylene.

media (Fig. 11.11(a) and (b)). This means that air and water vapor can pass nearly unhindered through the filtration media while larger molecules and aerosols cannot. Several methods exist for producing submicron fibrous media, such as electrospinning, islands-in-the-sea extrusion, bacterial synthesis, growth of nanoscale inorganic oxides onto supports, and so forth; however, the durability of these delicate nanoscale structures for flexible textile applications is questionable and is currently under investigation.

One of the most ambitious, cutting-edge research efforts to protect from aerosols and liquids involves a marriage of electrochemistry and mechanical filtration. While approaches to achieving ‘smart’ textiles like the one



11.11 (a) SEM of an electrospun web compared to a human hair; (b) high-resolution SEM showing the nanoscale diameter of the fibers.



11.12 Pictorial representation of a conducting interpenetrating fibrous network in its closed state (a) and open state (b). Figure courtesy of Dr Banahalli Ratna, Naval Research Laboratory.

described here are discussed in greater depth in Chapters 3, 7 and 10, the focus of this effort necessitates a brief description here. The project, managed and directed by Dr Banahalli Ratna at the Naval Research Laboratory, has developed an interpenetrating network (IPN) material (Fig. 11.12) composed of soft polyurethane interspersed with a conducting polymer network that can be reversibly switched between two conducting states by the application of a small potential (~ 1.0 V). The switchable states allow charged tethers to form complexes within the conducting polymer portion to either increase the material's porosity, or decrease it, on command. Chemical warfare protective clothing, or partial clothing sections, formed from this material will have normal permeability (breathability) for comfort while at the same time have the ability to instantaneously and reversibly lower their permeability to agent molecules by application of the small voltage. When the membrane is in its 'closed' state, it will block the transport of threat agents. When the threat is removed, a second voltage application will 'switch' the membrane to its 'open', breathable state. The open state allows the wearer comfort with low heat load, and rapid moisture vapor transport away from the body.

11.5 Conclusions

An ideal military protective ensemble would incorporate protection from detection, ballistics, toxic aerosols, toxic liquids and vapors, possess fire-retardant qualities, breathe like cotton, and be machine washable. Obviously

overcoming one deficiency is difficult in its own right, so when presented in bulk as an integrated system, the task might seem impossible. However, after the subtasks are separated and distributed into their respective areas, one can see that considerable progress is occurring in every facet of protection. To the skeptics that claim a wholly integrated protective system is impossible, I offer an old idiom: ‘How do you eat an elephant? One bite at a time.’

11.6 References

- BEHRENS, R. (2009) *Camoupedia: A Compendium of Research on Art, Architecture and Camouflage*. Dysart, IA: Bobolink Books.
- BIRCH, H. (2010) Iridescence in nature: how to disappear completely. *Chemistry World*, June: 42–45.
- CHIAO, C., CHUBB, C. and HANLON, R. (2007) Interactive effects of size, contrast, intensity and configuration of background objects in evoking disruptive camouflage in cuttlefish. *Vision Research*, 47: 2223–2235.
- CHO, A. (2006) High tech materials could render object invisible. *Science*, 312(5777): 1120.
- CORDESMAN, A. (2001) *Asymmetric and Terrorist Attacks with Chemical Weapons, in Defending America*. Washington, DC: Center for Strategic and International Studies.
- CORNWELL, J. (2003) *Hitler's Scientists: Science, War, and the Devil's Pact*. New York: Penguin.
- CRANE, D. (2006) Update: AAE IR/NV-stealth and visibility-stealth cloaking technology. *Defense Review*, 27 November.
- CUNNIFF, P. and AUERBACH, M. (2003) *High Performance 'M5' Fiber for Ballistics and Structural Composites*. US Army Soldier and Biological Chemical Command.
- DAVIES, N. (1973) *Air Filtration*. London: Academic Press.
- DONAHUE, K. (2003) *Chemical and Biological Barrier Materials for Collective Protection Shelters*. Soldier and Biological Chemical Command, Natick, MA, pp. 1–10.
- HINDS, W. (1999) *Aerosol Technology*, 2nd edn. New York: John Wiley & Sons, Inc.
- IUPAC (1996) *Terminology for Membranes and Membrane Processes*. Working Party on Membrane Nomenclature.
- KANNIK, P. (1968) *Military Uniforms of the World*. New York: Littlehampton Publishing.
- LEE, H. and OWENS, J. (2010) Design of superoleophobic NyCo. *Journal of Material Science*, 45: 3247–3252.
- LEE, H. and OWENS, J. (2010) Design of superoleophobic NyCo. *Journal of Material Science*, 45: 3247–3252.
- MACGILLIVRAY, L. (2010) *Metal–Organic Frameworks Design and Application*, 1st edn. New York: John Wiley & Sons.
- NCJRS (2001) Selection and application guide to personal body armor. *NIJ Guide*: 100–101.
- NIJ (2008) Ballistic resistance of body armor. NIJ standard-0101.06, US Department of Justice.
- NMAB (2003) Materials research to meet 21st century defense needs. National Materials Advisory Board. Washington, DC: National Academic Press.

- NORTHOLT, M. and BALTUSSEN, J. (2001) The tensile and compressive deformation of polymer and carbon fibers. *Journal of Applied Polymer Science*, 83: 508–538.
- RIVIN, D. and KENDRICK, C. (1997) Adsorption properties of vapor-protective fabrics containing activated carbon. *Carbon*, 35(9): 1295–1305.
- ROLANDO, M. and ROQUE, M. (2007) *Adsorption and Diffusion in Nanoporous Materials*. Puerto Rico: CRC Press.
- SARAF, S., LEE, H., MICHELSEN, S., OWENS, J., WILLIS, C., STONE, C. and WILUSZ, E. (2010) Superhydrophobic, superoleophobic, hydroentangled nonwoven fabric, in press.
- WAGNER, N. and BRADY, J. (2009) Shear thickening in colloidal dispersions. *Physics Today*, October: 27–32.
- WARD, I. and LADIZESKY, N. (1985) Ultra high modulus polyethylene composites. *Pure and Applied Chemistry*, 57(11): 1641–1649.
- YANG, Y., BAKER, J. and WARD, R. (1992) Decontamination of chemical warfare agents. *Chemistry Reviews*, 92: 1729–1743.

Developments in clothing protection technology

W. ZHONG,

University of Manitoba, Canada

and

N. PAN,

University of California, Davis, USA

Abstract: Clothing protective technology provides protection for millions of people from hazards at work or in emergency situations. Different types of protective clothing have been developed to protect us from various environmental hazards. The two major issues of protective clothing are its protective function and the comfort it provides as clothing. Crucial textile components for the design and development of protective clothing include fiber species, fabric structure and physical/chemical finish applied in the fabrication process. Since the design and/or functionalization of these components greatly influences the performance of protective clothing, much work has been concentrated on one or several of these components, and theories and simulation models have been developed to explain the mechanism of clothing protection. It is expected that nanotechnology and smart/intelligent textiles will be two heated topics in the future development of clothing protection.

Key words: clothing protection, clothing comfort, nanotechnology, smart/intelligent textiles.

12.1 Introduction

Through its protection of millions of people from hazards at work or in emergency situations, clothing protective technology may be the most important of the ‘personal protective technologies’ (PPT). It helps maintain the health and safety of people by reducing or eliminating hazardous exposures to heat, cold, dusts, toxins, radiations, impact and biohazards. Extensive efforts have been devoted to the research and development of new technology for clothing protection, in such fields as new materials, fabric structures and innovative treatments. This chapter will provide an overview of these development efforts and results, and of how they can enhance the function and/or comfort of protective clothing.

12.2 Key issues of protective clothing

Different types of protective clothing have been developed to protect us from various environmental hazards, such as extremely high/low temperatures, chemicals, micro-organisms, insects, UV radiation and so on. Despite its varied end uses, protective clothing has traditionally involved two major issues: its protective function and the comfort it provides as clothing.

When we speak of the protective function of clothing, we usually mean that what we wear will serve as an effective barrier against hazards. Depending on the nature of the hazards, the protective clothing may be designed to be waterproof, dust-impermeable, bulletproof, fireproof, etc. High performance fibers, special fabric structures or special finishes, etc. are generally regarded as able to render a clothing system protective, and are used for such a capacity. The design issues will be discussed in detail in the next chapter.

‘Comfort’, on the other hand, may mean more than is usually suggested by the word. Direct contact and interactions between textiles and the skin may cause reactions, or even damage and diseases [1], and may be responsible for skin irritation and intolerance caused by textiles, dermatitis caused by chemicals (i.e. dyes and finishes) and physical contact/friction, and so on. When we wear – or are advised to wear – a piece of clothing that is ‘protective’, we expect that it will be so ‘comfortable’ as never to cause us these problems. Now it is clear that such comfort can be derived from novel designs of the microclimate between clothing and the skin, which ensures thermal clothing comfort as well as comfort that necessarily goes with protective clothing.

12.2.1 Microclimate

Water escapes through the skin in two different ways: passive loss and sensible loss. From the deeper, highly hydrated layers of the epidermis and dermis, a passive flux of water takes place towards the more superficial stratum corneum (SC) layers, which have a relatively low water content. This is so-called transepidermal water loss (TEWL) [2]. Extensive research work has been published on the topic of TEWL [3–6]; however, knowledge about how textile materials influence TEWL is limited.

In 1987, Hatch *et al.* reported an *in vivo* study of water content in the surface layers of human SC and water evaporation from its surface due to the placement of fabrics on the skin for varying time periods [7]. A lightweight fabric placed on the skin produced no change in skin water content or evaporative water loss from the SC. Only for occluded treatments (e.g. fabric plus plastic film) did water content and evaporation increase as the covering fabrics remained for longer periods.

Water loss through the skin may also occur in the form of perspiration or sweat, secreted by the eccrine sweat glands deep in the dermis. Water evaporation via secretion absorbs heat, and thus helps regulate body temperature in response to environmental changes. For humans to feel comfortable, a fairly narrow range of surface temperature and humidity must be maintained in the air immediately surrounding the body. Clothing, therefore, plays an important role in regulating body temperature and controlling heat loss. The term *microclimate*, accordingly, has been used frequently to describe the environmental parameters that influence heat exchanges such as temperature, humidity and microspace air stream between the skin and clothing [8]. Microclimate is an important factor for wear comfort, and depends on properties such as moisture and heat transport through the clothing material, and on physiological and environmental conditions.

Clothing comfort has been extensively studied; however, not much has been done towards clarifying how the skin responds to the clothing fabric in various conditions. Hatch *et al.* published works revealing *in vivo* cutaneous and perceived comfort response to fabric [9–14]. Their work began with experiments in a simulated skin/fabric/microclimate system composed of a modified Kawabata Thermolabo apparatus housed in a controlled environmental chamber [11]. The three experimental fabrics (one cotton and two polyester fabrics with different fiber deniers) showed small differences in water vapor and air permeability as well as energy dissipation rates. The results suggested that these thermophysiological comfort parameters were related more to fabric structures than to fiber contents. Also, these researchers added, different mechanical and surface properties of fibers were found to contribute to variation in sensorial comfort of the experimental fabrics [9]. They then went on to document water content and blood flow in human skin under garments worn by exercising subjects in a hot and humid environment [10]; no significant differences were observed between the three experimental fabrics in terms of alteration in capillary blood flow, SC water content, skin evaporative water loss or skin temperature [12]. These researchers made further investigations, placing fabric patches directly on the volar forearm skin of the subjects instead of having them loosely worn by the subjects [13, 14]. The experiments revealed that, for normal skin, SC hydration generally increase as fabric moisture content increased.

Kwon *et al.* compared the physiological effects of the hydrophilic and hydrophobic properties of the fabrics worn by exercising and resting subjects with and without wind [15]. Three types of materials with different moisture regains (wool/cotton blend with high moisture regain, 100% cotton with intermediate regain, 100% polyester with low regain) combined to form a clothing ensemble for the test. The results indicated that hydrophilic properties of the fabrics were physiologically significant for reducing heat strain (including skin temperature, clothing microclimate temperature and

humidity) and pulse rate for both the exercising and resting subjects, especially when influenced by the wind.

Generally, the experiments and analysis on skin response to textile and clothing system have not yet led to commercial interventions. One reason is the difference from one subject to the other in terms of physical status and sensitivity. When it comes to the *in vitro* experiments, the difficulties lie in how to realistically represent the whole skin/fabric/microclimate system.

12.2.2 Skin reactions and irritations caused by textiles

Irritation of the skin as a result of its reaction to textiles, all too often due to chemicals or dyes, will be discussed in Chapter 21.

Skin irritation may also be caused by physical contact and friction between clothing and the skin. The frictional properties of the skin are of interest in the area of cosmetic products and clinical dermatology dealing with acute and chronic friction trauma such as blisters and calluses [16].

A study on skin friction properties involved human subjects of different gender and age [17]. Measurements were obtained from 11 anatomical regions, namely, the forehead, upper arm, volar and dorsal forearm, postauricular, palm, abdomen, upper and lower back, thigh and ankle. The dynamic friction coefficient did not vary significantly between age and sex groups but varied considerably from region to region. It was suggested that frictional properties of the skin are dependent more on water content or non-apparent sweating, and may be related to sebum secretion. A subsequent study showed that surface lipid content (SSL) is also related to these properties [18].

Other studies on the influence of skin friction on the perception of fabric texture and pleasantness under a series of environmental conditions from neutral to hot-dry and hot-humid also revealed that moisture on the skin surface increased skin friction [19] and that fiber type and moisture influenced fabric-to-skin friction measurements [20]. According to these reports, moisture on the skin is more important than the fiber type or fabric construction parameters in determining the nature and intensity of fabric-to-skin friction, and glabrous skin friction changes less with wetting than with hairy skin.

Recent studies have further clarified how moisture, sebum and emollient products are related to skin friction properties [21]. Elkhyat *et al.* recorded the influence of hydrophilic/hydrophobic balance (Hi/Ho) of the skin surface on the friction coefficient, using both *in vitro* and *in vivo* experiments [22]. They showed that the higher hydrophobia tendency of the surfaces, the lower the friction coefficient. The friction coefficient, therefore, may quantify the influence of lubricant/emollients/moisturizers applied to the skin. And the relationship between the friction coefficient and the hydrophilic/

hydrophobic balance can be reversed in the presence of water and sebum on the forehead.

To measure the frictional coefficient of the skin, use is now made of such commercial instruments as the UMT series Micro-Tribometer [23, 24] and the KES-SE Frictional Analyzer [25, 26]. However, measurements thus obtained may lack comparability, due to disagreement on which scientific law governs the relationship between physical pressure and skin friction. The classic Amonton's law [27], which stipulates that the friction coefficient remains unchanged under varying normal loads and speeds of the probe (i.e. the opposing material used to measure skin friction), has long been challenged by numerous researches including some recent ones [23, 26], in which the friction coefficient was found to be inversely proportional to load [28].

Compared to what has been achieved in the study of the frictional coefficient of the skin surface, far less work has been performed on the assessment of frictional force between the skin and fabric. Such assessment usually involves slowly pulling fabric samples across the surface of the skin (i.e. forearm) so as to record with a force transducer the frictional force required to pull each fabric across the skin. The pressure between the fabric and skin is often applied by suspending a weight to the free end of the fabric. The resulting irritation effects caused by friction can then be documented [19, 20]. Other methods for measuring skin/fabric frictions were achieved using a strain gauge [29], or strained gauged flexure couples arranged in such a way as to try to detect both the normal and frictional force [30]. Measurements can be made by giving the applied material a wipe with the right index finger.

Hatch summarized work performed to understand skin irritation caused by contact and/or friction of clothing or other textile materials [31]. It is reported that dermatological problems are linked to six fibers: (a) nylon, for contact dermatitis and contact urticaria, (b) wool, for acute and cumulative irritant dermatitis, aggravate atopic dermatitis, allergic contact dermatitis, and immulogic contact urticaria, (c) silk, for atopic dermatitis and contact urticaria, (d) glass fiber, for mechanical irritation, (e) spandex fiber and (f) rubber fiber. Some forms of dermatitis, as in the cases of nylon, spandex and rubber fibers, were often caused by dye, finish or fiber additive instead of fiber material itself.

A study on the effects of wearing diapers on the skin showed that skin wetness was proportional to diaper wetness, and, with increased skin wetness, coefficients of friction and abrasion damage would increase [32]. According to a study of the electrostatic potentials generated on the surface of the scrotal area, the accumulated electrostatic charges on the pants were due to the friction of the pants with the skin when different types of textile fabric were worn [33]. Polyester pants showed the highest potential while polycotton

pants produced less than half that level. The daytime readings were higher than those in the night, probably mainly due to the higher temperature and activities during the day. A related study even suggested that this electrostatic potential may be responsible for inhibited hair growth [34].

12.3 Developments in clothing protection

Crucial textile components for the design and development of protective clothing include fiber species, fabric structure and physical/chemical finish applied in the fabrication process. Since the design and/or functionalization of these components tremendously influence the performance of protective clothing, much work has been concentrated on one or several of these components. Theories and simulation models have been developed to explain the mechanism of clothing protection.

12.3.1 Textile components in the development of protective clothing

Textile fiber is the basic unit of textiles. In the last few decades, a wide variety of advanced fibers were developed for protective clothing. For example, fibers with high heat resistance were made for thermal protective clothing. Aramid fibers were manufactured from the long-chain synthetic polyamide in which at least 85% of the amide linkages are attached directly to two aromatic rings [35], namely the aromatic groups are linked into the backbone chain through either the 1, 3 positions (meta-aramid) or the 1, 4 positions (para-aramid). Nomex and Kevlar from Dupont are widely used meta- and para-aramid fibers, respectively. Meta-aramid fibers are known for their good thermal stability and long-time stability at high temperatures, which justify their extensive use in thermal protective clothing. Valued for their high tenacity and high modulus, Kevlar fibers, on the other hand, are frequently used in ballistic fabrics. Other high performance fibers for protective clothing include both organic fibers (polybenzimidazole fibers, high molecular weight polyethylene, etc.) and inorganic fibers (glass fibers, carbon fibers, etc.).

Alongside the development of new fiber species is the development of new fiber formats. The high surface area to volume ratio of nanofibers explains why they can be an ideal material for protective clothing against biochemicals and air contaminants. The woven, non-woven or knitted fabrics, when coated with nanofibrous membranes, can be made into protective clothing or masks that will present minimal impedance to moisture vapor diffusion required for evaporative cooling. The water vapor transmission test results showed that electrospun polyurethane webs were able to significantly improve the performance of protective clothing as a barrier to liquids,

and that air permeability would decrease with increasing electrospun web area density [36]. It was also demonstrated that a layered fabric system (electrospun polyurethane fiber web layered on spunbonded non-woven) with a web area density of 1.0 and 2.0 g/m² exhibited higher air permeability than most PPE (personal protective equipment) materials currently in use [37]. Zinc titanate nanofibers were also tested and found able to improve detoxification properties of protective clothing [38].

Fabric structure is another important textile component. One of the most frequently used fabric structures is the *multilayered*, so termed because such a structure is composed of a number of layers and able to provide multi-protection to the wearer. Multilayered fibers have been extensively used in thermal protective clothing as static air trapped between the layers provides excellent insulation. Recently, much research work has been performed to gain a better understanding of the heat and moisture transfer through the multilayered fabrics so as to ascertain a fabric structure that will contribute the highest level of safety and the largest degree of comfort [39–41]. Polytetrafluoroethylene (PTFE)/fabric laminates, for instance, have been used in waterproof, chemical/biological protective clothing, which is both protective and breathable [42, 43]. Composite fabric/system has been drawing increasingly eager attention from protective clothing researchers, and a variety of materials have been used for such composite fabric systems to bring in a synergy for the purpose of protection and/or comfort [44–46].

Various treatments and finishes have also been introduced to enhance the protection of clothing. Many flame retardants, including those based on phosphorus, have been used in treating cellulose fibers, which will be blended into inherent flame-resistant fibers to achieve both thermal protection and comfort [47–50]. Treatments that will help render the protective clothing antibacterial [51–53] and anti-insect [54–58] have been extensively studied. Nanotechnology [52, 53] and smart/intelligent materials [59–62] have found their applications in the treatment of fibers or fabrics, also for the purpose of enhanced protection.

12.3.2 Modeling and simulation for clothing protection

Simulation models have been developed to aid related efforts, often by precisely and vividly representing the transport process of hazardous particles penetrating the fabric structure [63]. These researches are important because they generate further knowledge on which to base further research, and are themselves cost-effective than the normal experimental tests.

The ability of a fibrous filter to collect aerosol particles is usually expressed in terms of its filtration efficiency, and the fraction of entering particles it retained. This efficiency is often derived from the aerosol filtration efficiency

of a single filter element (η), whose size and shape are chosen to best represent the microstructure and porosity of a given filtering material [64, 65]. The single fiber efficiency is the combined effects of the various mechanisms of capture, including direct interception, inertial impaction, diffusion deposition, gravitational settling, etc. [64, 65]. These mechanisms are not necessarily independent. Adhesive forces involved in the filtration process are also studied. They include Van der Waals forces [65, 66] and electrostatic forces [67, 68] between the particle and a fibrous filter.

The arrangement formats of fibers in a filter, however, always have great impact on the aerosol filtration since the fibers interact with each other and with the particles during the filtration process. The most difficult job in the study of aerosol filtration processes is the description of the heterogeneous fibrous structures. To account for the effect of fiber arrangement, two multifiber models were used to investigate the interception efficiency of fibrous filters composed of symmetrical arrays of fibers, including the parallel and staggered arrays [69, 70], thus enabling the filtration process to be simplified as a two-dimensional periodic flow. Shapiro [71] introduced an inclusion model, where the filter material was regarded as a uniform matrix containing a certain volumetric fraction of inclusion of a certain size. Both inside and outside the inclusion, the filter structure is assumed to be homogeneous, albeit with different porosities. Alternative approaches [72] involved a model where the filter media was represented by a two-dimensional distribution [73] of cells of varying packing density.

When the filter structure is defined, the flow field in the course of filtration can be characterized by such constitutive equations as the continuity equation and Darcy's law. The constitutive equations and the corresponding boundary conditions can be solved analytically or numerically to give the pressure field and velocity field. These relations, combined with expressions for the single fiber efficiency, allow calculation of the efficiency of each element of the filter (local efficiency), as well as their combination or averaging into the overall efficiency of filter materials [72, 74].

However, none of these models suffices to precisely describe the heterogeneous structure of a fibrous filter and the stochastic nature of aerosol behavior. Other discrete approaches have therefore been attempted to deal with problems involved in the description of heterogeneous structures. These approaches include the lattice Boltzmann (LB) model [75] and the cellular automata (CA) probabilistic model [76]. The CA models keep track of the many-body correlations and provide a description of the fluctuations, while the LB models are believed to be numerically more efficient and exhibit more flexibility to adjust the fluid parameters [76].

Then a statistical mechanics model, i.e. the Ising model combined with Monte Carlo (MC) simulation, was introduced as a new approach to the study of aerosol filtration by fibrous filters. The Ising model had earlier been

presented for the study of ferromagnetic phase transition [77]. Since then it has been frequently used to study a system consisting of interactive subsystems, each of which bears two interchangeable states [78–81]. In the Ising model, a real system is divided by a grid into a discrete system composed of a number of lattice cells. The filtration system is thus treated as a system made from such subsystems as fiber cells and aero particle cells that interact with each other through adhesion. The transport and deposition process of the particles in the fibrous substrate is due to interactions as well as the effect of moving air stream, resulting in each particle moving from one cell to the other. In general, such a change in the system's configuration is driven by the energy difference after and before the change, subject to the random fluctuations represented by the MC simulation. Allowing use of a simpler binary algorithm, the Ising model makes for greater simulation accuracy and efficiency.

Model description

To describe the filtration process through a fibrous filter, a discrete 3-D Ising model is proposed. The system is divided into a lattice of a number of cubic cells. The length of a single cubic cell can be chosen arbitrarily and, for the sake of convenience, is made to be equal to the diameter of a fiber.

To represent the possible states of each cell, two variables are introduced:

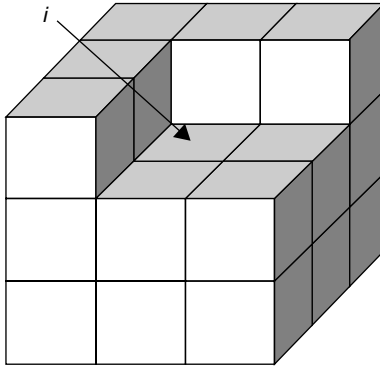
- 1 s_i , indicating whether a cell (i) is occupied by a particle ($s_i = 1$) or not ($s_i = 0$);
- 2 F_i , showing whether a cell (i) is filled with fibrous substrate ($F_i = 1$) or not ($F_i = 0$).

Energy of the system (the Hamiltonian) should be the summation of the energies of each single cell H_i , which in turn is the summation of the interactions between the cell i and its 26 nearest neighboring cubic cells (see Fig. 12.1), as

$$H_i = -A \sum_j s_i s_j - \left(B s_i F_i + C \sum_j s_i F_j \right) + G y_i \quad [12.1]$$

This equation takes into account all three types of interactions:

- 1 Cohesive interaction between neighboring particle cells, as shown in the first term on the right hand side of the equation, where A represents the cohesion energy between particles, and the summation of s values is over all nearest neighboring cells of cell i .
- 2 Adhesive interaction between particle and fiber substrate, shown as the terms in the bracket, where B and C correspond to the adhesion energies



12.1 A cell i in a 3-D Ising model with its neighbors.

between a particle and a fiber substrate in the same cell, and that in the nearest neighboring cells, respectively.

- 3 Gravitational effect of particles as shown in the last term, where G is the intensity of the gravity field and y_i the y -coordinate of cell i in the lattice.

The coefficients in equation [12.1] are determined in a manner described as follows:

It is assumed that the Van der Waals forces dominate the interactions between the fiber and the particles. According to the Lifshitz theory [82], the interaction energy between a particle (sphere) of diameter d_p and a surface, and that between two particles (spheres) with diameters d_{p1} and d_{p2} , can be expressed as equations [12.2] and [12.3], respectively:

$$W_{1,2} = \frac{h_{1,2}d_p}{12D} \quad [12.2]$$

$$W_{1,2} = \frac{h_{1,2}}{12D} \frac{d_{p1}d_{p2}}{(d_{p1} + d_{p2})} \quad [12.3]$$

where $h_{1,2}$ is the Hamaker constant, and D the distance between the particle(s) and the surface. An approximate expression for the Hamaker constant of two bodies (1 and 2) interacting across a medium 3, none of them being a conductor, is

$$h_{1,2} = \frac{3h\nu_e(n_1^2 - n_3^2)(n_2^2 - n_3^2)}{8\sqrt{2}(n_1^2 + n_3^2)^{1/2}(n_2^2 + n_3^2)^{1/2}[(n_1^2 + n_3^2)^{1/2} + (n_2^2 + n_3^2)^{1/2}]} + \frac{3}{4}k_B T \frac{\epsilon_1 - \epsilon_3}{\epsilon_1 + \epsilon_3} \frac{\epsilon_2 - \epsilon_3}{\epsilon_2 + \epsilon_3} \quad [12.4]$$

where h is the Planck's constant, ν_e is the main electronic adsorption frequency in the UV (assumed to be the same for the three bodies, and typically around $3 \times 10^{15} \text{ s}^{-1}$), n_i the refractive index of phase i , ϵ_i the static dielectric constant of phase i , k_B the Boltzmann constant, and T the absolute temperature.

Two constants, k_1 and k_2 , are used to represent the ratios of A/C and B/C , respectively.

$$k_1 = \frac{A}{C} = \frac{W_{1,1}}{W_{1,2}} = \frac{h_{1,1}}{h_{1,2}}, \quad k_2 = \frac{B}{C} = \frac{h_{1,2}/2D_2}{h_{1,2}/D_1} = \frac{D_1}{2D_2} \quad [12.5]$$

The ratio A/C is equal to the ratio of the cohesive energy between two particles to adhesive energy between a particle and fiber in neighboring cells. As the interaction distances in two cases are the same, the ratio is also equal to the ratio of the Hamaker constants in the two cases. B/C is the ratio of particle/fiber adhesive energy in the same cell to that in the neighboring cells, and therefore equals the ratio of the interaction distances. For interactions between a pair of neighboring particle and fiber cells, the distance, D_1 , is assumed to be one half of the cell length, while for interactions of particle/fiber within a cell, the distance, D_2 , depends on the scale of the surface roughness. In the present work, the value of C is determined by simulation to accommodate the experimental data. And the values of A and B are determined by equation [12.5].

The transportation process of aerosol particles through the fibrous substrate is usually accomplished by airflow in a certain velocity. The usual thermodynamic theories specify the considered bodies/systems in a state of absolute equilibrium, whereas aerosol particles transport through fibrous structures in airflow is conventionally categorized in aerodynamics, and it comes with substantial friction loss of transport characteristic of irreversibility. Therefore, dealing with such a problem we have, on the one hand, to make statistical calculations and, on the other, we are compelled to use mechanical energy terms like work of drag force. Assuming a quasi-equilibrium process this way, it is possible to extend MC simulation [79] to the case of aerosol particles transport through fibrous filters in an airflow:

When a particle is suspended in airflow of velocity V , through one time step in which air moves from its original cell to a neighboring cell, the particle can move in four different ways (Fig. 12.2), subject to different probabilities:

- 1 In the first case, the particle moves with the air stream to the neighboring cell. Accordingly, there is no relative velocity between particle and air stream during this time step, and the work done to the particle by airflow can be regarded as zero.
- 2 In the second case, the particle moves to a cell ahead of that of the air, with a velocity V relative to the air. The system energy change (dE) in

this time step includes both the change in Hamiltonian, dH , and the work done to the particle by airflow, W_A , as:

$$dE = dH + W_A = dH + F_D l \quad [12.6]$$

where l is the size of a cell, F_D is the drag force act on the particle with diameter d by the air stream and can be calculated according to the Stokes' law as

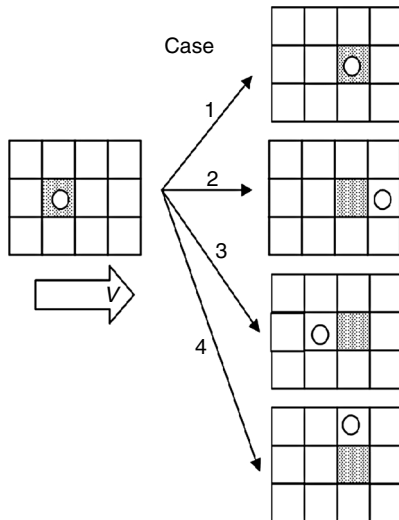
$$F_D = 3\pi\eta dV \quad [12.7]$$

where η is the viscosity of air which, at standard pressure and room temperature, is 1.81×10^{-5} Pa·s.

- 3 In case 3, the particle remains in the original cell despite the moving of air, the relative velocity of the particle to the air is $-V$. Therefore, the system energy change should be

$$dE = dH + F_D (-l) = dH + 3\pi\eta d(-l)(-V) = dH + 3\pi\eta dlV \quad [12.8]$$

- 4 In case 4, the particle may deviate from the air stream and move to other neighboring cells, as is the result of the combination of either the above three mechanisms or the diffusion. The influence of diffusion can be represented by the random effect of the MC simulation described in the next section.



12.2 Energy difference due to airflow.

The energy difference in each case is then used in the MC simulation to provide the probability for a cell changing its state at each time step.

In all the simulations (MC simulations) in the present study, for the sake of simplicity, movement of fibers is neglected. That is, the filtration process is assumed not to alter the internal structure of the fibrous filter, so that values of F for all the cells are kept constant in a simulation. Therefore, the process of aerosol filtration is the result of each particle moving from one cell to the other and/or depositing on the fiber substrate in a fiber cell. Procedures of the simulation are as follows:

- 1 Initial configuration is created by developing the lattice, within which the fibrous media are laid. The initial values of both F (1 or 0) and s (1 or 0) for each cell are also determined. A cell i is considered to be covered with fiber ($F = 1$) if the distance between the cell center and the fiber axis is smaller than the fiber radius.
- 2 All the particles in the space are scanned. For example, a particle cell i in the lattice is randomly selected. It can move in four different ways as described in the last section (also in Fig. 12.2). For each case, dE (energy difference between the configurations before and after the change) is calculated. Then the case with the lowest value of dE is selected as the most probable change. If a random number uniformly distributed between 0 and 1 is chosen and is smaller than the spin-flip probability, $p = \exp(-\beta \Delta E_T)$, the change of configuration takes place. Here, β is a constant inversely proportional to the absolute temperature.
- 3 An MC step ends when all the particles in the current state have been scanned. Then step 2 is repeated to start a new MC step until the whole simulation is terminated.

In the present study, an MC step is defined as the time in which air moves from one cell to a neighboring one with size l . Therefore, if the velocity of air is V , the relationship between an MC step and real time is

$$1 \text{ MC step} = \frac{1}{V} (\text{sec}) \quad [12.9]$$

Results and discussion

Based on the above description, a computational simulation algorithm is developed for the process of aerosol particles of different sizes filtering through isotropic fibrous filters with different fiber volume fractions.

Experimental data are adopted from the literature [83]; the filter used for testing is made from a polyester fiber, Dacron, of 12.9 μm in diameter. The filter fiber volume fraction is 27.1%. The particles are mono-disperse

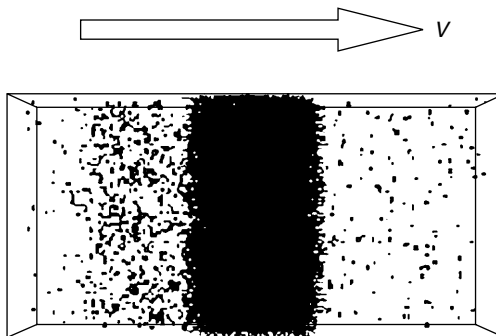
aerosols generated from DOP (dioctyle phthalate) solutions of different concentration to give different aerosol particle sizes.

To start the simulation, the length of a cubic cell is made to be equal to the fiber diameter, 12.9 μm . The fiber mat is constructed by generating a certain number of fibers whose center points and orientations are randomly determined. Next, the fiber volume fraction is represented by the ratio of the number of cells that are occupied by fibers to the total number of cells. The simulated system comprises a lattice of $228 \times 100 \times 50$, as shown in Fig. 12.3. The boundaries are periodical. In the space to the left of the fibrous filter, where the in-streams of the aerosols come from, the particles are regenerated after each MC step to maintain a constant input aerosol concentration C_{in} (the ratio of the number of particles to the total lattice cells on left sides of the filter). When output aerosol concentration C_{out} (the ratio of the number of particles to the total lattice cells on right sides of the filter) reaches equilibrium after certain MC steps, filtration efficiency of a fibrous filter is calculated as the ratio of C_{out} to C_{in} :

$$E_{\text{F}} = 1 - \frac{C_{\text{out}}}{C_{\text{in}}} \quad [12.10]$$

It is suggested that the adhesive force on a particle less than 10 μm is much greater than other forces that a particle experience [65]. The sizes of the particles modeled in this work are well below 10 μm . Gravity effect in equation [12.1] can therefore be neglected.

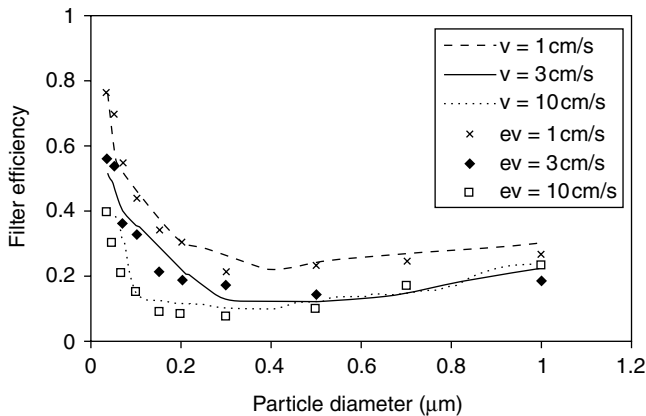
The parameters needed for the simulation are listed in Table 12.1. This model applies to different fibers and particles by taking account of the property parameters for different materials. It can also be seen that interactions between neighboring cells (A and C) are in a much smaller scale than those



12.3 A 3-D Ising model for the filtration process.

Table 12.1 Parameters for fiber and aerosol particle at room temperature (20°C)

	Density ρ (g/cm ³)	Refractive index n	Static dielectric constant ϵ	Simulation parameters			
				A	B	C	β
Fiber (Dacron)	1.35	3.0	1.61	2.23×10^{-3}	15	1.86×10^{-3}	40
Aerosol particle (DOP)	0.983	5.1	1.485				



12.4 Simulation and experimental results of filter efficiency vs. particle size; v represents the velocity of particles in simulated penetration, while ev is the velocity of particles in experiments.

within the same cell (B). This gap would be reduced in a finer lattice in cases of fibrous filters with more intricate structures, e.g. nanofiber filters.

Both simulation results (shown as continuous lines) and reported experimental data [83] (shown as discrete symbols) are shown in Fig. 12.4. They are in high accordance, indicating a good validity of the method.

Both the simulations and experiments show that, with the variation of particle size, the filtration behavior goes first through a diffusion regime, where filtration efficiency decreases with increase of particle size, as smaller particle size makes for better diffusion and thus better filtration efficiency. Then there is a regime of diffusion transiting to interception, and the efficiency goes down to a minimum, where the dominance of diffusion mechanism is taken over by interception, and then rises with the increase of particle size. Finally in an interception regime, filtration efficiency rises singularly with particle size. Combination of the above mechanisms in the simulation process is represented in the energy expression in equations

(12.6–12.8). To be specific, when the gravity effect can be neglected (for particle size below 10 μm):

- 1 Increased particle diameter d means higher adhesion between particle and fiber and the particles have fewer chances to deviate from the airflow. This leads to a more prominent impaction/interception mechanism.
- 2 With decreasing particle diameter, on the one hand, adhesion between particle and fiber is weakened, and it becomes easier to remove a deposited particle from the fiber. On the other hand, the effect of airflow on the particles diminishes, and the particles have more chances to fluctuate around the streamline. Both of these two factors contribute to enhanced diffusion.

Hence there are certain advantages of the present approach. First, the Ising model is capable of describing such complicated systems as aerosol filtration in fibrous structures in a simple binary form, accounting for all the physical mechanisms involved, without using such indirect parameters as single fiber efficiency, as is the case with classical filtration approaches, yet generating robotically informative results. Second, the approach is obviously able to depict the intricate interface between aerosol and fibrous media. This approach can be especially useful for explaining the effect of the interactions that occur at the interface within heterogeneous materials. Further, this model can be adapted to deal with more complicated cases, such as poly-disperse particles filtration through multilayer fibrous filters.

However, since this work is intended to deal with a particle/fiber system where movement of fibers is neglected for the sake of simplicity, the model requires further modification if it is to be applied to study aerosol-fiber systems with considerable fiber movement, in which the parameter F for each cell has to change accordingly to reflect the fiber movement.

12.4 Future trends

Protective clothing provides essential barriers to environmental hazards of different kinds, so as to maintain human safety and health. The developments of clothing protection technology have been focused on the design and development of new materials, structures and/or treatments to enhance clothing protection and comfort. These two key issues, protection and comfort, will continue to be the focus of research in the future. Theoretical and simulation work will also be a future trend, because they offer important design tools when experimental tests are costly, difficult or dangerous.

In addition, nanotechnology and smart/intelligent textiles will be two important topics in the future development of clothing protection: micro- or nano-encapsulation provide highly effectively methods of carrying various

active compounds such as antibacterial agents; the high surface-to-volume ratio of nanofibers makes them excellent barrier materials, while the high porosity of nanofibrous structures gives them excellent comfort; the incorporation of smart materials into protective clothing allows sensitive detection of hazards as well as programmable reactions to protect the end users of the protective clothing. As a result, these two highly interdisciplinary technologies are important for the developments in clothing protection technology in the future. A breakthrough in the clothing protection technology will likely depend on the extensive collaboration of researchers in a variety of areas, including material sciences, engineering, chemistry and biology.

12.5 References

1. ZHONG, W., *et al.*, Textiles and human skin, microclimate, cutaneous reactions: an overview. *Cutaneous and Ocular Toxicology*, 25(1) (2006): 23–39.
2. WILSON, D. R. and MAIBACH, H. I., Transepidermal water loss, a review. *In: Leveque, J. L. (ed.) Cutaneous Investigation in Health and Disease: Noninvasive Methods and Instrumentation*. New York: Marcel Dekker, 1989, pp. 113–133.
3. LEVIN, J. and MAIBACH, H., The correlation between transepidermal water loss and percutaneous absorption: an overview. *Journal of Controlled Release*, 103(2) (2005): 291–299.
4. FLUHR, J., *Bioengineering of the Skin: Water and Stratum Corneum*, 2nd edn., *Dermatology*. Boca Raton: CRC Press, 2005.
5. WARREN, R., *et al.*, Transepidermal water loss dynamics of human vulvar and thigh skin. *Skin Pharmacology and Physiology*, 18(3) (2005): 139–143.
6. WEIGMANN, H. J., *et al.*, Comparison of transepidermal water loss and spectroscopic absorbance to quantify changes of the stratum corneum after tape stripping. *Skin Pharmacology and Physiology*, 18(4) (2005): 180–185.
7. HATCH, K. L., WILSON, D. R. and MAIBACH, H. I., Fabric-caused changes in human skin – in vivo stratum-corneum water-content and water evaporation. *Textile Research Journal*, 57(10) (1987): 583–591.
8. CENA, K. and CLARK, J. A., *Bioengineering, Thermal Physiology, and Comfort*. Studies in Environmental Science. Amsterdam: Elsevier Scientific Pub. Co, 1981.
9. BARKER, R. L., *et al.*, *In vivo* cutaneous and perceived comfort response to fabric. 2. Mechanical and surface related comfort property determinations for 3 experimental knit fabrics. *Textile Research Journal*, 60(8) (1990): 492–494.
10. HATCH, K. L., *et al.*, *In vivo* cutaneous and perceived comfort response to fabric. 3. Water-content and blood-flow in human skin under garments worn by exercising subjects in a hot, humid environment. *Textile Research Journal*, 60(9) (1990): 510–519.
11. HATCH, K. L., *et al.*, *In vivo* cutaneous and perceived comfort response to fabric. 1. Thermophysiological comfort determinations for 3 experimental knit fabrics. *Textile Research Journal*, 60(7) (1990): 405–412.
12. MARKEE, N. L., *et al.*, *In vivo* cutaneous and perceived comfort response to fabric. 4. perceived sensations to 3 experimental garments worn by subjects exercising in a hot, humid environment. *Textile Research Journal*, 60(10) (1990): 561–568.

13. HATCH, K. L., *et al.*, *In vivo* cutaneous response to fabric. 5. Effect of fiber type and fabric moisture-content on stratum-corneum hydration. *Textile Research Journal*, 62(11) (1992): 638–647.
14. HATCH, K. L., *et al.*, *In vivo* cutaneous and perceived comfort response to fabric. 6. The effect of moist fabrics on stratum corneum hydration. *Textile Research Journal*, 67(12) (1997): 926–931.
15. KWON, A., *et al.*, Physiological significance of hydrophilic and hydrophobic textile materials during intermittent exercise in humans under the influence of warm ambient temperature with and without wind. *European Journal of Applied Physiology and Occupational Physiology*, 78(6) (1998): 487–493.
16. ELSNER, P., WILHELM, D. and MAIBACH, H. I., Frictional properties of human forearm and vulvar skin: influence of age and correlation with transepidermal water loss and capacitance. *Dermatologica*, 181(2) (1990): 88–91.
17. CUA, A. B., WILHELM, K. P. and MAIBACH, H. I., Frictional properties of human skin: relation to age, sex and anatomical region, stratum corneum hydration and transepidermal water loss. *British Journal of Dermatology*, 123(4) (1990): 473–479.
18. CUA, A. B., WILHELM, K. P. and MAIBACH, H. I., Skin surface lipid and skin friction: relation to age, sex and anatomical region. *Skin Pharmacology*, 8(5) (1995): 246–251.
19. GWOSDOW, A. R., *et al.*, Skin friction and fabric sensations in neutral and warm environments. *Textile Research Journal*, 56(9) (1986): 574–580.
20. KENINS, P., Influence of fiber-type and moisture on measured fabric-to-skin friction. *Textile Research Journal*, 64(12) (1994): 722–728.
21. SHEU, H. M., *et al.*, Human skin surface lipid film: an ultrastructural study and interaction with corneocytes and intercellular lipid lamellae of the stratum corneum. *British Journal of Dermatology*, 140(3) (1999): 385–391.
22. ELKHYAT, A., *et al.*, Influence of the hydrophobic and hydrophilic characteristics of sliding and slider surfaces on friction coefficient: in vivo human skin friction comparison. *Skin Research Technology*, 10(4) (2004): 215–221.
23. SIVAMANI, R. K., *et al.*, Friction coefficient of skin in real-time. *Skin Research Technology*, 9(3) (2003): 235–239.
24. SIVAMANI, R. K., *et al.*, Tribological testing of skin products: gender, age, and ethnicity on the volar forearm. *Skin Research Technology*, 9(4) (2003): 299–305.
25. KIM, J. J., *et al.*, Instrumental methods for measuring the surface frictional-properties of softener treated fabrics. *Textile Chemist and Colorist*, 25(8) (1993): 15–20.
26. EGAWA, M., *et al.*, The evaluation of skin friction using a frictional feel analyzer. *Skin Research Technology*, 8(1) (2002): 41–51.
27. WOLFRAM, L. J., Friction of skin. *Journal of the Society of Cosmetic Chemists*, 34(8) (1983): 465–476.
28. KOUDINE, A. A., *et al.*, Frictional properties of skin: proposal of a new approach. *International Journal of Cosmetic Sciences*, 22 (2000): 11–20.
29. NISHIMATSU, T., *et al.*, Measurement of active tactual motion in judging hand of materials of fabrics. *Sen-I Gakkaishi*, 54(9) (1998): 452–458.
30. GEE, M. G., *et al.*, A new friction measurement system for the frictional component of touch. *Wear*, 259 (2005): 1437–1442.

31. HATCH, K. L. and MAIBACH, H. I., Textile fiber dermatitis. *Contact Dermatitis*, 12(1) (1985): 1–11.
32. ZIMMERER, R. E., LAWSON, K. D., and CALVERT, C. J., The effects of wearing diapers on skin. *Pediatric Dermatology*, 3(2) (1986): 95–101.
33. SHAFIK, A., IBRAHIM, I. H. and ELSAYED, E. M., Effect of different types of textile fabric on spermatogenesis. 1. Electrostatic potentials generated on surface of human scrotum by wearing different types of fabric. *Andrologia*, 24(3) (1992): 145–147.
34. SHAFIK, A., Polyester but not cotton or wool textiles inhibit hair-growth. *Dermatology*, 187(4) (1993): 239–242.
35. *Textile Fiber Products Identification Act*, Federal Trade Commission (approved September 2, 1958, 85th Congress, 2d Sess.; 15 U.S.C. 70, 72 Stat. 1717).
36. LEE, S. and OBENDORF, S. K., Use of electrospun nanofiber web for protective textile materials as barriers to liquid penetration. *Textile Research Journal*, 77(9) (2007): 696–702.
37. LEE, S. and OBENDORF, S. K., Transport properties of layered fabric systems based on electrospun nanofibers. *Fibers and Polymers*, 8(5) (2007): 501–506.
38. RAMASESHAN, R. and RAMAKRISHNA, S., Zinc titanate nanofibers for the detoxification of chemical warfare simulants. *Journal of the American Ceramic Society*, 90(6) (2007): 1836–1842.
39. CHITRPHIROMSRI, P. and KUZNETSOV, A. V., Porous medium model for investigating transient heat and moisture transport in firefighter protective clothing under high-intensity thermal exposure. *Journal of Porous Media*, 8(5) (2005): 511–528.
40. KEISER, C. and ROSSI, R. M., Temperature analysis for the prediction of steam formation and transfer in multilayer thermal protective clothing at low level thermal radiation. *Textile Research Journal*, 78(11) (2008): 1025–1035.
41. LI, H. Y., ZHANG, W. Y. and P. Chem Ind. Research on multilayer fabric integrated thermal protective performance. *Proceedings of the 2007 International Conference on Advanced Fibers and Polymer Materials, Vols 1 and 2*. Beijing: Chemical Industry Press, 2007, pp. 334–337.
42. STULL, J. O. and MCMANUS, R. E., Evaluation of three chemical protective clothing materials for selected performance properties. In: Yarborough, P. and Nelson, C. N. (eds.) *Performance of Protective Clothing: Global Needs and Emerging Markets: 8th Symposium*. W Conshohocken: American Society Testing and Materials, 2005, pp. 3–14.
43. TURLER, E., *et al.*, Surgical gowns and drapes in the clinical practice: the discrepancies between requirements and reality. *Chirurg*, 71(11) (2000): 1409–1415.
44. BRZEZINSKI, S., *et al.*, Structure and properties of microporous polyurethane membranes designed for textile-polymeric composite systems. *Fibres and Textiles in Eastern Europe*, 13(6) (2005): 53–58.
45. HAO, L. C., YU, W. D. and Hong Kong Polytechnic University, Functional design and characterization of fire protective and heat insulating composite fabric. *86th Textile Institute World Conference*, Vol. 2, Conference Proceedings. Kowloon: Hong Kong Polytechnic University, 2008, U526–U533.
46. HAO, L. C., YU and W. D., Thermal radiation protective performance of aluminized fabrics for firefighting. *Proceedings of the Fiber Society 2009 Spring Conference*, Vols I and II. Shanghai: Donghua University Press, 2009, pp. 1010–1012.

47. YANG, C. and WU, X. L., Innovative finishing methods for cotton fleece using non-traditional phosphorus-containing flame retardants. In: Dragcevic, Z. (ed.) *Itc&Dc: 4th International Textile Clothing & Design Conference, Book of Proceedings – Magic World of Textiles*. Zagreb: University of Zagreb, Faculty of Textile Technology, 2008, pp. 487–492.
48. YANG, C. and YANG, H., Flame retardant finishing of nylon/cotton blend fabrics for military uniforms. In: Dragcevic, Z. (ed.) *Itc&Dc: 4th International Textile Clothing & Design Conference, Book of Proceedings – Magic World of Textiles*. Zagreb: University of Zagreb, Faculty of Textile Technology, 2008, pp. 493–498.
49. YANG, C. Q., New development in functional finishing of cotton textiles. In: Dragcevic, Z. (ed.) *Itc&Dc: 4th International Textile Clothing & Design Conference, Book of Proceedings – Magic World of Textiles*. Zagreb: University of Zagreb, Faculty of Textile Technology, 2008, pp. 3–21.
50. MARTINKOVA, L., Flame-resistant and anti-electrostatic knitted and woven fabrics manufactured by using new finishing applications. *Industria Textila*, 59(2) (2008): 73–79.
51. HONG, K. H. and SUN, G., Antimicrobial and chemical detoxifying functions of cotton fabrics containing different benzophenone derivatives. *Carbohydrate Polymers*, 71(4) (2008): 598–605.
52. LI, Y., *et al.*, Antimicrobial effect of surgical masks coated with nanoparticles. *Journal of Hospital Infection*, 62(1) (2006): 58–63.
53. GRANCARIC, A. M., TARBUK, A. and KOVACEK, I., Nanoparticles of activated natural zeolite on textiles for protection and therapy. In: Trilling, L. *et al.* (eds.) *Proceedings of the 1st WSEAS International Conference on Recent Advances in Nanotechnology*. Athens: World Scientific and Engineering Academy and Society, 2009, pp. 35–40.
54. FAULDE, M. and UEDELHOVEN, W., A new clothing impregnation method for personal protection against ticks and biting insects. *International Journal of Medical Microbiology*, 296 (2006): 225–229.
55. SCHRECK, C. E. and KLINE, D. L., Personal protection afforded by controlled-release topical repellents and permethrin-treated clothing against natural-populations of aedes-taeniorhynchus. *Journal of the American Mosquito Control Association*, 5(1) (1989): 77–80.
56. LANE, R. S., Treatment of clothing with a permethrin spray for personal protection against the western black-legged tick, Ixodes-Pacificus (Acari, Ixodidae). *Experimental and Applied Acarology*, 6(4) (1989): 343–352.
57. RENZ, A., ENYONG, P. and WEYLER, D., The efficacy of appropriate clothing and of deet-simulium-repellent as an individual protection against the transmission of onchocerciasis. *Tropical Medicine and Parasitology*, 38(3) (1987): 267.
58. SCHRECK, C. E., SNODDY, E. L. and SPIELMAN, A., Pressurized sprays of permethrin or deet on military clothing for personal protection against Ixodes-Dammini (Acari, Ixodidae). *Journal of Medical Entomology*, 23(4) (1986): 396–399.
59. DOLEZ, P. I. and VU-KHANH, T., Recent developments and needs in materials used for personal protective equipment and their testing. *International Journal of Occupational Safety and Ergonomics*, 15(4) (2009): 347–362.
60. LIZAK, P., *Textiles for Army*. ICMT '07: International Conference on Military Technologies, ed. V. Rerucha. Brno: University of Defence, 2007, pp. 661–666.

61. WANG, S. X., *et al.*, Effect of phase change materials on temperature and moisture distributions in clothing during exercise in cold environment. In: Li, Y. *et al.* (eds.) *Textile Bioengineering and Informatics Symposium Proceedings*, Vols 1 and 2. Kowloon: Hong Kong Polytechnic University, 2008, pp. 706–717.
62. CONGALTON, D., Shape memory alloys for use in thermally activated clothing systems. In: Walicki, E. (ed.) *Applied Mechanics and Engineering*, Vol. 4, Special Issue: 'Icer '99', 1999 – *Proceedings of the International Conference on Engineering Rheology Icer '99*. Zielona Gora: Technical University Press, 1999, pp. 423–428.
63. ZHONG, W. and PAN, N., Aerosol filtration by fibrous filters: a statistical mechanics approach. *Textile Research Journal*, 77(5) (2007): 284–289.
64. BROWN, R. C., *Air Filtration: An Integrated Approach to the Theory and Applications of Fibrous Filters*. Oxford and New York: Pergamon Press, 1993.
65. HINDS, W. C., *Aerosol Technology: Properties, Behavior, and Measurement of Airborne Particles*, 2nd edn. New York: Wiley, 1999.
66. KIRSH, V. A., Gravitational deposition of aerosol particles on a fibrous filter with account for the effect of van der Waals force. *Colloid Journal*, 63(1) (2001): 68–73.
67. THORPE, A. and BROWN, R. C., Performance of electrically augmented fibrous filters, measured with monodisperse aerosols. *Aerosol Science and Technology*, 37(3) (2003): 231–245.
68. WANG, C. S., Electrostatic forces in fibrous filters: a review. *Powder Technology*, 118(1–2) (2001): 166–170.
69. LIU, Z. G. and WANG, P. K., Pressure drop and interception efficiency of multifiber filters. *Aerosol Science and Technology*, 26(4) (1997): 313–325.
70. LIU, Z. G. and WANG, P. K., Numerical investigation of viscous flow fields around multifiber filters. *Aerosol Science and Technology*, 25(4) (1996): 375–391.
71. SHAPIRO, M., An analytical model for aerosol filtration by nonuniform filter media. *Journal of Aerosol Science*, 27(2) (1996): 263–280.
72. MASCHIO, C. and DE ARRUDA, A. C. F., Modeling of the efficiency of fibrous filters through numerical simulation and X-ray tomography. *Advanced Powder Technology*, 12(3) (2001), 311–329.
73. DHANIYALA, S. and LIU, B. Y. H., Theoretical modeling of filtration by nonuniform fibrous filters. *Aerosol Science and Technology*, 34(2) (2001): 170–178.
74. QUINTARD, M. and WHITAKER, S., Aerosol filtration: an analysis using the method of volume averaging. *Journal of Aerosol Science*, 26(8) (1995): 1227–1255.
75. PRZEKOP, R., MOSKAL, A. and GRADON, L., Lattice-Boltzmann approach for description of the structure of deposited particulate matter in fibrous filters. *Journal of Aerosol Science*, 34(2) (2003): 133–147.
76. CHOPARD, B. and MASSELOT, A., Cellular automata and lattice Boltzmann methods: a new approach to computational fluid dynamics and particle transport. *Future Generation Computer Systems*, 16(2–3) (1999): 249–257.
77. ISING, E., A contribution to the theory of ferromagnetism. *Zeitschrift für Physik*, 31 (1925): 253.
78. YEOMANS, J. M., *Statistical Mechanics of Phase Transitions*. Oxford Science Publications. Oxford and New York: Oxford University Press, 1992.

79. ZHONG, W., DING, X. and TANG, Z. L., Modeling and analyzing liquid wetting in fibrous assemblies. *Textile Research Journal*, 71(9) (2001): 762–766.
80. ZHONG, W., DING, X. and TANG, Z. L., Analysis of fluid flow through fibrous structures. *Textile Research Journal*, 72(9) (2002): 751–755.
81. ZHONG, W., PAN, N. and LUKAS, D., Stochastic modelling of tear behaviour of coated fabrics. *Modelling and Simulation in Materials Science and Engineering*, 12(2) (2004): 293–309.
82. ISRAELACHVILI, J. N., *Intermolecular and Surface Forces*, 2nd edn. London and Toronto: Academic Press, 1992.
83. LEE, K. W., *Filtration of submicron aerosols by fibrous filters*. Minneapolis: University of Minnesota Press, 1977.
84. KRIGBAUM, W. K. and DAWKINS, J. V., *Polymer Handbook*, 2nd edn. New York: Wiley, 1975.

New developments in functional medical textiles and their mechanism of action

J. V. EDWARDS,
ARS-USDA, USA

and

S. C. GOHEEN,
Pacific Northwest National Laboratory, USA

Abstract: Functional medical textiles are undergoing a revolution in structural design. Medical textiles as non-implantables, implantables and extracorporeals are playing central roles in healthcare improvements enhancing and prolonging the quality of life. Developments in the design of materials that function at the biological–material interface address material biocompatibility and bioactive function. A deeper understanding of the physiological, biochemical and biophysical milieus of biomaterials is being achieved in critical areas like wound healing, implant biocompatibility, dialysis and pressure ulcer prevention, which coupled with advances in nanotechnology holds great promise for tissue engineering and areas of biomaterial design for wound healing and prevention.

Key words: biomaterials, medical textiles, biocompatibility, implantables, non-implantables, extracorporeals, chronic wound dressings, pressure ulcer, hemorrhage control.

13.1 Introduction

The functional nature of medical textiles is implicit to its application and many medical textiles have a multifunctional capacity. Even throughout history we see more than a mere attempt to cover a wound to protect it from further injury (see *Wound Management and Dressings* by Stephen Thomas, London: Pharmaceutical Press, 1999). From the ancients emerged textiles that were treated with substances that are still being researched for their underlying folklore properties. As with most areas of modern technology that address critical needs for mankind, exponential growth of functional medical textiles is drawing upon an interdisciplinary vision that challenges the textile and biomaterials scientist with new approaches to design based on mechanism of action. This chapter addresses some of the current ideas in medical textiles in the areas of non-implantables, extracorporeals, and implantables.

13.2 Extracorporeals and implantables

Extracorporeal medical textiles are used in mechanical organs such as hemodialyzers, artificial livers and mechanical lungs. Hemodialyzers provide blood purification for end-stage renal failure, and the use of other artificial organs as temporary replacement of or as a supplement to the lung or liver. The aim then with these types of artificial organs is to provide restoration of homeostasis within the body due to lack of blood oxygenation or a metabolic crisis due to acute liver failure. Implantable fibers include materials placed in the body that are used for wound closure or replacement surgery. Some of the considerations that are involved in determining the biocompatibility of the textile material with the body are (a) biodegradability, (b) non-toxicity and (c) fiber size, porosity and tissue encapsulation.

The boundary between extracorporeal medical devices and implantable devices will likely become thinner with advances in understanding the role of nano-biomaterials in tissue engineering, which is creating the potential to regenerate tissues and organs, for example artificial bladders, cornea and engineered skin. Nanostructured synthetic matrices and biopolymers show promise to be the next generation of biomaterial scaffolds. In this regard, natural polymers including collagen, fibronectin and hyaluroinic acid are viewed as superior to some traditional synthetic polymers used in tissue engineering. Moreover, understanding the design and role of biomaterials in three-dimensional spatial cell organization and interaction with the extracellular matrix (ECM) is an expanding topic where the role of fiber functionality is being examined in tissue engineering. Nanofiber scaffolds that will make their way into artificial organs and tissue engineering are being developed through advances in electrospinning, phase separation and self-assembling biomolecules.

13.2.1 Artificial kidney

An interesting pictorial history of dialysis can be found at <http://www.homedialysis.org/learn/museum/>. The kidney was the first organ to be substituted by an artificial device as well as the first successfully transplanted organ [1]. Renal replacement therapy for end-stage renal disease occurs now almost exclusively with hollow-fiber dialyzers [2]. Highly efficient hollow fibers have replaced coil or laminate in dialyzer devices. The cross-section of a hollow-fiber-type dialyzer consists of 4000–20 000 hollow filaments having an external diameter of 200–300 μm . Blood flows inside of the fibers and the dialysate flows outside of the fibers. Kidney dialysis mimics the ability of the kidney to remove wastes from the body including urea and albumin.

Through diffusion small molecules or solutes are removed with sequential mass transfer from the dialyzer blood compartment through the membrane and into the dialysate compartment. A challenge in efficient dialysis is selective removal of proteins 10–30 kDa. Thus more efficient dialysis membranes need to be designed where proteins of MW around 20 kDa are removed while proteins around 70 kDa are allowed to remain in the blood compartment. Hemodialysis has also been shown to lead to chronic inflammation which is characterized by the presence of pro-inflammatory cytokines [3]. Moreover, pro-inflammatory cytokines have previously been shown to be released *in vivo* and *in vitro* when exposed to cellulose membranes. However, removal of large-scale toxins and cytokines has been reported through the use of continuous renal replacement therapies (CRRT) with high-flux, highly permeable biocompatible dialysis membranes [4]. In addition, Klein *et al.* [5] reported on a method for capturing anti-(Gal α 1–3Gal) antibodies formed from hyperacute rejection of pig xenografts by immobilized Gal α 1–3Gal oligomers derived from carrageenan. The use of bioactive epitopes containing galactose in an α –1–3 linkage were obtained from γ -carrageenan oligosaccharides which were immobilized on hydrazide-modified microporous nylon membranes. These subsequently were shown to decrease human anti-(Gal- α 1–3 Gal) antibody level in normal human plasma. Layers of needle-punched fabrics varying in density have been reported to efficiently remove waste materials as an alternative in dialyzer filters [6].

Solute removal is the key function of the hollow-fiber dialyzers. Cellulosic materials are used in 80% of the dialyzers with very good permeability for low molecular weight substances. Cellulosic membranes are particularly suitable for diffusion-based dialysis with efficient removal of water-soluble uremic solutes like urea and creatinine. Cuprophane is a regenerated cellulosic membrane which is the material of choice in kidney dialysis due to the highly efficient and selective removal of urea and creatinine while retaining nutritive molecules such as vitamin B-12 in the bloodstream [7]. Cuprophane membranes have been shown to be more reusable than polysulfone and associated with fewer incidents of hypotension [8]. Cellulosic high efficiency dialyzers have very high diffusive permeability values for small solutes but low water permeability [1]. Synthetic membranes, on the other hand, which include polysulfone, polyamide and polymethylmethacrylate, were initially formulated with high water permeability in response to concerns about selective solute removal and a need to achieve higher filtration rates. The pore size and pore distribution have been characterized recently for the manner in which distribution influences a membrane's sieving properties [6]. By contrasting the pore size distribution with the sieving coefficient versus molecular weight profile for membranes an optimal cut-off similar to the native kidney may

be attained [9]. For example, a draw back with high permeability membranes can be albumin loss if the pore size is too large and the distribution of pores is too broad.

Since diffusion is the main mass transfer mechanism for removal of small molecules in hemodialysis, mass transfer resistance to biological flow rate is quantified by blood compartment resistance, resistance due to the membrane itself and dialysate compartment resistance. Solute removal of urea, creatinine and phosphate from blood occurs only during hemodialysis from plasma water, thus mass transfer from the red blood cell fraction of water to the plasma water must occur. When the percentage of red blood cells increase in whole blood (increased hematocrit) there is a relative sequestration of solute with low red blood cell membrane diffusivity. In the dialysate compartment improved mass transfer efficiency has been achieved by improved membrane designs. Among the new textile designs that influence hollow-fiber perfusion of dialysate is fiber bundle spacing. Improvements in the membrane surface area available for mass exchange during dialysis have been addressed with spacer yarns and specific fiber undulation patterns in this way. Ronco *et al.* measured the effect of ‘microcrimping’ and spacer yarns on small-solute removal and dialysate flow distribution, and it was found the urea clearances were higher for dialyzers with microcrimped fibers and spacer yarns [10]. Thus both of these approaches increase the effective membrane surface area, thus improving on dialysate flow distribution.

13.2.2 Bioartificial liver

The liver has enormous regenerative potential, and it has been recognized that it may be possible to regenerate sufficient amounts *in vitro* to make tissue engineering a viable clinical alternative to transplantation [11]. A variety of approaches have been tried in this regard, and these include culturing with growth factors and three-dimensional scaffolds in bioreactors. The extracorporeal liver assisted device (ELAD) containing porcine hepatocytes circulates a patient’s plasma through a bioreactor that contains active hepatocytes [12]. Hepatocytes carry out many vital functions including catabolic reactions and detoxification. Some of the membranes used in the ELAD are similar to those used in kidney dialysis including cuprophane, hemophan and polysulfone. Blood from the patient flows through the cartridge where the device is designed to filter and purify the patient’s blood through membranes containing the cells and then back into the patient similar to kidney dialysis. Although mature hepatocytes have been seeded in implantable artificial livers using biocompatible matrices the transplantation functionality and efficiency in animals requires considerable improvement before moving into the clinic [13].

13.2.3 Mechanical lung

Mechanical lungs with microporous membranes consisting of polypropylene hollow fibers exchange gases including O_2 and CO_2 . Thus the gases pass through the pores of polypropylene hollow fibers but are not bubbled through the blood at extremely low pressure as has been done in the past. Closed-loop mechanical ventilation has the potential to provide more effective ventilatory support to patients with less complexity than conventional ventilation [14]. Microporous polypropylene hollow fiber is currently used for the manufacture of artificial lung membranes that exchange gases with blood but offer some hydrophobicity since polypropylene fibers exhibit comparatively good compatibility with blood and good gas permeability. Oxygen permeates the micropores of the fiber whereby the pressure gradient between blood and oxygen is near zero allowing red blood cells to capture oxygen by the diffusion process. The mechanical lung is principally used to replace lung function during heart surgery, and problems in its long-term use have been encountered due to a need for better membrane materials to prevent leakage of blood plasma.

13.3 Structure and composition: role of functionality in implantables

13.3.1 Biocompatibility

It would not be fair to say that the role of biomolecules in textile biocompatibility is fully understood. Rather, biomolecules and textiles are both so extremely diverse that all possible interactions are overwhelmingly extensive. But some basics can be discussed. It is well known that polymers and biopolymers interact partly due to their ionic and hydrophobic characteristics. Polar regions of biomolecules by intuition should be attracted to polar regions of textiles. Anions are attracted to cations, and hydrophobic regions are attracted to hydrophobic regions on the two types of molecules. As long as the solvent is aqueous, the hydrophilic (polar) moieties of the fibers and biopolymers, however, are often more attracted to water than to one another, and this is one feature that is commonly taken advantage of in the design of biocompatible fibers. Indeed, it has long been recognized that high water levels in a biomaterial provide a low interfacial free energy with blood and thereby reduce protein adsorption and cell adhesion on the surface [15].

Biocompatibility of materials that is understood well enough to control the interactions between the material and the surrounding biological milieu is a goal of biomaterial science. The issues that are involved in controlling the interactions between a living system and an implantable material

are complex. To attempt to briefly enumerate some of the effects that are included in biocompatibility the following may be considered:

- (a) The interfacial free energy [16], which involves the surface tension at the interface of the material and the biological fluid or tissue and the resulting dispersion and polar contributions of the interfacial free energies from protein adsorption, as well as the role of interfacial properties on cell adhesion. Thus, minimum interfacial free energy would result from increasing the polar surface free energy of the material.
- (b) The hydrophilic versus hydrophobic balance on the surface of the fiber. Hydrophobic surfaces tend to adsorb larger amounts of proteins than hydrophilic ones and it is thought that more hydrophilic surfaces would be more biologically compatible [16]. Thus wettability is one of the most important parameters in biomaterial design.
- (c) Chemical structures which include the nature of charge. For example, anionic surfaces tend to benefit biocompatibility from a standpoint of complement activation [17], albumin adsorption and macrophage distribution [18] or cell toxicity with respect to amines and their quaternary, secondary or primary structure [19].
- (d) The types and density of charge which cover the surface of a polymer can affect cytotoxicity. For example, Fishcer showed that the charge/monomer ratio of cationic polymer was directly proportional to their cytotoxicity where poly(diallyldimethyl ammonium chloride) (PDDA) was the most toxic and cationized albumin was the least toxic [20]. In addition it has been shown that certain cationic polymers like polybrene, protamine and poly-L-ornithine cause activation of the complement system whereas negatively charged polyanions like dextran sulfate, polyvinyl sulfate, chondroitin sulfate and poly(inosinic acid) inactivate C1 or C2 components of the classical pathway of complement activation [17]. Charged surfaces have been found to promote bone formation [21] and Anderson *et al.* showed that hydrophilic anionic biomaterials induce apoptosis of adherent macrophages [22].
- (e) Both molecular weight and conformational flexibility of the polymer influence biocompatibility. For example, lower molecular weight PEG coated surfaces show minimal protein adsorption, and polycations with a globular structure have good biocompatibility, whereas polymers with a more linear or branched and flexible structure, that is polylysine, showed a higher cell damaging effect [20].
- (f) Surface patterns have been found to generate different responses of a biological system and self-assembling monolayers have been studied for their use in fabricating 3-D nano and micro structures [23]. Surface roughness has been found to influence thrombogenicity.

13.3.2 Cardiovascular implantables

In recent years implantable textiles have been increasingly designed with a biologically active component. Implantable textiles have been designed with specific functions compatible with the surrounding tissue. The functions have been targeted to blood flow and cardiovascular pressure as well as the forces and interactions of surrounding tissue. These include sutures for dermal and tissue repair, fabrics that have traditionally been employed in heart repair as reinforcement meshes, vascular grafts, velours for blood contacting surfaces, fiber reinforcements for hard and soft polymer bone and ligament prosthetics and intraocular lenses. The usefulness of actual biologically active molecules as a part of the fiber's function in a tissue environment has been explored. Research in this area is a model for bridging bioactive molecules on fibers with performance textiles. Modern drug design approaches are based on enzyme and cell receptor recognition principles, and the analogous development of pharmacologically active molecules on textile fibers is targeted to biological recognition originating on the textile fiber. The concept of a bioactive fiber with pharmacological activity has been developed with implantable textiles in the cell adhesion domain.

The functionality of materials like polyester (PET) and expanded polytetrafluoroethylene (ePTFE) has been studied in the context of vascular grafts for replacement of diseased or damaged arteries for over 40 years [24]. PET and ePTFE are constructed into different fabric motifs suitable for vascular grafts and can be made into sheets, tubes and specific tailored forms. Since these fabrics are exposed to a wide range of stresses like bending, expansion, compression, rotation, and shear they have been extensively studied in both woven and knitted motifs for their failure modes. For example, burst strength, which is the ability of the fabric to resist internal pressure caused by blood flow and kink resistance, is affected by thread count. Bursting is also a potential problem where seams exist; however, ePTFE grafts are frequently modified with segmented or spiral rings. In addition it is necessary to obtain a balance between the strength that higher thread count affords and the loss in flexibility [25]. The thickness and tensile strength of the fabric are also important for the functionality of the graft such that thickness affects overall volume change of the device as well as porosity, permeability and kink resistance; whereas tensile strength affects the ability of the fabric to withstand the puncture of a needle, that is if the woven PET is too thin or does not have a high enough thread count the force of the sutures holding the stent in place on the graft wound result in a progressive tear [26].

13.3.3 Implantable biomaterials for tissue engineering

Biomaterials provide a three-dimensional structure for functional tissue to and from cells based on delivery of cells and mechanical support during tissue development. Bioactive molecules may be added to promote cell adhesion and proliferation or regulate cellular function. Three classes of biomaterials are used in tissue and organ engineering; these include proteinaceous and carbohydrate biopolymers – collagen, alginate, hyaluronic acid and chitosan; acellular tissues matrices including bladder and small-intestine submucosa; and synthetic polymers including polyglycolic acid (PGA), polylactic acid and polylactic-co-glycolic acid. The advantage of naturally occurring materials is their biological recognition. On the other hand synthetic polymers are advantageous due to the control in improving biocompatibility through design and manufacturing.

Electrospinning

Due to the fibrous structure of ECM proteins like collagen technologies including electrospinning, self-assembly and phase separation have been developed to achieve biomimetic properties conferred to tissues and organs using naturally occurring and synthetic materials. With electrospinning a non-woven material with nano-fibrous properties can be achieved that is not possible with other textile technologies. This is done with a polymer solution containing a spinneret, electric field and a target collector. A charged jet of polymer solution under the influence of an electric field is pulled in a straight line. As the jet diameter is reduced under a spiraling path due to electrical instability, and with solvent evaporation, a non-woven fibrous mat is collected. Various cells proliferate and maintain their integrity on nano-fibrous materials consisting of collagen, silk, fibroin and fibrinogen and synthetic polymers like poly(glycolic acid) (PGA), poly(lactic acid) (PLLA), poly(lactic acid-co-glycolic acid) (PLGA) and poly(ϵ caprolactone) (PCL). Electrospinning has been used to create highly porous scaffolds in various shapes, most recently in regenerative medicine, and has shown promise in application to functional nerve regeneration [27].

Self-assembly

Self-assembly on the other hand involves an autonomous organization of molecular components unique to the biomolecule without human devices and has led to the fabrication of novel biomaterials [28]. Biomolecules that form well-defined secondary structures like beta-sheet and alpha-helical conformation as is found with peptide, or micellar structures which form from lipids undergo self-assembly as a result of non-covalent bond forces including hydrogen bonds, ionic bonds and hydrophobic interactions. Collectively

these non-covalent interactions can form tight networks of macromolecular structure useful in material design. Self-assembly to form biomaterials is discussed here in the context of bioactive peptides.

Phase separation

Phase separation utilizes the thermodynamic instability of a homogeneous, multicomponent system to lower the system's free energy to achieve the equilibrium of the resulting material designed. Phase separation has been applied to the development of porous structures as tissue engineering scaffolds. For example, sublimation or replacement of a biomaterial and cellular system's solvent to fabricate a nano-fibrous scaffold made of alginate with cells can result in a nano-fibrous pore wall in the shape of a human ear. Here the solvent or phase change process in material design is effectively doing the work to increase the surface area or implement pore distribution. Phase separation has been used as an accompanying technology to computer assisted design of tissue scaffolds [29]. This approach has been used to mimic body parts at size levels ranging from nano-fibrous ECM architecture to macro/micro-pores and patient anatomical shapes [30]. Along similar lines it has been found that scaffold materials can be printed into a desired shape using inkjet technology, and it has been shown that living cells can also be printed using this technology so that a three-dimensional construct containing a precision arrangement of cells' growth factors and ECM can be printed.

13.4 The role of biomolecules in conferring bioactive function

13.4.1 Design of bioactive textiles

Numerous bioactive compounds including peptides, proteins, carbohydrates and lipids have been shown to retain their activity when conjugated to or formulated on textile fibers. Biologically active materials may be designed by conjugating bioactive compounds to a chemically reactive fiber with an understanding of retaining activity on the fiber. Four major classes of naturally occurring bioactive molecules include enzymes, peptides/proteins, carbohydrates and lipids, which offer various potential applications to performance textiles. These classes of bioactive molecules provide a myriad of potential high performance functionality for non-implantable, extracorporeal and implantable medical textiles.

Peptides

Peptides are perhaps the most versatile class of bioactive molecules within a diverse range of therapeutic and material applications. Peptides when

attached to wound dressings in the form of textile-related technology have found applications in chronic and burn wounds. Peptide analogs of the bio-active sequences of elastin and laminin when linked to alginate promoted proliferation of fibroblasts. Synthetic peptides that mimic thrombin have also been linked to alginate to give rise to accelerated wound healing.

Self-assembling peptides have received increased attention for their potential application in implantable materials. Self-assembling peptides are found naturally in silk, wool and collagen. Silk is a natural fibrous protein derived from the silk worm cocoon which has been used as a medical textile for centuries due to its excellent mechanical and tensile properties. Silk consists of a core protein silk fibroin and a glue-like coating of sericin proteins. Silk is a potentially excellent scaffolding material for tendon and ligament tissue engineering [31]. The beta-sheet or alpha-helix conformational motifs of these self-assembling peptides confer nanostructural properties that lend themselves to use in implantable biomaterials. An interesting example of these conformational motifs that gives rise to self-assembly is found in spider dragline silk formed from beta-sheet crystals. This peptide motif converts to a partial helical structure when the sequence undergoes oxidation at the side chain thiomethylene of methionine to the sulfoxide thereby triggering a change in conformation. The resulting self-assembly gives rise to a biomaterial that could be used as a surface coating.

Self-assembling peptides (termed sapeptides) are being studied as biomaterials in regenerative medicine. Sapeptides generally have an amphiphilic structure that presents as hydrophilic heads and hydrophobic tails forming beta-sheets, and thus can pack together due to the hydrophobic interaction in water forming double-layered beta-sheet nanofibers [28] similar to those discussed above in silk. Interesting, sapeptides show nanostructures resembling those of the ECM. Since the self-assembling peptide is composed of amino acids that are the body's natural building blocks they present negligible immune response and little inflammatory reactions *in vivo*. The self-assembling step is harmless and the versatility of the peptides similar to that of proteins.

Cell adhesion is important to cell spreading and migration and occurs within the ECM which is composed of proteins and glycoproteins like fibronectin, laminins, collagens and vitronectin. Cell surface receptors termed integrins bind ECM proteins to the matrix and mediate mechanical and chemical signals from it. In the early 1980s it was shown that the integrin binding and activation of these large proteins of the ECM resides in a short three amino acid sequence, arginine-glycine-aspartic acid (RGD) [32]. Since then the RGD sequence has been applied to textile surfaces through both covalent and non-covalent attachment. Dacron vascular grafts containing a 23 amino acid sequence with RGD (termed Peptide 2000) were prepared and used as a sewing cuff for artificial heart valves and vascular grafts. The RGD containing peptide promoted the formation of an endothelial-like

cell layer on both PET and PTFE vascular grafts [33]. It is noteworthy that nanostructural scaffolds with bioactive motifs such as the RGD cell adhesion peptides have been considered for use in numerous tissue engineering approaches. For example Horii designed self-assembling scaffolds functionalized for osteoblast cultures with 2-unit RGD binding sequences [34]. Some sapeptides which are promising scaffolds have similarity to RGD, that is RAD mimics RGD, and they have been derivatized with bioactive sequences as well [35]. On the other hand a variety of applications of self-assembled peptide in tissue engineering include cartilage repair [35], neural regeneration [36], regeneration of cardiac tissue [37] and rapid hemostasis [38]. Interestingly the title, “‘nano neural knitting’ a peptide scaffold for brain repair and axonal regeneration with return of functional vision’ [36], illustrates the promise of the technological applications of sapeptides. Since many of these scaffolds are beta-sheet conformation they do not prompt the body to mount an immune response, and they form a strong non-woven structure. Beta-sheet conformations self-assemble very rapidly and often form insoluble precipitates. Issues concerning the reproducibility resulting from random formation of beta-sheet self-assembled non-wovens, elastic architecture, and presentation to living tissue in high salt concentration to ensure more hydrophilic and aqueous compatibility need more work to fully realize the potential application of self-assembled peptides in tissue regeneration.

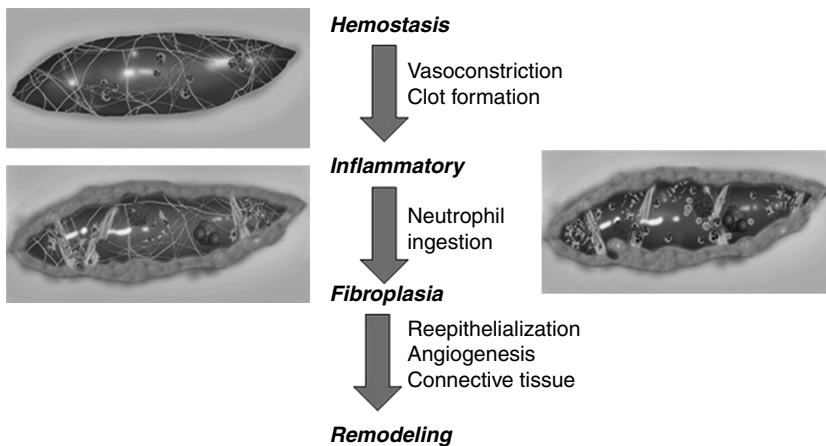
13.5 Non-implantables: wound dressings, pressure ulcers, hemorrhage control

Non-implantable medical textiles include those which are applied to the surface of the body. Examples of non-implantables include materials that are applied to or worn on the body for their hygienic, antimicrobial or decontamination properties; wound dressings used in wound and orthopedic care; hygienic incontinence devices which include disposable and non-disposable diapers, bed pads and high performance sheets used for pressure ulcer support surfaces; and protective clothing such as patient and medical personnel gowns and face masks. Improvements in the functional roles of each of these subgroups of non-implantables which will be treated here include (a) the development of improved battlefield and chronic wound dressings that target two separate parts of the wound-healing cascade; (b) development of decubitus-prevention devices for pressure ulcer patients and textiles that are compatible with pressure ulcer support mattresses; (c) improvements in creating antimicrobial surfaces against pathogenic bacteria viruses and fungi, and blood resistant protective environments.

13.5.1 Structure and composition: role of functionality in non-implantable medical textiles

Wound-healing materials

Progress in wound-healing science is reshaping the design of wound dressings. As shown in Fig. 13.1, wound healing is a complex cascade of molecular and cellular events [39]. During the coagulation phase following injury platelets initiate healing through the release of growth factors which diffuse from the wound to recruit inflammatory cells to the wound. Thus growth factors are responsible for the activation of immune cells, ECM deposition, collagen synthesis, and keratinocyte and fibroblast proliferation and migration. Neutrophils arrive on the scene early, and serve to clear the wound of bacteria and cellular debris. The arrival of neutrophils marks the onset of the inflammatory phase of wound healing, and under acute healing conditions lasts only a few days. However, in the chronic wound the period of growing neutrophil population is extended indefinitely. Inflammation is the second phase of healing and it is mostly regulated by cytokines which are secreted by macrophages. Cytokines control cellular chemotaxis, proliferation and differentiation. Macrophages also migrate to the wound site to destroy bacteria. However, an overabundance of cytokines and neutrophils prolongs the inflammatory phase and has a negative influence on healing. Granulation tissue, which consists of fibroblasts, epithelial cells and vascular endothelial cells, is formed about five days after injury. Fibroplasia is the last restorative stage of healing. Fibroplasia involves the combined effect of re-epithelialization, angiogenesis and connective tissue growth and it has been termed ‘a dynamic reciprocity of fibroblasts, cytokines, and ECM proteins’.



13.1 Stages of wound healing.

In a healthy person healing occurs in 21 days from coagulation, and the remodeling phase consisting of scar transformation based on collagen synthesis continues for months following injury.

Pressure ulcers

Pressure ulcers occur when occluded blood flow due to interfacial pressure between the body and a support surface results in internal tissue stress leading to ischemia [40]. Ischemia involves impaired transport of nutrients and waste products to and from cells. During ischemia cells accumulate toxic metabolites that are deposited in the tissue and increase the rate of cell death. If external loading is not relieved where healthy tissue is allowed to recover from the pressure, tissue necrosis will occur. The rapidity with which this inflammatory process may occur and worsen to form a bed sore (sometimes within hours) depends on a variety of intrinsic and extrinsic factors. Shearing and friction also initiate bedsores by causing skin to stretch and blood vessels to kink resulting in impaired blood circulation in the skin. The incidence of pressure ulcers increases markedly in individuals over 70 years of age [41]. This in part is because the collagen content of the dermis, which makes the subcutaneous fat resistant to mechanical forces, decreases with aging [42]. Additional aging effects of the skin that can exacerbate the problem are decreased skin microcirculation [43] and decreased moisture content in the stratum corneum [44].

Pressure ulcers can progress through four stages of wounds that are clinically identifiable [40, 44–46]. Stage I is characterized by redness, non-blanchable erythema, increased temperature and inconsistency of the epidermal layer of skin. Stage II is a partial thickness wound involving the dermis and characterized by swelling and formation of a blister, sore or shallow open crater. Stage III is characterized by full-thickness skin loss of the dermal layer down to subcutaneous fat tissue and it presents as a deep crater. Stage IV is a full-thickness skin loss down to the muscle or bone, presenting as a deep crater with visible muscle or bone and often accompanied by necrotic tissue and significant drainage.

Occlusive dressings

The concept that wounds heal best when kept dry was chiefly espoused in wound management up until the late 1950s because it was thought that bacterial infection could best be prevented by absorbing and removing all wound exudate. In the early 1960s Winter [47] and Hinman [48] showed that the rate of re-epithelialization increases in a moist wound versus a wound kept dry. Occlusion is the regulation of water vapor and gases from a wound to the atmosphere promoting a moist environment, which allows epidermal barrier function to be rapidly restored. Occlusion is a concept

in wound management that prompted a revolution during the 1970s in the production of new types of wound dressings that are still being developed. The finding that moist wounds heal faster than when desiccated and that collagen at the interface of the scab and dermis impedes epidermal cell movement prompted the development of occlusive dressings for wound management.

Wound occlusion requires careful regulation of the moisture balance of the wound with vapor permeability to avoid exceeding the absorbency limits of the dressing. Thus, occlusive dressing types have been developed depending on the nature of the wound and accompanying wound exudate. The theory of moist wound healing led to approximately eight to nine separate types of wound-dressing materials and devices useful for different wound treatment indications. Each of the material types that represent these distinct groups have molecular and mechanical characteristics that confer properties to promote healing under specifically defined clinical indications, and are often used for pressure ulcer treatment depending on the stage and drainage of the wound. The following briefly outlines some of their properties.

Thin films

Thin films are semipermeable, polyurethane membranes with acrylic adhesive. They are used to treat minor burns, pressure areas (Stage I), donor sites and post-operative wounds. They should not be used to treat deep cavity wounds, third-degree burns or infected wounds.

Sheet hydrogels

Sheet hydrogels are solid, non-adhesive gel sheets that consist of a network of cross-linked, hydrophilic polymers which can absorb large amounts of water without dissolving or losing their structural integrity. Thus, they have a fixed shape in contrast to amorphous gels. They can be used as a carrier for topical medications, and absorb their own weight of wound exudate. They are permeable to water vapor and oxygen, but not to water and bacteria, and afford good visibility of the wound due to their transparent nature. They can be used for light to moderately exudative wounds, and in the autolytic debridement of Stages II and III pressure sores. They should not be used with heavily exuding wounds.

Hydrocolloids

Hydrocolloids are semipermeable polyurethane films in the form of solid wafers that contain hydroactive particles as sodium carboxymethyl cellulose, which swells with exudate and forms a gel. They are impermeable to exudate, micro-organisms and oxygen. Moist conditions produced by hydrocolloids promote epithelialization. Hydrocolloid dressings are good for the treatment of shallow or superficial wounds with minimal to moderate exudates. They should not be used on wounds with dry eschar or very light exudate.

Semipermeable foam

Semipermeable foam is a soft, open cell hydrophobic, polyurethane foam sheet 6–8 mm thick. Cells of the foam are designed to absorb liquid by capillary action. They are permeable to gases and water vapor, but not to aqueous solutions and exudate. They absorb blood and tissue fluids while the aqueous component evaporates through the dressing. Cellular debris and proteinaceous material are trapped. They are used for leg and decubitus ulcers, sutured wounds, burns and donor sites. They should not be applied to wounds covered with a dry scab or hard black necrotic tissue.

Amorphous hydrogel

Amorphous hydrogels are similar in composition to sheet hydrogels in their polymer and water make-up. However, amorphous gels are not cross-linked. They usually contain small quantities of added ingredients such as collagen, alginate, copper ions, peptides and polysaccharides. The gels are clear, yellowish or blue from copper ions. Viscosity of the gel varies with body temperature. They are available as tubes, foil packets and impregnated gauze sponges, and are used for full-thickness wounds to maintain hydration. They may also be used on infected wounds or as wound filler. They should not be used on heavily draining wounds, and improper use may lead to peri-wound maceration.

Fillers

Calcium alginate is one of the fillers that consist of an absorbent fibrous fleece with sodium and calcium salts of alginic acid (ratio 80:20). Dextranomer beads consist of circular beads, 0.1–0.3 mm in diameter, when dry. The bead is a three-dimensional cross-linked dextran, and long chain polysaccharide. Fillers are used with heavily exuding wounds including chronic wounds such as leg ulcers, pressure sores and fungating carcinomas. They are indicated for use in heavily exuding wounds (Stages III and IV), wounds containing soft yellow slough, including infected surgical or post-traumatic wounds. They should not be used with minimally exuding wounds.

Contact layer dressings

Contact layer dressings are porous, non-absorbent and inert and designed to allow the passage of wound exudate for absorption by a secondary dressing. These types of dressing are for shallow or superficial wounds with minimal to moderate exudates, and are not recommended for cleaning the wound.

Gauze packing

Cotton gauze is used both as a primary and secondary wound dressing. Gauze is manufactured as bandages, sponges, tubular bandages and stockings. Improvements in low-linting and absorbent properties have been made. Gauze is still a standard of care for chronic wounds. It fills deep wound defects and is useful over wound gel to maintain a moist environment; but

it needs to be packed lightly. It may traumatize the wound if allowed to dry; therefore multiple small dry dressing wads in the wound cavity should be avoided. Cotton gauze may be wetted with saline solution to confer moist properties. It should possess a slight negative charge, which facilitates uptake of cationic proteases. It has absorbent and elastic properties for mobile body surfaces.

Wound vacuum assisted closure

Vacuum assisted closure is accomplished with polyurethane foam accompanied by vacuum negative pressure in the wound bed. The wound is filled with foam and sealed with a film. Vacuum tubing is inserted and used continuously. This approach is used on infected wounds and wounds with fistulae.

Chronic wounds

When wounds fail to heal the molecular and cellular environment of the chronic wound requires conversion to an acute wound so the ordinary sequential phases of wound healing can proceed. In June 2002 a meeting of wound-healing experts formulated an overview of the current status, role and key elements of wound bed preparation [49]. The subsequent reports in the literature from this meeting articulate well the concept of a systematic approach to wound bed preparation, which is based on an emphasis to decrease inflammatory cytokines and protease activity while increasing growth factor activity. Thus a challenge of current wound-dressing development is to promote the clinical action of wound bed preparation through addressing issues of high protease, and cytokine levels and increasing growth factor levels.

The design and preparation of interactive chronic wound dressings [50] has become increasingly important as part of a solution to addressing the critical worldwide health crisis of the growing number of chronic wound patients. In the United States alone there are over five million patients a year who suffer from chronic wounds due to the formation of decubitus bed sores brought on in the elderly nursing home or spinal chord paralysis patient. In addition, diabetes accounts for at least 60 000 patients annually who also suffer with foot ulcers. Since the mid-1990s the number of wound care products in the well-recognized groups outlined in Table 13.1 has expanded and new groups of products have also been marketed including tissue-engineered products [51, 52]. Recent efforts to develop wound dressings that do more than simply offer a moist wound environment for better healing have prompted most major wound-dressing companies to develop research and approaches on interactive chronic wound dressings. Interactive chronic wound dressings, which possess a mechanism-based mode of action, are targeted to biochemical events associated with pathogenesis of the chronic wound and are a part of good wound bed management.

Table 13.1 A list of functional characteristics and the corresponding structural properties needed to create a bed sore prevention incontinence device

Functional characteristics	Structural properties
Fiber orientation to optimize patient skin health	Fibers used as the weft of the material to impart smoothness are to be relatively more hydrophobic and finishes on fibers or cotton/synthetic blends having defined directionality are aligned to give less resistance to the stratum corneum of the skin and yield lower friction upon sliding. In contrast, fibers used as warp are more hydrophilic giving rise to more rapid moisture wicking away from the skin and sheet interface.
Low friction/high strength fibers	The coefficient of friction will be low for the surface in contact with the patient and higher for the surface in contact with the bed support to keep the pad or sheet from moving and causing creases while imparting less friction and shear force to the patient's skin.
Local deformation distribution/crease resistance	Cotton spacer fabric composed of a surface contact layer that wicks moisture away from the skin while relieving shear, an internal core will provide a hydrophobic wicking channel that drains to a hydrophilic, highly absorbent core and is resilient to shear and pressure. Finishes on sheet or bed pad cover stocks will impart wrinkle resistance to promote better pressure redistribution.
Water absorbency	Internal core of care sheet with cotton batting that is grafted with a super absorbent biopolymer, i.e. modified starch, polyethylene glycol, alginate, or similar polysaccharides.
Softness	A ratio of cotton blended with compatible polymeric fibers or addition of a silicone softening agent to the fabric finish that impart a soft hand.
Antimicrobial	An antimicrobial finish that provides a barrier to infection resulting from macerated skin or microbial contamination.

Skin substitutes, which are being increasingly used, contain both cellular and acellular components that appear to release or stimulate important cytokines and growth factors that have been associated with accelerated wound healing [52]. Some basic materials may also play a role in up-regulating growth factor and cytokine production and blocking destructive proteolysis. In this regard the biochemical and cellular interactions that promote more optimal wound healing have only recently been elucidated

for some of the occlusive dressings. For example, certain types of alginate dressings have been shown to activate human macrophages to secrete pro-inflammatory cytokines associated with accelerated healing [53]. Interactive wound-dressing materials may also be designed with the purpose of either entrapping or sequestering molecules from the wound bed and removing the deleterious activity from the wound bed as the wound dressing is removed, or stimulating the production of beneficial growth factors and cytokines through unique material properties. They may also be employed to improve recombinant growth factor applications. Impetus for material design of these dressings derives from advances in the understanding of the cellular and biochemical mechanisms underlying wound healing. With an improved understanding of the interaction of cytokines, growth factors and proteases in acute and chronic wounds [54–57] the molecular modes of action have been elucidated for dressing designs as balancing the biochemical events of inflammation in the chronic wound and accelerating healing. The use of polysaccharides, collagen and synthetic polymers in the design of new fibrous materials that optimize wound healing at the molecular level has stimulated research on dressing material interaction with wound cytokines [53], growth factors [58, 59], proteases [60–63], reactive oxygen species [64] and ECM proteins [65].

Sequestration of wound proteases and approaches to treating chronic dermal ulcers

The prolonged inflammatory phase characteristic of chronic wounds results in an overexuberant response of neutrophils, which contain proteases and free radical generating enzymes that have been implicated in mediating much of the tissue damage associated with chronic inflammatory diseases. Since neutrophils mediate a variety of chemotactic, proteolytic and oxidative events that have destructive activities in the chronic wound, therapeutic interventions have been proposed based on the proteolytic and oxidative mechanisms of neutrophil activity in the wound. Neutrophils contain both matrix metalloproteases and cationic serine proteases, which are two families of proteases that have been associated with a variety of inflammatory diseases, and have been implicated as destructive proteases that impede wound healing. The presence of elevated levels of these proteases in non-healing wounds has been associated with the degradation of important growth factors and fibronectin necessary for wound healing [66]. There is also a synergistic effect of further oxidative inactivation of endogenous protease inhibitors which leads to unchecked protease activity.

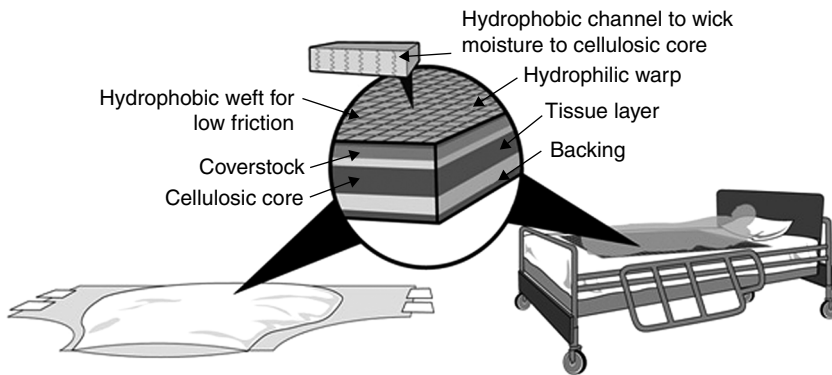
A protease sequestrant dressing's design for activity may be couched in a number of molecular motifs based on the structural features of the protease, which interferes with the healing process. The molecular features of the

material may be targeted to the protein's size, charge, active site and conformation to enhance selective binding of the protein to the dressing material and removal of the detrimental protein from the wound bed. Active wound dressings that have been designed to redress the biochemical imbalance of the chronic wound in this manner are composed of collagen and oxidized regenerated cellulose [67], nanocrystalline silver-coated high density polyethylene [63], deferrioxamine-linked cellulose [68], and electrophilic and ionically derivatized cotton [61].

13.5.2 Pressure ulcer prevention materials

As the population ages and the number of pressure ulcer patients increases [69–71], there is now a critical need to fill a serious gap in effective pressure ulcer prevention textiles [72]. The medical textiles at the interface of patient skin and medical treatment support surfaces include bed sheets, patient clothing, under pads and incontinence devices. The interfacial forces of pressure, shear and friction act at this common boundary to break down skin, occlude blood flow and create ischemia or inflammation, ultimately leading to tissue necrosis and a chronic wound pathology that can often result in death [73–75]. Pressure ulcers develop on the bony prominences of the body, and most pressure ulcer wounds are located on the sacrum or coccyx. Although there has been a huge effort in medicine to analyze and prevent bed sores with pressure relief support surfaces [76], efforts to control friction and moisture transport away from the patient's body have been considerably less [77]. For example, there is little mention in the standards for minimum care or reimbursable services in the United States Medicare codes with regard to hospital bed sheet criteria, and there have been very few randomized controlled trials on the use of incontinence pads with support surfaces [78, 79] to prompt improvements in moisture management and skin and textile friction control. Moreover, the effect of existing absorbent incontinence pads on pressure management mattresses has been characterized recently for their substantial adverse effect on pressure redistribution [80]. Moreover, whereas treatment and prevention often overlap in the care given to pressure ulcer patients [81], many of the seven–eight types of occlusive dressings (discussed above) used for decubitus treatment have not been studied for their compatibility with under pads, bed sheets, patient clothing and support surfaces.

With a few recent exceptions, the work previously reported on decubitus-prevention care sheets [81] and bed sheets [82] is scarce. The patent literature has a few examples of inventions for friction and combined incontinence control in care pads [83] and sheets [84, 85]. However, a variety of factors need to be considered in design of improved hospital bed sheets, bed pads, incontinence devices and medical textile compatible surfaces. Table 13.1 outlines



13.2 Diagram of a bed sheet and non-woven care sheet designed to wick moisture away from a patient's skin into an absorbent core while possessing a low coefficient of friction at the skin–textile interface. The design of incontinence devices for bed sore prevention is laid out in Table 13.1.

the structural properties required to give functional characteristics needed in care and bed sheets for improved decubitus prevention, and Fig. 13.2 illustrates the conventional design of incontinence devices and bed pads. Since the patient is in constant contact with the sheet or bed pad, these materials are very important in maintaining a proper microclimate. The skin can produce up to 1000 cm³ of perspiration an hour to maintain a constant body temperature between 33°C and 35°C which assures thermal comfort. Thus, perspiration should be moved to the outside, otherwise it condenses on the skin and within the sheet structure. It has been recently shown using corneometry in combination with friction experiments on a force plate that coefficients of friction (COFs) of skin against hospital textiles increase from very dry to normally moist skin by 33% [77]. Hence, skin abrasions and bed sores can have their origin in poor moisture management at the skin–textile interface. Although there have been a few recent biophysical and friction analysis tests directed toward understanding the interfacial forces of friction and pressure between skin and textiles, there have been very few literature reports on applying the concepts outlined in Table 13.1 to the design and testing of improved decubitus-prevention materials. Thus, there is great potential for improving medical textiles at the skin–textile interface in this regard.

13.5.3 Hemorrhage control dressings

Half of all deaths on the battlefield are caused by uncontrolled hemorrhage [86, 87]. In addition, high blood loss can lead to hypothermia, multiple organ failure and infection [88–90]. Thus, rapid hemostasis is essential for survival and recovery. The development of improved hemostatic agents

for use in lethal extremity arterial hemorrhages has increased over recent years [91].

The US Army Institute for Surgical Research (USAISR) and the Uniformed Services University of the Health Sciences has outlined ideal properties needed in a battlefield dressing [92]. These include the following: (a) being able to rapidly stop large vessel arterial and venous bleeding 2 min after application when applied to an actively bleeding wound through a pool of blood; (b) no requirement for mixing or pre-application preparation; (c) simplicity of application by wounded victim, buddy or medic; (d) light weight and durable; (e) long shelf life in extreme environments; (f) safe to use with no risk of injury to tissues or transmission of infection; and (g) inexpensive. With this list of ideal properties the question arises: Is there any deployed product capable of stopping or reducing groin arterial bleeding and preventing exsanguinations that otherwise could not be controlled by the standard gauze dressing? The dressings evaluated by the USAISR were the Army Field Dressing (a cotton product of long-standing use), Quikclot, HemCon, and Fibrin Sealant. Surface area coverage, sealant efficacy, adherence and adsorption capacity are all important factors in this challenging area of hemostasis since the geometry and anatomical location of the wounds can vary greatly, and factors in to the success of patient survival. The Army Field Dressing, which is the standard field dressing used by the military consists of two layers of gauze that wrap densely packed cotton. It absorbs a large volume of blood, and the cotton strands stimulate platelet aggregation. The prohibitive price of Fibrin Sealant which consists of fibrinogen and thrombin (\$500–\$1000 per dressing) prevents widespread deployment of this type of dressing. Quikclot is a granular mineral zeolite that rapidly absorbs water in an exothermic reaction [92]. Some improvements on zeolite-impregnated dressings in the form of the kaolin-impregnated gauze (Quikclot Combat Gauze) were made. Bentonite (WoundStat) also rapidly halts clotting [93, 94]. Kaolin and bentonite are clay minerals which act as sealants; however, they do not produce an exothermic reaction. It is also noteworthy that recently the relative thrombogenic effects of these aluminum phyllosilicate clay minerals have been examined, and questioned for their *in vivo* safety [95]. However, it is important to understand their mode of action as blood flow sealants, and in clotting. Furthermore considerable concern was registered about systemic vascular thrombogenesis shown by bentonite granules since the material was tested as loose granules at the locus of the wound bed and resulted in occlusive thrombi. HemCon, which is principally chitosan as previously described, has strong tissue adhesive properties that seal the wound and stops bleeding through promotion of platelet aggregation [92]. TaumaDex employs starch microspheres which seal blood flow upon application through a molecular sieve-like mechanism [96]. Surface area coverage, sealant efficacy, adherence and adsorption

capacity are all important factors in this challenging area of hemostasis since the geometry and anatomical location of the wounds can vary greatly, and is a factor in the success of patient survival.

13.6 References

1. CLARK, W. R., ROCHA, E. and RONCO, C., Solute removal by hollow-fiber dialyzers. *In: Ronco, C., Canaud, B. and Aljama, P. (eds.) Hemodiafiltration*, Vol. 158, *Contributions to Nephrology*. Basel: Karger, 2007, pp. 20–33.
2. CARRACEDO, J., RAMIREZ, R., MADUENO, J. A., SORIANO, S., RODRIGUEZ-BENOT, A., RODRIGUEZ, M., MARTIN-MALO, A. and ALJAMA, P., The acute-phase inflammatory process. *Kidney International*, 61 (2002): S89–S93.
3. GUILD, W. R., HARRISON, J. H., MERRILL, J. P. and MURRAY, J., Successful homotransplantation of the kidney in an identical twin. *Transactions of the American Clinical and Climatological Association*, 67 (1955): 167–173.
4. RONCO, C. J., Modalities of continuous renal replacement therapy: technical and clinical considerations. *Seminars in Dialysis*, 22(2) (March–April 2009): 114–122.
5. KLEIN, E., EULER, M. and VERCELLOTTI, J., Capture of anti-(Gal α 1-3Gal) antibodies by immobilized Gal α 1-3Gal oligomers derived from carrageenan. *Biotechnology and Applied Biochemistry*, 28 (1998): 189–199.
6. BERGMANN, L., Filter media for blood products, *Tech. Text. Int.*, 1 September 1992: 14–16.
7. CHATTERJI, P. R., Biomedical applications of synthetic polymers, *Journal of Scientific & Industrial Research*, 46(4) (1987): 168–171.
8. KADIRI, S., KEHINDE, Z., ARIJE, A. and SALAKO, B. L., The influence of cuprophane and polysulfone membranes on dialyzer reusability and intradialytic complications. *African Journal of Medicine and Medical Sciences*, 30 (2001): 191–194.
9. RONCO, C., BRENDOLAN, A., EVERARD, P., *et al.*, Cellulose triacetate: another membrane for continuous renal replacement therapy. *Journal of Nephrology*, 12 (1999): 241–247.
10. RONCO, C., BRENDOLAN, A., CREPALDI, C., RODIGHIERO, M., SCABARDI, M. and GHEZZI, P. M., Blood and dialysate flow distributions in hollow fiber hemodialyzers: a non-intrusive experimental study using MRI. *Journal of Biomechanical Engineering*, 125 (2003): 481–489.
11. BHANDARI, R. N., RICCALTON, L. A., LEWIS, A. L., FRY, J. R., HAMMOND, A. H., TENDLER, S. J. and SHAKESHEFF, K. M., Liver tissue engineering: a role for co-culture systems in modifying hepatocyte function and viability. *Tissue Engineering*, 7 (2001): 345–357.
12. ELLIS, A. J., HUGHES, R. D., WENDON, J. A., DUNNE, J., LANGLEY, P. G., KELLY, J. H., GISLASON, G. T., SUSSMAN, N. L. and WILLIAMS, R., Pilot-controlled trial of the extracorporeal liver assist device in acute liver failure. *Hepatology*, 24 (1996): 1445–1451.
13. KAUFMANN, P. M., KNESER, U., FIEGEL, H. C., KLUTH, D., HERBST, H. and ROGIER, X., Long-term hepatocyte transplantation using three-dimensional matrices. *Transplant Proceedings*, 31 (1999): 1928–1929.
14. TEHRANI, F. T., The origin of adaptive support ventilation. *International Journal of Artificial Organs*, 28(10) (2005): 1051–1052.

15. RATNER, B. D., HOFFMAN, A. S., HANSON, S. R., HARKER, L. A. and WHIFFEN, J. D., Blood-compatibility-water-content relationships for radiation-grafted hydrogels, *Journal of Polymer Science Polymer Symposium*, 66 (1979): 363–375.
16. ANDRADE, J. D., Interfacial phenomena and biomaterials. *Medical Instrumentation*, 7 (1973): 110–120.
17. RAEPPEL, E., HILL, H. U. and LOOS, M., Model of interaction of different polyanions with the first (C1, C1), the second (C2) and the fourth (C4) component of complement-1. Effect of fluid phase C1 and on C1 bound to EA or to EAC4. *Immunochemistry*, 13 (1976): 251–255.
18. SMETANA, JR., K., VACIK, J., HOUSKA, M., SOUCKOVA, D. and LUKAS, J., Macrophage recognition of polymers: effect of carboxylate groups. *Journal of Materials Science: Materials in Medicine*, 4 (1993): 526–529.
19. FERRUTI, P., KNOBLOCH, S., RANUCCI, E., GIANASI, E. and DUNCAN, R., A novel chemical modification of poly-L-lysine reducing toxicity while preserving cationic properties. *Proceedings of the International Symposium on Controlled Release of Bioactive Materials*, 24 (1997): 45–46.
20. FISCHER, D., LI, Y., AHLEMEYER, B., KRIEGLSTEIN, J. and KISSEL, T., *In vitro* cytotoxicity testing of polycations: influence of polymer structure on cell viability and hemolysis. *Biomaterials*, 24 (2003): 1121–1131.
21. PUELO, D. A. and NENCI, A., Understanding and controlling the bone-implant interface. *Biomaterials*, 20 (1999): 2311–2321.
22. BRODBECK, W. G., SHIVE, M. S., COLTON, E., MAKAYAMA, Y., MATSUDA, T. and ANDERSON, J. M., Influence of biomaterials surface chemistry on the apoptosis of adherent cells. *Journal of Biomedical Materials Research*, 55 (2001): 661–668.
23. CHAPMAN, R. C., OSTUNI, E., YAN, L. and WHITESIDES, G. M., Preparation of mixed self assembled monolayers (SAMS) that resist adsorption of proteins using the reaction of amines with a SAM that present interchain carboxylic anhydride groups. *Langmuir*, 16 (2000): 6927–6936.
24. CHARRIER, J. M., *Polymeric Materials and Processing*. Munich: Hanser, 1990.
25. MIURA, H., HISHIBE, T., YASUDA, K., *et al.*, The influence of node-fibril morphology on healing of high-porosity expanded polytetrafluoroethylene grafts. *European Surgical Research*, 34 (2002): 224–231.
26. UMSCHIED, T. and STELTER, W. J., Time-related alterations in shape, position, and structure of self-expanding, modular aortic stent-grafts: a 4-years single-center follow-up. *Journal of Endovascular Surgery*, 6 (1999): 17–32.
27. PANSERI, S., CUNHA, C., LOWERY, J. *et al.*, Electrospun micro and nanofiber tubes for functional nervous regeneration in sciatic nerve transections. *BMC Biotechnology*, 8 (2008): 39.
28. ZHANG, S., Fabrication of novel biomaterials through molecular self-assembly. *Nature Biotechnology*, 21 (2003): 1171–1178.
29. GIORDANO, R. A., WU, B. M., BORLAND, S. W., CIMA, L. G., SACHS, E. M. and CIMA, M. J., Mechanical properties of dense polylactic acid structures fabricated by three dimensional printing. *Journal of Biomaterials Science. Polymer Edition*, 8 (1996): 63–75.
30. MA, X., Biomimetic materials for tissue engineering. *Advanced Drug Delivery Reviews*, 60 (2008): 184–198.
31. ALTMAN, G. H., FIAZ, F., JAKUBA, C., CALABRO, T., HORAN, R. L., CHEN, J., LU, H., RICHMOND, J. and KAPLAN, D. L., Silk matrix for tissue engineered anterior cruciate ligaments. *Biomaterials*, 23 (2002): 4131–4141.

32. PIERSCHBACHER, M. D. and RUOSLATHI, E., Cell attachment of fibronectin can be duplicated by small synthetic fragments of the molecule, *Nature*, 309 (1984): 30–33.
33. TSCHOPP, J. F., CRAIG, W. S., TOLLEY, J., BLEVITT, J., MAZUR, C. and PEIRSCHBACHER, M. D., Therapeutic application of matrix biology. *Methods in Enzymology*, 245 (1994): 556–569.
34. HORII, A., WANG, X., GELAIN, F., *et al.*, Biological designer self-assembling peptide nanofiber scaffolds significantly enhance osteoblast proliferation, differentiation and 3-D migration. *PLoS ONE*, 2: e190.
35. KISIDAY, J., JIN, M., KURZ, B., *et al.*, Self-assembling peptide hydrogel fosters chondrocyte extracellular matrix production and cell division: implications for cartilage tissue repair. *Proceedings of the National Academy of Sciences USA*, 99 (2002): 9996–10001.
36. ELLIS-BEHNKE, R. G., LIANG, Y. X., YOU, S. S., *et al.*, Nano neuro knitting: peptide nanofiber scaffold for brain repair and axon regeneration with functional return of vision. *Proceedings of the National Academy of Sciences USA*, 103 (2006): 5054–5059.
37. GENOVE, E., HSHEN, C., ZHANG, S., *et al.*, The effect of functionalized self-assembling peptide scaffolds on human aortic endothelial cell function. *Biomaterials*, 26 (2005): 3341–3351.
38. ELLIS-BEHNKE, R. G., LIANG, Y. X., YOU, S. W., *et al.*, Nano hemostat solution: immediate hemostasis at the nanoscale. *Nanomedicine*, 2 (2006): 207–215.
39. CLARK, R. A. F., Wound repair: overview and general considerations. In: Clark, R. A. F. (ed.) *The Molecular and Cellular Biology of Wound Repair*. New York: Plenum Press, 1996, pp. 3–35.
40. WITKOWSKI, E. F. and PARISH, L. C., Histopathology of the decubitus ulcer. *Journal of the American Academy of Dermatology*, 696 (1982): 1014–1021.
41. LYDER, C. H. http://www.geriatricsreviewsyllabus.org/content/agscontent/ulcer6_m.htm.
42. RICHEY, M. L., RICHEY, H. K. and FENSKE, N. A., Aging-related skin changes: development and clinical meaning. *Geriatrics*, 43 (1988): 49–64.
43. RYAN, T. J., The microcirculation of the skin in old age. *Gerontologia Clinica*, 8 (1966): 327–337.
44. SINGER, A. J. and CLARK, R. A. F., JR., Cutaneous wound healing. *New England Journal of Medicine*, 341(10) (1999): 738–746.
45. LOCALIO, A. R., MARGOLIS, D. J., KAGAN, S. H., LOWE, R. A., KINOSIAN, B., ABBUHL, S., KAVESH, W., HOLMES, J. H., RUFFIN, A. and BAUMGARTEN, M., Use of photographs for the identification of pressure ulcers in elderly hospitalized patients: validity and reliability. *Wound Repair and Regeneration*, 14(4) (2006): 506–513.
46. EAGLESTEIN, W. H. and FALANGA, V., Chronic wounds. *Surgical Clinics of North America*, 77 (1997): 689–700.
47. WINTER, G. D., Formation of the scab and the rate of epithelization of superficial wounds in the skin of the young domestic pig. *Nature*, 193 (1962): 294.
48. HINMAN, C. D. and MAIBACH, H., Effect of air exposure and occlusion on experimental human skin wounds. *Nature*, 200 (1963): 377.
49. SCHULTZ, G. S., SIBBALD, R. G., FALANGA, V., AYELLO, E. A., DOWSETT, C., HARDING, K., ROMANELLI, M., STACEY, M. C., TEOT, L. and VANSCHIEDT, W., Wound bed preparation: a systematic approach to wound management. *Wound Repair and Regeneration*, 11 (2003): 1–28.

50. Draft Guidance for the Preparation of an IDE Submission for an Interactive Wound and Burn Dressing, in 817 Guidance for Interactive Wound Dressings, U.S. Food and Drug Administration Center for Devices and Radiological Health, 1995, pp. 1–5.
51. MORGAN, D., Wounds – what should a dressing formulary include? *Hospital Pharmacist*, 9 (2002): 261–266.
52. FALLING, V., ISAACS, C., PACKET, D., DOWNING, G., KOWTOW, N., BUTTER, E. B. and HARDEN-YOUNG, J., Wounding of bioengineer skin: cellular and molecular aspects after injury. *Journal of Investigative Dermatology*, 119 (2002): 653–660.
53. THOMAS, A., HARDING, K.G. and MOORE, K., Alginates from wound dressings activate human macrophages to secrete tumor necrosis factor- α . *Biomaterials*, 21 (2000): 1797–1802.
54. SCHULTZ, G. S., SIBBALD, R. G., FALANGA, V., AYELLO, E. A., DOWSETT, C., HARDING, K., ROMANELLI, M., STACEY, M. C., TEOT, L. and VANSCHIEDT, W., Wound bed preparation: a systematic approach to wound management. *Wound Rep. Reg.*, 11 (2003): 1–28.
55. MAST, B.A., SCHULTZ, G.S., Interactions of cytokines, growth factors and proteases in acute and chronic wounds, *Wound Repair and Regeneration*, 4 (1996): 411–420.
56. BAKER, E. A. and LEAPER, D. J., Proteinases, their inhibitors, and cytokine profiles in acute wound fluid. *Wound Repair and Regeneration*, 8 (2000): 392–398.
57. TRENGOVE, N. J., BIELEFELDT-OHMANN, H. and STACEY, M. C., Mitogenic activity and cytokine levels in non-healing and healing chronic leg ulcers. *Wound Repair and Regeneration*, 4 (1996): 234–239.
58. CHRISTOFOROU, C., LIN, X., BENNETT, S., CONNORS, D., SKALLA, W., MUSTOE T., LINEHAN, J., ARNOLD, F. and GUSKIN, E., Biodegradable positively charged ion exchange beads: a novel biomaterial for enhancing soft tissue repair. *Journal of Biomedical Materials Research*, 42 (1998): 376–386.
59. CONNORS, D., GIES, D., LIN, H., GRUSKIN E., MUSTOE, T. A. and TAWIL, N. J., Increase in wound breaking strength in rats in the presence of positively charged dextran beads correlates with an increase in endogenous transforming growth factor- β 1 and its receptor TGF β R1 in close proximity to the wound. *Wound Repair and Regeneration*, 8 (2000): 292–303.
60. CULLEN, B., SMITH, R. MCCULLOCH, E., SILCOCK, D. and MORRISON, L., Mechanism of action of PROMOGRAN, a protease modulating matrix, for the treatment of diabetic foot ulcers. *Wound Repair and Regeneration*, 10 (2002): 16–25.
61. EDWARDS, J. V., YAGER, D. R., COHEN, I. K., DIEGELMANN, R. F., MONTANTE, S., BERTONIERE, N. and BOPP, A. F., Modified cotton gauze dressings that selectively absorb neutrophil elastase activity in solution. *Wound Repair and Regeneration*, 9 (2001): 50–58.
62. EDWARDS, J. V., BATISTE, S. L., GIBBINS, E. M. and GOHEEN, S. C., Synthesis and activity of NH₂- and COOH-terminal elastase recognition sequences on cotton. *Journal of Peptide Research*, 54 (1999): 536–543.
63. WRIGHT, J. B., LAM, K., BURET, A. G., OLSON, M. E. and BURRELL, R. E., Early healing events in a porcine model of contaminated wounds: effects of nanocrystalline silver on matrix metalloproteinases, cell apoptosis, and healing. *Wound Repair and Regeneration*, 10 (2002): 141–151.
64. MOSELEY, R., LEAVER, M., WALKER, M., WADDINGTON, R. J., PARSONS, D., CHEN, W. Y. I. and EMBERY, G., Comparison of the antioxidant properties of HYAFF-11p75,

- AQUACEL and hyaluronan towards reactive oxygen species *in vitro*. *Biomaterials*, 23 (2002): 2255–2264.
65. KIRKER, K. R., LUO, Y., NIELSON, J. H., SHELBY, J. and PRESTWICH, G. D., Glycosaminoglycan hydrogel films as bio-interactive dressings for wound healing. *Biomaterials*, 23(17) (2002): 3661–3671.
 66. YAGER, D. and NWOMEH, B., The proteolytic environment of chronic wounds. *Wound Repair and Regeneration*, 7 (1999): 433–441.
 67. CULLEN, B., SMITH, R., MCCULLOCH, E., SILCOCK, D. and MORRISON, L., Mechanism of action of PROMOGRAN, a protease modulating matrix, for the treatment of diabetic foot ulcers. *Wound Repair and Regeneration*, 10 (2002): 16–25.
 68. MEYER-INGOLD, W., EICHNER, W., ETTNER, N. and SCHINK, M., Wound coverings for removal of interfering factors from wound fluid. United States Patent, 6,156,334, 2000.
 69. National Pressure Ulcer Advisory Panel, Pressure ulcers in America: prevalence, incidence, and implications for the future. An executive summary of the National Pressure Ulcer Advisory Panel Monograph. *Advances in Skin Wound Care*, 14 (2001): 208–215.
 70. RICHEY, M. L., RICHEY, H. K. and FENSKE, N. A., Aging-related skin changes: development and clinical meaning. *Geriatrics*, 43 (1988): 49–64.
 71. BAUMGARTEN, M., MARGOLIS, D. J., LOCALIO, A. R., KAGAN, S. H., LOWE, R. A., KNOSIAN, B., HOLMES, J. G., ABBUHL, B., KAVESH, W. and RUFFIN, A., Pressure ulcers among elderly patients early in the hospital stay. *Journal of Gerontology*, 61A(7) (2006): 749–754.
 72. ZHONG, W., XING, M. M. Q., PAN, N. and MAIBACH, H. I., Textiles and human skin, microclimate, cutaneous reactions: an overview. *Cutaneous and Ocular Toxicology*, 25 (2006): 1–17.
 73. BENNETT, L., KAVNER, D., LEE, B. Y., TRAINOR, F. S. and LEWIS, J. M., Shear vs pressure as causative factors in skin blood flow occlusion. *Archives of Physical Medicine and Rehabilitation*, 60 (1979): 309–314.
 74. BRIDEL, J., The aetiology of pressure sores. *Journal of Wound Care*, 2(4) (1993): 230–238.
 75. GERHARDT, L. C., MATTLE, N., SCHRADE, G. U., SPENCER, N. D. and DERLER, S., Study of skin-fabric interactions of relevance to decubitus: friction and contact-pressure measurements. *Skin Research Technology*, 14 (2008): 77–88.
 76. HOFFMAN, A., GEELKERKEN, R. H., WILLIE, J., HEMMING, J. J., HERMANS, J. and BRESLAU, P. J., Pressure sores and pressure-mattresses: controlled clinical trial. *Lancet*, 343 (1994): 568–571.
 77. GERHARDT, L.-C., STRASSLE, V., LENZ, A., SPENCER, N. D. and DERLER, S., Influence of epidermal hydration on the friction of human skin against textiles. *Journal of the Royal Society, Interface*, 5 (2008): 1317–1328.
 78. NEWMAN, D. K., FADER, M. and BLISS, D. Z., Managing incontinence using technology devices and products. *Nursing Research*, 53(6S) (2004): S42–S48.
 79. EREKSON, E. A., MEYER, S. A., MELICK, C. and MCLENNAN, M. T., Incontinence pads: recommending the best product-based wetback performance and price. *International Urogynecology Journal*, 19 (2008): 1411–1414.
 80. FADER, M., BAIN, D. and COTTENDEN, A., Effects of absorbent incontinence pads on pressure management mattresses. *Journal of Advanced Nursing*, 48(6) (2004): 569–574.

81. EROWELE, G. K. and EBIASAH, R., The prevention and treatment of pressure ulcers. *U.S. Pharmacist*, 2009. http://www.uspharmacist.com/continuing_education/ceview/test/lessonid/106088/.
82. ENOMAE, T., ASAKAWA, R., ONABE, F., YOSHIKAWA, M., FUKASAWA, H., HIYOSHI, K. and KURATA, T., Development of nursing care sheets of cellulosic nonwoven fabrics for aging society. *Textile Research Journal*, 76 (2006): 41–48.
83. PRYCYNSKA, E., LIPP-SYMONOWICZ, B., WIECZOREK, A., GASZYNSKI, W., KREKORA, K. and BITTNER-CZAPINSKA, E., Sheet fabrics with biophysical properties as elements of joint prevention in connection with first- and second-generation pneumatic anti-bedsores mattresses. *Fibres and Textiles in Eastern Europe*, 11(4) (2003): 50–53.
84. EILENDER, K. and STAND, M., Low friction multilayer pad. US Patent, 4,959,059, 25 September 1990.
86. LINDBERG, E. Patient sliding sheet with liquid absorbing layer. 5,787,523. 4 August 1998
86. BELLAMY, R. F., The causes of death in conventional land warfare: implications for combat casualty care research. *Military Medicine*, 149 (1984): 55–62.
87. CHAMPION, H. R., BELLAMY, R. F., ROBERTS, C. P. and LEPPANIEMI, A., A profile of combat injury. *Journal of Trauma*, 54 (2003): S13–S19.
88. SAUUA, A., MOORE, F. A., MOORE, E. E., HAENEL, J. B., READ, R. A. and LEZOTTE, D. C., Early predictors of post injury multiple organ failure. *Archives of Surgery*, 129 (1994): 39–45.
89. COSGRIFF, N., MOORE, E. E., SAUUA, A., KENNY-MOYNIHAN, M., BURCH, J. M. and GALLOWAY, B., Predicting life-threatening coagulopathy in the massively transfused trauma patient: hypothermia and acidosis revisited. *Journal of Trauma*, 42 (1997): 857–861; discussion 861–862.
90. HECKBART, S. R., VEDDER, N. B., HOFFMAN, W., *et al.*, Outcome after hemorrhage shock in trauma patients. *Journal of Trauma*, 45 (1998): 545–549.
91. ACHESON, E. M., KHEIRABADI, B. S., DEGUZMAN, R., DICK, E. J., JR. and HOLCOMB, J. B., Comparison of hemorrhage control agents applied to lethal extremity arterial hemorrhages in swine. *Journal of Trauma*, 59 (2005): 865–874; discussion 874–875.
92. PUSATERI, A. E., HOLCOMB, J. B., KHEIRABADI, B. S., ALAM, H. B., WADE, C. E. and RYAN, K. L., Making sense of the preclinical literature on advanced hemostatic products. *Journal of Trauma*, 60 (2006): 674–682.
93. WARD, K. R., TIBA, M. H., HOLBERT, W. H., BLOCHER, C. R., DRAUCHER, G. T., PROFFITT, E. K., BOWLIN, G. L., IVATURY, R. R. and DIEGELMANN, R. F., Comparison of a new hemostatic agent to current combat hemostatic agents in a swine model of lethal extremity arterial hemorrhage. *Journal of Trauma*, 63 (2007): 276–284.
94. http://www.z-medica.com/zmedica/hemostasis_zmedica.asp.
95. KHEIRABADI, B. S., MACE, J. E., IRASEMA, B., TERRAZAS, M. S., FEDYK, C. G., ESTEP, J. S., DUBICK, M. A. and BLACKBOURNE, L. H., Safety evaluation of new hemostatic agents, smectite granules, and kaolin-coated gauze in a vascular injury wound model in swine. *Journal of Trauma Injury, Infection, and Critical Care*, 668 (2010): 260–278.
96. GEGEL, B. T., BURGERT, J. M., LOCKHART, C., AUSTIN, R., III, DAVILA, A., DEEDS, J., HODGES, A., HOVER, A., ROY, J., SIMPSON, G., WEAVER, S., WOLFE, W. C. and JOHNSON, D., Effects of Celox and TraumaDEX on hemorrhage control in a porcine model. *AANA Journal*, 78 (2) (2010), 115–120.

Improving superhydrophobic coatings for textiles through chemical modifications

C. H. XUE,
University of California, Davis, USA

Abstract: This chapter provides an overview of superhydrophobic textiles with detailed illustrations of key principles of superhydrophobic textiles, chemical modification coating on fibers, and hydrophobization for improving superhydrophobicity and surface robustness of textiles. Applications of superhydrophobic textiles in practical and potential fields are discussed. Future trends of superhydrophobic textiles are also presented.

Key words: superhydrophobic surface, coating, textile, chemical modification, surface roughness.

14.1 Introduction

Superhydrophobic textiles recently attracted a lot of attention due to their simple fabrication, easy availability of raw materials, large-scale production of superhydrophobic surfaces (Xue *et al.*, 2008b) obtained possibly by industrialized techniques (Wang *et al.*, 2007; Xue *et al.*, 2009), and the potential applications of such surfaces in a variety of areas. They literally repel water, making water hardly stick to the surface and bounce off after an impact, and thereby such treatment can remove dust and surface contaminants very effectively, showing a self-cleaning effect like that of the lotus leaf (Barthlott and Neinhuis, 1997). Superhydrophobicity of textiles can not only provide protection from a wide variety of liquids but also prolong the lifetime of the fabrics due to the prevention of water wetting that causes fiber degradation (Xue *et al.*, 2008a). Superhydrophobic textiles with superoleophobic properties are desirable for oil repellency in industrial or household environments (Hoefnagels *et al.*, 2007; Leng *et al.*, 2009).

In the following context, I will discuss the key principles of superhydrophobic textiles, various ways to produce superhydrophobic coatings on textiles, and the role of chemical modifications in improving superhydrophobicity and robustness of textile surfaces. Then, commercially available superhydrophobic textile products and their corresponding applications are

reviewed. Future trends and suggestions in superhydrophobic surfaces on textiles are also presented.

14.2 Key principles of superhydrophobic textiles

A superhydrophobic surface is defined as having a water contact angle greater than 150° and a roll-off angle lower than 5° (Michielsen and Lee, 2007; Wu and Shi, 2006). There is now abundant evidence that combinations of topography and hydrophobic chemical structure produce surfaces with high contact angles with very low roll-off angles (Roach *et al.*, 2008; Zhang *et al.*, 2008b).

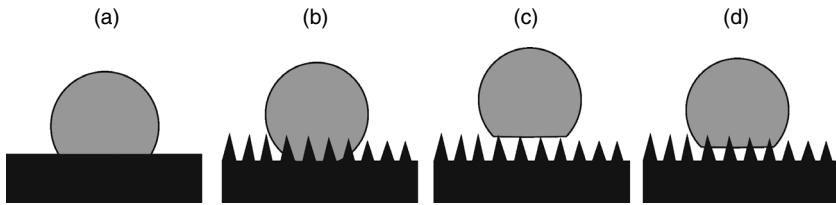
Theoretical models for liquid drops on topologically rough and chemically non-homogeneous surfaces have been established by different researchers (Cassie and Baxter, 1944; Wenzel, 1936, 1949) and these models have recently been used to rationalize the lotus effect (Cheng *et al.*, 2006; Crick and Parkin, 2009; Gao and McCarthy, 2006; Hou and Wang, 2009; Marmur, 2003; Qu *et al.*, 2008; Roach *et al.*, 2008). Water can interact with rough surfaces by contacting only the peaks of the roughened surface, wetting the peaks while leaving the valleys with air trapped, or by wetting the entire surface, both the peaks and valleys, as shown in Fig. 14.1(b–d). When water interacts with the surface by contacting only the peaks of the roughened surface, as shown in Fig. 14.1(c), the apparent contact angle, θ_{CB} , is given by the Cassie–Baxter equation for wetting on composite surfaces made of the solid and air (Cassie and Baxter, 1944),

$$\cos \theta_{CB} = f_s \cos \theta + f_a - 1, \quad [14.1]$$

where f_s is the fraction of projected planar area of the drop in contact with the solid. In the limit of $f_s \rightarrow 0$, the macroscopic contact angle θ_{CB} approaches 180° , leading to ideal superhydrophobic behavior. When water wets both peaks and valleys of a rough surface with uniform chemical composition, as shown in Fig. 14.1(b), the apparent contact angle of the drop, θ_w , is given by Wenzel's formula (Wenzel, 1936, 1949),

$$\cos \theta_w = \gamma \cos \theta, \quad [14.2]$$

where γ is the ratio of the actual area of liquid–solid contact to the projected area on the horizontal plane of the rough surface, and θ is the equilibrium contact angle of the liquid drop on the corresponding flat surface. Wenzel's equation predicts that roughness will amplify the intrinsic wetting behavior of a surface as determined by its surface chemistry. If the contact angle on the smooth surface is larger than 90° , roughness will further increase the observed contact angle. If it is less than 90° , roughness will reduce the



14.1 Schematic of the behavior of a droplet on a perfectly flat surface (a), and rough surfaces of wetting states: (b) Wenzel, (c) Cassie–Baxter, and (d) combined models.

observed contact angle. Equations [15.1] and [15.2] represent two possible equilibrium states of liquid drops on rough surfaces. Drops in the Cassie–Baxter state can easily roll because of low resistance from the air pockets. In contrast, drops in the Wenzel state can become ‘sticky’ from contacting the rough surface (Cheng *et al.*, 2006; Roach *et al.*, 2008) in that the interfacial area between solid and liquid is much larger than that on a flat surface, as shown schematically in Fig. 14.1(a) and (b). It is, however, possible to generate ‘sticky’ surfaces in the regime of Cassie and Baxter, usually by using a surface with high intrinsic contact angle hysteresis; the combined Cassie–Baxter/Wenzel state can also have large hysteresis as the interfacial area between solid and liquid can be at least as large as on a flat surface, as shown schematically in Fig. 14.1(d). For the surfaces with self-cleaning effect, it is generally believed that the two-level roughness, in combination with low surface energy, amplifies the apparent contact angle, lowering the hysteresis, and is responsible for the rolling behavior of the drops.

Most textiles are textured woven or knit structures consisting of nature or synthetic fibers with organic, elastic and usually micro-sized features, thus exhibiting some distinction from other solid surfaces in terms of creation of superhydrophobic surfaces. According to the main requirements for a superhydrophobic surface, there are two major methods of producing superhydrophobic textiles. The first method is to construct textiles with a big roughness factor through physical methods. The materials consisting of the substrate can be initially hydrophobic or created afterwards. The second method is to enhance the roughness of an intrinsic textured textile through chemical modifications, and then hydrophobize the roughness-enhanced textile surface by changing the surface chemistry or applying a hydrophobic material to lower the surface energy, or to generate a layer of nanoscopic fibrous or particle coating of materials with low surface energy on the micro-scope fibrous textiles. In addition, nanoscaled coating of materials with low surface energy through chemical modification can also be done to impart roughness and hydrophobicity onto fibers simultaneously, making textiles superhydrophobic. Superhydrophobic rough coatings for textiles through chemical modifications will be discussed in the following section.

14.3 Chemical modifications for fabricating rough surfaces on textiles

Rough surfaces can be constructed on textiles by attachment of micro or nanoparticles on fibers through sol-gel processing, hydrothermal synthesis, complex coating, layer-by-layer methods, and others. The particles used may be inorganic, organic or organic/inorganic hybrid. It is widely known that inorganic substances, such as ZnO, SiO₂, TiO₂ and the like, have lower affinity for organic substances, for example textile fibers. Therefore, for application of superhydrophobic textiles, it is very important to compatibilize the particles with the textile substrates through chemical modification to enhance the stability of the superhydrophobic coating on textiles as well as the robustness of superhydrophobicity during service.

14.3.1 Sol-gel processing

Sol-gel processing is a well recognized method for preparing gels and nanoparticles. Researches based on the sol-gel method to develop applications have resulted in technologies to obtain multilayered films, porous pillars, thin films, nanocrystalline materials, nanopowders, rough coatings and clusters for uses in paints, antiseptics, nanocomposites, drugs, biomedical implants and military components (Bae *et al.*, 2009; Daoud *et al.*, 2004; Xue *et al.*, 2008a). The surface roughness of the textiles fabricated via the sol-gel method can be easily tuned through changing the protocol of the method and the composition of the reaction mixture. Daoud (2004) prepared transparent and durable superhydrophobic surfaces on knit and woven cotton substrates of various dimensions at low temperatures using a modified silica sol. The silica sol is produced via cohydrolysis and polycondensation of a hexadecyltrimethoxysilane, tetraethoxyorthosilicate and 3-glycidoxypolytrimethoxysilane mixture. Leaching behavior of the hydrophobic properties by comparing the contact angle and water gain values before and after washing showed that after ten cycles of washing, the hydrophobic properties maintained well in the later wash cycles. The maintenance of the hydrophobic properties of the coating after repeated washing was attributed to the linking ability of 3-glycidoxypolytrimethoxysilane that promoted a high level of adhesion to the cotton substrates. Hoefnagels *et al.* (2007) reported the fabrication of biomimetic superhydrophobic cotton textiles by either one-step or two-step reactions to generate *in situ* silica particles with amine groups on their surfaces, which were covalently bonded to the cotton fibers; the amine groups were then utilized to hydrophobize the surface via the reaction with mono-epoxy-functionalized polydimethylsiloxane. When a perfluoralkyl silane was used for the surface modification, oleophobic textiles were obtained. Xue *et al.* (2008a) prepared superhydrophobic cotton

fabrics by sol-gel coating of TiO_2 and surface hydrophobization. It was found that the superhydrophobicity of the obtained fabrics relied on the roughness caused by the sol-gel coating rather than the concentration of TiO_2 . Yu *et al.* (2007) prepared a silica sol with appropriate particle size via alkaline hydrolysis of tetraethoxysilane in a mixture of ethanol and water, and synthesized a perfluorooctylated quaternary ammonium silane coupling agent. The silica sol and perfluorooctylated quaternary ammonium silane coupling agent were applied to cotton fabrics by conventional pad-dry-cure process. The fabrics treated with both silica sol and perfluorooctylated quaternary ammonium silane coupling agent showed high hydrophobicity and oleophobicity. Li *et al.* (2008) used water glass, a cheap and common industry product, as the precursor to prepare silica sol under acid catalyzed hydrolysis and condensation. After dip-coating the silica sol onto cotton surfaces, the surfaces were then modified with hexadecyltrimethoxysilane to gain a thin layer through a self-assembled process. As a result, the cotton fabrics treated with such processes showed superhydrophobicity. The superhydrophobic surfaces were made at low temperatures without expensive equipment and tedious processes.

Bae *et al.* (2009) have imparted superhydrophobicity to the hydrophilic cotton fabric by a combined treatment of silica nanoparticles and a cost-effective commercial water-repellent agent. For the cotton fabrics treated with silica nanoparticles of average diameter 378 nm, water contact angles above 130° could be easily obtained even with a very low water-repellent agent concentration of 0.1 wt% at which no hydrophobicity was exhibited for the neat cotton fabric treated with the water-repellent agent only.

Wang *et al.* (2008) have produced stable superhydrophobic surfaces with water contact angles over 170° and sliding angles below 7° by simply coating a particulate silica sol solution of co-hydrolyzed TEOS/fluorinated alkyl silane with $\text{NH}_3 \cdot \text{H}_2\text{O}$ on various substrates, including textile fabrics (e.g. polyester, wool and cotton) and electrospun nanofiber mats.

It should be mentioned that the above-mentioned superhydrophobic coatings through sol-gel method were mostly conducted on cotton textiles. It is well recognized that there are a lot of reactive hydroxyl groups on cotton fibers. Thus covalent bonds can be formed between coating and cotton substrate by condensation in sol-gel process and/or dehydration in curing process, making sol-gel coating robust on textiles.

14.3.2 Hydrothermal synthesis

Hydrothermal synthesis is a well-known method for the fabrication of nano/microscale materials. Researches on growing inorganic materials with all kinds of structure on organic materials to fabricate superhydrophobic surfaces on textiles were conducted. Xu and Cai (2008) employed

a hydrothermal method on cotton fabrics to create superhydrophobic surfaces. First, ZnO nanocrystals were prepared and applied on the cotton fibers. Subsequently, oriented ZnO nanorod arrays were fabricated on the fibers to form nanoscale roughness. Finally, the as-obtained fabrics were modified by n-dodecyltrimethoxysilane to obtain superhydrophobic surfaces. Their method showed a high degree of experimental reproducibility, and the fabrication processes were applied using inexpensive laboratory equipment usually employed for conventional textile processing. The researchers proposed that two factors contributed to the enhancement of the attachment between the cotton fiber substrate and the ZnO nanorods. N-dodecyltrimethoxysilane was infiltrated above and below the ZnO seed layer as binding agents when the cotton fabrics were immersed into n-dodecyltrimethoxysilane ethanol solution. The as-produced Si-OH groups in hydrolyzed n-dodecyltrimethoxysilane could react with both the ZnO seeds and the cotton fiber substrates since there are abundant hydroxyl groups on their surfaces. As a result, the ZnO seeds and the fiber substrate were tightly bound with each other. Furthermore, there are three hydroxyl groups in one hydrolyzed n-dodecyltrimethoxysilane molecule and hydrolyzed n-dodecyltrimethoxysilane could easily form cross-linked chains, thus the nanorods were firmly bundled and fixed on the ZnO seeding layer. The two layers created in this process successfully improved the fastness and stability of the ZnO nanorods on the cotton substrate.

14.3.3 Complex particle coating

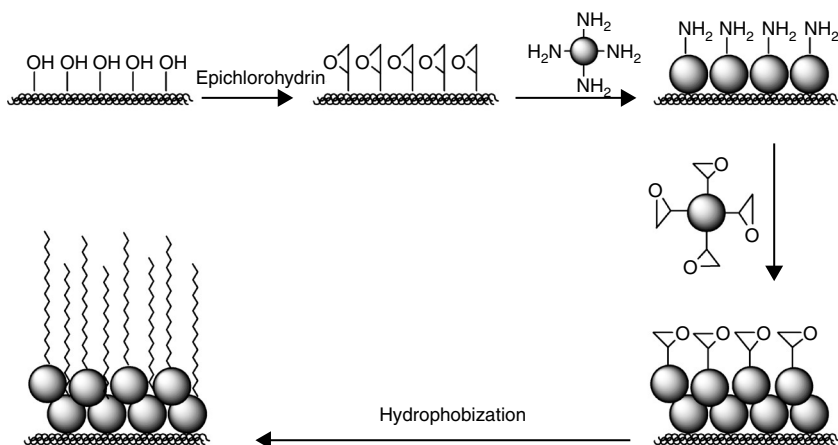
Well-defined coating of nano/micro particles on fibers is a promising way to make rough coatings on textile. In order to make the coating fast and the superhydrophobicity function durable, particles and/or textile substrates are usually modified by introduction of functional groups, such as carboxyl, amino, epoxy, hydroxyl, and so forth. By doing so, the particles and the textile fibers can compatibilize with each other by forming covalent bonds. In complex coating, particles with different functional groups can attach to each other by reaction, forming firm coating. And the remaining functional groups on the coating surface facilitate further hydrophobization with low-surface-energy materials.

Ramaratnam *et al.* (2007) prepared ultrahydrophobic textile surface via decorating fibers with a monolayer of reactive nanoparticles and non-fluorinated polymer. In their first step of the surface modification, silica particles covered with an ultrathin reactive layer of poly(glycidyl methacrylate), an epoxy containing polymer, were deposited on the fiber surface. The silica particles covered with epoxy functional groups are capable of reacting with the fiber surface containing complementary (e.g. carboxy, hydroxy) functionality and with hydrophobic polymers possessing the functional groups,

leading to affinity to the epoxy modified surface. During the second step, a hydrophobic polymer was grafted to the surface of the fibers and nanoparticles, and an ultrathin rough hydrophobic layer chemically anchored to the fiber boundary was generated.

We prepared superhydrophobic surfaces on cotton textiles by a complex coating of amino- and epoxy-functionalized silica nanoparticles on epoxy-functionalized cotton textiles to generate a dual-size surface roughness, followed by hydrophobization with stearic acid, 1H,1H,2H,2H-perfluorodecyltrichlorosilane, or their combination (Xue *et al.*, 2009), as shown in Fig. 14.2. The epoxy-functionalization of the cotton enhances the interaction between the fiber and the silica coating. The incorporation of the functionalized SiO₂ particles not only generates a firm dual-size rough surface but also facilitates the further hydrophobization of the surface. The achieved coating surfaces are robust and the superhydrophobicity of the cotton textiles is long lasting.

Leng *et al.* (2009) introduced raspberry-like, dual-size structures onto woven cotton fibers, leading to a triple-size surface structure. Relatively large silica particles were generated *in situ* and covalently bonded to the cotton fibers. After treatment with 3-aminopropyl-triethoxysiloxane and hydrochloric acid, the surface charge was turned positive due to the protonation of amine groups. Negatively charged silica nanoparticles were then electrostatically adsorbed onto the fiber surface. The obtained roughened structure was stabilized by SiCl₄ cross-linking, followed by surface modification with a perfluoroalkyl silane. The modified textiles were completely non-wettable by both water and hexadecane, which both showed high contact angles and low roll-off angles.



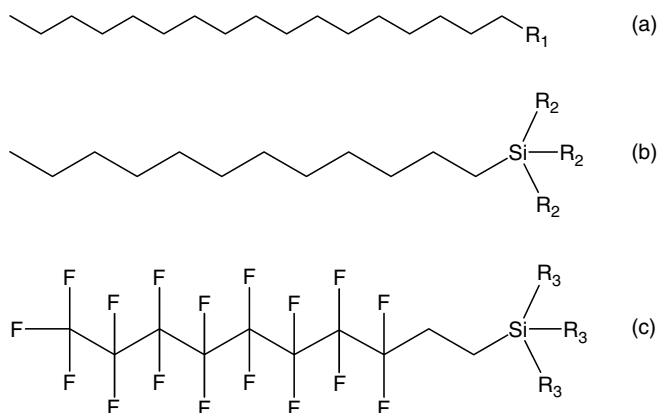
14.2 Schematic illustration of procedure for preparation of superhydrophobic surfaces on cotton substrate roughened by functionalized silica nanoparticles. Adapted from Xue *et al.* (2009).

14.4 Hydrophobization for lowering the surface energy of roughened textiles

After application of a roughening coating, most textiles cannot reach superhydrophobic state. It is necessary to lower the surface energy of the rough coated textiles. Until now, various low-surface-energy coatings have been developed to modify organic and inorganic rough surfaces, leading to fabrication of superhydrophobic surfaces, many of which are suitable for superhydrophobic coating on textiles. The commonly used reactive molecules for low-surface-energy modifications are long alkyl chain thiols, alkyl or fluorinated organic silanes, perfluorinated alkyl agents, long alkyl chain fatty acids, polymer, and polydimethylsiloxane, and so forth as shown of some examples in Fig. 14.3, or their combinations. Among others, commercially available products such as water-repellent agent and poly(acrylate-g-siloxane) textile finishing agent can also be used.

14.4.1 Hydrophobization with fluorinated molecules

In hydrophobization, the most commonly used chemicals were fluoroalkylsilanes due to their extremely low-surface-free energy and easy reaction of the silane groups with the hydroxyl groups on coatings. Large amount of superhydrophobic surfaces were based on the surface modification with fluoroalkylsilanes. Examples in this chapter focus mainly on superhydrophobic textiles. Hoefnagels (2007) *in situ* introduced silica particles to cotton



14.3 Examples of surface reactive molecules for low-surface-energy modifications: (a) long alkyl chain with R_1 groups, (b) long alkyl chain organic silanes with R_2 groups, and (c) long alkyl chain fluorinated silanes with R_3 groups, in which R_1 could be $-\text{SH}$, $-\text{OH}$, $-\text{COOH}$, $-\text{NH}_2$, and so forth; R_2 and R_3 could be $-\text{Cl}$, $-\text{OCH}_3$, $-\text{OCH}_2\text{CH}_3$; the length of these chains might be variable from C8 to C18.

fibers to generate a dual-size surface roughness, followed by introduction of a perfluoroalkyl chain of 1*H*,1*H*,2*H*,2*H*-perfluorodecyl trichlorosilane to the silica particle surface. The substrate becomes highly oleophobic, as demonstrated by a static contact angle of 140° and a roll-off angle of 24° for a 15 µL sunflower oil droplet. By introducing a nano/microparticle dual-size structure to the woven cotton fiber network followed by surface perfluorination with 1*H*,1*H*,2*H*,2*H*-perfluorodecyl trichlorosilane, the modified textiles were completely non-wettable by both water and hexadecane (Leng *et al.*, 2009). It should be noted that many superhydrophobic surfaces are poor in oil repellency. Up until now most superoleophobic surfaces, including superoleophobic textiles, are based on perfluorinated alkyl hydrophobization. Choi *et al.* (2009) developed a simple dip-coating process for delivering a conformal coating of fluorodecyl polyhedral oligomeric silsesquioxane molecules on commercial fabrics that exhibit reversible, deformation-dependent, tunable wettability, including the capacity to switch their surface wetting properties (between superrepellent and superwetting) against a wide range of polar and non-polar liquids.

14.4.2 Hydrophobization with alkyl molecules

Alkanethiol is a kind of active surfactant bearing a hydrophobic alkyl chain and a thiol group as a surface anchor. Zhang *et al.* (2004) employed n-dodecanethiol to modify the rough surface of gold or silver aggregates, fabricated by electrochemical deposition to prepare superhydrophobic surfaces. Their experiment shows that the contact angles can reach around 156° with a droplet of 4 µL after modification by SAMs of n-dodecanethiol on the silver aggregates (Shi *et al.*, 2007). Wang *et al.* (2007) modified normal commercial cloths with suitable gold micro/nanostructures. Surface hydrophobization was then carried out by immersing the as-prepared product in an ethanol solution of n-dodecanethiol, forming superhydrophobic cloths with the highest water contact angle of close to 180°.

Fluorochemicals have extremely low-surface-free energy. However, such compounds are high cost and have a potential risk for human health and for the environment. Hence, the development of non-fluorinated modifying agents or lowering the concentration of fluorochemicals used is very important for the fabrication of environmentally friendly coatings on textile substrates. In order to lower the risk and cost of fluorochemicals, stearic acid was combined with 1*H*,1*H*,2*H*,2*H*-perfluorodecyl trichlorosilane to lower the content of fluorochemical in hydrophobization of the TiO₂ particle or silica particle roughened cotton textiles, which is useful for industrial application of superhydrophobic textiles (Xue *et al.*, 2008a, 2008b, 2009).

Li *et al.* (2008) modified the silica coating with hexadecyltrimethoxysilane on cotton substrate prepared by sol-gel method using water glass.

The achieved product presented superhydrophobicity with a water contact angle higher than 151° . Xu and Cai (2008) modified the ZnO nanorod array film on cotton fabrics with a layer of n-dodecyltrimethoxysilane. The modified cotton fabrics exhibited superhydrophobicity with a contact angle of 161° for 8 μL water droplet and a roll-off angle of 9° for 40 μL water droplet. Most importantly, the hydrolyzed n-dodecyltrimethoxysilane can react with the ZnO seeds, the cotton fibers, and the nanorods. Therefore, the fastness and stability of the ZnO nanorods to the cotton substrate were largely improved.

14.4.3 Hydrophobization with non-fluorinated polymer

Ramaratnam *et al.* (2007) deposited a thin film coating of non-fluorinated hydrophobic polymer, which contains 29 wt% of styrene and 1.4 wt% of reactive maleic anhydride groups, on the poly(ethylene terephthalate) fabric covered with the epoxidized silica nanoparticle, leading to the generation of an ultrahydrophobic textile surface. The coating was permanently anchored to the fiber boundary due to the chemical attachment of the nanoparticles and polymers to the surface.

14.4.4 Hydrophobization with silicon compounds

Hoefnagels (2007) turned normally hydrophilic cotton superhydrophobic by *in situ* introducing silica particles to cotton fibers to generate a dual-size surface roughness, followed by hydrophobization with polydimethylsiloxane. The obtained superhydrophobic textile exhibits a static water contact angle of 155° for a 10 μL droplet. The roll-off angle of water droplets depends on the droplet volume, ranging from 7° for a droplet of 50 μL to 20° for a 7 μL droplet. Li *et al.* (2007) prepared superhydrophobic cellulose-based materials coupled with transparent, stable and nanoscale polymethylsiloxane coating by a simple process via chemical vapor deposition, followed by hydrolyzation and polymerization. In this research, polymethylsiloxane plays the role as not only hydrophobization but also nano-scaled silicone coating.

14.5 Nanoscaled coating of materials with low surface energy

Researches on nanoscaled coating of materials with low surface energy on fibers were also conducted. In this way, roughness and hydrophobicity can be imparted simultaneously onto fibers, making textiles superhydrophobic. Li *et al.* (2007) transformed hydrophilic cellulose into superhydrophobic cellulose by a process via chemical vapor deposition, followed by hydrolyzation

and polymerization. First, a sheet of cotton fabric was cleaned by ultrasonic washing in ethanol and water, respectively, and then dried. Second, the cotton fabric was placed in a sealed chamber for a set time, into which a saturated atmosphere of trichloromethylsilane was introduced. Next, the cotton fabric was withdrawn from the chamber and immersed into an aqueous solution of pyridine at room temperature to hydrolyze the remaining Si-Cl bonds. The cotton fabric was washed with water carefully to remove the excess reagents. Finally, the cotton fabric was treated in an oven at 150°C for 10 min. Subsequent polymerization of Si-OH results in a nanoscaled silicone coating tightly attached to the surface.

Zimmermann *et al.* (2008) prepared superhydrophobic textile fabrics by a one-step gas phase coating procedure by which a layer of polymethylsilsesquioxane nanofilaments was grown onto the individual textile fibers. A total of 11 textile fabrics made from natural and manmade fibers were successfully coated and their superhydrophobic properties evaluated by the water shedding angle technique. A thorough investigation of the commercially relevant poly(ethylene terephthalate) fabric revealed an unparalleled long-term water resistance and stability of the superhydrophobic effect. Because of the special surface geometry generated by the nanoscopic, fibrous coating on the microscopic, fibrous textiles, the coated fabric remains completely dry even after two months of full immersion in water and stays superhydrophobic even after continuous rubbing with a skin simulating friction partner under significant load. Furthermore, important textile parameters such as tensile strength, color and haptics are unaffected by the silicone nanofilament coating.

Zhang *et al.* (2008a) described a simple and economical method of obtaining a superhydrophobic surface on wool textile by a comb-like polymer comprising acrylate and organic siloxane. The combination of acrylate and organic siloxane could exhibit some unique characteristics: first, the acrylate polymer chains could contribute to the increase of the cohesiveness and film forming properties; second, the long Si-O-Si chains, characterized by their low surface energy, could be utilized to enhance the water repellency; third, the Si-O-Si chains could immigrate towards the surface of the outer layers, resulting in forming a surface with roughness in nanosize scale. To achieve this goal, the poly(acrylate-g-siloxane) was prepared by emulsion copolymerization of acrylate with silicone oligomers containing a double bond. After being treated with the resulting emulsion, the wool textile could exhibit excellent superhydrophobicity.

Liu *et al.* (2007) fabricated artificial lotus-leaf structures on cotton substrates via the controlled assembly of carbon nanotubes onto the surface of cotton substrates. Both pristine carbon nanotubes and surface modified carbon nanotubes with poly(butylacrylate) shells were used as building blocks to form artificial structures on cotton similar to a lotus-leaf surface

at the nanoscale. Cotton fabrics have been endowed with superhydrophobic properties.

14.6 Applications

The researches on superhydrophobic textile surfaces are driven by various functional applications. Superhydrophobic coatings on textiles not only can improve the performance of conventional textile materials by surface modification, but also bring about new functions which are not available for the textiles themselves.

14.6.1 Water repellence

In most studies, the waterproofing of textiles is considered to be among the primary potential applications for the superhydrophobic effect. Textiles with a superhydrophobic coating could find applications as water-resistant apparel and be useful for any kind of application where textile surfaces are exposed to the environment. An advantage of superhydrophobic textiles is that the fibrous structure can be maintained to keep the substrate breathable, which is preferable to the traditional waterproof textiles coated with rubbers, plastics, sealing agents or conventional wet-chemical finish using fluorocarbons. Additional benefits of the superhydrophobic effect on textiles could include a plastron layer (Zimmermann *et al.*, 2008). This thin layer of air forms on many natural superhydrophobic surfaces upon immersion in water. On the one hand, the ability to support a plastron layer would prevent wetting of the textile even upon full immersion in water; on the other hand, it would significantly reduce the frictional drag in water. And it is convenient for users to get their mobile marquees, awnings, umbrellas, and so forth with water shedding effect easily stored even after a shower.

14.6.2 Self-cleaning

After some time textile surfaces in a natural environment usually get contaminated. Cleaning them requires extensive effort; additionally, often surfactants are applied with negative effects on the environment. The creation of textiles that can clean themselves or have anti-contamination properties has long been a dream for human beings. These textiles are usually called 'self-cleaning clothes' and the research related to the creation of self-cleaning clothes has been a hot topic for several decades (Liu *et al.*, 2007). In fact, the technology for creating self-cleaning textiles has developed rapidly in recent years. Currently, there are two main techniques used in the production of self-cleaning textiles, which are similar to that of self-cleaning coating (Parkin and Palgrave, 2005). One is the production of surfaces that

can break down, decompose or even ‘digest’ dirt, and another is the production of surfaces with repellent properties. The common route to fabricate both of these two types of self-cleaning textiles is to treat the target textile substrates with self-cleaning coatings. Self-cleaning textiles are divided into two categories: superhydrophobic textiles and hydrophilic textiles with photocatalytic properties for the destruction of organic dirt.

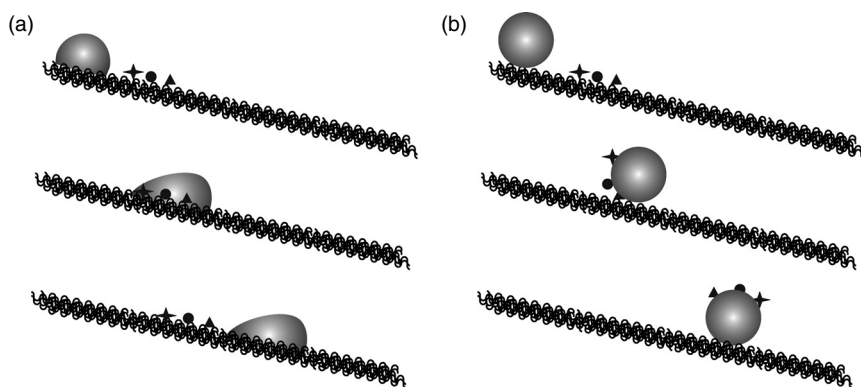
Daoud and Xin (2004) reported the surface treatment of cotton textiles with titania nanoparticles. After using a simple dipping-drying procedure, a thin film of titania nanoparticles was formed on the cotton fiber surface. Owing to the high photocatalytic activity of titania nanoparticles in breaking down dirt molecules, pollutants and micro-organisms, these treated cotton fabrics were expected to be ideal materials for self-cleaning fabrics. This method has been employed by many researchers to fabricate self-cleaning cotton (Bozzi *et al.*, 2005a; Yuranova *et al.*, 2006), polyester (Bozzi *et al.*, 2005b) and wool (Daoud *et al.*, 2008; Tung and Daoud, 2009) textiles.

However, the high photocatalytic activity of the titania nanoparticles also presents several potential problems that must be taken into consideration before these types of self-cleaning textiles are made into commercial products. The first problem with this approach is that photocatalytic coatings generate free radicals under UV irradiation (Linsebigler *et al.*, 1995), and these free radicals might damage human skin, accelerating the ageing of skin and even causing skin cancers (Liu *et al.*, 2007). The other problem with this approach is that these free radicals would probably damage the textile fibers, causing the degradation and decomposition of textiles. As an alternative, a safer strategy is the utilization of repellent coatings to create self-cleaning textiles.

Superhydrophobic textiles with self-cleaning property are prepared mostly based on the ‘lotus effect’ of plants. As shown in Fig. 14.4, when a droplet of water rolls off the surface of superhydrophobic textiles, it takes away the dust on the surfaces, while on normal hydrophobic textiles, the dust remains on the surfaces.

Superhydrophobic textile surfaces with self-cleaning effects have been fabricated by mimicking the behavior of the lotus-leaf and other desert plants, which have rough surfaces combined with hydrophobic surface chemistry. Several approaches described in previous sections of this chapter have been industrialized and transformed into some proprietary technologies. Products with self-cleaning property such as shirts, blouses, skirts and trousers that shrug off ketchup, mustard, red wine and coffee (Forbes, 2008) have already been produced.

With Mincor TX TT, BASF for the first time prepared textiles with a genuine self-cleaning effect based on nanostructured surfaces like its model in nature (Anon, 2007; Steigelmann, 2007). This finishing material endows technical textiles for awnings, sunshades, sails and tents with the



14.4 Water droplets rolling through surfaces with dust on: (a) normal hydrophobic textiles and (b) superhydrophobic textiles with self-cleaning properties.

same self-cleaning effect as the lotus plant. What on the surface of the plant leaves are tiny papillae, on treated textiles are innumerable particles with a diameter of under 100 nm embedded in a carrier matrix. Whether in nature or technology, the effect is the same: these tiny particles keep water droplets and particles of dirt at bay. The dirt particles are carried along by the water droplets and are washed away without the need for detergents or scrubbing. In 2006, polyester awning fabrics finished with Mincor TX TT were very successful in achieving the transition from the laboratory to practical applications, and fabrics for sunshades and sails treated with Mincor TX TT are also promising. Applications of Mincor to washable fabrics, such as cotton, to produce dirt-repellent clothing are also welcome.

Nano-Care (Forbes, 2008) is a finish applied to fabrics developed by inventor and entrepreneur David Soane, now made by his company Nano-Tex. The fabrics made of Nano-Care treated fibers or threads repel molecules of liquid, dirt or perspiration. This idea was inspired by the fuzz on a peach, which was called the Nano-Care effect. Nano-Care's 'fuzz' is made of minuscule whiskers attached to the cotton threads.

Another company, Swiss firm Schoeller Textil AG, calls its technology NanoSphere (Forbes, 2008). The system has nanoscopic particles of silica or of a polymer on the clothing fibers and these particles provide the lotus-like bumpy roughness, making textiles superhydrophobic with self-cleaning effect.

When rain falls on lotus leaves, water beads up with a high contact angle. The water drops promptly roll off the leaves, collecting dirt along the way, leaving the substrates in the original dry state. When self-cleaning textiles become widely available, marquees, awnings, sails, textile roofs in modern architecture, and so forth with lotus effect are expected to constitute the biggest market.

14.6.3 Multifunctionalization

Textiles with more than one function would have their value added, as is true with superhydrophobic textiles. Xue *et al.* (2008a) prepared superhydrophobic textiles with UV-shielding property through incorporation of TiO_2 particles by titania sol coating. Tomšič *et al.* (2008) prepared multifunctional, water- and oil-repellent and anti-microbial finishes for cotton fibers from a commercially available fluoroalkylfunctional water-borne siloxane, nanosized silver and a reactive organic-inorganic binder. Vilčnik *et al.* (2009) fabricated hydrophobic and oleophobic sol-gel coatings with a long-lasting passive anti-bacterial effect for cotton fabrics without the addition of any anti-bacterial agents. The prepared fabrics have long-lasting low-surface-energy values, owing to the excellent adherence of the finishes on cotton fabrics and to the structure of the coatings, with 1H,1H,2H,2H-perfluorooctyltriethoxysilane acting in a specific role. The main cause of the passive anti-bacterial effect of the unwashed fabrics was the ability of the coatings to repel water. In fact, superhydrophobic surfaces have found their application in anti-biofouling (Marmur, 2006; Zhang *et al.*, 2008b) on submerged surfaces, e.g. ships' hulls, because the ability of organisms to adhere to superhydrophobic surfaces is much decreased. Hence, superhydrophobic textiles might also find future application as anti-microbial coatings.

14.7 Future trends

With increased research activities on superhydrophobic surfaces, many efforts have been devoted in the fabrication of superhydrophobic coatings on textiles. Although several publications have revealed the robustness of the superhydrophobic coating on textiles and the durability of superhydrophobicity, there is still much work to be done to put superhydrophobic textiles into real application.

The advantage of using textile substrates to fabricate superhydrophobic surfaces relies on the easy manipulation of a large production area and rich raw materials with many different properties. It is necessary to maintain the properties of the substrate in a way that makes it suitable for its original purpose. Such techniques could result in excellent robustness of coatings with durable superhydrophobicity, without altering the physico-chemical properties, color and hand of the textiles, which would be highly beneficial to the final products.

Again, talking about self-cleaning surfaces, many publications take the example of removing dust by water. But for textiles in application, it is not so simple. First, the contamination is complex, which may not be fly ash but water slurry or kitchen oil. In this case washable or oil-repellent textiles are preferable. Second, the contamination may be caused by heavily pressed

attachment of smudge. In this case, the self-cleaning function will not perform properly on that spot again until the smudge is removed. A lotus-leaf repairs itself after scratch because it has tiny wax crystals on the surface which grow back. Self-healing materials have been prepared in other fields. Fabricating textiles with self-healing superhydrophobicity may not be impossible.

Superhydrophobic textiles with other functions have been fabricated as described earlier in this chapter. Multifunctional textiles are greatly appreciated by a more discerning and demanding consumer market due to the addition of high value, and will be one of the primary investigations on textile functionalization. Surfaces with tunable superhydrophobicity (Bhushan, 2009; Choi *et al.*, 2009) have been reported, which might trigger the investigation of superhydrophobic coatings on textiles with stimulus tunable wettability to fabricate smart textiles.

Finally, environmental issues should be taken into account when preparing superhydrophobic textiles. It has been recognized that some fluorochemicals have potential risks for human health and for the environment. Hence, the development of non-fluorinated modifying agents is preferable for the fabrication of environmentally friendly coatings on textile substrates.

14.8 References

- ANON. (2007) Emulating nature – self-cleaning effects for textiles. *Focus on Surfactants*, 7: 4.
- BAE, G. Y., MIN, B. G., JEONG, Y. G., LEE, S. C., JANG, J. H. and KOO, G. H. (2009) Superhydrophobicity of cotton fabrics treated with silica nanoparticles and water-repellent agent. *Journal of Colloid and Interface Science*, 337(1): 170–175.
- BARTHLOTT, W. and NEINHUIS, C. (1997) Purity of the sacred lotus, or escape from contamination in biological surfaces. *Planta*, 202(1): 1–8.
- BHUSHAN, B. (2009) Biomimetics: lessons from nature—an overview. *Philosophical Transactions of the Royal Society A – Mathematical Physical and Engineering Sciences*, 367(1893): 1445–1486.
- BOZZI, A., YURANOVA, T., GUASQUILLO, I., LAUB, D. and KIWI, J. (2005a) Self-cleaning of modified cotton textiles by TiO₂ at low temperatures under daylight irradiation. *Journal of Photochemistry and Photobiology A-Chemistry*, 174(2): 156–164.
- BOZZI, A., YURANOVA, T. and KIWI, J. (2005b) Self-cleaning of wool-polyamide and polyester textiles by TiO₂-rutile modification under daylight irradiation at ambient temperature. *Journal of Photochemistry and Photobiology A-Chemistry*, 172(1): 27–34.
- CASSIE, A. B. D. and BAXTER, S. (1944) Wettability of porous surfaces. *Transactions of the Faraday Society*, 40: 546–551.
- CHENG, Y. T., RODAK, D. E., WONG, C. A. and HAYDEN, C. A. (2006) Effects of micro- and nano-structures on the self-cleaning behaviour of lotus leaves. *Nanotechnology*, 17(5): 1359–1362.
- CHOI, W., TUTEJA, A., CHHATRE, S., MABRY, J. M., COHEN, R. E. and MCKINLEY, G. H. (2009) Fabrics with tunable oleophobicity. *Advanced Materials*, 21(21): 2190–2195.

- CRICK, C. R. and PARKIN, I. P. (2009) A single step route to superhydrophobic surfaces through aerosol assisted deposition of rough polymer surfaces: duplicating the lotus effect. *Journal of Materials Chemistry*, 19(8): 1074–1076.
- DAOUD, W. A., LEUNG, S. K., TUNG, W. S., XIN, J. H., CHEUK, K. and QI, K. (2008) Self-cleaning keratins. *Chemistry of Materials*, 20(4): 1242–1244.
- DAOUD, W. A. and XIN, J. H. (2004) Nucleation and growth of anatase crystallites on cotton fabrics at low temperatures. *Journal of the American Ceramic Society*, 87(5): 953–955.
- DAOUD, W. A., XIN, J. H. and TAO, X. M. (2004) Superhydrophobic silica nanocomposite coating by a low-temperature process. *Journal of the American Ceramic Society*, 87(9): 1782–1784.
- FORBES, P. (2008) Self-cleaning materials: lotus leaf-inspired nanotechnology. *Scientific American Magazine*, 8, <http://www.scientificamerican.com/article.cfm?id=self-cleaning-materials>.
- GAO, L. C. and MCCARTHY, T. J. (2006) 'Artificial lotus leaf prepared using a 1945 patent and a commercial textile. *Langmuir*, 22(14): 5998–6000.
- HOEFNAGELS, H. F., WU, D., DE WITH, G. and MING, W. (2007) Biomimetic superhydrophobic and highly oleophobic cotton textiles. *Langmuir*, 23(26): 13158–13163.
- HOU, W. X. and WANG, Q. H. (2009) Stable polytetrafluoroethylene superhydrophobic surface with lotus-leaf structure. *Journal of Colloid and Interface Science*, 333(1): 400–403.
- LENG, B. X., SHAO, Z. Z., DE WITH, G. and MING, W. H. (2009) Superoleophobic cotton textiles. *Langmuir*, 25(4): 2456–2460.
- LI, S. H., XIE, H. B., ZHANG, S. B. and WANG, X. H. (2007) Facile transformation of hydrophilic cellulose into superhydrophobic cellulose. *Chemical Communications*, 43(46): 4857–4859.
- LI, Z. X., XING, Y. J. and DAI, J. J. (2008) Superhydrophobic surfaces prepared from water glass and non-fluorinated alkylsilane on cotton substrates. *Applied Surface Science*, 254(7): 2131–2135.
- LINSEBIGLER, A. L., LU, G. Q. and YATES, J. T. (1995) Photocatalysis on TiO_2 surfaces – principles, mechanisms, and selected results. *Chemical Reviews*, 95(3): 735–758.
- LIU, Y. Y., WANG, R. H., LU, H. F., LI, L., KONG, Y. Y., QI, K. H. and XIN, J. H. (2007) Artificial lotus leaf structures from assembling carbon nanotubes and their applications in hydrophobic textiles. *Journal of Materials Chemistry*, 17(11): 1071–1078.
- MARMUR, A. (2003) Wetting on hydrophobic rough surfaces: to be heterogeneous or not to be? *Langmuir*, 19(20): 8343–8348.
- MARMUR, A. (2006) Super-hydrophobicity fundamentals: implications to biofouling prevention. *Biofouling*, 22(2): 107–115.
- MICHELSEN, S. and LEE, H. J. (2007) Design of a superhydrophobic surface using woven structures. *Langmuir*, 23(11): 6004–6010.
- PARKIN, I. P. and PALGRAVE, R. G. (2005) Self-cleaning coatings. *Journal of Materials Chemistry*, 15(17): 1689–1695.
- QU, M. N., ZHAO, G. Y., CAO, X. P. and ZHANG, J. Y. (2008) Biomimetic fabrication of lotus-leaf-like structured polyaniline film with stable superhydrophobic and conductive properties. *Langmuir*, 24(8): 4185–4189.
- RAMARATNAM, K., TSYALKOVSKY, V., KLEP, V. and LUZINOV, I. (2007) Ultrahydrophobic textile surface via decorating fibers with monolayer of reactive nanoparticles and non-fluorinated polymer. *Chemical Communications*, 43: 4510–4512.

- ROACH, P., SHIRTCLIFFE, N. J. and NEWTON, M. I. (2008) Progress in superhydrophobic surface development. *Soft Matter*, 4(2): 224–240.
- SHI, F., NIU, J., LIU, J. L., LIU, F., WANG, Z. Q., FENG, X. Q. and ZHANG, X. (2007) Towards understanding why a superhydrophobic coating is needed by water striders. *Advanced Materials*, 19(17): 2257–2261.
- STEIGELMANN, M. (2007) Emulating nature – self-cleaning effects for textiles. *Science Around Us: A News Service Provided by BASF*, <http://www.basf.com/group/corporate/en/news-and-media-relations/science-around-us/mincor/story>.
- TOMŠIĆ, B., SIMONČIĆ, B., OREL, B., CERNE, L., TAVČER, P. F., ZORKO, M., JERMAN, I., VILČNIK, A. and KOVAC, J. (2008) Sol-gel coating of cellulose fibres with antimicrobial and repellent properties. *Journal of Sol-Gel Science and Technology*, 47(1): 44–57.
- TUNG, W. S. and DAOUD, W. A. (2009) Photocatalytic self-cleaning keratins: a feasibility study. *Acta Biomaterialia*, 5(1): 50–56.
- VILČNIK, A., JERMAN, I., VUK, A. S., KOZELJ, M., OREL, B., TOMŠIĆ, B., SIMONČIĆ, B. and KOVAC, J. (2009) Structural properties and antibacterial effects of hydrophobic and oleophobic sol-gel coatings for cotton fabrics. *Langmuir*, 25(10): 5869–5880.
- WANG, H. X., FANG, J., CHENG, T., DING, J., QU, L. T., DAI, L. M., WANG, X. G. and LIN, T. (2008) One-step coating of fluoro-containing silica nanoparticles for universal generation of surface superhydrophobicity. *Chemical Communications*, 44(7): 877–879.
- WANG, T., HU, X. G. and DONG, S. J. (2007) A general route to transform normal hydrophilic cloths into superhydrophobic surfaces. *Chemical Communications*, 43(18): 1849–1851.
- WENZEL, R. N. (1936) Resistance of solid surfaces to wetting by water. *Industrial and Engineering Chemistry*, 28(8): 988–994.
- WENZEL, R. N. (1949) Surface roughness and contact angle. *Journal of Physical and Colloid Chemistry*, 53(9): 1466–1467.
- WU, X. F. and SHI, G. Q. (2006) Production and characterization of stable superhydrophobic surfaces based on copper hydroxide nanoneedles mimicking the legs of water striders. *Journal of Physical Chemistry B*, 110(23): 11247–11252.
- XU, B. and CAI, Z. S. (2008) Fabrication of a superhydrophobic ZnO nanorod array film on cotton fabrics via a wet chemical route and hydrophobic modification. *Applied Surface Science*, 254(18): 5899–5904.
- XUE, C. H., JIA, S. T., CHEN, H. Z. and WANG, M. (2008a) Superhydrophobic cotton fabrics prepared by sol-gel coating of TiO₂ and surface hydrophobization. *Science and Technology of Advanced Materials*, 9(3): 035001.
- XUE, C. H., JIA, S. T., ZHANG, J. and TIAN, L. Q. (2009) Superhydrophobic surfaces on cotton textiles by complex coating of silica nanoparticles and hydrophobization. *Thin Solid Films*, 517(16): 4593–4598.
- XUE, C. H., JIA, S. T., ZHANG, J., TIAN, L. Q., CHEN, H. Z. and WANG, M. (2008b) Preparation of superhydrophobic surfaces on cotton textiles. *Science and Technology of Advanced Materials*, 9(3): 035008.
- YU, M., GU, G. T., MENG, W. D. and QING, F. L. (2007) Superhydrophobic cotton fabric coating based on a complex layer of silica nanoparticles and perfluorooctylated quaternary ammonium silane coupling agent. *Applied Surface Science*, 253(7): 3669–3673.
- YURANOVA, T., MOSTEO, R., BANDARA, J., LAUB, D. and KIWI, J. (2006) Self-cleaning cotton textiles surfaces modified by photoactive SiO₂/TiO₂ coating. *Journal of Molecular Catalysis A-Chemical*, 244(1–2): 160–167.

- ZHANG, B. T., LIU, B. L., DENG, X. B., CAO, S. S., HOU, X. H. and CHEN, H. L. (2008a) Fabricating superhydrophobic surfaces by molecular accumulation of polysiloxane on the wool textile finishing. *Colloid and Polymer Science*, 286(4): 453–457.
- ZHANG, X., SHI, F., NIU, J., JIANG, Y. G. and WANG, Z. Q. (2008b) Superhydrophobic surfaces: from structural control to functional application. *Journal of Materials Chemistry*, 18(6): 621–633.
- ZHANG, X., SHI, F., YU, X., LIU, H., FU, Y., WANG, Z. Q., JIANG, L. and LI, X. Y. (2004) Polyelectrolyte multilayer as matrix for electrochemical deposition of gold clusters: toward super-hydrophobic surface. *Journal of the American Chemical Society*, 126(10): 3064–3065.
- ZIMMERMANN, J., REIFLER, F. A., FORTUNATO, G., GERHARDT, L.-C. and SEEGER, S. (2008) A simple, one-step approach to durable and robust superhydrophobic textiles. *Advanced Functional Materials*, 18(4): 3662–3669.

Improving superhydrophobic textile materials

H. J. LEE,
North Carolina State University, USA

Abstract: Since the wettability of a solid surface is determined by two parameters, the chemical composition and the geometrical structure of a rough surface, the combination of these two factors are used for the development of superhydrophobic surfaces. In this chapter, the relationships among contact angles, surface tension and surface roughness are reviewed; the physical surface modifications for the design of superhydrophobic surfaces are discussed; the wetting behavior of a rough surface is compared with that of a smooth surface; the relationship between the contact-angle hysteresis and the roll-off angle is analyzed, and the preparation of superhydrophobic surfaces using textile structures is discussed.

Key words: wetting behavior, surface modification, contact angle, surface tension, textile, superhydrophobic, self-cleaning.

15.1 Introduction

Science and technology related to superhydrophobicity have recently attracted considerable attention due to their potential applications in medical devices as well as in industrial materials. The idea of superhydrophobicity was introduced in 1940s by A. Cassie who was interested in enhanced water repellency.¹ This amazing water repellency has been used in the textile industry ever since.

A superhydrophobic surface is defined as having a water contact angle greater than 150° .² The high contact angle is obtained by a combination of surface chemistry and surface roughness, while the roll-off angle depends on the droplet size and the receding contact angle.³ A water droplet easily rolls off a superhydrophobic surface, such as lotus-leaves, washing dirt off in the process and effectively cleaning the surface. This unusual wetting behavior is called self-cleaning or the 'lotus effect' although there are two different types of water-repellent plant leaves: the first type is macroscopically smooth leaves such as the lotus, and the second type is hair-covered leaves such as lady's mantle.⁴ Water droplets completely run off both plant leaves even after heavy rain. Although this phenomenon is observed on other plant leaves besides the lotus plant leaves, the ability has been termed

the lotus effect. For these surfaces, since water droplets roll off easily, they remove dirt off the leaves and effectively keep the surface clean and dry.⁵

This chapter focuses on the physical surface modification and design of superhydrophobic surfaces, compares the wetting behavior of a rough surface with that of a smooth surface, analyzes the relationship between the contact-angle hysteresis and the sliding angles of water droplets, and discusses the preparation of superhydrophobic surfaces using textile structures. Since the wettability of a solid surface is determined by two parameters, the chemical composition and the geometrical structure of a rough surface, the combination of these two factors are used for the development of superhydrophobic surface.⁶ On the other hand, in this chapter, a superhydrophobic rough surface is designed using a plain woven and hydroentangled non-woven structure. In addition, the wetting behavior of the superhydrophobic woven fabric is compared with that of other materials having a flat surface or a rough surface made of a woven fabric with monofilament yarns.

15.2 Physical modification for superhydrophobic textiles

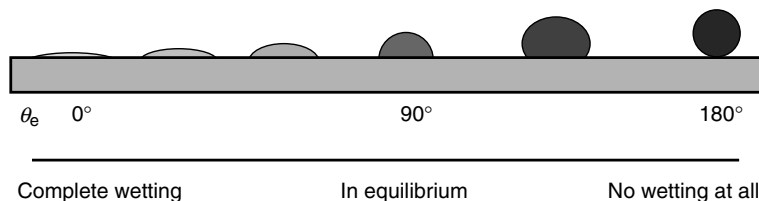
15.2.1 Surface tension and contact angle

Although it is hard to measure the surface tension of a solid directly, it is easy to measure its contact angles (Fig. 15.1). Therefore, the contact angles of polymers and organic layers can be used for the prediction of surface tension and wetting behavior for various liquids.^{7–9}

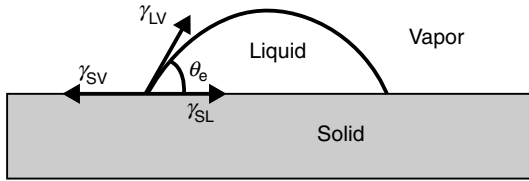
The relation between the surface tension and contact angle is obtained by the Young equation:¹⁰

$$\frac{\gamma_{SV} - \gamma_{SL}}{\gamma_{LV}} = \cos \theta_e \quad [15.1]$$

where γ is the surface tension and SV, SL and LV are the solid–vapor, the solid–liquid and the liquid–vapor interfaces, respectively (Fig. 15.2). According to Young’s equation, the contact angle is a well-defined property that depends on the surface tension coefficients of solid, liquid and gas.



15.1 Contact angle and wettability.



15.2 A drop on a flat surface.

The right-hand side of equation [15.1] and γ_{LV} can be obtained from experimental measurements, leaving two unknowns, γ_{SV} and γ_{SL} . When θ_e for a test liquid $> 20^\circ$, it is assumed that $\gamma_{SV} \approx \gamma_s$ and $\gamma_{LV} \approx \gamma_L$ and equation [15.1] can then be reformulated as:¹¹

$$\frac{\gamma_s - \gamma_{SL}}{\gamma_L} = \cos \theta_e \quad [15.2]$$

Likewise, the thermodynamic work of adhesion, W_{SL}^a , can be explained by the Dupre equation as:

$$W_{SL}^a = \gamma_s^a + \gamma_L^a - \gamma_{SL}^a \quad [15.3]$$

Combining equations [15.2] and [15.3] results in the Dupre–Young equation:

$$W_{SL}^a = \gamma_s^a + \gamma_L^a - \gamma_{SL}^a = \gamma_L^a (1 + \cos \theta) \quad [15.4]$$

According to Fowkes, the interfacial tension between solid and liquid is given by the following equation when only dispersion interactions are present:¹²

$$\gamma_{SL}^{LW} = (\sqrt{\gamma_s^{LW}} - \sqrt{\gamma_L^{LW}})^2 \quad [15.5]$$

The geometric mean of the liquid and solid surface tension is used to calculate the thermodynamic work of Lifshitz–van der Waals (LW) components:¹³

$$W_{SL}^{LW} = 2\sqrt{\gamma_L^{LW} \gamma_s^{LW}} \quad [15.6]$$

Meanwhile, the addition of intermolecular forces at interfaces is equal to a surface tension of a material as shown in equation [15.7].¹⁴

$$\gamma = \gamma^d + \gamma^p + \gamma^H + \gamma^{ind} + \gamma^m + \dots \quad [15.7]$$

where d, p, H, ind and m mean London dispersion forces, permanent dipoles, hydrogen bonds, induced dipoles and metallic interaction, respectively. Since the first three components in equation [15.7] are the major factors

determining the surface tension of most materials, we can use these group contribution methods to calculate γ_s and γ_L :

$$\gamma_s = \gamma_s^d + \gamma_s^p + \gamma_s^H \quad [15.8]$$

$$\gamma_L = \gamma_L^d + \gamma_L^p + \gamma_L^H \quad [15.9]$$

Combining equations [15.4], [15.6], [15.8] and [15.9] gives:

$$\begin{aligned} \gamma_L (1 + \cos \theta) &= \gamma_L^d (1 + \cos \theta) + \gamma_L^p (1 + \cos \theta) + \gamma_L^H (1 + \cos \theta) \\ &= 2(\sqrt{\gamma_s^d \cdot \gamma_L^d} + \sqrt{\gamma_s^p \cdot \gamma_L^p} + \sqrt{\gamma_s^H \cdot \gamma_L^H}) \end{aligned} \quad [15.10]$$

15.2.2 Rough wetting

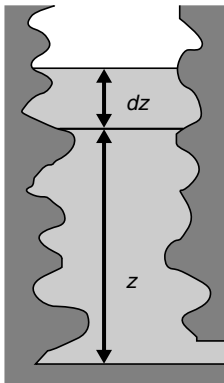
Wettability of rough surfaces

The Young equation is valid for only wetting of smooth surfaces, but real solids are not perfectly flat. The surface structure affects wettability, for example when a surface of solid is superhydrophobic, liquid droplets are in contact with the upper part of a rough surface and the lower part is filled with air. In this chapter, we study the apparent contact angle of a drop deposited on a textured surface, and finally characterize a hydrophobic surface.

Bico *et al.* presented a possible function of the roughness when a textured surface is in contact with liquid as shown in Fig. 15.3.¹⁵ The liquid will be in equilibrium when:

$$(\gamma_{SL} - \gamma_s)(r - \Phi_s) + \gamma_L (1 - \Phi_s) \approx 0 \quad [15.11]$$

since the total liquid quantity z decreases through adsorption when dE/dz is positive and increases when negative.



15.3 Rough surface of a liquid reservoir.

Using the Young equation, equation [15.11] can be reformed as:

$$\cos \theta_r = \frac{1 - \Phi_s}{r - \Phi_s} \quad [15.12]$$

Equation [15.12] defines a critical contact angle between zero and $\pi/2$, since $r \geq 1$ and $\Phi_s \leq 1$. For example, the surface should be completely wet when r approaches one since the contact angle becomes zero, but the contact angle will be close to 90° when $r \gg 1$ or $r > 1$ and $\Phi_s \ll 1$.

Hydrophobicity on rough surfaces

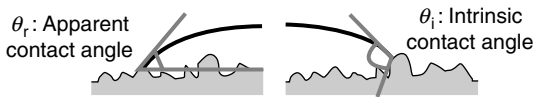
Roughness makes a significant contribution to the wetting behavior of a surface.^{16–18} When the surface is roughened the minimization of liquid surface free energy results in two possible contact angles, the Wenzel apparent contact angle or the Cassie–Baxter apparent contact angle.^{19,20} Figure 15.4 shows the apparent contact angle on a rough surface.

In Wenzel's approach the liquid fills the grooves on the rough surface (Fig. 15.5a). According to Wenzel, the liquid contact angle at a rough surface can be described as:

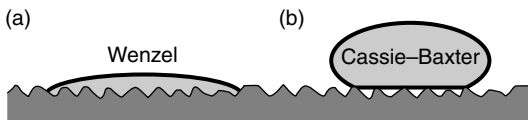
$$\cos \theta_r^w = r \cos \theta_e \quad [15.13]$$

Here, r is the ratio of the total wet area of a rough surface to the apparent surface area in contact with the water droplet ($r > 1$). If the Young contact angle is smaller than a critical contact angle θ_c , the liquid is sucked into contact with the rough surface. According to equation [15.13], for large r , the rough surface is dry when the contact angle on a flat surface exceeds 90° .

The Cassie and Baxter model is an extended form of the Wenzel model to include porous surfaces. In this model a liquid sits on a composite surface made of a solid and air. Therefore, the liquid does not fill the grooves of a



15.4 A drop on a rough surface.



15.5 A liquid drop (a) wetting the grooves of a rough surface (Wenzel model) and (b) sitting at the top of a rough surface (Cassie–Baxter model).

rough solid. In their paper published in 1944, Cassie and Baxter suggested that:

$$\cos \theta_r^{\text{CB}} = f_1 \cos \theta_e - f_2 \quad [15.14]$$

where f_1 is the surface area of the liquid in contact with the solid divided by the projected area, and f_2 is the surface area of the liquid in contact with air trapped in the pores of the rough surface divided by the projected area. When there is no trapped air, f_1 is identical to the value of r in the Wenzel model. Recognizing this, equation [15.14] has recently been rewritten as follows:

$$\begin{aligned} f_1 &= r_f f \\ f_2 &= 1 - f \\ \cos \theta_r^{\text{CB}} &= r_f f \cos \theta_e + f - 1 \end{aligned} \quad [15.15]$$

where f is the fraction of the projected area of the solid surface in contact with the liquid and r_f is defined by analogy with the Wenzel model.²¹ It is important to note that r_f in equation [15.15] is not the roughness ratio of the total surface, but only of that in contact with the liquid. In this form of the Cassie–Baxter equation, the contributions of surface roughness and of trapped air are much clearer than in the other forms of the equation.

Recently, many authors used another approach for the Cassie–Baxter equation to describe contact angles of droplets on heterogeneous rough surfaces that have composite interfaces.²² In the modified Cassie and Baxter model the liquid forms a composite surface made of solid, liquid and air; and the liquid does not fill the grooves on the rough surface (Fig. 15.5b).²³ When the top of a rough surface is completely flat, the following equation describes the apparent contact angle on a rough surface:²⁴

$$\cos \theta_r^{\text{CB}} = \Phi_1 \cos \theta_1 + \Phi_2 \cos \theta_2 \quad [15.16]$$

where θ_r^{CB} is the apparent contact angle at a heterogeneous rough surface composed of two different materials and θ_1 and θ_2 are the droplet contact angles on the two surfaces. A unit area of the surface has a unit surface area fraction Φ_1 with a contact angle θ_1 and an area fraction Φ_2 with a contact angle θ_2 . When this rough surface consists of only two materials $\Phi_2 = 1 - \Phi_1$. If the liquid does not completely wet the surface, Φ_2 represents the trapped air with $\theta_2 = 180^\circ$. Equation [15.14] can be modified as:²⁵

$$\cos \theta_r^{\text{CB}} = \Phi_s (\cos \theta_e + 1) - 1 \quad [15.17]$$

where Φ_s is the ratio of the rough surface area in contact with a liquid drop to the total surface covered by a liquid drop. Smaller Φ_s increases θ_r^{CB} and

makes the surface more hydrophobic. For an apparent contact angle of water on Teflon™ to be greater than 150° (superhydrophobic), the fraction of the surface in contact with water must be less than 26%.²⁶

Modeling of artificial lotus fabric

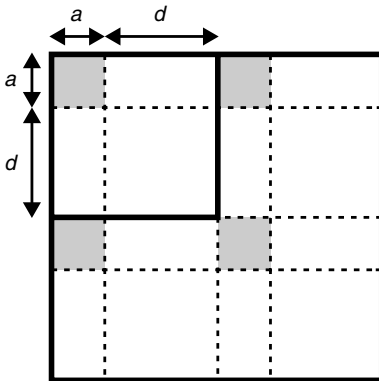
Although most studies of the lotus effect have been carried out on inorganic materials, textile materials having a rough surface can also be superhydrophobic by the lotus effect.^{27,28} In this case, the protruding fibers of woven or knitted fabric, flock fibers of flock fabric, or surface fibers of non-woven fabric can be regarded as grooves of rough surfaces.²⁹ Figure 15.6 shows the upper-sectional view of a roughness pattern when the grooves are thought of as square pillars sticking up from a fabric substrate.^{30,31}

The pillar cross-sectional area is a^2 , the distance between two pillars is d , and the height of pillar is h . In an analysis of the superhydrophobic effect, Patankar has provided two equations to describe the surface based on the Wenzel and the Cassie–Baxter models:^{32,33}

$$\cos\theta_r^w = \left(\left(\frac{a}{a+d} \right)^2 \frac{4h}{a} + 1 \right) \cos\theta_e \quad [15.18]$$

$$\cos\theta_r^{CB} = \left(\frac{a}{a+d} \right)^2 (\cos\theta_e + 1) - 1 \quad [15.19]$$

As a numerical example, if a smooth surface is hydrophobic ($\theta_e = 120^\circ$), the width of a pillar is 10 μm and the height of the pillar is 1 mm, the distance between two pillars, d , has to be $0.014 \text{ mm} < d < 0.24 \text{ mm}$ for a superhydrophobic surface.



15.6 Upper-sectional view of roughness pattern.

15.2.3 Contact-angle hysteresis

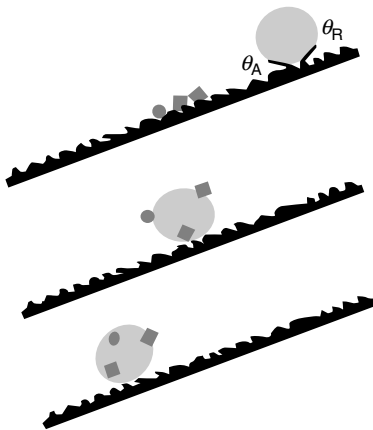
When the volume of a liquid drop placed on the surface is steadily increased until the contact line advances, the contact line begins to move. The contact angle observed when it just begins to move is the advancing contact angle (θ_A). On the other hand, when the liquid droplet is retracted steadily until the contact line recedes, the contact line begins to move again. The contact angle observed when the contact line is just set in motion by this process is defined as the receding contact angle (θ_R).³⁴ Alternatively, if the surface with a drop on it is slightly tilted, the drop remains with different contact angles at the front and the back of the drop. Barthlott and Neihuis suggested that the receding contact angle of a water droplet easily reaches the advancing contact angle on a self-cleaning rough surface when the surface is slightly tilted.³⁵ Thus, the drop easily rolls off this surface, washing dirt off and cleaning the surface in the process as shown in the right side of Fig. 15.7.

Roll-off angle

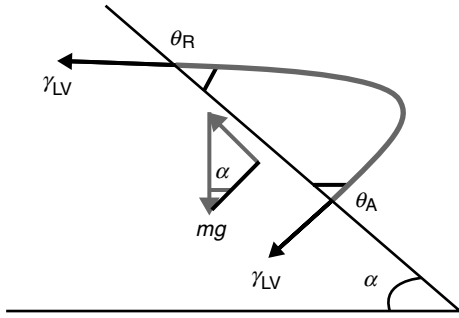
The sliding angle of droplets, α , on smooth surface can be described as:³⁶

$$mg \sin \alpha = k 2 \pi R \quad [15.20]$$

where R is the radius of the contact circle, m is the mass of the droplet, g is the gravitational acceleration and k is a proportionality constant. Roura and Fort demonstrated the work due to the external forces on a drop in Fig. 15.8.³⁷



15.7 Self-cleaning effect by superhydrophobicity.



15.8 Water drops on a tilted surface.

Figure 15.8 shows that the advancing contact angle is always greater than the receding contact angle on a tilted surface. This condition was described by Furmidge as:

$$mg \sin \alpha \approx -2R\gamma_{LV}(\cos \theta_A - \cos \theta_R) \quad [15.21]$$

When the surface is tilted, the sliding angle increases until the drop begins to move and equation [15.21] can be expressed in terms of working energy. As mentioned before, it is assumed that the receding contact angle and the advancing contact angle seem to be close to their minimum and maximum values, respectively, when the drop begins to roll off ($\alpha = \alpha_c$):

$$mg \sin \alpha_c \approx -2R\gamma_{LV}(\cos \theta_{A(max)} - \cos \theta_{R(min)}) \quad [15.22]$$

Equation [15.22] shows an energy balance when the solid surface is progressively inclined and the drop begins to move at α_c . In this situation, gravity can supply the necessary energy to develop the back wetted surface, and thereby the energy used to create a unit area of this surface is $-2R\gamma_{LV}(\cos \theta_{A(max)} - \cos \theta_{R(min)})$. Although the contact angle changes continuously along the contact line, equation [15.22] can be approximately calculated. The constant k in equation [15.20] is related to contact-angle hysteresis and the interfacial surface tension between water and vapor.

When the surface is superhydrophobic and a droplet is very small, the droplet is close to spherical.

$$m = \frac{4}{3}\pi(R')^3 \rho \quad [15.23]$$

where ρ is the density of water and R' is the radius of droplet. By multiplying $g \sin \alpha_c$ to both sides we can describe the relationship between the radius of the contact circle and the radius of droplet sliding on a smooth surface as:

$$mg \sin \alpha_c = \frac{4}{3}\pi(R')^3 \rho g \sin \alpha_c \quad [15.24]$$

Substituting equation [15.24] into equation [15.22], we obtain:

$$\sin \alpha_c = k'(\cos \theta_{A(\max)} - \cos \theta_{R(\min)}) \quad [15.25]$$

where k' is constant. Referring to equation [15.22], k' is related to the radius of the contact circle, the interfacial surface tension between water and vapor, and the contact-angle hysteresis.

Contact-angle hysteresis

Contact-angle hysteresis, $\Delta\theta_H$, is defined as the difference between advancing contact angle, θ_A , and receding contact angle, θ_R , that is $\Delta\theta_H = \theta_A - \theta_R$. The gain factor, which is often used to understand the relationship between contact-angle hystereses and roll-off angle, is considered as the rate of variation of the contact-angle hysteresis at any operating point.³⁸ The Wenzel gain factor graph shows gain factors equal to the roughness factors for the region close to $\theta_e = 90^\circ$, and the gain factors dramatically increase on either side of this region. The Cassie–Baxter gain factors increase from zero to maximum value of one. The Wenzel equation gives a change in the Wenzel contact angle, $\Delta\theta_H^W$, caused by a change in the contact angle on the smooth surface, $\Delta\theta_H$, as:

$$\Delta\theta_H^W = r \left(\frac{\sin \theta_e}{\sin \theta_r^W} \right) \Delta\theta_H = G_e^W \Delta\theta_H \quad [15.26]$$

where G_e^W is the Wenzel gain factor, and is $\partial\theta_r^W / \partial\theta_e$. The gain factor is very useful since it separates the idea of the equilibrium contact angle increase occurring by surface topography from the observed contact angle. Using the Wenzel equation we can obtain the Wenzel gain factor as follows:

$$G_e^W = \frac{r \sin \theta_e}{\sin \theta_r^W} = \frac{r \sin \theta_e}{\sqrt{1 - r^2 \cos^2 \theta_e}} \quad [15.27]$$

When a contact angle θ_e is close to 90° the Wenzel gain factor is approximately unity. Since the effect of roughness is proportional to the radian contact angle changes, the Wenzel gain factor rapidly increases as the roughness factor increases.

Likewise, the Cassie–Baxter equation gives a change in the Cassie–Baxter contact angle, $\Delta\theta_H^{CB}$, caused by a change in the contact angle on the smooth surface, $\Delta\theta_H$, as:

$$\Delta\theta_H^{CB} = \Phi_s \left(\frac{\sin \theta_e}{\sin \theta_r^{CB}} \right) \Delta\theta_H = G_e^{CB} \Delta\theta_H \quad [15.28]$$

In a similar manner as above, a Cassie–Baxter gain factor, G_e^{CB} , can be obtained by the Cassie–Baxter equation as follows:

$$G_e^{CB} = \frac{\Phi_s \sin \theta_e}{\sin \theta_r^{CB}} = \frac{\Phi_s \sin \theta_e}{\sqrt{1 - [\Phi_s (\cos \theta_e + 1) - 1]^2}} \quad [15.29]$$

Since $\Phi_s \leq 1$, $G_e^{CB} \leq 1$. The θ_e used in equations [15.26] and [15.28] can be either the advancing or receding contact angles. Thus, the contact-angle hystereses are:

$$\Delta \theta_H^W = G_e^W \Delta \theta_H \quad [15.30]$$

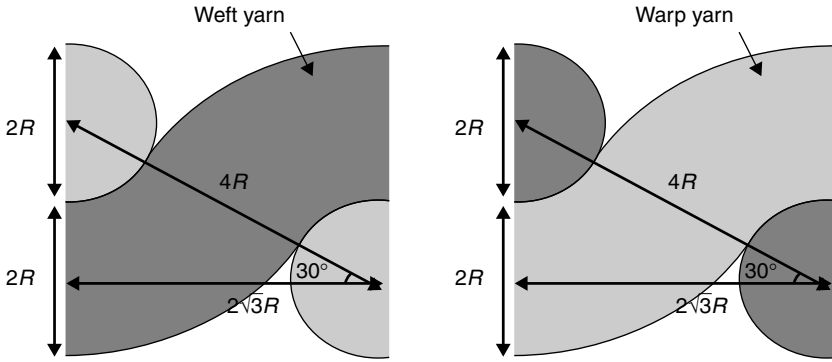
$$\Delta \theta_H^{CB} = G_e^{CB} \Delta \theta_H \quad [15.31]$$

According to McHale, the gain factor, G_e^{CB} , is an attenuation of any contact-angle hysteresis, while hysteresis increases on a Wenzel-type surface. As a numerical example, if the average contact angle on the smooth surface is 70° and the contact-angle hysteresis is 50° , then a roughness factor of 1.9 gives a Wenzel contact angle of 50° and a gain factor of 4.3 so that the hysteresis on the rough surface will be increased to 172° . However, when θ_e is 120° and $\Phi_s = 1\%$ after roughening, a Cassie–Baxter surface gives an apparent contact angle of 162° and a gain factor of 0.03, reducing the contact-angle hysteresis on the rough surface to 9.5° .

15.2.4 Preparation of superhydrophobic rough surfaces

To make a superhydrophobic surface, we first need to make the surface hydrophobic and create the appropriate roughness. As mentioned in the introduction, since $\cos \theta_r^W = r \cos \theta_e$, θ_r^W goes towards 180° when $\theta_e > 90^\circ$ and the surface has proper roughness. In other words, a hydrophobic surface becomes more hydrophobic when roughness, r , increases. Figure 15.9 shows a cross-sectional view of a model of a plain woven fabric made from monofilament yarns. The surface area of a single round monofilament yarn in the unit fabric can be calculated based on Fig. 15.9.

For this rough surface, r is defined using flux integral. As shown in Fig. 15.9, the distance from the center of a weft yarn to the center of an adjacent weft yarn is $4R$; in the same manner, the distance from the center of a warp yarn to the center of an adjacent warp yarn is $4R$; and the distance from the center of a weft yarn to the center of an adjacent warp yarn is $2R$. Hence, according to Pythagoras's theorem, the vector from the center of one weft yarn to the center of an adjacent weft yarn makes a 30° angle to the plane



15.9 The cross-section views of a plain woven fabric: at the warp yarn direction and at the weft yarn direction.

of the fabric. Using flux integral, the area of one yarn in the unit fabric is calculated as:

$$r(u, v) = (2R + R \cos v) \cos ui + (2R + R \cos v) \sin uj + R \cos vk$$

$$r_u = -(2R + R \cos v) \sin ui + (2R + R \cos v) \cos uj$$

$$r_v = -R \sin v \cos ui - R \sin v \sin uj + R \cos vk$$

$$r_u \times r_v = R(2R + R \cos v) \cos u \cos vi + R(2R + R \cos v) \sin u \cos vj + R(2R + R \cos v) \sin vk$$

$$|r_u \times r_v| = R(2R + R \cos v)$$

$$A_{\text{yarn in unit area}} = \frac{\int_0^{2\pi} \int_0^{2\pi} R(2R + R \cos v) du dv}{3}$$

$$A_{\text{yarn in unit area}} = \frac{8\pi^2 R^2}{3} = A_{\text{weft yarn in unit area}} = A_{\text{warp yarn in unit area}} \quad [15.32]$$

where R is the radius of yarn, A is the area, i, j and k are the vectors to x, y , and z axis directions, respectively, and u and v are the notations for the variables of integration. Then, we determine the true fabric surface area as follows:

$$A_{\text{fabric}}^{\text{real}} = A_{\text{weft yarn in unit area}} + A_{\text{warp yarn in unit area}} \quad [15.33]$$

where $A_{\text{fabric}}^{\text{real}}$ is the intrinsic area of the unit fabric determined by the area of yarn surfaces. We have two yarns in the unit area. Substituting equation [15.32] into equation [15.33] gives:

$$A_{\text{fabric}}^{\text{real}} = 52.64R^2 \quad [15.34]$$

The apparent surface area is just equal to the area of a plane tangent to the top surface.

$$A_{\text{fabric}}^{\text{apparent}} = 2\sqrt{3}R \times 2\sqrt{3}R = 12R^2 \quad [15.35]$$

where $A_{\text{fabric}}^{\text{apparent}}$ is the apparent area of the unit fabric shown in Fig. 15.9. Finally, the roughness, r , is just the ratio of these areas:

$$r = \frac{A_{\text{fabric}}^{\text{real}}}{A_{\text{fabric}}^{\text{apparent}}} = \frac{52.64R^2}{12R^2} = 4.39 \quad [15.36]$$

Next, we look at a plain woven fabric made of multifilament yarns. Clearly, a multifilament yarn will have even higher values of r , since the space between the fibers will increase the real surface area while the apparent surface area remains the same. In this case, equation [15.32] becomes:

$$A_{\text{fabric}}^{\text{real}} = A_{\text{multi}} \approx 52.64R \times NR_f \quad [15.37]$$

where N is the number of filament fibers, R is the radius of the yarn, and R_f is the radius of the filament fibers. Substituting equation [15.37] into equation [15.36] yields:

$$r = \frac{A_{\text{fabric}}^{\text{real}}}{A_{\text{fabric}}^{\text{apparent}}} \approx \frac{4\pi NR_f}{3R} = 4.39 \frac{NR_f}{R} \quad [15.38]$$

When $N = 1$, $R_f = R$. Otherwise, $R_f < R$ but $NR_f > R$. For example, a plain woven fabric could have $R \approx 150 \mu\text{m}$, $N > 70$, and $R_f \approx 10 \mu\text{m}$. Substituting these values into equation [15.38] gives $r > 20.48$. Since $r > 20.48$ for the multifilament fabric, we again expect that the surface is rough enough to be superhydrophobic when $\theta_e \geq 92.5^\circ$ for this plain woven fabric.

According to Cassie and Baxter, the Wenzel model is a special case of the Cassie–Baxter equation where $f_2 = 0$ in equation [15.14]. For a material with a smooth surface water contact angle of 93° , for example, the Wenzel surface roughness, r , must be greater than 16.5 for the apparent contact angle to exceed 150° . However, according to Marmur, the minimization of the free energy requires that, for a hydrophobic surface with $f = 1$, $\theta_e = 180^\circ$ in equation [15.15]. Since the only material known with $\theta_e = 180^\circ$ is air or vacuum,

f cannot be equal to one. In other words, the Wenzel model is invalid for hydrophobic surfaces. In order to develop superhydrophobic surfaces, we need to use a different approach, namely the Cassie–Baxter model.

We begin with an analysis of f , the fraction of the projected area in contact with the water droplet. For parallel cylinders viewed normal to the cylinders' axes there are two cases: (a) the cylinders are packed tightly together, or (b) they are separated by some distance, as shown in Fig. 15.10. In case (a), the distance from the center on one cylinder to the center of the next is $2R$, where R is the radius of the cylinder. In case (b), by analogy, the center-to-center distance is considered to be $2(R + d)$. In case (a), Marmur showed that $f = \sin \alpha$ where α is the angle between the top of the cylinder and the liquid contact line and $\alpha = \pi - \theta_e$. In case (b), $f = R \sin \alpha / (R + d)$; and in both cases, $r_f = \alpha / \sin \alpha$. Therefore, using simple differentials we obtain $d(f r_f) / df = (\cos \alpha)^{-1}$ and $d^2(f r_f) / df^2 > 0$ in both (a) and (b). According to Marmur, under these conditions, there is a minimum surface free energy on each surface such that $\alpha = \pi - \theta_e$. Substitution of f and r_f with the case (b) into equation [15.15] results in:

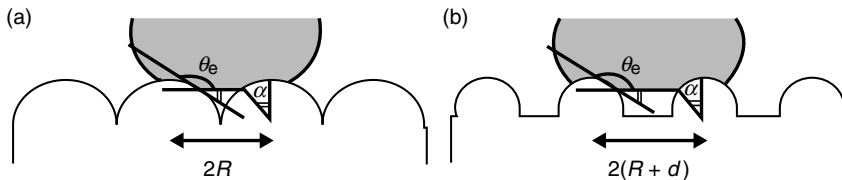
$$\cos \theta_r^{\text{CB}} = - \left(\frac{R}{R+d} \right) \alpha \cos \alpha + \left(\frac{R}{R+d} \right) \sin \alpha - 1 \quad [15.39]$$

On substituting $\pi - \theta_e$ for α , we obtain:

$$\cos \theta_r^{\text{CB}} = \left(\frac{R}{R+d} \right) (\pi - \theta_e) \cos \theta_e + \left(\frac{R}{R+d} \right) \sin \theta_e - 1 \quad [15.40]$$

For $\theta_e > 90^\circ$, θ_r^{CB} increases with increasing d . For example, when $\theta_e = 120^\circ$ and $d = 0$, the fibers are closely packed and $\theta_r^{\text{CB}} = 131^\circ$; for $d = R$, $\theta_r^{\text{CB}} = 146^\circ$; and for $d = 2R$, $\theta_r^{\text{CB}} = 152^\circ$.

We consider two cases for solving equation [15.40]. First, we solve it for a monofilament plain woven fabric shown in Fig. 15.9. Again, according to Pythagoras's theorem, the angle that a weft yarn (or warp yarn) makes with the fabric plane in traveling from one warp yarn (or weft yarn) to another is 30° . Therefore, the distance from the top of a weft yarn (or warp yarn) to the top of an adjacent warp yarn (or weft yarn) is $2\sqrt{3}R$. From this geometric consideration, the center-to-center distance of adjacent cylinders in



15.10 A liquid drop sitting on (a) cylinders packed tightly and (b) cylinders separated by a distance, $2d$. $\alpha = \pi - \theta_e$.

Table 15.1 Comparison of predicted and measured apparent contact angles of hydrophobic and superhydrophobic woven surfaces

Sample	Apparent contact angle (degree)	
	Fluoroamine-grafted nylon woven fabric	
	Predicted	Measured
Monofilament woven fabric	$118 \leq \theta_r \leq 134$	$130 \leq \theta_r \leq 138$
Multifilament yarn	$123 \leq \theta_r \leq 138$	N/M*
Multifilament woven fabric	$146 \leq \theta_r \leq 158$	$160 \leq \theta_r \leq 168$

* Not measured.

equation [15.40], $2(R + d)$, is equal to $2\sqrt{3}R$, and $f = \sin \alpha / \sqrt{3}$. Substituting these values into equation [15.40] along with the measured contact angles from the flat nylon films, we find $118^\circ \leq \theta_r^{\text{CB}} \leq 134^\circ$ for the fluoroamine grafted monofilament woven fabric. These values are in good agreement with the measured values shown in Table 15.1.

In the second case, we again extend the analysis to a multifilament fabric. We begin by determining the apparent contact angle of the liquid with the multifilament yarns. For example, if the fiber spacing is approximately equal to the fiber diameter, that is $2d \approx 2R_f$, where R_f is the fiber radius, substituting R_f for R and d into equation [15.40] carries out θ_r^{CB} ranging from 123° to 138° for the fluoroamine-grafted single fiber. Then, using these values as the effective contact angles for the yarns in the woven structure and re-solving equation [15.40] with R being the yarn radius and $d = R(\sqrt{3} - 1)$ such that $2(R + d) = 2\sqrt{3}R$ as before. We obtained $146^\circ \leq \theta_r^{\text{CB}} \leq 158^\circ$ for the fluoroamine-grafted fabric. As seen in Table 15.1, the measured values are slightly larger than our predicted values. This is probably due to the real value of d being larger than the values chosen in this analysis.

15.3 Applications

15.3.1 Research review

Over the last 15 years, many studies of superhydrophobicity and contact-angle hysteresis have been performed. Recently, Zhu *et al.* developed a superhydrophobic surface by electrospinning using a hydrophilic material, poly(hydroxybutyrate-co-hydroxyvalerate) (PHBV).³⁹ Gao and McCarthy made artificial superhydrophobic surfaces with conventional polyester and microfiber polyester fabrics rendered hydrophobic by using a simple patented water-repellent silicone coating procedure.⁴⁰ Lee and

Michielsens developed superhydrophobic surfaces via the flocking process and achieved contact angles as high as 178° .⁴¹ Jopp *et al.* researched the wetting behavior of water droplets on periodically structured hydrophobic surfaces and the effect of structure geometry.⁴² Liu *et al.* studied the creation of stable superhydrophobic surfaces using vertically aligned carbon nanotubes.⁴³ Nakajima *et al.* prepared superhydrophobic thin films with TiO_2 photocatalyst by coating a fluoroalkyl silane onto the original films.⁴⁴ Zhai *et al.* demonstrated that the superhydrophobic behavior of the lotus leaf structure can be achieved by creating a semifluorinated silane coated polyelectrolyte multilayer surface.⁴⁵ Han *et al.* created a superhydrophobic surface using a block copolymer micelle solution and silica nanoparticles. He also provided a strategy for the fabrication of a wettability-controlled organic–inorganic hybrid. Many other studies of superhydrophobicity have been accomplished in inorganic materials.⁴⁶ Huang *et al.* showed a superhydrophobic surface from nanostructure materials can be applied to microfluidic devices by preparing a stable superhydrophobic surface via aligned carbon nanotubes (CNTs) coated with a zinc oxide (ZnO) thin film.⁴⁷ Shang *et al.* prepared optically transparent superhydrophobic silica-based films on glass substrates by making a nanoscale rough surface using nanoclusters and nanoparticles.⁴⁸ Shi *et al.* obtained a superhydrophobic surface by modifying a silver covered silicon wafer with a self-assembled monolayer of n-dodecanethiol.⁴⁹ Although most studies of the lotus effect have been carried out on inorganic materials, organic composite materials having a rough surface can also be superhydrophobic by using the lotus effect. Jeong *et al.* fabricated micro/nanoscale hierarchical structures using a molding technique.⁵⁰ To modify an organic film surface and create superhydrophobicity, Kim *et al.* used He plasma and CF_x nanoparticle coatings and Fresnais *et al.* applied CF_4 and O_2 plasma.^{51,52}

15.3.2 New product development

Successful product design and development result in products that can be sold profitably. However, profitability is often difficult to evaluate quickly and directly. The following five specific dimensions related to profit can be used to evaluate the performance of product design and development: product quality, product cost, development time, development cost and market feasibility. Since these factors present huge challenges for product designers, only a few companies are successful in their product development in high-tech product markets. In developing new high-tech textile products based on such excellent superhydrophobic materials or the surface modifying technologies introduced in this research, the product designer should search potential markets in which to apply the developed materials or technologies. For new high-tech product designs, the new materials or technologies

should fit easily into existing products or processes. Therefore, new product development often uses modifications of generic materials to easily access the potential markets.

15.3.3 Market approach

Superhydrophobic textile fabrics developed in this research can be used as new platform products. Platform products are generally built near an existing technological system. The technology platform shown in the previous section has already demonstrated its usefulness in mass production and its huge potential for the existing markets as well as new markets. Therefore, product design built on a technology platform is simpler than product design built on technology-push products. In designing a new technology-push product, a designer begins to work with a novel material or a unique technology to look for potential markets where the material or the technology can be applied. The potential markets for the new products consisting of self-cleaning surfaces are shown in Table 15.2.

The product design cannot be successful if the technology does not offer a clear competitive advantage satisfying customers' needs. For example, stain-release children's wear has to maintain soft hand, dimensional stability after 30 launderings, and colorfastness to saliva and perspiration. Self-cleaning convertible tops have to consist of coating materials having good durability after car washing, sunlight and high or low temperature exposure. Self-cleaning roofs have to be well designed to enhance the lotus effect while maintaining the original external appearance. Superhydrophobic-oleophobic surgical gowns need materials having appropriate softness, high thermal conductivity and perspiration permeability. In developing artificial organs, it is important to design the new products while considering the biocompatibility for their applications. Therefore, the prototype

Table 15.2 Potential markets and new products using self-cleaning technologies

Potential markets	Possible new products
Protective equipment	Self-cleaning outerwear, shoes, bags, individual and collective protection gear
Residential interiors and exteriors	Self-cleaning outdoor furniture, windows, roofs; Stain-release carpets, paint, wallpaper, etc.
Automotive interiors and exteriors	Self-cleaning auto glass, body shells, convertible tops
Biomedical textiles	Oil and water-release medical gowns, stain-release bed clothes; artificial organs such as blood vessels and scaffold, etc.

samples of new biotextile products have to be evaluated through *in vitro* and *in vivo* tests.

15.4 Future trends

Wetting behavior of solid materials has recently attracted a great deal of interest from both academia and industry. This interest extends beyond the bio-inspired, lotus leaf property of superhydrophobicity to materials that exhibit similar properties to oils, thus dubbed superoleophobic properties. The applications of such materials are far-reaching and include medical clothing, protective gear and high performance technical textiles. As a surface with a water contact angle exceeding 150° is called a superhydrophobic surface, we define a surface having an oil contact angle over 150° as a superoleophobic surface. Since the wettability of a solid surface is determined by two parameters, the chemical composition and the geometrical structure of a rough surface, the combination of these two factors can also be used for the development of a superoleophobic surface.

In order to design a superoleophobic surface, two predominant rough wetting models are used: the Wenzel model and the Cassie–Baxter model. In the Wenzel model a liquid fills the grooves of a rough surface and completely wets the surface, while in the Cassie–Baxter model, a liquid sits on top of the surface and repels the liquid. As mentioned, to create a Cassie–Baxter surface, the Young contact angle of a liquid, θ_e , must be greater than 90° . Analysis of the Cassie–Baxter model for assessing feasibility of superoleophobicity yields equation [15.10]. Since the surface tensions of dodecane and most polymeric surfaces are determined by London dispersion forces, this equation can be simplified to:

$$\gamma_L (1 + \cos \theta_e) = 2\sqrt{\gamma_s \cdot \gamma_L} \quad [15.41]$$

Substituting $\gamma_L = 25.4$ dyne/cm for dodecane into equation [15.41] suggests γ_s must be smaller than 6.35 dyne/cm, and a smooth surface having $\gamma_s \leq 6.35$ dyne/cm can be oleophobic ($\theta_e > 90^\circ$). Since most solid surfaces typically possess $\gamma_s > 6.35$ dyne/cm, the Cassie–Baxter model does not allow for permanent superoleophobicity under normal circumstances. On a metastable Cassie–Baxter surface, a liquid initially sits on top of the surface due to the minimization of surface energy caused by air pockets inside the grooves of the rough surface. However, the liquid is drawn into contact with the rough surface over time, with the time to absorption being dependent on the surface tension and volume of the liquid, and the surface tension and surface morphology of the solid. Hence, a superoleophobic surface can be produced by designing a metastable Cassie–Baxter surface.

15.5 References

1. CASSIE, A. B. D. and BAXTER, S., Large contact angles of plant and animal surfaces. *Nature (London)*, 155 (1945): 21–22.
2. WU, X. and SHI, G., Production and characterization of stable superhydrophobic surfaces based on copper hydroxide nanoneedles mimicking the legs of water striders. *Journal of Physical Chemistry B*, 110 (2006): 11247–11252.
3. NEINHUIS, C. and BARTHLOTT, W., Characterization and distribution of water-repellent, self-cleaning plant surfaces. *Annals of Botany*, 79 (1997): 667–677.
4. OTTEN, A. and HERMINGHAUS, S., How plants keep dry: a physicist's point of view. *Langmuir*, 20 (2004): 2405–2408.
5. FUERSTNER, R., BARTHLOTT, W., NEINHUIS, C. and WALZEL, P., Wetting and self-cleaning properties of artificial superhydrophobic surfaces. *Langmuir*, 21 (2005): 956–961.
6. NICOLAS, M., GUITTARD, F. and GERIBALDI, S., Stable superhydrophobic and lipophobic conjugated polymers films. *Langmuir*, 22 (2006): 3081–3088.
7. LEE, H. J. and MICHELSEN, S., Lotus effect: superhydrophobicity. *Journal of the Textile Institute*, 97 (2006): 455–462.
8. MICHELSEN, S. and LEE, H. J., Design of a superhydrophobic surface using woven structures. *Langmuir*, 23 (2007): 6004–6010.
9. LEE, H. J. and OWENS, J. R., Design of superhydrophobic ultraoleophobic NyCo. *Journal of Materials Science*, 45 (2010): 3247–3253.
10. PAL, S., WEISS, H., KELLER, H. and MUELLER-PLATHE, F., Effect of nanostructure on the properties of water at the water-hydrophobic interface: a molecular dynamics simulation. *Langmuir*, 21 (2005): 3699–3709.
11. BALKENEDE, A. R., VAN DE BOOGAARD, H. J. A. P., SCHOLTEN, M. and WILLARD, N. P., Evaluation of different approaches to assess the surface tension of low-energy solids by means of contact angle measurements. *Langmuir*, 14 (1998): 5907–5912.
12. FOWKES, F. M., Additivity of intermolecular forces at interfaces. I. determination of the contribution to surface and interfacial tensions of dispersion forces in various liquids. *Journal of Physical Chemistry*, 67 (1963): 2538–2541.
13. OSTROVSKAYA, L., PODESTA, A., MILANI, P. and RALCHENKO, V., Influence of surface morphology on the wettability of cluster-assembled carbon films. *Europhysics Letters*, 63 (2003): 401–407.
14. BARTON, A. F. M., *CRC Handbook of Solubility Parameters and Other Cohesion Parameters*. Boca Raton, FL: CRC Press, Inc., 1983.
15. BICO, J., TORDEUX, C. and QUERE, D., Rough wetting. *Europhysics Letters*, 55 (2001): 214–220.
16. YOSHIMITSU, Z., NAKAJIMA, A., WATANABE, T. and HASHIMOTO, K., Effects of surface structure on the hydrophobicity and sliding behavior of water droplets. *Langmuir*, 18 (2002): 5818–5822.
17. SUN, T., FENG, L., GAO, X. and JIANG, L., Bioinspired surfaces with special wettability. *Accounts of Chemical Research*, 38 (2005): 644–652.
18. ROSARIO, R., GUST, D., GARCIA, A. A., HAYES, M., TARACI, J. L., CLEMENT, T., DAILEY, J. W. and PICRAUX, S. T., Lotus effect amplifies light-induced contact angle switching. *Journal of Physical Chemistry B*, 108 (2004): 12640–12642.

19. SUN, M., LUO, C., XU, L., JI, H., OUYANG, Q., YU, D. and CHEN, Y., Artificial lotus leaf by nanocasting. *Langmuir*, 21 (2005): 8978–8981.
20. ZHENG, Q., YU, Y. and ZHAO, Z., Effects of hydraulic pressure on the stability and transition of wetting modes of superhydrophobic surfaces. *Langmuir*, 21 (2005): 12207–12212.
21. MARMUR, A., Wetting on hydrophobic rough surfaces: to be heterogeneous or not to be? *Langmuir*, 19 (2003): 8343–8348.
22. WU, X., ZHENG, L. and WU, D., Fabrication of superhydrophobic surfaces from microstructured zno-based surfaces via a wet-chemical route. *Langmuir*, 21 (2005): 2665–2667.
23. ZHAO, X., JIANG, P., XIE, S., FENG, J., GAO, Y., WANG, J., LIU, D., SONG, L., LIU, L., DOU, X., LUO, X., ZHANG, Z., XIANG, Y., ZHOU, W. and WANG, G., Patterned anodic aluminium oxide fabricated with a Ta mask. *Nanotechnology*, 17 (2006): 35–39.
24. KRUPENKIN, T. N., TAYLOR, J. A., SCHNEIDER, T. M. and YANG, S., From rolling ball to complete wetting: the dynamic tuning of liquids on nanostructured surfaces. *Langmuir*, 20 (2004): 3824–3827.
25. MCHALE, G., AQIL, S., SHIRTCLIFFE, N. J., NEWTON, M. I. and Erbil H. Y., Analysis of droplet evaporation on a superhydrophobic surface. *Langmuir*, 21 (2005): 11053–11060.
26. KIM, J. and KIM, C. J., A surface-tension driven micropump for low voltage and low power operations. *Microelectromechanical Systems*, 11 (2002): 454–461.
27. MA, M., MAO, Y., GUPTA, M., GLEASON, K. K. and RUTLEDGE, G. C., Superhydrophobic fabrics produced by electrospinning and chemical vapor deposition. *Macromolecules*, 38 (2005): 9742–9748.
28. SINGH, A., STEELY, L. and ALLCOCK, H. R., Poly[bis(2,2,2-trifluoroethoxy)phosphazene] superhydrophobic nanofibers. *Langmuir*, 21 (2005): 11604–11607.
29. VOGELAAR, L., LAMMERTINK, R. G. H. and WESSLING, M., Superhydrophobic surfaces having two-fold adjustable roughness prepared in a single step. *Langmuir*, 22 (2006): 3125–3130.
30. HE, B., PATANKAR, N. A. and LEE, J., Multiple equilibrium droplet shapes and design criterion for rough hydrophobic surfaces. *Langmuir*, 19 (2003): 4999–5003.
31. DUPUIS, A. and YEOMANS, J. M., Modeling droplets on superhydrophobic surfaces: equilibrium states and transitions. *Langmuir*, 21 (2005): 2624–2629.
32. PATANKAR, N. A., On the modeling of hydrophobic contact angles on rough surfaces. *Langmuir*, 19 (2003): 1249–1253.
33. LEE, J., HE, B. and PATANKAR, N. A., A roughness-based wettability switching membrane device for hydrophobic surfaces. *Journal of Micromechanics and Microengineering*, 15 (2005): 591–600.
34. WANG, X. D., PENG, X. F., LU, J. F., LIU, T. and WANG, B. X., Contact angle hysteresis on rough solid surfaces. *Heat Transfer – Asian Research*, 33 (2004): 201–210.
35. BARTHOLOTT, W. and NEIHUIS, C., Purity of the sacred lotus, or escape from contamination in biological surfaces. *Planta*, 202 (1997): 1–8.
36. MIWA, M., NAKAJIMA, A., FUJISHIMA, A., HASHIMOTO, K. and WATANABE, T., Effects of the surface roughness on sliding angles of water droplets on superhydrophobic surfaces. *Langmuir*, 16 (2004): 5754–5760.
37. ROURA, P. and FORT, J., Effects of the surface roughness on sliding angles of water droplets on superhydrophobic surfaces. *Langmuir*, 18 (2002): 566–569.

38. MCHALE, G., SHIRTCLIFFE, N. J. and NEWTON, M. I., Contact-angle hysteresis on super-hydrophobic surfaces. *Langmuir*, 20 (2004): 10146–10149.
39. ZHU, M., ZUO, W., YU, H., YANG, W. and CHEN, Y., Superhydrophobic surface directly created by electrospinning based on hydrophilic material. *Journal of Materials Science*, 41 (2006): 3793–3797.
40. GAO, L. and MCCARTHY, T. J., ‘Artificial Lotus Leaf’ prepared using a 1945 patent and a commercial textile. *Langmuir*, 22 (2006): 5998–6000.
41. LEE, H. J. and MICHIENSEN, S., Preparation of a superhydrophobic rough surface. *Journal of Polymer Science. Part B: Polymer Physics*, 45 (2007): 253–261.
42. JOPP, J., GRUELL, H. and YERUSHALMI-ROZEN, R., Wetting behavior of water droplets on hydrophobic microtextures of comparable size. *Langmuir*, 20 (2004): 10015–10019.
43. LAU, K. K. S., BICO, J., TEO, K. B. K., CHHOWALLA, M., AMARATUNGA, G. J., MILNE, W. I., MCFINLEY, G. H. and GLEASON, K. K., Superhydrophobic carbon nanotube forests. *Nano Letters*, 3 (2003): 1701–1705.
44. NAKAJIMA, A., HASHIMOTO, K. and WATANABE, T., Transparent superhydrophobic thin films with self-cleaning properties. *Langmuir*, 16 (2005): 7044–7047.
45. ZHAI, L., CEBECI F. C., ROBERT, E. C. and RUBNER, M. F., Stable superhydrophobic coatings from polyelectrolyte multilayer. *Nano Letters*, 4 (2004): 1349–1353.
46. HAN, J. T., XU, X. and CHO, K., Diverse access to artificial superhydrophobic surfaces using block copolymers. *Langmuir*, 21 (2005): 6662–6665.
47. HUANG, L., LAU, S. P., YANG, H. Y., LEONG, E. S. P. and YU, S. F., Stable superhydrophobic surface via carbon nanotubes coated with a ZnO thin film. *Journal of Physical Chemistry B*, 109 (2005): 7746–7748.
48. SHANG, H. M., WANG, Y., LIMMER, S. J., CHOU, T. P., TAKAHASHI, K. and CAO, G. Z., Optically transparent superhydrophobic silica-based films. *Thin Solid Films*, 472 (2005): 37–43.
49. SHI, F., SONG, Y., NIU, J., XIA, X., WANG, Z. and ZHANG, X., Facile method to fabricate a large-scale superhydrophobic surface by galvanic cell reaction. *Chemical Materials*, 18 (2006): 1365–1368.
50. JEONG, H. E., LEE, S. H., KIM, J. K. and SUH, K. Y., Nanoengineered multiscale hierarchical structures with tailored wetting properties. *Langmuir*, 22 (2006): 1640–1645.
51. KIM, S. H., KIM, J., KANG, B. and UHM, H., Superhydrophobic CF_4 coating via in-line atmospheric RF plasma of $\text{He}-\text{CF}_4-\text{H}_2$. *Langmuir*, 21 (2005): 12213–12217.
52. FRESNAIS, J., CHAPEL, J. P. and PONCIN-EPAILARD, F., Synthesis of transparent superhydrophobic polyethylene surfaces. *Surface and Coatings Technology*, 200 (2006): 5296–5305.

Antibacterial textile materials for medical applications

G. SUN,

University of California, Davis, USA

Abstract: This chapter discusses antimicrobial textiles for medical applications with focuses on proper antimicrobial performance, application requirements and expected benefits of the functional medical textiles. Several major antimicrobial agents and technologies for medical textiles, including quaternary ammonium salts, silver and other metals and halamine compounds, are discussed. Photo-sensitive antimicrobial agents, such as titanium dioxide and dyes, are outlined as new antimicrobial technologies. The trends of future development in this area are addressed based on different applications in medical textiles.

Key words: antimicrobial textiles, reusable and disposable, medical textiles, durable.

16.1 Introduction

Antimicrobial textiles have attracted a lot of research activities in recent years, with the goals of reducing transmission of infectious diseases and improving the life quality of human beings. Textile materials for medical applications have particular requirements on antimicrobial performance in terms of killing power, speed and effectiveness against the range of micro-organisms such as bacteria, viruses and even spores, which are quite different from the needs for consumer products. Various biocides are also available with claimed antimicrobial functions against pathogens when applied onto fabrics and fibers. The chapter provides detailed discussions of antimicrobial performance, application requirements and expected benefits of the functional medical textiles. As examples, the performance and limitations of quaternary ammonium salts (QAS), silver and other metals, halamine compounds and their treated fabrics are discussed in detail. Some latest approaches using photo-induced agents, such as titanium dioxide and dyes, are outlined as new antimicrobial technologies. The trends of future development in this area are addressed based on different applications in medical textiles.

16.2 Principles of antimicrobial textiles

16.2.1 Medical textiles and transmission of diseases

Medical textiles include healthcare worker uniforms, patient dresses, linens, wipes, wraps and, more importantly, surgical gowns and drapes. Most medical textiles such as uniforms, surgical gown and drapes are used as a physical barrier to protect healthcare personnel and patients from transmission of diseases. According to the fabric materials used in the medical textile products, non-woven and woven fabrics are the two options, which also lead to so-called disposable (single use) and reusable materials based on use patterns. Most doctors' uniforms, linens, patient and nurse dresses are made of woven fabrics and are reusable products, which should be repeatedly disinfected and laundered after wearing. Surgical gowns, drapes and wraps can be made by either woven or non-woven fabrics, and thus are either single use or reusable products. After usage, reusable ones are disinfected, washed and then sterilized for reuse, while disposable ones will be sterilized for disposal.

Current medical textiles are primarily serving as a defensive barrier for wearers to prevent penetration of potentially infectious liquids and particles through the system, regardless of the fabric structures. Improved biological protections and increased barrier performance of the medical textiles lead to increased heat stress to wearers as a result. Moreover, barrier textiles can block the penetration of liquids but cannot completely protect healthcare workers and patients from infections, because micro-organisms can survive on textiles for days or even months, which can still cause transmission and infection to humans (Neely, 2000; Neely and Maley, 2000; Neely and Orloff, 2001; Treacle *et al.*, 2009; Wilson *et al.*, 2007; Yazgi *et al.*, 2009). Contact transmission of diseases is one of the most important routes of hospital-related infections (Lingaas and Fagernes, 2009). Recent studies on medical white coats revealed that many uniforms worn by doctors, nurses and healthcare personnel do carry *Staphylococcus aureus* methicillin-resistant *S. aureus* (MRSA), and vancomycin-resistant enterococci (VRE). This could be one of the potential routes of transmission of the supergerm that is currently resistant to all antibiotics in hospitals in the UK and many other countries. Clothing materials not only can carry micro-organisms but also can transmit them into every corner of daily life since doctors and nurses often travel from seeing patients in hospitals to going home with family members. The solution to reduce material-related infections is to develop antibacterial textiles that can completely inactivate any micro-organisms upon surface contact (Borkow and Gabbay, 2008). Theoretical risk assessment research has shown that ideal antimicrobial textiles could possibly reduce the risk of transmission of infectious diseases in hospitals (Nicas and Sun, 2006).

However, not all so-called antimicrobial functions can provide proper protection against the transmission of pathogens. Antimicrobial functions cover a broad range of performance from instant and complete kill to only inhibition of infectious diseases.

16.2.2 Difference in antimicrobial performance

Antimicrobial functions on textiles could involve inhibition of micro-organism growth, or complete inactions of bacteria by a long contact time or by a short time of contact, and rapid kill of a broad spectrum of pathogens (bacteria, viruses, fungi and yeasts). If antimicrobial textiles only inhibit growth of micro-organisms, which are useful in the control of biodegradation of the products and preservation of textiles while also providing odor control functions (reducing body odor), these products are called *biostatic* materials. With such materials, growth rates and numbers of micro-organisms can be significantly reduced, but live bacteria or pathogens may still be found on their surfaces. Although the infection rates could be reduced, the residual micro-organisms still could cause transmission of infections at a certain level. Thus, the prevention of infection of disease in hospitals (nosocomial infection) cannot be achieved by using such materials as medical textiles.

Textile products that can provide total inactivation of a broad spectrum of micro-organisms by a short contact time are called *biocidal* (antibacterial) textiles. Such an antimicrobial function is the strongest among all antimicrobial claims and thus the ideal one for medical textiles, particularly for biologically protective products. Only textiles possessing such functions could ensure complete disinfection of diseases on the surfaces, prevent transmissions of infectious diseases caused by surface contacts on textile products, and result in reduced risks of infections in hospitals. In reality, most antimicrobial textiles currently available on the market do not have this function, and development of such biologically protective materials is the long-term goal for textile scientists.

16.2.3 Requirements for antimicrobial medical textiles

Generally speaking, medical textiles such as surgical gowns, drapes, linens, upholsteries and uniforms for doctors, nurses and patient dresses, should all possess the biocidal functions. Since most medical textiles are worn in close skin and long-term contact, human safety is a particular concern, especially in the products with biocidal functions. As explained earlier, ideal medical textiles should possess biocidal functions that could provide rapid inactivation to a broad spectrum of micro-organisms without inducing any potential resistance; the biocidal textile should be absolutely safe to the human body

without skin irritation and sensation; the biocidal functions should be durable against at least 50 repeated launderings; the functions could be refreshable or rechargeable during laundry or a simple process; and the biocidal functions should be compatible with other desired functions such as waterproofing and antistatic properties. As a matter of fact, there is no such ideal product currently available. The only biocidal technology that could provide performance close to these requirements is halamine chemistry (Sun and Worley, 2005).

Washing durability of antimicrobial functions on textiles is a key requirement for reusable uniforms, linens and surgical products. In order to provide the durable functions sufficient amounts of biocides should be incorporated into the textiles chemically or physically, to be slowly released to provide the function for the required duration. Such a mechanism is called a slow-releasing mechanism. Most biocides discussed in the later section, such as QAS and silver, are in this category. Another method is to use reversible redox reactions on surfaces of textiles, the so-called regeneration process. Precursors of biocides will be grafted onto the surfaces of fibers, which then can be converted to biocidal form after charging and recharging with an activating agent. If biocidal functions are provided by oxidative reactions between the reactive sites on the textiles and micro-organisms, chlorine or oxygen bleach can serve as a charging/activating agent. Halamine technology is a representative of such a mechanism (Sun and Worley, 2005).

16.3 The development of antibacterial textiles

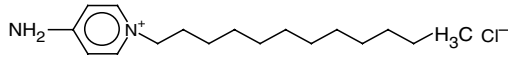
16.3.1 Current antimicrobial technologies

Antimicrobial functions on textiles could be achieved by chemically or physically incorporating antimicrobial agents into textiles. Chemical incorporation of these agents could use reactions that can build covalent, ionic or even strong inter-molecular interactions between fibers and the agents depending on the specific chemical structures. The chemically bounded biocides on textiles usually can survive more repeated washings and provide good washing durability. The biocides can be coated onto or blended into textiles physically to provide the desired durable functions. Antimicrobial agents that can be applied onto textile materials include organic biocides such as phenols, quaternary ammoniums salts, peptides and halamines, as well as inorganic compounds containing silver and copper ions. Several popular antimicrobial agents are discussed below.

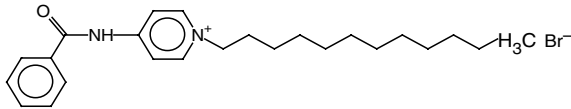
16.3.2 QAS and similar compounds

QAS are ionic compounds having a quaternary ammonium nitrogen, four alkyl or aryl groups connected to this nitrogen, and an anionic ion such as

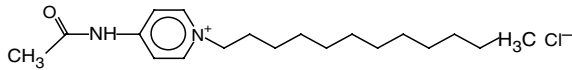
chloride or bromide. Among four alkyl groups, one is a long alkyl chain group containing more than eight hydrocarbons and also serves as the hydrophobic group. Hydrophobic groups on QAS tend to affect their antimicrobial functions (Tiller *et al.*, 2001; Zhao and Sun, 2007). With stronger hydrophobicity, the more powerful antimicrobial functions the QAS has (Zhao and Sun, 2008) (Fig. 16.1 and Table 16.1). Many QAS compounds have surfactant functions. QAS are effective biocides when used in aqueous solutions and as liquid disinfectants. When QAS are chemically connected to fiber



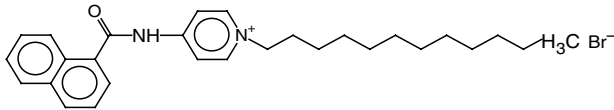
4-Amino-N-laurylpyridinium chloride (ALPC)



4-Benzoylamino-N-dodecylpyridinium bromide (BADPB)



4-Acetylamino-N-laurylpyridinium chloride (AALPC)



4-(1-Naphthoylamino)-N-dodecylpyridinium bromide (NADPB)

16.1 Structures of different QAS (Zhao and Sun, 2008).

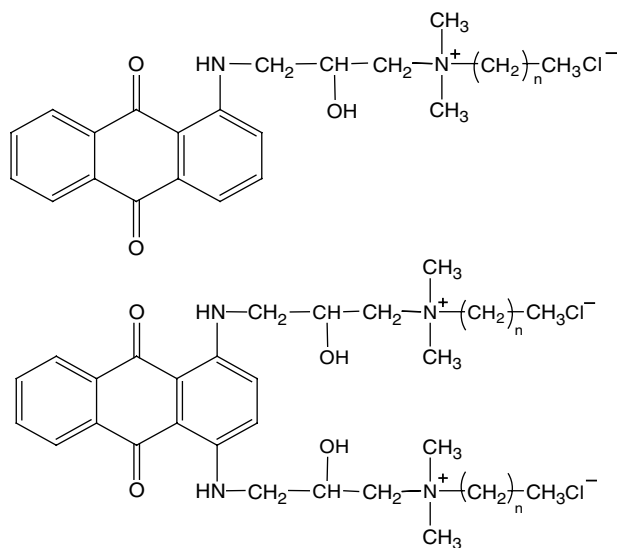
Table 16.1 Antimicrobial effects of the QAS (Zhao and Sun, 2008)

QAS	Concentration to cause a 6-log reduction of bacteria in contact time			
	1 min (<i>E. coli</i>) (ppm)	5 min (<i>E. coli</i>) (ppm)	1 min (<i>S. aureus</i>) (ppm)	5 min (<i>S. aureus</i>) (ppm)
ALPC	100	100	100	50
AALPC	100	100	100	50
BADPB	50	50	50	10
NADPB	50	10	50	10

surfaces their functions can be impeded depending on how they are connected and the final structures of QAS on surfaces. Physically incorporated QAS in fibers can provide antimicrobial functions by gradually releasing them from fiber's surfaces during usage, which could provide the intended functions of the materials but may present a durability concern.

QAS based antimicrobial textiles have been widely reported by researchers since 1970s (Isquith *et al.*, 1972) and more recently (Cai and Sun, 2004; Kim and Sun, 2002; Son and Sun, 2003; Son *et al.*, 2006; Zhao and Sun, 2008). Commercial QAS finishing agents have been developed and marketed, and the most popular one is Dow Corning 5700, which employs siloxyl groups to bind QAS to cellulose surfaces. QAS could be chemically incorporated to nylon and protein fibers (Son and Sun, 2003; Zhu and Sun, 2004; Zhao and Sun, 2007) and acrylic fibers (Cai and Sun, 2004; Kim and Sun, 2002) directly with ionic interactions, or by bridging with other reactive groups to cellulose (Son *et al.*, 2006); all provide the textiles with proper antimicrobial functions and durability, particularly washing durability.

Due to their effective antimicrobial functions, the QAS moieties were introduced onto polymer surfaces and dye molecules to produce functional polymers or dyes (Liu and Sun, 2008a; Ma *et al.*, 2003; Tiller *et al.*, 2001). When QAS structures are covalently connected to anthraquinone dyes (Fig. 16.2), the new dye molecules exhibited excellent biocidal properties in diluted solutions. However, when these dyes are incorporated onto acrylic fibers, following a basic dyeing process, the dyed fabrics showed limited



16.2 Structure of the antimicrobial colorants ($n = 3, 7, 11$ or 15) (Liu and Sun, 2008a).

antimicrobial properties, and these properties could be affected by surfactants and other species in water (Liu and Sun, 2009b). Results indicated that surface fixed QAS compounds or combined QAS molecules had reduced antimicrobial functions. Only the dissociated QAS could demonstrate the ideal antimicrobial functions, and this result is consistent with the accepted antimicrobial mechanisms of QAS (Hashemi and Sun, 2010). In fact, this limitation is pretty universal to all QAS antimicrobial agents.

16.3.3 Silver ion or other metals

Silver antimicrobial agents might be the most popular biocides employed in textiles and many different medical materials. Silver is well known for its antimicrobial functions and has a superior safety record for human beings since silverware has been used for 1000 years. Silver can be applied onto surfaces of fibers and textiles in different forms such as ions, nanoparticles and even layering. In whatever form silver is used, the silver ion is responsible for providing antimicrobial functions. The generally recognized mechanism is reaction between silver ions and sulfhydryl groups in proteins, resulting in expiration of micro-organisms.

Direct incorporation of silver ions onto textiles can be achieved easily by using silver salts and chelating agents. For example, cyclodextrin was grafted onto cotton fabrics, which then was employed to incorporate silver ion onto the fabrics. The slowly released silver ions from this fabric could provide proper and durable antimicrobial functions (Bajpai *et al.*, 2010). Silver chloride particles were embedded into silica sol matrix, which were then treated onto cotton fabrics. The finished cotton fabrics demonstrated antimicrobial functions (Tomsic *et al.*, 2009). Any acid groups that can form stable salt structures with silver ions could be incorporated into fibers. The representative example was the antimicrobial silk produced with different acid groups (Tsukada *et al.*, 2003).

In recent years, developments of nanotechnologies have enabled formation of nanoparticles, nanolayers of silver metal on surfaces of textiles. Silver layer was coated onto polyamide fiber surfaces by reacting aldehyde groups that were chemically incorporated onto the fibers with silver ions, the so-called Tollens reaction (Textor *et al.*, 2010). The treated fabrics showed proper antimicrobial functions against *E. coli* after 30 washes. Plasma sputtering is another process that can deposit a nanolayer of silver onto surfaces of polyamide fibers. In this process, energetic particles are collided onto silver material with high impact, which can cause silver single atoms to be emitted and then collected on the polyamide fiber surfaces (Hegemann *et al.*, 2009). These silver-coated fabrics can provide more than 14 days' slow release of silver ions in water. Plasma treatment was used to coat silver onto cotton/polyester fabrics as well, and the treated fabrics demonstrated

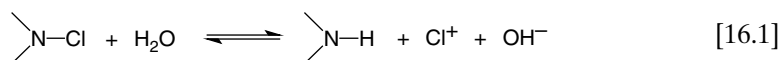
antimicrobial functions against *L. innocua* (LRGIA 01) strain (Chadeau *et al.*, 2010). Similarly, gamma irradiation can also impart silver nanoparticles to surfaces of fibers (Chang *et al.*, 2009). *In situ* formed silver nanoparticles were incorporated into acrylic fibers to provide the desired functions (Sreekumar *et al.*, 2009).

These surface coated silver nanoparticles or layering or particles embedded in fibers can all release silver ions slowly during usage, which provide durable antimicrobial functions. While silver is on the surfaces of the fibers, the metal can be affected by reactive chemicals, particularly bleaching agents, which is a concern for medical use textiles since chlorine bleach is widely used as a disinfectant.

Several metal oxides including copper and zinc oxide particles have also shown antimicrobial functions and been applied onto surfaces of textiles (Abramov *et al.*, 2009; Lee, 2009; Michels *et al.*, 2008).

16.3.4 Halamine chemistry

Halamine compounds have been widely used as water disinfectants in the swimming pool industry due to their ability to slowly release free chlorine in water (Worley and Williams, 1988). Later, halamine structures were proven biocidal by Williams *et al.* (1988), and could serve as water disinfectants themselves. This led to applications of the halamine chemistry on solid materials such as polymers and textiles (Sun and Worley, 2006, Sun *et al.*,



2001a). The halamine reactions in water (Equation [16.1]) and on solid surfaces (Equation [16.2]) are shown above.

Halamine structures are mostly available from heterocyclic compounds containing N-Cl or N-Br bonds, including imide, amide, and amine halamine bonds. The stabilities of halamine bonds are in an order of imide halamine < amide halamine < amine halamine. Reactivity of the halamine structures is in a reverse order of the stability (Sun and Worley, 2006). The representative cyclic halamine precursor structures widely used in textile treatments are compounds containing 5,5-dimethyl hydantoin and 2,2,5,5-tetramethyl-imidazolidin-4-one moieties (Badrossamay and Sun, 2009; Kou *et al.*, 2009; Qian and Sun, 2003; Sun *et al.*, 2001a, 2001b). These precursors or monomers were covalently incorporated onto polymers by

forming hemiacetal bonds (Qian and Sun, 2003; Sun *et al.*, 2001a), grafting (Sun *et al.*, 2001b) or siloxyl structures (Ren *et al.*, 2009) onto cellulose and other fibers. The monomers containing vinyl groups were employed in graft polymerization of polypropylene, and the products were extruded and then converted into biocidal polypropylene fibers (Badrossamay and Sun, 2009).

Beside cyclic halamine compounds, acyclic amide and amine structures also proved effective antimicrobial agents (Liu and Sun, 2008b; Luo and Sun, 2006). In fact, even the simplest acrylamide and methacrylamide could be employed in treatment of textiles, and the treated materials could be chlorinated to biocidal halamine structures (Badrossamay, 2009; Liu and Sun, 2008c, Liu and Sun, 2009a). The acyclic halamine structures on textiles are less stable than the cyclic halamine structures in general, but still can survive a few recharges in diluted chlorine bleach solutions.

16.4 Performance of antibacterial textiles

Antimicrobial textiles are considered as effective tools in the prevention of transmission of diseases in hospitals and should be used as personal protective gear in healthcare facilities. Thus these materials are expected to inactivate a broad spectrum of micro-organisms and prevent nosocomial infections caused by contact and cross transmission of pathogens through textile materials. In addition, these materials should also retain proper liquid barrier properties to block penetration of body fluids and blood. In order to prevent cross transmission of micro-organisms by contact, the textiles should provide quick or instant and complete kill to the germs since any surviving pathogen is infectious. If textiles could provide instant contact kill to pathogens, liquid barrier requirements on many current medical textiles could be reduced, which could increase the air permeability and comfort of the products. Thus, the ideal antimicrobial textiles for medical use should possess the following properties: quick and complete kill to bacteria and viruses; non-toxic and non-irritating; not generating resistance from micro-organisms; environmentally friendly; durable and reusable.

Currently developed antimicrobial technologies and textiles provide a wide range of antimicrobial functions according to antimicrobial mechanisms and the biocides employed in the materials. Some of the biocides such as QAS and silver ions may need to have sufficient amount and certain contact time to provide desired functions. Other biocides may be more effective against certain micro-organisms but not so effective to inactivate others. The textiles that cannot completely and quickly inactivate a broad spectrum of pathogens may still have applications in medical fields, but mostly limited to hygiene purposes. In general, antimicrobial functions consume biocides in the materials. Exposure to air and environment could result in bacterial

contacts with or consumption of the biocides. In order to achieve durable functions, significant amount of biocides should be imbedded into the fibers and slowly released during use. Another option is to follow the regeneration process and chemically recharge or (re)activate the functions on surfaces of the textiles (Sun and Worley, 2005).

Cotton and cotton polyester blend fabrics treated with halamine structures demonstrated almost instant biocidal functions (6-log reduction of bacteria in 2 min) against a broad spectrum of micro-organisms and could be recharged by chlorine bleach (Sun *et al.*, 2001a). Halamine treated textiles kill micro-organisms by an oxidation or chlorine transfer mechanism which then would not lead to generation of resistance from the germs after a long term of usage. More importantly, these halamine structures are rechargeable on textiles with a diluted chlorine bleach, which is also a US EPA certified biocide used in commercial laundering. However, halamine structures have limitations as well, including color bleaching functions, low thermal stability and low UV stability. Therefore, applications of halamine structures on reusable surgical gowns and drapes are almost impossible since these products are all sterilized under high temperatures.

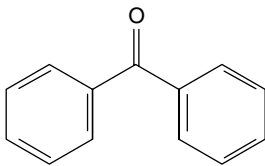
In addition, biocides if not chemically bonded to fibers could be released into water in laundering, and possibly enter the waste water stream, such as rivers and ground water. If their biocidal functions still exist they will affect the biological system in the environment, thus presenting potential environmental concerns (Brar *et al.*, 2010). Biocidal functional textiles should not be used in certain consumer products that have close skin contact, since the textiles might provide an overclean environment and become harmful to humans. Thus, users of biocidal textiles should be informed of the environmental and human safety concerns. Ideally, green or greener antimicrobial technologies without the above concerns should be developed.

16.5 New antimicrobial technologies

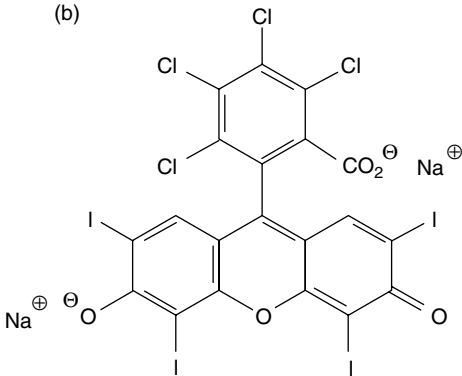
More recently, photo-sensitive agents have shown proper antimicrobial functions on surfaces of polymers and textiles when exposed to UVA and daylight (Hong and Sun, 2008, 2010; Hong *et al.*, 2010; Qi *et al.*, 2006). Titanium dioxide can be coated onto textile surfaces and when exposed to light the materials demonstrate antimicrobial or self-cleaning functions (Daoud and Xin, 2004; Qi, *et al.*, 2006). More interestingly, some of the dye compounds also exhibited antimicrobial functions in the dark after being exposed to UVA light (Hong and Sun, 2008). The photo-sensitizers could be incorporated onto cotton, protein and nylon fibers, as well as polyurethane coating, and the products showed proper biocidal functions (Fig. 16.3 and Table 16.2).

Based on the findings some anthraquinone compounds were investigated for the same functions (Fig. 16.3), and results indicated that these

(a)



(b)



16.3 Photo-sensitizers (a) benzophenone (BP) and (b) Rose Bengal (RB) (Hong and Sun, 2010).

Table 16.2 Antimicrobial abilities of BP/PU and RB/PU coated leather samples under fluorescent light (Hong and Sun, 2010)

<i>E. coli</i>	Dilution ratio of bacteria solution after contact time of 90 min				Reduction of bacteria (%)
	10	10 ²	10 ³	10 ⁴	
Blank	∞	∞	164	21	–
BP-0 or RB-0	∞	79	7	3	–
BP-4	0	0	0	0	>99.9999
RB-4	0	0	0	0	>99.9999

dye compounds also could provide photo-induced antimicrobial functions on textiles and coating surfaces (Hong, 2007). The photo-induced antimicrobial functions on these acid-dyed or photo-sensitizer incorporated fabrics are due to radicals generated by these active agents on fabrics, which also lead to the formation of reactive oxygen species (ROS) in air. With the existence of moisture, ROS will produce H₂O₂ on surfaces of the fabrics, which could provide antimicrobial functions in the dark if the materials have been exposed to light (Liu and Sun, 2011). Such materials could be applied as medical use textiles and coatings on desktops and leather surfaces.

Natural dyes also exhibited antimicrobial functions on dyed textiles under certain conditions (Alihosseini *et al.*, 2008; Gupta *et al.*, 2004). Antimicrobial colorants will be specifically discussed in detail in another chapter in this book and not dealt with further here.

16.6 Applications of antimicrobial textiles

16.6.1 Protective clothing and linen products

Antimicrobial functions on medical textiles will help to reduce nosocomial infections caused by contact transmission of diseases from textiles. As stated earlier, the biocidal functions on the textiles could provide personal protection against various pathogens. Thus, most researchers believe that medical textiles such as doctors' and nurses' uniforms, patient dresses and hospital linen products should possess biocidal functions in order to protect patients and more importantly healthcare workers. In addition, biological (biocidal) protective functions are also important for military uniforms. Since most of the uniforms are reusable the biocidal functions on the uniforms should be able to survive at least 50 repeated launderings. To meet such a requirement, technologies that can provide rechargeable biocidal functions will be important.

16.6.2 Surgical gowns and drapes

Surgical gowns and drapes, of course, should possess biocidal functions as well. However, these products belong to category Ib according to CDC guidelines as medical devices. More importantly, according to CDC guidelines, these surgical products should be sterilized by high temperature/pressure or chemicals before being reused. The sterilization processes may be detrimental to some biocides on the treated fabrics. The halamine structures are the most powerful biocides on textiles so far but are not thermally stable. Thus, technologies that can incorporate thermally stable biocidal functions onto surgical gowns and drapes are still under investigation. However, silver ion and QAS are thermally stable and can survive the sterilization processes. The only concern is their ability to provide the biocidal effects on the materials.

16.7 Future trends

Antimicrobial textiles for biological protection are needed for many applications, including medical textiles, sportswear, hygiene products and military uniforms. Green antimicrobial technology is a new direction for future development with the understanding that the antimicrobial textiles should be safe to humans and the environment, cost less energy to produce and be reusable and recyclable. Antibacterial technologies that can be employed in surgical gowns and drapes should be developed to meet the requirement of sterilization. Overall, the development of perfect biocidal textiles is still a challenge to textile scientists.

16.8 Acknowledgments

The author is grateful to financial support from the National Science Foundation (DMI 9733981 and CTS 0424716) and the National Textile Center (S06-CD01).

16.9 References

- ABRAMOV, O. V., GEDANKEN, A., KOLTYPIN, Y., *et al.* (2009) Pilot scale sonochemical coating of nanoparticles onto textiles to produce biocidal fabrics. *Surface and Coatings Technology*, 204: 718–722.
- ALIHOSSEINI, F., JU, K. S., LANGO, J., HAMMOCK, B. D. and SUN, G. (2008) Antibacterial colorants – characterization of prodiginines and their applications on textile materials. *Biotechnology Progress*, 24(3): 742–747.
- BADROSSAMAY, R. Z. and SUN, G. (2009) Durable and rechargeable biocidal polypropylene polymers and fibers prepared by using reactive extrusion. *Journal of Biomedical Materials Research: Part B – Applied Biomaterials*, 89B: 93–101.
- BAJPAI, M., GUPTA, P. and BAJPAI, S. K. (2010) Silver(I) ions loaded cyclodextrin-grafted-cotton fabric with excellent antimicrobial property. *Fibers and Polymers*, 11: 8–13.
- BORKOW, G. and GABBAY, J. (2008) Biocidal textiles can help fight nosocomial infections. *Medical Hypotheses*, 70: 990–994.
- BRAR, S. K., VERMA, M., TYAGI, R. D. and SURAMPALLI, R. Y. (2010) Engineered nanoparticles in wastewater and wastewater sludge – evidence and impacts. *Waste Management*, 30: 504–520.
- CAL, Z. S. and SUN, G. (2004) Antimicrobial finishing of acrilan fabrics with cetylpyridinium chloride. *Journal of Applied Polymer Science*, 94: 243–247.
- CHADEAU, E., OULAHAL, N., DUBOST, L., *et al.* (2010) Anti-listeria innocua activity of silver functionalised textile prepared with plasma technology. *Food Control*, 21: 505–512.
- CHANG, S. Q., KANG, B., DAI, Y. D., *et al.* (2009) Synthesis of antimicrobial silver nanoparticles on silk fibers via gamma-radiation. *Journal of Applied Polymer Science*, 112(4): 2511–2515.
- DAOUD, W. A. and XIN, J. H. (2004) Low temperature sol-gel processed photocatalytic titania coating. *Journal of Sol-Gel Science and Technology*, 29(1): 25–29.
- GUPTA, D., KHARE, S. K. and LAHA, A. (2004) Antimicrobial properties of natural dyes against gram-negative bacteria. *Coloration Technology*, 120: 167–171.
- HASHEMI, N. and SUN, G. (2010) Intermolecular interactions between surfactants and cationic dyes and effect on antimicrobial properties. *Industrial and Engineering Chemistry Research*, 49: 8347–8352.
- HEGEMANN, D., AMBERG, M., RITTER, A. and HEUBERGER, M. (2009) Recent developments in ag-metallised textile plasma sputtering. *Materials Technology*, 24–41.
- HONG, K.H. and SUN G. (2007) Photocatalytic Functional Cotton Fabrics Containing Benzophenone Chromophoric Groups. *Journal of Applied Polymer Science*, V106: 2661–2667.
- HONG, K. H. and SUN, G. (2008) Antimicrobial and chemical detoxifying functions of cotton fabrics containing different benzophenone derivatives. *Carbohydrate Polymers*, 71: 598–605.

- HONG, K. H. and SUN, G. (2010) Photoactive antimicrobial agents/polyurethane finished leather. *Journal of Applied Polymer Science*, 115: 1138–1144.
- HONG, K. H., LIU, N. and SUN, G. (2009) UV-induced graft polymerization of acrylamide on cellulose by using immobilized benzophenone as a photo-initiator. *European Polymer Journal*, V45: 2443–2449.
- ISQUITH, A. J., ABBOTT, E. A. and WALTERS, P. A. (1972) Surface-bonded antimicrobial activity of an organosilicon quaternary ammonium chloride. *Applied Microbiology*, 24: 859–863.
- KIM, Y. H. and SUN, G. (2002) Functional finishing of acrylic and cationic dyeable fabrics intermolecular interactions. *Textile Research Journal*, 72(12): 1052–1056.
- KOU, L., LIANG, J., REN, X. H., *et al.* (2009) Novel N-halamine silanes. *Colloids and Surfaces A-Physicochemical and Engineering Aspects*, 345(1–3): 88–94.
- LEE, S. (2009) Multifunctionality of layered fabric systems based on electrospun polyurethane/zinc oxide nanocomposite fibers. *Journal of Applied Polymer Science*, 114: 3652–3658.
- LINGAAS, E. and FAGERNES, M. (2009) Development of a method to measure bacterial transfer from hands. *Journal of Hospital Infection*, 72: 43–49.
- LIU, J. and SUN, G. (2008a) The synthesis of novel cationic anthraquinone dyes with high potent antimicrobial activity. *Dyes and Pigments*, 77(2): 380–386.
- LIU, S. and SUN, G. (2008b) Biocidal acyclic halamine polymers: conversion of acrylamide grafted cotton to acyclic halamine. *Journal of Applied Polymer Science*, 108: 3480–3486.
- LIU, S. and SUN, G. (2008c) Functional modification of poly(ethylene terephthalate) with an allyl monomer: chemistry and structure characterization. *Polymer*, 49: 5225–5232.
- LIU, S. and SUN, G. (2009a) New N-halamine polymeric biocides: N-chlorination of acyclic amide grafted cellulose. *Industrial and Engineering Chemistry Research*, 48(2): 613–618.
- LIU, J. and SUN, G. (2009b) The biocidal properties of anthraquininoid dyes. *Dyes and Pigments*, 81: 231–234.
- LIU, N. and SUN, G. (2011) Production of reactive oxygen species by photo-active anthraquinone compounds and their application in wastewater treatment. *Industrial and Engineering Chemistry Research*, in press.
- LUO, J. and SUN, Y. (2006) Acyclic N-halamine-based fibrous materials: preparation, characterization, and biocidal functions. *Journal of Polymer Science Part A: Polymer Chemistry*, 44: 3588–3600.
- MA, M. H., SUN, Y. Y. and SUN, G. (2003) Antimicrobial cationic dyes. Part 1: synthesis and characterization. *Dyes and Pigments*, V58: 27–35.
- MICHELS, H., MORAN, W. and MICHEL, J. (2008) Antimicrobial properties of copper alloy surfaces, with a focus on hospital-acquired infections. *International Journal of Metalcasting*, 2: 47–56.
- NEELY, A. N. (2000) A survey of gram-negative bacteria survival on hospital fabrics and plastics. *Journal of Burn Care and Rehabilitation*, 21: 523–527.
- NEELY, A. N. and MALEY, M. P. (2000) Survival of enterococci and staphylococci on hospital fabrics and plastic. *Journal of Clinical Microbiology*, 38: 724–726.
- NEELY, A. N. and ORLOFF, M. M. (2001) Survival of some medically important fungi on hospital fabrics and plastics. *Journal of Clinical Microbiology*, 39: 3360–3361.

- NICAS, M. and SUN, G. (2006) An integrated model of infection risk in a health-care environment. *Risk Analysis*, 26(4): 1185–1096.
- QI, K., DAOUD, W. A., XIN, J. H., MAK, C. L., TANG, W. and CHEUNG, W. P. (2006) Self-cleaning cotton. *Journal of Materials Chemistry*, 16: 4567–4574.
- QIAN, L. and SUN, G. (2003) Durable and regenerable antimicrobial textiles: synthesis and applications of 3-methylol-2,2,5,5-tetramethyl-imidazolidin-4-one (MTMIO). *Journal of Applied Polymer Science*, 89: 2418–2425.
- REN, X., AKDAG, A., KOCER, H. B., WORLEY, S. D., BROUGHTON, R. M. and HUANG, T. S. (2009) N-halamine-coated cotton for antimicrobial and detoxification applications. *Carbohydrate Polymers*, 78: 220–226.
- SON, Y. A. and SUN, G. (2003) Durable antimicrobial nylon 66 fabrics: ionic interactions with quaternary ammonium salts. *Journal of Applied Polymer Science*, 90: 2194–2199.
- SON, Y. A., KIM, B. S., RAVIKUMAR, K., *et al.* (2006) Imparting durable antimicrobial properties to cotton fabrics using quaternary ammonium salts through 4-aminobenzenesulfonic acid-chloro-triazine adduct. *European Polymer Journal*, 42: 3059–3067.
- SREEKUMAR, T. V., DAS, A., CHANDRA, L., *et al.* (2009) Inherently colored antimicrobial fibers employing silver nanoparticles. *Journal of Biomedical Nanotechnology*, 5(1): 115–120.
- SUN, G. and WORLEY, S. D. (2005) Chemistry of durable and regenerable biocidal textiles. *Journal of Chemical Education*, 82(1): 60–64.
- SUN, G. and WORLEY, S. D. (2006) Halamine chemistry and its applications in biocidal textiles and polymers. In: *Modified Fibers with Medical and Specialty Applications*, ed. Vincent Edwards, J., Buschle-Diller, G. and Goheen, S. Dordrecht: Springer, pp. 81–89.
- SUN, G., XU, X., BICKETT, J. R. and WILLIAMS, J. F. (2001a) Durable and regenerable antimicrobial finishing of fabrics with a new hydantoin derivative. *Industrial Engineering Chemistry Research*, 41: 1016–1021.
- SUN, Y. Y., CHEN, T. Y., WORLEY, S. D. and SUN, G. (2001b) Novel refreshable N-halamine polymeric biocides-containing imidazolidin-4-one derivatives. *Journal of Polymer Science, Polymer Chemistry*, 39(18): 3073–3084.
- TEXTOR, T., FOU DA, M. M. G. and MAHLTIG, B. (2010) Deposition of durable thin silver layers onto polyamides employing a heterogeneous Tollens' reaction. *Applied Surface Science*, 256: 2337–2342.
- TILLER, J., LIAO, C.-J., LEWIS, K. and KLIBANOV, A. M. (2001) Designing surfaces that kill bacteria on contact. *Proceedings of the National Academy of Science of the USA*, 98: 5981–5985.
- TOMSIC, B., SIMONCIC, B., OREL, B., *et al.* (2009) Antimicrobial activity of AgCl embedded in a silica matrix on cotton fabric. *Carbohydrate Polymers*, 75(4): 618–626.
- TREACLE, A. M., THOM, K. A., FURUNO, J. P., *et al.* (2009) Bacterial contamination of health care workers' white coats. *American Journal of Infection Control*, 37: 101–105.
- TSUKADA, M., ARAI, T., COLONNA, G. M., *et al.* (2003) Preparation of metal-containing protein fibers and their antimicrobial properties. *Journal of Applied Polymer Science*, 89(3): 638–644.
- WILLIAM, D. E., ELDER, E. D. and WORLEY, S. D. (1988) Is free halogen necessary for disinfection? *Applied and Environmental Microbiology*, 54(10): 2583–2585.

- WILSON, J. A., LOVEDAY, H. P., HOFFMAN, P. N., *et al.* (2007) Uniform: an evidence review of the microbiological significance of uniforms and uniform policy in the prevention and control of healthcare-associated infections. Report to the Department of Health (England), *Journal of Hospital Infection*, 66: 301–307.
- WORLEY, S. D. and WILLIAMS, D. E. (1988) Halamine water disinfectants. *CRC Critical Review Environmental Control*, 18: 133–175.
- YAZGI, H., UYANIK, M. H., ERTEK, M., *et al.* (2009) Survival of certain nosocomial infectious agents on the surfaces of various covering materials. *Turkish Journal of Medical Sciences*, 39: 619–622.
- ZHAO, T. and SUN, G. (2007) Antimicrobial finishing of wool fabrics with quaternary aminopyridinium salts. *Journal of Applied Polymer Science*, 103: 482–486.
- ZHAO, T. and SUN, G. (2008) Hydrophobicity and antimicrobial activities of quaternary pyridinium salts. *Journal of Applied Microbiology*, 104: 824–830.
- ZHU, P. and SUN, G. (2004) Antimicrobial finishing of wool fabrics: using quaternary ammonium salts. *Journal of Applied Polymer Science*, 93: 1037–1041.

F. ALIHOSSEINI and G. SUN,
University of California, Davis, USA

Abstract: Many colorants, whether natural or synthetic, possess some inherent functions in addition to their colors. These properties can be utilized in textile dyeing processes to bring the particular functions to textiles. In other words, dyeing textiles with these colorants can combine dyeing and functional finishing, a greener process than current separated wet treatments in terms of reduced generation of waste water and consumption of energy. Antimicrobial colorants are one of the functional colorants that have been widely employed in textile applications. This chapter provides a review on antimicrobial colorants with detailed discussions of synthetic and natural colorants, as well as some colorants produced from micro-organisms and photo-active colorants.

Key words: antimicrobial, colorants, dyes, natural, synthetic, photo-induced.

17.1 Introduction

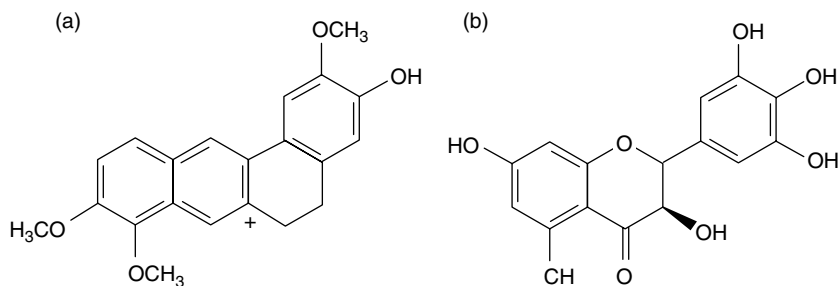
There has been an increased interest in antimicrobial textiles, which has led to a rapid development of antimicrobial technologies for textiles and polymers in recent years (Alihosseini and Sun, 2008; Gao and Cranston, 2008; Kenawy *et al.*, 2007; Sun and Worley, 2005; Sun *et al.*, 2001). Although most of the processes employ different biocides on fabrics (Gao and Cranston, 2008; Sun *et al.*, 2001) a significant amount of research efforts have been spent on studying antimicrobial properties of natural and synthetic dyes (Liu and Sun, 2008; Ma *et al.*, 2003; Sayed and El-Gaby, 2001). Using antimicrobial dyes to incorporate functions to textiles has the advantage of combining both finishing and dyeing processes together, which could reduce energy and water usages in wet treatment of textiles and so constitutes a green and eco-friendly technology for textile manufacturing processes (Gao and Cranston, 2008).

Natural colorants from plants with antimicrobial properties have been widely used as both herbal medicines and dyes for at least 4000 years. For example, black kohl or green malachite were used as cosmetics and also to cure or prevent eye diseases as well (Shafik and Elseesy, 2003). Henna (*Lawsonia inermis*) was used for tattoo or hair dyeing, and was also used

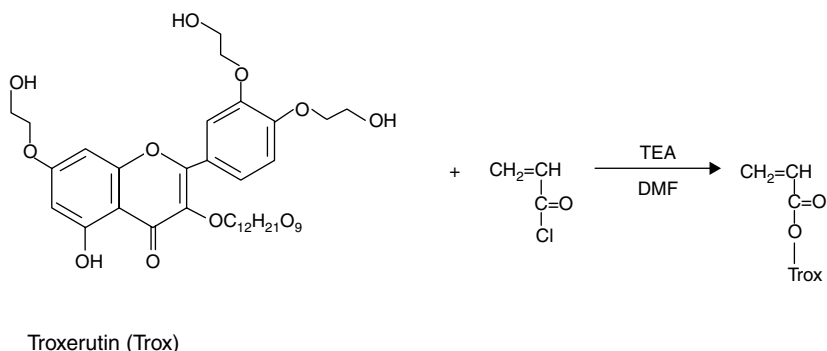
medicinally as an astringent and to cure diarrhea and open wounds. Onion, radish and wine were other well-known antimicrobial agents used in disinfection or sanitizing objects. Turmeric (*Curcuma longa*) was applied to close open wounds and was also used to dye skin and cloth (Aboelsoud, 2010; McKenna, 1998). Colorant extracts from rhubarb and aloe have been employed as laxatives for centuries. The main derivatives in the roots of *Lithospermum erythrorhizon*, shikonin, alkanin and other shikonon derivatives were used as an intensive red colorant. The water-soluble extract had remarkable anti-inflammatory and calming effects (Debnath *et al.*, 2006). Tannin-based natural dyes from *Punica granatum* are reported as potent antimicrobial agents. A natural colorant extracted from the stems and leaves of Taming, *Mahonia napaulensis* D.C., belongs to the family *Berberidaceae*, which has been used in India to dye cotton, silk and wool fabrics. The major components in the extracted colorant are two isoquinoline alkaloid colorants named Berberine and Jatrorrhizine and a flavonol, ampelopsin (Fig. 17.1). These compounds have shown antifungal and antibacterial activities and have been used to treat localized skin and mucosal infection. Taming-dyed fabrics showed 83.33% antifungal activity against growth of *Trichoderma*, a known pathogen (Bajpai and Vankar, 2007).

Natural flavonoid compounds such as troxerutin (Fig. 17.2) could be modified to become reactive with polymers and bring both antioxidant and antimicrobial functions to polyamide fabrics. Troxerutin was used as a protective agent on vein walls against the development of varicose veins. Troxerutin-treated bandage could slowly release the compound and result in reduced healing time of venous ulcers (Constantin *et al.*, 2008). Silk fabric dyed with extracts from *M. citrifolia*, *T. grandis* and *T. catappa* showed good color fastness and antimicrobial properties, causing 25–65% reduction against *Escherichia coli* (Prusty *et al.*, 2010).

In the first half of the nineteenth century, scientists started to synthesize natural products. The synthesis of quinine, a valuable natural anti-malarial medicine, led to the accidental synthesis of the first synthetic dye 'Aniline'



17.1 Chemical structure of (a) berberine and (b) ampelopsin (flavonol).



17.2 Converting troxerutin to vinyl monomer.

(Wainwright, 2008). Synthetic dyes were employed in staining and distinguishing different classes of gram-positive and gram-negative bacteria due to the fact that these colorants could dye skin. Different classes of bacteria absorb different dyes. Gram-positive bacteria have an outer cell layer of peptidoglycan that absorbs the purple crystal violet while gram-negative bacteria have a membrane in their outer layer which prevents the peptidoglycan from the stain (Fung and Miller, 1973; Wainwright, 2008, 2001). During this period of time, Ehrlich discovered the antibacterial activity of methylene blue (Albert *et al.*, 1949). The synthesis of methylene blue was the beginning of the production of numerous synthetic dyes such as mepacrine, a yellow acridine derivative that was used as an antibacterial agent in the treatment of various bacterial infections (Albert *et al.*, 1949).

The use of antimicrobial dyes on textile fabrics for protecting clothing started in 1941 for military purposes. In the warm and humid weather of tropical islands, certain textile materials, particularly natural fibers, caused an increase in microbial infections (Chun and Gamble, 2007; Russell and Chopara, 1996). Antimicrobial dyes have attracted more attention in recent years due to the latest developments in functional textiles, as well as concerns about outbreaks of various diseases. This chapter provides a review on the synthetic and natural antimicrobial colorants, their historical development and applications as well as latest progress.

17.2 Synthetic antibacterial colorants

17.2.1 Acridines

Acridines were the first group of synthetic dyes used as antimicrobial agents. A study on the relationship between structure and activity of acridine-based compounds revealed that cationic type character especially in neutral pH is a key parameter for the antimicrobial activities. This strong

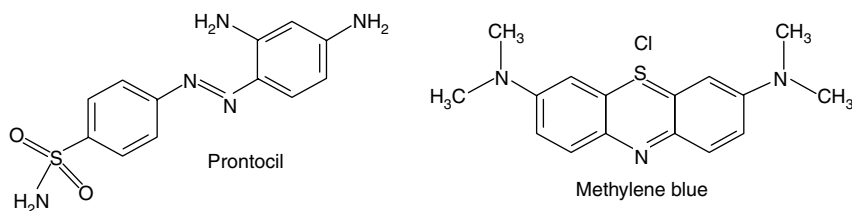
cationic entity could easily attach to different anionic sites on the surface of micro-organism cells. Acridines also act as an intercalating agent that binds to DNA and inhibits bacteria by preventing the synthesizing of DNA. It is also known that some of these dyes are photo-sensitizers and have the ability to generate singlet oxygen under the light to kill the bacteria (Albert *et al.*, 1949; Giorgio *et al.*, 2008; Wainwright, 2001).

Acridine, acroflavin, acridine yellow G, anthracine derivatives and anthraquinones were used as photo-induced antimicrobial agents on dyed nylon fabrics (Michielsen *et al.*, 2007). Nylon fabric was coated with polyacrylic acid (PAA) as a mediator polymer, and then diamine was incorporated to PAA, which can covalently bond more dyes and increase the antimicrobial activities. Acridine yellow G showed the best results on nylon fabrics and the dyed fabrics were able to inactivate all the viruses and bacteria (Michielsen *et al.*, 2007).

17.2.2 Sulfamid-based dyes

In the early twentieth century, Gerhart Domagk started to examine the antibacterial activity of synthetic sulfonamides, which led him to discover Prontosil, a red azo dye, in 1932. It could destroy streptococci (Fig. 17.3).

Later on, more active derivatives of Prontosil were synthesized, which were used to treat scarlet fever, cellulite and wound infections. Domagk received a Nobel Prize for his discovery in 1939. The drug also cured Franklin D. Roosevelt Jr. of an infection, which was an important step in its acceptance as a drug (Bishop, 1936). Due to their excellent antimicrobial activity, several attempts were made to bind sulfamide dyes to fabric surfaces to enhance their functional properties. It is known that sulfanamide dyes have antimicrobial activity only *in vivo*. The azo bond could be reduced *in vivo*, and the active part of the dye molecule, sulfanamide structural moiety which interferes with bacterial metabolism and kills the bacteria, was released. Sulfonamide dyes were used as the main wound disinfectant during the Second World War (Cooper, 2004).



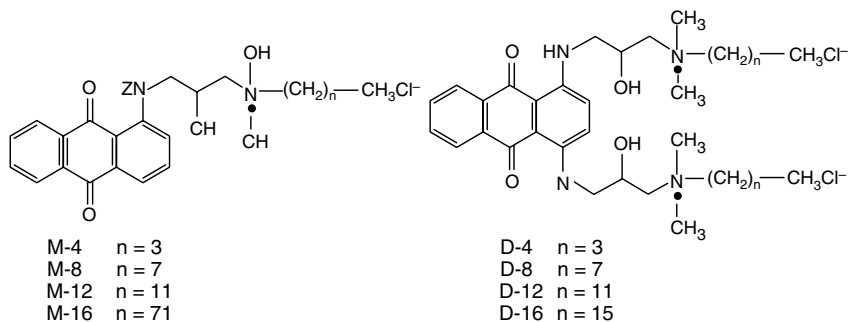
17.3 Chemical structures of prontosil and methylene blue.

Besides acridines and sulfonamide dyes, some other dyes such as triphenylmethane, brilliant green and crystal violet are also used as skin disinfectants or in wounds and burns treatments. A combination of these dyes was applied for bactericidal treatment of the umbilical cord stump in newborn babies (Janssen *et al.*, 2003). Phloxine B, an acid dye and a color additive in food, drugs and cosmetics, is another newly reported synthetic dye which can significantly inhibit the growth of *Staphylococcus aureus* (Rasooly and Weisz, 2002).

17.2.3 Quaternary ammonium antibacterial dyes

Quaternary ammonium salts (QAS) are cationic compounds containing alkyl groups in a chain length of C8–C18, which are water soluble and can be used as disinfectants in textile industries. All of these compounds are membrane active agents and can damage cell walls of gram-positive bacteria. The damaged membrane could lead to leakage of intracellular constituents, resulting in cytolysis (Russell and Chopara, 1996). QAS have been successfully applied on wool and nylon fabrics and possess durable and powerful antibacterial activity (Kim and Sun, 2000, 2001; Zhao and Sun, 2007, 2008).

Two series of dyes containing both anthraquinone and QAS groups were reported, with a long alkyl chain varying from C4 to C12. The dyes with alkyl chain length longer than C8 showed good antimicrobial activities against both *E. coli* and *S. aureus* (Ma *et al.*, 2003; Ma and Sun, 2004). However, the washing durability and hydrolytic stability of the dyes were very limited since the anthraquinone and QAS were connected by an amide bond, which could be hydrolyzed in alkaline solution (Ma and Sun, 2005). To overcome the low hydrolytic stability of the amide bond, two new series of dyes were synthesized (Fig. 17.4) using amine bond as a new connection between the anthraquinone and QAS groups. These dyes are very stable under both alkaline and acidic conditions (Liu and Sun, 2008), and have



17.4 Chemical structures of antimicrobial cationic dyes (Liu and Sun, 2008).

different alkyl chains with different lengths varying from C4 to C16. The dyes containing alkyl chain lengths of C8 and C12 demonstrated the most powerful antimicrobial activity, and the dyes with two quaternary ammoniums sites were stronger than these with one site in antimicrobial activities. The minimum inhibition concentration of the dyes was as low as 10 ppm in solutions (Liu and Sun, 2008).

An antimicrobial reactive dye that can work on cellulosic fabrics as well as nylon, silk and wool fabrics was produced with QAS as biocidal site (Zhao *et al.*, 2008). The dye showed the desired antimicrobial functions in solutions, but when it was incorporated to fabrics, the antimicrobial functions were unexpectedly lost. No matter what process, reactive or basic dyeing, was employed the dyed fabrics lost antimicrobial functions even though the dyes are strong biocides *in vitro*. Several factors could cause this effect. One is that only surface dyes could be in contact with bacteria cells and provide the functions, while they also can be easily washed off during laundering. Another reason may be that all detergents are anionic compounds which could form insoluble ion pairs with the cationic sites. Most QAS exhibit the functions in dissociated ionic form in solutions. Anionic surfactants could form precipitates with QAS in solutions and could thus reduce the antimicrobial efficacy (Liu and Sun, 2008).

However, if the anionic surfactant concentration is higher than its CMC (critical micelle concentration) the biocidal functions of the QAS will not be affected (Hashemi and Sun, 2010). It was also found that the immobilized QAS on substrates still demonstrated the functions (Tiller *et al.*, 2001). In addition, some cationic species such as calcium and magnesium could also affect antimicrobial properties of the dyes (Hashemi and Sun, 2010). The comparison of antibacterial efficacy of pyridinium structures revealed that more hydrophobic moieties could increase antimicrobial power of the substrates (Zhao *et al.*, 2008).

17.3 Natural antimicrobial colorants

Natural colorants can be grouped based on their sources, methods of application, colors and chemical structures. They are mainly in the category of phenolic compounds, which play an important role in the growth and reproduction of plants and serve as defense systems against pathogens and predators. Many of them possess antioxidant activity and have shown remarkable antibacterial, anti-inflammatory and anticancer functions. In fact, many of the plants that can produce natural colorants have been known for their medicinal and herbal applications. These phenolic compounds based on their various structural moieties can be categorized into groups such as quinones, flavonoids, tannins, lignanes, curcuminoids, coumarins, stilbenes and their subgroups (Chenghaiah *et al.*, 2010; Dweck, 2002; Huang and Cai, 2009).

17.3.1 Quinones

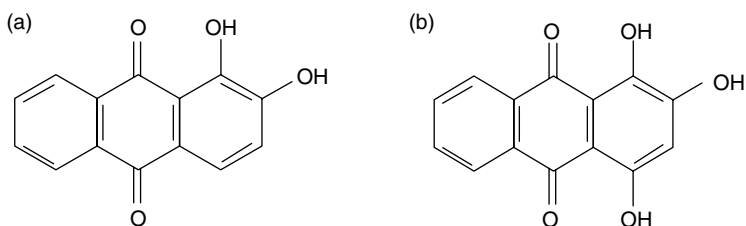
Quinone-type compounds including anthraquinones, naphthoquinones, phenanthraquinones and benzoquinones are naturally occurring in plants with remarkable therapeutic applications (Dweck, 2002; Huang and Cai, 2009; Chenghaiah *et al.*, 2010). These compounds are the basis of many of the ancient natural dyes (Chenghaiah *et al.*, 2010). In addition, they have been used as medicines due to their antibacterial, antiviral or antifungal activities (Huang and Cai, 2009).

Anthraquinones

Anthraquinones are the largest class of naturally occurring quinones and contain some of the most important natural colorants such as alizarin, purpurin, munjistin, emodin, chrysophanol, aloe-emodin, physcion, rhein, etc. They exist in the form of hydroxyanthraquinones and usually have 1–3 hydroxyl groups. These quinone dyes could form complexes with different metal salts resulting in very good color fastness (Cai *et al.*, 2006; Huang and Cai, 2009).

Alizarin and purpurin (Fig. 17.5) are two main anthraquinone-type colorants found in the root and tubers of *Rubia tinctorum* (Common Madder), *R. peregrine* (Wild Madder), *R. cordifolia* (Indian Madder), and *R. munjista*. Madder has been cultivated and used as a source of red dyes in Asia, Europe and America. In fact the oldest sample of madder dyed cotton found in Egypt belongs to the third millennium bc (De Santis and Moresi, 2007; Puchalska *et al.*, 2003). Other colorants found in these plants include munjistin, pseudopurpurin, xanthopurpurin, ruberythric acid and rubiadin (Sanyova and Reisse, 2006).

Alizarin and purpurin were found in glycoside or monosaccharide form in the plants. Part of alizarin can be extracted directly from the root of three-year-old plants while the higher yield of colorants especially purpurin could be obtained from the plants after two years' storage. During this storage time fermentation occurs and enzymes hydrolyze the glycoside and yield



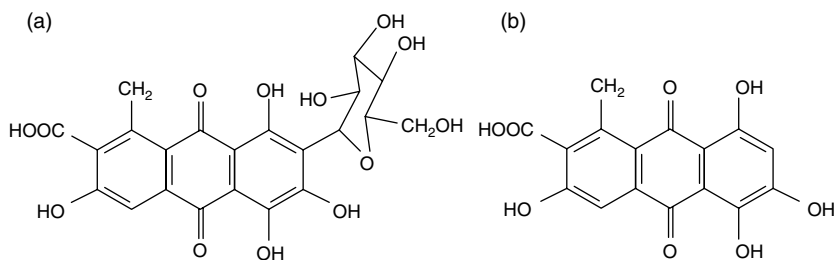
17.5 Chemical structure of (a) alizarin and (b) purpurin.

the free anthraquinone red dyes. In fermentation process particles stick together and form a solid mass called lake. The enzymatic process is considered the best since acidic or basic hydrolysis leads to the formation of a mutagenic compound called lucidin (Bechtold and Mussak, 2009; Chenciner, 2000). Madder has been used to dye wool, leather and cotton and can also be used as a food colorant. Alizarin known as Pigment Red 83 was one of the first colorants synthesized and commercialized in 1863 (Chenghaiah *et al.*, 2010; De Santis and Moresi, 2007).

Alizarin and purpurin have antimicrobial and antifungal activity against different pathogenic bacteria (Bechtold and Mussak, 2009; Chenciner, 2000). Wool fibers dyed with madder have shown higher insect resistance against carpet beetles (Park *et al.*, 2005). Purpurin even reveals an antigenotoxic effect against a range of different environmental carcinogens such as heterocyclic amines (Marczylo *et al.*, 1999). In medicinal application, madder has been used in skin care products with astringent, tonic, vulnerary and antiseptic functions. It can be used to clean open wounds and treat skin diseases, especially tubercular conditions of the skin and mucous tissues. Several studies on the safety of these compounds as phytopharmaceutical and food colorants have shown that only lucidin among these structures is mutagenic (Dweck, 2002).

Carminic acid (Fig. 17.6) is another important hydroxyanthraquinone-based colorant, which is derived from cochineal and has been used to dye wool, silk and cotton fabrics. Its brilliant red color with great light fastness could suppress many similar synthetic ones used in textiles (Taylor, 1986). Carminic acid consists of an anthraquinone with a sugar moiety attached to it. Treatment of carminic acid with an aluminum salt produces aluminum lake or carmine. Carminic acid is water soluble, and an acid stable colorant. Its aluminum lake, carmine, is soluble in alkaline media and has higher stability to heat, light and oxygen. In alkaline conditions carmine provides a blue-red shade (Cosentino *et al.*, 2005).

Although cochineal has shown antimicrobial activity against *S. aureus*, the dyed wool fabric did not provide any antimicrobial activity. However,



17.6 Chemical structures of (a) carminic acid and (b) kermesic acid.

the wool fabrics dyed with cochineal and some metal mordant revealed up to 100% antimicrobial functions depends on the type of metals (Bae and Huh, 2006).

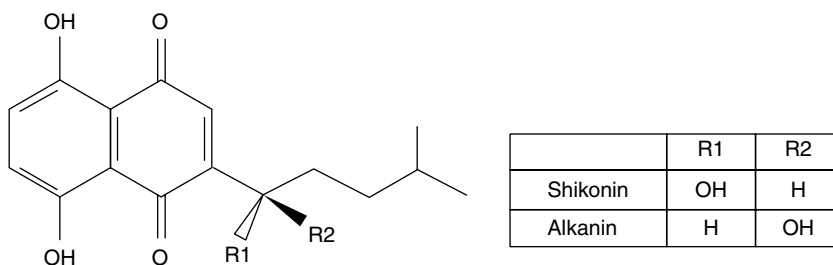
Naphthoquinones

Another main class of quinone colorants are naphthoquinones including shikonin, alkannin, juglone and lawsone (Chenghaiah *et al.*, 2010; Dweck, 2002). Shikonin (Fig. 17.7) is a naturally occurring naphthoquinone found in the dried root of the plant *Lithospermum erythrorhizon*. The s-enantiomer form of this pigment known as alkannin (Fig. 17.7) was also identified in the root of the plant *Alkanna tinctoria* (Okamoto *et al.*, 1995; Papageorgiou *et al.*, 1999). These two red pigments have traditionally been used as natural colorants in textile, food and cosmetic industries. Besides their use as pigments, shikonin and its derivatives have been used as a medicine for antimicrobial, anti-inflammatory and anti-tumor purposes. They also have shown ability to heal wounds, burns and hemorrhoids via proliferation of granulation tissue (Kamei *et al.*, 2002; Ordoudi *et al.*, 2011).

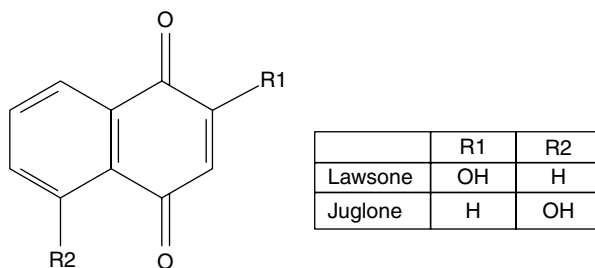
Shikonin is the first natural colorant that has been commercially produced by a plant cell culture method to supply the cosmetic industry in Japan since 1983 (Fujita *et al.*, 1983; Singh, 2010). Shikonin was loaded into PCL/PTMC (poly(epsilon-caprolactone)/poly(trimethylene carbonate)) nanofibers via electrospinning method. The fibers showed a sustained release of shikonin over a 48 h period with no sign of losing activity, thus ideal for drug delivery or in pads for wound healing (Han *et al.*, 2009).

Lawsone, a major colorant component extracted from *Lawsonia inermis* (Henna), and Juglone, extracted from walnut (*Juglans*), are the two most prominent members of naphthoquinone-type dyes (Fig. 17.8) (Endrini, 2002, 2007). This compound is well known for its cosmetic use to dye hair, nails and skin while it is been used to color textiles including leather, wool and silk (Shafik and Elseesy, 2003).

Juglone, an isomer of Lawsone, occurs in the leaves, root and bark of *Juglans regia* (English walnut, Persian walnut and Californian walnut),



17.7 Chemical structures of shikonin and alkanin.



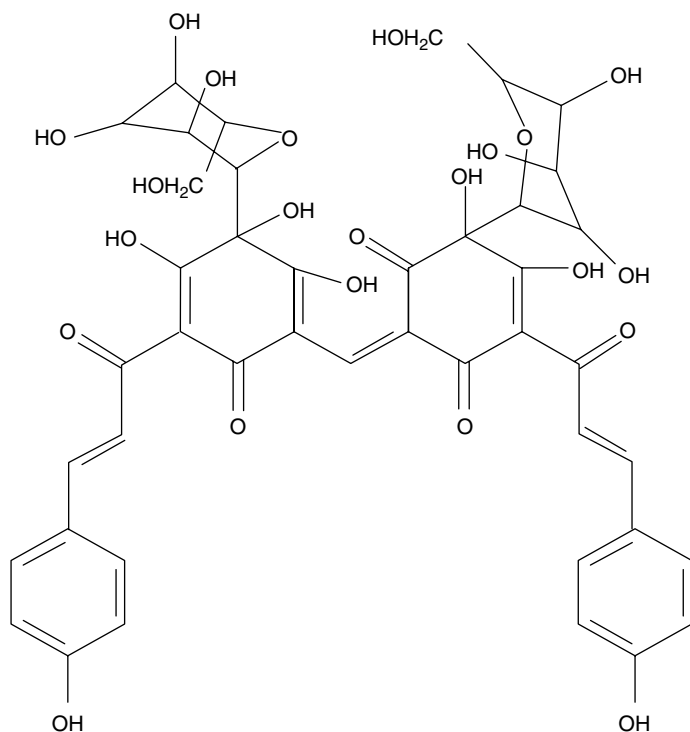
17.8 Chemical structures of lawsone and juglone.

J. cinerea (butternut and white walnut) and particularly *J. nigra* (black walnut) (Ali *et al.*, 2009; Inbaraj and Chignell, 2004). Juglone, with a dark reddish brown color, is mostly used to dye fabrics and hair, and is known as C.I Natural Brown 7 as well. Lawsone and juglone as members of the quinone-type compound family are found to possess antibacterial, antifungal, antiviral and antineoplastic activities. They could also inhibit tumor cell growth (Al-Rubiay *et al.*, 2008; Chenghaiah *et al.*, 2010; Endrini *et al.*, 2007). Their bioactivities are considered to be related to their high protein binding ability. They can covalently bind to the proteins, especially keratin in hair and skin through Michael addition reactions. Henna in particular has anti-inflammatory effects and traditionally has been used as a cooling agent and astringent to treat skin infections such as boils, burns and bruises. Juglone traditionally has been used for many years as a treatment for localized, topical fungal infections such as ringworm (Al-Rubiay *et al.*, 2008; Dweck, 2002; Endrini *et al.*, 2002; Sarkar and Dhandapani, 2009).

Benzoquinones

Carthamin (Natural Red 26) (Fig. 17.9) is a benzoquinone-based metabolite of safflower with the botanical name of *Carthamus tinctorius* L. Flower petals of the plant contain two main colors, the water-insoluble red Carthamin and a water-soluble yellow dye carthamidin. At the beginning the base compound in plant is yellow and as the flower grows, the yellow color oxidizes to a red oil-soluble colorant (Carthamin) (Ekin, 2005; Kim and Paik, 1997). The yield of Carthamin is about 0.4% of the flower petals while safflower yellow content is 26–36%. Safflower has been widely cultivated for its oil seed in industry but traditionally its petals have been used as a dye for textiles, cosmetics, coloring and flavoring of foods and drinks (Ekin, 2005).

Its extract is used as a harmless colorant in the cosmetic industry and shows a good light and washing fastness on dyed cotton and silk fabrics (Kim and Paik, 1997; Koren, 2001). In recent years, the traditional medicinal aspect of Carthamin has received attention as a cure for menstrual



17.9 Chemical structure of carthamin.

problems, cardiovascular disease and pain and swelling associated with trauma (Hiramatsu *et al.*, 2009; Kanehira *et al.*, 1990; Kim and Paik, 1997; Siva, 2007). Experimental results have shown that Carthamin has free radical scavenging activity against superoxide, hydroxyl and 1,1-diphenyl-2-picrylhydrazyl (DPPH) radicals and singlet oxygen which inhibits oxidative damage to lipids, proteins and nucleic acids. Quenching the free radicals involved in aging can result in a neuroprotective effect against neuron loss in forms of dementia including Alzheimer's (Hiramatsu *et al.*, 2009).

Carthamin is unstable in water and irreversibly changes to an unknown yellow-brown component. It is also unstable upon exposure to visible and ultraviolet (UV) light, oxygen and in the pH conditions out of 1.5–5.5 (Kanehira *et al.*, 1990; Kim and Paik, 1997).

Quinolones have been identified as rapid biocidal compounds. They can change the cell membrane permeability which leads to cytoplasmic leakage and cell death. They can be toxic by their ability to form free radicals. They can undergo one or two electron reduction to form semiquinones or hydroquinones respectively. The semiquinones could be toxic per se or they can react with molecular oxygen and form the superoxide anion

radical and regenerate the parent quinone which then can be reduced again (Chenghaiah *et al.*, 2010).

17.3.2 Flavonoids

Flavonoids are one of the most abundant groups of the natural phenolic compounds in plants, which provide color and protection against UV-B irradiation. They have been found in flowers, leaves, fruit and seeds as well as tea, wine, propolis and honey (Cushnie and Lamb, 2005). They have been widely used to dye fabrics; in fact, they make up almost 50% of all the natural colorants listed in the color index, although their light fastness is not high and falls below other classes of natural dyes such as anthraquinones and indigoids (Crews, 1987; Cristea and Vilarem, 2006; Cushnie and Lamb, 2005).

The core structure of the flavonoid compounds is the 2-phenylbenzo[α]pyrene or flavone nucleus comprising two benzene rings (A and B) linked by a three-carbon bridge that usually forms a heterocyclic pyrane C-ring. The flavonoids, based on the degree of oxidation and functional groups of C-ring, are divided into different classes. These classes are defined based on the existence of hydroxyl-containing side chain on the C-ring. The first class is the 3-desoxy flavonoid including chalcone, flavanones and flavones, and the second class is 3-hydroxy flavonoid consisting of flavonols, anthocyanidins, leucoanthocyanidins and flavonols or catechins (Brown, 1980; Cushnie and Lamb, 2005; Shils *et al.*, 2006). Most of the flavonoids in plants exist in various glycoside form or other conjugates such as sulfates (Zhang *et al.*, 2007). Some of the flavonoids, for example quercetin, have been reported to have over 70 glycosidic combinations. These glycoside forms can be hydrolyzed in a dyeing bath to aglycone form and bind to the fabrics (Brown, 1980; Guinot *et al.*, 2008), although some studies mentioned that glycoside form can dye the fabrics as well (Surowieca *et al.*, 2003; Zhang *et al.*, 2007).

Flavonoids are usually yellow in color, except for anthocyanins, with a spectrum of colors from yellow to red, violet and blue (Stintzing and Carle, 2004). In addition, many flavonoids possess antibacterial, anti-inflammatory, anticarcinogenic and enzyme inhibition activities and were used for centuries to cure diseases (Cushnie and Lamb, 2005; Krolicka *et al.*, 2008). For example, propolis containing galanin and pinocembrin has been used for treatment of sores and ulcers (Cushnie and Lamb, 2005). *Ginkgo biloba* extract containing flavonoid compounds has been used in Korea as a natural antimicrobial agent in herbal medicine. In a recent study the extract was applied to bedclothes made from Tencel Jacquard fabrics (cellulosic-based fabric). The treated fabric showed 98.2% antimicrobial activity against *S. aureus*. Adding silicone as a softener to the *G. biloba*-treated fabric increased the antimicrobial activity to 100% and this activity was maintained after 30 consecutive launderings (Jang and Lee, 2010). Chitosan fibers were grafted

with flavonoids and the functionalized polymer showed antioxidant activity and higher antimicrobial effect against *Bacillus subtilis* and *Pseudomonas aeruginosa* (Sousa *et al.*, 2009).

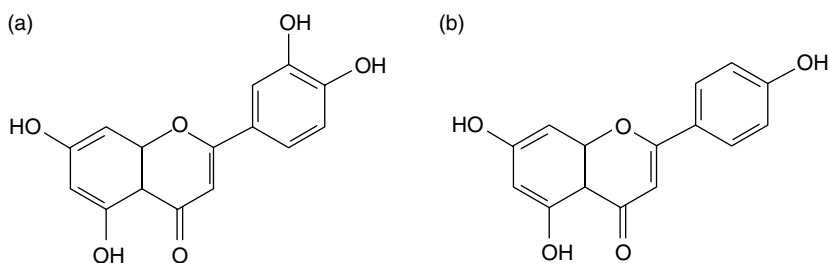
Flavones

Flavones are the most popular colorants used as textile dyes due to their often high light fastness (Ferreira *et al.*, 2004). The most common flavones are apigenin, luteolin and their glycosides (Fig. 17.10). Luteolin and its derivatives named luteolin 7-glucoside and 5-deoxyluteolin were identified as yellow colorants in fabrics belonging to pre-Colombian Andes cultures (Zhang *et al.*, 2007). Usually flavones such as luteolin and its derivatives have higher light and thermal stability compared to other flavonols such as quercetin (Crews, 1987; Shils *et al.*, 2006). Their higher stability might be related to the absence of a hydroxyl group on position 3 compared to presence of OH group in flavonols (Zhang *et al.*, 2010). The color fading rate on fabric is fast initially, followed by a slower constant rate like most dyes (Crews, 1987).

Weld with the botanical name of *Reseda luteola* L. is a native Euro-Asian plant and has been used as the best source of natural yellow colorant for silk and wool with the highest light fastness (Angelini *et al.*, 2003; Crews, 1987; Woelfl *et al.*, 2010). In addition it was used as a pigment in painting and in manuscripts. In both applications, metal cations were used as a mordant to increase the stability of the color (Amat *et al.*, 2009). The chrome complex has shown higher fastness due to quenching effect of chrome (Cerrato *et al.*, 2002; Crews, 1987; Zhang *et al.*, 2010). Extract of weld has been applied for treating wounds and chronic skin disorders. It has shown anti-inflammatory and antimicrobial properties (Ramos *et al.*, 2006).

Flavonols

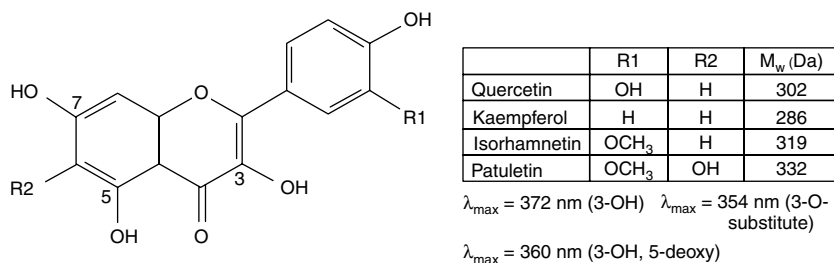
Flavonols are the most abundant yellow colorants. There are a variety of different sources of flavonols, but only a few of them produced a sufficient



17.10 (a) Luteolin ($M = 286$ Da, $\lambda_{\max} = 348$ nm) and (b) apigenin ($M = 270$ Da, $\lambda_{\max} = 337$ nm).

quantity of dyes with relatively good color fastness (Zhang *et al.*, 2010). Flavonols can easily chelate with metal cations due to the presence of neighboring hydroxyl–keto functional groups (Bajpai and Vankar, 2007). Quercetin and kaempferol are the predominant flavonols followed by morin, fisetin, myricetin, isorhamnetin and their glycoside derivatives (Fig. 17.11). Flavonols usually have brilliant yellow color and have been mainly used to dye wool and silk fabric since ancient times. The characteristic UV-Vis maximum absorption bands of morin are 378 and 261 nm. Quercetin-like structures have UV spectrum with maximum absorption at 258, 278, 358 nm (Siva, 2007).

Green tea, red grapes, onion especially red onion and leafy vegetable, and berries are the main source of quercetin. Onion skin contains a mixture of quercetin, kaempferol and quercetin-3-o-glucoside and has been used to dye wool and silk (Wei *et al.*, 1990). Tea has been used to dye cotton and jute using copper sulfate or ferrous sulfate as mordants. Marigold (*Tagetes patula* L.) has been used in European countries to achieve dark yellow colors on cotton- and protein-based fabrics. The color has shown good light and excellent washing fastness. In addition, marigold extract contains lutein, a carotenoid colorant which has been used as food colorant for pigmentation of poultry skin and eggs and for protection against certain eye diseases (Krinsky and Johnson, 2005). The flowers have shown antifungal and antimicrobial activities (Guinot *et al.*, 2008). Flavonols including quercetin and morin have the ability to associate with Al (III) as mordant which increases their photo stability. Forming complex with metals reduces the electron density on the chromophore and enhances the resistance to photo oxidation, which leads to higher light fastness (Guinot *et al.*, 2008). Many flavonoids such as quercetin, morin and myricetin have been reported to form fluorescent chelates with metals (Chang *et al.*, 2003; Surowieca *et al.*, 2003). Quercetin has been used in SiO₂ particle probe (Frederice *et al.*, 2010) and anodic aluminum oxide-nano composites to produce sensitive fluorescent probes for detecting aluminum ion (Chang *et al.*, 2003).



17.11 Chemical structures of main flavonol colorants.

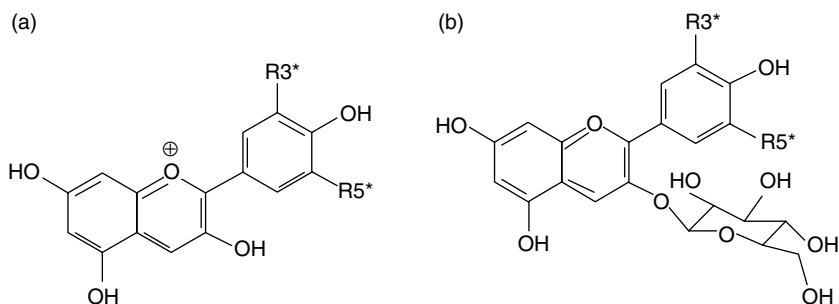
Antimicrobial functions of flavonoids

Flavonoids have shown antioxidant, anti-inflammatory, anti-allergic, anti-carcinogenic and antimicrobial functions (Sarkar and Dhandapani, 2009). Flavonols in diet have been reported to reduce the risk of heart disease and cancer (de Vries *et al.*, 1998). Among flavonoids, flavonols and some of the flavones have shown activity against Methicillin-resistant *S. aureus* (MRSA), while other compounds such as flavonones, flavonols, isoflavones, chalcones and biflavones were inactive. None of the glycoside forms of the compounds showed any activity against micro-organisms (Chang *et al.*, 2003; Cushnie and Lamb, 2005; Krollicka *et al.*, 2008). One study on the relationship between flavonoid structure and their antibacterial activity indicated that the active flavonoids were polyhydroxylated. They have common C4 keto group and hydroxyl groups at positions C3, C5 and C7 and contain at least one hydroxyl group on ring B (de Vries *et al.*, 1998). The higher degree of hydroxylation of the A and B rings result in higher antioxidant and higher radical scavenging activities (Cai *et al.*, 2006). Myricetin is the only flavonol which possesses antimicrobial activity against gram-negative bacteria *Burkholderia cepacia* and *Klebsiella pneumonia*. The hydroxyl group at C3 position is a main parameter for bio-activity of flavonols and replacing this group with other substitute groups such as glycoside will suppress the activity. For flavones, this hydroxyl group is not the key, as in the case of luteolin and flavones (Xu and Lee, 2001).

17.3.3 Anthocyanins

Anthocyanins are the most important flavonoid colorants in plants and mostly occur in floral tissues. The six main aglycone anthocyanin chromophores and their glycosides (Fig. 17.12) are pelargonidin, cyanidin, delphinidin, peonidin, petunidin and malvidin (Stintzing and Carle, 2004). Some of them are covalently linked to flavonol glycoside co-pigments. This intermolecular co-pigmentation enhances and stabilizes the color. For example, the stable bluish color of *Ceanothus* and *agapanthus praecox* flowers is related to the delphinidin glycoside linked to a kaempferol triglycoside. The colorant has a maximum absorption at 680 nm, as well as bands at 536, 576 and 615 nm. The reported ratio of flavonol to anthocyanin in the complex is 8:1.6 (Harborne and Williams, 2001; Yoshitama, 1978). Pigment-co-pigment complexes are mostly linked together by hydrogen bonding but rarely via covalent linkage through organic acids (Harborne and Williams, 2001). Chelation between anthocyanin and metal cation can increase stability as well (Stintzing and Carle, 2004).

Anthocyanins are the only category of flavonoid colorants that cover a variety of shades from orange-red (pelargonidin) in reddish to blue-violet



	R3*	R5*	(a) λ_{\max} (nm)	(b) λ_{\max} (nm)
Pelargonidin	H	H	520	516
Cyanidin	OH	H	535	530
Delphinidin	OH	OH	546	543
Peonidin	OCH ₃	OH	532	536
Malvidin	OCH ₃	OCH ₃	542	546

17.12 Chemical structure of anthocyanidine colorants (a) and their glycoside form (b).

(delphinidin) color of grapes and blueberries (Stintzing and Carle, 2004). The hydroxylated anthocyanins have bathochromic shift while methylation or glycosidation of OH at position 3 reduces the maximum absorption band and increases the solubility and stability of the color. Aglycone forms of anthocyanins are rarely found in fresh plant materials (Stintzing and Carle, 2004; Wrolstad *et al.*, 2005).

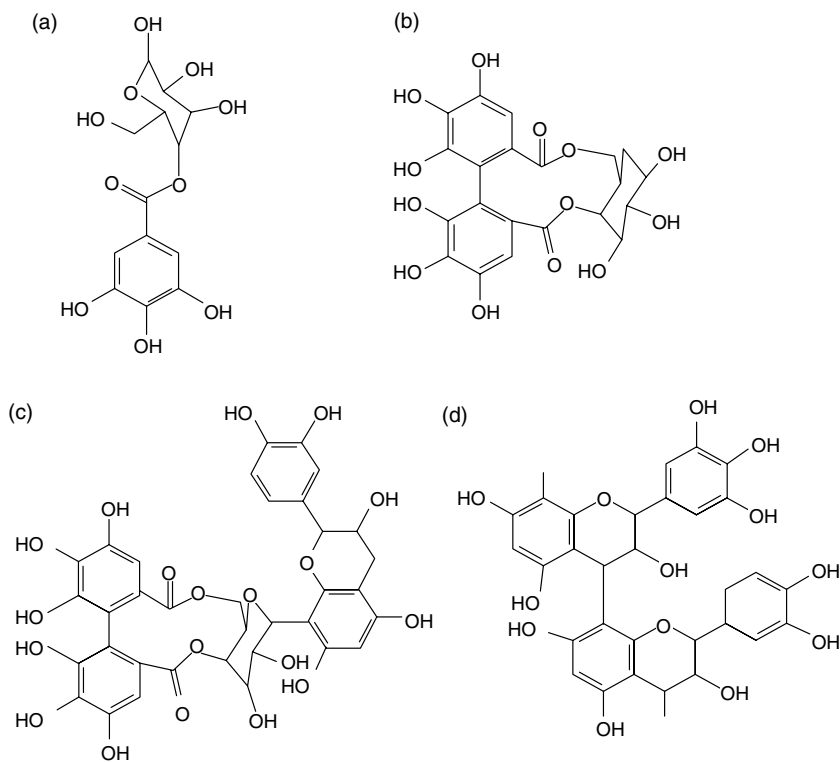
Despite the variety of colors and high abundance in nature, they were rarely used as textile colorants due to degradation during processing and storage. Cotton fabric dyed with anthocyanins extracted from grape pomace using tannic acid as mordant, and the combination of the mordant with anthocyanins provided different red-violet color with good washing fastness. However, the dyed fabric did not have good light fastness (Bechtold *et al.*, 2007).

17.3.4 Tannins

Tannins are concentrated in bark, wood, leaves, fruit, roots and seeds of different plants. Their production is increased in plants with sickness so it is assumed to provide protection against infections and insects. Tannins are natural water-soluble polyphenolic compounds with light yellow or white color. In textiles they are well-known mordant dyes for brown and black colors (Ferreira *et al.*, 2004; Joshi *et al.*, 2009; Khanbabaee and van Ree, 2001). Tannins are applied on fabric as cationic dyes and have also been used in the production of inks (iron gallate ink) (Khanbabaee and van Ree, 2001).

Tannins are widely used as tanning agents in preparing leather, herbal medicine, textile dyes and antioxidants in the food industry (Khanbabaee and van Ree, 2001). They have antiviral, antimicrobial, anti-inflammatory and especially, anti-tumor activity and could be used as astringent, antiseptic and haemostatic agents (Joshi *et al.*, 2009). Tannins divide into four major groups based on their chemical structure: *Gallotannins*, *ellagitannins*, *complex tannins* and *condensed tannins* (Fig. 17.13). The first three groups contain galloyl moieties and their derivatives are attached to a variety of polyol-, catechin- and triterpenoid core structures. Many types of tannins in these categories can be hydrolyzed after treatment with hot water (Khanbabaee and van Ree, 2001).

Pomegranate (*Punica granatum* L.) is rich in hydrolyzable tannins including punicalagin (80–85% w/w), ellagic acid (EA; 1.3% w/w), punicalin and EA-glycosides (hexoside, rhamnoside and pentoside) (Sarkar and Dhandapani, 2009; Seeram *et al.*, 2005b). Besides its use as fruit and juice,



17.13 Chemical structures of (a) gallotannins, (b) ellagitannins, (c) complex and (d) condensed tannins.

pomegranate fruit husk/peels have been used in dyeing wool, silk and cotton fabrics for 1000 years. In addition it has shown antimicrobial activities on cotton and wool fabrics with good laundry durability and light fastness (Joshi *et al.*, 2009; Lee *et al.*, 2009; Seeram *et al.*, 2005a). The antibacterial activities of pomegranate extract are possibly related to EA and tannin components. EA has been reported as an antioxidant, antimicrobial, anti-inflammatory, antiviral, or anticarcinogen agent and has showed inhibitory effect on the microbes when applied on textile materials (Lee *et al.*, 2009; Sarkar and Dhandapani, 2009; Seeram *et al.*, 2005b).

Quercus infectoria (QI) is another tannin-rich plant which has been used with alum and copper mordants to dye cotton fabrics. The dyed fabric with 12% concentration (owf, on weight of fiber) showed antimicrobial activity (70–90%) against gram-negative bacterium *E. coli* and gram-positive bacterium *B. subtilis*. The antibacterial activity of treated cotton fabric with QI was not durable to laundering but the mordanted samples retain 80–100% activity after five launderings. The cotton textiles treated with QI can be used as anti-odor textiles for sportswear and household products (Gupta, 2008; Gupta and Laha, 2007; Sarkar and Dhandapani, 2009). QI is also known as an ideal tanning material in the leather industry (Dıđrak *et al.*, 1999).

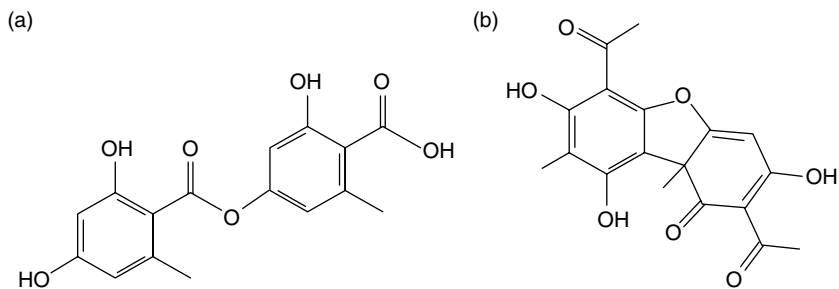
It has also been reported that wool and silk fabrics dyed with extract of black tea, peony, clove, *Coptis chinensis* and gallnut extracts showed excellent antimicrobial activity against *S. aureus* (96.8–99.9%). All the fabrics dyed, except the one dyed with peony extract, could also kill *K. pneumonia* (95.7–99.9%) (Lee *et al.*, 2009). The antimicrobial activity of black tea, peony and galls extracts might be due to tannins.

17.4 Antimicrobial colorants from micro-organisms

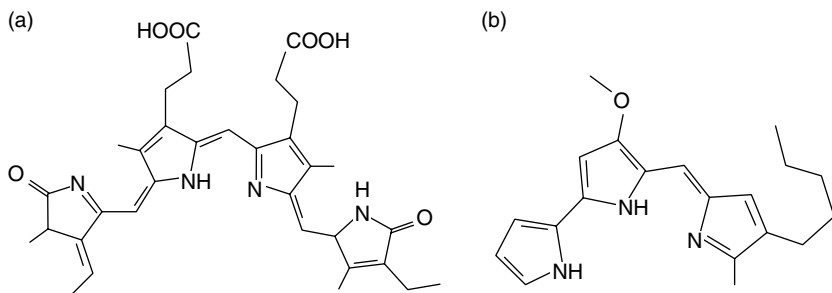
Micro-organisms such as fungi and bacteria are a key source of natural colorants. Colorants are secondary metabolites from micro-organisms which have no effect on the cell growth of fungi but serve different functions based on their structures. For example, they can have a protective function against light or can be used as a cofactor in biochemical reactions. Use of fungi colorant in foodstuff is not a novel practice. Different water-soluble natural colorants from fungi such as red pigment from *Monascus* and yellow carotenoids from *Dunaliella salina* have already been used as food colorants (Mapari *et al.*, 2005). Many colorants resulting from micro-organisms, such as ones with quinine structures, possess significant antibiotic and antibacterial activity and are used as herbal medicines. Although some of these antimicrobial colorants have been reported, researchers have renewed interest in looking for alternatives to current synthetic dyes and novel antimicrobial dyes in recent years (Molinski and Faulkner, 1988; Richardson *et al.*, 1998).

Lichens are a combination of fungi and algae and have been used to dye fabrics for a long time. Like anthocyanins, they have different color shades from yellows, oranges and browns to reds, pinks and purples, but their washing and light fastness is better. The colorant extracted from *Rocella tinctoria* was used as an alternative for royal purple from shellfish (Hancock and Boxworth, 1997). The main natural colorants from the lichen extracts, *Leconora tartarula*, *Ochrolechia tartarea* and *R. tinctoria*, are depsides. For example, lecanoric acid is known as Natural Red 28. The other most common yellow colorant from lichens is usnic acid (Fig. 17.14). Usnic acid and depsides have shown antimicrobial activities against gram-positive bacteria and some pathogenic fungi (Dawson, 2007; Schmeda-Hirschman *et al.*, 2008). It also has anti-inflammatory, anti-insect and preserving properties and can absorb UV light. Usnic acid has been used as a herbal medicine and recently has been marketed in the USA as an ingredient for weight reduction (Dawson, 2007; Hobbs, 1990).

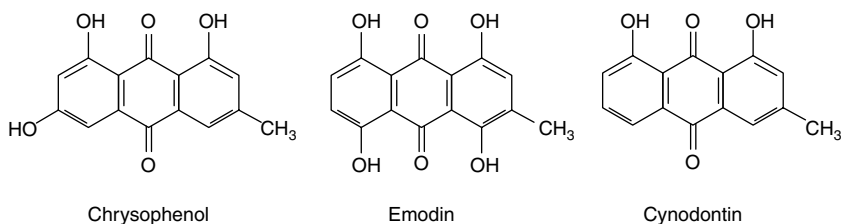
Phycocyanobilin (Fig. 17.15) is a colorant from *spirulina*, a blue-green algae, which has been used for many years to dye fabrics. Research on bacterial production of prodigiosin compounds (Fig. 17.15) showed that fabrics dyed with this compound, including wool, nylon, silk and acrylic fibers, exhibited good antibacterial activities (Alihosseini *et al.*, 2008).



17.14 Chemical structures of (a) lecanoric acid and (b) usnic acid.



17.15 Chemical structures of (a) phycocyanobilin and (b) prodigiosin.



17.16 Anthraquinones produced by *C. lunata*.

The dyed fabrics could kill gram-negative bacterium *E. coli* which was not reported before. The antimicrobial power of the dyed fabric increased under exposure to UV light, suggesting that photo-induced reactions on the colorant could be a cause of its antimicrobial activity (Alihosseini *et al.*, 2008, 2010). Genetic modification of the bacterium increased the yields of prodigiosin compounds to 81% and improved selectivity of the pigment production with 97% purity (Alihosseini *et al.*, 2010). This result is important to commercial applications as it can simplify the purification step. In another study, colorants resulted from five different fungi were used to dye cotton and leather fabrics, with the dyed fabrics showing 50% antibacterial activity with post-mordanting (Velmurugan *et al.*, 2009).

Colorants isolated from fungi and bacteria could be chemically modified to produce new bio-based colorants for textile products. In other words, these chemicals can serve as building blocks for bio-based colorants. One example is a strain of *Curvularia lunata*, which is capable of producing three anthraquinones: cynodontin, helminthosporin and chysophanol (Fig. 17.16). Cynodontin was converted successfully to two anthraquinone biocolorants: 'Disperse blue 7' and 'Acid green 28'. The properties of these biocolorants applied to knitted polyamides were compared with those of conventional colorants and found to be identical in all respects (Hobson and Wales, 1998).

17.5 Photo-activated antimicrobial colorants

Photo-sensitizers and some dyes with special structures can become activated upon exposure to UV or daylight, and the activated (excited) forms of the compounds can react with other substrate and result in very reactive species such as singlet oxygen and radicals. The color is the result of absorption of specific wavelengths of light by the chemical. The molecule absorbs light, and as a result, one or more electrons will be excited to a higher energy, non-bonding or anti-bonding molecular orbital. The excited compound will be in a structure possessing bi-radicals in triplet status. The triplet bi-radicals can collide with another bi-radical-oxygen in the air to produce singlet oxygen

or peroxide and consequently hydroxyl radicals, which could cause bacterial cell damage or necrosis (Maisch *et al.*, 2004; Wainwright, 2008). Synthetic positively charged photo-sensitizers such as methylene blue and toluidine blue and natural ones including porphyrins and phthalocyanines have shown antibacterial activity against both gram-positive and gram-negative bacteria (Maisch *et al.*, 2004). Antimicrobial properties of porphyrin grafted nylon fabrics with limited activity against bacteria were reported. Although this dye showed better antimicrobial effect in free form under the light, the amount of singlet oxygen produced by the dye bound to the fabric was not enough to kill all bacteria in a short contact time (Bozja *et al.*, 2003; Sherrill *et al.*, 2003). The samples need high light intensity and longer exposure to get better antimicrobial effects. In addition, some photo-sensitizers, usually a conjugate chromophore, can be excited by longer wavelength UV or fluorescent lights to provide antimicrobial effects as well (Decraene *et al.*, 2008; Hong and Sun, 2007, 2008). Rose bengal in the mixture of dye/PVA (poly vinyl alcohol) hydrogel showed photo-active antimicrobial functions under both fluorescent and UVA (365 nm) light against both *E. coli* and *S. aureus* (Hong and Sun, 2010a). Leather coated with this photo-sensitizer showed durable antimicrobial activity to abrasion and light (Hong and Sun, 2010b). In other application, photo-sensitizer applied on fabrics was used as radical initiator to graft polymer onto the fabrics (Liu *et al.*, 2010). These antimicrobial colorants are advantageous in medical use textiles for prevention of cross-transmission of infectious diseases through hard and soft surface areas.

17.6 References

- ABOELSOU, N. H. (2010) Herbal medicine in ancient Egypt. *Journal of Medicinal Plants Research*, 4(2): 82–86.
- ALBERT, A., RUBBO, S. D. and BURVILL, M. I. (1949) The influence of chemical constitution on antibacterial activity: a survey of heterocyclic bases, with special reference to benzquinolines, phenanthridines, benzacridines, quinolines and pyridines. *British Journal of Experimental Pathology*, 30(3): 159–175.
- ALI, S., HUSSAIN, T. and NAWAZ, R. (2009) Optimization of alkaline extraction of natural dye from henna leaves and its dyeing on cotton by exhaust method. *Journal of Cleaner Production*, 17(1): 61–66.
- ALIHOSSEINI, F. and SUN, G. (2008) Recent progresses in antibacterial dyes. *Household and Personal Care Today*, 4: 17–21.
- ALIHOSSEINI, F., JU, K. S., LANGO, J., HAMMOCK, B. D. and SUN, G. (2008) Antibacterial colorants: characterization of prodiginines and their applications on textile materials. *Biotechnology Progress*, 24: 742–747.
- ALIHOSSEINI, F., LANGO, J., JU, K. S., HAMMOCK, B. D. and SUN, G. (2010) Mutation of bacterium *Vibrio gazogenes* for selective preparation of colorants. *Biotechnology Progress*, 26(2): 352–360.
- AL-RUBIAY, K. K., JABER, N. N., AL-MHAAWE, B. H. and ALRUBAIY, L. K. (2008) Antimicrobial efficacy of henna extracts. *Oman Medical Journal*, 23(4): 253–256.

- AMAT, A., CLEMENTI, C., DE ANGELIS, F., SGAMELLOTTI, A. and FANTACCI, S. (2009) Absorption and emission of the apigenin and luteolin flavonoids: a TDDFT investigation. *Journal of Physical Chemistry A*, 113: 15118–15126.
- ANGELINI, L. G., BERTOLI, A., ROLANDELLI, S. and PISTELLI, L. (2003) Agronomic potential of *Reseda luteola* L. as new crop for natural dyes in textiles production. *Industrial Crops and Products*, 17(3): 199–207.
- BAE, J.-S. and HUH, M.-W. (2006) The dyeability and antibacterial activity of wool fabric dyed with Cochineal. *Journal of Korean Society of Dyers and Finishers*, 18(50): 22–29.
- BAJPAI, D. and VANKAR, P. S. (2007) Antifungal textile dyeing with mahonia napaulensis D.C. leaves extract based on its antifungal activity. *Fibers and Polymers*, 8(5): 487–494.
- BECHTOLD, T., MAHMUD-ALI, A. and MUSSAK, R. (2007) Anthocyanin dyes extracted from grape pomace for the purpose of textile dyeing. *Journal of the Science of Food and Agriculture*, 87(14): 2589–2595.
- BECHTOLD, T. and MUSSAK, R. (2009) *Handbook of Natural Colorants*, Wiley Series in Renewable Resource. Chichester: John Wiley & Sons.
- BISHOP, J. M. (1936) *How to Win the Nobel Prize: An Unexpected Life in Science*. Cambridge, MA: Harvard University Press.
- BOZJA, J., SHERRILL, J., MICHELSEN, S. and STOJILJKOVIC, I. (2003) Porphyrin-based, light-activated antimicrobial materials. *Journal of Polymer Science Part A: Polymer Chemistry*, 41(15): 2297–2303.
- BROWN, J. P. (1980) A review of the genetic effects of naturally occurring flavonoids, anthraquinones and related compounds. *Mutation Research*, 75: 243–277.
- CAI, Y.-Z., SUN, M., XING, J., LUO, Q. and CORKE, H. (2006) Structure–radical scavenging activity relationships of phenolic compounds from traditional Chinese medicinal plants. *Life Sciences*, 78: 2872–2888.
- CERRATO, A., DE SANTIS, D. and MORESI, M. (2002) Production of luteolin extracts from *Reseda luteola* and assessment of their dyeing properties. *Journal of the Science of Food and Agriculture*, 82: 1189–1199.
- CHANG, X., WANG, S., LUO, H. and GONG, G. (2003) Study on fluorescence characteristic of quercetin–nanoporous anodic aluminum oxide composites. *Journal of Fluorescence*, 13(5): 421–425.
- CHENCINER, R. (2000) *Madder Red: A History of Luxury and Trade*. Richmond: Curzon Press.
- CHENGHAIAH, B., MALLIKARJUNARAO, K., MAHESHKUMAR, K., ALAGUSUNDARAM, M. and CHETTY, C. M. (2010) Medicinal importance of natural dyes. *International Journal of PharmTech Research*, 2(1): 144–154.
- CHUN, D. T. W. and GAMBLE, G. R. (2007) Textile technology, using the reactive dye method to covalently attach antibacterial compounds to cotton. *Journal of Cotton Science*, 11: 154–158.
- CONSTANTIN, M., FUNDUEANU, G. and NICHIFOR, M. (2008) Synthesis and characterization of novel flavonoid based biomaterials. *Revue Roumaine de Chimie*, 53(9): 753–758.
- COOPER, R. (2004) A review of the evidence for the use of topical antimicrobial agents in wound care. <http://www.worldwidewounds.com/2004/february/Cooper/Topical-Antimicrobial-Agents.html>
- COSENTINO, H. M., FONTENELE, R. S. and DEL MASTRO, N. L. (2005) Stability of γ -irradiated carmine. *Physica Scripta*, T118: 223–224.

- CREWS, P. C. (1987) The fading rates of some natural dyes. *Studies in Conservation*, 32: 65–72.
- CRISTEA, D. and VILAREM, G. (2006) Improving light fastness of natural dyes on cotton yarn. *Dyes and Pigments*, 70: 238–245.
- CUSHNIE, P. T. and LAMB, A. J. (2005) Review, antimicrobial activity of flavonoids. *International Journal of Antimicrobial Agents*, 26: 343–356.
- DAWSON, T. L. (2007) Light-harvesting and light-protecting pigments in simple life forms. *Society of Dyers and Colourists, Coloration Technology*, 123: 129–142.
- DEBNATH, M., MALIK, C. P. and BISEN, P. S. (2006) Micropropagation: a tool for the production of high quality plant-based medicines. *Current Pharmaceutical*, 7(1): 33–49.
- DECREAENE, V., PRATTEN, J. and WILSON, M. (2008) Novel light-activated antimicrobial coatings are effective against surface-deposited *S. aureus*. *Current Microbiology*, 57(4): 269–273.
- DE SANTIS, D. and MORESI, M. (2007) Production of alizarin extracts from *Rubia tinctorum* and assessment of their dyeing properties. *Industrial Crops and Products*, 26: 151–162.
- DE VRIES, J. H., HOLLMAN, P. C., MEYBOOM, S., BUYSMAN, M. N. C. P., ZOCK, P. L., VAN STAVEREN, W. A. and KATAN, M. B. (1998) Plasma concentrations and urinary excretion of the antioxidant flavonols quercetin and kaempferol as biomarkers for dietary intake 1–3. *American Journal of Clinical Nutrition*, 68: 60–65.
- DIĞRAK, M., ALMA, M. H., İLÇİM, A. and ŞEN, S. (1999) Antibacterial and antifungal effects of various commercial plant extracts. *Pharmaceutical Biology*, 37(3): 216–220.
- DWECK, A. C. (2002) Natural ingredients for coloring and styling. *International Journal of Cosmetic Science*, 24: 287–302.
- EKIN, Z. (2005) Resurgence of safflower (*Carthamus tinctorius* L.) utilization: a global view. *Journal of Agronomy*, 4(2): 83–87.
- ENDRINI, S., RAHMAT, A., ISMAIL, P. and YUN HIN, T.-Y. (2002) Anticarcinogenic properties and antioxidant activity of henna (*Lawsonia inermis*). *Journal of Medicine and Science*, 2(4): 194–197.
- ENDRINI, S., RAHMAT, A., ISMAIL, P. and YUN HIN, T.-Y. (2007) Comparing the cytotoxicity properties and mechanism of *Lawsonia inermis* and *Strobilanthes crispus* extract against several cancer cell lines. *Journal of Medical Sciences*, 7(7): 1098–1102.
- FERREIRA, E., HULME, A. N., MCNAB, H. and QUYUE, A. (2004) The natural constituents of historical textile dyes. *Chemical Society Reviews*, 33: 329–336.
- FREDERICE, R., FERREIRA, A. P. G. and GEHLEN, M. H. (2010) Molecular fluorescence in silica particles doped with quercetin-Al³⁺ complexes. *Journal of the Brazilian Chemical Society*, 21(7): 1213–1217.
- FUJITA, Y., MAEDA, Y., SUGA, C. and MORIMOTO, T. (1983) Production of shikonin derivatives by cell suspension cultures of *Lithospermum erythrorhizon*. III. Comparison of shikonin derivatives of cultured cells and ko-shikon. *Plant Cell Reports*, 2: 192–193.
- FUNG, D. Y. C. and MILLER, R. D. (1973) Effect of dyes on bacterial growth. *Applied and Environmental Microbiology*, 25: 793–799.
- GAO, Y. and CRANSTON, R. (2008) Recent advances in antimicrobial treatments of textiles. *Textile Research Journal*, 78: 60–72.
- GIORGIO, C. D., NIKOYAN, A., DECOME, L., BOTTA, C., ROBIN, M., REBOUL, J. P., SABATIER, A. S., MATTA, A. and DE MÉO, M. (2008) DNA-damaging activity and mutagenicity of 16 newly synthesized thiazolo[5,4-*a*]acridine derivatives with high photo-inducible

- cytotoxicity. *Mutation Research/Genetic Toxicology and Environmental Mutagenesis*, 650(2): 104–114.
- GUINOT, P., GARGADENNEC, A., VALETTE, G., FRUCHIER, A. and ANDARY, C. (2008) Primary flavonoids in marigold dye. *Phytochemical Analysis*, 19: 46–51.
- GUPTA, D. and LAHA, A. (2007) Antimicrobial activity of cotton fabric treated with *Quercus infectoria* extract. *Indian Journal of Fiber and Textile Research*, 32(1): 88–92.
- GUPTA, S. (2008) Blocking odor with renewable and botanical resources. *Journal for Asia on Textile and Apparel*. <http://www.adsaleata.com/Publicity/ePub/lang-eng/article-2326/asid-77/Article.aspx>
- HAN, J., CHEN, T. X., BRANFORD-WHITE, C. J. and ZHU, L. M. (2009) Electrospun shikonin-loaded PCL/PTMC composite fiber mats with potential biomedical applications. *Pharmaceutical Nanotechnology*, 382(1–2): 215–221.
- HANCOCK, M. and BOXWORTH, A. (1997) *Potential for Colorants from Plant Sources in England and Wales*. Arable Crops and Horticulture Division, ST106, CB28NN, Cambridge.
- HARBORNE, J. B. and WILLIAMS, C. A. (2001) Anthocyanins and other flavonoids. *Natural Product Reports*, 18: 310–333.
- HASHEMI, N. and SUN, G. (2010) Intermolecular interactions between surfactants and cationic dyes and effect on antimicrobial properties. *Industrial and Engineering Chemistry Research*, 49: 8347–8352.
- HIRAMATSU, M., TAKAHASHI, T., KOMATSU, M., KIDO, T. and KASAHARA, Y. (2009) Antioxidant and neuroprotective activities of Mogami-benibana (Safflower, *Carthamus tinctorius* Linne). *Neurochemical Research*, 34: 795–805.
- HOBBS, C. (1990) *Usnea the Herbal Antibiotic*. Santa Cruz: Botanica Press.
- HOBSON, D. K. and WALES, D. S. (1998) Green colorants. *Journal of the Society of Dyers and Colourists*, 114: 42–44.
- HONG, K. H. and SUN, G. (2007) Preparation and properties of benzophenone chromophoric group branched polymer for self-decontamination. *Polymer Engineering and Science*, 47(11): 1750–1755.
- HONG, K. H. and SUN, G. (2008) Antimicrobial and chemical detoxifying functions of cotton fabrics containing different benzophenone derivatives. *Carbohydrate Polymer*, 71: 598–605.
- HONG, K. H. and SUN, G. (2010a) Photoactive antimicrobial PVA hydrogel prepared by freeze-thawing process for wound dressing. *Journal of Applied Polymer Science*, 116: 2418–2424.
- HONG, K. H. and SUN, G. (2010b) Photoactive antimicrobial agents/polyurethane finished leather. *Journal of Applied Polymer Science*, 115: 1138–1144.
- HUANG, W.-Y. and CAI, Y.-Z. (2009) Natural phenolic compounds from medicinal herbs and dietary plants: potential use for cancer prevention. *Nutrition and Cancer*, 62(1): 1–20.
- INBARAJ, J. J. and CHIGNELL, C. F. (2004) Cytotoxic action of juglone and plumbagin: a mechanistic study using HaCaT keratinocytes. *Chemical Research in Toxicology*, 17: 55–62.
- JANG, Y. J. and LEE, J. S. (2010) Antimicrobial treatment properties of tencel acquard fabrics treated with ginkgo biloba extract and silicon softener. *Fibers and Polymers*, 11(3): 422–430.

- JANSSEN, P. A., SELWOOD, B. L., DOBSON, S. R., PEACOCK, D. and THIESSEN, P. N. (2003) To dye or not to dye: a randomized, clinical trial of a triple dye/alcohol regime versus dry cord care. *Pediatrics*, 111(1): 15–20.
- JOSHI, M., WAZED, S. and PURWAR, R. (2009) Ecofriendly antimicrobial finishing of textiles using bioactive agents based on natural products. *Indian Journal of Fiber and Textile Research*, 34: 295–304.
- KAMEI, R., KITAGAWA, Y., KADOKURA, M., HATTORI, F., HAZEKI, O., EBINA, Y., NISHIHARA, T. and OIKAWA, S. (2002) Shikonin stimulates glucose uptake in 3T3–L1 adipocytes via an insulin-independent tyrosine kinase pathway. *Biochemical and Biophysical Research Communication*, 292: 642–651.
- KANEHIRA, T., NARUSE, A., FUKUSHIMA, A. and SAITO K. (1990) Decomposition of carthamin in aqueous solutions: influence of temperature, pH, light, buffer systems, external gas phases, metal ions, and certain chemicals. *Zeitschrift für Lebensmittel-Untersuchung und -Forschung*, 190: 299–305.
- KENAWY, E. R., WORLEY, S. D. and BROUGHTON, R. (2007) The chemistry and applications of antimicrobial polymers: a state-of-the-art review. *Biomacromolecules*, 8(5): 1359–1384.
- KHANBABAEE, K. and VAN REE, T. (2001) Tannins: classification and definition. *Natural Product Reports*, 18: 641–649.
- KIM, J.-B. and PAIK, Y.-S. (1997) Stability of carthamin from *Carthamus tinctorius* in aqueous solution: pH and temperature effects. *Archives of Pharmacal Research*, 20(6): 643–646.
- KIM, Y. H. and SUN, G. (2000) Dye molecules as bridges for functional modifications of nylon: antimicrobial functions. *Textile Research Journal*, 70(8): 728–733.
- KIM, Y. H. and SUN, G. (2001) Durable antimicrobial finishing of nylon fabrics with acid dyes and a quaternary ammonium salt. *Textile Research Journal*, 71(4): 318–323.
- KOREN, Z. C. (2001) A successful talmudic-flavored high-performance liquid chromatographic analysis of carthamin from red safflower dyeing. *Dyes in History and Archaeology*, 16/17: 158–166.
- KRINSKY, N. I. and JOHNSON, E. J. (2005) Carotenoid actions and their relation to health and disease. *Molecular Aspects of Medicine*, 26(6): 459–516.
- KROLICKA, A., SZPITTER, A., GILGENAST, E., ROMANIK, G., KAMINSKI, M. and LOJKOWSKA, E. (2008) Stimulation of antibacterial naphthoquinones and flavonoids accumulation in carnivorous plants grown *in vitro* by addition of elicitors. *Enzyme and Microbial Technology*, 42: 216–221.
- LEE, Y.-H., HWANG, E.-K. and KIM, H.-D. (2009) Colorimetric assay and antibacterial activity of cotton, silk, and wool fabrics dyed with peony, pomegranate, clove, *Coptis chinensis* and gallnut extracts. *Materials*, 2: 10–21.
- LIU, J. and SUN, G. (2008) The synthesis of novel cationic anthraquinone dyes with high potent antimicrobial activity. *Dyes and Pigments*, 77(2): 380–386.
- LIU, N., SUN, G., GAAN, S. and RUPPER, P. (2010) Controllable surface modifications of polyamide by photo-induced graft polymerization using immobilized photo-initiators. *Journal of Applied Polymer Science*, 116: 3629–3637.
- MA, M. and SUN, G. (2004) Antimicrobial cationic dyes. Part 2: thermal and hydrolytic stability. *Dyes and Pigments*, 63(1): 39–49.
- MA, M. and SUN, G. (2005) Antimicrobial cationic dyes. Part 3: simultaneous dyeing and antimicrobial finishing of acrylic fabrics. *Dyes and Pigments*, 66(1): 33–41.

- MA, M., SUN, Y. and SUN, G. (2003) Antimicrobial cationic dyes. Part 1: synthesis and characterization. *Dyes and Pigments*, 58(1): 27–35.
- MAISCH, T., SZEIMIES, R.-M., JORI, G. and ABELS, C. (2004) Antibacterial photodynamic therapy in dermatology. *Photochemical and Photobiological Science*, 3: 907–917.
- MAPARI, S. A. S., NIELSEN, K. F., LARSEN, T. O., FRISVAD, J. C., MEYER, A. S. and THRANE, U. (2005) Exploring fungal biodiversity for the production of water-soluble pigments as potential natural food colorants. *Current Opinion in Biotechnology*, 16(2): 109–238.
- MARCZYLO, T. H., HAYATSU, T., ARIMOTO-KOBAYASHI, S., TADA, M., FUJITA, K.-I., KAMATAKI, T., NAKAYAMA, K. and HAYATSU, H. (1999) Protection against the bacterial mutagenicity of heterocyclic amines by purpurin, a natural anthraquinone pigment. *Mutation Research/Genetic Toxicology and Environmental Mutagenesis*, 444(2): 451–461.
- MCKENNA, J. (1998) *Natural Alternatives to Antibiotics*. New York: Avery Publishing Group.
- MICHIELSEN, S., CHURCHWARD, G., BOZIA, J., STOJILOKIVIC, I. and ANIC, S. (2007) Light activated antiviral materials and devices and methods for decontaminating virus infected environments. US Patent 20070238660.
- MOLINSKI, T. F. and FAULKNER, D. J. (1988) An antibacterial pigment from the sponge *Dendrilla membranosa*. *Tetrahedron Letter*, 29: 2137–2138.
- OKAMOTO, T., YAZAKI, K. and TABATA, M. (1995) Biosynthesis of shikonin derivatives from L-Phenylalanine via deoxyshikonin in *lithospermum* cell cultures and cell-free extracts. *Phytochemistry*, 38(1): 83–88.
- ORDOUDI, S. A., TSERMENTSELI, S. K., NENADIS, N., ASSIMOPOULOU, A. N., TSIMIDOU, M. Z. and PAPAGEORGIOU, V. P. (2011) Structure-radical scavenging activity relationship of alkannin/shikonin deriv. *Food Chemistry*, 124(1): 171–176.
- PAPAGEORGIOU, V. P., ASSIMOPOULOU, A. N., COULADOUROU, E. A., HEPWORTH, D. and NICOLAOU, K. C. (1999) The chemistry and biology of alkannin, shikonin, and related naphthazarin natural products. *Angewandte Chemie (International Edition in English)*, 38: 270–300.
- PARK, J. H., GATEWOOD, B. M. and RAMASWAMY, G. N. (2005) Naturally occurring quinones and flavonoid dyes for wool: insect feeding deterrents. *Journal of Applied Polymer Science*, 98(1): 322–328.
- PRUSTY, A. K., DAS, T., NAYAK, A. and DAS, N. B. (2010) Colorimetric analysis and antimicrobial study of natural dyes and dyed silk. *Journal of Cleaner Production*, 18: 1750–1756.
- PUCHALSKA, M., ORLIŃSKA, M., ACKACHA, M. A., POŁEĆ-PAWLAK, K. and JAROSZ, M. (2003) Identification of anthraquinone coloring matters in natural red dyes by electrospray mass spectrometry coupled to capillary electrophoresis. *Journal of Mass Spectrometry*, 38: 1252–1258.
- RAMOS, F. A., TAKAISHI, Y., SHIROTORI, M., KAWAGUCHI, Y., TSUCHIYA, K., SHIBATA, H., HIGUTI, T., TADOKORO, T. and TAKEUCHI, M. (2006) Antibacterial and antioxidant activities of quercetin oxidation products from yellow onion (*Allium cepa*) skin. *Journal of Agriculture and Food Chemistry*, 54(10): 3551–3557.
- RASOOLY, A. and WEISZ, A. (2002) *In vitro* antibacterial activities of phloxine B and other halogenated fluoresceins against methicillin-resistant *Staphylococcus aureus*. *Antimicrobial Agents and Chemotherapy*, 46(11): 3650–3653.

- RICHARDSON, W., SCHMIDT, T. M. and NEALSON, K. H. (1998) Identification of an anthraquinone pigment and a hydroxystilbene antibiotic from *Xenorhabdus luminescens*. *Applied and Environmental Microbiology*, 54(6): 1602–1605.
- RUSSELL, A. D. and CHOPARA, I. (1996) *Understanding Antibacterial Action and Resistance*. Chichester: Ellis Horwood.
- SANYOVA, J. and REISSE, J. (2006) Development of a mild method for the extraction of anthraquinones from their aluminum complexes in madder lakes prior to HPLC analysis. *Journal of Cultural Heritage*, 7(4): 229–235.
- SARKAR, A. K. and DHANDAPANI, R. (2009) Study of natural colorants as antibacterial agents on natural fibers. *Journal of Natural Fibers*, 6: 46–55.
- SAYED, Z. and EL-GABY, M. S. A. (2001) Synthesis of novel dyestuffs containing sulpho-
namido moieties and their application on wool and polyamide fibers. *Coloration Technology*, 117(5): 293–297.
- SCHMEDA-HIRSCHMAN, G., TAPIA, A., LIMA, B., PERTINO, M., SORTINO, M., ZACCHINO, S., DE ARIAS, A. R. and FERESIN, G. E. (2008) A new antifungal and antiprotozoal dep-
side from the Andean lichen *Protosnea poeppigii*. *Phytotherapy Research*, 22(3): 349–355.
- SEERAM, N. P., ADAMS, L. S., HENNING, S. M., NIU, Y., ZHANG, Y., NAIR, M. G. and HEBER, D. (2005a) *In vitro* antiproliferative, apoptotic and antioxidant activities of punicalagin, ellagic acid and a total pomegranate tannin extract are enhanced in combination with other polyphenols as found in pomegranate juice. *Journal of Nutritional Biochemistry*, 16(6): 360–367.
- SEERAM, N. P., LEE, R., HARDY, M. and HEBER, D. (2005b) Rapid large scale purification of ellagitannins from pomegranate husk, a by-product of the commercial juice industry. *Separation and Purification Technology*, 41(1): 49–55.
- SHAFIK, A. and ELSEESY, W. R. (2003) *Medicine in Ancient Egypt: History and Practice of Medicine in Non-Western Cultures*. Dordrecht: Springer.
- SHERILL, J., MICHELSEN, S. and STOJILJKOVIC, I. (2003) Grafting of light-activated antimicrobial materials to nylon films. *Journal of Polymer Science Part A: Polymer Chemistry*, 41(1): 41–47.
- SHILS, E., SHIKE, M., ROSS, A. C., CABALLERO, B. and COUSINS, R. J. (2006) *Modern Nutrition in Health and Disease*. Philadelphia: Lippincott Williams and Wilkins.
- SINGH, M. (2010) Biotechnology a boon to textile industry. <http://biotechsector.com/>
- SIVA, R. (2007) Status of natural dyes and dye-yielding plants in India. *Current Science*, 92(7): 916–925.
- STINTZING, F. C. and CARLE, R. (2004) Functional properties of anthocyanins and betalains in plants, food and in human nutrition. *Trends in Food Science and Technology*, 15(1): 19–38.
- SOSA, F., GUEBITZ, G. M. and KOKOL, V. (2009) Antimicrobial and antioxidant properties of chitosan enzymatically functionalized with flavonoids. *Process Biochemistry*, 44: 749–756.
- SUN, G. and WORLEY, S. D. (2005) Chemistry of durable and regenerable biocidal textiles. *Journal of Chemical Education*, 82(1): 60–64.
- SUN, G., XU, X., BICKETT, J. R. and WILLIAMS, J. F. (2001) Durable and regenerable antibacterial finishing of fabrics with a new hydantoin derivative. *Industrial Engineering Chemistry Research*, 41: 1016–1021.
- SUROWIECA, I., O-GAWRYŚB, J., BIESAGAA, M., TROJANOWICZAB, M., HUTTAC, M., HALKOC, R. and U-WALCZA, K. (2003) Identification of natural dyestuff in archeological

- coptic textiles by HPLC with fluorescence detection. *Analytical Letters*, 36(6): 1211–1229.
- TAYLOR, G. W. (1986) Natural dyes in textile applications. *Review of Progress in Coloration*, 16: 53–61.
- TILLER, J. C., LIAO, C.-J., LEWIS, K. and KLIBANOV, A. M. (2001) Designing surfaces that kill bacteria on contact. *Proceedings of the National Academy of Science*, 22: 5981–5985.
- VELMURUGAN, P., CHAE, J.-C., LAKSHMANAPERUMALSAMY, P., YUN, B.-S., LEE, K.-J. and OH, B.-T. (2009) Assessment of the dyeing properties of pigments from five fungi and anti-bacterial activity of dyed cotton fabric and leather. *Journal of the Society of Dyers and Colourists*, 125: 334–341.
- WAINWRIGHT, M. (2001) Acridine: a neglected antibacterial chromophore. *Journal of Antimicrobial Chemotherapy*, 47: 1–13.
- WAINWRIGHT, M. (2008) Dyes in the development of drugs and pharmaceuticals. *Dyes and Pigments*, 76: 782–589.
- WEI, H., TYE, L., BRESNICK, E. and BIRT, D. F. (1990) Inhibitory effect of apigenin, a plant flavonoid, on epidermal ornithine decarboxylase and skin tumor promotion in mice. *Cancer Research*, 50: 499–502.
- WOELFL, U., S-HAARHAUS, B., MERFORT, I. and SCHEMP, C. M. (2010) *Reseda luteola* L. extract displays antiproliferative and pro-apoptotic activities that are related to its major flavonoids. *Phytotherapy Research*, 24: 1033–1036.
- WROLSTAD, R. E., DURST, R. W. and LEE, J. (2005) Tracking color and pigment changes in anthocyanin products. *Trends in Food Science and Technology*, 16(9): 423–428.
- XU, H. X. and LEE, S. F. (2001) Activity of plant flavonoids against antibiotic-resistant bacteria. *Phytotherapy Research*, 15: 39–43.
- YOSHITAMA, K. (1978) Blue and purple anthocyanins isolated from the flowers of *Tradescantia reflexa*. *Botanical Magazine, Tokyo*, 91: 207–212.
- ZHANG, X., BOYTNER, R., CABRERA, J. L. and LAURSEN, R. (2007) Identification of yellow dye types in pre-Columbian Andean textiles. *Analytical Chemistry*, 79: 1575–1582.
- ZHANG, X., CARDON, D., CABRERA, J. L. and LAURSEN, R. (2010) The role of glycosides in the light-stabilization of 3-hydroxyflavone (flavonol) dyes as revealed by HPLC. *Microchimica Acta*, 169: 327–334.
- ZHAO, T. and SUN, G. (2007) Antimicrobial finishing of wool fabrics with quaternary aminopyridinium salts. *Journal of Applied Polymer Science*, 103(1): 482–486.
- ZHAO, T. and SUN, G. (2008) Hydrophobicity and antimicrobial activities of quaternary pyridinium salts. *Journal of Applied Microbiology*, 104: 824–830.
- ZHAO, T., SUN, G. and SONG, X. (2008) An antimicrobial cationic reactive dye: synthesis and applications on cellulosic fibers. *Journal of Applied Polymer Science*, 108(3): 1917–1923.

Pyrethroid-laden textiles for protection from biting insects

D. G. HAYES,
University of Tennessee, USA

Abstract: This chapter provides an overview of long-lasting insecticidal nets (LLINs) and other insecticide-laden textiles for the prevention of vector-borne diseases. The chapter first reviews the diseases, including malaria, that plague tropical and subtropical developing countries; diseases carried by arthropods such as mosquitoes and fleas. The insecticides, such as pyrethroids, that are employed to combat biting insects are also discussed. The underlying textile technology and applications for factory-prepared wash-durable insecticide-laden textiles, particularly LLINs, and approaches for derivatizing textiles on site to prepare wash-durable insecticidal textiles are then presented. Future areas of focus for insecticide-laden textiles, such as textiles to combat pyrethroid-resistant mosquitoes, are then discussed.

Key words: arthropods, long-lasting insecticidal nets, malaria, mosquitoes, pyrethroids.

18.1 Introduction

Malaria, dengue fever and other tropical diseases carried by biting arthropods such as mosquitoes, ticks and fleas have greatly affected life expectancy, infant mortality, quality of life and work productivity in many developing countries in Africa, Southern Asia, and Central and South America. An effective means of combating these diseases are textiles (e.g. bednets and curtains) that contain insecticides, particularly pyrethroids such as permethrin, α -cypermethrin or deltamethrin. For the textiles to be effective, they need to withstand several months or years of extreme weather and washing, and should be inexpensive and readily distributed from the factory to the remote villages in tropical or subtropical regions. This need has led to the development of long-lasting insecticidal nets, or LLINs. In addition, insecticide-laden textiles are important for vector protection worldwide for employment in outdoor recreation and occupational work (e.g. military, forestry and agricultural uses).

This chapter focuses upon LLINs. The first section reviews vector-borne diseases, insecticides incorporated into textiles, particularly pyrethroids, and an overview of the applications and needs of insecticidal textiles. Section 18.2

provides the key issues for insecticide-laden textiles while Section 18.3 provides state-of-the-art information on the preparation and employment of insecticidal textiles prepared in the factory, with the emphasis placed on LLINs, including an evaluation of their effectiveness and the methodology employed for their assessment. The next section describes methods for the *in situ* preparation of insecticide-laden textiles. Section 18.5 provides a description of future directions, including a discussion of the treatment of pyrethroid-resistant vectors. Resources for further information and references are given in the final two sections.

18.1.1 Biting insects and diseases they carry

Diseases transferred to humans through contact with biting insects, particularly mosquitoes, have plagued humanity throughout recorded history (Table 18.1). The most prominent of the diseases and the disease serving as a primary focus for this chapter is malaria, which can rapidly lead to high fever, organ failure (e.g. of the spleen and kidneys), coma and even death within hours of infection. In 2009, of the 243 000 000 cases of malaria reported, 863 000 resulted in death, with 89% of fatalities residing in Africa, 6% in the Middle East/Southwest Asia and 5% in Southeast Asia (WHO, 2009c). The severity of symptoms and progression of symptoms is particularly strong for children, who account for 85% of the fatalities (WHO, 2009c). The disease initiates through infection by the parasite *Plasmodium falciparum* or other members of the *Plasmodium* genus, with infection by *P. falciparum* generating the most severe symptoms (Enayati and Hemingway, 2010). Parasites are carried to their human hosts by mosquitoes, particularly by the species *Anopheles gambiae* in Africa and the Middle East and by other members of the genus *Anopheles* worldwide (Enayati and Hemingway, 2010). Global efforts have greatly impacted the fight against malaria, with additional impact expected in the years to come. Agencies and organizations such as the Bill and Melinda Gates Foundation, the Global Fund to Fight AIDS, Tuberculosis and Malaria, the US President's Malaria Initiative (USA), and Roll Back Malaria have funded a global research effort to develop improved medicines and vaccines, diagnoses and vector control technologies (i.e. insecticide-treated nets (ITNs), clothing and textiles, the main focus of this chapter, indoor residual spraying, or IRS, and larval control agents) and to more effectively and abundantly distribute the medicines, vaccines, vector control agents and technological information (i.e. education) to the people and places where they are needed. The funding for malaria control is currently at US\$1.7 billion in 2009, a 5.6-fold increase in funding from 2003 (WHO, 2009c). Pyrethroids are the most commonly employed vector control agent for the combat of malaria (WHO, 2009a) (Table 18.1).

Table 18.1 Vector-borne diseases and associated vector control agents

Disease	Regions of prominence	Vectors	Vector control agents
Malaria	Africa, Southern Asia, Central America, Caribbean	<i>Anopheles</i> sp. (e.g. <i>A. gambiae</i>) mosquitoes	Pyrethroids; organophosphates, DDT
Chagas	Central and South America	Blood-sucking triatomine 'kissing' bug (genus <i>Triatominae</i>)	Pyrethroids
Dengue	Central and South America, Caribbean, Southern Asia, Middle East, Africa	<i>Aedes</i> sp. (<i>Ae. aegypti</i> , <i>Ae. albopictus</i>) mosquitoes	Organophosphates, pyrethroids
Japanese encephalitis	Southeast Asia	<i>Culex tritaeniorhynchus</i> mosquitoes	Organophosphates, pyrethroids
Leishmaniasis	Central America, Middle East	Sand fly (subfamily Phlebotominae)	Pyrethroids
Lyme disease	USA and Northern Hemisphere	Black-legged, or 'deer' ticks (genus <i>Ixodes</i>)	Repellents (e.g. DEET), pyrethroids (permethrin)
Lymphatic filariasis	Middle East, Africa, Southern Asia, Central and South America	<i>Aedes</i> , <i>Culex</i> , <i>Anopheles</i> , and <i>Mansonia</i> mosquitoes	Organophosphates; pyrethroids
West Nile disease	North America and worldwide	<i>Culex</i> sp. (e.g. <i>C. pipiens</i>) mosquitoes	Organophosphates; pyrethroids

Source: (WHO, 2009a).

Dengue fever is a disease of increasing abundance and concern to several developing countries in the subtropics: Central and South American, Africa, the Middle East and Southeast Asia (Knox and Scott, 2009) (Table 18.1). The above-mentioned regions contain 2.5 billion people, equal to 40% of the world's population. Approximately 50 million cases of dengue infection are reported annually, with 500 000 'dengue hemorrhagic fever' cases reported (Knox and Scott, 2009). Epidemics have become more widespread in recent years (e.g. in Puerto Rico, 1986 and 1998), fueled by the unplanned growth of urban populations (Bennett *et al.*, 2010). Symptoms of this disease include severe headache, fever, rash and muscle and joint pains, earning it the nicknames 'break-bone fever' and 'bonecrusher disease'. Dengue is caused by four related but distinct viruses belonging to the genus *Flavivirus*, and is transmitted by *Aedes* mosquitoes, particularly *A. aegypti* and *A. albopictus*, both of which are known to pose high contact rates with humans (Knox and Scott, 2009). Currently, no vaccines or treatment protocols exist to treat dengue fever, although vaccines are currently undergoing clinical trials. There are no strategies for screening for dengue, due in part to the long (3–14 day) incubation period existing before symptoms appear (Knox and Scott, 2009). To date, vector control in individual households through insecticide-treated curtains and bednets is an important strategy in combating dengue. Although organophosphates are the most commonly used pesticides in the treatment of dengue, pyrethroid usage for dengue vector control is common (WHO, 2009a) (Table 18.1).

Chagas disease, prominent in South and Central America (Table 18.1), is reported to have infected 8–11 million people in 2009 (Nakagawa, 2009). Chagas has two phases. During the first 'acute' phase, symptoms are typically mild, consisting of a fever and perhaps swelling at the site of the insect bite or one of the eyelids. Then, the disease will go into remission for several weeks or years, and resurface as a 'chronic' phase, where it may affect the digestive system (e.g. liver, colon, esophagus), cause irregular heartbeats, or affect the nervous system, with a mortality rate of 5–15% (Nakagawa, 2009). Infected children are particularly at risk. The disease is caused by the flagellate protozoan *Trypanosoma cruzi*, transmitted by the blood-sucking triatomine bug (genus *Triatominae*), or 'kissing bug,' which hides in crevices, roofs or walls during the daytime, and typically bites humans at night. Therefore, bednets are an important preventative measure. However, approximately 20% of transmissions are through blood transfusions or breast milk. Pyrethroids are the most commonly used insecticide for chagas vector control, applied in sprays and onto bednets (Nakagawa, 2009; WHO, 2009a) (Table 18.1).

Leishmaniasis, a disease prominent in many subtropical regions throughout the world that affects approximately 12 million people annually, is caused by protozoan parasites of the genus *Leishmania* and is transmitted by the

female sand fly (subfamily *Phlebotominae*), a tiny insect 2–3 mm in length (WHO, 2009b). The disease is known to promote skin lesions which resemble leprosy and often leave permanent scars. The visceral form of leishmania typically kills 60 000 people annually. It leads to the swelling of the spleen and liver, and can cause anemia, leading to high fever and weight loss. No vaccines are available to date. The main insecticides used to combat the sandfly in the fight to prevent leishmania are pyrethroids (WHO, 2009a) (Table 18.1).

Lymphatic filariasis, prominent in subtropical regions worldwide, is reported to have affected 120 million people in 2009, 40 million with serious symptoms (WHO, 2010). The disease attacks the lymphatic system, causing enlargement (i.e. ‘elephantiasis’) of the entire leg or arm, the genitals, vulva and breasts. No vaccine is available. The parasite which causes the disease, the thread-like filarial nematode worms of the superfamily *Filarioidea*, is transmitted to humans through the bites of mosquitoes (Table 18.1). Pyrethroids are one of the most prominent vector control agents (Table 18.1) due to their effectiveness in controlling mosquitoes (WHO, 2009a).

West Nile disease is of growing concern in the USA due to a recent outbreak in the past decade (663 serious cases and 30 deaths reported in 2009), but has also been reported in Europe and throughout the world (CDC, 2010c). It often leads to moderate symptoms such as abdominal pain, fever, diarrhea, muscle aches and nausea, but can also cause damage of muscle and brain tissues (i.e. encephalitis), loss of consciousness and death. It is caused by a virus within the same family of the parasite that causes dengue fever (genus *Flavivirus*; the family *Flaviviridae*) and is transmitted to humans, animals and birds by mosquitoes (*Culex* sp.). Human-to-human transmission can also occur, through blood transfusions and breast milk. Pyrethroids and organophosphates are the most commonly used insecticides. A major concern for the future control of this disease is the growing population of insecticide-resistant mosquitoes (Kasai *et al.*, 2009). Japanese encephalitis is a similar disease prominent in Southeast Asia, caused by a parasite from the same family (*Flaviviridae*) (CDC, 2010a).

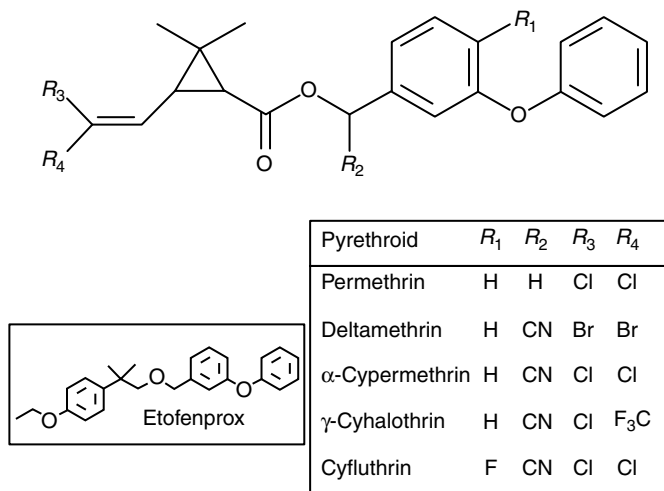
Lyme disease, prominent in the USA (28 000 cases reported in 2008), but encountered worldwide (particularly in the Northern hemisphere), is attributed to a gram-negative spirochetal bacteria of the genus *Borrelia*, transmitted to humans through bites by black-legged, or deer, ticks (genus *Ixodes*) (CDC, 2010b). If detected early the disease can be treated through antibiotics, and provides mild symptoms: fever, headache, fatigue and depression. It is readily detected by a characteristic circular skin rash called ‘erythema migrans’. However, if not treated early, Lyme disease can cause more severe symptoms that involve the joints, heart and nervous system (e.g. facial palsy). Ticks also transmit other diseases, such as Rocky Mountain spotted fever. Pyrethroids, particularly permethrin, are effective tick control agents (Table 18.1).

In conclusion, vector control is a critical component in the fight to end malaria and other debilitating diseases that affect subtropical regions and reduce the quality of life for its inhabitants. Pyrethroids, discussed in the next section, are the main insecticide employed for vector control, through their use in indoor spraying and in bednets, curtains, clothing and other protective textiles.

18.1.2 Pyrethroids and other insecticides

Pyrethroids, chemical agents that disable and frequently kill mosquitoes upon contact, refer to a class of homologous compounds that mimic the chemical structure of pyrethrum, a naturally occurring insecticide derived from the crushed flower petals of dried daisy (*Chrysanthemum cinerariifolium*) that consists of six different esters (Hayes *et al.*, 2009). Pyrethrin consists of esters formed between cyclopropane-containing carboxylic acids and cyclopenteneolone alcohol groups (Spurlock and Lee, 2008). Due to the poor photostability of the pyrethrin esters, synthetic pyrethroids were created which contain halogen atoms within the cyclopropane-carboxylic acid moieties and substitution of the alcohol groups with those containing oxydibenzene groups (Spurlock and Lee, 2008). The chemical structures of synthetic pyrethroids approved by the World Health Organization (WHO) for employment in mosquito control for the prevention of malaria are given in Fig. 18.1. Of the pyrethroids depicted in the figure, permethrin was the first one produced, dating to the early 1970s, and is an example of a 'Type I' pyrethroid (Spurlock and Lee, 2008). The others, with the exception of etofenprox, contain a cyano group bonded to the hydroxyl-containing carbon atom of the alcohol moiety of pyrethroids and are classified as 'Type II'. Both Type I and II pyrethroids attack the nervous systems of vectors, through disrupting the function of voltage-sensitive sodium channels, which are membrane proteins responsible for function in nerve cells (Shafer *et al.*, 2005). Type II pyrethroids have an additional biochemical function: they inhibit the neurotransmitter GABA in mosquitoes, and may inhibit chlorine ion channels as well (Burr and Ray, 2004). Type I and II pyrethroids possess other differences in the physiological responses they cause in mosquitoes (Lautraite and Sargent, 2009). Due to their hydrophobic nature (octanol-water partition coefficient, or 'log P', values of 6.0 (Spurlock and Lee, 2008)), pyrethroids are poorly water-soluble and thus are produced as (oil-in-water) emulsions or suspensions.

Pyrethroids generally impose low toxicity to humans, mammals and the ecosystem (Lautraite and Sargent, 2009). In mammals, they are quickly catabolized and excreted in the urine and feces and therefore do not bioaccumulate. They are poorly absorbed by skin and are not linked to cancer (Barlow *et al.*, 2001; Cecchine *et al.*, 2000). Only a few health problems



18.1 Chemical structure of pyrethroids employed to combat biting insects. Stereochemistry is not shown.

have been reported (Kolaczinski and Curtis, 2004). They do not bioaccumulate in the atmosphere, being degraded by sunlight and chemicals in the atmosphere within 48 hours, or in groundwater, due to their poor solubility. However, due to their non-polar nature, pyrethroids are strongly adsorbed by soil and sediment particles, which has led to several recent reports of toxicity to aquatic organisms, particularly fish, crustaceans and insects (Lopez *et al.*, 2005; Shamim *et al.*, 2008; Werner and Moran, 2008; Wong, 2006). A major problem is that although their concentrations in sediments is very low (making their measurement challenging), the threshold concentration for acute toxicity is also very low, on the order of nanograms to micrograms per liter (Werner and Moran, 2008). Also the pyrethroids listed in Fig. 18.1 are ultraviolet-stable, allowing for their long-term persistence in liquid or solid systems, and indirectly allowing for pesticide resistance to occur (Kawada, 2009).

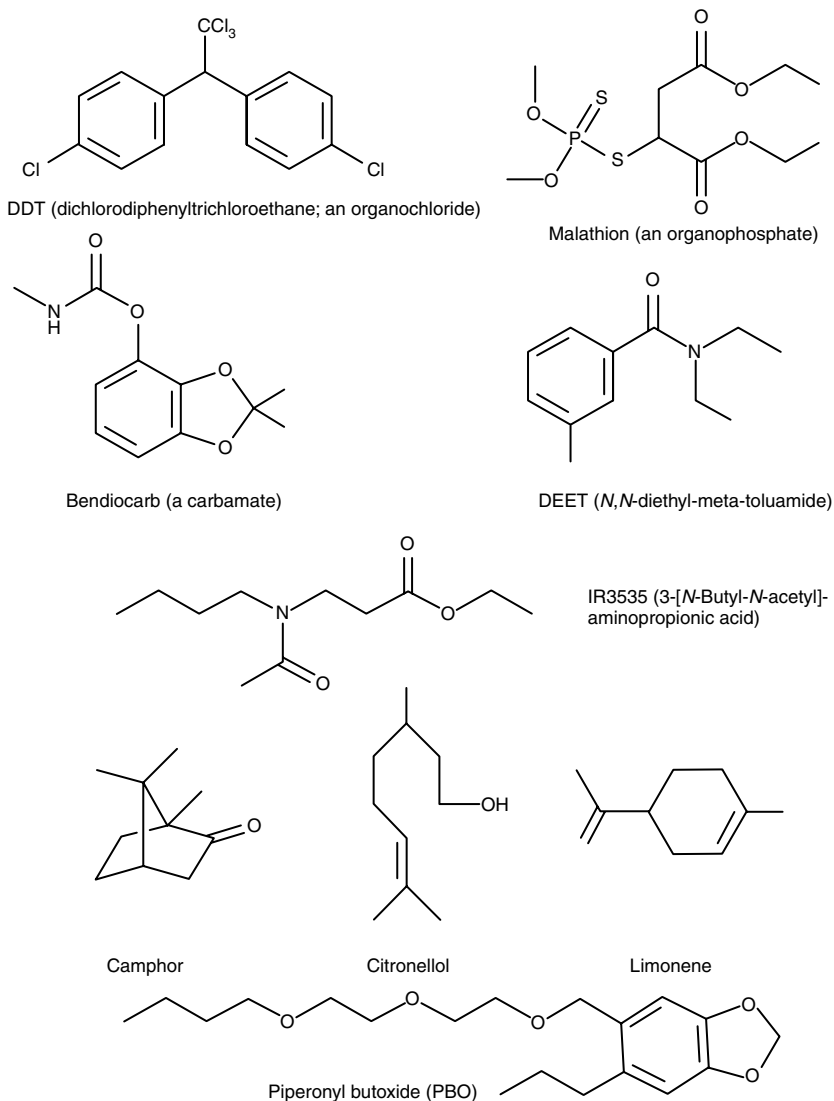
Of the pyrethroids depicted in Fig. 18.1, the most frequently used for vector control in 2006/2007 is α-cypermethrin, followed by permethrin, deltamethrin and λ-cyhalothrin (WHO, 2009a). The usage of etofenprox and cyfluthrin is approximately two-fold smaller (WHO, 2009a). Permethrin is commonly employed by the US military to protect its personnel (Cecchine *et al.*, 2000). The pyrethroids differ significantly in their ability to combat malaria. For instance, permethrin has strong repellency effects and is reported to work rapidly (Abdel-Mohdy *et al.*, 2008; WHOPES, 2005). Etofenprox also has a high repellency (WHOPES, 2005). Deltamethrin (and λ-cyhalothrin) more effectively kill mosquitoes but does not impart as rapid of a response as permethrin (Giroux *et al.*, 2006; Hougard *et al.*, 2003). The

behavior of α -cypermethrin is intermediate of that described above for permethrin and deltamethrin; moreover, it has a rapid rate of effectiveness and a high mortality imparted (Hougard *et al.*, 2003). To achieve comparable levels of efficacy, differences in concentration of pyrethroid are typically required, as an approximate scale (milligram of agent per square meter of netting) 10–15, 15–25, 20–40, and 200–500 for λ -cyhalothrin, deltamethrin, α -cypermethrin and permethrin, respectively (Jawara *et al.*, 1998; WHOPES, 2007a). Deltamethrin has the advantage over permethrin that it is less susceptible toward metabolic resistance in malaria mosquitoes (WHOPES, 2008).

Commercial pyrethroids typically are diastereomeric mixtures, with chiral carbon atoms existing in the cyclopropane ring, and carbon attached to the R_2 group in Fig. 18.1 (Perez-Fernandez *et al.*, 2010). Several of the commercial pyrethroids are isomerically enriched, such as λ -cyhalothrin and α -cypermethrin (Spurlock and Lee, 2008). Also, several pyrethroids possess *cis/trans* isomerization within their alkene groups, such as those in Fig. 18.1. For example, in the permethrin formulation employed to prepare the Olyset® Net, a commercial long-lasting insecticide bednet (described below), the *cis/trans* isomer ratio is 50/50 to 30/70. The stereochemistry strongly determines the toxicity of pyrethroids toward vectors, particularly the chirality of the carbon atom containing the R_2 group in Fig. 18.1 (Perez-Fernandez *et al.*, 2010), and strongly affects their biodegradability (Nillos *et al.*, 2008).

Frequently, pyrethroids are formulated with piperonyl butoxide, or PBO, since the latter acts as a ‘synergist’, increasing the potency of the pyrethroid, particularly for encountering insecticide-resistant pests (Fakoorziba *et al.*, 2009; Romero *et al.*, 2009). The chemical structure of PBO is given in Fig. 18.2. PBO inhibits cytochrome P450 monooxygenase, enzymes which act to detoxify many chemicals *in vivo* (Fakoorziba *et al.*, 2009; Romero *et al.*, 2009). Of note, PBO is being used in the PermaNet 3.0, an LLIN being used for vector control in regions containing pesticide-resistant *Anopheles* mosquitoes (discussed below). The inhibitory activity of PBO is also a concern since similar oxidase enzymes are in humans. Also, PBO has been reported to be a carcinogen (Muguruma *et al.*, 2007). However, a recent report demonstrates that the usage of pyrethroid/PBO mixtures has led to very few toxicological problems for humans (Osimitz *et al.*, 2009).

In addition to mosquitoes (e.g. *Anopheles*, *Culex*, and *Aedes* sp.), pyrethroids (commonly permethrin) are well-known agents for protection against fleas, mites, chiggers, ticks (carriers of Lyme disease and tick-borne encephalitis), roaches and termites, and are found in a variety of commercial lawn and garden and pet care products (Bissinger and Roe, 2010). For example, permethrin is a key ingredient of the tick control product Damminix® and the mite control product MiteArrest® (EcoHealth, Inc., Boston, MA).



18.2 Chemical structure of insecticides, repellents and synergist.

In addition to pyrethroids, organophosphates (e.g. malathion) and carbamates (e.g. bendiocarb) are also commonly employed for mosquito control in the fight against malaria (WHO, 2009a). Their chemical structures are given in Fig. 18.2. Both organophosphates and carbamates inactivate the nervous system of mosquitoes through inhibiting the enzyme cholinesterase. In the mid-twentieth century, DDT (dichlorodiphenyltrichloroethane, depicted in Fig. 18.2), an organochlorine, was employed successfully for IRS, greatly

reducing the frequency and mortality rate (Enayati and Hemingway, 2010). Since the ratification of the Stockholm Convention on persistent organic pollutants in 2004, the use of DDT, known to bioaccumulate in the fatty tissues of lower and higher organisms, animals and humans, has been limited mainly to Africa and India (WHO, 2009a). However, organochlorines (i.e. DDT) remain the most abundantly used insecticide (3962 metric tons in 2006–2007), followed by organophosphates (795 tons), pyrethroids (229 tons) and carbamates (16 tons) (WHO, 2009a). However, for insecticide treatment of textiles, pyrethroids were the primary chemical agent used (WHO, 2009a).

Although the focus of this chapter is on the employment of pyrethroids, a short discussion of vector repellents is warranted. The most commonly used repellent for mosquitoes, ticks and sand flies is DEET (*N,N*-diethyl-metotoluamide), depicted chemically in Fig. 18.2. DEET is used worldwide and is generally considered safe, with only minor toxicological impact on humans typically reported (e.g. skin rash, digestive discomfort if ingested in large quantities) (Sudakin and Trevathan, 2003). For DEET to be effective, it must be in a vapor form. Fortunately, DEET is quite volatile. A recently developed repellent, IR3535 (3-[*N*-butyl-*N*-acetyl]-aminopropionic acid; Merck, Rahway, NJ USA, Fig. 18.2) has received recent attention (Faulde *et al.*, 2010). It is structurally similar to the amino acid alanine and has been classified by the US Environmental Protection Agency (EPA) as a biopesticide. However, alternative insecticides continue to be developed for combating insecticide-resistant vectors and reducing unwanted side-effects or environmental damage (Lopez *et al.*, 2005; Zaim and Guillet, 2002). One example is the larvacide spinosad, a material produced by the fermentation of the bacterium *Saccharopolyspora spinosa* (*Actinomycetales*) via extraction-based purification from the fermentation broth. It acts as a nicotinic agonist, resulting in neuron excitation, and has low acute toxicity to the gastrointestinal tract, skin or lungs (WHOPES, 2007b). Natural oils from aromatic plants such as peppermint, citronella and eucalyptus oils, enriched in terpenes and terpenoid, such as citronellol, limonene and camphor, have been receiving increased attention as natural repellents (Nerio Luz *et al.*, 2010). An alternative approach is the production of transgenic mosquitoes, genetically modified to be refractory to malaria infection (Kokoza *et al.*, 2010; Olson and Franz, 2009).

18.1.3 Application and effectiveness of insecticide-treated textiles

In combating vector-borne diseases (Section 18.1.1) with pyrethroids or other insecticides (Section 18.1.2), IRS, larval control agents, and ITNs, clothing and textiles have been the main approaches. The agents, materials or technologies must be delivered to people on the ‘front line’ in the fight (Africa, the Middle East, Southern Asia, and Central and South

America) in a means that will be inexpensive, due to low-to-modest household incomes, through a robust distribution system. Bednets are particularly important since most vector activity occurs at night (Pates and Curtis, 2005). It is well established that bednets treated with pyrethroids are very effective in reducing the occurrence of malaria and other vector-borne diseases (Pates and Curtis, 2005). In fact, ITNs reduce the malarial mortality rate by 17–43% (Binka and Akweongo, 2006).

Another related need for vector-protective textiles is for those who frequent vector-populated environments due to work- or recreational-related activities, such as military personnel, agricultural and forestry personnel, environmental scientists and outdoor sporting enthusiasts. These applications apply to North American and Europe, and indeed the entire world, to reduce the spread of disease, loss of worker productivity due to illness, and the socio-economic impact of outdoor recreation.

18.2 Key issues of insecticide-laden textiles

A problem with the use of ITNs and other insecticide-laden textiles is that the insecticide molecules ('active ingredient') contained in the netting are readily removed when washed with detergent solution, leading to a reduction of bioactivity by at least 50% (Kroeger *et al.*, 2004; Somboon *et al.*, 1995). Thus, conventional ITNs need to be repeatedly retreated to remain effective (Frances *et al.*, 2003; Kroeger *et al.*, 2004; Miller *et al.*, 1991). Alternatively, wash-durable, or LLINs have been prepared either in the factory or through *in situ* treatments. Both approaches are described below. In addition to long-term effectiveness without the need of retreatment, LLINs and other wash-durable vector-protective textiles lead to the lower release of pyrethroids and pesticides into the environment. As the world's use of natural resources, including water, increases, thus creating stress on the ecosystem, the minimization of environmental impact is essential.

An additional issue for ITNs in the prevention of vector-borne diseases is increasing their local use, and providing a viable infrastructure for their procurement, delivery and distribution. This has been a major problem for LLINs prepared in European or Asian factories throughout the past decade. A separate section below is devoted to this topic.

18.3 Factory-produced LLINs and textiles for protection from biting insects

18.3.1 Measurement of the effectiveness of LLINs

In the evaluation of LLINs, the WHO Pesticide Evaluation Scheme (WHOPES) has developed a three-tier system for their certification

(WHOPES, 2005). For Phase I, the effectiveness of the LLINs after several washing cycles must meet specified benchmarks. The bioactivity of the nets is evaluated by a WHO ‘cone’ assay, where a population of at least 50 vectors is exposed to a 25 × 25 cm LLIN sample. The vectors that are ‘knocked-down’ at 30 min, 60 min and 24 h are measured, and referred to as KD30, KD60 and mortality, respectively. Using a standardized washing protocol, LLINs washed 20 times must promote >80% mortality and/or >95% KD60; otherwise, the LLIN is considered to be ‘exhausted’ (WHOPES, 2008). (Of note, a recent study shows that LLINs are more wash-durable when exposed to hand-washing rather than via a washing machine (Sreehari *et al.*, 2009).) Alternatively, a new ‘tunnel’ procedure can be used to replace the ‘cone’ assays which does better in quantifying the effect of repellency by pyrethroids (WHOPES, 2005). A recent study recommends usage of ‘median knock-down time’ (MKDT) as a replacement to KD30 or KD60 since it is directly correlated with the pyrethroid concentration remaining on the net when plotted on semilog paper (Skovmand *et al.*, 2008). Also, the release of pyrethroid through washing is monitored by measuring the concentration of pyrethroid (or other active ingredient) remaining on the LLIN using gas or liquid chromatography (Perez-Fernandez *et al.*, 2010). A recent study concludes the most useful means of expressing the surface concentration of LLINs is mg of active ingredient per kilogram of net; however, milligram per square meter remains commonly employed. Phase II and III involve small- and large-scale field studies, respectively. Achievement of Phase II demonstrates the LLINs strongly impact the vector behavior and are safe. LLINs achieving Phase I and II approval are referred to as receiving ‘time-limited interim recommendation’. Phase III LLINs promote safe protection for 3–5 years and are accepted by local communities.

18.3.2 Factory-prepared LLINs

LLINs prepared in the factory receiving approval by WHOPES for the treatment of malaria and other vector-borne diseases are given in Table 18.2. The Olyset® Net and PermaNet products can be considered as ‘second’ generation, meaning the current products were reformulated to improve performance of first-generation products, the latter of which received approval between 2000 and 2004. The others listed in the table either received approval, sought approval, or are undergoing approval by WHOPES during 2006–2010. Most LLINs employ the pyrethroids deltamethrin or α -cypermethrin as active ingredient, with the Olyset® Net, which employs permethrin, being an exception.

The most common and traditional material for the bednets is polyester, with a few employing polyethylene (DuraNet, Olyset® Net, and MAGNET). Both polymers are non-polar and semi-crystalline, containing

both crystalline and amorphous morphological regions (WHOPES, 2008). Polyesters (primarily polyethylene terephthalate) remain the material of choice due to their high strength, low cost and global availability (Lickfield *et al.*, 2010). Polyester LLINs are made from 75 or 100 denier multifilament yarn that is flat or textured (Lickfield *et al.*, 2010). Polyesters have several advantages compared to polyethylene: better stability to ultraviolet light, strong, resistant to chemicals and are easily washed (Lickfield *et al.*, 2010). Polyethylene (typically high-density polyethylene, or HDPE) possesses a lower melting point temperature, allowing it to be more thermally bondable. This property makes polyethylene the material of choice for LLINs prepared by impregnation into the yarn prior to extrusion. Polyethylene is also advantageous in terms of being lightweight (density of 0.95 kg m^{-3} , compared to 1.38 kg m^{-3} for polyester), and having quick drying characteristics, and strong resistance to chemicals, perspiration, rot and weather. An ultraviolet light protective agent is typically added to polyethylene. Other disadvantages of polyethylene include its 'plastic-like' feel to the skin compared to polyesters and its low ability to be dyed (unless pigments are incorporated into the yarn). Of great importance, insecticide-impregnated polyethylene LLINs regenerate their activity slowly after washing (requiring 3–7 days) due to the slow diffusion of pyrethroids adsorbed to the highly hydrophobic polymer matrix (Lickfield *et al.*, 2010). Also, the availability of 75–150 denier polyethylene (as used for LLINs) is lower, and thus the price is higher, compared to polyester (Lickfield *et al.*, 2010). Polypropylene has also been suggested as a possible LLIN material due to its strength (Lickfield *et al.*, 2010).

Pyrethroid (i.e. active ingredient) molecules reside in two states: entrapped within the polymeric matrix and 'free' pyrethroid which resides at the surface. As a portion of the second population is removed through washing (via detergents driving the solubilization of pyrethroids into water through micelle formation), a fraction of entrapped pyrethroid will migrate to the surface through diffusion, suggesting entrapped pyrethroid acts as a reservoir. However, through successive washings, the less thoroughly entrapped pyrethroids are more likely to diffuse to the surface. Hence as the number of washings increase, the population of entrapped pyrethroids is more comprehensively entrapped, retarding the diffusion of pyrethroid to the surface. Also, molecules contained in the LLINs that facilitate diffusion of entrapped pyrethroids, such as residual surfactants and detergents occurring in the pyrethroid emulsion or suspension preparations and in the finishing of the textiles, are more likely to be removed through the washing, further exacerbating the diffusion rate. As stated elsewhere, 'the mechanisms by which active ingredient is transferred from the surface of netting to the sites of activity within mosquitoes do not appear to be well established' (WHOPES, 2008).

Table 18.2 Commercially available LLINs that contain pyrethroids as 'active ingredients'

LLIN product	Manufacturer	Pyrethroid	Pyrethroid concentration, mg m ⁻² (g kg ⁻¹)	Pyrethroid incorporation method	LLIN material	Fiber thickness, denier	WHOPES recommendation
DawaPlus 2.0	Tana Netting (by SiamDutch), Bangkok, Thailand	Deltamethrin	80 (2.66)	Type 3	Polyester	75 or 100	Time-limited interim recommendation
DuraNet	Clarke Products (Roselle, IL, USA)	α -Cypermethrin	261 (5.5)	Type 1	Polyethylene	150	Time-limited interim recommendation (undergoing Phase III evaluation)
ICON-MAXX-Net	Syngenta (Basel, Switzerland)	λ -Cyhalothrin	50	Type 3	Polyester	NA	Applied for, but did not receive approval
Interceptor	BASF (Ludwigshafen, Germany)	α -Cypermethrin	175	Type 2	Polyester	NA	Time-limited interim recommendation (undergoing Phase III evaluation)
LifeNet™	Bayer Crop Science (Lyon, France)	Deltamethrin	NA	Type 1	Polyethylene	NA	Undergoing Phase I evaluation
MAGNET	VKA Polymers (Tamil Nadu, India)	α -Cypermethrin	NA	Type 1	Polyethylene	NA	Undergoing Phase I evaluation
Netprotect	Bestnet Europe (London, UK)	Deltamethrin	68 (1.8)	Type 1	Polyethylene	110	Time-limited interim recommendation (undergoing Phase III evaluation)

Continued

Table 18.2 Continued

LLIN product	Manufacturer	Pyrethroid	Pyrethroid concentration, mg m ⁻² (g kg ⁻¹)	Pyrethroid incorporation method	LLIN material	Fiber thickness, denier	WHOPES recommendation
Olyset Net 2.0	Sumitomo Chemicals Co., Ltd (Tokyo, Japan)	Permethrin	1000 (20)	Type 1	Polyethylene	>150	Fully recommended for 3 years
PermaNet 2.0	Vestergaard-Frandsen, SA (Lausanne, Switzerland)	Deltamethrin	55 (1.4)	Type 2	Polyester	100	Fully recommended for 5 years
PermaNet 3.0	Vestergaard-Frandsen, SA (Lausanne, Switzerland)	Deltamethrin	180 (4.0)	Type 2	Polyester	100	Time-limited interim recommendation
Royal Sentry™	Disease Control Technologies, USA	NA	NA	NA	NA	NA	Undergoing Phase I evaluation
YORKOOL® LLITN	Tianjin Yorkool, Tianjin, China	Deltamethrin	55 (2.11)	NA	Polyester	50, 75, or 100	Undergoing Phase I evaluation

Notes: 'NA' indicates data not available. WHOPES: World Health Organization Pesticides Evaluation Scheme. Pyrethroid incorporation method: Type 1: incorporated into yarns; Type 2: coated onto the netting (pad frame); Type 3: pyrethroid suspension and binder applied to netting: spraying for Dawa, and coating of slow-release capsule suspension of pyrethroid onto binder-treated net for ICON. For DawaPlus 2.0, an LLIN product formed from 75 denier yarn is also available with a pyrethroid concentration of 80 mg m⁻² (2.00 g kg⁻¹). For Netprotect, pyrethroid concentration listed is for a 136 mesh version of product. For a 200 mesh Netprotect, the pyrethroid concentration was 79 mg m⁻² (1.8 g kg⁻¹). For PermaNet 2.0, an additional product consisting of 75 denier fibers and a pyrethroid concentration of 1.8 g kg⁻¹ is also available. For PermaNet 3.0, values tabulated are for the roof portion. The side panels contain 75 denier fibers with deltamethrin concentrations of 2.8 g kg⁻¹ (i.e. 118 mg m⁻² for the upperpart and 85 mg m⁻² for the lower part, reflecting the higher density of the knitting for the upper part compared to the lower part). Also for the PermaNet 3.0, a synergist, PBO, is incorporated into the fibers employed for the roof at 25 g kg⁻¹.

Sources: Banek *et al.*, 2010; Tangu *et al.*, 2010; WHOPES, 2007b, 2008, 2009, 2010a.

The commercial LLINs can be divided into three categories when assessing the means of incorporating the active ingredient (pyrethroid) (Dev, 2009; WHOPEs, 2008). The first (referred to as 'Type 1') is prepared by incorporating the insecticide into the (monofilament polyethylene) fibers prior to extrusion and knitting. 'The insecticide ... migrates through the threads of the net by diffusion' (WHOPEs, 2010a). Examples of this category are the Olyset® Net (Sumitomo Chemicals Co. Ltd, Tokyo, Japan), DuraNet (Clarke Products, Roselle, IL USA), LifeNet™ (Bayer Crop Science, Lyons, France), MAGNET (VKA Polymers, Tamil Nadu, India), and the Netprotect (Bestnet Europe, London, UK; Table 18.2). A detailed description for the Netprotect is representative of the Type 1 LLIN preparation process: the mixing of HDPE chips and 'master batches' of additives, including UV protectants and active ingredient (deltamethrin), followed by extrusion, passing through a spinneret, cooling, stretching and heating to prepare the yarn (Bestnet Europe, 2010). The second category ('Type 2') is the coating of the knitted yarn with insecticide and binder during the 'pad frame' operation. The latter term refers to a finishing process, often used for the impregnation, or 'padding', of dye, through the application of NaOH solution containing a wetting agent to induce chemical bonds and a film builder, then heating at ~80°C, followed by applying tension to stretch the textile. (A recent patent suggests the use of a heat-drying process operated at 150–190°C to replace the latter step (Hataipitisuk, 2007).) Examples include the PermaNet (Vestergaard-Frandsen, SA, Lausanne, Switzerland) and Interceptor (BASF, Ludwigshafen, Germany). The third category is the coating of the knitted yarn with pesticide and binder as the final stage of preparation. The DawaPlus (Tana Netting, Bangkok, Thailand) adopts this approach. Typically the encapsulation and binding agents employed are proprietary (WHOPEs, 2008). Common binders used in industry include cross-linkable acrylic polymers or copolymers, copoly(styrene-butadiene), or copoly(ethylene-vinyl acetate) (Anderson and Daniels, 2003).

The Olyset® Net was the first LLIN to be submitted for approval by WHOPEs. The product, wide mesh (4 × 4 mm), is made of high-density monofilament polyethylene yarn (50 g m⁻²), containing 2% (w/w) permethrin (WHOPEs, 2010a). Reviewed elsewhere, the Olyset® Net is recommended by WHOPEs for use in malaria prevention for a three-year period, and is effective in prevention of dengue and leishmaniasis (Itoh, 2005; Itoh *et al.*, 2009; Kasili *et al.*, 2010). A recent study showed that the Olyset® Net was active for seven years, but only if the net was treated carefully (e.g. holes were repaired) (Malima *et al.*, 2008). Both the DuraNet and Netprotect, using α -cypermethrin and deltamethrin as insecticide, respectively (Table 18.1), are prepared similarly. Both have received WHOPEs Phase I approval (WHOPEs, 2008). In contrast to the other Type 1 LLINs, Netprotect is made from both medium-density polyethylene and HDPE

(WHOPES, 2008). The MAGNET LN (VKA Polymers, Tamil Nadu, India) and LifeNet™ (Bayer Crop Science, Lyons, France) Type 1 LLINs, containing α -cypermethrin and deltamethrin as pesticide, respectively, are currently undergoing WHOPES Phase I trials (Table 18.2).

Type 2 LLINs are equally as common as Type 1 nets. The PermaNet manufactured by Vestergaard-Frandsen (Switzerland) was the second LLIN to seek approval by WHOPES. Version 2.0 has received WHOPES certification for three to five years (WHOPES, 2009) (Table 18.2). PermaNet products contain deltamethrin as active ingredient, which 'is bound in a resin coating that reduces the amount of insecticide lost during routine washing' of the polyester net (WHOPES, 2009). PermaNet is also reported to be effective in combating dengue, leishmaniasis, chagas and lymphatic filariasis (Vestergaard-Frandsen, 2010). The PermaNet 3.0 employs a synergist, PBO (discussed in Section 18.1.2), to increase effectiveness against pyrethroid-resistant vectors (discussed in detail below). The Interceptor (Type 2) LLIN has received 'interim recommendation' (WHOPES, 2007b), with Phase III trials ongoing. A recent field trial in Liberia suggests the Interceptor LLIN lost only 22% of its active ingredient, α -cypermethrin, with household usage remaining at 94% after one year of continual usage (Banek *et al.*, 2010).

The PermaNet 3.0 is a new product aimed for vector protection in regions plagued with pyrethroid-resistant mosquitoes. The product has received WHOPES Phase I and II approval but 'cannot be considered as a tool to control mosquito populations resistant to pyrethroids or to prevent the spread of pyrethroid resistance' (WHOPES, 2009). In addition to deltamethrin, PermaNet 3.0 utilizes the synergist PBO (described in Section 18.1.2) to affect oxygenase- and esterase-based resistance mechanisms, which are important mechanisms in *Culex quinquefasciatus*, the underlying vector for filariasis (WHOPES, 2009). The net combines two fabrics: a roof with knitted 100 denier monofilament polyethylene and side panels with more densely knitted 75-denier multifilament polyester. The latter contains a higher dosage of pyrethroid. A report from a recent field study focusing upon pyrethroid-resistant *Culex* mosquitoes in Tanzania demonstrated the PermaNet 3.0 did not significantly outperform the PermaNet 2.0 (Tungu *et al.*, 2010).

The DawaPlus® 2.0 is the only Type 3 factory-prepared LLIN to have received approval by WHOPES (WHOPES, 2010a). It is prepared by coating an aqueous solution of deltamethrin suspension concentrate and a proprietary binder onto knitted multifilament polyester fibers through spraying nets tumbling in an industrial scale washing machine. The binder is same as used in K-O TAB 123 (discussed in Section 18.4). A similar approach was used to prepare the ICON-MAXX-Net, using a slow-release capsule suspension of λ -cyhalothrin, ICON10 CS, and the same binder as employed in the product ICON-MAXX mosquito treatment test (WHOPES, 2009). Due

to a high level of variability in performance, the ICON-MAXX net did not receive WHOPES approval (WHOPES, 2009).

18.3.3 Effectiveness of LLINs in controlling vector-borne diseases

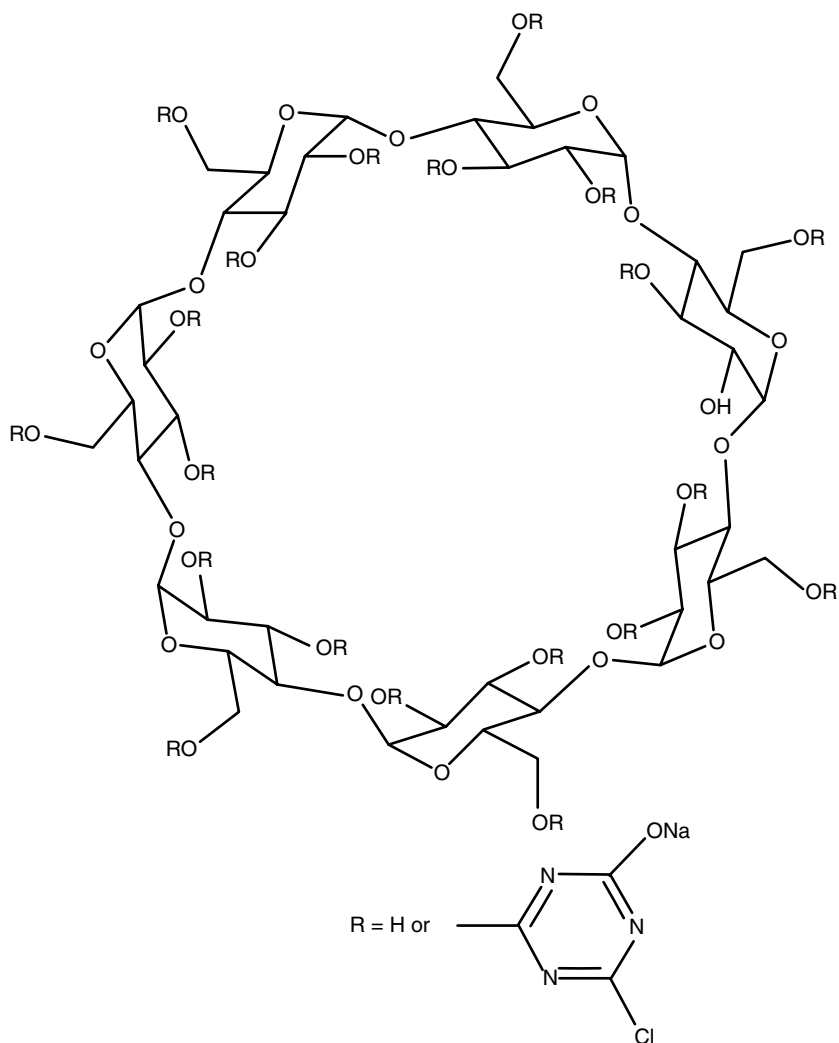
As described in a recent review published in 2008, the distribution of LLINs in tropical settings was problematic due to their relatively high costs compared to untreated nets, making them unaffordable for many households in developing countries, and the difficulty for the logistics of their transport from European or Asian factories to remote villages in Africa, Southern Asia, and other remote subtropical regions (Hayes *et al.*, 2009). The distribution of LLINs has improved in recent years due to the influx of funds from the Gates Foundation, UNICEF, the Global Fund, USAID, the European Union and other private sources. An economic study suggests the annual cost for LLINs is on par with ITN, and suggests local campaigns for LLIN distribution and usage can be effective (Yukich *et al.*, 2008). However, a recent study suggests the employment of LLINs in a household does not equate to total coverage in neighboring households (Gu and Novak Robert, 2009). In Tanzania, LLIN usage was skewed toward households with higher incomes, due to economic motivation and negative perceptions in rural areas on the safety of pyrethroids (Matovu *et al.*, 2009). The latter trends are significant because whole community usage is important for effective vector control using LLINs (Curtis *et al.*, 2006). In addition, a recent study found that the LLINs can be used for non-intended purposes, such as for catching fish (Minakawa *et al.*, 2008). Therefore, a recent assessment suggests the improved control against malaria through increased LLIN distribution will be uneven (Gu and Novak Robert, 2009). The main finding from the recent epidemiological field studies cited above is that the most important factor for LLIN effectiveness is their ability to maximize vector mortality through the engagement of vectors with the LLINs (Gu and Novak Robert, 2009; Siebert *et al.*, 2009). Moreover, LLINs which repel but do not kill mosquitoes may put non-LLIN users in the vicinity at a higher risk for bites. Interestingly, the PermaNet led to a higher degree of engagement, hence mortality, compared to the Olyset® Net (Siebert *et al.*, 2009).

18.3.4 Factory-produced textiles for protection from biting insects

In addition to LLINs, technology to prepare insecticide-laden textiles has been developed which is more applicable for military and outdoor occupation and recreational purposes due to their higher costs. Regarding military textiles, typically consisting of 80–100% cotton for uniforms, the standard

procedures employed for incorporation of pyrethroid (usually permethrin) reflect the three incorporation methods listed for LLINs in Section 18.3.2: incorporation into the fibers through heat and salt gradients (similar to Type 1 preparation), the impregnation of textiles after dyeing but before the tailoring of the textile by soaking textiles in aqueous pyrethroid and binder solution followed by in-process heating at $\sim 130^{\circ}\text{C}$, ('polymer-coated', similar to Type 2), and the dipping or spraying of the tailored textiles with aqueous permethrin solution followed by air drying as an end-of-line process, similar to Type 3 (Faulde *et al.*, 2003). A disadvantage of the last method is an increase of skin exposure to pyrethroids weakly adsorbed to the textile (Faulde *et al.*, 2003). However, an advantage of the dipping method is that it can be deployed in the field (described in Section 18.4). Military battle dress uniforms treated via 'polymer-coating' performed quite well, withstanding 50–100 washes yet retaining effective mortality, knock-down and repellency against mosquitoes (*Ae. aegypti*) and ticks (*Ixodes ricinus*) (Faulde and Uedelhoven, 2006; Faulde *et al.*, 2003; Faulde *et al.*, 2006). The 'polymer-coating' method has been employed to incorporate repellents, DEET and IR3535, producing textiles protective against *Aedes* mosquitoes and ticks for one year in the absence of washing and weathering extremes, with the DEET-derivatized cotton fabric performing best (Faulde *et al.*, 2010).

An effective approach has been to use cyclodextrins, cyclic oligosaccharides produced during enzymatic degradation of starches. Cyclodextrins, due to their cage-like structure, form inclusion compounds with several hydrophobic organic and inorganic compounds. In particular, monochlorotriazinyl- β -cyclodextrin (CDMCT), the first derivatized cyclodextrin produced on an industrial scale, is effectively conjugated to textile materials such as cotton. As depicted in Fig. 18.3, CDMCT contains seven glucose units (hence its naming as a β -cyclodextrin) conjugated through 1,4-glycosidic bonds. They form a truncated conical shape, with a thickness and internal diameter of ~ 0.78 nm. The grafting reaction typically consists of soaking cotton textiles into alkaline aqueous CDMCT/sodium carbonate solution at room temperature and atmospheric pressure, removing excess water from the textiles, heating the textiles in an oven at 130°C for 15 min using dry heat, and rinsing the textiles with deionized water to remove free CDMCT. The reaction occurs via nucleophilic substitution, resulting in the loss of the chlorotriazine ring's Cl atom and the formation of an ether bond at the ring position of the departing Cl atom with a hydroxyl group of cotton. Insecticide is then incorporated into the interior cavity of cyclodextrins through soaking the textiles in methanolic or ethanolic insecticide solution for several hours, and then perhaps rinsed with water or methanolic or ethanolic solution to remove non-included insecticide. Results show that cotton treated with CDMCT containing permethrin, cypermethrin or prallethrin were effective wash-durable textiles for protection against *Anopheles* and



18.3 Chemical structure of CDMCT.

Aedes mosquitoes, with the majority of pyrethroid retained on the cloth after several washing cycles (Abdel-Mohdy *et al.*, 2008; Romi *et al.*, 2005). Although the knock-down and mortality activity of the derivatized textiles was slower than control ITNs, their repellency was faster (Abdel-Mohdy *et al.*, 2008). CDMCT-derivatized cotton containing the repellent DEET inside the cyclodextrin cavities was poorly effective and wash-durable, due in part to the inability of included DEET molecules to evaporate (Romi *et al.*, 2005). But recently, α -cyclodextrin containing 2-undecanone, a natural repellent, performed well in protecting against German cockroaches due to

the lowering of the repellent's volatility through inclusion in the cyclodextrin ring (Whang and Tonelli, 2008). As an alternative to CDMCT, pyrethroid/cyclodextrin complexes can be incorporated into bednets through impregnation using a binder such as poly(vinyl alcohol), resulting in an effective wash-durable LLIN (Mount and Green, 2001).

For outdoor recreation and occupation use, in 2003, Insect Shield LLC (2010, Greensboro, NC) developed a process to treat clothing products with permethrin. Several commercially available apparel product lines are available. Insect Shield is now registered with the US EPA to provide effective protection from mosquitoes, ticks, fleas and flies through 70 washings for both outdoor civilian and military use.

18.4 *In situ* treatment of bednets and other textiles to enable protection from biting insects

Due to the logistics issues raised for the effective distribution of LLINs in Section 18.3.3, *in situ* treatments of locally available nets have been investigated. This approach, similar to Type 3 LLIN preparation (Section 18.3.2) except for its operation occurring in the field rather than the factory, is also important for the retreatment of LLINs that have lost their bioactivity. Two commercial products have been developed which have received WHOPES time-limited interim recommendation: K-O TAB 1,2,3[®] (Bayer Crop Science) and ICON-MAXX (Syngenta) (WHOPES, 2007b, 2008). Both products employ water-soluble capsules containing pyrethroid preparations (deltamethrin and λ -cyhalothrin for K-O TAB and ICON, respectively). Recent studies show that K-O TAB is effective for treatment of polyester and polyethylene nets, on par with the performance of the PermaNet (Oxborough *et al.*, 2009; Yates *et al.*, 2005). K-O TAB-treated cotton resulted in a high retention of deltamethrin in the net, but a lower mosquito mortality rate, reflecting the residence of deltamethrin in the interior of the fibers (Oxborough *et al.*, 2009). K-O TAB treatment of nylon was ineffective (Oxborough *et al.*, 2009). Therefore the ability to prepare an *in situ* treatment kit that is universally applicable to all textile types is challenging. The US military employs a dipping method similar to that described above for K-O TAB and ICON-MAXX to treat uniforms in the field known as the 'Individual Dynamic Absorption (IDA) Kit', NSN 6840-01-345-0237 (AFPMB, 2009).

In a related approach, Hayes and co-workers developed an *in situ* preparation method based on co-adsorption of pyrethroid and free-radical polymerizable water-soluble monomer or oligomer (Zhuang *et al.*, 2008). An aqueous solution of monomer, 2-hydroxy ethyl methacrylate (HEMA), or its oligomers (0.4 mol monomer L⁻¹), and pyrethroid suspension or emulsion (with deltamethrin employed in the cited study) is prepared on site for the derivatization. Then the net was soaked in the aqueous solution for a few

minutes, and then removed of its excess water. *In situ* oligomerization was enacted by exposing the treated net to sunlight and/or warm ambient temperatures. The ITNs synthesized in the laboratory produced 70–90% mortality after six successive washes and $\geq 70\%$ of their original deltamethrin content, both benchmarks of which are comparable to the performance of first-generation commercial LLIN products. A cost analysis indicated that chemicals required for the derivatization solution would cost only an additional US\$1.15 beyond the cost of the pyrethroid.

In addition to nets and clothing, insecticide-laden textiles can also take the form of patches that can be attached directly to arms or legs, or to clothing (Emmrich *et al.*, 2006). The patches are made of rayon, polyester and polypropylene. The patent literature also contains examples of insecticide-laden textiles for use as covers for containers that store food or water, shoes and blankets (Uemura and Ogawa, 2008; Vestergaard-Frandsen and Skovmand, 2003; Vestergaard-Frandsen *et al.*, 2003).

18.5 Future trends

An important future trend is the development of new insecticides to alleviate concern over the release of pyrethroids to the environment and to address pyrethroid resistance among vectors. An example is the use of incorporation of metals into polyester (Han, 2009). Interest in natural insecticides such as citronellol is anticipated to increase.

A major concern is the spread of pyrethroid resistance among mosquito populations. Two major types of resistance occur: ‘knock-down resistance’, referring to the ability of vectors to reside on pyrethroid-laden textiles for longer periods of time (i.e. lower repellency), and metabolic resistance, where vectors have enzyme systems to counteract the activity of the pyrethroids. The PermaNet 3.0 (described in Section 18.3.2) serves as an example of the approach to combat pyrethroid-resistant mosquitoes, employing the synergist PBO. To date the PermaNet 3.0 has not been shown to be uniquely effective against pyrethroid-resistant mosquitoes. An alternative approach is to employ repellents such as DEET or organophosphates such as ‘chlorpyrifos Me’ or carbamates (Faulde *et al.*, 2010; N’Guessan *et al.*, 2010; Vestergaard-Frandsen, 2009), either in neat form or in combination with pyrethroids, as active ingredients for vector-protective textiles. Vestergaard-Frandsen (2009), the producer of the PermaNet, recently received a patent describing the use of tents containing two different nets separated from each other by a significantly large distance, one laden with pyrethroid and synergist and the other carbamate for combating pyrethroid-resistant mosquitoes.

An additional need is for field-deployable methodologies to measure the concentration of pyrethroid contained by textiles, to evaluate their effectiveness and identify the need for retreatment. Typically, pyrethroid is quantified

chromatographically (Section 18.1.3). Along these lines, an enzyme-linked immunosorbent assay, or ELISA, has been developed to measure the delta-methrin concentration of cotton (Soltan *et al.*, 2009).

Nanotechnology is anticipated to produce new polymeric matrices for insecticide-laden textiles and delivery systems to enable incorporation of pesticides. An example of the former includes polylactic acid/cellulose nanocomposites (Frey *et al.*, 2010). Recent approaches in the patent literature for nanoscale derivatization of textiles with pyrethroids or repellents focus upon microencapsulation technology (Mathis and Sladek, 2007; Takahashi *et al.*, 2005; Xin and Bin, 2009).

18.6 Sources of further information and advice

Information on vector-borne diseases is available through the WHO and the CDC, with additional information available through Roll Back Malaria. Information on pesticides, including pyrethroids, is available at the WHO website (WHO, 2009a) and in a recent American Chemical Society (ACS) Symposium Series book (Clark *et al.*, 2009). The latter also provides an overview of pyrethroid-resistant vectors. Recent concerns of the persistence and ultimate effect of pyrethroids on the ecosystem have been reviewed in a recent ACS Symposium Series book (Gan *et al.*, 2008). The best resource for learning about LLINs and their testing requirements is through the WHOPES website (WHOPES, 2010b). Protective textiles employed by the USA military are provided through the Armed Forces Pest Management Board (specifically, see AFPMB (2009)).

18.7 References

- ABDEL-MOHDY, F. A., FOUADA, M. M. G., REHAN, M. F. and ALY, A. S. (2008) Repellency of controlled-release treated cotton fabrics based on cypermethrin and prallethrin. *Carbohydrate Polymers*, 73: 92–97.
- AFPMB (2009) Personal protective measures against insects and other arthropods of military significance (Technical Guide No. 36). Washington, DC, Armed Forces Pest Management Board (USA). Available from: http://www.afpmb.org/coweb/guidance_targets/ppms/TG36/TG36.pdf [Accessed 8 June 2010].
- ANDERSON, C. D. and DANIELS, E. S. (2003) Emulsion and applications of latex. *RAPRA Review Reports*, 14: 1–32.
- BANEK, K. E., KILIAN, A. and ALLAN, R. (2010) Evaluation of Interceptor long-lasting insecticidal nets in eight communities in Liberia. *Malaria Journal*, 9: 84.
- BARLOW, S. M., SULLIVAN, F. M. and LINES, J. (2001) Risk assessment of the use of delta-methrin on bednets for the prevention of malaria. *Food and Chemical Toxicology*, 39: 407–422.
- BENNETT, S. N., DRUMMOND, A. J., KAPAN, D. D., SUCHARD, M. A., MUNOZ-JORDAN, J. L., PYBUS, O. G., HOLMES, E. C. and GUBLER, D. J. (2010) Epidemic dynamics revealed in dengue evolution. *Molecular Biology and Evolution*, 27: 811–818.

- BESTNET EUROPE (2010) Netprotect, London. Available from: <http://www.bestneteurope.com/Products/Netprotect®.aspx> [Accessed 9 June 2010].
- BINKA, F. and AKWONGO, P. (2006) Prevention of malaria using ITNs: potential for achieving the millennium development goals. *Current Molecular Medicine*, 6: 261–267.
- BISSINGER, B. W. and ROE, R. M. (2010) Tick repellents: past, present, and future. *Pesticide Biochemistry and Physiology*, 96: 63–79.
- BURR, S. A. and RAY, D. E. (2004) Structure-activity and interaction effects of 14 different pyrethroids on voltage-gated chloride ion channels. *Toxicology Science*, 77: 341–346.
- CDC (2010a) Japanese encephalitis, Atlanta, Center for Disease Control (USA). Available from: <http://www.cdc.gov/ncidod/dvbid/jencephalitis/index.htm> [Accessed 9 June 2010].
- CDC (2010b) Lyme disease, Atlanta, Center for Disease Control (USA). Available from: <http://www.cdc.gov/ncidod/dvbid/lyme> [Accessed 9 June 2010].
- CDC (2010c) West Nile virus, Atlanta, Center for Disease Control (USA). Available from: <http://www.cdc.gov/westnile/> [Accessed 9 June 2010].
- CECCHINE, G., GOLOMB, B. A., HILBORNE, L. H., SPEKTOR, D. M. and ANTHONY, C. R. (2000) *A Review of the Scientific Literature as it Pertains to Gulf War Illnesses, Volume 8: Pesticides*. Santa Monica, CA, USA: Rand Corporation.
- CLARK, J. M., BLOOMQUIST, J. R., KAWADA, H. and editors (2009) *Advances in Human Vector Control (ACS Symposium Series 1014)*. Washington, DC: American Chemical Society.
- CURTIS, C. F., MAXWELL, C. A., MAGESA, S. M., RWEGOSHORA, R. T. and WILKES, T. J. (2006) Insecticide-treated bed-nets for malaria mosquito control. *Journal of the American Mosquito Control Association*, 22: 501–506.
- DEV, V. (2009) Long-lasting insecticidal nets for malaria control. *Current Science*, 97: 469–470.
- EMMRICH, R. R., KONGSHAUG, P., HELDING, E. M. and ROPIAK, D. T. (2006) Wearable insect-repelling patch. USA, 2006–359089.
- ENAYATI, A. and HEMINGWAY, J. (2010) Malaria management: past, present, and future. *Annual Review of Entomology*, 55: 569–591.
- FAKOORZIBA, M. R., EGHBAL, F. and VIJAYAN, V. A. (2009) Synergist efficacy of piperonyl butoxide with deltamethrin as pyrethroid insecticide on *Culex tritaeniorhynchus* (Diptera: Culicidae) and other mosquito species. *Environmental Toxicology*, 24: 19–24.
- FAULDE, M. K., ALBIEZ, G. and NEHRING, O. (2010) Insecticidal, acaricidal and repellent effects of DEET- and IR3535-impregnated bed nets using a novel long-lasting polymer-coating technique. *Parasitology Research*, 106: 957–965.
- FAULDE, M. K., UEDELHOVEN, W. M., MALERIUS, M. and ROBBINS, R. G. (2006) Factory-based permethrin impregnation of uniforms: residual activity against *Aedes aegypti* and *Ixodes ricinus* in battle dress uniforms worn under field conditions, and cross-contamination during the laundering and storage process. *Military Medicine*, 171: 472–477.
- FAULDE, M. K. and UEDELHOVEN, W. (2006) A new clothing impregnation method for personal protection against ticks and biting insects. *International Journal of Medical Microbiology*, 296 (Suppl 40): 225–229.
- FAULDE, M. K., UEDELHOVEN, W. M. and ROBBINS, R. G. (2003) Contact toxicity and residual activity of different permethrin-based fabric impregnation methods for *Aedes*

- aegypti* (Diptera: Culicidae), *Ixodes ricinus* (Acari: Ixodidae), and *Lepisma saccharina* (Thysanura: Lepismatidae). *Journal of Medical Entomology*, 40: 935–941.
- FRANCES, S. P., WATSON, K. and CONSTABLE, B. G. (2003) Comparative toxicity of permethrin- and bifenthrin-treated cloth fabric for *Anopheles farauti* and *Aedes aegypti*. *Journal of the American Mosquito Control Association*, 19: 275–278.
- FREY, M. W., XIANG, C., HOFFMANN, M. P., TAYLOR, A. G. and GARDNER, J. (2010) Biodegradable agrochemical delivery system using polymeric materials. WO, 2010039865.
- GAN, J., SPURLOCK, F., HENDLEY, P., WESTON, D. P. and editors (2008) *Synthetic Pyrethroids: Occurrence and Behavior in Aquatic Environments (ACS Symposium Series 991)*. Washington, DC: American Chemical Society.
- GIROUX, P., WALKER, E. and MILLER, J. R. (2006) Comparison of mode of action of PermaNet and Olyset insecticide treated bednets. *Entomological Society of America Annual Meeting*, December 10–13, The Indiana Convention Center and RCA Dome Indianapolis, Indiana.
- GU, W. and NOVAK ROBERT, J. (2009) Predicting the impact of insecticide-treated bed nets on malaria transmission: the devil is in the detail. *Malaria Journal*, 8: 256.
- HAN, G. S. (2009) Method for manufacturing fabric and clothes for preventing biting of mosquitoes. South Korea, KR 912636.
- HATAIPITISUK, R. (2007) Process for coating fiber or fabric with insecticide using a temperature of 150–190°C for drying. US, 2007009563.
- HAYES, D. G., GERHARDT, R. R. and WADSWORTH, L. C. (2009) Long-lasting insecticide-treated nets for mosquito control: alternate preparation approaches. *AATCC Review*, 9: 33–36.
- HOUGARD, J. M., DUCHON, S., DARREIT, F., ZAIM, M., ROGIER, C. and GUILLET, P. (2003) Comparative performances, under laboratory conditions, of seven pyrethroid insecticides used for impregnation of mosquito nets. *Bulletin of the WHO*, 81: 324–333.
- INSECT SHIELD LLC (2010) Insect shield, Greensboro, NC USA. Available from: <http://www.insectshield.com/> [Accessed 9 June 2010].
- ITOH, T. (2005) Olyset net, a long lasting insecticidal net for malaria control. In: Clark, J. M. and Ohkawa, H. (eds.) *New Discoveries in Agrochemicals (ACS Symposium Series 892)*. Washington, DC: American Chemical Society, pp. 326–333.
- ITOH, T., SHONO, Y., LUCAS, J. R. and ISHIWATARI, T. (2009) Olyset net: a long lasting insecticidal net for vector control. In: Clark, J. M., Bloomquist, J. R. and Kawada, H. (eds.) *Advances in Human Vector Control (ACS Symposium Series 1014)*. Washington, DC: American Chemical Society, pp. 153–159.
- JAWARA, M., MCBEATH, J., LINES, J. D., PINDER, M., SANYANG, F. and GREENWOOD, B. M. (1998) Comparison of bednets treated with alphacypermethrin, permethrin or lambda-cyhalothrin against *Anopheles gambiae* in the Gambia. *Medical and Veterinary Entomology*, 12: 60–66.
- KASAI, S., ISHII, N., NATSUAKI, M., FUKUTOMI, H., KOMAGATA, O., KOBAYASHI, M. and TOMITA, T. (2009) Monitoring of KDR-mediated pyrethroid resistance in head louse colonies in Japan. In: Clark, J. M., Bloomquist, J. R. and Kawada, H. (eds.) *Advances in Human Vector Control (ACS Symposium Series 1014)*. Washington, DC: American Chemical Society, pp. 217–224.
- KASILI, S., KUTIMA, H., MWANDAWIRO, C., ngumbi PHILIP, M., anjili CHRISTOPHER, O. and ENAYATI, A. A. (2010) Laboratory and semi-field evaluation of long-lasting insecticidal nets against leishmaniasis vector, *Phlebotomus (Phlebotomus duboscqi)* in Kenya. *Journal of Vector Borne Diseases*, 47: 1–10.

- KAWADA, H. (2009) An inconvenient truth of pyrethroid: does it have a promising future? In: Clark, J. M., Bloomquist, J. R. and Kawada, H. (eds.) *Advances in Human Vector Control (ACS Symposium Series, 1014)*. Washington, DC: American Chemical Society, pp. 171–190.
- KNOX, T. B. and SCOTT, T. W. (2009) Vector control for prevention of dengue: current status and future strategies. In: Clark, J. M., Bloomquist, J. R. and Kawada, H. (eds.) *Advances in Human Vector Control (ACS Symposium Series 1014)*. Washington, DC: American Chemical Society, pp. 39–57.
- KOKOZA, V., AHMED, A., SHIN, S. W., OKAFOR, N., ZOU, Z. and RAIKHEL, A. S. (2010) Blocking of plasmodium transmission by cooperative action of cecropin A and defensin A in transgenic *Aedes aegypti* mosquitoes. *Proceedings of the National Academy of Science USA Early Edition*, 12 April: 1–6.
- KOLACZINSKI, J. H. and CURTIS, C. F. (2004) Chronic illness as a result of low-level exposure to synthetic pyrethroid insecticides: a review of the debate. *Food and Chemical Toxicology*, 42: 697–706.
- KROEGER, A., SKOVMAND, O., PHAN, Q. C. and BOEWONO, D. T. (2004) Combined field and laboratory evaluation of a long-term impregnated bednet, PermaNet®. *Transactions of the Royal Society of Tropical Medicine and Hygiene*, 98: 152–155.
- LAUTRAITE, S. and SARGENT, D. (2009) Pyrethroids toxicology – a review of attributes and current issues. *Bayer CropScience Journal*, 62: 195–210.
- LICKFIELD, D. K., ALEXANDER, D. and BUTENHOFF, A. (2010) A review of important polymer and yarn selection parameters for the production of warp knit mosquito net fabrics. Washington, DC, NetMark Africa. Available from: <http://www.netmarkafrica.org/news/LLIN%20Textile%20Review.pdf> [Accessed 9 June 2010].
- LOPEZ, O., FERNANDEZ-BOLANOS, J. G. and GIL, M. V. (2005) New trends in pest control: the search for greener insecticides. *Green Chemistry*, 7: 431–442.
- MALIMA, R. C., MAGESA, S. M., TUNGU, P. K., MWINGIRA, V., MAGOGO, F. S., SUDI, W., MOSHA, F. W., CURTIS, C. F., MAXWELL, C. and ROWLAND, M. (2008) An experimental hut evaluation of Olyset nets against anopheline mosquitoes after seven years use in Tanzanian villages. *Malaria Journal*, 7: 38.
- MATHIS, R. and SLADEK, H.-J. (2007) Microencapsulation of insect repellents for fibers and textiles and preparation of fiber with long lasting wash-proofed insect repellent properties. EP, 1845186.
- MATOVU, F., GOODMAN, C., WISEMAN, V. and MWENGEE, W. (2009) How equitable is bed net ownership and utilisation in Tanzania? A practical application of the principles of horizontal and vertical equity. *Malaria Journal*, 8: 109.
- MILLER, J. E., LINDSAY, S. W. and ARMSTRONG, J. (1991) Experimental hut trials of bed-nets impregnated with synthetic pyrethroid or organophosphate Insecticide for mosquito control in the Gambia. *Medical and Veterinary Entomology*, 5: 465–476.
- MINAKAWA, N., DIDA GABRIEL, O., SONYE GORGE, O., FUTAMI, K. and KANEKO, S. (2008) Unforeseen misuses of bed nets in fishing villages along Lake Victoria. *Malaria Journal*, 7: 165.
- MOUNT, D. L. and GREEN, M. D. (2001) Insecticide-impregnated fabric. WO, 2001058261.
- MUGURUMA, M., UNAMI, A., KANKI, M., KUROIWA, Y., NISHIMURA, J., DEWA, Y., UMEMURA, T., OISHI, Y. and MITSUMORI, K. (2007) Possible involvement of oxidative stress in piperonyl butoxide induced hepatocarcinogenesis in rats. *Toxicology*, 236: 61–75.
- N'GUESSAN, R., BOKO, P., ODJO, A., CHABI, J., AKOGBETO, M. and ROWLAND, M. (2010) Control of pyrethroid and DDT-resistant *Anopheles gambiae* by application of indoor

- residual spraying or mosquito nets treated with a long-lasting organophosphate insecticide, chlorpyrifos-methyl. *Malaria Journal*, 9: 44.
- NAKAGAWA, J. (2009) Current status and challenges of Chagas disease control initiatives in the Americas. In: Clark, J. M., Bloomquist, J. R. and Kawada, H. (eds.) *Advances in Human Vector Control (ACS Symposium Series 1014)*. Washington, DC: American Chemical Society, pp. 59–71.
- NERIO LUZ, S., OLIVERO-VERBEL, J. and STASHENKO, E. (2010) Repellent activity of essential oils: a review. *Bioresource Technology*, 101: 372–378.
- NILLOS, M. G., GAN, J. and SCHLENK, D. (2008) Chemical analysis and enantioselective toxicity of pyrethroids. In: Gan, J., Spurlock, F., Hendley, P. and Weston, D. P. (eds.) *Synthetic Pyrethroids: Occurrence and Behavior in Aquatic Environments (ACS Symposium Series 991)*. Washington, DC: American Chemical Society, pp. 400–414.
- OLSON, K. E. and FRANZ, A. W. E. (2009) Controlling dengue virus transmission in the field with genetically modified mosquitoes. In: Clark, J. M., Bloomquist, J. R. and Kawada, H. (eds.) *Advances in Human Vector Control (ACS Symposium Series 1014)*. Washington, DC: American Chemical Society, pp. 123–141.
- OSIMITZ, T. G., SOMMERS, N. and KINGSTON, R. (2009) Human exposure to insecticide products containing pyrethrins and piperonyl butoxide (2001–2003). *Food and Chemical Toxicology*, 47: 1406–1415.
- OXBOROUGH, R. M., WEIR, V., IRISH, S., KAUR, H., N'GUESSAN, R., BOKO, P., ODJO, A., METONNOU, C., YATES, A., AKOGBETO, M. and ROWLAND, M. W. (2009) Is K-O Tab 1–2–3 long lasting on non-polyester mosquito nets? *Acta Tropica*, 112: 49–53.
- PATES, H. and CURTIS, C. (2005) Mosquito behavior and vector control. *Annual Review of Entomology*, 50: 53–70.
- PEREZ-FERNANDEZ, V., GARCIA, M. A. and MARINA, M. L. (2010) Characteristics and enantiomeric analysis of chiral pyrethroids. *Journal of Chromatography A*, 1217: 968–989.
- ROMERO, A., POTTER, M. F. and HAYNES, K. F. (2009) Evaluation of piperonyl butoxide as a deltamethrin synergist for pyrethroid-resistant bed bugs. *Journal of Economic Entomology*, 102: 2310–2315.
- ROMI, R., LO NOSTRO, P., BOCCI, E., RIDI, F. and BAGLIONI, P. (2005) Bioengineering of a cellulosic fabric for insecticide delivery via grafted cyclodextrin. *Biotechnology Progress*, 21: 1724–1730.
- SHAFFER, T. J., MEYER, D. A. and CROFTON, K. M. (2005) Developmental neurotoxicity of pyrethroid insecticides: critical review and future research needs. *Environmental Health Perspectives*, 113: 123–137.
- SHAMIM, M. T., HOFFMANN, M. D., MELENDEZ, J. and RUHMAN, M. A. (2008) Ecological risk characterization for the synthetic pyrethroids. In: Gan, J., Spurlock, F., Hendley, P. and Weston, D. P. (eds.) *Synthetic Pyrethroids: Occurrence and Behavior in Aquatic Environments (ACS Symposium Series 991)*. Washington, DC: American Chemical Society, pp. 257–309.
- SIEGERT, P. Y., WALKER, E. and MILLER, J. R. (2009) Differential behavioral responses of *Anopheles gambiae* (Diptera: Culicidae) modulate mortality caused by pyrethroid-treated bednets. *Journal of Economic Entomology*, 102: 2061–2071.
- SKOVMAND, O., BONNET, J., PIGEON, O. and CORBEL, V. (2008) Median knock-down time as a new method for evaluating insecticide-treated textiles for mosquito control. *Malaria Journal*, 7: 114.

- SOLTAN, H. R., ABD EL-MEGEED, F. A., MUSTAFA, F. I. and ISMAIL, H. M. (2009) Analysis of photochemically induced cotton bound residues of deltamethrin by an immuno-assay technique. *Journal of AOAC International*, 92: 1815–1820.
- SOMBOON, P., LINES, J., ARAMRATTANA, A., CHITPRAROP, U., PRAJAKWONG, S. and KHAMBOONRUANG, C. (1995) Entomological evaluation of community-wide use of lambdacyhalothrin impregnated bed nets against malaria in a border area of north-west Thailand. *Transactions of the Royal Society of Tropical Medicine and Hygiene*, 89: 248–254.
- SPURLOCK, F. and LEE, M. (2008) Synthetic pyrethroid use patterns, properties, and environmental effects. In: Gan, J., Spurlock, F., Hendley, P. and Weston, D. P. (eds.) *Synthetic Pyrethroids: Occurrence and Behavior in Aquatic Environments (ACS Symposium Series 991)*. Washington, DC, American Chemical Society, pp. 3–25.
- SREEHARI, U., RAGHAVENDRA, K., RIZVI, M. M. A. and DASH, A. P. (2009) Wash resistance and efficacy of three long-lasting insecticidal nets assessed from bioassays on *Anopheles culicifacies* and *Anopheles stephensi*. *Tropical Medicine & International Health*, 14: 597–602.
- SUDAKIN, D. L. and TREVATHAN, W. R. (2003) DEET: a review and update of safety and risk in the general population. *Journal of Toxicology. Clinical Toxicology*, 41: 831–839.
- TAKAHASHI, T., TAGUCHI, Y. and TANAKA, M. (2005) Preparation of polyurea microcapsules containing pyrethroid insecticide with hexamethylene diisocyanate uretidione and isocyanurate. *Journal of Chemical Engineering Japan*, 38: 929–936.
- TUNGU, P., MAGESA, S., MAXWELL, C., MALIMA, R., MASUE, D., SUDI, W., MYAMBA, J., PIGEON, O. and ROWLAND, M. (2010) Evaluation of PermaNet 3.0 a deltamethrin-PBO combination net against *Anopheles gambiae* and pyrethroid resistant *Culex quinquefasciatus* mosquitoes: an experimental hut trial in Tanzania. *Malaria Journal*, 9: 21.
- UEMURA, S. and OGAWA, T. (2008) Insecticide-volatilizing tool to attach to shoe. Japan, JP 3140153.
- VESTERGAARD-FRANSEN, M. (2009) Room with two counter-resistant insecticidal objects. WO, 2009059603.
- VESTERGAARD-FRANSEN, M. (2010) PermaNet, Lausanne, Switzerland. Available from: <http://www.vestergaard-frandsen.com/permanet/> [Accessed 9 June 2010].
- VESTERGAARD-FRANSEN, M. and SKOVMAND, O. (2003) Pesticidal blanket. WO, 2003055307.
- VESTERGAARD-FRANSEN, M., VESTERGAARD-FRANSEN, T. and SKOVMAND, O. (2003) Protective cover for food and water storage containers. European Patent, EP 1356732.
- WERNER, I. and MORAN, K. (2008) Effects of pyrethroid insecticides on aquatic organisms. In: Gan, J., Spurlock, F., Hendley, P. and Weston, D. P. (eds.) *Synthetic Pyrethroids: Occurrence and Behavior in Aquatic Environments (ACS Symposium Series 991)*. Washington, DC: American Chemical Society, pp. 310–334.
- WHANG, H. S. and TONELLI, A. (2008) Release characteristics of the non-toxic insect repellent 2-undecanone from its crystalline inclusion compound with α -cyclodextrin. *Journal of Inclusion Phenomena and Macrocyclic Chemistry*, 62: 127–134.

- WHO (2009a) *Global insecticide use for vector-borne disease control*, 4th edn. Geneva: World Health Organization. Available from: http://whqlibdoc.who.int/publications/2009/9789241598781_eng.pdf [Accessed 31 January 2011].
- WHO (2009b) *Leishmaniasis*. Geneva: World Health Organization. Available from: <http://www.who.int/leishmaniasis/en/> [Accessed 9 June 2010].
- WHO (2009c) *World malaria report 2009*. Geneva: World Health Organization. Available from: <http://www.who.int/malaria/publications> [Accessed 9 June 2010].
- WHO (2010) *Filariasis*. Geneva: World Health Organization. Available from: <http://www.who.int/topics/filariasis/en/> [Accessed 9 June 2010].
- WHOPES (2005) *Guidelines for the laboratory and field testing of long-lasting insecticidal mosquito nets*. Geneva: World Health Organization Pesticide Evaluation Scheme. Available from: http://whqlibdoc.who.int/hq/2005/WHO_CDS_WHOPES_GCDPP_2005.11.pdf [Accessed 9 June 2010].
- WHOPES (2007a) *Introduction: Malaria accounts for a large part of the disease burden of poor countries*. Geneva: World Health Organization Pesticide Evaluation Scheme. Available from: http://www.who.int/malaria/docs/whopes/safety_pt_mn_eng.pdf [Accessed 9 June 2010].
- WHOPES (2007b) *Report of the 10th WHOPES Working Group Meeting (2006)*. Geneva: World Health Organization Pesticide Evaluation Scheme. Available from: http://whqlibdoc.who.int/hq/2007/WHO_CDS_NTD_WHOPES_2007_1_eng.pdf [Accessed 9 June 2010].
- WHOPES (2008) *Report of the 11th WHOPES Working Group Meeting (2007)*. Geneva: World Health Organization Pesticide Evaluation Scheme. Available from: http://whqlibdoc.who.int/hq/2008/WHO_HTM_NTD_WHOPES_2008.1_eng.pdf [Accessed 9 June 2010].
- WHOPES (2009) *Report of the 12th WHOPES Working Group Meeting (2008)*. Geneva: World Health Organization Pesticide Evaluation Scheme. Available from: http://whqlibdoc.who.int/hq/2009/WHO_HTM_NTD_WHOPES_2009_1_eng.pdf; <http://www.who.int/whopes/resources/en/> [Accessed 9 June 2010].
- WHOPES (2010a) *Report of the 13th WHOPES Working Group Meeting (2009)*. Geneva: World Health Organization Pesticide Evaluation Scheme. Available from: http://whqlibdoc.who.int/publications/2009/9789241598712_eng.pdf [Accessed 9 June 2010].
- WHOPES (2010b), WHOPES: links and resources. Geneva: World Health Organization Pesticide Evaluation Scheme. Available from: http://whqlibdoc.who.int/hq/2009/WHO_HTM_NTD_WHOPES_2009_1_eng.pdf; <http://www.who.int/whopes/resources/en/> [Accessed 9 June 2010].
- WONG, C. S. (2006) Environmental fate processes and biochemical transformations of chiral emerging organic pollutants. *Analytical and Bioanalytical Chemistry*, 386: 544–558.
- XIN, J. H. and BIN, F. (2009) Insect-repellent fabrics having nanocapsules with pyrethroid. US, 2009010977.
- YATES, A., N'GUESSAN, R., KAUR, H., AKOGBÉTO, M. and ROWLAND, M. (2005) Evaluation of KO-Tab 1–2–3®: a wash-resistant 'dip-it-yourself' insecticide formulation for long-lasting treatment of mosquito nets. *Malaria Journal*, 4: 1–9.
- YUKICH, J. O., LENGELER, C., TEDIOSI, F., BROWN, N., MULLIGAN, J.-A., CHAVASSE, D., STEVENS, W., JUSTINO, J., CONTEH, L., MAHARAJ, R., ERSKINE, M., Mueller DIRK, H., WISEMAN, V.,

- GHEBREMESKEL, T., ZEROM, M., GOODMAN, C., MCGUIRE, D., URRUTIA JUAN, M., SAKHO, F., HANSON, K. and SHARP, B. (2008) Costs and consequences of large-scale vector control for malaria. *Malaria Journal*, 7: 258.
- ZAIM, M. and GUILLET, P. (2002) Alternate insecticides: an urgent need. *Trends in Parasitology*, 18: 161–163.
- ZHUANG, F., CHITTUR, K. K., HAYES, D. G., MOUNT, D. L. and SMITH, S. C. (2008) Simple and inexpensive preparation of long-lasting insecticidal nets via co-adsorption of pyrethroid and oligomer. *Textile Research Journal*, 78: 595–603.

Improving the functionality of clothing through novel pesticide protection

S. K. OBENDORF,
Cornell University, USA

Abstract: Chemical protection is needed to reduce occupational chemical exposure for individuals involved with mixing, loading and applying pesticide. Protection is provided by chemical protective materials that function by means of barrier (i.e. no permeation or penetration), repellency, or adsorption mechanisms, or a combination of these approaches. Basic mechanisms have been used to define novel approaches for pesticide-protective clothing including microporous and nanofibrous membranes as well as self-decontamination materials based upon N-halamines, metal oxides and polyoxometalates.

Key words: protective clothing, membrane, nanofiber, metal oxide, polyoxometalate.

19.1 Introduction to human exposure

19.1.1 Health effects

Chemicals may enter the body through a variety of routes including ingestion of food or in drinking water, inhalation and absorption through the skin. Although food safety issues have gained high visibility, occupational exposure for people involved with mixing, loading or application of pesticides is also a major health issue. Dermal absorption, rather than inhalation or ingestion, is the primary route for occupational chemical exposure.

Pesticide exposure levels are influenced by a variety of factors such as wind, type of activity, method and rate of application, duration of exposure and worker hygiene. Distribution patterns on worker's garments vary with method of application, equipment used and environmental conditions. Studies of garments after pesticide application with air-blast sprayers showed a general trend of higher exposure levels on the upper body (forearm, shoulder, chest, neck) rather than the lower body (DeJonge *et al.*, 1985). Coffman *et al.* (1999) observed the highest concentration on the neck, upper arm and shoulder in a diagonal pattern from upper right shoulder (spraying arm) to lower left torso. The use of a hooded sprayer with high volume, low concentration output produced considerably less contamination than an air-assist

sprayer. Nigg *et al.* (1990) found higher deposition on the thigh rather than chest when a canopied tractor was used to pull the air-blast sprayer.

A wide variety of health hazards related to common pesticides are known. Local effects of pesticides include irritation, allergic contact dermatitis, photo irritation, photo allergic contact dermatitis and contact urticaria. Systemic effects include seizures, aplastic anemia, various neurological symptoms, cognitive and psychomotor dysfunction, sterility and some rare fatalities (Kamel and Hoppin, 2004; Tripp *et al.*, 2007).

Over 16 000 pesticide products are used in the United States (NIOSH, 2009). Pesticides such as methyl parathion, *O,O*-dimethyl *O*-4-nitrophenyl phosphorothioate, can cause severe poisoning effects in humans and is classified as extremely hazardous, or Class IA (Tomlin, 1997; WHO, 2002). Therefore its use has been restricted in the United States since 1978; it can now be applied only as an agricultural insecticide by a certified individual (Abou-Donia, 1994). Restriction is necessary because methyl parathion and other pesticides inhibit the acetyl cholinesterase enzyme by blocking the binding site on the enzyme (Levin and Rodnitzky, 1976; Tafuri and Roberts, 1987). Blocked acetyl cholinesterase enzyme binding sites leads to high levels of acetylcholine, which can result in death from asphyxiation. Aside from the neurotoxic effects, methyl parathion is also toxic to several organs, such as the liver, and to cardiovascular and muscular systems (Garcia *et al.*, 2003). Additionally, methyl parathion exposure can lead to lowered concentration, slower information processing time, memory and speech impairment, depression and anxiety (Levin and Rodnitzky, 1976). It is important to find better personal protective equipment (PPE) and strategies to limit human exposures to such pesticides.

19.1.2 Mitigation strategies

Agencies such as the Environmental Protection Agency (EPA) and United States Department of Agriculture (USDA) develop mitigation strategy systems to reduce occupational pesticide exposure. Although specific guidelines vary with individual chemicals and situations, these measures combine several closely related approaches to create practical and enforceable procedural modifications. General criteria include: use of PPE, engineering controls, limit of exposure time or reduction of active ingredient, and establishment of buffer zones. Garment materials can range from highly specialized protective suits to conventional woven cotton/polyester work clothing.

The use of PPE directly limits exposure. However, clothing that limits pesticide exposure also limits water vapor transmission and contributes to discomfort or heat stress. In order to allow increased ventilation, workers wearing more occlusive garments inadvertently decrease their personal

protection by not closing them properly. For such reasons, some workers prefer more traditional types of garments such as denim coveralls.

19.1.3 Chemical protective clothing systems

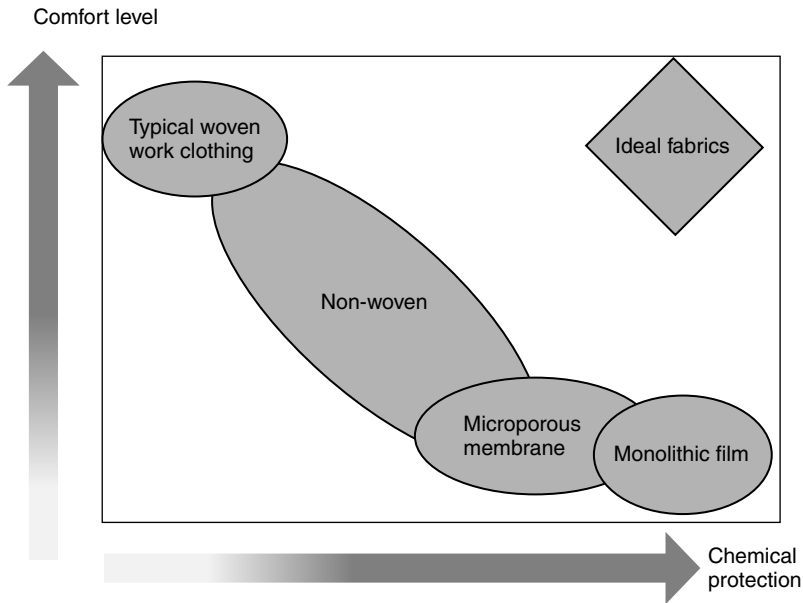
US EPA guidelines suggest the use of basis PPE that include coveralls, apron, broad-brimmed waterproof hat, boots, rubber gloves, goggles, face shields or respirators. These items are constructed of a variety of material types from highly specialized selectively permeable membranes to everyday clothing fabrics. They can be disposable or reusable, each with benefits and drawbacks depending on the situation, working environment, user groups and toxicity of the pesticide governing the specific choices of PPE. The Center for Disease Control and Prevention (CDC) recommends that people working as mixers, loaders and applicators of pesticides wear protective clothing according to the EPA guidelines (CDC, 2005).

Performance specifications for chemical protective body garments, ASTM F2669–09, were developed by the American Society for Testing and Materials (ASTM, 2009). Materials are categorized into three different levels based on average penetration values for a given challenge chemical. Properties are material and seam resistance to penetration by liquid under pressure, resistance to permeation (in the absence of applied pressure), breaking and tearing strength.

Protective garments function primarily by barrier (no permeation or penetration), repellency, adsorption or a combination of these mechanisms. Thus, chemicals are kept away from the skin by retention in the fabric structure or rolling off the outside layer without penetration. Lee and Obendorf (2007a) show the relationship between protective properties and air permeability for materials including typical woven work fabrics, non-wovens, microporous membranes and laminated fabrics (see Fig. 19.1).

19.2 Mechanisms for chemical protection

Textile structures have highly complex three-dimensional lattices with overall material properties derived from a combination of fiber chemistry and geometry, degree of open spaces, and tightness in yarn and weave. Pesticide penetration is governed by properties of the material (content and structure) as well as the physical and chemical properties of the challenge chemical. Contamination may occur through a combination of permeation, penetration and sorption. Structural and chemical characteristics of the material determine which mechanism will dominate when exposed to a specific liquid challenge chemical. Many different materials are used for PPE including monolithic polymeric films for glove, non-woven disposable fabrics, woven fabrics, and laminated or coated fabrics.



19.1 Protection/comfort model (Lee and Obendorf, 2007a).

19.2.1 Barriers to permeation of liquids

Protective garments, such as gloves, act primarily as barriers to chemical permeation. Permeation involves the sequential absorption of molecules, diffusion of absorbed molecules followed by desorption. From Fick's Second Law, the diffusion rate of a given chemical through a material is proportional to the concentration difference through the material:

$$\frac{d\varphi}{dt} = D \frac{d^2\varphi}{dx^2} \quad [19.1]$$

where φ is concentration, t is time, D is diffusion coefficient, and x is diffusion distance. Chemically resistant gloves or suits designed for high levels of exposure are commonly made from monolithic film or use a film or coating as part of a system. Common materials for reusable suits and gloves include: butyl rubber, nitrile, neoprene and chlorinated polyethylene (Raheel, 1994, p. 262). For these materials, the type and concentration of the carrier solvent is the most important determinant of permeation of pesticides (Schwope *et al.*, 1992).

Permeation predictive models have been developed to estimate the movement of solvents through polymeric materials used for chemical protective clothing (Evans and Hardy, 2004; Evans *et al.*, 2008; Goydan *et al.*, 1988; Zellers, 1993; Zellers and Zhang, 1993). The relative affinity of a polymer

and solvent can be assessed using Hansen three-dimensional solubility parameters; thus researchers studied their correlation with permeation data (Zellers, 1993; Zellers and Zhang, 1993). The model for solubility and permeation of organic solvents in polymeric glove material was improved using a combination of Hansen solubility parameters and the polymer solution theory of Flory–Rehner (Evans and Hardy, 2004; Evans *et al.*, 2008; Zellers, 1993):

$$\left(\frac{V_m A}{RT} + \chi_s \right) \phi_m^2 = -[\ln(1 - \phi_m) + \phi_m] \quad [19.2]$$

where ϕ_m is the volume fraction of polymer in the polymer/solvent system, χ_s is the Flory Higgins polymer interaction parameter (a constant often set between 0.3 and 0.4), V_m is the molar volume of solvent, and A is defined for a specific polymer (solute) and solvent:

$$A = \left[a(\delta_{d1} - \delta_{d2})^2 + b(\delta_{p1} - \delta_{p2})^2 + (\delta_{h1} - \delta_{h2})^2 \right]^{1/2} \quad [19.3]$$

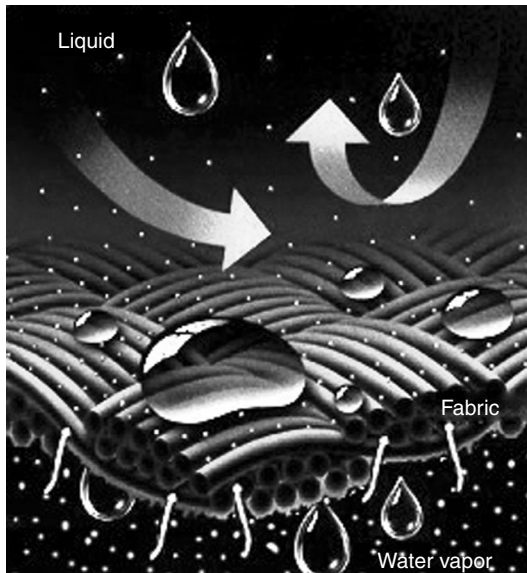
where subscripts 1 and 2 stand for the solute and solvent respectively, a and b are weighting factors, δ is the individual solubility parameters where d represents dispersion, p polar, h hydrogen bonding. High correlations are observed to the solvent-polymer interactive term $\chi \phi_p^2$ for steady-state permeation rates, breakthrough times, and lag times for butyl gloves (Evans *et al.*, 2008) and elastomeric Viton gloves (Evans and Hardy, 2004).

Monolithic materials such as nitrile glove materials are usually impermeable in both directions. The type of carrier solvent and concentration are the primary factors to impact permeation of the active ingredient. There are no universally effective glove barrier materials against active ingredients in solvents such as alcohols, ketones, aliphatic and aromatic petroleum distillates. However, in general nitrile, butyl and Silver Shield® materials were more effective than polyvinyl chloride and natural rubber (Schwope, 1986; Schwope *et al.*, 1992).

Upon contact with chemicals, various processes can occur such as chemical degradation and penetration, as well as permeation. Degradation can result from dissolution of the material, chemical reaction with the material, or chemical leaching. Cracking, shrinking or loss in mechanical properties can occur. Penetration is the passage of liquid chemical through pores or over openings such as holes, punctures, cracks or seams.

19.2.2 Repellency and sorption of liquids

Interaction between the textile surface and the liquid challenge chemical is governed by characteristics including chemical composition, surface configuration and fiber roughness, pore geometry of the textile, and liquid



19.2 Interaction of textile material with challenge liquid.

parameters such as surface tension and viscosity. In order to understand the penetration of pesticides through protective materials, it is necessary to understand the mechanisms of interaction between challenge liquids and textile surfaces (see Fig. 19.2). The processes of surface wetting and wicking form an important foundation for understanding the two major mechanisms for protective clothing materials, sorption and repellency.

Penetration into or through the fabric occurs if the material is 'wettable'. In wetting, the fiber–air interface is displaced by a fiber–liquid interface. Spontaneous wetting is the flow of a liquid over a solid surface toward thermodynamic equilibrium in the absence of external forces. The displacement of a fiber–air interface with a fiber–liquid interface is characterized by the contact angle θ formed between the liquid and solid and their surface energies. The Young-Dupré equation describes this equilibrium at the solid–liquid interface:

$$\gamma_{SV} - \gamma_{SL} = \gamma_{LV} \cos \theta \quad [19.4]$$

where γ is interfacial tension; subscripts S, L, and V denote solid, liquid, and vapor phases; θ is the equilibrium contact angle. Wettability increases with decreasing contact angle, or increasing $\cos \theta$. The surface tension at the maximum value for $\cos \theta$ is the critical surface tension of a solid (γ_c), a constant property of a given solid. Thus, spontaneous spreading and wetting occurs when the liquid surface tension is less than or equal to the critical

surface tension of the solid. If wetting does occur, capillary force-driven wicking allows the flow of liquid through a porous material (Hsieh, 1995; Kissa, 1996; Miller, 1977; Miller and Tyomkin, 1994).

19.2.3 Liquid penetration through porous materials

After wetting of fibers assembled with capillary spaces between them occurs, capillary forces drive the spontaneous flow of the liquid through the porous substrate, in the wicking process. Pesticide penetration is defined as the flow of a chemical through pores, or other discontinuities in the material such as closures or other imperfections. The flow of a liquid through a fibrous material may be described using a capillary bundle model with the Laplace and Poiseuille equations. The Laplace equation gives the pressure of fluid in a capillary:

$$P = 2\gamma \frac{\cos \theta}{r} \quad [19.5]$$

where P is pressure, γ is liquid surface tension, θ is solid/liquid contact angle, and r is pore radius. As described by the Laplace equation, positive capillary pressure (and thus liquid flow) occurs when $\cos \theta$ is positive; the contact angle is between 0° and 90° .

The Poiseuille equation shows the inverse relationship between the flow rate in a tube (capillary) and the distance that the liquid travels:

$$Q = \frac{\pi r^4}{8\eta} \cdot \frac{dp}{dl} \quad [19.6]$$

where Q is liquid flow rate, r is pore radius, l is pore length, η is viscosity, p is pressure.

Porosity (Φ) is defined as the fraction of void space in a porous medium:

$$\Phi = \frac{1 - \rho_b}{\rho_s} \quad [19.7]$$

where ρ_b is fabric density and ρ_s is fiber density. It is an important material property for sorption, flow of liquids, and vapor transmission. Fabric density (solid volume fraction) can be calculated by:

$$\rho_b = \frac{m / \rho_s}{at} \quad [19.8]$$

where m is the mass of the fabric, ρ_s is fiber density, a is area of fabric, and t is fabric thickness.

When the entire pore space is filled with the absorbed liquid, the material is saturated and has reached the maximum adsorption capacity (C_m):

$$C_m = \frac{\rho_l}{\rho_s} \cdot \frac{\varphi}{1 - \varphi} \quad [19.9]$$

where ρ_l is liquid density, ρ_s is fiber density, and φ is the fraction of volume made up of pores (void) defined by equation [19.7] (Chatterjee, 1985, p. 40).

Sorption by a material is governed by inter- and intra-fiber spaces where liquids are retained through capillary forces. When fabrics have the same weave structure, yet different fiber contents, the adsorption capacity can be also quite different due to different fiber pore structures. Pore geometry and connectivity, however, is not easily described (Hsieh, 1995). Pore sizes for woven fabrics commonly have a bimodal distribution. Large sizes represent the inter-yarn spaces, whereas the inter-fiber spaces are reflected by smaller spaces (Lee and Obendorf, 2007a; Miller and Tyomkin, 1994). For woven (Tencel) and non-woven (polyethylene) fabrics with similar solid volume fraction (0.386, 0.399 respectively), Lee and Obendorf (2007a) observed different water vapor transmission rates (20 and 15 g/h m²) and through-pore size distributions. The woven fabric showed a range of pore diameters of 6.5–114.4 μm , whereas the non-woven ranged from 0.3 to 6.2 μm , all pores smaller than the lower bound of the woven distribution. They demonstrated that a property such as water vapor transmission rate cannot be linked solely to a characteristic such as solid volume fraction but must also include pore size and fiber hydrophobicity. Researchers have created statistical models to predict qualities of comfort and protection based on basic physical properties of fabrics and challenge liquids (Lee and Obendorf, 2001, 2005).

Liquid properties such as surface tension and viscosity play an important role in penetration and may be more influential in penetration than chemical composition of the active ingredient. In commercially produced pesticide formulations, ingredients (adjuvants) are often added to alter the liquid properties of the solution and increase wettability in the target environment.

Non-woven fabrics

Models for performance of non-woven fabrics have been developed. The penetration of repellent finished fabrics is driven by one main property, surface tension difference between the fiber substrate and the challenge liquid ($\gamma_{\text{diff}} = \gamma_s - \gamma_L$), whereas that of untreated fabrics appears to be affected by various liquid/fabric properties (Lee and Obendorf, 2001). Repellent finished

fabrics with low surface energies function through a repellency mechanism regardless of the fiber type or fabric porosity. On the other hand, untreated fabrics go through repellency, wicking and absorbency processes that are affected by not only liquid–medium surface interaction but also other fabric/liquid parameters. For fabrics with a surface tension difference ($\gamma_s - \gamma_L$) below -13 mN/m, no penetration was observed for a series of non-woven fabrics; this may be an empirical diverging point determining penetration mechanisms of individual fabrics when no pressure is applied. When γ_s is very small, for instance, due to repellent finish, thus γ_{diff} is equal to or less than -13 mN/m, fabric performance is governed by repellency. The process is driven mainly by one factor, liquid–medium surface interaction (wetting and wicking). Thus, a model for pesticide penetration is as follows:

$$\text{if } \gamma_{\text{diff}} \leq -13 \text{ mN/m, } P = 0 \quad [19.10]$$

When γ_s is large, thus γ_{diff} is greater than -13 mN/m, fabric performance is governed by a combination of repellency, wicking and absorbency mechanisms, which are affected by various additional fabric/liquid parameters. For untreated (no fluorocarbon finish) materials, pesticide penetration increased with increased surface tension difference, decreased solid volume fraction, and decreased fabric thickness (Lee and Obendorf, 2001). An empirical model has been presented to predict pesticide penetration for untreated non-woven fabrics. The regression equation is:

$$P = 18 + 0.24 \gamma_{\text{diff}} - 30 \rho_b - 22 t - 0.010 (\gamma_{\text{diff}})^2 \quad [19.11]$$

where γ_{diff} is the surface tension difference; ρ_b is the solid volume fraction in equation [19.8]; t is the fabric thickness. Pesticide penetration increases as the difference in surface tension between fabric and pesticide mixture gets larger, whereas penetration increases with decreased solid volume fraction and fabric thickness.

For the relationship between fabric barrier performance and thermal comfort properties, research shows that, in general, a negative relationship exists between fabric protection performance and air permeability for untreated non-woven fabrics (Lee and Obendorf, 2001). A statistical model predicting air permeability based on fabric thickness and solid volume fraction was developed. The regression equation was:

$$\text{Air permeability} = 1370 - 9933 t + 4289 \rho_b + 14791 t^2 - 12771 \rho_b^2 \quad [19.12]$$

where t is the fabric thickness; ρ_b is the solid volume fraction. This could be useful in estimating thermal comfort based on simple measurements of

fabric parameters. An empirical model that related air permeability of fabric and fabric protection performance was presented:

$$\text{Air permeability} = 435 - 9 \text{ Protection} + 0.05 (\text{Protection})^2 \quad [19.13]$$

Woven fabrics

Modeling of liquid penetration through woven fabrics has used fabric cover factor, yarn twist factor and yarn packing factor as possible predictor variables, in an attempt to describe the complex capillary geometry of woven textiles with parameters that can easily be derived from basic fabric characteristics (Lee and Obendorf, 2005). Cover factor is a measure of fabric tightness and describes compactness of the weaving of a given yarn system, which could represent the relative magnitude of inter-yarn space of a given fabric. Cover factor was calculated from fabric counts and yarn diameters using the following equation:

$$C = ed_1 + pd_2 - epd_1d_2 \quad [19.14]$$

where C represents cover factor of the fabric; e is number of warp yarns over 1 in of fabric width; p is number of filling yarns over 1 in of fabric width; d_1 is diameter of the warp yarn (in); d_2 is diameter of the filling yarn (in).

Relative magnitude of inter-fiber space could be quantified by textile parameters such as yarn twist factor or yarn packing factor. Twist factor is a measure of 'twist hardness' of yarn and describes compactness in yarns of the same size. Twist factor was calculated using the following equation:

$$t_w = \frac{\text{tpi}}{\sqrt{N_e}} \quad [19.15]$$

where t_w represents twist factor of the yarn; tpi is the twist in turns per inch; N_e is yarn number in the cotton system. Average twist factors of warp and filling yarns for each specimen ranged from 2.53 to 5.30 (Lee and Obendorf, 2005).

Wicking height was measured for each combination of pesticide mixtures and woven fabrics to reflect the complex fabric-liquid interactions. Average wicking heights of warp and filling direction for each combination ranged from 0.2 to 8.8 cm (Lee and Obendorf, 2005).

Surface energy of the solid, γ_s , is a property that reflects the chemical nature of the solid surface, and such inherent fiber characteristics contribute to wetting and liquid transport properties. In this study, critical surface tension of fiber was used as a predictor variable to represent surface free energy of the solid (Lee and Obendorf, 2005).

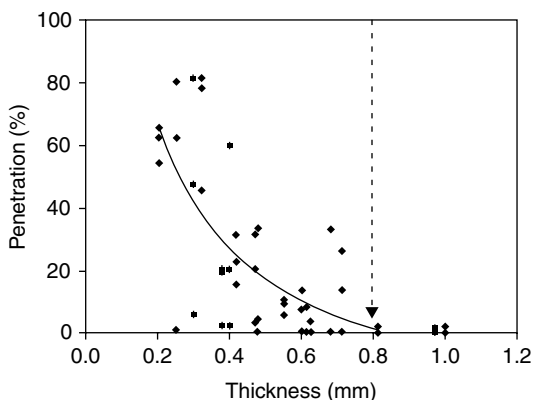
To develop a statistical model for pesticide penetration through woven fabrics, regression analyses were performed using those fabric/liquid parameters

(Lee and Obendorf, 2005). The final model selected to predict pesticide penetration through woven fabrics was a polynomial model with linear terms of cover factor, twist factor, critical surface tension of fiber, viscosity of pesticide mixture, and wicking, and quadratic terms of cover factor, twist factor, critical surface tension of fiber, and wicking:

$$P = 11 - 97C - 22t_w + 0.7\eta - 5\gamma_s - 4w + 874C^2 + 13t_w^2 - 0.6\gamma_s^2 + 1.5w^2 \quad [19.16]$$

where C is fabric cover factor; t_w is yarn twist factor; η is viscosity of pesticide mixture (mPa s); γ_s is critical surface tension of fiber (mN/m); w is wicking height (cm). Influence of surface tension of liquid, solid volume fraction, and yarn packing factor were shown to be insignificant at the 5% significance level for these experimental conditions. Fiber swelling from absorption of liquid or the complex interactions of fibers with liquid causes shifting of fibers and changes of the pore structure, which results in an increase in penetration with increased viscosity of the challenge liquid (Miller and Schwartz, 2001; Rajagopalan *et al.*, 2001).

Fabric thickness was one of the highly influential factors affecting liquid penetration of woven fabric as a singular parameter (Lee and Obendorf, 2005). Fabrics with thickness above 0.8 mm showed very little or no penetration regardless of other fabric/liquid parameters for the experimental conditions (see Fig. 19.3); therefore, fabric thickness as a single factor is a dominant factor in the penetration phenomenon of woven work clothing fabrics. However, further statistical modeling processing to find a model with multiple variables for a better fit revealed that influence of fabric thickness decreases once other fabric parameters are entered into the model, which indicates that fabric parameters are interrelated. Consequently, influence



19.3 Relationship between fabric thickness and pesticide penetration (Lee and Obendorf, 2005).

of fabric thickness was insignificant at the 5% significance level when other textile parameters are present, thus replaced by a combination of fabric cover factor and yarn twist factor in the final model.

Lee and Obendorf (2005) found cover factor and twist factor were better parameters in describing the geometry of woven fabrics than solid volume fraction. Pesticide penetration increases as fabric cover factor and yarn twist factor decrease.

Fabric air permeability is a characteristic closely related to comfort performance of fabric. To develop a statistical model predicting air permeability from basic textile parameters, regression analyses were performed using fabric thickness, fabric cover factor, yarn twist factor, yarn packing factor and solid volume fraction as independent variables (Lee and Obendorf, 2005). The final model selected to predict air permeability of fabric was a polynomial model with linear terms of fabric thickness, cover factor, twist factor, and packing factor, and quadratic terms of fabric thickness, cover factor, and packing factor:

$$\text{Air permeability} = 17 - 127C - 130t - 12t_w - 161\phi + 957C^2 + 229t^2 + 904\phi^2 \quad [19.17]$$

where C is fabric cover factor in equation [19.14]; t is fabric thickness (mm); t_w is yarn twist factor; ϕ is yarn packing factor. Yarn packing factor ϕ is the ratio of total fiber area to actual yarn area in the cross-section of a multifilament yarn:

$$\phi = \frac{4N_t}{\pi \cdot d^2 \rho \cdot S} \quad [19.18]$$

where ϕ represents packing factor of the yarn; d is diameter of the fiber (cm); ρ is density of the fiber (g/cm^3); N_t is linear density of the yarn (tex); S is the constant, 10^5 .

19.3 Development of novel pesticide-protective clothing

19.3.1 Enhanced repellency

A fabric that displays repellency has a critical surface tension that is lower than that of the liquid, creating a bead on the surface, which can roll off rather than penetrate the internal fabric structure. Finishes such as fluorocarbons are applied to fabric surfaces to lower the surface tension thus reducing wetting; these finishes reduce penetration for pesticide-protective clothing (Laughlin *et al.*, 1986). Nanotechnology is being used by the textile industry to upgrade chemical finishing. Electrospraying processes provide control of agglomeration of nanoparticles improving performance (Güneşoğlu *et al.*, 2010). Layer-by-layer

deposition has been used to self-assemble nanoparticles on the surfaces of fibers to develop functional textiles of protective clothing (Hyde *et al.*, 2005).

19.3.2 Enhanced sorption

Many textile structures have the ability to retain liquids and other chemicals via sorption providing protection by trapping a contaminant within a fibrous matrix limiting dermal contact. This is the mechanism of activated carbon used in military garments. Washable woven garments made from cotton often blended with other fibers such as polyester are popular garments for pesticide applicators, especially those working in hot environments; this traditional work clothing functions by sorption to reduce dermal pesticide exposure (Obendorf *et al.*, 2003; Welch and Obendorf, 1997). Many agricultural workers prefer traditional work clothing for its comfort, cost and availability (DeJonge *et al.*, 1985). Although the National Institute for Occupational Safety and Health (NIOSH, 2009) reports that work clothing such as long-sleeved shirts and long pants can provide 90% protection, dermal pesticide exposure even on a comparatively small scale can have dramatic health effects (Thongsinthusak and Frank, 2007). Therefore, there is a continued effort to develop specialized barriers or selective membranes to provide higher levels of protection.

Treatment of traditional non-barrier textiles with chemical finishes such as starch or carboxymethyl cellulose increase sorption properties while also decreasing transfer by rubbing and enhance removal of contaminants by laundering (Csiszár *et al.*, 1998; Obendorf *et al.*, 1991; Obendorf and Ko, 1997). Increased fabric thickness/weight can also be used to trap additional liquids within the fabric structure thus reducing penetration (see Fig. 19.3). Following this reasoning, layering of clothing materials has been shown to offer increased protection (Crossmore and Obendorf, 1992; Laughlin *et al.*, 1986).

Researchers have shown that textile treatments such as renewable starch finish or durable carboxymethylation of cotton increase the amount of pesticide adsorbed by the fabrics. Both treatments also are effective in enhancing the decontamination of cotton fabrics with laundering. The addition of enzymes such as amylase also improves decontamination (Csiszár *et al.*, 1998; Ko and Obendorf, 1997). Cyclodextrins are also used to enhance sorption of toxins on fibrous structures (Martel *et al.*, 2002).

19.3.3 Membranes

Microporous membranes

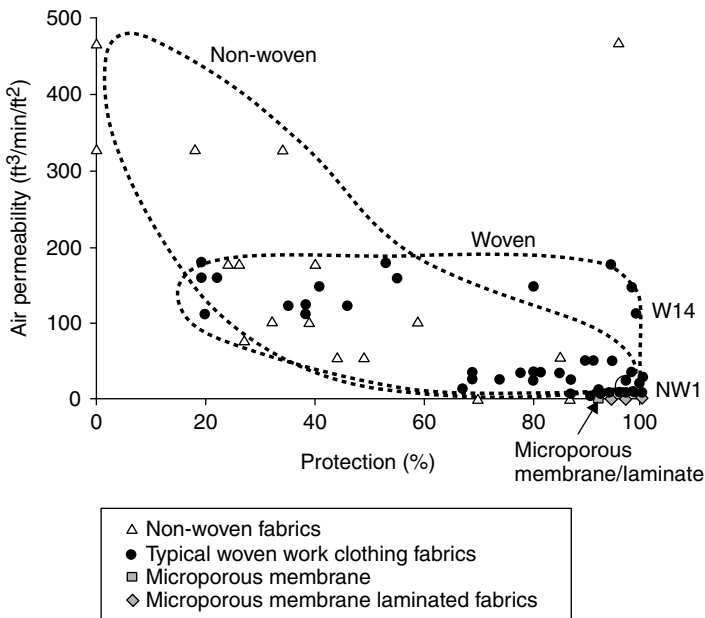
An approach to achieving a balance between chemical protection and comfort is to limit pore size. Microporous membranes that allow vapor penetration but prevent liquid penetration alleviate the thermal discomfort often associated with traditional barrier materials while maintaining a high degree of chemical protection (Shaw and Hill, 1990). When laminated to

conventional fabric structures, these materials were shown to have higher barrier properties than their unlaminated woven and non-woven counterparts, or the membrane alone (see Fig. 19.4) (Branson *et al.*, 1986; Lee and Obendorf, 2007a). Although microporous membranes and laminates have very low air permeability, their water vapor transmission rate was comparable to most non-wovens (Lee and Obendorf, 2007a). Pore size and pore size distribution are important parameters determining water vapor transport. Engineering the pore size can provide increased thermal comfort while maintaining high protection for liquid chemical penetration.

Selectivity (α) of a membrane or material can be defined as the ratio of water vapor permeability P_w to toxic agent permeability P_t :

$$\alpha = \frac{P_w}{P_t} \quad [19.16]$$

Although effective barriers to pesticide penetration for tasks with high risk of spilling or large volume contamination, full-body chemical suits of a barrier material limit water vapor transport causing heat stress and fatigue, unless a cooling device is included. Thus, they are often inappropriate for



19.4 Relationship between protection performance and air permeability for non-woven, woven, microporous membranes and laminates (Lee and Obendorf, 2007a). W14, a woven fabric, and NW1, a non-woven fabric that have similar protection and solid volume fraction but different air permeability and moisture vapor transport that was shown to be related to pore size and pore size distribution.

extended use outdoors at elevated temperatures. In Californian agriculture, full-body chemical resistant suits are not permitted at temperatures exceeding 30°C during the day (26°C night) (Thongsinthusak and Frank, 2007).

Selectively permeable membranes

Membranes that have selective permeability have been developed that are permeable to water vapor and impermeable to more hydrophobic chemical challenges. Perfluoro-sulfonic polymers (e.g. Nafion®) and sulfonated polyaryles (e.g. sulfonated polyetherketones) show characteristic hydrophilic/hydrophobic nano-separations, especially in the presence of water. While the hydrophobic domain provides morphological stability, the hydrated hydrophilic domain is responsible for the transport of water of hydration. Such polyelectrolyte membranes were evaluated by Rivin *et al.* (2004) for use as permselective diffusion barriers in protective fabrics giving insight into the complex interactions between solvent and polymers.

Membranes have also been developed by filling the pores of a porous substrate film with a polymer with different solubility (Yamaguchi *et al.*, 1991). Due to the solubility differences the membrane has selective permeability. The pores of a hydrophobic host membrane such as polypropylene can be filled with a polyelectrolyte that is hydrophilic while it retards permeation by organic compounds. This forms a polymer composite membrane with the cross-linked gel filling the nanopores of the host hydrophobic membrane. Such membranes have been developed using porous polypropylene and polyelectrolytes such as poly(acrylic acid), poly(methacrylic acid), poly(acrylamide) and poly (2-hydroxyethyl methacrylate) (Y. M. Lee *et al.*, 1989; Yamaguchi *et al.*, 1991; Yamaguchi *et al.*, 1994). Using this approach, highly selective nanocomposite membranes have been developed that exhibit high water-transport rate and low toxic agent transport rate for breathable protective clothing. H. Chen *et al.* (2006, 2007) have shown that membranes with oriented polyelectrolyte nanodomains exhibit enhanced transport properties useful in chemical protective materials.

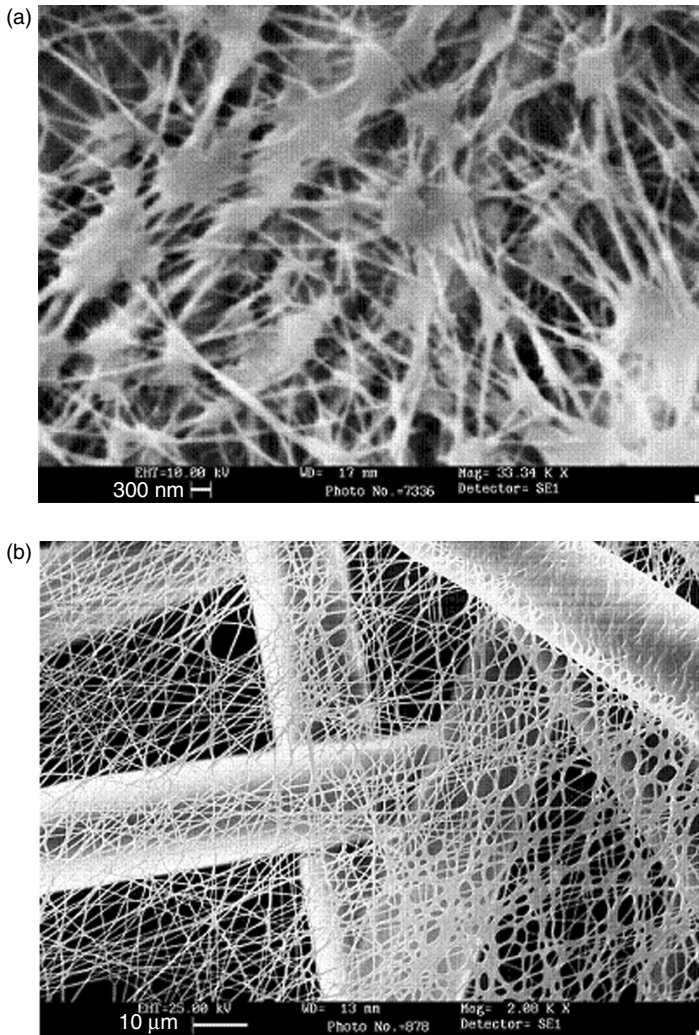
A selective membrane has been developed using a cross-linked lyotropic liquid crystal–butyl rubber composite membrane that appears to function by molecular size discrimination rather than differences in solubility (Lu *et al.*, 2008). This new membrane was evaluated for reduction in vapor transport of dimethyl methylphosphonate (DMMP); it is believed that the membrane has an effective pore size of around 0.57 nm due to the nanostructure of the composite material.

Nanofibrous membranes

Electrospun fiber webs and laminates have been developed to provide smaller pore size between fibers allowing enhanced protection while

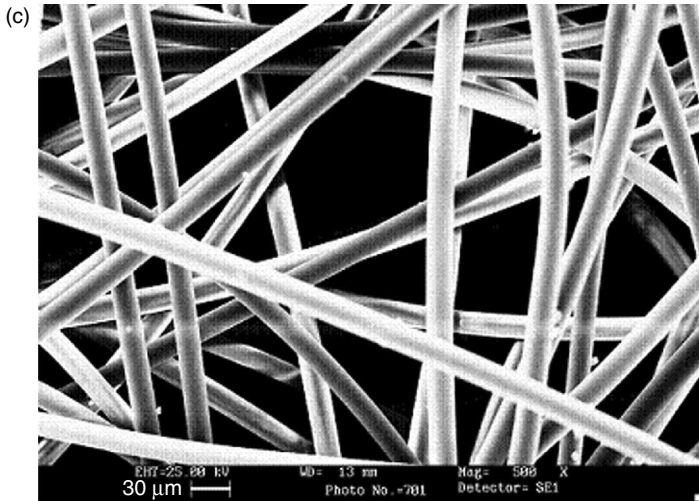
maintaining high water vapor transport (Lee and Obendorf, 2006, 2007c). Schreuder-Gibson *et al.* (2002) demonstrated the enhancement of aerosol protection using a fine layer of electrospun fibers that increased aerosol particle protection without significant change in the moisture vapor transport.

Electrospinning is an effective and promising technique for the production of fibers, with diameters from 40 to 5000 nm (Doshi and Reneker, 1995; Reneker



19.5 Comparison of SEM micrographs; (a) microporous membrane, (b) layered fabric system with electrospun polyurethane nanofiber web, and (c) spunbonded non-woven (Lee and Obendorf, 2007c).

Continued



19.5 Continued.

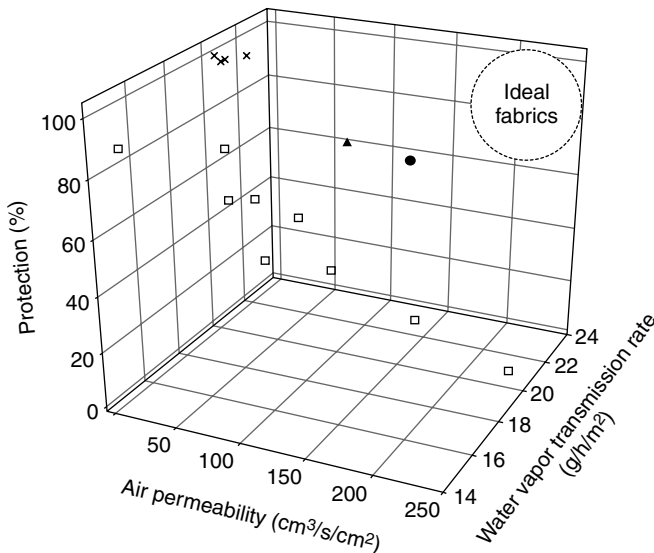
and Chun, 1996). Nanofibers have great potential for application in filtration, membrane and protective clothing applications due to the large surface area and the small inter-fiber pore sizes (Lee and Obendorf, 2007b, 2007c).

Layered structures with electrospun nanofiber web gave protection performance lower than microporous materials but higher than most non-wovens (see Fig. 19.5). Air permeability of layered fabric systems was higher than microporous materials and many conventional non-wovens used for PPE. For moisture vapor transport, layered fabric systems gave a similar range as conventional non-wovens (see Fig. 19.6) (Lee and Obendorf, 2007c).

19.3.4 Multifunctional materials with self-decontaminating properties

Pesticides may contaminate clothing and skin directly during application in the field or by indirect contact with contaminated surfaces. Elevated temperatures with perspiration and other dermal secretions increase the potential for transfer of pesticides to clothing and skin (Nelson *et al.*, 1993). Pesticides adsorbed on clothing can be transferred with friction (Obendorf *et al.*, 1994). This is a critical factor when donning and doffing a contaminated garment since toxic chemicals may be transferred to people and their immediate environment. Studies of pesticide residues in homes confirm accumulation on surfaces especially on carpets with large fiber surface areas. Residues found as settled dust confirm that chemicals may be redistributed within a household (Obendorf *et al.*, 2006).

Decontamination is the removal of chemicals from exposed clothing systems. For protective clothing worn by operators applying pesticides, this is



19.6 Air permeability, water vapor transmission rate and protection performance against pesticide mixture (Prowl® 3.3 EC) of layered fabric systems with electrospun nanofiber web compared with existing PPE materials; (●) layered fabric system with $1.0 \text{ g}/\text{m}^2$ web area density, (▲) layered fabric system with $2.0 \text{ g}/\text{m}^2$ web area density, (x) microporous membrane and laminated fabrics, (□) non-woven fabrics (Lee and Obendorf, 2007c).

most often accomplished by laundering (Laughlin, 1993). Removal of pesticide soils is a complex system involving material, chemical and structural factors. Formulation, active ingredients and concentration of pesticides, fiber type and washing conditions impact effectiveness. Pesticides from contaminated protective clothing have been found distributed on the surfaces of both cotton and polyester, as well as inside the cotton lumen (Obendorf and Solbrig, 1986). One laundering cycle removed most of the surface residue for the fiber surfaces of cotton and polyester (McQueen *et al.*, 2000). Even properly used, garments may still contaminate the wearer during doffing. Thus, it may be useful to employ textile treatments that reduce the toxicity of contaminants through oxidation or destructive adsorption. These self-decontaminating properties could reduce the toxicity of chemicals even before the laundering process.

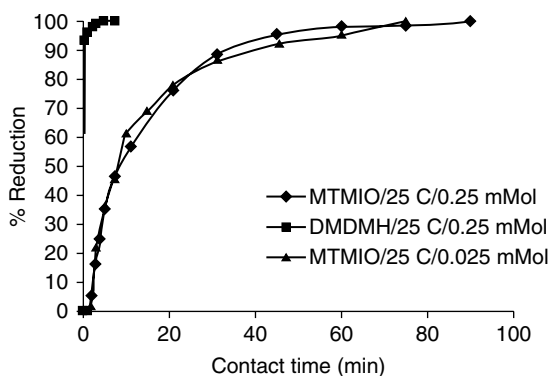
Self-decontaminating fabric treatments, which decompose pesticides on contact may provide enhanced dermal protection as well as limit garment mediated contamination. Materials with self-decontaminating treatments are a promising approach to comfortable yet protective clothing systems. This class of materials incorporates compounds with detoxifying properties

(such as oxidation) onto protective textiles. By converting pesticides to potentially less harmful forms on contact, the efficacy of porous materials for limiting dermal pesticide contamination may be enhanced.

N-halamines

Organic polymeric compounds with oxidative properties are promising candidates for detoxifying pesticides on protective clothing. *N*-halamine compounds, which derive their efficacy from disassociation of chloramines bonds (N-Cl) have demonstrated the ability to oxidize commonly used carbamate pesticides which contain sulfur bonds such as aldicarb and methomyl (Fei *et al.*, 2006). Researchers have demonstrated their ability to convert alcohols to ketones, sulfides to sulfoxides and sulfones, and cyanides to carbon dioxide and water (Sun and Xu, 1998). These materials also have biocidal properties (Qian and Sun, 2005). *N*-halamine polymers can be grafted onto polyester/cotton and exhibit durable and rechargeable properties when reactivated with a chlorine treatment (Ko *et al.*, 2000; Sun and Xu, 1998; Sun and Sun, 2001).

Three forms of chloramine bonds are imide, amide and amine halamines. The bond stability was found to be inversely related to reaction rate with aldicarb (imide halamine > amide halamine > amine halamine) (Fei *et al.*, 2006) as well as biocidal properties (Qian and Sun, 2005). The imide bond which is found in 1,3 dimethylol-5,5-dimethylhydantoin (DMDMH) dissociates readily and reacts the fastest with aldicarb compared to the amide and amine bond types. Researchers have shown the decrease in aldicarb concentration with exposure to *N*-halamines and the oxidation of the thio bond to sulfoxide ($-\text{SO}-$) and later sulfone ($-\text{SO}_2$) (see Fig. 19.7). Researchers



19.7 Degradation of aldicarb by DMDMH- and MTMIO-treated fabrics (5 g of fabrics in 20 mL of 0.25 mMol and 0.025 mMol aldicarb at 25°C) (Fei *et al.*, 2006).

have developed both imide and amide N-halamine treatments for fabrics; DMDMH contains predominantly imide bonds, whereas the 3-methylol 2,2,5,5-tetramethyl imidozalidin 4-one (MTMIO) treated fabrics contain amine halamine structures. The imide halamines, though more reactive, are significantly less durable than the amines with repeated laundering.

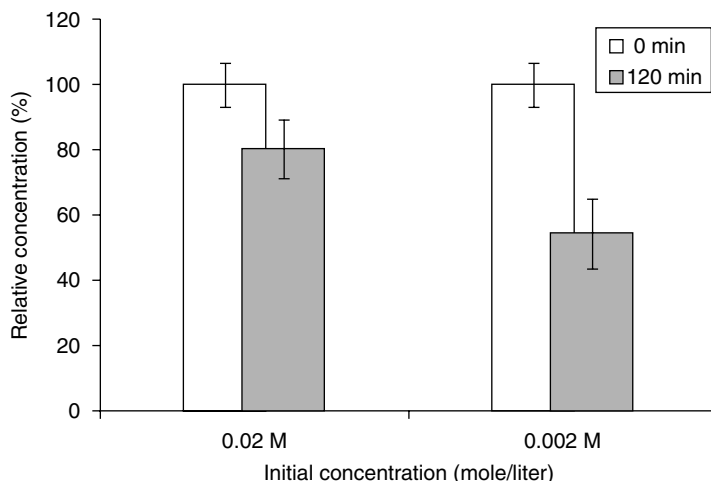
Bleaching reactivates all three types of N-halamines. A mixture of highly reactive imide and stable amine compounds may provide the desired properties of both compounds. It is possible that the amine halamines may be able to recharge the imide halamines on the fabric surface (Qian and Sun, 2005).

Self-decontamination of polyacrylonitrile (PAN) electrospun fibers has been achieved using surface oximation (L. Chen *et al.*, 2009). Using excess hydroxylamine, the PAN fibers were functionalized by forming polyacrylamidoxime (PAAO). In the presence of water, these nucleophilic amidoxime groups hydrolyze organophosphate pesticides. Thus, these functionalized fibers are possible candidates for use in self-detoxifying fabrics.

Metal oxides

Photocatalytic oxidation is one of the most effective ways to decompose alkenes and other volatile organic compounds. Titanium dioxide, TiO_2 , is a well known metal oxide with photocatalytic properties; it has been incorporated into non-woven filtration fabrics to aid in degradation of volatile organic compounds (Park *et al.*, 2006). In this system, the metal oxides act as a photocatalyst in the presence of UV light. TiO_2 has been incorporated in both textile fibers and finishes. Cotton fabrics that were treated with aqueous TiO_2 in a silicone finishing solution aided in the decomposition of gaseous ammonia (Dong *et al.*, 2006), and electrospun PAN fibers containing TiO_2 nanoparticles degrade aldicarb (Woo and Obendorf, 2010; see Fig. 19.8). Titanium dioxide has been proven to degrade mixed pesticides including methyl parathion (Senthilnathan and Philip, 2009). In the outdoor environment, with the combination of elevated temperatures during the summer growing season, direct sunlight and moisture, these self-decontaminating properties of textiles may be effective in increasing personal protection.

Nanocrystalline materials exhibit a wide array of unusual properties; one of these unusual features is enhanced surface chemical reactivity toward incoming adsorbates (Li and Klabunde, 1991). Nanocrystalline MgO , CaO and Al_2O_3 adsorb polar organics such as aldehydes and ketones in very high capacities (Khaleel *et al.*, 1999). The chemical reactivity of adsorbates on the nanoparticles has been shown to follow a two-step decomposition mechanism. The first step is adsorption of the toxic agent on the surface by means of physisorption, and the second step is chemical decomposition. This two-step mechanism substantially enhances the detoxification abilities of the nanoparticles.



19.8 Degradation of aldicarb solution with reaction time in the presence of UV and TiO₂ nanofiber (Woo and Obendorf, 2010).

Magnesium oxide in nanocrystalline form (particle size ≤ 8 nm, aggregate size $3.3 \mu\text{m}$) has a large reactive surface area due to polyhedral shapes and high proportion of corner/edge sites compared to typical polycrystalline material (Klabunde *et al.*, 1996). The surface morphology of the MgO structure is very important; higher numbers of defects and corners of small nanoparticles provide high surface reactivity (Klabunde *et al.*, 1996). High surface area combined with high surface reactivity gives these materials great potential for use in decontamination of toxic substances by dissociative chemisorptions termed 'destructive adsorption'.

Nanoparticles of metal oxides such as MgO exhibit unique properties that are related to particle size (Koper *et al.*, 1993; Klabunde *et al.*, 1996). Particle sizes are dependent on the formation methods. Chemists reported several methods for the preparation of metal oxides. The most popular one is a conventional preparation using boiling water and vacuuming treatments (CP), and the other is an aerogel method using hydrolysis and thermal treatments with autoclaving (AP). The unique characteristics between the particles made by the two methods are their surface area and crystal size. Aerogel-prepared (AP) nanoparticles have larger surface area and smaller crystals compared with conventional prepared (CP) ones; for example, CP-MgO has $150 \text{ m}^2/\text{g}$ of surface area and 8 nm of crystal size and AP-MgO has $400 \text{ m}^2/\text{g}$ and 4 nm (Rajagopalan *et al.*, 2002).

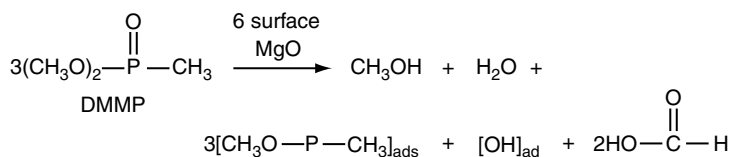
Metal oxides have been shown to degrade various organic compounds including paraoxon and other pesticides (Klabunde *et al.*, 1996; Li and Klabunde, 1991; Rajagopalan *et al.*, 2002), and military agents such as GD, VX and HD (Decker and Klabunde, 1996; Rajagopalan *et al.*, 2002; Wagner

et al., 2000, 2001). Nanocrystalline MgO reacts faster and in higher capacity than activated carbon, a commonly used material for chemical and military protective clothing (Khaleel *et al.*, 1999; Rajagopalan *et al.*, 2002).

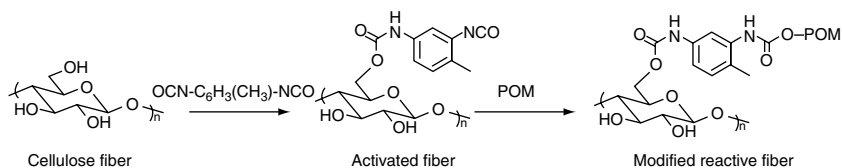
Magnesium oxide (MgO) has been shown to degrade organophosphate including DMMP a chemical agent stimulant (Li and Klabunde, 1991) and paraoxon (Rajagopalan *et al.*, 2002) through a surface stoichiometric process rather than catalytic. It is believed to cleave the P–S bond or P–O bond of organophosphates. The mechanism involves –OH groups that are bound to the Mg metal on the surface of the MgO structure. First of all, oxygen from the MgO matrix attaches to the phosphorous of the DMMP. Surface –OH group results in methanol being released from the reaction. Methanol dissociates on the surface, and the adsorbed CH₃O group is oxidized by DMMP thus releasing formic acid as the main volatile product. About two surface MgO moieties are used in the decomposition of one DMMP molecule. Water, formic acid, methanol, adsorbed –OH and the remaining portion of the DMMP molecule containing phosphorous adsorbed onto the surface of the MgO are the products of the degradation reaction (see Fig. 19.9). The water formed could possibly dissociate to provide more surface –OH groups to promote further reactions. It is believed that the presence of small amounts of water is beneficial for the decontamination process. The non-volatile product is immobilized on the MgO surface bound by two bridging oxygen atoms with the empirical formula of C₂H₆PO₃MgO. This mechanism indicates that the MgO surface moieties then will be blocked from further participation in the reaction.

Polyoxometalates

Polyoxometalates (POM) are negatively charged metalate anions in the form of nanoclusters. They consist of transition metal ions bonded to other ligands, generally oxygen atoms (Hill and Prosser-McCarthy, 1995; Müller and Roy, 2003). POM are in their highest oxidation state with the general formula XM₁₂O₄₀^{x–8} where X is Si⁴⁺, P⁵⁺, etc. and M can be tungsten, molybdenum and vanadium, etc. These transition metal–oxygen cluster complexes are relevant because of their oxidation-reduction chemistry and their relevance as environmentally benign catalysis. They have been known and used



19.9 Overall balanced reaction of DMMP with surface MgO. The products of this reaction are methanol, water, non-volatile product, adsorbed –OH group, and two formic acid molecules (Li and Klabunde, 1991).



19.10 Cross-linking POM to cellulose.

in the chemistry laboratories for nearly 200 years, but with the advances in materials science and nanotechnology, POM are beginning to be considered as unique chemical species that could turn from very special molecules to very useful materials. With sizes just one order of magnitude smaller than the smallest of living biological structures such as the *Rhinovirus*, i.e. ~ 20 nm, POMs are not colloids but soluble polynuclear species. They have structural and topological features in common with transition metal oxides and have similar reduction-oxidation reaction, electron transfer and ion transport behavior. In all these respects, POM can be generically considered as the perfect models for quantum-sized transition metal oxide nanoparticles. POMs are inexpensive, easy to synthesize, non-toxic, have catalytic nature, and can be incorporated on fabrics.

The Keggin-type POM $\text{H}_5\text{PV}_2\text{Mo}_{10}\text{O}_{40}$ has been deposited on cotton, polyacrylic and nylon fabrics (Xu *et al.*, 2000). Acting as a redox-based, radical chain initiator, they catalyzed O_2 -based oxidation (aerobic) of representative air toxins, acetaldehyde and 1-propanethiol. These fabrics offer self-deodorizing and self-decontamination properties. POM can be cross-linked to cellulose thus to cotton fibers (see Fig. 19.10).

Nanohybrid membranes based on POM $\text{H}_5\text{PV}_2\text{Mo}_{10}\text{O}_{40}$ and a poly(vinyl alcohol)/polyethyleneimine (PVA/PEI) blend have been prepared as a chemical and biological protective, permeable membrane material (Wu *et al.*, 2009). $\text{H}_5\text{PV}_2\text{Mo}_{10}\text{O}_{40}$ nanoparticles were incorporated on electrospun fibrous materials using toluene diisocyanate as a cross-linker. Oxidation of 2-chloroethyl-ethyl sulfide (CEES) was observed with the significant color change from orange to blue. In addition to oxidation of CEES, these membranes exhibited antibacterial properties against both gram-negative and gram-positive bacteria.

19.4 References

- ABOU-DONIA, M. B. (1994) Organophosphorus pesticides. *In*: Chang, L. W. and Dyer, R. S. (eds.) *Handbook of Neurotoxicology*. New York: Marcel Dekker, pp. 419–473.
- ASTM INTERNATIONAL (2009) ASTM F2669–09 Performance specification for protective clothing worn by operators applying pesticides. *ASTM Book of Standards*, Volume 11.03, ASTM International, West Conshohocken, PA. Available at: <http://www.astm.org/Standards/F2669.htm> [accessed 15 July 2008].

- BRANSON, D., AYERS, G. S. and HENRY, M. S. (1986) Effectiveness of selected work fabrics as barriers to pesticide penetration. In: Barker, R. L. and Colletta, G. C. (eds.) *Performance of Protective Clothing*, ASTM STP 900. Philadelphia, PA: American Society for Testing and Materials, pp. 114–120.
- CENTERS FOR DISEASE CONTROL AND PREVENTION (CDC) (2005) Worker fact sheet: pesticide safety guidance for mixers, loaders, and applicators. Available from: <http://www.cdc.gov/> [Accessed 15 July 2008].
- CHATTERJEE, P. K. (1985) *Absorbency*. New York: Elsevier.
- CHEN, H., PALMESE, G. R. and ELABD, Y. A. (2006) Membranes with oriented polyelectrolyte nanodomains. *Chemical Materials*, 18: 4875–4881.
- CHEN, H., PALMESE, G. R. and ELABD, Y. A. (2007) Electrosensitive permeability of membranes with oriented polyelectrolyte nanodomains. *Macromolecules*, 40: 781–782.
- CHEN, L., BROMBERG, L., SCHREUDER-GIBSON, H., WALKER, J., HATTON, T. A. and RUTLEDGE, G. C. (2009) Chemical protective fabrics via surface oxidation of electrospun polyacrylonitrile fiber mats. *Journal of Materials Chemistry*, 19: 2432–2438.
- COFFMAN, C. W., OBENDORF, S. K. and DERKSEN, R. C. (1999) Pesticide deposition on coveralls during vineyard applications. *Archives of Environmental Contamination and Toxicology*, 37: 273–279.
- CROSSMORE, D. G. and OBENDORF, S. K. (1992) Pesticide protection through layered clothing systems. In: McBriarty, J. P. and Henry, N. W. (eds.) *Performance of Protective Clothing: Fourth Volume*, ASTM STP 1133. Philadelphia: American Society for Testing and Materials, pp. 210–220.
- CSISZÁR, E., BORSA, J., RACZ, I. and OBENDORF, S. K. (1998) Reduction in human exposure to pesticide using traditional work clothing fabrics with chemical finishing: carboxymethylation and starch. *Archives of Environmental Contamination and Toxicology*, 35: 129–134.
- DECKER, S. and KLABUNDE, K. J. (1996) Enhancing effect of Fe_2O_3 on the ability of nanocrystalline calcium oxide to adsorb SO_2 . *Journal of the American Chemical Society*, 118: 12465–12466.
- DEJONGE, J. O., AYERS, G. and BRANSON, D. H. (1985) Pesticide deposition patterns on garments during air-blast spraying. *Home Economics Research Journal*, 14: 262–268.
- DONG, Y., BAI, Z., ZHANG, L., LIU, R. and ZHU, T. (2006) Finishing of cotton fabrics with aqueous nano-titanium dioxide dispersion and the decomposition of gaseous ammonia by ultraviolet irradiation. *Journal of Applied Polymer Science*, 99: 286–291.
- DOSHI, J. and RENEKER, D. H. (1995) Electrospinning process and applications of electrospun fibers. *Journal of Electrostatics*, 35: 151–160.
- EVANS, K. M. and HARDY, J. K. (2004) Predicting solubility and permeation properties of organic solvents in Viton glove material using Hansen's solubility parameters. *Journal of Applied Polymer Science*, 93: 2688–2698.
- EVANS, K. M., GUO, W. and HARDY, J. (2008) Modeling solubility parameters and permeation data of organic solvents versus butyl gloves from four manufacturers. *Journal of Applied Polymer Science*, 109: 3867–3877.
- FEL, X., GAO, P., SHIBAMOTO, T. and SUN, G. (2006) Pesticide detoxifying functions of N-halamine fabrics. *Archives of Environmental Contamination and Toxicology*, 51: 509–514.
- GARCIA, S. J., ABU-QARE, A. W., MEEKER-O'CONNELL, W. A., BORTON, A. J. and ABOU-DONIA, M. B. (2003) Methyl parathion: a review of health effects. *Journal of Toxicology and Environmental Health B*, 6: 185–210.

- GOYDAN, R., SCHWARTZ, A. D., REID, R. C., KRISHNAMURTHY, S. and WONG, K. (1988) Approaches to predicting the cumulative permeation of chemicals through protective clothing polymers. In: Mansdorf, S. Z., Sager, R. and Neilsen, A. P. (eds.) *Performance of protective clothing*, ASTM STP 989. Philadelphia, PA: American Society for Testing and Materials, pp. 257–268.
- GÜNEŞOĞLU, C., KUT, D. and ORHAN, M. (2010) Performing the electrospraying process for the application of textile nano finishing particles. *Textile Research Journal*, 80: 106–115.
- HILL, C. L. and PROSSER-MCCARTH, C. M. (1995) Homogeneous catalysis by transition metal oxygen anion clusters. *Coordination Chemistry Reviews*, 143: 407–455.
- HSIEH, Y. (1995) Liquid transport in fabric structures. *Textile Research Journal*, 65: 299–307.
- HYDE, K., RUSA, M. and HINESTROZA, J. (2005) Layer-by-layer deposition of polyelectrolyte nanolayers on natural fibres: cotton. *Nanotechnology*, 16: S422–S428.
- KAMEL, F. and HOPPIN, J. (2004) Association of pesticide exposure with neurologic dysfunction and disease. *Environmental Health Perspectives*, 112: 950–958.
- KHALEEL, A., KAPOORA, P. N. and KLABUNDE, K. J. (1999) Nanocrystalline metal oxides as new adsorbents for air purification. *Nanostructured Materials*, 11: 459–468.
- KISSA, E. (1996) Wetting and wicking. *Textile Research Journal*, 66: 660–668.
- KLABUNDE, K. J., STARK, J., KOPER, O., MOHS, C., PARK, D. G., DECKER, S., JIANG, Y., LAGADIC, I. and ZHANG, D. (1996) Nanocrystals as stoichiometric reagents with unique surface chemistry. *Journal of Physical Chemistry*, 100: 12142–12153.
- KO, L. L. and OBENDORF, S. K. (1997) Effect of starch on reducing the retention of methyl parathion by cotton and polyester fabrics in agricultural protective clothing. *Journal of Environmental Science and Health B*, B32: 283–294.
- KO, L. L., SHIBAMOTO, T. and SUN, G. (2000) A novel detoxifying pesticide protective clothing for agricultural workers. *Textile Chemist and Colorist and American Dye-stuff Reporter*, 32 (2):34–38.
- KOPER, O., LI, Y.-W. and KLABUNDE, K. J. (1993) Destructive adsorption of chlorinated hydrocarbons on ultrafine (nanoscale) particles of calcium oxide. *Chemical Materials*, 5: 500–505.
- LAUGHLIN, J. M. (1993) Decontaminating pesticide protective clothing. *Reviews of Environmental Contamination and Toxicology*, 130: 79–94.
- LAUGHLIN, J. M., EASLEY, C. B., GOLD, R. E. and HILL, R. M. (1986) Fabric parameters and pesticide characteristics that impact on dermal exposure of applicators. In: Barker, R. L. and Colletta, G. C. (eds.) *Performance of Protective Clothing*, ASTM STP 900. Philadelphia: American Society for Testing and Materials, pp. 136–150.
- LEE, S. and OBENDORF, S. K. (2001) A statistical model to predict penetration through nonwoven chemical protective fabrics. *Textile Research Journal*, 71: 1000–1009.
- LEE, S. and OBENDORF, S. K. (2005) Statistical model of pesticide penetration through woven work clothing fabrics. *Archives of Environmental Contamination and Toxicology*, 49: 266–273.
- LEE, S. and OBENDORF, S. K. (2006) Developing protective textile materials as barriers to liquid penetration using melt-spinning. *Journal of Applied Polymer Science*, 102: 3430–3437.
- LEE, S. and OBENDORF, S. K. (2007a) Barrier effectiveness and thermal comfort of protective clothing materials. *Journal of the Textile Institute*, 98: 87–97.
- LEE, S. and OBENDORF, S. K. (2007b) Use of electrospun nanofiber web for protective textile materials as barriers to liquid Penetration. *Textile Research Journal*, 77: 696–702.

- LEE, S. and OBENDORF, S. K. (2007c) Transport properties of layered fabric systems based on electrospun nanofibers. *Fibers and Polymers*, 8: 501–506.
- LEE, Y. M., BOURGEOIS, D. and BELFORT, G. (1989) Sorption, diffusion, and pervaporation of organics in polymer membranes. *Journal of Membrane Science*, 44: 161–181.
- LEVIN, H. S. and RODNITZKY, R. L. (1976) Behavioral effects of organophosphate pesticides in man. *Clinical Toxicology*, 9: 391–405.
- LI, Y.-X. and KLABUNDE, K. J. (1991) Nanoscale metal oxide particles as chemical reagents. Destructive adsorption of a chemical agent stimulant, dimethyl methylphosphonate, on heat-treated magnesium oxide. *Langmuir*, 7: 1388–1393.
- LU, X., NGUYEN, V., ZENG, X., ELLIOTT, B. J. and GIN, D. L. (2008) Selective rejection of a water-soluble nerve agent stimulant using a nanoporous lyotropic liquid crystal–butyl rubber vapor barrier material: evidence for a molecular size-discrimination mechanism. *Journal of Membrane Science*, 318: 397–404.
- MARTEL, B., THUAUT, P. L., BERTINI, S., CRINI, G., BACQUET, M., TORRI, G. and MORCELLET, M. (2002) Grafting of cyclodextrins onto polypropylene nonwoven fabrics for the manufacture of reactive filters. III. Study of the sorption properties. *Journal of Applied Polymer Science*, 85: 1771–1778.
- MCQUEEN, R. H., LAING, R. M., NIVEN, B. E. and WEBSTER, J. (2000) Revising the definition of satisfactory performance for chemical protection for agricultural workers. In: Nelson, C. N. and Henry, N. W. (eds.) *Performance of Protective Clothing: Issues and Priorities for the 21st Century: Seventh Volume*, ASTM STP 1386. West Conshohocken, PA: American Society for Testing Materials, pp. 102–116.
- MILLER, A. and SCHWARTZ, P. (2001) Forced flow percolation for modeling of liquid penetration of barrier materials. *Journal of the Textile Institute*, 92: 53–62.
- MILLER, B. (1977) The wetting of fibers. In: Schick M. J. (ed.) *Surface Characteristics of Fibers and Textiles, Part II*. New York: Marcel Dekker, pp. 417–445.
- MILLER, B. and TYOMKIN, I. (1994) Liquid wetting, transport, and retention properties of fibrous assemblies. *Textile Research Journal*, 64: 55–57.
- MÜLLER, A. and ROY, S. (2003) En route from the mystery of molybdenum blue via related manipulatable building blocks to aspects of materials science. *Coordination Chemistry Reviews*, 245: 153–166.
- NATIONAL INSTITUTE FOR OCCUPATIONAL SAFETY AND HEALTH NIOSH (2009) Pesticide illness and injury surveillance. Available from: <http://www.cdc.gov/niosh/topics/pesticides/> [Accessed 10 August 2009].
- NELSON, C., BRAATEN, A. and FLEEKER, J. (1993) The effect of synthetic dermal secretion on transfer and dissipation of the insecticide aldicarb from granular formulation to fabric. *Archives of Environmental Contamination and Toxicology*, 24: 513–516.
- NIGG, H. N., STAMPER, J. H., EASTER, E. P., MAHON, W. D. and DEJONGE, J. O. (1990) Protection afforded citrus pesticide applicators by coveralls. *Archives of Environmental Contamination and Toxicology*, 19: 635–639.
- OBENDORF, S. K. and SOLBRIG, C. M. (1986) Distribution of malathion and methyl parathion on unfinished and durable-press cotton/polyester fabrics before and after laundering as determined by electron microscopy. In: Barker, R. L. and Colletta, G. C. (eds.) *Performance of Protective Clothing* ASTM-STP 900, Philadelphia, PA: American Society for Testing Materials, pp. 187–204.
- OBENDORF, S. K., KASUNICK, R. S., RAVICHANDRAN, V., BORSA, J. and COFFMAN, C. W. (1991) Starch as a renewable finish to improve the pesticide-protective properties of

- conventional workclothes. *Archives of Environmental Contamination and Toxicology*, 21: 10–16.
- OBENDORF, S. K., LEMLEY, A. T., HEDGE, A., KLINE, A. A., TAN, K. and DOKUCHAYEVA, T. (2006) Distribution of pesticide residue within homes in central New York state. *Archives of Environmental Contamination and Toxicology*, 50: 31–44.
- OBENDORF, S. K., LOVE, A. M. and KNOX, T. (1994) Use of a crocking test method to measure the transfer of pesticide from contaminated clothing. *Clothing and Textiles Research Journal*, 12(2): 1–5.
- OBENDORF, S. K., CSISZÁR, E., MANEEFUANGFOO, D. and BORSA, J. (2003) Kinetic study of transport of pesticide from contaminated fabric through a model skin. *Archives of Environmental Contamination and Toxicology*, 45: 283–288.
- OBENDORF, S. K. and KO, L. L. (1997) Effect of starch on reducing the retention of methyl parathion by cotton and polyester fabrics in agricultural protective clothing. *Journal of Environmental Science and Health B*, 32: 283–294.
- PARK, O. H., KIM, C. S. and CHO, H. H. (2006) Development of a photoreactive fabric filter for simultaneous removal of VOCs and fine particles. *Korean Journal of Chemical Engineering*, 23: 194–198.
- QIAN, L. and SUN, G. (2005) Durable and regenerable antimicrobial textiles: chlorine transfer among halamine structures. *Industrial and Engineering Chemical Research*, 44: 852–856.
- RAHEEL, M. (1994) *Protective Clothing Systems and Materials*. New York: Marcel Dekker.
- RIVIN, D., MEERMEIER, G., SCHNEIDER, N. S., VISHNYAKOV, A. and NEIMARK, A. V. (2004) Simultaneous transport of water and organic molecules through polyelectrolyte membranes. *Journal of Physical Chemistry B*, 108: 8900–8909.
- RAJAGOPALAN, D., ANEJA, A. P. and MARCHAL, J. (2001) Modeling capillary flow in complex geometries. *Textile Research Journal*, 71: 813–821.
- RAJAGOPALAN, S., KOPER, O., DECKER, S. and KLABUNDE, K. J. (2002) Nanocrystalline metal oxides as destructive adsorbents for organophosphorus compounds at ambient temperatures. *Chemistry*, 8: 2602–2607.
- RENEKER, D. H. and CHUN, I. (1996) Nanometre diameter fibres of polymer, produced by electrospinning. *Nanotechnology*, 7: 216–223.
- SCHREUDER-GIBSON, H., GIBSON, P., SENEAL, K., SENNETT, M., WALKER, J., YEOMANS, W., ZIEGLER, D. and TSAI, P. P. (2002) Protective textile materials based on electrospun nanofiber. *Journal of Advanced Materials*, 34: 44–55.
- SCHWOPE, A. D. (1986) Permeation of chemicals through the skin. In: Barker, R. L. and Colletta, G. C. (eds.) *Performance of Protective Clothing*, ASTM STP 900. Philadelphia: American Society for Testing and Materials, pp. 221–234.
- SCHWOPE, A. D., GOYDAN, R., EHNTOLT, D. J., FRANK, U. and NIELSEN, A. P. (1992) Resistance of glove materials to permeation by agricultural pesticides. *American Industrial Hygiene Association Journal*, 53: 352–361.
- SENTHILNATHAN, J. and PHILIP, L. (2009) Removal of mixed pesticides from drinking water system by photodegradation using suspended and immobilized TiO₂. *Journal of Environmental Science and Health B*, 44: 262–270.
- SHAW, A. and HILL, K. R. (1990) Variability in sorption of diazinon through microporous fabrics. *Bulletin of Environmental Contamination and Toxicology*, 45: 500–506.
- SUN, Y. Y. and SUN, G. (2001) Novel regenerable N-halamine polymeric biocides. I. Synthesis, characterization, and antibacterial activity of hydantoin containing polymers. *Journal of Applied Polymer Science*, 80: 2460–2467.

- SUN, G. and XU, X. (1998) Durable and regenerable antibacterial finishing of fabrics: biocidal properties. *Textile Chemist and Colorist*, 30(6): 26–30.
- TAFURI, J. and ROBERTS, J. (1987) Organophosphate poisoning. *Annals of Emergency Medicine*, 16: 193–202.
- THONGSINTHUSAK, T. and FRANK, J. P. (2007) Developing pesticide exposure mitigation strategies. In: Krieger, R., Seiber, J. and Ragsdale, N. (eds.) *Assessing Exposures and Reducing Risks to People from the Use of Pesticides*. Washington, DC: American Chemical Society, pp. 98–110.
- TOMLIN, C. D. S. (1997) *The Pesticide Manual*, 11th edn. Surrey, UK: British Crop Protection Council.
- TRIPP, J. M., KARTONO, F. and MAIBACH, H. I. (2007) Percutaneous penetration of pesticides: clinical ramifications. In: Krieger, A. R., Seiber, J. and Ragsdale, N. (eds.) *Assessing Exposures and Reducing Risks to People from the Use of Pesticides*. Washington DC: American Chemical Society.
- WAGNER, G. W., KOPER, O. B., LUCAS, E., DECKER, S. and KLABUNDE, K. J. (2000) Reactions of VX, GD, and HD with nanosize CaO: autocatalytic dehydrohalogenation of HD. *Journal of Physical Chemistry B*, 104: 5118–5123.
- WAGNER, G. W., PROCELL, L. R., O'CONNOR, R. J., MUNAVALLI, S., CARNES, C. L., KAPOOR, P. N. and KLABUNDE, K. J. (2001) Reactions of VX, GB, and HD with nanosize Al_2O_3 : formation of aluminophosphonates. *Journal of the American Chemical Society*, 123: 1636–1644.
- WELCH, L. and OBENDORF, S. K. (1997) Limiting dermal exposure of workers to pesticides from contaminated clothing. In: Stull, J. O. and Schwoppe, A. D. (eds.) *Performance of Protective Clothing: Sixth volume*, ASTM STP 1273. West Conshohocken, PA: American Society for Testing Materials, pp. 158–165.
- WOO, D. J. and OBENDORF, S. K. (2010) Unpublished data.
- WORLD HEALTH ORGANIZATION (WHO) (2002) *WHO recommended classification of pesticides by hazard and guidelines to classification 2000–2002*. Geneva: WHO/PCS/01.5.
- WU, K. H., YU, P. Y., YANG, C. C., WANG, G. P. and CHAO, C. M. (2009) Preparation and characterization of polyoxometalate-modified poly(vinyl alcohol)/polyethyleneimine hybrids as a chemical and biological self-detoxifying material. *Polymer Degradation and Stability*, 94: 1411–1418.
- XU, L., BORING, E. and HILL, C. L. (2000) Polyoxometalate-modified fabrics: new catalytic materials for low-temperature aerobic oxidation. *Journal of Catalysis*, 195: 394–405.
- YAMAGUCHI, T., NAKAO, S. and KIMURA, S. (1991) Plasma-graft filling polymerization: preparation of a new type of pervaporation membrane for organic liquid mixtures. *Macromolecules*, 24: 5522–5527.
- YAMAGUCHI, T., YAMAHARA, S., NAKAO, S. and KIMURA, S. (1994) Preparation of pervaporation membranes for removal of dissolved organics from water by plasma-graft filling polymerization. *Journal of Membrane Science*, 95: 39–49.
- ZELLERS, E. T. (1993) 3-Dimensional solubility parameters and chemical protective clothing permeation. 1. Modeling the solubility of organic-solvents in Viton (R) gloves. *Journal of Applied Polymer Science*, 50: 513–530.
- ZELLERS, E. T. and ZHANG, G. Z. (1993) 3-Dimensional solubility parameters and chemical protective clothing permeation. 2. Modeling diffusion-coefficients, breakthrough times, and steady-state permeation rates of organic-solvents in Viton (R) gloves. *Journal of Applied Polymer Science*, 50: 531–540.

Biomechanics in skin/clothing interactions

M. XING and W. ZHONG,
University of Manitoba, Canada

and

N. PAN,
University of California, Davis, USA

Abstract: Skin/clothing interactions or abrasions lead to discomfort or blistering. These irritations may turn out to be critical in athletic competitions or military missions. However, despite the theoretical and practical importance of the problem, no research has been published investigating the connections between skin abnormalities and the physical properties of the fabric (elastic modulus, thickness, mass density, and friction coefficients), or between the initial gap and relative interaction intensity between skin and fabric. This chapter therefore seeks to fill this gap by describing two models of skin/fabric interactions and how these interactions may lead to skin injuries.

Key words: biomechanics, skin/clothing interactions, friction blistering, finite element methods.

20.1 Introduction

Skin abrasion leads to hot spots [1]; even mild abnormality in garment/skin regulatory interaction could result in discomfort, with consequences such as itching, rashes and blistering. These irritations can prove to be critical in athletic competition or military operations, when reduced performance or mobility [2–5] has adverse, or even fatal, consequences [6]. This alone necessitates a thorough investigation and understanding of interactions between garment and skin under various conditions. There has been a long string of research papers devoted to this subject. A recent review article [7] focuses on methods of studying and assessing the skin's response to fabrics in static contact, in terms of changes in capillary blood flow and skin hydration. More thorough investigations on skin blisters due to friction under controlled conditions have been reported [8], followed by laboratory studies on the treatment of such blisters [9]. Another report examined the pathophysiology, prevention and treatment of blisters caused by friction [10]. Other studies investigated the influence of skin friction on the perception of fabric texture and pleasantness under a series of environmental conditions from neutral to hot-dry and hot-humid, and one conclusion is that moisture (not

liquid sweat) on the skin surface increases significantly the skin friction [11]. Others analyzed the friction effects of skin in contact with different types of materials and found that friction coefficients varied from 0.37 (skin/nylon), 0.61 (skin/silicone) [12] to 0.9 (skin/rubber hoses) [13]. Still others applied numerical methods to simulate the friction contact effects of soft tissues such as pigskin, and reported that specimens subjected to specimens/platen friction may experience 50% greater stress than those that experienced frictionless contact between specimens [14–16]. A finite element (FE) model was developed by Hendriks *et al.* to characterize the non-linear mechanical responses of human skin to suction at various pressure levels [17–19].

Skin friction blisters, a frequent dermatological injury associated with intensive abrasion of skin against other surfaces, can inactivate an otherwise healthy individual, and be of significant consequence for such intensive events as sport and military operations: for infantry soldiers carrying heavy equipment and supplies over long distances, blisters can account for 48% of the total injuries [20].

From a mechanical approach, abrasion will lead to ‘sore spots’, portions of the skin suffering excessive stress and strain, and will eventually result in blistering [21]. The blisters are caused by frictional forces which mechanically separate the surface epidermal cells from the stratum spinosum [2]. Hydrostatic pressure then causes the area of separation to fill with a fluid similar in composition to plasma but with a lower protein level [22].

In the late 1950s and early 1970s [2, 6, 23–25], friction blisters became one of the main focuses of skin research and a special apparatus was designed for creating friction blisters. The instrument consists of a rubbing head to which various materials (including textiles) may be attached. The head can be moved over the surface of any chosen skin site at a selected stroking rate under a given compressive load. The effect of skin moisture was also studied: a dry or nearly dry skin reduced the friction, intermediate degrees of moisture increased friction, and highly moist or completely wet skin decreased the friction again.

The geometry of the rubbing head, its weight and the material attached to it all affect the friction coefficient measurements [26]. Sivamani *et al.* [27, 28] utilized the UMT Series Micro-Tribometer, a tribology instrument that permits real-time monitoring and calculation of the important parameters in friction studies, to conduct tests on abdominal skin samples of four healthy volunteers. They concluded that skin friction appears to be dependent on additional factors, such as age, anatomical site and skin hydration; the choice of the probe and the test apparatus also influence the measurement [27, 28] and Amonton’s law does not provide an accurate description of the skin surface [29].

Emollients and antiperspirants alleviated blistering. For instance, Darrigrand *et al.* and Reynolds *et al.* [30, 31] showed that antiperspirants

reduced sweat rates and tended to decrease blisters, in spite of their side effect of introducing irritant dermatitis. However, antiperspirants used with emollients abated irritant dermatitis but did not reduce total foot-sweat accumulation, occurrence of hot spots, or appearance and severity of blisters as the emollients may have altered the antiperspirant's chemical properties. In addition, the emollients may have acted as moisturizing agents, thus increasing the friction [32], and macerating the stratum corneum [33].

The effects of clothing on blistering have also been documented. Herring and Richie [34] conducted a double-blind study to determine the effect of sock fiber composition on the frequency and size of blistering events in long-distance runners. The two socks were identical except in their fiber content: one was 100% acrylic, while the other was 100% natural cotton. The acrylic fiber socks were associated with fewer blisters and smaller blister size compared to cotton socks.

An ulcer formation hypothesis [35] can also be applied to the formation of blisters from a mechanical perspective. The plantar foot experiences a distributed shear and compressive stresses due to joint tangential and vertical forces. As a result, affected skin may slip (i) toward, (ii) away from or (iii) parallel to (i.e. a region in which no slip occurs) each other. The friction coefficient is defined as the ratio of the tangential/vertical forces, and blister formation is inhibited if the frictional coefficient is below a critical minimum (μ_{Rmin}).

Despite extensive friction blister studies, the prevalence or severity of friction blisters remains difficult to predict and prevent. The reasons may lie in the variations of skin condition (surface roughness, hydration, adhesion between skin layers, etc.) among individuals as well as among different anatomical locations on the same individual [36]. These variations may have pronounced effects on the dynamic contact of skin against outer-materials, and may ultimately dictate the occurrence and severity of blisters.

However, no studies investigating the connections between skin abnormalities and the physical properties of the fabric (elastic modulus, thickness, mass density and friction coefficients), or between the initial gap and relative interaction intensity between skin and fabric, have been reported, in spite of the theoretical and practical importance of the problem. This chapter, therefore, will describe two models of skin/fabric interactions and will discuss how these interactions may lead to skin injuries. Specifically, the first model focuses on the dynamic interactions between a fabric sleeve and a rotating arm model, accounting for the above factors, by developing an explicit finite element (EFE) model to simulate the problem. To facilitate a comparison of the numerical results, all the Von-Mises stresses are normalized into relative values. The second model is a blistering model again using the EFE method. For given shear and normal forces, this model is able to account for the influences of the friction coefficient, stiffness of the

abrasion material, non-linear dynamic contact between skin and the material, and even the blistering geometry. The static and dynamic responses of the blister are obtained through mode frequency, sweeping frequency harmonic analysis, and highly non-linear contact dynamics. The stresses on the hot spots are also compared to account for the effects of friction coefficients and material stiffness.

20.2 An explicit finite element model of skin/sleeve interactions during arm rotation

20.2.1 Method

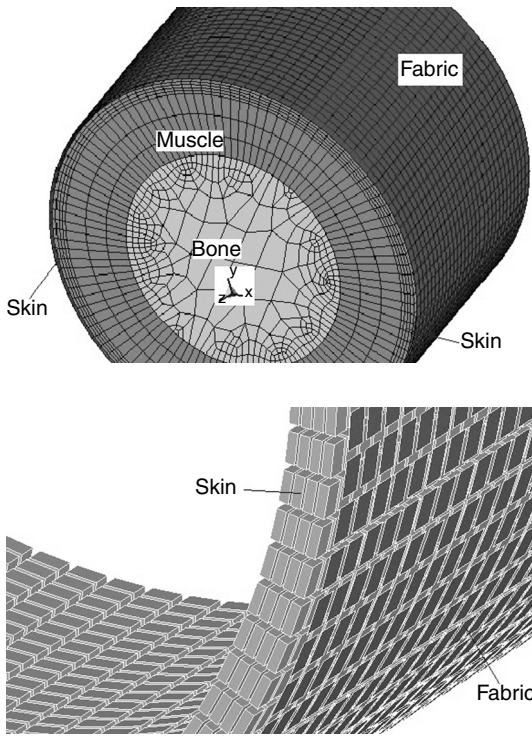
System description/analytical model

A part of the forearm (Fig. 20.1(a) and (b)) with an idealized cylindrical shape is taken as the base for simulation. For a problem like this, a two-dimensional model would be unable to effectively account for the interaction of fabric with skin. In a 2-D model, the beam or line element must be used to represent the fabric. It is difficult to calculate the line element dynamic contact where the cross-sectional area of the line element is required, as it calls for 3-D model. The current model adopted, therefore, is 3-D, consisting of the fabric sleeve, and skin, muscle and bone forming the forearm, so as to be closer to the actual structure [37]. The sleeve is cylindrical in shape and larger than the forearm; the gap between the two means that gravity causes the sleeve to drop onto the forearm, providing the initial impact.

Also, if the model only includes the skin and fabric components and ignores the muscle and bone, defining the boundary conditions of the inner side of the skin, which interacts with the muscle, is somewhat problematic. If the normal displacement of the inner skin is constrained, then the reaction force will be greater than the actual value at large angular displacement due to the unrealistic boundary constraint. The skin layer is very sensitive to these constraints, since it is extremely thin. Furthermore, normal constraints may cause the fabric to interact with skin to induce a radial displacement. If no normal constraint is assigned, however, continued simulation of the dynamic interaction will become difficult.

The initial configuration of the model is as follows:

- (a) The arm is inside the sleeve coaxially so that there is an initial gap between the sleeve and skin.
- (b) Upon rotation of the arm at a given initial angular speed, the sleeve first drops freely under gravity.
- (c) The falling sleeve then strikes the skin on the still rotating arm.



20.1 (a) Schematics of the FE model for the skin–fabric–arm system under an arm rotation. (b) A local view of the skin and fabric contact in the model.

One of the key issues in our simulation is how to deal with the contact between skin and fabric. The uncertain and more or less oscillating nature of the contact and the soft, flexible and hyperelastic behavior of the skin present significant difficulties in simulation. We employed the augmented Lagrange algorithm (ALA), instead of the Lagrange multipliers or the penalty algorithm, to overcome this problem.

So the total potential energy variation of the system during the whole dynamic interaction process can be expressed as [38, 39],

$$\delta\Psi = \int_{\Gamma} [(\lambda_N + \varepsilon_N g_N) \delta g_N + (\lambda_T + \varepsilon_T g_T) \delta g_T] dA \quad [20.1]$$

Here λ_N and λ_T are the Lagrange multipliers, ε_N and ε_T are the associated penalty parameters, and δg_N and δg_T are the virtual displacements. The subscripts N and T denote the normal and tangent directions, respectively, $\lambda_T \delta g_T$ reflects the tangential sticking; the gap $g_N \geq 0$ assures no penetration of fabric into the skin; and $\lambda_N \leq 0$ indicates a compressive normal stress

(fabric pressure on the arm). $g_N \lambda_N = 0$ is required so that if the gap is non-zero $g_N > 0$, then $\lambda_N = 0$, no contact taking place. And if the gap is zero, the contact normal force $\neq 0$.

Equation [20.1] can be considered as a generalization of the Lagrange multiplier method where an additional term involving the contact tractions is added to the variation equation. The ALA method will alleviate the ill-conditions (difficulties in convergence) in the penalty and Lagrange methods.

In addition to the ALA, an automatic surface to surface contact method is used with suitable penalty parameters and stiffness factors so as to prevent the fabric from penetrating into itself at large deformation and maintaining the stability of the fabric/skin contact algorithm. The skin is considered to be the master/target and the fabric to be the slave/contact objects in the contact algorithm. In the case of fabric self-contact, however, fabric is treated as both. To ascertain the status of skin/fabric contact at every stage, much finer skin and fabric elements are adopted and the elements in the normal contact direction are treated with special care. All contacts in the normal direction are assumed as plane contact; otherwise the contact stresses (both tangent and normal) will approach a singular state.

Thus the global dynamic equation is

$$[K + K_c]\{u\} + [M]\{\ddot{u}\} = \{f_e\} \quad [20.2]$$

Here $[K]$ is the structural stiffness matrix, $[K_c]$ is contact stiffness matrix, $[M]$ is mass matrix and $\{f_e\}$ is external force matrix (gravity); $\{u\}$ is displacement matrix and $\{\ddot{u}\}$ is acceleration matrix. The second term in the left-hand side accounts for the inertial force.

The boundary conditions are as follows:

for the bone: $U_x, U_y, U_z = 0$, and $R_x, R_y = 0$ (R : rotation degree of freedom)
for the muscle: $U_z = 0$

The initial condition is as follows:

An initial angular velocity ω_z is given for bone, muscle and skin at $t = 0$.

In this EFE model, the arm is represented by solid elements with skin thickness 2 mm measured by 20 MHz ultrasound [40], whereas the fabric sleeve is represented by shell elements with a thickness 0.5 mm. The bending stiffness of fabric is

$$D = \frac{Eh^3}{12(1-\nu^2)} \quad [20.3]$$

where E is the elastic modulus, h is the fabric thickness, and ν is Poisson's ratio [41].

The skin's stress-strain curve exhibits a pseudoelasticity, and hence the corresponding strain-energy [42]. In our model, a time-independent, isotropic and hyperelastic constitutive model is used for skin according to [41, 43], and the Mooney-Rivlin two-parameter constitutive equation [18, 44] is employed with two-parameter C_{10} and C_{11} to represent the hyperelastic properties of the skin. The bone is considered to be a rigid body, since the elastic modulus of the bone is much larger than that of the muscle or skin. Since our focus is on the interaction between skin and fabric in a very short time, the *muscle* under the skin is presumed to be elastic.

Numerical resolution/software

Four numerical simulations, a , b , c and d , under different conditions, are performed to investigate the interactions between skin and fabric as the forearm is turning by a certain number of degrees in one direction or in alternating directions over a given period of time. Each simulation examines the influence of one parameter at four different levels as detailed in Table 20.1. During calculation, the skin surface nodes experiencing maximum Von-Mises shear stress are located and recorded based on the hypothesis that a higher maximum stress is more likely to cause greater skin irritation. So that different simulation results can be easily compared, normalization is then performed by dividing all other stress values with the corresponding maximum stress in each run, and the normalized relative stresses are plotted against time to illustrate the interactions between the skin and the fabric sleeve during the process. The EFE analyses are performed using commercial FE software (pre-processor: ANSYS V.6.1, Explicit solver: DYNA3D, post-processor: PostGL).

Model parameters

Ranges of the parameters for each simulation are listed in Table 20.1.

It is noted that for Simulations a and b , the arm rotation around axis Z (arm central rotation axis as shown in Fig. 20.1 (a)) is in alternating directions; from 0 to 0.1 s, the arm rotates in one direction for an angular displacement of $\pi/2$, i.e. at a constant angular velocity of 15.7 rad/s; then from 0.1 to 0.2 s, the arm reverses in the opposite direction from $\pi/2$ to $\pi/2$. In other words, the angular speed doubled to 31.4 rad/s upon reversing the rotation direction. This is different from Simulations c and d , where the arm turns from 0 to $\pi/2$ in 0.12 s in one direction only.

The two hyperelastic material properties of the skin are taken from [18] as $C_{10} = \text{KPa}$ and $C_{11} = 100 \text{ KPa}$, input into the card of DYNA3D. For muscle, the normal modulus E_n is 1 MPa and tangential modulus E_t 5 KPa adopted

Table 20.1 Parameters/ranges for four simulations

Variables		Fabric modulus (MPa)	Fabric/skin uniform initial gap (mm)	Fabric/skin friction	Fabric density (10 ⁻⁴ g/mm ³)	Forearm rotation		
						Range (rad)	Total time (s)	Speed (rad/s)
Simulation	<i>a</i>	200, 400, 600, 800	2.0	0.3	6.0	0 to $\pi/2$ $\pi/2$ to $-\pi/2$	0 to 0.1 0.1 to 0.2	15.7 31.4
	<i>b</i>	400	1.0	0.0, 0.2, 0.3, 0.5	3.0	0 to $\pi/2$ $\pi/2$ to $-\pi/2$	0 to 0.1 0.1 to 0.2	15.7 31.4
	<i>c</i>	600	0.8, 3, 6, 8	0.3	5.0	0 to $\pi/2$	0.12	13.1
	<i>d</i>	500	7.0	0.4	2.0, 4.0, 6.0, 8.0	0 to $\pi/2$	0.12	13.1

Table 20.2 Relative maximum Von-Mises stress with the second set skin parameters under varying fabric elastic modulus at the arm reversing point around $t = 0.1$ s

Elastic modulus (MPa)	200	400	600	800
Stress peak (normalized)	0.61	0.67	0.75	1

Table 20.3 Normalized maximum Von-Mises stress with the second set skin parameters under varying frictional coefficients at arm reversing point around $t = 0.1$ s

Elastic modulus (MPa)	200	400	600	800
Stress peak (normalized)	0.46	0.73	0.81	1

from [45]. Thus, computational time is drastically reduced without too much compromise in accuracy. In addition, the contact relationship between parts is classified as perfect bonding (bone/muscle, muscle/skin), and dynamic sliding with friction (skin/fabric), respectively.

Material properties of biological system tissues usually vary greatly from experimental conditions and samples; thus, in order to test the significance of the results and to evaluate their dependence on the model parameter, we take a second set of skin parameter $C_{10} = 7.1$ KPa and $C_{11} = 34$ KPa [18] to simulate the effects of elastic modulus and frictional coefficients on fabric. The results are shown in Tables 20.2 and 20.3.

20.2.2 Results

In order to evaluate the shear stress or friction force, the maxima Von-Mises stress (effective shear stress) is used to characterize the skin/fabric

interactions in these numerical simulations. The Von-Mises stress is defined as a function of deviated principal stress:

$$\sigma_e = \left[(\sigma_1 - \sigma_2)^2 + (\sigma_2 - \sigma_3)^2 + (\sigma_3 - \sigma_1)^2 \right]^{1/2} \quad [20.4a]$$

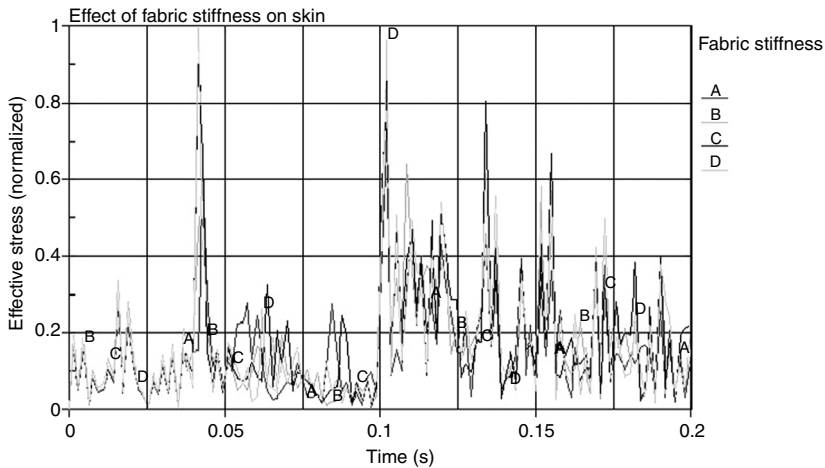
or

$$\sigma_e = \left[(\sigma_x - \sigma_y)^2 + (\sigma_y - \sigma_z)^2 + (\sigma_z - \sigma_x)^2 + 6(\sigma_{xy}^2 + \sigma_{yz}^2 + \sigma_{xz}^2) \right]^{1/2} \quad [20.4b]$$

where σ_i is the i^{th} principal stress, σ_j are the normal stresses at $j = x, y, z$ axes, and $\sigma_{xy,zy,xy}$ are the corresponding shear stresses, respectively.

With the hypothesis that the largest stresses contribute most significantly to skin discomfort, in our simulations we focus on the contact points suffering maximum stresses during arm rotation. In other words, in the following plots, we only provide the time when, not where, the maximum stress occurs on the skin at different levels of the related parameters.

Figure 20.2 shows the results for Simulation *a*, where the normalized maximum effective shear stress at the skin/fabric contact interface is plotted as a function of time at four different fabric elastic modulus levels (A: 200 MPa, B: 400 MPa, C: 600 MPa, D: 800 MPa). It is clear that in this case, all the fabric sleeves strike the arm at the same time as indicated by the peaks at around $t = 0.04$ s, and the second group of peaks occur at the time the rotation direction reverses. Fabric elastic modulus exerts significant influence on the shear response of the skin, and the doubling of the rotation speed at the second period clearly impacted the shear stresses.



20.2 Normalized effective shear stress as a function of time at four different fabric modulus levels for Simulation *a*: (A) 200 MPa; (B) 400 MPa; (C) 600 MPa; and (D) 800 MPa.

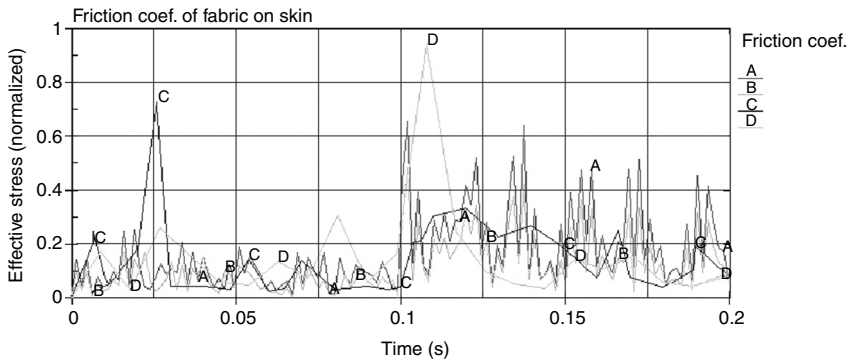
To examine the effects of the fabric/skin friction coefficients on the results, four different fabric/skin friction coefficients are used for Simulation *b*. and the normalized effective shear stresses are plotted against time in Fig. 20.3. Once again, the differences between the two periods of different angular speeds are apparent.

For Fig. 20.3, some curves are shown in more zigzag formats: this is a result of the different sampling frequencies employed during the simulation, which were changed depending on the complexities of each case. However, we used the same number of data points in each graph so as to facilitate comparison among the curves. In other words, some curves are smoother because fewer points were used.

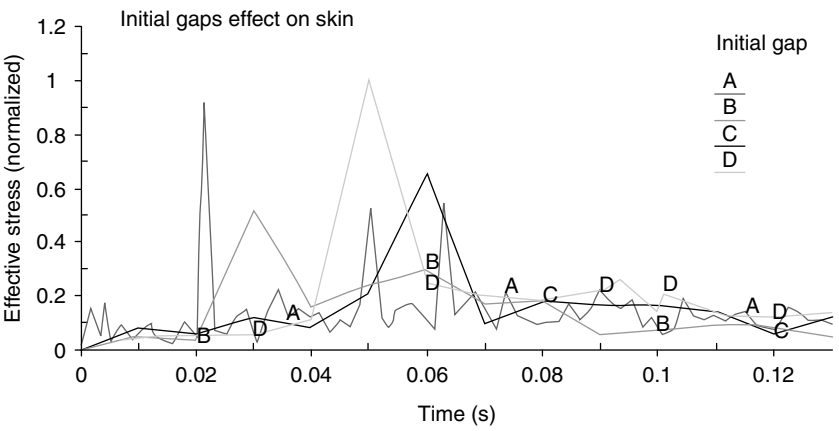
Results in Fig. 20.3 show that the fabric friction coefficients have a significant impact on the skin/fabric interactions. The maximum shear stress corresponds to the value of the friction coefficients, except the anomalous peak *C* with friction coefficient 0.2 at near 0.025 s, a more specific explanation of which is provided in the discussion section.

Effects of initial gap between the fabric and skin are depicted in Fig. 20.4 at four initial gaps: 0.8 (A), 3 (B), 6 (C), and 8 mm (D). The four first-strike peaks take place according to their corresponding initial gaps, yet with samples C and D the sequence was reversed. This shows that the maximum Von-Mises shear stresses are significantly greater with initial gaps of 0.8 and 8 mm than with a gap of 3 and 6 mm, respectively.

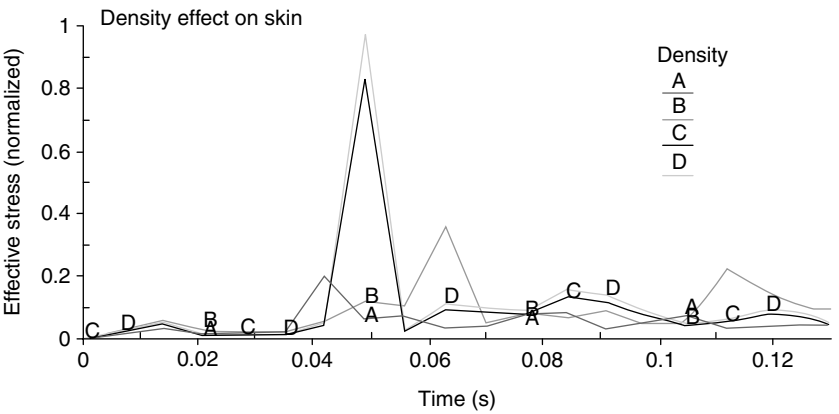
Note that curve A with initial gaps of 0.8 mm in Fig. 20.4 shows more peaks than other curves. This is not a result of numerical instability. For explicit computation, when the lost energy is smaller than 5% of the initial energy, the result is considered stable. In our simulation, the ratio of final energy to initial energy is close to 1.0. In fact, if we observe that the initial gap in this case is the smallest, 0.8 mm, this tighter arrangement between



20.3 Normalized effective stresses at different friction coefficients as a function of time for Simulation *b*: (A) 0.3; (B) 0; (C) 0.2; (D) 0.5.



20.4 Predicted effective shear stresses at different initial gap between fabric and skin as a function of the rotating time for Simulation c: (A) 0.8 mm; (B) 3 mm; (C) 6 mm; and (D) 8 mm.

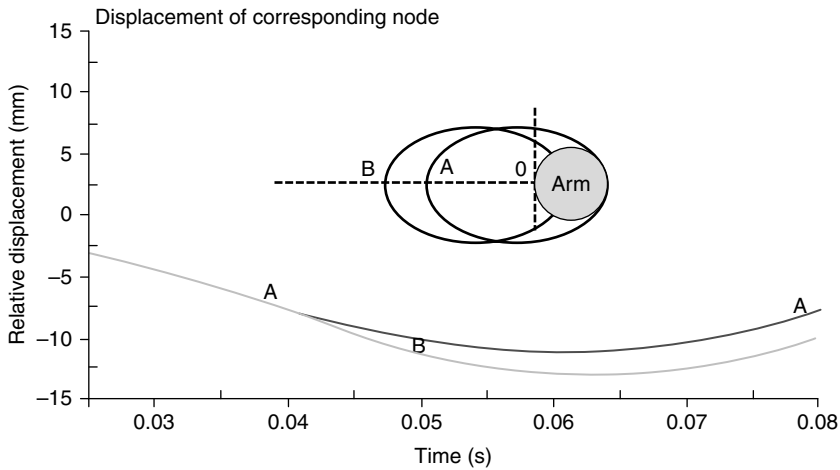


20.5 Predicated normalized stress response with different fabric density as a function of rotation time for Simulation d: (A) 2×10^{-4} g/mm³, (B) 4×10^{-4} g/mm³, (C) 6×10^{-4} g/mm³, and (D) 8×10^{-4} g/mm³.

the skin and sleeve likely leads to more frequent interactions, and thus more peaks.

The effect of fabric density is calculated as seen in Fig. 20.5, where, when the arm is given a constant angular velocity of 13.1 rad/s, the stress magnitude in general increases with an increasing fabric density. The first-strike peaks should occur at the same time the peaks for samples A and B, however, occurred earlier or later.

Figure 20.6 shows that the fabric B which has a lower elastic modulus and consequently is in closer contact with the rotating arm, exhibits a larger displacement due to its more pliable shape conformity.



20.6 Displacements of the sleeves away from the arm contacting point as a function of time at different levels of fabric elastic modulus: (A) elastic modulus: 800 MPa and (B) elastic modulus: 200 MPa.

In order to further validate the results of the simulation, we adopt the second set of skin mechanical parameters $C_{10} = 7.1$ KPa and $C_{11} = 34$ KPa [18] to confirm the effects of both fabric elastic modulus and friction coefficients on the peak Von-Mises stress, and the predictions are tabulated in Tables 20.2 and 20.3. We once again found pronounced peak stresses around the time $t = 0.1$ s, the point when the turning direction of the arm is reversing and thus generating excessive angular acceleration. This result bears close similarities to what was observed in the predictions using the first set of skin parameters above.

20.2.3 Discussion and conclusions

As mentioned above, during each simulation, we first scanned all the nodes of the fabric/skin contacts to identify the maximum stress to plot against time. Therefore, we only examined *when* and *how much*, but not *where*, a maximum stress takes place.

Next, the rotation of the arm is a circular motion. For the fabric sleeve to follow this circular motion, we have included a centripetal force distributed over the fabric in the model, pushing it toward the center of the circular path. The magnitude of the centripetal force is equal to the mass m of the fabric times its velocity squared V^2 divided by the radius r of its path: $F = mV^2/r$. Obviously this force plays an important role during the fabric/skin interactions.

The effects of fabric tensile modulus studied in Simulation *a* are plotted in Fig. 20.2, which is shown to have exerted a significant influence on the shear (frictional) response of the skin.

There are two major peak locations. The first is located at $t \approx 0.04$ s, which is most likely the point where the fabrics first strike the skin. Obviously, a stiffer fabric would generate a greater impact stress. However, the exact first-strike time cannot be readily estimated by Newton's Law alone, i.e. by considering fabric free falling from the height of a given initial gap, as the deformation of fabrics and fabric self-interaction may affect the first-strike time.

Nonetheless, this fabric/skin first-strike time is clearly important and will be discussed again in other simulations below.

After the first strike, from $t = 0.05$ to 0.1 s, it is the least stiff fabric A that generates the highest shear stress, as for a given centripetal force, a less stiff fabric in general maintains a better or tighter contact with the skin during a stable circular motion, hence the greater frictional force.

Another interesting point is at $t \geq 0.1$ s, when reversed arm rotation starts, the higher acceleration and greater centripetal force intensify the fabric/skin impact and the peak frictional forces for all the four samples as mentioned before. It reveals that fabric/skin interactions are often highly dynamic or bumpy in nature as illustrated in Fig. 20.2 (B), rather than just being cases of smooth or static friction.

These characteristics are also indicated in Fig. 20.3, where different friction coefficients are adopted. Generally speaking, when the friction coefficient is smaller, the corresponding shear stress will be lower. However, the higher acceleration and greater centripetal force in the reverse period again causes greater skin/fabric interactions for all the samples in Fig. 20.3 (A)–(D). There are reasons to consider the unusually high peak C with friction coefficient 0.2 at 0.025 s as anomalous; the potential fabric local folding and wrinkling at the fabric/skin interface is likely to result in penalty force and singular stress effect at fabric element edge.

In Simulations *c* and *d*, a constant angular speed $\omega = 13.1$ rad/s is chosen. The effects of the initial gap between fabric and skin are studied in Simulation *c* as shown in Fig. 20.4. It is shown that samples A, B and C strike the skin at different times according to their respective gaps; namely, the smaller the gap, the earlier the first strike. The deviation of sample D, however, again highlights the complexity of the whole process. In terms of the magnitude of impact, although a fabric with larger initial gap, and thus higher impact speed, will generate larger effective stress on the skin, the question of why the very close initial gap (0.8 mm) also leads to a significant peak of effective stress on the contact surface has yet to be resolved. This may suggest that when a garment is excessively tight or loose, greater shear stresses could be generated at the skin/fabric contact interface. Further evidence is still required to verify this hypothesis. If the peaks corresponding to different initial gaps in the first time period (0–0.6 s) are excluded, the rest of the four curves are quite similar to each other, as a consequence of the

same fabrics moving at the constant angular speed 13.1 rad/s. Another possible reason may be the low impact speed on the skin: the fabric would then have a tighter contact on the skin, and a greater static friction might have contributed to an increased skin surface stress. However, once fabrics settle down, they all show quite smooth interactions with the skin, in contrast with Simulations *a* and *b* where reversed arm rotation does indeed complicate the situation.

Fabric density also exhibits considerable influences on the results as examined in Simulation *d* with Fig. 20.5. Since the skin surface node with maximum effective stress is our focus in the simulation, variations of the first peak time for samples A and B are reasonable because the initial location for this node may be different for each test. Magnitudes of initial impact on the skin are exactly proportional to their mass as predicted by Newton's Law. The rest of the process is a relatively smooth ride for all samples.

With the hypothesis that the largest stresses contribute most significantly to skin discomfort, in our simulations we focus on the contact points suffering maximum stresses during the rotation of the arm and the changing of direction. It is clear from the results that an increase in fabric elastic modulus, friction coefficient, initial gap and fabric density will all increase the skin stress. Our results should provide guidance for analyzing the skin discomfort caused by fabrics. However, the complexity and random nature of the skin/fabric interactions also generate deviations from the trends predicted above in terms of the time of the first stress peak, the fluctuation of stresses during the arm rotating, and the singular stress state at the boundary.

In fact, a simple analysis below can explain some of the apparent anomalies. For simplicity, the skin/fabric contact model is reduced to 2-D as shown in Fig. 20.7. It is also assumed that the initial local contact area is very small and contact only happens very briefly. Thus the rotation angular displacement of the skin could be neglected. Applying Coulomb's friction law, shear traction can be determined from [46]:

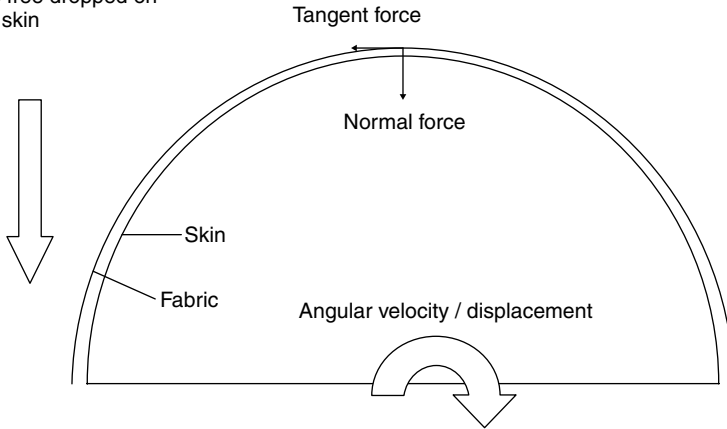
$$T_x = 2\mu F_{\text{normal}} \sqrt{a^2 - x^2} / (\pi a^2) \quad [20.5]$$

Expanding equation [20.5] at zero respective to $(x/a)^2$ leads to

$$T_x \approx 2\mu F_{\text{normal}} \frac{1}{\pi a} \left[1 - 1/2 \left(\frac{x}{a} \right)^2 \right] \quad [20.6]$$

where T_x is the tangent force along the local contact area, μ the friction coefficient, F_{normal} the local normal force of contact, a the approximate length of contact area, and x the distance from the center to the edge of the contact area, and $-a < x < a$.

Fabric free dropped on
to the skin



20.7 Initial contact between fabric and skin with a velocity.

Our simulation results also indicate that at initial contact stage the curvature radius of the fabric with a smaller elastic modulus is lower than that of the fabric with a larger elastic modulus, so that the initial contact length a with smaller modulus will be longer than that with larger modulus, and the tangent force gives the relationship $T_{x\text{largestif}} \geq T_{x\text{smallstif}}$, as has been shown in the simulation results in Figs 20.2 and 20.6.

Finally, we have employed a second set of skin properties to check the influences of both fabric elastic modulus and frictional coefficients. The results shown in Tables 20.2 and 20.3 are consistent with those corresponding to the first set of skin parameters.

The simulations carried out for this study focus on the rotation of the arm, a movement frequently performed in daily life. Analysis of the model has for the first time revealed how variations of such related factors as the elastic modulus, friction coefficients, density of the fabric, and initial gap between skin and fabric contribute to the frictional stresses and presumably to the levels of discomfort caused by the friction between skin and cloth during movement.

Obviously, this report only represents an initial attempt at tackling an extremely complex phenomenon. Our model simulated only a 0.2 s transient process. Time consumption was one consideration (each calculation takes about 15 h on a computer with dual CPUs and 2 GB memory). Also, it is widely believed that transient process is critical in studying human sensations. We assume that a simulation carried out over a longer period and with an integral parameter besides instantaneous values would provide additional information.

Furthermore, different models have been proposed to describe the behavior of skin, including isotropic viscoelastic and hyperelastic theories [41, 43], as well as the more realistic porelastic model proposed by Wu *et al.* [15, 16].

Finally, we will conduct some experiments in order to validate and improve the numerical model, selecting more appropriate material properties and constitutive equations. We will also deal with the fabric edge singular stress and the problem of fabric contact penetration. Our ultimate aim is to work with interested companies to simulate the dynamic interactions between sports garments and the entire human body [47, 48].

20.3 Skin friction blistering: computer model

20.3.1 Model and material properties

Blister geometry model

As shown in Fig. 20.8, the blister in the model consists of three parts: (i) roofed skin, (ii) blister fluid and (iii) basal cell layer. The roofed layer is composed of stratum granulosum, stratum corneum and a small segment of amorphous cellular debris [2]. The blister is considered as an ellipsoid shape with a circular base, whose radius is viewed as the longer axis and set as 3 mm. The height of the blister is the shorter axis. We simulated the dynamics of the blister model using the ANSYS system (v.10.0, ANSYS Inc., Canonsburg, PA, USA, 2005) [49].

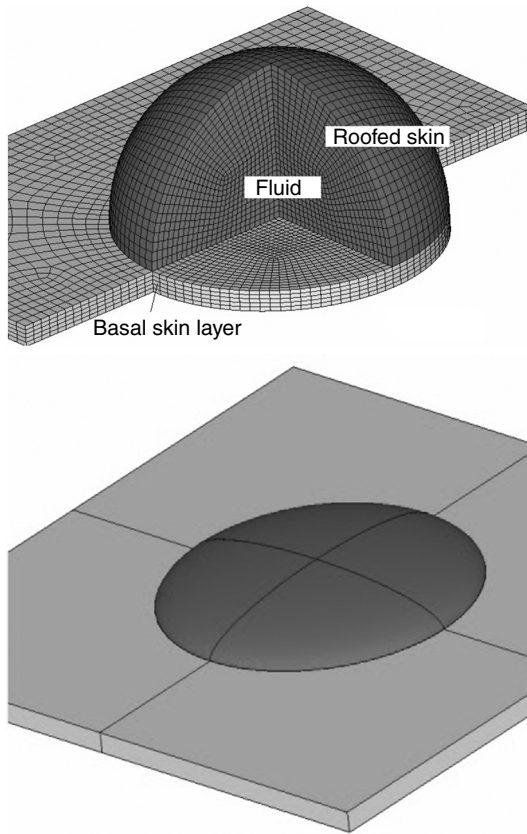
The thickness of roofed skin is 55 μm taking into account the thickness of the stratum corneum of the sole [50]. The basal skin layer is 1.6 mm thick as measured by ultrasound (20 MHz) [40]. The blister fluid is contained in the cavity between roofed skin and the basal skin layer. During the computation, the lateral surface (3-D) or sides (2-D) of the basal skin layer are given displacement constraints.

Material properties

The elastic modulus of roofed skin is about 13 MPa measured using the *in vivo* dynamic (sonic) method [51], and the skin is assumed to be isotropic. For a simulation of steady or transient time span (a time much shorter than the skin relax time), a linear elastic constitutive behavior can be assumed. The Poisson ratio is taken as 0.4 [50]. The blister fluid is more or less like the plasma derived from blood with bulk modulus: 2150 MPa and apparent viscosity: 1.1×10^{-9} MPa.s [6].

Contact algorithm

Materials contact skin with different friction coefficients and the effects on blisters are highly significant [34, 52]. Such contact is an extremely non-linear dynamic problem. The ALA is employed to cope with the challenges through use of the Lagrange multipliers or penalty parameters. So the total potential energy (virtual work) of the system can be expressed as [38, 39],



20.8 The 3-D blister with different radius ratio (a) 0.9 with FE, (b) 0.2 in solid model.

$$\delta \Psi = \int_{\Gamma} [(\lambda_N + \varepsilon_N g_N) \delta g_N + (\lambda_T + \varepsilon_T g_T) \delta g_T] dA \quad [20.7]$$

where λ_N and λ_T are the Lagrange multipliers, ε_N and ε_T are the associated penalty parameters, and δg_N and δg_T are the virtual displacements. The subscripts N and T denote the normal and tangent directions respectively. Equation [20.7] can be considered as a generalization of the Lagrange multiplier method where an additional term involving the contact tractions is added to the variational equation.

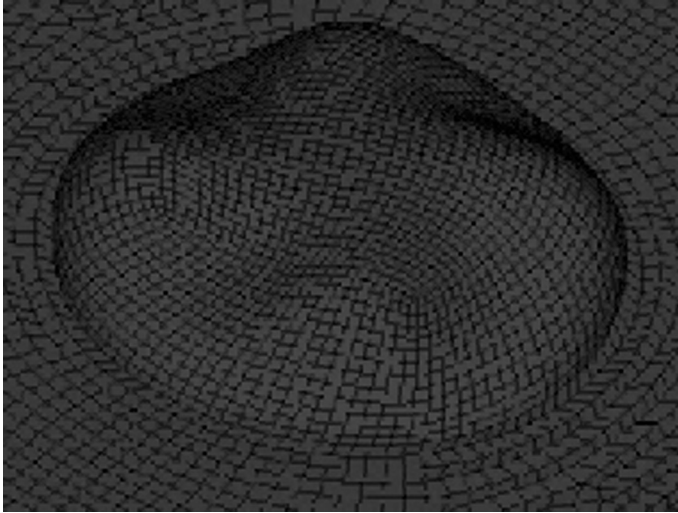
20.3.2 Results

The model designed in this way is executed as a 3-D model with a radius ratio of 0.5. The mode natural frequencies calculated are shown in Table 20.4,

Table 20.4 The modal natural frequencies for the model from 1st to 6th order to account for resonance frequency

Order	1st	2nd	3rd	4th	5th	6th
Frequency (Hz)	28.38	30.61	30.64	30.74	32.44	34.66

The lowest frequency 28.38 Hz is far higher than those occurred in sports competition.



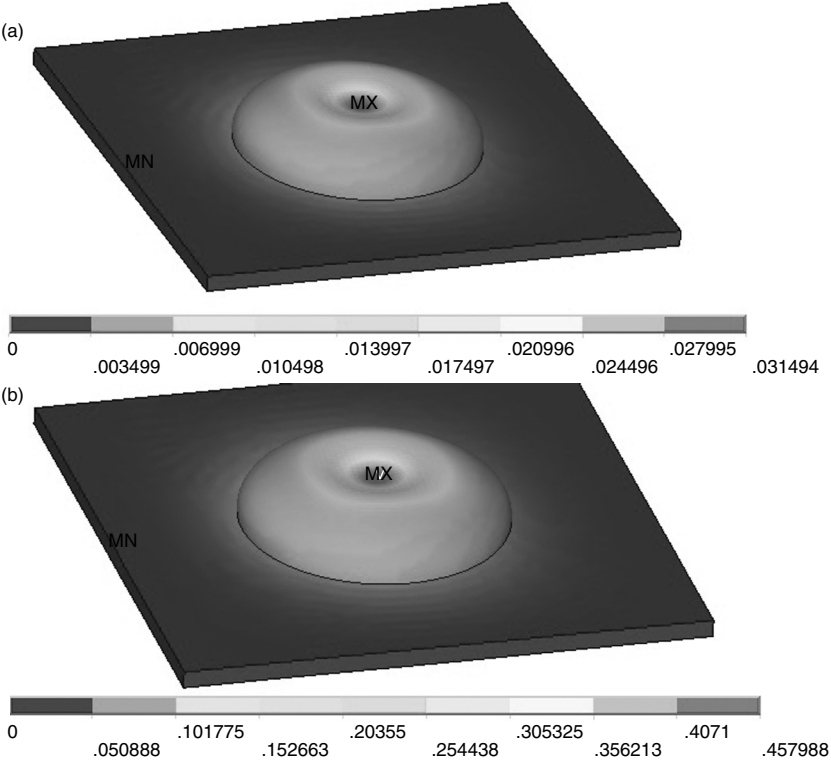
20.9 1st order modal shape with frequency 28.38 Hz. When the loading frequency reaches this value, the blister shape will be excited.

and detailed descriptions of the mode and harmonic analysis are provided in Section 20.3.3. The lowest modal frequency is 28.38 Hz with a modal shape (resonance) shown in Fig. 20.9.

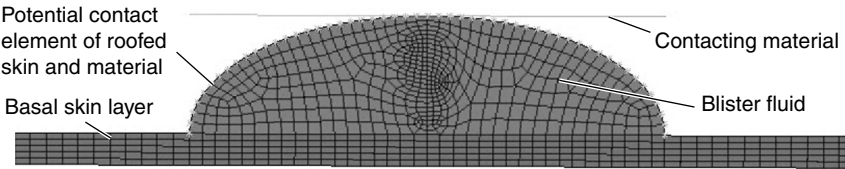
Figure 20.10 (a) and (b) shows the model harmonic analysis with sweeping frequency from 1 to 7 Hz. The loads are 0.1 and 0.01 N respectively along the normal and tangential directions on the tip of the blister. From the figures, the maximum displacement at 1.6 Hz is 0.031 mm in Fig. 20.10 (a), less than 0.46 mm at 6 Hz in Fig. 20.10 (b).

To account for the effects of material properties on blistering in terms of the contacting friction coefficient and stiffness, we simplify the blister into a 2-D FE model with radius ratio 0.5 (Fig. 20.11) for ease of illustration.

In the 2-D model, line elements are used for the roofed skin and contacting material domain, the fluid elements are employed in the blister fluid domain, and the plane elements are in the basal skin layer. To maintain displacement continuity, displacement constrained equations are applied to the interfaces between the roofed skin and blister blood, blister fluid and basal skin layer, respectively.

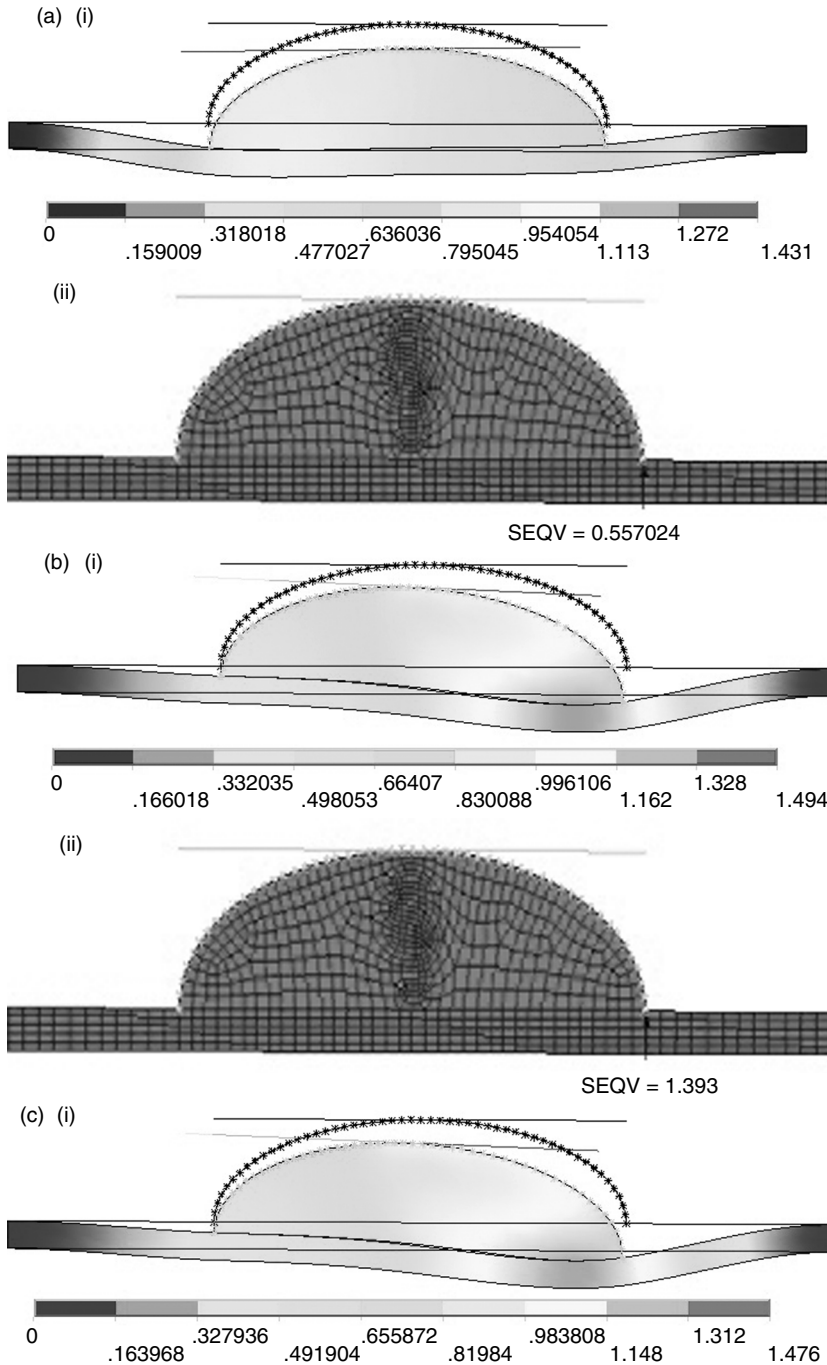


20.10 Displacement of the blister at different frequencies of excitation: (a) 1.6 Hz and (b) 6 Hz. Blister displacement increased in response to the frequency changing from 1.6 to 6 Hz.

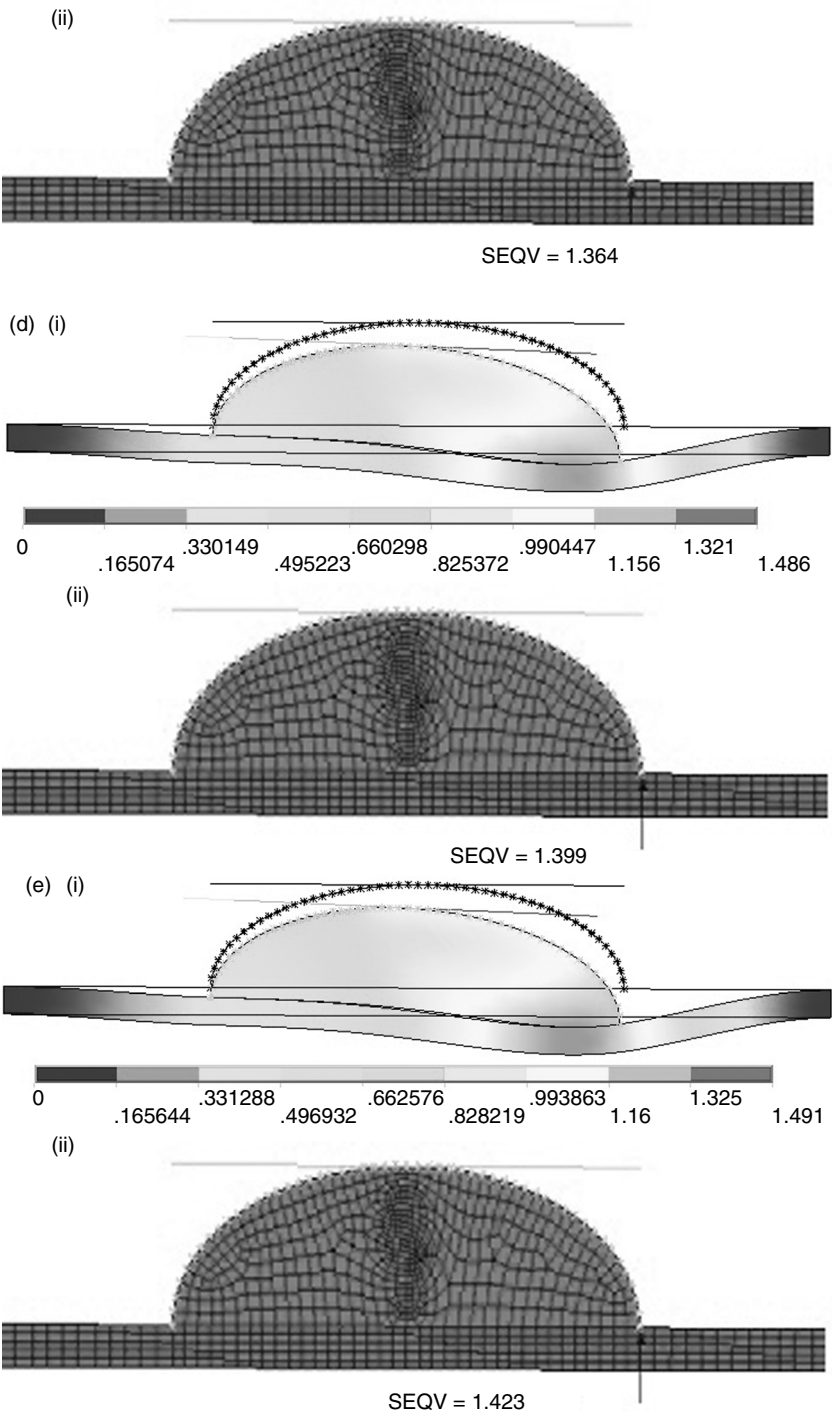


20.11 A 2-D FE model of a blister. When force or displacement is loaded on the contacting material, a blister will be formed. Different friction coefficients and contact stiffness could be compared.

Two equal compressive forces are applied at both ends of the contacting material in a vertical direction. We assume that the displacement is constrained by the two ends of the basal skin layer. The contact algorithm is used to study the interactions between the contacting material and roofed



20.12 The displacement and hot spot stress at five friction coefficient levels. In panels (a) to (e), image (i) shows blister displacement and image (ii) shows Von-Mises stress of the hot spot. Friction coefficients are: (a) 0, (b) 0.1, (c) 0.2, (d) 0.3 and (e) 0.4. The effect of friction coefficient on blister displacement and stress can be compared.

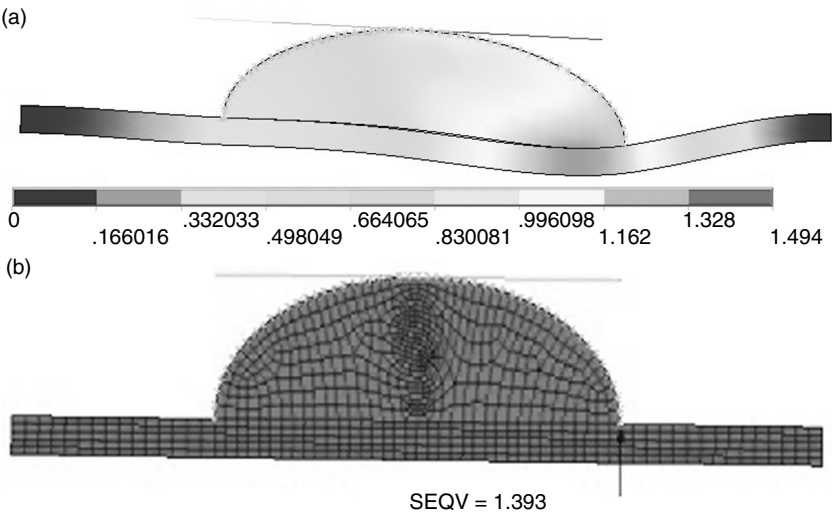


20.12 Continued.

Table 20.5 The maximum tangential friction stress (τ_m) and normal pressure (P_n) at different friction coefficients

	μ				
	0	0.1	0.2	0.3	0.4
τ_m (MPa)	0	0.069	0.044	0.050	0.053
P_n (MPa)	0.175	1.548	0.852	0.843	0.840

Friction stress (τ_m) and normal pressure (P_n) are critical to blister formation. To compare the effect of the friction coefficient, τ_m and P_n are calculated.



20.13 (a) The displacement of the blister and (b) the stress of the hot spot. To account for the stiffness effect of the contacting materials, the elastic modulus from 80 to 120 MPa of the worn outer skin is compared for blister deformation and stress.

skin. The contacting materials have an elastic modulus of 100 MPa and a Poisson ratio of 0.3. The two compressive forces are 0.1 N each and a 1 mm horizontal displacement is added to the contacting material in order to generate the friction movement. The blister responses are obtained with frictional coefficient at 0 (frictionless), 0.1, 0.2, 0.3 and 0.4 respectively as shown in Fig. 20.12.

The maximum tangential friction stress τ_m and normal pressure P_n occurred on the top contact point of the blister shown in Table 20.5.

With the same friction coefficient 0.1 and the same compressive loads, the elastic modulus of the contacting materials changes to 80, 100, and 120 MPa, the respective results of Von-Mises stress in hot spots and displacement of blister show no significant changes; as a result, only data from 120 MPa are provided in Fig. 20.13.

20.3.3 Discussion

Friction blisters are a common problem in long-distance running [5] and infantry road marching [20], and as such underline the significance of understanding the dynamic response of the skin under intensive loading. Based on the numerical model, the eigen equation for the system can be established as

$$[K|\phi] - [\lambda|M|\phi] = [0] \quad [20.8]$$

where $[K]$, $[M]$, $[\lambda]$, $[\phi]$, and $[0]$ are, respectively, the stiffness matrix, mass matrix, eigen value matrix, corresponding mode shape matrix, null matrix of the FE assemblage [53].

We first computed the natural frequency of the skin system by finding the eigen frequency from equation [20.8], as this frequency closely relates to the resonance, which has arisen due to the coincidence between the natural and the loading frequencies and leading to much greater deformation and stress, finally resulting in broken blisters.

We assume the gait frequency is from 1 Hz (normal walk) to 7 Hz (fast run). From the mode analysis result, the 1st order natural frequency is >20 Hz (Table 20.4). It means the loadings with human gait frequency cannot cause resonance, and are consequently unable to lead to the mode shape shown in Fig. 20.9.

Furthermore, to account for the frequency effects on blistering, a normal force 0.1 N and tangential force 0.01 N were loaded on the top point of the blister simultaneously. Then a sweeping frequency harmonic analysis as in equation [20.9] was conducted to investigate the blister deformation at different frequency values.

$$[K|\phi] - [\lambda|M|\phi] = [F] \quad [20.9]$$

where the forces are modulated by multiplying with a harmonic term $\sin(\omega t)$ with ω as the angular frequency and t the time, i.e. $F_i = A \sin(\omega t)$ with A as the force amplitude.

The displacement amplitudes of blisters at 1.6 and 6 Hz are extracted and compared as shown in Fig. 20.10. The displacement amplitude at 6 Hz is 15-fold greater than that at 1.6 Hz. It suggests that the displacement amplitude of the blister is non-linearly proportional to the loading frequency before the resonance frequency. That is, although the same forces are loaded on the skin, a fast runner is more susceptible to blister formation than a normal walker. Although this is a seemingly simple fact, no experiments or theoretical analyses have been carried out to demonstrate it.

Next, since blistering results from the friction interactions between skin and contact materials, the frictional coefficient contributes to a large degree

to the process. Because of the blister symmetry about the related axis, a 2-D FE model was employed here to examine the effects. We consider the deformation and the Von-Mises stress [54] at one hot point at interaction;

$$\sigma_e = \left[(\sigma_1 - \sigma_2)^2 + (\sigma_2 - \sigma_3)^2 + (\sigma_3 - \sigma_1)^2 \right]^{1/2}$$

or

$$\sigma_e = \left[(\sigma_x - \sigma_y)^2 + (\sigma_y - \sigma_z)^2 + (\sigma_z - \sigma_x)^2 + 6(\sigma_{xy}^2 + \sigma_{yz}^2 + \sigma_{zx}^2) \right]^{1/2} \quad [20.10]$$

where σ_i is the i^{th} principal stress, σ_j are stresses at $j = x, y, z$ axes, respectively, and $\sigma_{xy,zy,xz}$ are the corresponding shear stresses.

The effects of the frictional coefficient are calculated (Fig. 20.12), where five levels of the frictional coefficient from 0.0 to 0.4 are represented by the panels (a) to (e); in each panel, the upper image (i) shows blister displacement while the lower image (ii) represents the Von-Mises stress. Results are summarized in Table 20.5.

From the figures and the table of results, it is clear that the influence of the frictional coefficient μ is not monotonic. In Table 20.5, both stress τ_m and normal force P_n reach their corresponding maximum values at $\mu = 0.1$. Since the range of μ in our study – 0.0 to 0.4 – covers a wide range, our conclusion seems valid in general, except perhaps in the cases where the μ value becomes excessive.

The stiffness of the contact materials is also a concern in blister forming and breaking. Some interesting results are obtained from our simulations. When the elastic modulus of contact material increased from 80 to 100 MPa, then to 120 MPa under the same loads and friction coefficient, the tangential friction stress and normal pressure, displacement presented almost no change (as shown in Fig. 20.13). The result is somewhat different from the experiment [34] where different materials show different blistering scenarios. However, from our simulations, the elastic modulus shows no pronounced difference under the calculated range. With the complicated blister forming process, in the above experiments, the different blister events with various contact materials may arise from the difference in the moisture level of the material.

20.3.4 Summary

Due to experimental difficulties and variations in skin, we designed a non-linear dynamic FE model to simulate the deformation of the blister and stress under various loading conditions. From the mode and harmonic analysis, we can concluded that since our gait frequencies (both walking and running) are far below the lowest natural frequency of a blister, human activities are unlikely to lead to blister resonance, presumably with consequences such as broken blisters. Our analysis also indicates that increased frequency will lead

to monotonically increasing deformation and stress of the blister. However, increasing the friction coefficient does not necessarily cause greater stress or displacement of blister hot spots. In fact, there is a local maximum friction stress and Von-Mises stress at certain friction coefficient values. Furthermore, the change of elastic modulus in contact material (within 20–30% range) has not generated significant effects on either the deformation or the Von-Mises stress. The model and method provided here have been shown to be robust in evaluating material properties to prevent blistering. As an ongoing project, we will use different fabrics with variable periodic tension forces on skin to investigate the influences and also to further verify our model, avoiding unfounded generalizations regarding the value of the model.

20.4 References

1. BRUCE, C. M., The role of topical lubrication in the prevention of skin friction in physically challenged athletes. *Journal of Sports Chiropractic and Rehabilitation*, 14(2) (2000): 37–41.
2. SULZBERGER, M. B., *et al.*, Studies on blisters produced by friction. I. Results of linear rubbing and twisting technics. *Journal of Investigative Dermatology*, 47(5) (1966): 456–465 contd.
3. REYNOLDS, K., *et al.*, Injuries and risk factors in an 18-day Marine winter mountain training exercise. *Military Medicine*, 165(12) (2000): 905–910.
4. REYNOLDS, K. L., *et al.*, Injuries and risk factors in a 100-mile (161-km) infantry road march. *Preventative Medicine*, 28(2) (1999): 167–173.
5. MAILLER, E. A. and ADAMS, B. B., The wear and tear of 26.2: dermatological injuries reported on marathon day. *British Journal of Sports Medicine*, 38(4) (2004): 498–501.
6. AKERS, W. A. and SULZBERGER, M. B., The friction blister. *Military Medicine*, 137(1) (1972): 1–7.
7. HATCH, K. L., MARKEE, N. L. and MAIBACH, H. I., Skin response to fabric: a review of studies and assessment methods. *Clothing Textile Research Journal*, 10(4) (1992): 54–63.
8. NAYLOR, P. F., Experimental friction blisters. *British Journal of Dermatology*, 67(10) (1955): 327–342.
9. CORTESE, T. A., JR., *et al.*, Treatment of friction blisters: an experimental study. *Archives of Dermatology*, 97(6) (1968): 717–721.
10. KNAPIK, J. J., *et al.*, Friction blisters – pathophysiology, prevention and treatment. *Sports Medicine*, 20(3) (1995): 136–147.
11. GWOSDOW, A. R., *et al.*, Skin friction and fabric sensations in neutral and warm environments. *Textile Research Journal*, 56(9) (1986): 574–580.
12. ZHANG, M. and MAK, A. F., *In vivo* friction properties of human skin. *Prosthetics and Orthotics International*, 23(2) (1999): 135–141.
13. SEO, N. J. and ARMSTRONG, T. J., Friction coefficients in a longitudinal direction between the finger pad and selected materials for different normal forces and curvatures. *Ergonomics*, 52(5) (2009): 609–616.
14. WU, J. Z., DONG, R. G. and SCHOPPER, A. W., Analysis of effects of friction on the deformation behavior of soft tissues in unconfined compression tests. *Journal of Biomechanics*, 37(1) (2004): 147–155.

15. WU, J. Z., *et al.*, Nonlinear and viscoelastic characteristics of skin under compression: experiment and analysis. *Bio-Medical Materials and Engineering*, 13(4) (2003): 373–385.
16. WU, J. Z., *et al.*, Analysis of skin deformation profiles during sinusoidal vibration of fingerpad. *Annals of Biomedical Engineering*, 31(7) (2003): 867–878.
17. HENDRIKS, F. M., *et al.*, A numerical-experimental method to characterize the non-linear mechanical behaviour of human skin. *Skin Research and Technology*, 9(3) (2003): 274–283.
18. HENDRIKS, F. M., *et al.*, Influence of hydration and experimental length scale on the mechanical response of human skin in vivo, using optical coherence tomography. *Skin Research and Technology*, 10(4) (2004): 231–241.
19. XING, M., *et al.*, Skin friction blistering: computer model. *Skin Research and Technology*, 13(3) (2007): 310–316.
20. REYNOLDS, K. L., WHITE, J. S., KNAPIK, J. J., WITT, C. E. and AMOROSO, P. J., Injuries and risk factors in a 100-mile (161-km) infantry road march. *Preventative Medicine*, 28(2) (1999): 167–173.
21. BRUECK, C., The role of topical lubrication in the prevention of skin friction in physically challenged athletes. *Journal of Sports Chiropractic and Rehabilitation*, 14(2) (2000): 37–41.
22. KNAPIK, J. J., REYNOLDS, K. L., DUPLANTIS, K. L. and JONES, B. H., Friction blisters. Pathophysiology, prevention and treatment. *Sports Medicine*, 20(3) (1995): 136–147.
23. CORTESE, T. A., JR., SAMS, JR., W. M. and SULZBERGER, M. B., Studies on blisters produced by friction. II. The blister fluid. *Journal of Investigative Dermatology*, 50(1) (1968): 47–53.
24. SULZBERGER, M. B. and CORTESE, T. A., Observations on the blister base. *British Journal of Clinical Practice*, 22(6) (1968): 249–250.
25. NAYLOR, P. F. D., The skin surface and friction. *British Journal of Dermatology*, 67 (1955): 239–248.
26. GITIS, N. and SIVAMANI, R., Tribometry of skin. *Tribology Transactions*, 47 (2004): 1–9.
27. SIVAMANI, R. K., GOODMAN, J., GITIS, N. V. and MAIBACH, H. I., Coefficient of friction: tribological studies in man – an overview. *Skin Research and Technology*, 9(3) (2003): 227–234.
28. SIVAMANI, R. K., WU, G. C., GITIS, N. V. and MAIBACH, H. I., Tribological testing of skin products: gender, age, and ethnicity on the volar forearm. *Skin Research and Technology*, 9(4) (2003): 299–305.
29. SIVAMANI, R. K., GOODMAN, J., GITIS, N. V. and MAIBACH, H. I., Friction coefficient of skin in real-time. *Skin Research and Technology*, 9(3) (2003): 235–239.
30. DARRIGRAND, A., REYNOLDS, K., JACKSON, R., HAMLET, M. and ROBERTS, D., Efficacy of antiperspirants on feet. *Military Medicine*, 157(5) (1992): 256–259.
31. REYNOLDS, K., DARRIGRAND, A., ROBERTS, D., KNAPIK, J., POLLARD, J., DUPLANTIS, K. and JONES, B., Effects of an antiperspirant with emollients on foot-sweat accumulation and blister formation while walking in the heat. *Journal of the American Academy of Dermatology*, 33(4) (1995): 626–630.
32. NACHT, S., CLOSE, J., YEUNG, D. and GANS, E. H., Skin friction coefficient – changes induced by skin hydration and emollient application and correlation with perceived skin feel. *Journal of the Society of Cosmetic Chemists*, 32(2) (1981): 55–65.
33. AKERS, W. A., Sulzberger on friction blistering. *International Journal of Dermatology*, 16(5) (1977): 369–372.

34. HERRING, K. M. and RICHIE, D. H., JR., Friction blisters and sock fiber composition. A double-blind study. *Journal of the American Podiatric Medical Association*, 80(2) (1990): 63–71.
35. DAVIS, B. L., Foot ulceration: hypotheses concerning shear and vertical forces acting on adjacent regions of skin. *Medical Hypotheses*, 40(1) (1993): 44–47.
36. ZHONG, W., XING, M., PAN, N. and MAIBACH, H. I., Textiles and human skin, microclimate, cutaneous reactions: overview. *Journal of Toxicology: Cutaneous and Ocular Toxicology*, 25(1) (2006): 23–39.
37. XING, M. M. Q., *et al.*, An EFE model on skin-sleeve interactions during arm rotation. *Journal of Biomechanical Engineering – Transactions ASME*, 128(6) (2006): 872–878.
38. ZAVARISE, G., WRIGGERS, P. and SCHREFLER, B. A., On augmented Lagrangian algorithms for thermomechanical contact problems with friction. *International Journal for Numerical Methods in Engineering*, 38(17) (1995): 2929–2949.
39. WRIGGERS, P. and ZAVARISE, G., Application of augmented Lagrangian techniques for nonlinear constitutive laws in contact interfaces. *Communications in Numerical Methods in Engineering*, 9(10) (1993): 815–824.
40. BLACK, M. M., A modified radiographic method for measuring skin thickness. *British Journal of Dermatology*, 81(9) (1969): 661–666.
41. FUNG, Y. C., *Biomechanics-Mechanical Properties of Living Tissues*. New York: Springer, 1984.
42. TONG, P. and FUNG, Y. C., The stress-strain relationship for the skin. *Journal of Biomechanics*, 9(10) (1976): 649–657.
43. GAMBAROTTA, L., *et al.*, *In vivo* experimental testing and model identification of human scalp skin. *Journal of Biomechanics*, 38(11) (2005): 2237–2247.
44. AGACHE, P. and HUMBERT, P., *Measuring the Skin*. Berlin: Springer-Verlag, 2004.
45. BLEMKER, S. S., PINSKY, P. M. and DELP, S. L., A 3D model of muscle reveals the causes of nonuniform strains in the biceps brachii. *Journal of Biomechanics*, 38(4) (2005): 657–665.
46. JAGER, J., Half-planes without coupling under contact loading. *Archives of Applied Mechanics*, 67(4) (1997): 247–259.
47. KENINS, P., Influence of fiber type and moisture on measured fabric-to-skin friction. *Textile Research Journal*, 64 (1994): 722–728.
48. RIDGE, M. D. and WRIGHT, V., Mechanical properties of skin: a bioengineering study of skin structure. *Journal of Applied Physiology*, 21(5) (1966): 1602–1606.
49. XING, M., *et al.*, Skin friction blistering: computer model. *Skin Research and Technology*, 13(3) (2007): 310–316.
50. PIERRE AGACHE, P. H. (ed.), foreword by Howard I. Maibach, *Measuring the Skin: Non-invasive Investigations, Physiology, Normal Constants*. Berlin and New York: Springer, 2004, pp. 748–749.
51. TAKENOCHI, M., SUZUKI, H., and TAGAMI, H., Hydration characteristics of pathologic stratum corneum – evaluation of bound water. *Journal of Investigative Dermatology*, 87(5) (1986): 574–576.
52. KNAPIK, J. J., *et al.*, Influence of boot-sock systems on frequency and severity of foot blisters. *Military Medicine*, 161(10) (1996): 594–598.
53. BATHE, K.-J., *Finite Element Procedures in Engineering Analysis*. New York: Prentice Hall, Englewood Cliffs, 1982, pp. 557–559.
54. LOVE, A. E. H., *A Treatise on the Mathematical Theory of Elasticity*, 4th edn. New York: Dover Publications, 1944.

Transdermal permeation of textile dyes and chemicals

W. ZHONG and M. XING,
University of Manitoba, Canada
and

N. PAN,
University of California, Davis, USA

Abstract: Direct contact and interactions between textiles and skin may cause adverse reactions, including dermatitis induced by chemicals or dyes that remain/reside in the textiles worn next to the skin. Despite the fact that textile dyes/chemicals may provoke irritations when in contact with human skin or when they penetrate the human skin, there has been little reported work to investigate the fundamentals or the mechanisms in the process of transdermal permeation of chemicals. This chapter also introduces studies on the process of transdermal drug delivery, both experimental and numerical. These reports may provide useful tools for the study of textile dyes/chemicals transdermal permeation in the future.

Key words: transdermal permeation, textile dye, drug delivery, stochastic modeling.

21.1 Introduction

The skin is a large barrier organ that protects the human body from environmental hazards (heat, cold, chemicals, mechanical forces, etc.) while maintaining the integrity of the body, whereas the clothing system provides an extra layer(s) of barrier to enhance the aesthetic, thermophysiological and sensorial comfort of the wearer. However, direct contact and interactions between textiles and skin may evoke adverse reactions, even damage or diseases. One of the skin irritation reactions to textiles is dermatitis caused by chemicals or dyes that remain/reside in the textiles worn next to the skin. This chapter starts with an introduction of the key issues of textile dyes/chemicals and skin irritations. There has been little reported work to investigate the fundamentals or process of transdermal permeation of textile dyes/chemicals, while considerable work has been performed to study the transdermal permeation of drugs, which provides useful tools for the study of textile dyes/chemicals transdermal permeation. Therefore, an *in vitro* study of transdermal drug permeation is delineated and its results

analyzed. A stochastic model is also introduced to simulate the process of transdermal permeation of drugs.

21.2 Key issues of textile dyes/chemicals and skin irritations

Numerous chemicals may be incorporated into textiles and clothing during the processes from fiber formation, spinning and fabric construction to dyeing and finishing. These chemicals, when in contact with human skin, may cause allergic contact dermatitis (ACD). Hatch and Maibach [1] reviewed the occurrence of dermatological problems induced by consumer exposure to dyes on clothing, and 31 dyes, mainly dispersed with anthraquinone or azo structures, were found to cause ACD. Subsequently they reviewed the literature concerning textile-dye dermatitis published during the decade before, and four new dye allergens were identified [2]. Studies on ACD prevalence, discussing the amount of ACD cases presented in population, were summarized in 2000 [3]. Most studies, however, were conducted in Europe, primarily Italy. And all the tests were performed by placing a dye mostly dispersed dye with unknown purity, instead of a dyed fabric, directly on the skin.

Accordingly, Hatch *et al.* adopted the term 'textile-dye ACD' in contrast to 'colored-textile ACD' [4], because the former involves more complicated factors, such as dye molecules transferred or released from textiles to the skin and perspiration fastness of the dyes. It was also reported that dyes to which a patient was patch test positive were infrequently identified in the fabric suspected to be the cause of the skin problems [5]. This means that further investigation is desirable in the diagnosis and management of textile-dye ACD.

They further reviewed textile chemical finish dermatitis [6]. Chemicals used on fabrics to improve ten performance characteristics have been detected to have resulted in irritant or ACD. The most significant problem is associated with formaldehyde and N-methylol compounds for durable press fabrics. An updated review on textile dermatitis evoked by resins, additives and fibers ended in 1994 [7]. Textile formaldehyde resins for durable press finish was still the focus, because formaldehyde released from the resin was believed to be the causal agent.

Hatch provided a list of those textile chemicals (dyes, finishes and additives) reported to cause textile dermatitis and the types of fabrics on which these chemicals are most likely to present [8]. Clinical aspects of textile dermatitis and methods available to identify the specific chemical causing a skin problem were also covered. However, the extent of the skin problems caused by textile associated chemicals is hard to define and predict because of a number of factors including variation of skin's sensitivity, capacity of

absorption and reaction among different people, transfer of irritant chemicals from textiles to skin, synergy of sweating, pressure and friction, etc.

Despite the fact that textile dyes/chemicals may provoke irritations by contact with human skin or penetrate into the human skin, there has been little reported work to investigate the fundamentals or the mechanisms in the process of transdermal permeation of chemicals. On the other hand, considerable work has been performed to study the transdermal permeation of pharmaceutical drugs, regarded as an efficient way to administrate medicines that can cause side effects if taken orally. These works, both experimental and numerical, provide useful tools for the study of textile dyes/chemicals transdermal permeation in the future [9].

21.3 An *in vitro* study of transdermal drug permeation

Topical drug application has been widely used to manage skin diseases as well as treating a variety of local and systemic disorders [10, 11]. It is particularly useful for the administrations of drugs that could cause side effects if taken orally. For example, estrogens are effective in treating post-menopause estrogen deficiency, which could lead to osteoporosis, bone fracture and atherosclerosis [12]. However, large doses of estrogen are needed to reach a therapeutic requirement. Adverse effects include elevated hepatic protein during liver metabolic reaction and abnormal fluctuation of hormone in blood [13]. These undesirable effects can be minimized in transdermal absorption [14].

In most studies on the transdermal permeation of drugs, skin was investigated as a single unit, so that knowledge of drug absorption and its properties of transport in stratum corneum (SC), epidermis and dermis is lacking. As a result of the combined use of mathematical model and *in vitro* human skin estradiol transport experiments, our work is an effort to explore the transport properties of the three sub-structures of the skin.

21.3.1 Materials and methods

[¹⁴C]-Estradiol, [4-¹⁴C]-NEC-127 estradiol (molecular weight: 272) with a specific activity of 54.1 mCi/mmol was obtained from DuPont NEN (lot number 3188-151SP), and was kept at 0–4°C until used. The formulation was estradiol 10%, vehicle 90% including ethanal 80%, PEG (propylene glycol 20%). Use of radioactivity was necessary to distinguish between the estradiol [¹⁴C-] which was absorbed through the skin and the estradiol which is a natural constituent of the human body. The single dose was 15 µl/cm² with 0.02 µCi/dose. The diffusion cell was a flow through cell design with 1 cm² diffusion area and 3 ml reservoir fluid. Incubation temperature was 37°C and skin surface temperature 32°C.

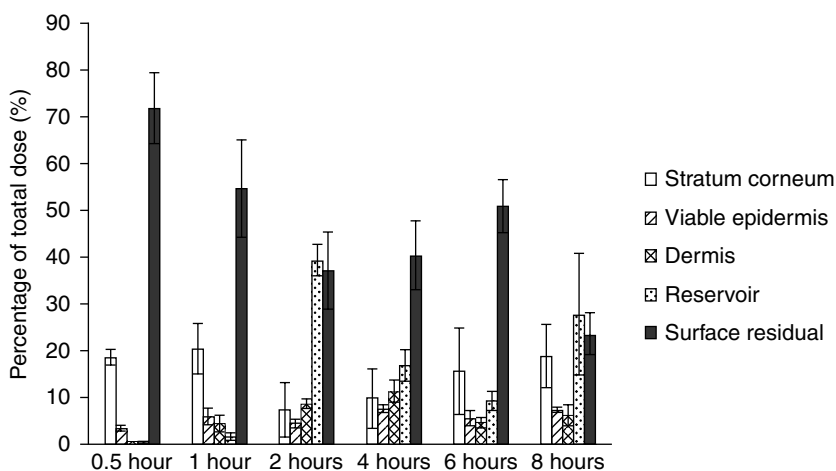
Human skin from four donors obtained by amputation was frozen, stored at -20°C and thawed prior to processing. Following removal of the subcutaneous fat by blunt dissection, individual portions were immersed in water at 60°C for 45 s. The receptor chambers were kept at 37°C throughout the experiment. The samples were taken from the cell at 0.5, 1, 2, 8 h for treatment of SC, epidermis, and viable epidermis (VE) separately. After specified hours, the dose sites were washed using cotton balls (Sherwood Medical, St. Louis, MO), Ivory liquid soap (Procter & Gamble, Cincinnati, OH) and distilled water.

Tape stripping was done after skin washing to analyze the residual dose. The dosed skin was stripped with Scotch[®] cellophane tape 5912 clear (3M Commercial Supply Division, St. Paul, MN) ten times and SC removed for residual chemical. These tapes were then individually placed in borosilicate glass vials with 5 ml of methanol overnight, then 10 ml of scintillation cocktail added for radioactivity assay. The VE was gently stripped with a thin blade, and finally the remaining dermis was assayed.

All samples were measured using a model Tri-Carb 2900 TR (Packard Instruments). Wash samples, skin and receptor fluid were mixed directly with Universal Scintillation Cocktail (ICN Biomedicals, Costa Mesa, CA) for radioactivity assay.

21.3.2 Results and discussion

A summary of the transport and absorption results is given in Tables 21.1 to 21.6 and Fig. 21.1. The initial dose of estradiol for each sample was $15.17\text{ }\mu\text{g}$



21.1 Estradiol transdermal absorption at different times (\pm S.D., $n = 4$).

Table 21.1 After 0.5-h diffusion the residual estradiol in layers (\pm S.D., $n = 4$)

Mass balance	Dose	Surface residual (\pm S.D.)	Stratum corneum (\pm S.D.)	Viable epidermis (\pm S.D.)	Dermis (\pm S.D.)	Reservoir fluid (\pm S.D.)	Total
Percentage	100%	71.65 \pm 7.48	18.63 \pm 1.66	3.45 \pm 0.57	0.59 \pm 0.07	0.41 \pm 0.06	94.72
μ g	15.17	10.87 \pm 1.13	2.83 \pm 0.25	0.52 \pm 0.09	0.090 \pm 0.01	0.062 \pm 0.01	14.37
Average cumulative transported drug (μ g)		14.37	3.5	0.67	0.15	0.06	

Table 21.2 After 1-h diffusion the residual estradiol in layers (\pm S.D., $n = 4$)

Mass balance	Dose	Surface residual (\pm S.D.)	Stratum corneum (\pm S.D.)	Viable epidermis (\pm S.D.)	Dermis (\pm S.D.)	Reservoir fluid (\pm S.D.)	Total
Percentage	100%	54.63 \pm 10.22	20.43 \pm 5.29	6.01 \pm 1.80	4.52 \pm 1.72	1.80 \pm 0.72	87.38
μ g	15.17	8.29 \pm 1.55	3.10 \pm 0.80	0.91 \pm 0.27	0.69 \pm 0.26	0.27 \pm 0.11	13.26
Average cumulative transported drug (μ g)		13.26	4.97	1.87	0.96	0.27	

Table 21.3 After 2-h diffusion the residual estradiol in layers (\pm S.D., $n = 4$)

Mass balance	Dose	Surface residual (\pm S.D.)	Stratum corneum (\pm S.D.)	Viable epidermis (\pm S.D.)	Dermis (\pm S.D.)	Reservoir fluid (\pm S.D.)	Total
Percentage	100%	37.01 \pm 8.08	7.36 \pm 5.70	4.5 \pm 0.88	8.65 \pm 0.98	39.18 \pm 3.35	96.7
μ g	15.17	5.61 \pm 1.23	1.12 \pm 0.86	0.68 \pm 0.13	1.31 \pm 0.15	5.94 \pm 0.51	14.67
Average cumulative transported drug (μ g)		14.67	9.06	7.94	7.26	5.94	

Table 21.4 After 4-h diffusion the residual estradiol in layers (\pm S.D., $n = 4$)

Mass balance	Dose	Surface residual (\pm S.D.)	Stratum corneum (\pm S.D.)	Viable epidermis (\pm S.D.)	Dermis (\pm S.D.)	Reservoir fluid (\pm S.D.)	Total
Percentage	100%	40.33 \pm 7.24	9.92 \pm 6.30	7.65 \pm 0.90	11.31 \pm 2.39	16.88 \pm 3.35	86.08
μ g	15.17	6.12 \pm 1.10	1.50 \pm 0.96	1.16 \pm 0.14	1.72 \pm 0.36	2.56 \pm 0.51	13.06
Average cumulative transported drug (μ g)		13.06	6.94	5.44	4.28	5.56	

Table 21.5 After 6-h diffusion the residual estradiol in layers (\pm S.D., $n = 4$)

Mass balance	Dose	Surface residual (\pm S.D.)	Stratum corneum (\pm S.D.)	Viable epidermis (\pm S.D.)	Dermis (\pm S.D.)	Reservoir fluid (\pm S.D.)	Total
Percentage	100%	50.85 \pm 5.57	15.58 \pm 9.22	5.57 \pm 1.65	4.73 \pm 1.06	9.27 \pm 2.04	85.99
μ g	15.17	7.71 \pm 0.84	2.36 \pm 1.40	0.84 \pm 0.25	0.72 \pm 0.16	1.41 \pm 0.31	13.04
Average cumulative transported drug (μ g)		13.04	5.33	2.97	2.13	1.41	

Table 21.6 After 8-h diffusion the residual estradiol in layers (\pm S.D., $n = 4$)

Mass balance	Dose	Surface residual (±S.D.)	Stratum corneum (±S.D.)	Viable epidermis (±S.D.)	Reservoir fluid (±S.D.)	Total
Percentage	100%	23.64 ± 4.50	18.73 ± 6.64	7.43 ± 0.57	6.20 ± 2.15	27.75 ± 12.93
μg	15.17	3.59 ± 0.68	2.84 ± 1.00	1.13 ± 0.09	0.94 ± 0.32	4.21 ± 1.96
Average cumulative transported drug (μg)		12.70	9.11	6.27	5.14	4.2

(100%). Estradiol absorption in SC reached $2.83 \pm 0.25 \mu\text{g}$ ($18.63 \pm 1.66\%$) after 30 min, peaked at $3.10 \pm 0.8 \mu\text{g}$ ($20.43 \pm 5.29\%$) around 1 h, and then gradually decreased, with a small increase of $2.84 \pm 1.0 \mu\text{g}$ ($18.73 \pm 6.64\%$) at the end of the 8-h period. For the epidermis, however, estradiol absorption peaked at the end of the fourth hour, increasing from $0.52 \pm 0.09 \mu\text{g}$ ($3.45 \pm 0.57\%$) at 30 min to $1.16 \pm 0.14 \mu\text{g}$ ($7.65 \pm 0.90\%$) at the end of 4 h, and to $1.13 \pm 0.09 \mu\text{g}$ ($7.43 \pm 0.57\%$) at the end of the 8-h period. Almost the same pattern existed in the case of the dermis, where absorption peaked at $1.72 \pm 0.36 \mu\text{g}$ ($11.31 \pm 2.39\%$) within 4 h. The estradiol contained in reservoir fluid reached its maximum of $5.94 \pm 0.51 \mu\text{g}$ ($39.18 \pm 3.25\%$) at the end of the second hour, then sharply decreased to $1.41 \pm 0.31 \mu\text{g}$ ($9.27 \pm 2.04\%$) at the end of the sixth hour, but again quickly rose to $4.21 \pm 1.96 \mu\text{g}$ ($27.75 \pm 12.93\%$) at the end of the eighth hour. The cumulative transported estradiol is presented in Tables 21.1 to 21.6. For SC, the peaks (9.06 and 9.11) were reached at the end of the second hour, and the end of the eighth hour, respectively, with their accompanying valleys $6.94 \mu\text{g}$ and $5.33 \mu\text{g}$ at the end of the fourth hour and the end of the sixth hour, respectively. The epidermis and dermis showed transport tendencies similar to SC. They arrived at their maximums of cumulative transported drug at the end of the second and eighth hour, respectively.

Use of the percutaneous route is, as we know, an effective approach to estrogen replacement: it helps diminish side effects resulting from conventional oral estrogen, and enhances patient compliance and satisfaction because the drug release can be properly controlled. Our research revealed that the transport of estradiol through the skin varied significantly from SC to epidermis and to dermis ($p < 0.001$, power = 0.99, ANOVA). Such knowledge of the transport properties of the various layers of the skin provides us with a guide in drug administration. Up to now, however, related research is lacking, so that most researchers still regard the skin as a single unit in their transdermal researches of estrogen. In order to investigate the percutaneous absorption of estradiol, our research included the design of an experiment using extracted radioactive ^{14}C estradiol to evaluate the effects of the drug delivered to the various layers: SC, VE and dermis. By the combination of equations [21.1] and [21.2], it is possible to obtain the diffusion coefficient (J_s), permeability, lag time, and partition coefficient (Table 21.7):

$$J_s = \frac{Dk_m C_0}{\delta} = k_p C_0 \quad [21.1a]$$

$$D = \frac{\delta^2}{6\tau} \quad [21.1b]$$

Table 21.7 The percutaneous absorption parameters of estrogen

	Stratum corneum	Epidermis	Dermis
Thickness (μm)	17	100	500
D (cm ² /h)	1.1×10^{-7}	2.1×10^{-6}	2.0×10^{-5}
K_p (cm/h)	1.14×10^{-3}	7.8×10^{-4}	6.4×10^{-4}
τ (h)	4.2	8	20.8
K_m	17.6	3.7	1.6
$K_{\text{skin/i}}$	2.4		

where D is the diffusion constant within the skin (cm²/h); δ , the thickness (cm) of the human stratum; τ , the lag time (h); K_p , the permeability coefficient through the skin (cm/h); K_m , the skin–vehicle partition coefficient of the drug; and C_0 , the initial concentration of the drug in the test formulation (μg/cm). The solution of Fick’s Second Law [15] is as follows:

$$\frac{Q}{AC} = S[(U)t - 1/6 - \frac{2}{\pi} \sum_{n=1}^{\infty} \frac{(-1)^n}{n^2} \exp(-Un^2\pi^2t)] \quad [21.2]$$

where Q is the accumulative amount of flow through the membrane as measured in the experiment, A is the skin diffusion area (here 1 cm²), and C is the given concentration in the donor cell; S and U are fitted parameters based on the experiment.

The approximate partition coefficients of skin as a complete layer were obtained,

$$K_{\text{skin/i}} = K_{\text{sc/i}} \frac{\delta_{\text{sc}}}{\delta_{\text{skin}}} + K_{\text{ve/i}} \frac{\delta_{\text{ve}}}{\delta_{\text{skin}}} + K_{\text{de/i}} \frac{\delta_{\text{de}}}{\delta_{\text{skin}}} \quad [21.3]$$

All calculated absorption parameters of estrogen are summarized in Table 21.7.

21.4 Stochastic modeling for transdermal drug delivery

To evaluate the efficiency of transdermal drug delivery, extensive work has been performed in studying the process of percutaneous transport or permeation [16]. Both *in vivo* and *in vitro* tests have been conducted [17]. However, experimentation associated with the field of drug delivery is inherently time consuming. Therefore, modeling the process of transdermal

drug delivery is important by reducing the experimental runs, to increase performance in the design of new products, and to develop scientific understanding of the transport process.

Many models have been developed for transdermal drug delivery. Compartment pharmacokinetic models describe the skin as a series of two pseudo-homogeneous membranes (compartments) representing the SC and the VE, respectively. In two-compartment pharmacokinetic models, transport characterized by different transfer rates occurs between four well-stirred compartments: vehicle, SC, epidermis and cutaneous blood [18]. In one-compartment models, only SC is represented as the primary barrier to transdermal permeation, and transport occurs between three well-stirred compartments of vehicle, SC and cutaneous blood [19, 20].

Other models consider the SC a biphasic arrangement of corneocytes (keratinized cellular remnants of epithelial differentiation) interposed with intercellular lipid lamellae, rather than a homogeneous membrane. These are known as 'bricks-and-mortar' models, where the bricks and mortar respectively corresponding to the corneocytes and surrounding intercellular lipid bilayers. Then the governing equations of transport or diffusion are usually numerically analyzed by finite difference methods [21] or finite element methods [22].

Recently stochastic techniques like the random walk model are used to represent the molecular diffusion through SC [23]. The advantage of these models is that they are capable of representing the stochastic nature of the process of diffusion.

Another stochastic approach, the Monte Carlo (MC) technique combined with Cellular Automata (CA), has been used in modeling the process of drug dissolution for a soluble binary drug delivery system [24, 25]. CA is a class of discrete models in which an assembly of objects is allowed to change according to a set of rules. Each object, or a grid cell, can assume a state value from a prescribed set. The state of the grid cells is changed depending on its value and inputs of other connected or neighboring grid cells according to prescribed rules or transfer functions. This approach provides simple tools for studies of complex systems and has been used in a variety of problems including life sciences [26, 27]. However, it has not been used to study transdermal drug delivery.

Here we explore the application of MC methods and CA for investigating the transdermal drug delivery through human skin *in vitro*. In the discrete model of CA, the discrete units in the model are capable of changing their states stochastically according to a set of rules, representing the evolution of the system. A two-dimensional (2-D) discrete model is developed based on the 'bricks-and-mortar' setting. The diffusion of drug molecules from the vehicle to the SC is depicted in a morphologically realistic SC structure. For validation, the predictions generated by the presented model are compared with the *in vitro* experiment on percutaneous absorption of radioactive $^{17}\beta$ -estradiol, as described in the previous section.

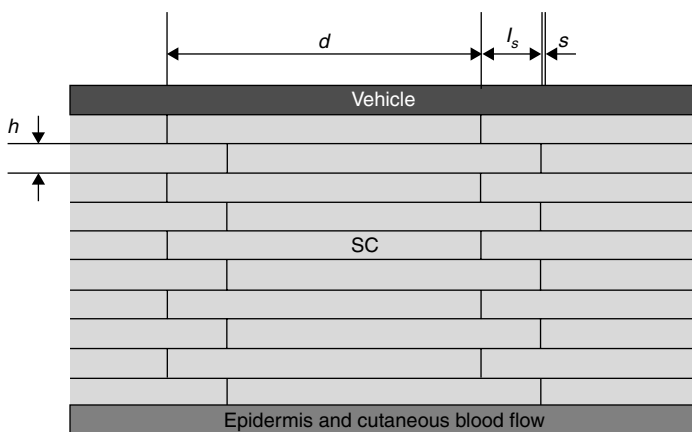
21.4.1 Model description

SC geometry is modeled in a simple case as a 2-D staggered ‘bricks-and-mortar’ structure, as shown in Fig. 21.2. The SC consists of N layers of corneocytes with width d and thickness h . The amount of lateral shift between adjacent corneocyte layers is l_s . The lipid lamella is of thickness s in both horizontal and vertical directions. The diffusion of drug molecules across the SC will occur in the pathway of lipid lamella.

For simulations presented here, we use realistic *in vitro* SC values adapted from the literature [17, 21]: $N = 15$, $d = 31.2 \mu\text{m}$, $h = 1 \mu\text{m}$, $s = 0.1 \mu\text{m}$, $l_s = 6 \mu\text{m}$.

In a 2-D CA model for transdermal drug delivery, the transport process of drug molecules occurs in a 2-D lattice consisting of discrete square units (or grid cells). The size of a grid cell is chosen to be equal to the thickness of the lipid lamella s , which is the smallest in the characteristic sizes of the SC structures. The lattice is developed so that a grid cell is occupied either by corneocytes or lipid lamella, that is, no corneocytes and lipid lamella coexist in any single grid cell. Then three variables are used to represent the states of each grid cell:

- (i) N_i is designated to be 1 or 0, representing a grid cell i occupied by corneocytes or not.
- (ii) L_i is designated to be 1 or 0, representing the grid cell i occupied by lipid lamella or not.
- (iii) C_i is the local concentration (number) of drug molecules in a grid cell. It may have different values in three different cases:



21.2 Staggered bricks-and-mortar model for SC.

Case I: For a grid cell occupied by corneocytes, therefore, $N_i = 1$, $L_i = 0$, $C_i = 0$, as we assumed that corneocytes are impervious to diffusion of drug molecules.

Case II: For a grid cell occupied by lipid lamella, that is, $N_i = 0$, $L_i = 1$, the range of C_i is between 0 and C_{SC} , which indicates the solubility of the drug in SC.

Case III: For a grid cell occupied by neither corneocytes nor lipid lamella, that is, the grid cell could be a cell for vehicle ($N_i = 0$, $L_i = 0$), the range of C_i is between 0 and C_v , which indicates the solubility of the drug in vehicle.

Here, the ratio of drug molecules solubility in SC and vehicle C_{SC}/C_v corresponds to the partition coefficient.

For these variables, N_i and L_i for all grid cells are set at initial configuration and will remain unchanged throughout the simulation, representing a stable state and structure of the SC during the drug delivery process. However, the variable C_i for each grid cell changes with time according to a set of rules as expounded in the following section to represent the diffusion process.

The modeling approach for diffusion is adapted from Barat *et al.* [24], where a number of molecules are allowed to move from one grid cell i to a neighboring one according to a gradient dependent probability p :

$$p = \frac{C_i - C_j}{C_i} \quad [21.4]$$

where C_i is the local concentration for grid cell i , and C_j the local concentration for a neighboring cell. During the simulation, each of the grid cells has four neighbors, and therefore, has four possible moves. Then the move associated with the highest value of p will be regarded as the most probable move, and will be compared with a random number (between 0 and 1). If the probability p is higher than the generated random number, the move will be accepted and performed.

The number of molecules that move from one site to a neighboring one at a time is given by:

$$N = p * X \quad [21.5]$$

where X is a variable uniformly distributed between one and the maximum number of particles allowed on the grid cell, C_{max} :

$$C_{max} = \begin{cases} C_{SC}, & \text{for lipid grid cells} \\ C_v, & \text{for vehicle grid cells} \end{cases} \quad [21.6]$$

Here, C_v is determined by the physiochemical properties of the drug, and can be calculated as:

$$C_v = \frac{DN_A}{M_w N_c} \quad [21.7]$$

where D is the applied dose of the drug, N_A is the Avogadro's constant (6.022×10^{23}), M_w is the molecular weight of the drug, and N_c is the number of vehicle grid cells. And the C_{sc} can be determined by C_v and partition coefficient k , as

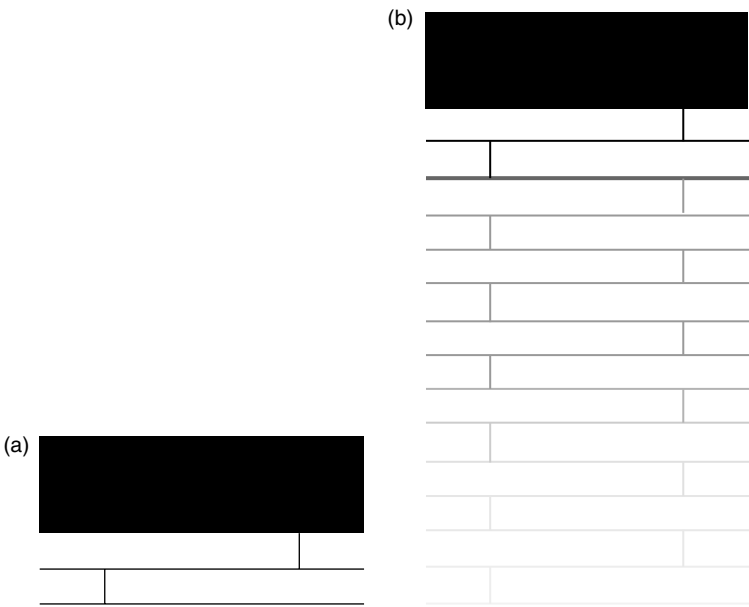
$$k = \frac{C_{sc}}{C_v} \quad [21.8]$$

Within each time step (MC step) of the simulation, all grid cells that contain at least one drug molecule ($C_i \neq 0$) will be scanned for possible changes in their concentration in the way described above. The steps will be repeated until equilibrium or terminated manually.

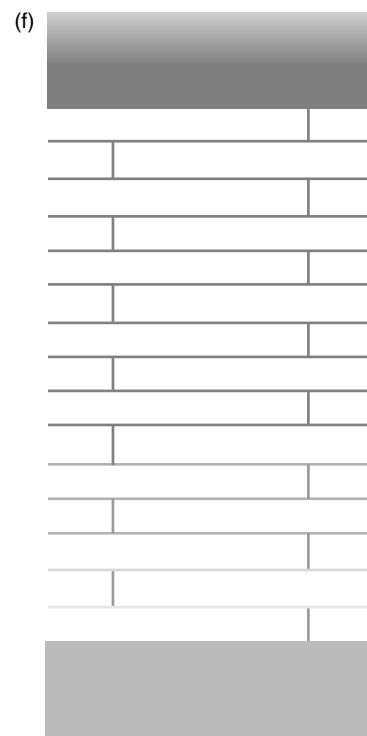
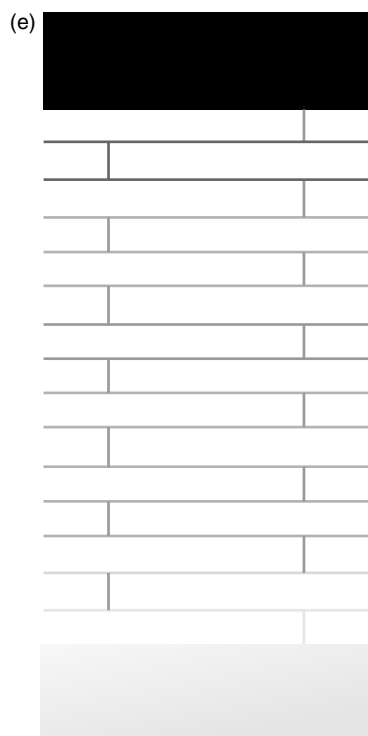
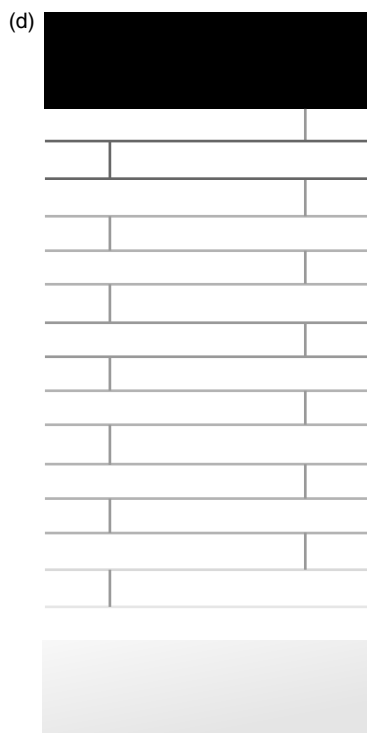
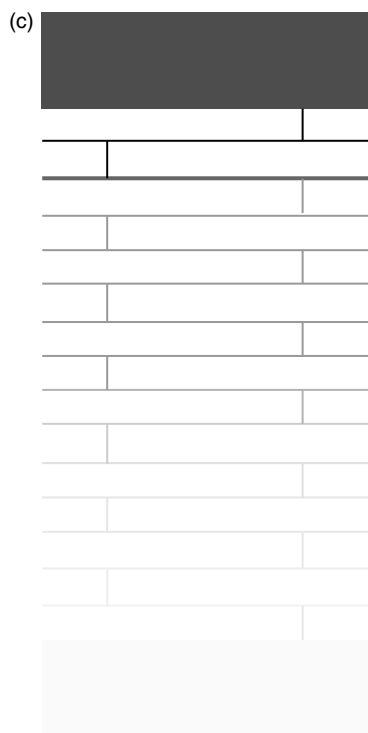
21.4.2 Results and discussion

A computer simulation algorithm was developed for the process of transdermal drug delivery based on the previous section of model description along with the simulation parameters. In simulations described here, 1 real time second is correspondent to 50 MC steps.

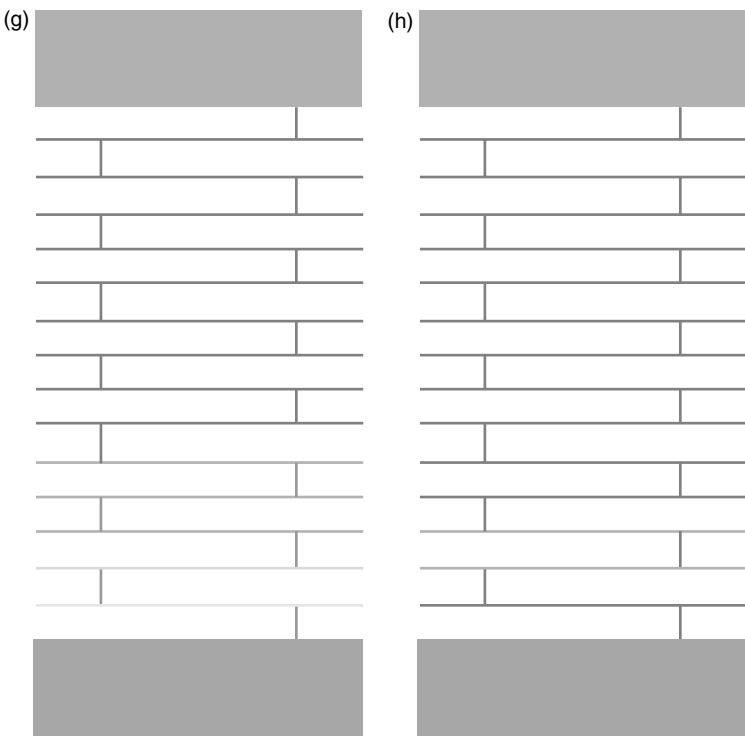
Simulated penetration of drug into a section of the staggered 'bricks-and-mortar' structure of SC after different penetration times is shown in Fig. 21.3.



21.3 Simulated penetration of drug into a section of the staggered 'bricks-and-mortar' structure of SC after different penetration times: (a) 40 s, (b) 15 min, (c) 30 min, (d) 45 min, (e) 1 h, (f) 2 h, (g) 4 h and (h) 8 h.



21.3 Continued.



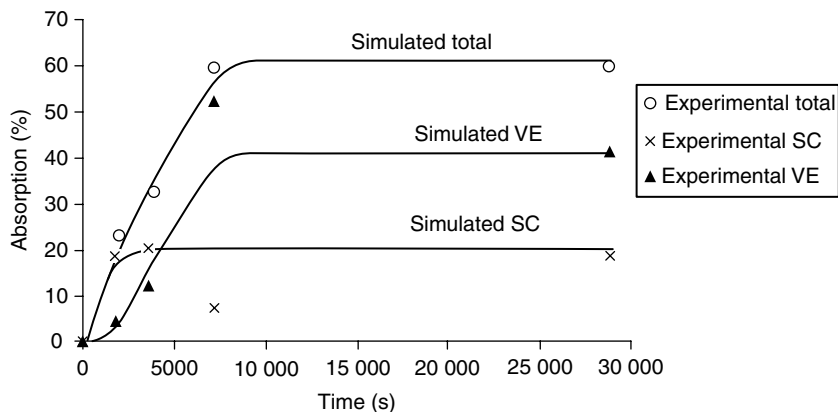
21.3 Continued.

The grey level in the shades is proportional to the local drug concentration. It can be seen from Fig. 21.3 that the drug diffuses at a high speed at the beginning because of high concentration difference, then slows down and reaches equilibrium after about 2 h when concentration difference becomes negligible. The permeation percentage finally reaches a plateau, as shown in Fig. 21.4.

Figure 21.4 shows a comparison between experimental and simulation results of drug absorptions in different layers of epidermis vs. time. The simulated results are shown as continuous lines while experimental data are in discrete symbols. The absorptions in SC and VE were obtained through tape stripping and radiation assay as described previously. And the total absorptions were calculated as the summation of both SC and VE absorption. Both experimental and simulation results agree well, demonstrating the potential use and power of the current approach in studying the process of transdermal drug delivery or percutaneous absorption.

21.5 Conclusion

Despite the demonstrated fact that textile dyes/chemicals cause adverse consequences in contacting human skin and the potential permeation into



21.4 Comparison between experimental and simulation results of drug absorptions in different layers of epidermis vs. time.

the human skin, there has been little reported work to investigate the fundamentals or process of transdermal permeation of chemicals. However, considerable work has been performed to study the transdermal permeation of medical drugs and thus provides useful tools for the study of textile dyes/chemicals transdermal permeation in the future.

Currently, in most transport models for the research of estradiol transdermal absorption, the skin is regarded as a single layer, and the related transport parameters have been the result of taking account of its average conditions. Our research revealed that the identical drug has induced significantly different outcomes in the various sub-layers (i.e. SC, epidermis and dermis) of the skin, and the knowledge of such difference obviously benefits future transdermal drug delivery research, an effort that will render it possible for hormone therapy to be an efficient and safe clinical practice. The experimental approaches and the mathematical model proposed in this study help obtain the transport parameters and predict the transport properties for the complex structure of multiple sub-layer skin.

More specifically we presented a stochastic model based on MC methods and CA to study the molecular transport process through the SC of the human skin, which is a typical process in transdermal drug delivery. The diffusion of drug molecules from the vehicle to the SC is depicted in a morphologically realistic SC structure based on the 'bricks-and-mortar' model. The simulation results agree with the experimental data, showing that the drug diffuses at a high speed at the beginning because of a greater concentration difference, then slows down and reaches an equilibrium after about 2 h when concentration difference disappears.

Clearly the experimental and simulation approaches are useful not only in studying the process of transdermal drug delivery, but also in investigating transdermal permeation of textile dyes/chemicals.

21.6 References

1. HATCH, K. L. and MAIBACH, H. I., Textile dye dermatitis: a review. *Journal of the American Academy of Dermatology*, 12(6) (1985): 1079–1092.
2. HATCH, K. L. and MAIBACH, H. I., Textile dye dermatitis. *Journal of the American Academy of Dermatology*, 32(4) (1995): 631–639.
3. HATCH, K. L. and MAIBACH, H. I., Textile dye allergic contact dermatitis prevalence. *Contact Dermatology*, 42(4) (2000): 187–195.
4. HATCH, K. L., MOTSCI, H. and MAIBACH, H. I., Textile-dye and colored-textile allergic contact dermatitis. *Exogenous Dermatology*, 2 (2003): 206–209.
5. HATCH, K. L., MOTSCI, H. and MAIBACH, H. I., Disperse dyes in fabrics of patients patch-test-positive to disperse dyes. *American Journal of Contact Dermatology*, 14(4) (2003): 205–212.
6. HATCH, K. L. and MAIBACH, H. I., Textile chemical finish dermatitis. *Contact Dermatology*, 14(1) (1986): 1–13.
7. HATCH, K. L. and MAIBACH, H. I., Textile dermatitis – an update .1. Resins, additives and fibers. *Contact Dermatology*, 32(6) (1995): 319–326.
8. HATCH, K. L. and MAIBACH, H. I., Textiles. In: L. Kanerva, *et al.* (eds.) *Handbook of Occupational Dermatology*. Berlin: Springer Verlag, 2000, pp. 622–636.
9. ZHONG, W., *et al.*, Textiles and human skin, microclimate, cutaneous reactions: an overview. *Cutaneous and Ocular Toxicology*, 25(1) (2006): 23–39.
10. XING, M. M. Q., *et al.*, *In vitro* human topical bioactive drug transdermal absorption: estradiol. *Cutaneous and Ocular Toxicology*, 28(4) (2009): 171–175.
11. BRONAUGH, R. L. and MAIBACH, H. I. (eds.), *Percutaneous Absorption: Drugs, Cosmetics, Mechanisms, Methods*, 4th edn. Boca Raton, FL: Taylor and Francis, 2005.
12. BIRGE, S. J., The use of estrogen in older women. *Clinics in Geriatric Medicine*, 19(3) (2003): 617–627.
13. POWERS, M. S., *et al.*, Pharmacokinetics and pharmacodynamics of transdermal dosage forms of 17-beta-estradiol – comparison with conventional oral estrogens used for hormone replacement. *American Journal of Obstetrics & Gynecology*, 152(8) (1985): 1099–1106.
14. JEWELEWICZ, R., New developments in topical estrogen therapy. *Fertility and Sterility*, 67(1) (1997): 1–12.
15. CRANK, J., *Mathematics of Diffusion*. Oxford: Oxford University Press, 1975, pp. 47–48.
16. ZHONG, W., *et al.*, A stochastic model for transepidermal drug delivery. *Skin Research and Technology*, 15(4) (2009): 407–411.
17. AGACHE, P. and HUMBERT, P., *Measuring the Skin*. Berlin: Springer, 2004.
18. MCCARLEY, K. D. and BUNGE, A. L., Physiologically relevant two-compartment pharmacokinetic models for skin. *Journal of Pharmaceutical Sciences*, 89(9) (2000): 1212–1235.
19. MCCARLEY, K. D. and BUNGE, A. L., Physiologically relevant one-compartment pharmacokinetic models for skin. 1. Development of models. *Journal of Pharmaceutical Sciences*, 87(4) (1998): 470–481.
20. REDDY, M. B., MCCARLEY, K. D. and BUNGE, A. L., Physiologically relevant one-compartment pharmacokinetic models for skin. 2. Comparison of models when combined with a systemic pharmacokinetic model. *Journal of Pharmaceutical Sciences*, 87(4) (1998): 482–490.

21. WANG, T. F., KASTING, G. B. and NITSCHKE, J. M., A multiphase microscopic diffusion model for stratum corneum permeability. I. Formulation, solution, and illustrative results for representative compounds. *Journal of Pharmaceutical Sciences*, 95(3) (2006): 620–648.
22. FRASCH, H. F. and BARBERO, A. M., Steady-state flux and lag time in the stratum corneum lipid pathway: results from finite element models. *Journal of Pharmaceutical Sciences*, 92(11) (2003): 2196–2207.
23. FRASCH, H. F., A random walk model of skin permeation. *Risk Analysis*, 22(2) (2002): 265–276.
24. BARAT, A., RUSKIN, H. J. and CRANE, M., Probabilistic methods for drug dissolution. Part 2. Modelling a soluble binary drug delivery system dissolving *in vitro*. *Simulation Modelling Practice and Theory*, 14(7) (2006): 857–873.
25. BARAT, A., RUSKIN, H. J. and CRANE, M., Probabilistic models for drug dissolution. Part 1. Review of Monte Carlo and stochastic cellular automata approaches. *Simulation Modelling Practice and Theory*, 14(7) (2006): 843–856.
26. WOLFRAM, S., *Theory and Applications of Cellular Automata*. Singapore: World Scientific, 1986.
27. CHOPARD, B. and DROZ, M., *Cellular Automata Modeling of Physical Systems*. Cambridge: Cambridge University Press, 1998.

- AA30B, 216, 218
AA40B, 217
AA50B, 214, 216
AA30R, 218
AA50R, 214, 216
AAMA30B, 218
AATCC *see* American Association of
Textile Chemists and Colorists
AATCC 183–1998, 48, 51
AATCC Test Method 115–2005, 40
AATCC Test Method 134–2006, 40
absorption, 257
acceleration correction, 84
acridines, 378–9, 380
acrylamide, 200
activated carbon, 259
active camouflage, 251, 252
active drag, 232, 235
active-wear clothing, 176
adaptive camouflage *see* active camouflage
Add-Delete, 74
adsorption, 257–9
Aedes mosquitoes, 407
aerogel method, 454
aerosol filtration media, 264
aerospace textiles, 175
air permeability, 445, 450
air plasma treatment, 20–1
ALA method *see* augmented Lagrange
algorithm method
alizarin, 382–3
chemical structure, 382
alkanethiol, 328
allergic contact dermatitis (ACD), 490
alumina, 259
American Association of Textile
Chemists and Colorists, 39
American Society of Testing and
Materials (ASTM), 39
ammonium polyphosphate (APP), 113
Amonton's law, 273
amorphous hydrogel, 307
ANOVA, 495
ANSYS system, 477
ANSYS V.6.1, 468
anthraquinone, 490
antibacterial colorants
chemical structure
alizarin and purpurin, 382
anthocyanidine colorants and
their glycoside form, 391
berberine and ampelopsin, 377
carthamin, 386
cationic dyes, 380
curminic acid and kermesic acid,
383
flavonol colorants, 389
gallotannins, ellagitannins, com-
plex and condensed tannins, 392
lawsone and juglone, 385
lecanoric acid and usnic acid, 394
luteolin, 388
phycocyanobilin and prodigiosin,
394
prontosil and methylene blue, 379
shikonin and alkanin, 384
micro-organisms, 393–5
anthraquinones produced by
C. lunata, 395
natural antibacterial colorants, 381–3
anthocyanins, 390–1
flavonoids, 387–90
quinones, 382–7
tannins, 391–3

- antibacterial colorant (*cont.*)
 - photo-activated antibacterial colorants, 395–6
 - synthetic antibacterial colorants, 378–81
 - acridines, 378–9
 - quaternary ammonium antibacterial dyes, 380–1
 - sulfamid-based dyes, 379–80
 - textiles, 376–96
 - converting Troxerutin to vinyl monomer, 378
- antimicrobial textiles
 - applications
 - protective clothing and linen products, 371
 - surgical gowns and drapes, 371
 - benzophenone and Rose Bengal
 - antimicrobial abilities, 370
 - photo-sensitisers, 370
 - development, 363–8
 - Halamine chemistry, 367–8
 - silver ion or other metals, 366–7
 - future trends, 371
 - medical applications, 360–71
 - performance, 368–9
 - principles, 361–3
 - difference in antimicrobial performance, 362
 - medical textiles and diseases
 - transmission, 361–2
 - requirements for antimicrobial medical textiles, 362–3
 - quaternary ammonium salts, 363–6
 - antimicrobial colorants structure, 365
 - antimicrobial effects, 364
 - similar compounds, 363–6
 - structures, 364
 - technologies, 363, 369–70
 - current, 363
 - new, 369–70
- antistatic agents, 32, 33–4
- antistatic textiles, 27–42
 - evaluation, 39–41
 - direct methods, 39–40
 - fabric cling test, 41
 - indirect methods, 40
 - simulation methods, 40–1
 - future trends, 41–2
 - effect of washing on surface anti-static coating, 42
 - R711 nanoparticulates, 42
 - principles, 28–32
 - key principles, 31–2
 - static charge generation mechanisms, 28–31
 - triboelectric series, 30
 - role, 33
 - types, 33–9
 - dimethyloldihydroxyethyleneurea and dimethylolethyleneurea, 36
 - durable, 35–8
 - graft polymerisation, 38
 - monomers with non-ionic or ionic groups, 37
 - non-durable, 34–5
 - phosphoric acid esters, 35
 - polyamines with polyoxyethylene groups, 36
 - polyhydroxypolyamines, 36
 - quaternary ammoniums, 34
- Aquablade swimwear, 230
- aramid fibres, 274
- aramids, 105–7
- Army Field Dressing, 313
- aromatic polyamides *see* aramids
- aromatic polyester fibre, 110
- artificial kidney, 294–6
- AS/NZS 4399, 48, 50
- ash test, 40
- ASTM 6603, 51
- ASTM D 6544, 51
- ASTM F2669–09, 436
- atomic force microscopy (AFM), 10–11
- attenuated total reflectance (ATR), 15
- augmented Lagrange algorithm
 - method, 466
- automotive textiles, 177
- Avogadro's constant, 500
- Avora, 109
- axis-aligned bounding box (AABB), 85
- B-spline skinning, 65
- ballistic and fragmentation
 - protection, 253
- ballistics, 253–255

- bamboo-carbon modified polyesters (BCMP), 191–2
- BASF, 332
- Basofil, 107
- battlefield dressing, 313
- bentonite, 313
- bio-ceramics, 191–2
- bioactive textiles, 301–3
- bioartificial liver, 296
- biocidal textiles, 362
- biocides, 363, 366, 368
- biocompatibility, 297–8
- biomechanics
 - skin/fabric interactions, 462–86
 - computer model: skin friction blistering, 477–86
 - EFE model of skin/sleeve interactions during arm rotation, 465–77
- biostatic materials, 362
- bisphenol A bis(diphenyl phosphate), 113
- body scanning, 65
- Boltzmann constant, 279
- Boltzmann statistics, 28–9
- breathable fabric, 165, 208
- British Redcoat uniforms, 250
- Broglie wavelength, 9
- brominated flame retardants, 113
- burst strength, 299
- BVD Company, 229
- calcium alginate, 307
- camera calibration, 67–9, 68
- camouflage, 250–3
- capillary rise method, 19
- carbon nanotubes (CNTs), 355
- cardiovascular implantables, 299
- Cassie–Baxter contact angle, 344, 349
- Cassie–Baxter equation, 321, 345, 348, 349, 351, 352
- Cassie–Baxter model, 344–5, 346
- CDC guidelines, 371
- cell adhesion, 302
- Cellular Automata (CA), 497
- cellular automata probabilistic model, 276
- cellulose, 116
 - cellulose-based textiles
 - finishing treatments, 116–20
 - flame retardancy with sulfur derivatives, 119
 - grafting flame retardant monomers to cellulose, 119–20
 - inorganic phosphates, 116–17
 - organophosphorus compounds, 117–19
- Centre for Disease Control and Prevention (CDC), 436
- ceramic nanoparticulates, 41–2
- Chagas disease, 407
- chain stripping, 102
- charge-induced charge separation, 31
- chelating agents, 366
- chemical and biological warfare (CBW) agents, 255
- chemical modifications
 - improving superhydrophobic coatings for textiles, 320–35
 - applications, 331–4
 - chemical modifications for fabricating rough surfaces on textiles, 323–6
 - future trends, 334–5
 - hydrophobisation for lowering the rough textiles surface energy, 327–9
 - materials with low surface energy
 - nanoscaled coating, 329–31
 - superhydrophobic textiles key principles, 321–2
- chemical vapour deposition, 5
- chemicals *see* textiles dyes
- chemisorption, 258
- chitosan, 219, 220, 286–7, 313
- 2-chloroethyl-ethyl sulphide (CEES), 456
- chronic dermal ulcers, 310–11
- Chrysanthemum cinerarifolium*, 409
- clothing
 - ultraviolet protection, 45–57
 - environment and fabric use, 55–6
 - fabric colour, dyes and UV absorbers, 53–5
 - fabric type and construction, 51–3
 - outlook, 56–7

- clothing (*cont.*)
 - sun-protective clothing standards, 50–1
 - UPF *in vitro* and *in vivo* testing, 48–50
- clothing protection technology, 269–85
 - developments, 274–84
 - cell *i* in a 3-D Ising model with its neighbours, 278
 - 3-D Ising model for filtration process, 282
 - energy difference due to airflow, 280
 - filter efficiency vs particle size simulation and experimental results, 283
 - model description, 277–81
 - modelling and simulation, 275–85
 - parameters for fibre and aerosol particle, 283
 - textile components, 274–5
 - future trends, 284–5
 - key issues of protective clothing, 270–4
 - microclimate, 270–2
 - skin reactions and irritations caused by textiles, 272–4
- colorants *see* antibacterial colorants
- comfort factor, 164
- condensed phase action, 104
- conductive textiles, 27–42
 - evaluation, 39–41
 - direct methods, 39–40
 - fabric cling test, 41
 - indirect methods, 40
 - simulation methods, 40–1
 - future trends, 41–2
 - effect of washing on surface anti-static coating, 42
 - R711 nanoparticulates, 42
 - principles, 28–32
 - key principles, 31–2
 - static charge generation, 28–31
 - triboelectric series, 30
 - role, 33
 - types, 38–9
- conductivity, 40
- constitutive equations, 276
- contact-angle, 236–8, 341–3, 349–50
 - hysteresis, 349–50
 - defined, 349
 - measurement, 16–18
 - surface tension, 341–3
 - drop on a flat surface, 342
 - wettability, 341
- contact-induced charge separation, 28–9
- contact layer dressings, 307
- continuous renal replacement therapies (CRRT), 295
- cotton fabrics, 141
- cross-linking, 102
- Cuprophane, 295
- Curcuma longa*, 377
- CVD *see* chemical vapour deposition
- cyclodextrins, 446
- cylindrical mapping, 81–2
- 3D body imaging
 - collision detection and response, 85–9
 - edge–edge collision, 88
 - edge–edge collision detection and response, 87–9
 - point-triangle collision, 86–7
 - subject surface vertex and a panel triangle collision, 86
 - functional textiles, 64–94
 - future trends, 93–4
 - sewability and fit assessment, 91–3
 - sewability of the pattern, 93
 - virtual dressing integrated system, 92
- stereovision, 66–72
 - data flow diagram, 68
 - foreground segmentation and coarse/refined disparity map, 72
 - pair of stereo images, 68
 - stereo imaging system setup, 67
 - stereo matching, 69–72
 - stereo matching algorithm, 70
 - system calibration, 67–9
 - system setup, 66–7
- surface modelling, 72–80
 - 3D surface models, 80
 - data resampling, 72–4

- edge collapse, 76
- initial mesh generation, 74–5
- Loop's evaluation rule for a vertex point, 78
- mesh simplification, 75–7
- mesh subdivision and optimisation, 77–80
- mesh subdivision by mesh split, 77
- modified Loop's evaluation rule for an edge point, 78
- optimised control mesh, subdivision mesh, and shaded model, 79
- original scan data, 73
- simplified mesh and its shaded model, 77
- triangulation of torso, 75
- virtual dressing, 80–91
 - adaptive sewing force, 83–5
 - body skeleton and initial positioning of panels, 81
 - hanging cloth with different strain control methods, 90
 - image series, 91
 - initial positioning and panel rolling, 80–3
 - merging nodes/particles on seam-lines, 85
 - multi-panel positioning, 83
 - self-rolling through cylindrical mapping, 82
 - sewing force, 84
 - strain control and size stability, 89–91
 - strain control through velocity adjustment, 90
- Dacron, 229
- Dacron vascular grafts, 302–3
- Darcy's law, 276
- DawaPlus, 419
- DawaPlus 2.0, 420–1
- decabromodiphenyl ether (DecaBDE), 121, 122
- Defender-M, 250
- Deflexion, 255
- Degussa, 41
- Delaunay triangulation algorithm, 73–4
- deltamethrin, 410, 419
- DEMEP, 121
- dengue fever, 407
- denticles, 230
- desert marine, 250
- dextranomer beads, 307
- dichlorotribromophenyl phosphate (DCTBPP), 115
- dielectric barrier discharge (DBD), 20
- diffusion, 263–4
- dimethyloldihydroxyethyleneurea, 36
- dimethylolethyleneurea, 36
- 3-(dimethylphosphono)-N-methylolpropionamide (DMPMP), 117, 118
- DIN 53 923, 18
- dioctyle phthalate (DOP), 282
- direct coupling reaction, 6
- 'dirty bombs,' 260
- disparity gradients, 71–2
- disparity space image (DSI), 69
- Dow Corning 5700, 365
- Dr Scholl's Memory Fit, 152
- dressing simulation, 80
 - see also* virtual dressing
- dry heat loss, 165
- dual-sensitive (temperature and pH sensitive) polymers/hydrogels, 202–4
- Du Pont, 229
- DuPont NEN, 491
- Dupre equation, 342
- Dupre–Young equation, 342
- durable antistatic finishes, 36–8
- DuraNet, 415, 419
- dyes, 53–5, 379–81
 - quaternary ammonium, 380–81
 - sulfamid-based, 379–80
 - see also* textiles dyes
- DYNA3D, 468
- Dyneema, 253, 254
- edge collapse, 75–6
- edge points, 77
- edge–edge collision, 87–9
- electrical-active shape memory fabric, 137
- electroactuating fibres, 219–21
- electroless deposition, 6–7

- electromagnetic radiation, 185
- electron spectroscopy for chemical analysis (ESCA) *see* x-ray photoelectron spectroscopy
- electrospinning, 300, 449–50
- electrostatic attraction, 264
- Electrostatic Discharge (ESD) Association, 39
- electrostatic induction *see* charge-induced charge separation
- EN 13758–13751, 51
- EN 13758–13752, 51
- encapsulation, 260–1, 262
- end-scission, 102
- Environmental Protection Agency, 435
- EPA *see* Environmental Protection Agency
- estradiol, 491
 - residual in layers after 0.5-h diffusion, 493
 - residual in layers after 4-h diffusion, 494
 - transdermal absorption at different times, 492
- estrogens, 491
 - percutaneous absorption parameters, 496
- Exolit 5060, 113
- expanded polytetrafluoroethylene, 299
- expanded polytetrafluoroethylene composites, 262
- extracorporeal liver assisted device (ELAD), 296
- extracorporeal medical textiles, 294–97
- fabric blends, 100
- fabric cling test, 40–1
- fabric colour, 53–5
- fabric porosity, 53
- fabric structure, 275
- far infrared, 186
- far infrared textiles, 184–94
 - applications, 192–3
 - sportswear, 192
 - therapeutic, 192–3
 - warmth, 193
 - benefits and limitations, 193–4
 - FIR in relation to functional textiles, 190–2
 - bio-ceramics, 191–2
 - FIR fibres and fabrics, 190–1
 - FIR therapy, 186–90
 - FIR health effects, 187–90
 - phototherapy, 186–7
 - future trends, 194
 - IR principles, 185–6
 - electromagnetic radiation
 - principles, 185
 - far infrared, 186
 - location and breakdown within the electromagnetic spectrum, 186
 - overview, 184–5
- Fastskin, 230, 239
- Fastskin FSII, 230
- FE model *see* finite element model
- fibres, 198
- Fibrin Sealant, 313
- fibrous aerosol filters, 263, 264
- Fick's Second Law, 437, 496
- fillers, 307
- filtration efficiency, 275–6, 282–3
- finite element method, 464
- finite element model, 463
- Fir-Tex, 191, 193
- FIR therapy, 186–90
- fire-retardant textiles, 250
- fit assessment, 91–3
- flame retardant additives, 103–5
- flame retardant functional textiles, 98–123
 - additives, 103–5
 - fibres from addition of non-reactive additive to polymer, 111–14
 - additives for wet spun fibres, 113–14
 - melt additives, 111–13
 - phosphorous-containing flame-retardant additive, 114
- finishing treatments, 114–21
 - ammonium salts of phosphoric and polyphosphoric acid, 117
 - cyclic phosphonate compounds for thermosol application, 115

- guanidine phosphate salts, 117
- hydroxyl functional oligomeric organophosphorus compound, 119
- natural fibre fabrics, 116–21
- organophosphorus flame retardants for cellulose, 118
- synthetic fibre fabrics, 114–16
- flame retardation of textile materials, 105–21
 - aromatic polyester, 110
 - fibres from inherently flame retardant polymers, 105–11
 - inherently flame retardant polymers, 106
 - inherently flame retardant polymers fibre properties, 111
 - phosphorus-containing monomers for polyester, 109
- flammability and thermal behaviour, 99–102
 - fabric construction, 99–100
 - textile fibre types, 100–1
 - thermal behaviour of polymers, 101–2
- test standards, 122–3
 - standard test methods, 123
- flame retardant polyesters, 109
- flame retardants, 98–123
 - addition of non-reactive additive to polymer, 111–14
 - environmental issues, 121–2
 - finishing treatments, 114–21
 - flammability and thermal behaviour, 99–102
 - test standards, 122–3
 - textile materials, 105–21
 - types, chemistry and mode of action of additives, 103–5
- flame retardation, 98–123
- Flamestab NOR 116, 113
- flammability, 99–102
 - textile fibre, 100–1
- Flammentin FMB, 117
- flavonoids, 387–90
 - antimicrobial functions, 390
 - flavones, 388
 - flavonols, 388–9
- Flory–Rehner polymer solution theory, 438
- Flovan CGN, 117
- fluid mechanics, 231–4
- fluoroalkylsilanes, 327
- fluorocarbons, 445
- form drag *see* pressure drag
- formaldehyde resins, 490
- Fortron, 108
- Fourier-transform infrared spectroscopy (FT-IR), 15
- friction blisters, 463
- friction coefficient, 272–3
- functional clothing, 64
- functional medical textiles
 - bioactive textiles design, 301–3
 - biomolecules in conferring bioactive function, 301–3
 - developments and their mechanism of action, 293–314
 - extracorporeals and implantables, 294–7
 - artificial kidney, 294–6
 - bioartificial liver, 296
 - mechanical lung, 297
 - non-implantables, 303–14
 - bed sheet and non-woven care sheet designed to wick moisture away, 312
 - bed sore prevention incontinence device, 309
 - haemorrhage control dressings, 312–14
 - pressure ulcer prevention materials, 311–12
 - stages of wound healing, 304
 - structure and composition, 304–11
 - structure and composition, 297–301
 - biocompatibility, 297–8
 - cardiovascular implantables, 299
 - implantable biomaterials for tissue engineering, 300–1
- functional shape memory textiles, 131–57
- future trends, 155–7
- SMA applications in textiles, 133–8
 - effect on textiles, 134–8

- functional shape memory textiles (*cont.*)
 - electrical-active shape memory fabric, 137
 - functionality of insulating property, 136
 - pseudoelasticity, 133
 - shape memory dress with SMA wires, 136
 - shape memory fabric with SMA wires, 135
 - shape recovery fabric with nitinol SMA wires, 135
 - smart garment with SMA wires, 137
- SMA shape memory mechanisms, 132–3
 - one-way and two-way SME, 132
- SMP applications, 140–55
 - basic fabric parameter, 147
 - crease retention, 141
 - easy wear and perfect match, 150
 - end-capped SMPU oligomers synthesis, 140
 - fibre spinning, 144–5
 - good shape retention, 142
 - improved dimensional stability, 143
 - moisture-responsive SMPs for sweat intelligent management, 155
 - Nike ‘Sphere React’ shirt with smart vent structure, 154
 - pressure of enlarged fabrics to ‘wearer,’ 149
 - shape memory foams, 151–2
 - shape memory hollow fibre, 146
 - shape memory nano-fibres, 151
 - shape memory textiles with good damping properties, 152
 - smart breathability, 152–3
 - SMP coating, 140–4
 - SMP fabrics and garments, 146–51
 - SMP fibres prepared by wet and melt spinning, 145
 - SMPU fibre stress–strain curve vs other synthetic fibres, 145
 - SMPU oligomers reaction with cotton, 140
 - strain recovery ratio, 147
 - synthesis routine of SMPU with pyridine units, 154
 - textile products made of shape memory foams, 152
 - untreated and treated wool fabrics, 142
 - water/moisture-driven SME, 153–5
 - wrinkle-free effect, 141
- SMP shape memory mechanisms, 138–9
 - thermal active SME, 139
- strain recovery ratio
 - 100% cotton knitted fabric, 148
 - 100% shape memory knitted fabric, 147
 - 50% SM fibre and 50% cotton knitted fabric, 148
- untreated and treated wool fabrics texture, 144
- see also* shape memory alloys; shape memory polymers
- functional smart textiles
 - using stimuli-sensitive polymers, 198–21
 - drawbacks and limitations of current SSP/hydrogels, 204–5
 - smart functional textile, 205–21
 - stimuli-sensitive polymers, 198–204
- functional textiles
 - 3D body imaging and fit, 64–94
 - future trends, 93–4
 - sewability and fit assessment, 91–3
 - stereovision, 66–72
 - surface modelling, 72–80
 - virtual dressing, 80–91
 - flame retardant, 98–123
 - environmental issues, 121–2
 - flammability and thermal behaviour, 99–102
 - test standards, 122–3
 - textile materials, 105–121
 - types, chemistry and mode of action, 103–5
- surface modifications, 3–24
 - applications, 19–23
 - future trends, 23–4
 - physical and chemical characterisation, 8–19
 - types, 4–7

- gain factor, 349
- gas-phase action, 103
- Gauss–Seidel iteration, 89–90
- gauze packing, 307–8
- glass fibre, 108, 273
- Gore-tex, 262
- graft polymerisation, 6, 37
- grafting, 6
- grid density, 73
- Gulf stream stitch, 229

- haemorrhage control
 - dressings, 312–14
- Halamine chemistry, 363, 367–8
- halogen-based flame retardants, 103
- halogen compounds, 111
- Hamaker constant, 278, 279
- HBCD *see* hexabromocyclododecane
- HDPE *see* high-density polyethylene
- heat-induced charge separation, 31
- heat release rates, 101
- Heim, 109
- HemCon, 313
- hemodialyzers, 294
- henna *see* *Lawsonia inermis*
- hexabromocyclododecane, 121
- hexafluorozirconate, 120
- high-density polyethylene, 416
- high-performance fibre poly{diimid
azopyridinylene(dihydroxy)
phenylene} *see* M-5 fibre
- hoefnagels, 329
- Honestometer, 39–40
- hydrated salts, 169
- hydrocolloids, 306
- hydrophilic monomers, 37
- hydrophobisation, 327–9
 - alkyl molecules, 328–9
 - fluorinated molecules, 327–8
 - non-fluorinated polymer, 329
 - silicon compounds, 329
 - surface reactive molecules for low-
surface-energy modifications, 327
- hydrothermal synthesis, 324–5
- hydroxy-functional organophosphorus
oligomer (HFPO), 118, 119
- hydroxymethyl phosphinyl propanoic
acid, 110

- ICON-MAXX, 424
- impermeable fabrics, 165
- implantables, 294–7
 - implantable biomaterials for tissue
engineering, 300–1
 - electrospinning, 300
 - phase separation, 301
 - self-assembly, 300–1
 - role of functionality, 297–1
 - biocompatibility, 297–8
 - cardiovascular implantables,
299
- inertial impaction, 263
- infrared functional textiles *see* far
infrared textiles
- inherently flame retardant fibres, 99,
105–11
- inherently flame retardant polyesters,
109–10
- inherently flame retardant polymers,
105, 106, 111
- inorganic phosphates, 116–17
- insecticides, 409–14
 - insecticide-laden textiles key issues,
414
 - pyrethroids, 409–13
 - chemical structure, 410
 - repellents and synergist chemical
structure, 412
 - treated textiles application and
effectiveness, 413–14
- insects
 - diseases, 405–9
 - Chagas disease, 407
 - dengue fever, 407
 - leishmaniasis, 407–8
 - Lyme disease, 408
 - lymphatic filariasis, 408
 - vector-borne diseases and associ-
ated vector control agents, 406
 - West Nile disease, 408
 - pyrethroid-laden textiles protection
from biting, 404–26
 - bednets *in situ* treatment and
other textiles, 424–25
 - factory-produced long-lasting insecti-
cidal nets and textiles, 414–24
 - future trends, 425–26

- insects (*cont.*)
 - insecticide-laden textiles key issues, 414
 - insecticide-treated textiles application and effectiveness, 413–14
 - insecticides, repellents and synergist chemical structure, 412
 - pyrethroids and other insecticides, 409–13
 - pyrethroids chemical structure, 410
- integrins, 302
- intelligent-polymers *see* stimuli-sensitive polymers (SSP)
- interactive chronic wound dressings, 308, 310
- interception, 263
- Interceptor, 419
- International Standards Organisation (ISO), 39
- interpenetrating network (IPN) material, 266
- interpenetrating polymer networks (IPN), 204
- invisibility cloak, 253
- IR light, 185
- iridescence, 252
- Ising model, 276–7

- Jacobi iteration, 89–90
- Jantzen Company, 228, 229
- Joint-Service Lightweight Integrated Suit Technology (JSLIST), 250

- K-O TAB 1-2-3, 424
- kaolin, 313
- Kappaflam P 31, 115
- Kawabata Thermolabo apparatus, 271
- Keggin-type POM, 456
- Kermel, 105
- KES-SE Frictional Analyzer, 273
- Kevlar, 105, 250, 253, 255, 274
- kidney *see* artificial kidney

- Lagrange multiplier method, 466, 467, 477
- lake, 383
- Laplace equation, 440
- Lastex, 229

- latent heat, 166
- lattice Boltzmann model, 276
- Lawsonia inermis*, 376–7
- leishmaniasis, 407–8
- LifeNet, 420
- Lifshitz theory, 278
- Lifshitz–van der Waals (LW), 342
- light therapy *see* phototherapy
- limiting oxygen index (LOI), 101
- liquid absorptive capacity, 16, 18
- liver *see* bioartificial liver
- LLINs *see* long-lasting insecticidal nets
- long-lasting insecticidal nets, 414–21
 - effectiveness in controlling vector-borne diseases, 421
 - effectiveness measurement, 414–15
 - factory-prepared, 415–21
 - commercially available LLINs that contain pyrethroids, 417–18
- Loop's subdivision algorithm, 77–80
- lotus effect, 340
- low-level laser therapy (LLLT), 187, 194
- lower critical solution temperature (LCST), 199
- lucidin, 383
- lung *see* mechanical lung
- Lycra, 229
- Lyme disease, 408, 411
- lymphatic filariasis, 408
- LZR Pulse fabric, 231
- LZR racer swimwear, 231

- M-5 fibre, 254
 - chemical structure, 255
- m-aramid, 101
- MA30B, 217
- MAD system, 235
- Magellan Systems International LLC, 254
- magnesium oxide (MgO), 455
- MAGNET, 415, 419
- marigold *see Tagetes patula* L.
- mechanical filtration, 261
- mechanical lung, 297
- median knock-down time (MKDT), 415
- medical textiles, 177, 361–2
- melamine fibres, 107
- melt additives, 111–13

- membranes, 261, 262, 446–50, 451
 - microporous membranes, 446–8
 - relationship between protection performance and air permeability, 447
 - nanofibrous membranes, 448–50, 451
 - air permeability, water vapour transmission rate and protection performance against pesticide mixture, 451
 - microporous membrane vs fabric and non-woven SEM micrographs, 449–50
 - selectively permeable membranes, 448
- mesh simplification, 75–7
- mesh triangulation, 74–5
- meta-aramid fibres, 105, 274
- metal oxides, 453–5
 - aldicarb solution degradation with reaction time, 454
- metal–organic frameworks (MOF), 259–60
- metamaterials, 252–3
- methacryloyloxyethyl orthophosphorotetra ethyl diamidate, 119
- methicillin-resistant *Staphylococcus aureus* (MRSA), 361, 390
- methyl parathion, 435
- micro-encapsulation, 284–5
- Micro-Tribometer, 273
- microcirculation, 187
- microclimate, 270–2
- microencapsulated PCM, 173–4, 175
 - core-shell schematic, 173
- MicroPCMs *see* microencapsulated PCM
- microporous polypropylene hollow fibre, 297
- military textiles, 249–67
 - aerosols, 260–6
 - aerosol capture mechanisms, 263
 - alumina membrane, 262
 - conducting interpenetrating fibrous network, 266
 - electrospun web vs human hair, 265
 - expanded polytetrafluoroethylene, 264
 - meltblown glass fibre aerosol filtration media, 262
 - size exclusion membrane, 261
 - ballistics, 253–5
 - camouflage, 250–3
 - chemical structures of M-5 and PBO fibres, 255
 - toxic chemicals, 255–66
 - bulk toxic or burning liquids, 256–7
 - gases and vapours, 257–60
 - microwave-treated 50:50 nylon:cotton, 258
 - MOF filled with adsorbate, 260
 - water and dodecane drop-let on treated 50:50 woven nylon:cotton, 257
 - USA fielded camouflage, fielded ballistic protection and fielded CBW agent protection, 251
- Mincor TX TT, 332, 333
- minimal erythema doses (MEDs), 48–9
- modacrylics, 108
- moderately flammable fibres, 100
- monochlorotriazinyl- β -cyclodextrin (CDMCT), 422
 - chemical structure, 423
- Monte Carlo simulation, 276, 279, 281
- Monte Carlo technique, 497
- Mooney-Rivlin 2-parameter constitutive equation, 468
- multilayered fibres, 275
- N-tert*-butylacrylamide (NTBA), 200
- N-halamines, 452–3
 - aldicarb degradation by DMDMH- and MTMIOP-treated fabrics, 452
- N-N'* diethyl amino ethyl methacrylate, 202
- Nafion, 448
- Nano-Care, 333
- nano-encapsulation, 284–5
- 'nano neural knitting', 303
- NanoSphere, 333
- nanotechnology, 445
- National Institute for Occupational Safety and Health (NIOSH), 446

- natural fibre fabrics, 116–21
- Navier–Stokes equation, 261
- Netprotect, 419
- Newstar, 105
- N,N*-methylene bisacrylamide (MBA), 201
- Noflan, 120
- Nomex, 101, 105, 274
- non-durable antistatic agents, 34–5
- non-implantables, 303–14
 - bed sore prevention incontinence device, 309
 - haemorrhage control dressings, 312–14
 - pressure ulcer prevention materials, 311–12
 - structure and composition, 304–11
 - occlusive dressings, 305–10
 - pressure ulcers, 305
 - stages of wound-healing, 304
 - wound-healing materials, 304–5
 - wound proteases sequestration and approaches to treating chronic dermal ulcers, 310–11
- non-woven fabrics, 441–3
- normalised cross-correlation (NCC), 69
- novel pesticide protection clothing
 - aldicarb
 - degradation by DMDMH-and MTMIOP-treated fabrics, 452
 - solution degradation with reaction time, 454
 - development, 445–56
 - air permeability, water vapour transmission rate and protection performance against pesticide mixture, 451
 - enhanced repellency, 445–6
 - enhanced sorption, 446
 - membranes, 446–50, 451
 - microporous membrane vs fabric and non-woven SEM micrographs, 449–50
 - relationship between protection performance and air permeability, 447
 - human exposure, 434–6
 - chemical protective clothing systems, 436
 - health effects, 434–5
 - mitigation strategies, 435–6
 - improving the functionality, 434–56
 - liquid penetration through porous materials, 440–45
 - non-woven fabrics, 441–3
 - relationship between fabric thickness and pesticide penetration, 444
 - woven fabrics, 443–5
 - mechanisms for chemical protection, 436–45
 - barriers to liquids permeation, 437–8
 - protection/comfort model, 437
 - repellency and liquids sorption, 438–40
 - textile material interaction with challenge liquid, 439
 - multifunctional materials with self-decontaminating properties, 450–6
 - cross-linking POM to cellulose, 456
 - DMMP overall balanced reaction with surface MgO, 455
 - metal oxides, 453–5
 - N-halamines, 452–3
 - polyoxometalates, 455–6
- NSN 6840–6801–346–0237, 424
- nylon, 229, 273
- nylon 6,6, 229
- nylon fabrics, 114
- O, O*-dimethyl *O*-4-nitrophenyl phosphorothioate, 435
- occlusion, 305–6
- occlusive dressings, 305–10
 - amorphous hydrogel, 307
 - chronic wounds, 308–10
 - contact layer dressings, 307
 - fillers, 307
 - gauze packing, 307–8
 - hydrocolloids, 306
 - semipermeable foam, 307
 - sheet hydrogels, 306
 - thin films, 306

- wound vacuum assisted closure, 308
- octabromodiphenyl ether (OctaBDE), 121
- oil repellency, 21–2
- Olyset Net, 415, 419
- organophosphorus compounds, 117–19
- orthophosphoric acid, 119
- output aerosol concentration, 282
- oxidised polyacrylonitrile fibres, 108
- P84, 107
- P-N Synergism, 104
- para-aramid, 254
- para-aramid fibres, 105
- passive camouflage, 251
- passive drag, 232, 234–5
- PCM *see* phase-change materials
- penalty algorithm, 466
- Penalty methods, 467
- pentabromodiphenyl ether (PentaBDE), 121
- peptides, 301–3
- Peptite 2000, 302
- performance swimwear, 226–46
 - biomechanics of swimming, 231–6
 - drag force associated with swimming, 231–4
 - drag force measurement, 234–5
 - swimwear design and drag force, 236
 - development, 227–31
 - design, 229–31
 - effect on swimming performance, 231
 - history, 227–8
 - materials used, 228–9
 - effect of innovative swimwear on swimming performance, 236–45
 - contact angles for different types of fabrics, 237
 - drag force and physiological and biomechanical responses, 238–45
 - water repellency, 236–8
 - future trends, 245–6
 - studies on innovative performance swimwear and wetsuits, 241–4
- PermaNet, 415, 419
- PermaNet 3.0, 420
- permethrin, 410, 411
- persistent organic pollutants (POPs), 122
- personal protective equipment, 275, 435
- personal protective technologies (PPT), 269
- pesticide penetration, 440, 445
- pH-responsive fibres, 210–19
 - cross-linking, 210–11
 - cycles of swelling and de-swelling, 217
 - equilibrium swelling without any load and retractive force during de-swelling, 215
 - fibres with physical cross-links, 213–19
 - modification of an existing precursor fibre, 211–13
- pH-responsive polymers, 201–2
- phase-change material microcapsules (PCMMCs), 192
- phase-change materials
 - applications of PCM incorporated textiles, 175–7
 - active-wear clothing, 176
 - aerospace textiles, 175
 - automotive textiles, 177
 - cotton fabrics with microcapsules, 176
 - medical textiles, 177
 - other areas, 177
 - incorporation in textile structure, 172–5
 - coating, 174
 - core-shell microencapsulation, 173
 - fibre technology, 175
 - lamination, 174
 - microencapsulation, 173–4
 - process, 166–7
 - heating and cooling cycles, 167
 - phase-change cycles, 166
- thermo-regulating textiles, 163–78
 - applications, 175–7
 - challenges, 177–8
 - thermal comfort and clothing, 164–5
 - thermo-physiological comfort, 168
- types, 168–72
 - hydrated salts, 169

- phase-change materials (*cont.*)
 - influence of molecular weight on heat of fusion, 172
 - latent heat storage materials and their thermal properties, 170
 - linear hydrocarbons thermal properties, 171
 - long chain hydrocarbons, 169–71
 - organic and inorganic PCMs, 169
 - polyethylene glycol, 171
- phase separation, 301
- Phloxine B, 380
- phosphinic acid derivatives, 113
- phosphoramidates, 119
- phosphoric acid esters, 34–5
- photobiomodulation, 187
- photocatalytic coatings, 23
- photocatalytic oxidation, 453
- phototherapy, 186–7, 194
- PHPA *see* polyhydroxypolyamines
- physical vapour deposition, 4
- physisorption, 258
- pigment Red 83 *see* alizarin
- piperonyl butoxide (PBO), 411
- Planck's constant, 279
- plasma, 37
- plasma sputtering, 366
- plasma surface modification, 7
- point-triangle collision, 86–7
- Poiseuille equations, 440
- poly(2-hydroxypropylene spirocyclic pentaerythritol bisphosphonate) (PPBPB), 115
- poly(*N*-isopropylacrylamide) (PNIPAm), 199, 204
 - chemical structure, 200
- poly(*p*-phenylene-2,6-benzobisoxazole) (PBO), 254
 - chemical structure, 255
- poly-phenylene benzobisoxazole, 108
- polyacrylic acid (PAA), 201–2, 379
- polyacrylonitrile fabrics, 115–16
- polyacrylonitrile (PAN) fibres, 211–12, 453
- polyamides, 112
- polyamines, 36
- polybenzimidazole (PBI), 107–8
- polyepoxides, 36
- polyester, 229
- polyester fabrics, 114–15
- polyether ether ketone (PEEK) composites, 262
- polyetherimide, 107
- polyethylene glycol, 171
- polyethylene paraffin compound (PPC), 171–2
- polyethylene terephthalate (PET), 299
- poly(hydroxybutyrate-co-hydroxyvalerate), 354
- polyhydroxypolyamines, 36–7
- polyimide fibre, 107
- polyolefin fibres, 113
- polyoxometalates, 455–6
 - cross-linking to cellulose, 456
 - DMMP overall balanced reaction with surface MgO, 455
- polyphenylene sulphide fibres, 108
- polyvinyl chlorides, 108
- polyvinylidene fluoride, 31
- POM *see* polyoxometalates
- pomegranate *see* *Punica granatum* L.
- porosity, 440
- PostGL, 468
- Potts model, 103
- PPE *see* personal protective equipment
- pressure drag, 232–3, 236
- pressure-induced charge separation, 31
- pressure ulcers, 305
 - bed sheet and non-woven care sheet designed to wick moisture away, 312
 - bed sore prevention incontinence device, 309
 - prevention materials, 311–12
- Proban CC, 117
- Procon, 108
- Prontosil, 379
- protease sequestrant dressing, 310–11
- pseudoelasticity, 133
- Punica granatum* L., 392
- PVD *see* physical vapour deposition
- pyrethroids, 409
- pyrethroid-laden textiles

- bednets *in situ* treatment and other textiles, 424–5
- chemical structure
 - insecticides, repellents and synergist, 412
 - monochlorotriazinyl- β -cyclodextrin, 423
 - pyrethroids, 410
- factory-produced long-lasting insecticidal nets, 414–21
 - commercially available LLINs that contain pyrethroids, 417–18
 - effectiveness in controlling vector-borne diseases, 421
 - effectiveness measurement, 414–15
 - factory-prepared, 415–21
- factory-produced textiles, 421–4
- future trends, 425–6
- protection from biting insects, 404–26
 - biting insects and diseases they carry, 405–9
 - insecticide-laden textiles key issues, 414
 - insecticide-treated textiles application and effectiveness, 413–14
 - pyrethroids and other insecticides, 409–13
 - vector-borne diseases and associated vector control agents, 406
- pyrethroids, 407, 409–13
 - chemical structure, 410
- pyroelectric effect, 31
- PYRON, 108
- Pyrovatex CP, 117
- Pyrovatim PBS, 117
- Pythagoras's theorem, 349, 352
- QAS *see* quaternary ammonium salts
- quadric error metrics, 75
- quaternary ammonium salts, 363–6, 380–1
 - antimicrobial effects, 364
 - structures, 364
- quaternary ammoniums, 34, 35
- Quercus infectoria* (QI), 393
- Quikclot, 313
- Quikclot Combat Gauze, 313
- quinolones, 386–7
- quinones, 382–7
 - anthraquinones, 382–4
 - benzoquinones, 385–7
 - naphthoquinones, 384–5
- R711 silica nanoparticulates, 41–2
- random-chain scission, 102
- random walk model, 497
- Rayleigh criterion, 8
- REACH *see* Registration, Evaluation, Authorisation and Restriction of Chemicals
- reactive oxygen species (ROS), 370
- readily flammable fibres, 100
- regeneration process, 363
- Registration, Evaluation, Authorisation and Restriction of Chemicals, 122
- regularisation parameter, 72
- relatively non-flammable fibres, 100
- resistivity, 40
- resorcinol bis(diphenyl phosphate), 113
- Restriction of Hazardous Substances (RoHS), 122
- Reynolds number, 233
- Rhinovirus*, 456
- roll-off angle, 347–9
 - self-cleaning effect by superhydrophobicity, 347
 - water drops on a tilted surface, 348
- rubber fibre, 273
- Ryton, 108
- sapeptides *see* self-assembling peptides
- SC *see* stratum corneum
- 'scaffolding' effect, 100
- scanning electron microscopy (SEM), 9–10
- Scotch cellophane tape 5912, 492
- Securus fibre, 152
- self-assembling peptides, 302
- self-assembly, 300–1
- self-cleaning, 340
- self-cleaning clothes, 331
- self-rolling, 81–2
- semipermeable foam, 307
- sewability, 91–3

- sewing forces, 83–5
- shape memory alloys
 - applications in textiles, 133–8
 - pseudoelasticity, 133
 - effect on textiles, 134–8
 - electrical-active shape memory fabric, 137
 - electro-active shape memory textile products, 137
 - functionality of insulating property, 136
 - other textile products, 136
 - problems, 138
 - shape memory clothing, 135–6
 - shape memory dress with SMA wires, 136
 - shape memory fabrics, 134–5
 - shape memory of a fabric with SMA wires, 135
 - shape memory yarn, 134
 - shape recovery of a fabric with nitinol SMA wires, 135
 - smart garment with SMA wires, 137
 - shape memory mechanisms, 132–3
 - one-way and two-way SME, 132
- shape memory clothing, 135–6
- shape memory effect, 131, 132–3, 156
- shape memory fabrics, 134–5
- shape memory foams, 151–2
- shape memory materials (SMMs), 131–57
 - future trends, 155–7
 - SMA applications in textiles, 133–8
 - SMA shape memory mechanisms, 132–3
 - SMP applications in textiles, 140–55
 - SMP shape memory mechanisms, 138–9
- shape memory nano-fibres, 151
- shape memory polymers
 - applications in textiles, 140–55
 - basic fabric parameter, 147
 - coating, 140–4
 - crease retention, 141
 - easy wear and perfect match, 150
 - end-capped SMPU oligomers
 - synthesis, 140
 - fabrics and garments, 146–51
 - fibers prepared by wet and melt spinning, 145
 - fibre spinning, 144–5
 - improved dimensional stability, 143
 - moisture-responsive SMPs for sweat intelligent management, 155
 - Nike ‘Sphere React’ shirt with smart vent structure, 154
 - pattern with good shape retention, 142
 - pressure of enlarged fabrics to ‘wearer’, 149
 - shape memory foam textile products, 152
 - shape memory foams, 151–2
 - shape memory hollow fibre, 146
 - shape memory nano-fibres, 151
 - shape memory textiles with good damping properties, 152
 - smart breathability, 152–3
 - SMPU fibre stress–strain curve vs other synthetic fibres, 145
 - SMPU oligomers reaction with cotton, 140
 - SMPU synthesis routine, 154
 - strain recovery ratio, 147
 - untreated/treated wool fabrics
 - SEM images, 142
 - water/moisture-driven SME, 153–5
 - wrinkle-free effect, 141
 - shape memory mechanisms, 138–9
 - thermal active SME, 139
 - untreated and treated wool fabrics
 - SEM images, 142
- shape memory polyurethane, 140–1
 - synthesis routine with pyridine units, 154
- shape memory yarn, 134
- shear-thickening fluids (STF), 254–5
- sheet hydrogels, 306
- shikonin, 384
- silica gels, 259
- silk, 120–1, 273, 302
- silver, 363, 366–67
- silver salts, 366
- simulation, 40–1
- single fibre efficiency, 276

- single wall carbon nano-tubes (SWCNT), 219
- skin/fabric interactions
 - biomechanics, 462–86
 - blister, 477
 - 3-D blister with different radius ratio, 478
 - 2-D FE model, 480
 - displacement and hot spot stress, 483
 - displacement at different frequencies, 480
 - geometry model, 477
 - computer model: skin friction blistering, 477–86
 - contact algorithm, 477–8
 - displacement and hot spot stress at five friction coefficient levels, 481–2
 - material properties, 477
 - maximum tangential friction stress and normal pressure at different friction coefficient, 483
 - modal natural frequencies, 479
 - model and material properties, 477–8
 - 1st order modal shape with frequency, 479
- EFE model of skin/sleeve interactions
 - during arm rotation, 465–77
- FE model for skin–fabric–arm system under an arm rotation, 466
- initial contact between fabric and skin with a velocity, 476
- method, 465–9
- model parameters, 468–9
- numerical resolution/software, 468
- parameters/ranges for four simulations, 469
- shear stresses at different initial gap between fabric and skin, 472
- sleeves displacements away from the arm contacting point, 473
- stress response with different fabric density, 472
- system description/analytical model, 465–8
- maximum Von-Mises stress
 - normalised with the second set skin parameters, 469
 - relative with the second set skin parameters, 469
 - normalised effective shear stress
 - different fabric modulus levels, 470
 - different friction coefficients, 471
- skin friction drag, 232, 236
- skin irritation, 272–4
- skin substitutes, 309–10
- slow-releasing mechanism, 363
- SMA *see* shape memory alloys
- SMA wires, 134–5, 137
- Small Vision System, 67
- smart garment, 137
- smart-polymers *see* stimuli-sensitive polymers (SSP)
- SME *see* shape memory effect
- SMP *see* shape memory polymers
- SMP fibre spinning, 144–5
- SMPU *see* shape memory polyurethane
- ‘soft deletion’ strategy, 77
- soft rigid armour, 253
- soft wearable armour, 253
- sol-gel, 7
 - processing, 323–4
- Spandex, 229
- spandex fibre, 273
- Spectra, 253
- Spectra/Dyneema, 250
- Speedo, 226, 230, 231, 239
- ‘Sphere React Shirt,’ 153–5
- Staphylococcus aureus*, 380, 383
- static charges, 27, 28–31
- static dielectric constant, 279
- stereo matching, 69–72
 - algorithm, 70
 - example, 72
- stereovision, 66–72
- stimuli-responsive polymers *see* stimuli-sensitive polymers (SSP)
- stimuli-sensitive polymers (SSP), 198–121, 198–204
 - approaches to improve the response, 205
 - conversion to fibres, 208–21
 - change in shape of different SSP fibres, 211

- stimuli-sensitive polymers (SSP) (*cont.*)
- cyclability behaviour of modified acrylic fibre, 213
 - electroactuating fibres, 219–21
 - functionalised SWCNT on magnitude and strain rate of composite fibres, 221
 - modified PAN fibre chemical structure, 212
 - pH-responsive fibres, 210–19
 - proposed structure of the copolymers and fibre, 214
 - rate of transition and transition temperatures of SSP fibres, 210
 - SSP fibre produced from poly(NTBA:Am::27:73) copolymer, 209
 - SWCNT/chitosan composite fibres
 - response towards change in applied voltage, 220
 - SWCNT concentration on tenacity of SWCNT/chitosan composite fibre, 219
 - temperature-responsive fibres, 209–10
 - drawbacks and limitations of current SSP/hydrogels, 204–5
 - dual-sensitive (temperature and pH sensitive) polymers/hydrogels, 202–4
 - integration to textiles, 206–8
 - coated yarn rate of transition, 207
 - coated yarn structures, 206–7
 - responsive breathable fabric, 208
 - water-vapour transmission for coated fabrics, 208
 - mechanism of action, 199
 - pH-responsive polymers, 201–2, 203
 - commonly used polymer systems, 203
 - mechanism of action, 202
 - smart functional textile, 205–21
 - temperature-responsive polymers, 199–201
 - copolymer structure, 201
 - PNIPAm chemical structure, 200
 - Stoke's law, 280
 - stratum corneum, 491
 - stroke distance, 238–9, 240
 - stroke rate, 239, 240
 - subject surface, 85
 - sulfur derivatives, 119
 - sum of squared differences (SSD), 71
 - sun-protective clothing
 - standards, 50–1
 - see also* ultraviolet-blocking fabrics
 - sunlight, 185
 - Sunshen fabric, 229
 - superhydrophobic surface, 321
 - superhydrophobic textile, 340–57
 - applications, 354–7
 - market approach, 356–7
 - new product development, 355–6
 - potential markets and new products using self-cleaning technologies, 356
 - research review, 354–5
 - contact-angle, 341–3, 349–50
 - drop on a flat surface, 342
 - hysteresis, 349–50
 - surface tension, 341–3
 - wettability, 341
 - future trends, 357
 - physical modification, 341–4
 - roll-off angle, 347–9
 - self-cleaning effect by superhydrophobicity, 347
 - water drops on a tilted surface, 348
 - rough surfaces, 343–6
 - contact angle, 344
 - hydrophobicity, 344–6
 - liquid drop, 344
 - liquid reservoir, 343
 - wettability, 343–4
 - rough wetting, 343–7
 - artificial lotus fabric modelling, 346–7
 - roughness pattern upper-sectional view, 346
 - superhydrophobic rough surfaces
 - preparation, 349–53
 - liquid drop sitting on cylinders, 352
 - plain woven fabric cross-section, 350
 - predicted vs measured apparent contact angles of woven surfaces, 353

- superhydrophobic textiles
 - applications, 331–4
 - multifunctionalisation, 334
 - self-cleaning, 331–3
 - water droplets rolling through surfaces with dust, 333
 - water repellence, 331
 - chemical modifications for fabricating rough surfaces, 323–6
 - complex particle coating, 325–6
 - hydrothermal synthesis, 324–5
 - procedure for preparation on cotton substrate, 326
 - sol-gel processing, 323–4
 - future trends, 334–5
 - hydrophobisation for lowering the rough textiles surface energy, 327–9
 - alkyl molecules, 328–9
 - fluorinated molecules, 327–8
 - non-fluorinated polymer, 329
 - silicon compounds, 329
 - surface reactive molecules for low-surface-energy modifications, 327
 - improving through chemical modifications, 320–35
 - key principles, 321–2
 - droplet behaviour on a flat surface, 322
 - materials with low surface energy
 - nanoscaled coating, 329–31
- superhydrophobicity, 22
- ‘surface flash,’ 100
- surface modelling, 72–80
- surface modifications
 - applications for functional textiles, 19–23
 - biomedical applications, 19–20
 - conductivity and antistatic properties, 22–3
 - increasing hydrophilic character, 20–1
 - photocatalytic coatings, 23
 - UV-protection, 23
 - water and oil repellency, 21–2
 - improving textile functionality, 3–24
 - future trends, 23–4
 - physical and chemical characterisation, 8–19
 - microscopic techniques, 8–11
 - atomic force microscopy, 10–11
 - polyester non-woven, 8
 - resolution, 8
 - scanning electron microscopy, 9–10
 - untreated polypropylene non-woven, 10
 - spectroscopic techniques, 11–15
 - contact angle measurement, 17
 - effective depth and take-off angle, 14
 - Fourier-transform infrared spectroscopy, 15
 - photoionisation process energy diagram, 13
 - x-ray photoelectron spectroscopy, 11–15
 - XPS measurements schematic set-up, 12
 - types, 4–7
 - plasma technology, 7
 - vapour deposition, 4–5
 - chemical vapour deposition, 5
 - CVD process schematic, 5
 - physical vapour deposition, 4
 - PVD process schematic, 4
 - wet surface modification techniques, 6–7
 - electroless deposition, 6–7
 - grafting, 6
 - sol-gel, 7
 - wetting and wicking of modified textiles, 15–19
 - capillary rise method, 19
 - contact angle measurement, 16–18
 - liquid absorptive capacity, 18
 - water droplet on silicone surface, 17
- survey scan, 14
- swimming velocity, 239, 240
- swimwear, 226
 - history, 227–8
 - see also* performance swimwear
- synthetic antibacterial colorants, 378–81
- synthetic fibre fabrics, 114–16

- Tagetes patula* L., 389
 TaumaDex, 313
 Technora, 105
 Teflon, 346
 Teijinconex, 105
 temperature-responsive fibres, 209–10
 temperature-responsive polymers, 199–201
 tetrabromobisphenol A (TBBPA), 121
 tetrakis (hydroxymethyl) phosphonium chloride (THPC), 117, 118
 textile fibre, 100–1, 274
 textiles
 antibacterial colorants, 376–96
 micro-organisms, 393–5
 natural, 381–93
 photo-activated, 395–6
 synthetic, 378–81
 textiles, 376–96
 superhydrophobic, 320–35
 key principles, 321–2
 thermo-regulating with phase-change materials, 163–78
 applications of PCM incorporated textiles, 175–7
 challenges, 177–8
 how PCMs work, 166–7
 incorporation in textile structure, 172–5
 thermal comfort and clothing, 164–5
 thermo-physiological comfort, 168
 types, 168–72
 see also pyrethroid-laden textiles
 textiles dyes
 and chemicals transdermal permeation, 489–503
 skin irritations key issues, 490–1
 stochastic modelling for transdermal drug delivery, 496–502, 503
 drug absorptions experimental vs simulation results, 503
 drug simulated penetration into a bricks-and-mortar structure section, 500–2
 model description, 498–500
 staggered bricks-and-mortar model, 498
 transdermal drug permeation
 in vitro study, 491–6
 estradiol residual in layers after 0.5-h diffusion, 493
 estradiol residual in layers after 4-h diffusion, 494
 estradiol transdermal absorption at different times, 492
 estrogen percutaneous absorption parameters, 496
 materials and methods, 491–2
 textiles dyes and chemicals, 489–503
 skin irritations key issues, 490–1

- stochastic modelling for transdermal drug delivery, 496–502, 503
- transdermal drug permeation *in vitro* study, 491–6
- transepidermal water loss (TEWL), 270
- Trevira CS, 109
- Tri-Carb 2900 TR, 492
- triboelectric effect, 28
- triboelectric series, 29, 30
- tripwires, 230
- tris (tribromoneopentyl) phosphate, 113
- Trypanosoma cruzi*, 407
- turmeric *see Curcuma longa*
- Twaron, 105, 253
- twist factor, 443
- Type III ballistic protection, 253
- TYR, 226, 230, 239
- Ultem, 107
- ultra-high-surface area (UHSA) adsorbents, 259
- ultraviolet absorbers, 53–5
- ultraviolet-blocking fabrics, 45–57
 - environment and fabric use, 55–6
 - fabric colour, dyes and UV absorbers, 53–5
 - fabric type and construction, 51–3
 - outlook, 56–7
 - sun-protective clothing standards, 50–1
 - UPF *in vitro* and *in vivo* testing, 48–50
- ultraviolet dosimetry, 50
- ultraviolet protection, 23, 45–57
 - see also* ultraviolet-blocking fabrics
- ultraviolet protection factor (UPF), 45–57
 - environment and fabric use, 55–6
 - fabric colour, dyes and UV absorbers, 53–5
 - fabric type and construction, 51–3
 - in vitro* and *in vivo* testing, 48–50
 - outlook, 56–7
 - sun-protective clothing standards, 50–1
- ultraviolet radiation, 45–7
- UMT Series Micro-Tribometer, 463
- United States Department of Agriculture (USDA), 435
- Universal Scintillation Cocktail, 492
- UPF *see* ultraviolet protection factor
- US Environmental Protection Agency, 413
- US EPA *see* US Environmental Protection Agency
- Van der Waals forces, 278
- vancomycin-resistant enterococci (VRE), 361
- VE *see* viable epidermis
- Vectran, 110
- Vectran HT, 110
- Vectran UM, 110
- velocity perturbation method, 235
- vertex points, 77
- viable epidermis, 492
- virtual dressing, 66, 80–91, 92
- Viscose FR, 113
- Visil, 113
- Von-Mises stress, 468, 473
 - defined, 470
- Vyrene, 229
- water repellency, 21–2
- water-vapour transmission rate (WVTR), 208
- wave drag *see* wave-making resistance
- wave-making resistance, 233–4
- Weissmuller model, 229
- Wenzel contact angle, 344, 349
- Wenzel model, 344–5, 346, 352
- Wenzel's equation, 321
- West Nile disease, 408
- wet surface modification, 6–7
- wetsuit, 240, 245
- WHO *see* World Health Organisation
- WHO Pesticide Evaluation Scheme, 414–15
- WHOPES *see* WHO Pesticide Evaluation Scheme
- wool, 273
- wool fabrics, 142, 143

- wool textiles, 120
- work function, 13
- World Health Organisation, 409
- wound-healing materials, 304–5
- wound vacuum assisted closure, 308
- WoundStat, 313
- woven fabrics, 443–5
 - relationship between fabric thickness and pesticide penetration, 444
- X-Fiber, 105
- x-ray photoelectron spectroscopy (XPS), 11–15
- Young–Dupré equation, 439
- Young equation, 341, 343, 344
- zeolite, 259, 313
- Zipro, 120
- Zylon, 108